SSC-398

ASSESSMENT OF RELIABILITY
OF SHIP STRUCTURES

DTIC QUALITY INSPECTED 2

SHIP STRUCTURE COMMITTEE
1997

SHIP STRUCTURE COMMITTEE

The SHIP STRUCTURE COMMITTEE is constituted to prosecute a research program to improve the hull structures of ships and other marine structures by an extension of knowledge pertaining to design, materials, and methods of construction.

RADM J. C. Card, USCG (Chairman)
Chief, Office of Marine Safety, Security
  and Environmental Protection
U. S. Coast Guard

Mr. John Grinstead
Director, Policy and Legislation
Marine Regulatory Directorate
Transport Canada

Mr. Edwin B. Schimler
Associate Administrator for Ship-
  building and Technology Development
Maritime Administration

Dr. Donald Liu
Senior Vice President
American Bureau of Shipping

Mr. Robert McCarthy
Director, Survivability and Structural
  Integrity Group (SEA 03P)
Naval Sea Systems Command

Mr. Thomas Connors
Acting Director of Engineering (N7)
Military Sealift Command

Dr. Ross Grahm
Head, Hydronautics Section
Defence Research Establishment-Atlantic

EXECUTIVE DIRECTOR

CDR Stephen E. Sharpe, USCG
LT Tom Miller, USCG

CONTRACTING OFFICER TECHNICAL REPRESENTATIVE

Mr. William J. Siekierka
Naval Sea Systems Command

SHIP STRUCTURE SUBCOMMITTEE

The SHIP STRUCTURE SUBCOMMITTEE acts for the Ship Structure Committee on technical matters by providing technical coordination for determinating the goals and objectives of the program and by evaluating and interpreting the results in terms of structural design, construction, and operation.

MILITARY SEALIFT COMMAND

Mr. Robert E. Van Jones (Chairman)
Mr. Rickard A. Anderson
Mr. Michael W. Touma
Mr. Jeffrey E. Beach

MARITIME ADMINISTRATION

Mr. Frederick Seibold
Mr. Richard P. Voelker
Mr. Chao H. Lin
Dr. Walter M. Maclean

U. S. COAST GUARD

CAPT George Wright
Mr. Walter Lincoln
Mr. Rubin Sheinberg

AMERICAN BUREAU OF SHIPPING

Mr. Glenn Ashe
Mr. John F. Conlon
Mr. Phillip G. Rynn
Mr. William Hanzalek

NAVAL SEA SYSTEMS COMMAND

Mr. W. Thomas Packard
Mr. Charles L. Null
Mr. Edward Kadala
Mr. Allen H. Engle

TRANSPORT CANADA

Mr. Peter Timonin
Mr. Felix Connolly
Mr. Francois Lamanque

DEFENCE RESEARCH ESTABLISHMENT ATLANTIC

Dr. Neil Pegg
LCDR Stephen Gibson
Dr. Roger Hollingshead
Mr. John Porter

SHIP STRUCTURE SUBCOMMITTEE LIAISON MEMBERS

SOCIETY OF NAVAL ARCHITECTS AND
  MARINE ENGINEERS
Dr. William Sandberg

CANADA CENTRE FOR MINERALS AND
  ENERGY TECHNOLOGIES
Dr. William R. Tyson

U. S. NAVAL ACADEMY
Dr. Ramswar Bhattacharyya

U. S. MERCHANT MARINE ACADEMY
Dr. C. B. Kim

U. S. COAST GUARD ACADEMY
CDR Bruce R. Mustain

U. S. TECHNICAL ADIVSORY GROUP TO THE
  INTERNATIONAL STANDARDS ORGANIZATION
CAPT Charles Piersall

AMERICAN WELDING SOCIETY
Mr. Richard French

NATIONAL ACADEMY OF SCIENCES -
  MARINE BOARD
Dr. Robert Sielski

NATIONAL ACADEMY OF SCIENCES -
  COMMITTEE ON MARINE STRUCTURES
Dr. John Landes

WELDING RESEARCH COUNCIL
Dr. Martin Prager

AMERICAN IRON AND STEEL INSTITUTE
Mr. Alexander D. Wilson

OFFICE OF NAVAL RESEARCH
Dr. Yapa D. S. Rajapaske

MASSACHUSETTS INSTITUTE OF TECHNOLOGY
CAPT Alan J. Brown

STUDENT MEMBER
Mr. Jason Miller
Massachusetts Institute of Technology

Ship

Structure

Committee

An Interagency Advisory Committee

SSC-398
SR1344

April 30, 1997

ASSESSMENT OF RELIABILITY OF SHIP STRUCTURES

This work forms part of a series of Ship Structure Committee tasks in the structural reliability area. Previous work covered assessment of uncertainties associated with hull ultimate failure, uncertainties in stress analysis, uncertainties in strength models, probabilistic loads and load combinations. In addition, an introduction to structural reliability theory, a demonstration of probability based design procedures, and demonstration prototype design code have been funded.

This report presents a set of methodologies for assessing existing surface ship structural reliability. Areas included cover wave loads and load combinations, hull strength, the estimation of ship failure probabilities, fatigue reliability, and safety level selection. Methods for dealing with non-linearity associated with both loads and strength are presented. In addition to incorporating the results of previous work, the report presents additional information and developments in the various topic areas. In several cases results have been presented in the form of design charts and equations with worked out examples. Applications are made to four ships: two cruisers, a tanker, and an SL-7. For each of these ships loads, strength, reliability, and sensitivity to parameters have been estimated.

The report includes general guidelines for identifying significant parameters affecting reliability as well as recommendations. A set of 10 appendices provides more detail on selected topics.

J. C. CARD
Rear Admiral, U.S. Coast Guard
Chairman, Ship Structure Committee

Technical Report Documentation Page

1. Report No. SSC-398	2. Government Accession No. PB97-141584	3. Recipient's Catalog No.	
4. Title and Subtitle Assessment of Reliability of Existing Ship Structures		5. Report Date 1997	
		6. Performing Organization Code	
		8. Performing Organization Report No.	
7. Author(s) A.Mansour, P.Wirsching, M. Luckett, A. Plumpton, et al.			
9. Performing Agency Name and Address Mansour Engineering, Inc. Attn: A.E. Mansour 14 Maybeck Twin Drive Berkeley, CA 94708		10. Work Unit No. (TRAIS)	
		11. Contract or Grant No. N00024-94-C-4059	
		13. Type of Report and Period Covered	
12. Sponsoring Agency Name and Address Ship Structure Committee U. S. Coast Guard (G-MSE/SSC) 2100 Second St. S.W. Washington, DC 21\0593-0001		Final	
		14. Sponsoring Agency Code G-M	

15. Supplementary Notes

Sponsored by the Ship Structure Committee. Jointly funded by SSC agency members. The U.S. Navy was the contracting agent for the Ship Structure Committee for this project.

16. Abstract

A detailed approach has been developed for assessing structural safety and reliability of ships. The methodology provides a means for determining reliability levels associated with a hull girder, stiffened panel and unstiffened plate modes of failure. Procedures for esimating the non-linear extreme sea loads and structural strength which are required for the reliability analysis have been developed. Fatigue reliability of ship structural details was also addressed and further developed.

The methodology was demonstrated on four ships; two cruisers, a double hull tanker and an SL-7 containership. Reliability levels associated with each mode of failure of these ships were determined and compared. Sensitivity analysis has been conducted which provides sensitivity of a safety index to variations in design variables associated with extreme loading conditions as well as with fatigue loads.

Recommendations are made of target reliability levels for each ship type and failure mode. Design variables that have the highest impact on reliability have been identified and some guidelines are provided for improving design criteria.

17. Key Words reliability models, loads, ship structural details, structural reliability, stiffened plates, extreme loads, design criteria	18. Distribution Statement Distribution unlimited, available from: National Technical Information Service U.S. Department of Commerce Springfield, VA 22151 (703)487-4690		
19. Security Classif. (of this report) Unclassified	20. SECURITY CLASSIF. (of this page) Unclassified	21. No. of Pages 424	22. Price $57.00-paper

Form DOT F 1700.7 (8/72)   Reproduction of form and completed page is authorized.

United States Department of Commerce
Technology Administration
National Institute of Standards and Technology
Metric Program, Gaithersburg, MD 20899

NIST

METRIC CONVERSION CARD

Approximate Conversions to Metric Measures

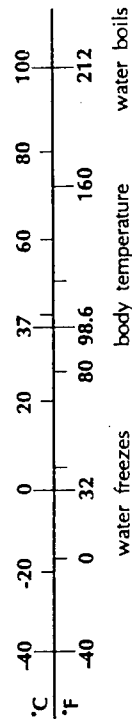| Symbol	When You Know	Multiply by	To Find	Symbol
LENGTH				
in	inches	2.5	centimeters	cm
ft	feet	30	centimeters	cm
yd	yards	0.9	meters	m
mi	miles	1.6	kilometers	km
AREA				
in^2	square inches	6.5	square centimeters	cm^2
ft^2	square feet	0.09	square meters	m^2
yd^2	square yards	0.8	square meters	m^2
mi^2	square miles	2.6	square kilometers	km^2
	acres	0.4	hectares	ha
MASS (weight)				
oz	ounces	28	grams	g
lb	pounds	0.45	kilograms	kg
	short tons (2000 lb)	0.9	metric ton	t
VOLUME				
tsp	teaspoons	5	milliliters	mL
Tbsp	tablespoons	15	milliliters	mL
in^3	cubic inches	16	milliliters	mL
fl oz	fluid ounces	30	milliliters	mL
c	cups	0.24	liters	L
pt	pints	0.47	liters	L
qt	quarts	0.95	liters	L
gal	gallons	3.8	liters	L
ft^3	cubic feet	0.03	cubic meters	m^3
yd^3	cubic yards	0.76	cubic meters	m^3
TEMPERATURE (exact)				
°F	degrees Fahrenheit	subtract 32, multiply by 5/9	degrees Celsius	°C
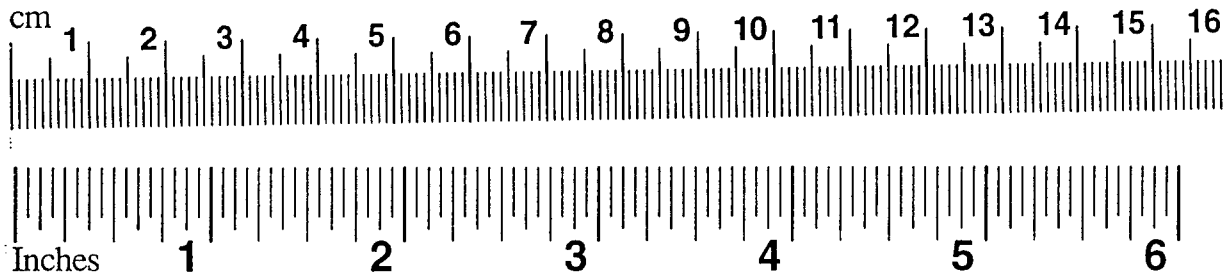
Approximate Conversions from Metric Measures

Symbol	When You Know	Multiply by	To Find	Symbol
LENGTH				
mm	millimeters	0.04	inches	in
cm	centimeters	0.4	inches	in
m	meters	3.3	feet	ft
m	meters	1.1	yards	yd
km	kilometers	0.6	miles	mi
AREA				
cm^2	square centimeters	0.16	square inches	in^2
m^2	square meters	1.2	square yards	yd^2
km^2	square kilometers	0.4	square miles	mi^2
ha	hectares ($10,000\ m^2$)	2.5	acres	
MASS (weight)				
g	grams	0.035	ounces	oz
kg	kilograms	2.2	pounds	lb
t	metric ton ($1,000\ kg$)	1.1	short tons	
VOLUME				
mL	milliliters	0.03	fluid ounces	fl oz
mL	milliliters	0.06	cubic inches	in^3
L	liters	2.1	pints	pt
L	liters	1.06	quarts	qt
L	liters	0.26	gallons	gal
m^3	cubic meters	35	cubic feet	ft^3
m^3	cubic meters	1.3	cubic yards	yd^3
TEMPERATURE (exact)				
°C	degrees Celsius	multiply by 9/5, add 32	degrees Fahrenheit	°F

Temperature scale:

°C	-40	-20	0	20	37	60	80	100
°F	-40	0	32	80	98.6	160	212	

water freezes · body temperature · water boils

ASSESSMENT OF
RELIABILITY OF SHIP STRUCTURES

TABLE OF CONTENTS

Page

ABSTRACT

TABLE OF CONTENTS

APPENDICES

A. EXTREME LOADS AND LOAD COMBINATIONS

B. SKEWNESS, KURTOSIS AND ZERO UPCROSSING RATE OF COMBINED RESPONSE

C. INFORMATION ON AVAILABLE COMPUTER CODES FOR RELIABILITY CALCULATIONS

D. GENERAL INFORMATION ON FOUR SHIPS

E. COLLECTED LOAD DATA ON FOUR SHIPS

F. CALREL OUTPUT FILE

G. PARAMETRIC STUDY AND COMPARISONS OF RELIABILITY INDICES

H. SENSITIVITY ANALYSIS RESULTS

I. THE LOGNORMAL FORMAT

J. CRITICAL VARIABLES BASED ON SENSITIVITY ANALYSIS

1. INTRODUCTION

1.1 Objectives

The objectives of this study are detailed as follows:

1. Provide a methodology for assessing the reliability level of the structure of existing ships. The computerized methodology will estimate failure probabilities associated with each identified failure mode.

2. Select four ships and perform reliability analysis relative to each identified failure mode for each select ship.

3. Recommend minimum acceptable reliability levels for each ship type and failure mode to be used as guidelines for ship designers for future ships.

4. Provide a methodology for performing sensitivity analysis of reliability levels to variations in design parameters, i.e., loads and stresses, materials and strength, and geometry of the structure.

5. On the basis of the sensitivity analysis performed, recommend design strategies that are likely to have the highest payoffs in terms of reliability.

A detailed methodology for reliability assessment has been developed. A data base has been assembled for developing estimates of structural strength of ships as well as wave induced loads, both in short term and over a ship's lifetime. With these data, it is possible to conduct a comprehensive reliability analysis. The results of the reliability analysis can be conceptually divided into two main sections. First, the "level of safety" can be estimated for a wide variety of ship loading conditions. This "level of safety" is quantified as either a safety index (β) or, equivalently, a probability of failure. Second, information can be gathered on the sensitivity of the safety index (or probability of failure) to changes in the input variables. These variables include the strength of the structure, the various loadings imposed on the structure, and load combination factors which account for the correlations between different loadings.

The methodology has been applied to four ships. Two of them are military vessels and two are commercial ships. The two military ships — *Cruiser 1* and *Cruiser 2* — have a common hull form and very similar structures. *Cruiser 1* is about 15 percent heavier than *Cruiser 2* and it has a significant portion of its structure made out of high-strength steel in an attempt to reduce this weight growth. The third ship is the *SL-7*, a fast containership design. The fourth ship, *Tanker*, is a double-hull petroleum tanker operating along the west coast of the United Stated. Table 1.1.1 shows the particulars of the four ships.

	Cruiser 1	Cruiser 2	SL-7	Tanker
Length, BP (ft)	529.0	529.0	880.5	625.0
Beam (ft)	55.0	55.0	105.5	96.0
Draft (ft)	24.0	19.8	30.0	34.0
Displacement (LT)	9680	7996	47760	44513

Table 1.1.1 — Particulars for the Four Ships

The safety of each of the subject ships will be assessed in a variety of conditions. These cases include several failure modes, two loading conditions, and two time frames. The safety of each ship will be quantified by the safety index. The resulting data can then be analyzed to uncover patterns. Also, it is possible to infer from these results and other information available in the literature what is currently considered an acceptable level of reliability.

In addition to computing safety indices, the reliability analysis procedure also generates a variety of sensitivity data that can be used to make assessments on variable importance. By analyzing these data, one can make judgments about whether or not some variables can be assumed to be deterministic quantities. Also, these data can give one a general idea as to the effects on the safety of the ship due to modifications of any of the variables (e.g., decreasing the stillwater bending moment).

Throughout the analysis of the results, an important thread is that of comparison. Since the exact same procedures produce the results for all cases and all ships, comparing the *relative* values of various outputs should yield valid conclusions. This is true despite inevitable inaccuracies in the analysis. Comparisons will be drawn between military-designed versus commercially-designed ships, between the use of high-strength versus mild steel in conctruction, between failure modes, and between loading conditions. The object of such comparisons will be to discern some sort of pattern in the data. These patterns can then be assessed and some generalizations and conclusions drawn.

1.2 Report Organization

The next chapter of the report (Chapter 2) describes the methodology developed for assessing structural reliability of ships. This chapter is divided into three main sections; the first on methodology for constructing probabilistic models of non-linear wave loads and load combinations (section 2.2), the second on methodology for constructing statistical models for non-linear hull strength (section 2.3) and the third on methodology for estimating ship failure probabilities (section 2.4).

Chapters 3, 4, 5 and 6 are concerned with the application of the methodology developed in section 2 to four ships. Specifically, Chapter 3 describes the load results for the four ships, Chapter 4 shows the strength results of the four ships and Chapters 5 and 6 give

the reliability and sensitivity analysis results, respectively. Chapter 7 describes the methodology for fatigue reliability and the results of application to the four ships. In Chapter 8, target reliabilities are recommended based on the results of this project as well as information available in the literature. The report ends with recommendations for improvements and some concluding remarks in Chapter 9.

It is highly recommended to the reader to read first the report "Introduction to Structural Reliability Theory", Ship Structure Committee report SSC-351 (1990) prior to reading this report. SSC-351 explains the basic background on reliability theory and provides in some detail the derivation of some of the equations given in this report.

1.3   Historical Review — Ship Structure Committee Previous and Future Work

A complete description of SSC previous and future work on reliability thrust area is given in the report, "Research Recommendations for FY 1996-1997" by the Committee on Marine Structures, Marine Board, National Research Council (National Academy Press, 1995). The following are excerpted from that reference in order to provide a historical review and background.

On June 17, 1987, the CMS convened an ad hoc committee with experts in the subject areas of marine structures and structural reliability. The consensus of that group was that the SSC should have a long-range program in reliability to develop a probability-based design approach for ship structures. following that meeting, the CMS formulated a four-phase program, which began in FY 1989. This program has been modified since that time to reflect the results of the first phases and to add a fifth and a sixth phase, but it remains a principal thrust area of the CMS.

The SSC also is committed to supporting the reliability thrust. The goal is development of technology to support preparation of a probability-based design code for ships. The program is described later in this section. Because reliability-based design criteria promise to improve structural efficiency, a U.S. Navy panel is studying this approach. Reliability projects proposed for SSC funding provide a sound basis for a much larger, three-pronged effort that would include computer simulation, towing-tank tests, and full-scale trials. Predicting environmental loads and the responses of complex marine structures is extremely difficult. Because assumptions and simplifications are frequently introduced, uncertainty and risk can follow. A research program initiated by the SSC to develop design criteria for marine structures is addressing uncertainties in loads. Many other research projects in structural reliability supported by the SSC either have been or are being completed. This thrust area is expected to develop the fundamental reference for (1) the development of a probability-based ship-structure design code, (2) the definition of procedures for performing failure analysis, and (3) reliability analysis for existing ships.

The development and implementation of probability-based structural design procedures have been under way in other areas since the early 1960s. In addition to the

existing design procedure that is based on the concept of a working stress, a probability-based load and resistance factor design procedure was issued by the American Institute for Steel Construction in 1986, with a second edition published in 1993. Further, the American Petroleum Institute has recommended this technology for offshore structures with their publication RP2A, "Recommended Practice for Design, Fabrication, and Installation of Fixed Offshore Structures."

The development of probability-based design codes in other areas appears to have stimulated important advances in structural design. In addition, the codes become a living document that can be revised to include new sources of information and to reflect additional statistical data on loads and load effects. It is a top-down approach that actively encourages the collection of better data.

Final design decisions about materials, sizes, and arrangements should be based on experience, regardless of the overall approach. The main advantage of a probabilistic approach as a design method is that it provides a mechanism for taking advantage of all relevant information. Probabilistic methods allow engineers to make decisions based on a quantitative description of uncertainty, in addition to reaching a consensus in structural design based on experience and judgment. The process of developing reliability technology for marine structures unifies the thrusts of many other active and recommended projects that had appeared to be unrelated in earlier times.

The advantages of new probabilistic design strategies are expected to produce a more balanced design and allow use of different safety levels (or safety factors) that depend on the predicted accuracy of various loads and structural capabilities.

To kick off the program, the SSC cosponsored a symposium and funded a tutorial on structural reliability to inform the marine community of this new technology. Sponsored by the SSC and the Society of Naval Architects and Marine Engineers, the Marine Structural Reliability Symposium was held in Arlington, Virginia, in October 1987. It attracted experts from around the world and provided a forum for assessing the state of the art in reliability methods. The report, "An Introduction to Structural Reliability Theory" (SSC-351), is a tutorial on applying reliability to marine structures. A 1-week seminar, in which the draft document was presented to SSC participants and colleagues, was held in San Francisco in January 1988 and repeated in Washington, D.C., in October 1990.

A multiyear research program is under way to apply reliability technology and develop probability-based design criteria for ship structures. The program represents a major sustained effort that will make significant changes in structural design, improve the reliability of ship structures, and permit the results of research to be more easily incorporated into future designs. The program consists of the following projects recommended by the CMS.

Probability-Based Design Approach for Ship Structures

Phase 1: Demonstration Project A demonstration project, "Probability-Based Ship Design Procedures: A Demonstration" (SSC-368), was completed in 1993. The study compares a hull girder designed by present conventional American Bureau of Shipping rules with a design that uses probability-based procedures, illustrating the applications of this approach and identifying its advantages and problems. The project report will be useful for information, instruction, and future reference.

Phase 2: Loads and Load Combinations The Phase 2 project, "Probability-Based Ship Design: Loads and Load Combinations" (SSC-373), which defines ship design loads suitable for use in reliability analysis, was completed in 1993. This study includes statistical distributions of extreme wave loads, fatigue loads, and modeling errors. Load-combination issues that require further investigation are addressed in this project.

Modeling errors were addressed in the project, "Uncertainties in Stress Analysis on Marine Structures" (SSC-363), which was completed in 1991. The project's materials counterpart, "Uncertainty in Strength Models for Marine Structures" (SSC-375), was completed in 1993.

Phase 3: Implementation The third phase of probability-based design approaches is Project SR-1345, "Probability-Based Design: Implementation of Design Guidelines for Ships," which developed a more detailed probability-based design procedure for ships. Load models provided by the Phase 2 project were combined with strength formulations from the supporting project, "Uncertainty in Strength Models for Marine Structures" (SSC-375). This project developed design procedures based on reliability considerations similar to reliability-based design procedures used for other structural applications worldwide. The procedures included provisions for ultimate strength of hull girders; design of stiffened panels; fatigue of details (typically connections); and buckling.

The first part of Project SR-1344, "Assessment of Reliability of Existing Ship Structures (Phase 1)," is now complete, and it will be useful for the Phase 3 reliability project. Phase 2 of Project SR-1344 began in 1994 and this report is the final report on this project.

Phase 4: Synthesis of the Reliability Thrust Area The four phase will provide a summary and synthesis of the various projects in the reliability thrust area, including the complementary projects in design methods and load uncertainties. There have been several programs and several investigators, and there is now a need to put all of the pieces together. The synthesis will provide a summary of reliability technology for specific application to (1) design code development, (2) failure analysis, and (3) reliability assessment of existing designs. Project SR-1362, "Probability-Based Design: Synthesis of the Reliability Thrust Area," has been initiated by the CMS.

Phase 5: LRFD Design Practice Several SSC projects have introduced load and resistance factor design. It is time now to put this design procedure into practice. Proposed Project 96-4, "Probability-Based Design (Phase 5): Load and Resistance Factor Design (LRFD) Methods for Ship Structures," will include a rigorous and complete code calibration for the design of ship structure. The resulting load and resistance factor design criteria, including all failure modes, will be written in a code style that is suitable for the direct use of practicing engineers. This phase should have higher priority than the phase for novel hull-form design, but the two research projects may be performed concurrently.

Phase 6: Novel Hull Forms and Environments The sixth phase will address reliability-based design processes for novel structures. Project 96D-O, "Probability-Based Design (Phase 6): Novel Hull Forms and Environments," is proposed for Phase 6. The term "novel" in this project applies to unconventional hull forms or structures subject to uncommon environments. The premise of the project is that in novel situations, first principles must be applied, because these designs cannot be based on extrapolation or interpolation of current practice or existing structures, as implied in the third phase. This project will determine whether the current data base, existing structural reliability literature, and practice contain the necessary elements to probabilistically assess the performance and safety of ship structures that have unusual forms or are subject to uncommon environments.

Reliability of Existing Ship Structures

Knowledge of the probabilistic characteristics of important failure modes would be useful in developing rational probability-based design criteria. This information could be used on an ad hoc basis to review or revise present procedures or to develop an entire design-criteria document. For successful implementation of a load and resistance factor design code, an estimation of modeling bias is required. In support of efforts to develop this information, the CMS recommends Project 96-20, "Experiments on Stiffened Panel Collapse and Estimation of Modeling Bias." This research should provide, for example, the much needed uncertainty data on stiffened panel collapse. In order to develop a method for the kind of failure definition needed to calculate structural reliability, Project 96-3, "Failure Definition for Structural Reliability Assessment," has been proposed. In support of this effort, Project SR-1380, "Post Yield Strength of Structural Members," is intended to provide additional means to verify the load-carrying capacity of structural components.

2. METHODOLOGY FOR ASSESSING STRUCTURAL RELIABILITY OF SHIPS

This chapter consists of three main sections. The first is concerned with the development of probabilistic models of non-linear wave loads and load combinations. The second describes a methodology for determining hull primary (global), secondary (stiffened panel) and tertiary (unstiffened plate) strength. The third section defines methods of estimating ship structural failure probability based on the load and strength information developed in the two earlier sections.

In addition to the computer codes necessary to determine the non-linear wave loads (SOST), the non-linear hull strength (ALPS/ISUM) and the probability of failure (CALREL), simple formulations are presented at the end of each section that allow the approximate estimation of the non-linear wave loads, the non-linear hull strength and the failure probability.

2.1 Methodology for Constructing Probabilistic Models of Wave Loads and Load Combinations

Estimating wave-induced loads, particularly vertical bending moment, is one of the most important tasks in ship design. In the book, *Principles of Naval Architecture* (Lewis, ed., 1989), Paulling suggests that there are four methods by which wave-induced loads can be determined:

a. approximate methods

b. strain and/or pressure measurements of full scale ships

c. laboratory measures of loads on models

d. direct computation of wave induced fluid loads

Historically, approximate methods have been the most commonly used design tool for the prediction of a characteristic extreme load which the ship must be designed to resist. The well known static balance procedure is perhaps the best example of an approximate method. The static balance procedure, and any approximate method, has also been checked by both full scale measurements and model data in an attempt to ensure reliability in design.

Approximate methods are, as the name suggests, approximate, however. The advent of nonconventional hull forms, the desire for optimal structural design, and advancing analytical capability has helped motivate work in the area of direct computation of wave induced loads. A variety of approaches has been explored here, each with varying degrees of success. Often the assumptions required to make these approaches tractable can lead to significant limitations and inaccuracies. This realization is of extreme importance in the application of analytical tools to the problem of wave induced motions and loads. Any

analytical tool, applied beyond its limits of applicability, suffers performance problems and becomes little more than an approximate method.

The prediction of wave induced loads (and motions) using direct analytical methods became more attractive after the publication of St. Denis and Pierson's paper, "On the Motion of Ships in Confused Seas", in 1953. In this paper, St. Denis and Pierson suggest that the principle of linear superposition can be applied to the ship-motion problem. The response of a ship in irregular waves can then be taken as the summation of the individual responses to the regular waves which form the confused sea.

This assumption of linearity, along with several other significant assumptions led to the development of what is now called strip theory. Salveson *et al.* (1970) and Gerritsma *et al.* (1967) presented two important papers in the development of strip theory. According to Salveson *et al.*, if linear superposition is a valid assumption, the "complex problem of predicting ship motions and sea loads in a seaway can be reduced to the two problems: (i) the prediction of the ship motions and loads in regular sinusoidal waves and (ii) the prediction of the statistical responses in irregular waves using the regular wave results." While the analytical development of linear strip theory will not be presented here, the assumptions associated with the development will be summarized. First, it is assumed that the oscillatory motions are both linear and harmonic. For a ship with lateral symmetry, vertical plane responses are taken as uncoupled with respect to lateral type responses. All viscous effects are ignored. In order to reduce the three-dimensional problem to a two-dimensional problem, the response frequency is assumed to be relatively high. Furthermore, all higher order terms in the resulting equations are neglected — again, the theory is linear.

While these assumptions seem, and are, severe, linear strip theory has shown good agreement with model and full scale tests for small excitations and responses. For larger motions, however, both the wave excitation and the ship response are non-linear. A linear prediction procedure has little hope of providing accurate results in this case. Clarke (1986) shows that this is, in fact, the case. In extreme seas, linear strip theory tends to over-predict responses. Clarke suggests that linear strip theory's 'wall-sided' assumption is the main reason for this observation. As an example, he presents the British narrow beam *Leander* class. At a probability corresponding to once in a ship life, the associated relative motion is approximately 2.6 times the freeboard at the bow. Linear strip theory assigns buoyancy to the station at the bow according to the wall sided assumption (i.e., infinite freeboard, constant beam). It is not surprising, then, that the bending moment associated with this probability level is over-predicted. Further comparison with model and full scale data shows that linear strip theory tends to, in general, under-predict sagging moments, and over-predict hogging moments. As it is linear, classic strip theory cannot distinguish between hogging and sagging moments. This is a significant limitation of classic strip theory.

The difference between sagging and hogging bending moments can be quite large, particularly for ships with fine forms, such as warships and containerships (Clarke, 1986). Given this difference, a reasonable design procedure must depend upon separate predictions of the hogging and sagging bending moments. This requirement is the motivation behind a

quadratic strip theory, developed primarily by J. J. Jensen (1979, 1992, 1993) at the Technical University of Denmark. Jensen's second order strip theory provides an analytical method for the prediction of the non-linear vertical responses of ships. This method does predict different values for the hogging and sagging moments. A portion of the work described in this report was dedicated to the application of SOST (Second Order Strip Theory), a computer program implimenting the quadratic theory) to four specific ships of interest.

The next section will highlight the theory underlying the quadratic theory, and discuss limitations of the theory. The following section (2.1.2) will describe a simple formulation for determining slightly non-linear extreme wave loads and load combinations that do not depend on the use of the SOST code. This section is followed by design charts that may assist in determining hog/sag moments acting on a ship. In the final section of this chapter, slamming loads are discussed together with the computer code SLAM.

2.1.1   An Overview of the Second Order Strip Theory (SOST):

The quadratic strip theory is based upon the same underlying assumptions as linear strip theory; the difference between linear strip theory and quadratic strip theory is that in the quadratic theory, the second order terms in the perturbational expansion of the governing equations are not discarded. The linear terms in the analysis are identical to those of linear strip theory. Second order terms arise from the non-linearities in the exciting waves, the non-vertical sides of the ship, and the non-linear hydrodynamic forces (Jensen and Pedersen, 1979). The response is still taken to be two uncoupled problems, one in the vertical plane and one in the 'lateral plane' (sway, roll and yaw and associated loads). The vertical motions and loads are of primary interest in the design phase and are developed in the quadratic theory. Its starting point is the classical linear strip theory formulation of Salvesen, Tuck and Faltinsen (1970), which has already been mentioned.

A basic approximation of strip theory is that the hydrodynamic force p_z (x,t) exerted on the ship hull per unit length can be interpreted as the sum of the change in momentum of the added mass of water, the damping due to energy dissipation in generated waves, and the restoring term:

$$p_z(x,t) = -\left[\frac{D}{Dt}\left\{m(z^*,x)\frac{Dz^*}{Dt}\right\} + N(z^*,x)\frac{Dz^*}{Dt} + \int_{-T}^{-z^*} B(z,x)\frac{\partial p}{\partial z}\bigg|_{z+w} dz\right] \quad (2.1.1)$$

Here, the operator $\frac{D}{Dt}$, is the total derivative with respect to time t:

$$\frac{D}{Dt} \equiv \frac{d}{dt} - V\frac{d}{dx}$$

where
V = forward speed of the ship

$z^*(x,t)$ = $w(x,t) - h(x,t)$

$w(x,t)$ = absolute displacement of the ship in the vertical direction

$h(x,t)$ = water surface elevation, corrected for the Smith effect

m = added mass per unit length

N = damping per unit length

$B(z,x)$ = breadth of the ship

$T(x)$ = draft of the ship

p = Froude-Krylov fluid pressure (ignoring diffraction effects)

For more information on Froude-Krylov pressure, Smith effect and Lewis transformation, please refer to Jensen and Pedersen, 1979.

In order to show the nature of the non-linearities in the resulting analysis, eqn. (2.1.1) is expanded by a perturbational method, taking into account both first and second order terms in relative displacement z^*, total displacement w, and water surface elevation h. In the expansion, the waterline breadth B, the added mass m, and the damping N are all evaluated around $z^* = 0$, and terms which are linear in z^* are included, resulting in linear and quadratic components of $p_z(x,t)$.

For deep water waves, the water surface elevation and pressure which (approximately) fulfill the free surface boundary condition can also be expressed as sums of linear and quadratic terms:

$$h(x,t) = h^{(1)} + h^{(2)}$$

or

$$h(x,t) = \sum_{i=1}^{n} a_i \cos \Psi_i + \frac{1}{4} \sum_{i=1}^{n} \sum_{j=1}^{n} a_i a_j \left[\left(k_i + k_j \right) \cos \left(\Psi_i + \Psi_j \right) - \left| k_i - k_j \right| \cos \left(\Psi_i - \Psi_j \right) \right] \quad (2.1.2)$$

where

$$\Psi_i = k_i x \cos \phi - \omega_i^e t + \theta_i$$
$$\omega_i^e = \omega_i - k_i V \cos \phi$$
$$\omega_i = \sqrt{g k_i}$$

and
a_i = wave amplitudes

k_i = wave number

ω_i = wave frequency

$$g = \text{the acceleration of gravity}$$
$$\phi = \text{angle of encounter}$$
$$\theta_i = \text{an arbitrary phase lag}$$
$$\omega_i^e = \text{frequency of encounter}$$

Together, these approximations lead to

$$p_z(x, z^*, t) = p_z^{(1)} + p_z^{(2)} \tag{2.1.3}$$

where $p_z^{(1)}$ are linear terms and $p_z^{(2)}$ are quadratic terms.

For a given system of incoming waves, the ship motions can be found from eqn. (2.1.3) by solving the equilibrium equations. The expression for wave induced bending moment takes the form:

$$M(x, t) = M^{(1)}(x, t) + M^{(2)}(x, t) + \ldots \tag{2.1.4}$$

where

$$M^{(1)}(x, t) = \sum_{i=1}^{n} \left\{ \left[\xi_i \, M_i^c(x) - \xi_{i+n} \, M_i^s(x) \right] \cos \omega_i^e \, t + \left[\xi_i \, M_i^s(x) - \xi_{i+n} \, M_i^c(x) \right] \sin \omega_i^e \, t \right\} \tag{2.1.5}$$

and

$$
\begin{aligned}
M^{(2)}(x, t) = \sum_{i=1}^{n}\sum_{j=1}^{n} \Big\{ &\left[\left(\xi_i \xi_j - \xi_{i+n}\xi_{j+1} \right) M_{it}^{c+}(x) - \left(\xi_i \xi_{j+n} + \xi_{i+n}\xi_j \right) M_{it}^{s+}(x) \right] \cos\left(\omega_i^e + \omega_j^e \right) t \\
+ &\left[\left(\xi_i \xi_j + \xi_{i+n}\xi_{j+1} \right) M_{it}^{c-}(x) + \left(\xi_i \xi_{j+n} - \xi_{i+n}\xi_j \right) M_{it}^{s-}(x) \right] \cos\left(\omega_i^e - \omega_j^e \right) t \\
+ &\left[\left(\xi_i \xi_j - \xi_{i+n}\xi_{j+1} \right) M_{it}^{s+}(x) + \left(\xi_i \xi_{j+n} + \xi_{i+n}\xi_j \right) M_{it}^{c+}(x) \right] \sin\left(\omega_i^e + \omega_j^e \right) t \\
+ &\left[\left(\xi_i \xi_j + \xi_{i+n}\xi_{j+1} \right) M_{it}^{s-}(x) - \left(\xi_i \xi_{j+n} - \xi_{i+n}\xi_j \right) M_{it}^{c-}(x) \right] \sin\left(\omega_i^e - \omega_j^e \right) t \Big\}
\end{aligned}
\tag{2.1.6}
$$

In eqn. (2.1.6), the wave amplitude and phase lag have been introduced as:

$$\xi_k = a_k \cos\theta_k \quad \text{and} \quad \xi_{k+n} = a_k \sin\theta$$

The analytical expressions for the coefficients M_i^α, $M_{it}^{\alpha\pm}$; $\alpha = c, s$ are given in the paper by Jensen and Pedersen (1979). The evaluation of these coefficients requires the application of a procedure to determine the added mass and damping coefficients (m and N) at each station. While more complex and accurate procedures exist, the simple Lewis transformation is used in the SOST code. It has been shown that the use of more accurate methods do not produce

significant improvements in the results. (Lewis form solutions for added mass and damping do not show good agreement with experimental results for ships with large bulbous bows, however.)

In the SOST code, Jensen has provided means to generate short term and long term statistical predictions of specific responses. These predictions are based upon Hermite series approximations, using the first four moments of the response as input (mean, standard deviation, skewness and kurtosis). The specifics of these procedures are described in Jensen and Pedersen (1979) and will not be repeated here.

2.1.2 Simple Formulations for Determining Slightly Non-linear Extreme Wave Loads and Load Combinations:

In an earlier Ship Structure Committee project (SR-1337), the problem of extreme loads (linear) and load combinations was investigated. The work was published in a Ship Structure Committee report SSC-373 and in a Journal of Ship Research paper (Mansour, 1994). Although this section of the report is concerned mainly with the estimation of slightly non-linear extreme wave loads, a brief review of the load combination method is described in the next few paragraphs. The details of the method are given in Appendix A. A list of nomenclature used in sections 2.1.2 and 2.1.3 is given at the end of this section.

A simple format was adopted for the load combination:

$$f_c = f_1 + K f_2 \qquad\qquad f_1 > f_2 \qquad\qquad (2.1.7)$$

where f_1 are the individual extreme loads and K is a load combination factor. The load combination factor K was found to depend on the correlation coefficient ρ of the two load components, their ratio and the frequency content of the processes from which the two loads are determined (Mansour, 1994). More specifically, it was found that K takes the form:

$$K = \frac{m_r}{r}\left[m_c\left(1 + r^2 + 2\rho_{12}r\right)^{\frac{1}{2}} - 1\right] \qquad\qquad (2.1.8)$$

where

ρ_{12} = correlation coefficient between the two load components

r = σ_2/σ_1 = ratio of the standard deviations of the loads

$$m_r = \sqrt{\frac{\ln v_{01}T}{\ln v_{02}T}} \qquad\qquad (2.1.9)$$

$$m_c = \sqrt{\dfrac{\ln v_{0c}T}{\ln v_{01}T}} \qquad\qquad (2.1.10)$$

σ_i = standard deviations of the loads, $i = 1,2$

v_{0i} = rate of zero upcrossing of the load processes, $i = 1,2,c$

Expressions for the correlation coefficient ρ_{12} are given in Mansour (1994) and Appendix A. The factors, m_r and m_c were found to be close to unity in the case of combining two low frequency loads resulting from rigid body motion of a ship such as vertical and horizontal moments or vertical and torsional moments. When combining springing and vertical moments, the factor m_r must be computed using the zero upcrossing rates of the two underlying processes and time T spent in the sea state under consideration as indicated by eqn. (2.1.9).

In this section, load format similar to that given by eqn. (2.1.7) is sought for slightly non-linear extreme loads. First, however, the extreme value f of a slightly non-linear and non-Gaussian load will be determined. Although the developed formulation is general, the application will concentrate on combining loads (or moments) acting on a ship. The non-linearities in this case manifests itself in the difference between hog and sag moments. Such a difference becomes more important in the case of fine form ships with large flare such as container vessels and naval ships. These vessels exhibit large differences between hog and sag moments, particularly in high sea states. Measurements on actual ships have shown such a trend as can be seen from Figures 2.1.1 and 2.1.2 published by Hackmann (1979) and Clarke (1986). These figures, among others, confirmed that larger sagging moment must be considered in the design of these vessels, and, indeed rules of classification societies have been modified to reflect a larger sagging moment.
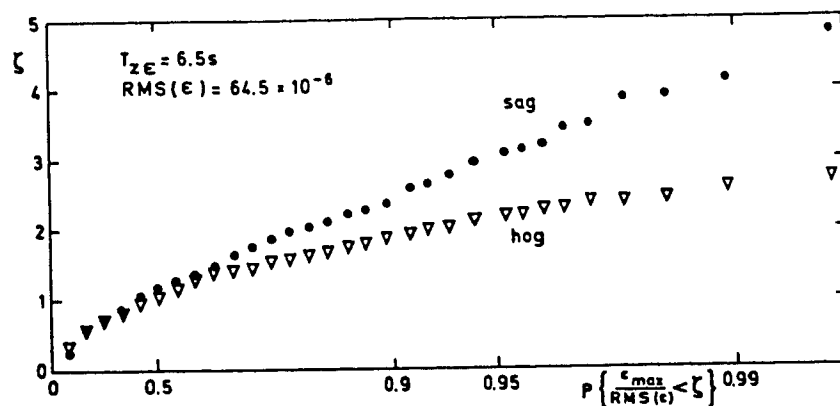
Figure 2.1.1   Short-term statistical representation of the wave induced bending strain ε derived from Northern Atlantic measurements on CTS TOKYO EXPRESS (1018 GMT Dec. 27, 1973). A low pass filter was applied to remove contributions from the 2-node vibration taking place at 5 rad/s. After Hackmann (1979).
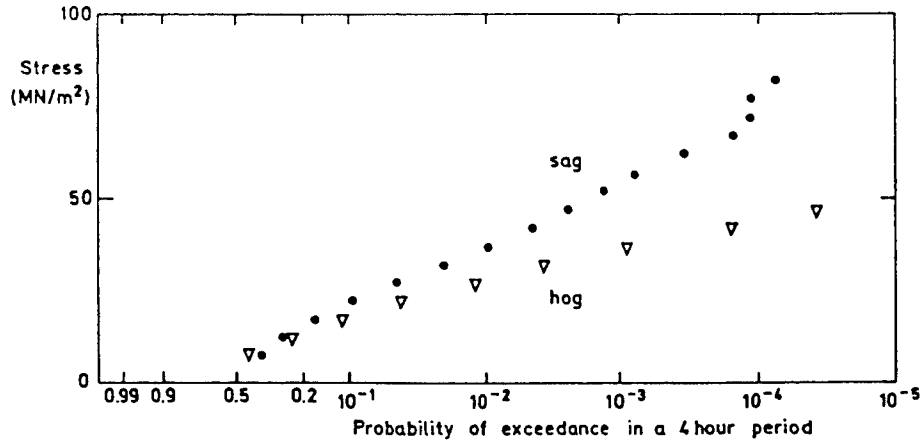
Figure 2.1.2   Gumbel plot of long-term deck stress measurements in a narrow beam
LEANDER Class frigate. A probability of exceedance of $2 \cdot 10^{-5}$ corresponds to
a 20 years' period. After Clarke (1986).

As discussed earlier, linear strip theory is unable to predict the difference between hog
and sag moments.

A second order strip theory developed by Jensen and Pedersen (1979) and further
investigated by Jensen et al. (1981, 1990, 1992, 1993) is able and can be used to predict the
rapid increase of the sagging moment with sea states. The theory compares well with the
experimental data (see, e.g., Jensen et al., 1979, 1990) and exhibits clearly the difference
between hog and sag moments.

According to the linear theory and the associated extreme value statistics, the most
probable extreme load (MPEL) as well as other characteristic loads in a stationary sea,
depend only on the first two moments of the load probability distribution, i.e., the mean and
the standard deviation. In many cases, the mean is either zero or can be taken as zero without
loss of generality. The most probable extreme value (MPEV) thus depends only on the
standard deviation, and, for Rayleigh distributed peaks, is given in the form:

$$\text{MPEV} = \sigma\sqrt{2\ln v_0 T} \qquad (2.1.11)$$

where $v_0 T = N$ = number of peaks and σ is the standard deviation of the load.

The quadratic theory, however, gives, as will be shown later, a MPEV as well as other
characteristic values that depend also on the higher order statistical moments. Of special
importance are the first four moments. These are: the mean, the standard deviation, the
skewness (third moment) and the kurtosis (fourth moment). The skewness measures the
deviation from symmetry of the probability density function of the underlying load process;
zero being a symmetrical density (like, e.g., Gaussian). The kurtosis measures the peakness
of the density function relative to the Gaussian density which has a kurtosis of three. These

four moments are found to characterize rather accurately the MPEV as well as other characteristic values for slightly non-linear wave loads.

In both cases, linear and non-linear, the extreme values will also depend on the frequency content of the underlying load processes. More specifically, for narrow-band processes, the frequency content will influence the number of peaks N where $N = v_0 T$ and v_0 is the rate of zero upcrossing of the process. T is the period of time over which the extreme value is estimated.

The objective of this section is to derive a simple equation similar to eqn. (2.1.11), to estimate the MPEV (and other characteristic values) for slightly non-linear loads; and to approximately combine the loads using a simple format similar to that given by eqns. (2.1.7) and (2.1.8). The developed equations for the slightly non-linear extreme loads will capture the important non-linear characteristics, though some approximations will be necessary due to the emphasis on simplicity.

The most probable extreme value and other characteristic values — slightly non-linear loads:

A slightly non-linear (non-Gaussian) response process $M(t)$ of a marine structure can be expressed in a stationary sea in the form of an N-term Hermite series of a standard Gaussian process $U(t)$, see, e.g., Winterstein (1988) and Jensen, Mansour and Pedersen (1991):

$$\frac{M(t)-\mu}{\sigma} = M_0(t) = k \left[U(t) + \sum_{n=3}^{N} c_n \, He_{n-1} \, (U(t)) \right] \qquad (2.1.12)$$

where $k = k(c_n)$ is a scaling factor to ensure that $M_0(t)$ has a unit variance and the coefficients c_n control the shape of the standardized distribution. Expanding (2.1.12) up to $N = 4$, one gets:

$$M = \mu + k \, \sigma \left[U + c_3 \left(U^2 - 1 \right) + c_4 \left(U^3 - 3U \right) \right] \qquad (2.1.13)$$

The argument t is omitted for brevity. μ here indicates the mean of the process, e.g., the wave bending moment.

Equivalently, a polynomial in the standard Guassian process $U(t)$ can be used to model $M(t)$:

$$M = a_0 + \sum_{i=1}^{3} a_i \, U^i \qquad (2.1.14)$$

One advantage of using the cubic Hermite series eqn. (2.1.13) is that the response is expressed explicitly in terms of the mean μ and standard deviation σ of the response, and that the coefficients c_3 and c_4 can be approximately related to the skewness α and kurtosis β of the response using Gram-Charlier series and a coefficient matching procedure (see Winterstein, 1988):

$$\alpha \simeq 6\,c_3\,(1 + 6\,c_4) \tag{2.1.15}$$

and

$$\beta \simeq \frac{2}{3}\left[\left(18c_4 + 1\right)^2 - 1\right] + 3 \tag{2.1.16}$$

This means that the response process $M(t)$ is expressed explicitly, albeit approximately, by the first four statistical moments (mean, standard deviation, skewness and kurtosis).

The polynomial representation of the response given by eqn. (2.1.14) can be made equivalent to the Hermite representation given by eqn. (2.1.13), by matching the coefficients of the two series, i.e.,

$$
\begin{aligned}
c_3 &= a_2\,(a_1 + 3a_3)^{-1}\\
c_4 &= a_3\,(a_1 + 3a_3)^{-1}\\
k\sigma &= a_1 + 3a_3\\
\mu &= a_0 + a_2
\end{aligned}
\tag{2.1.17}
$$

and the variance σ^2 is given by Jensen, Mansour and Pedersen (1991)

$$\sigma^2 = a_1^2 + 2a_2^2 + 15a_3^3 + 6a_1a_3 \tag{2.1.18}$$

From the four lowest statistical moments, the a_i can be determined via eqns. (2.1.15), (2.1.16) and (2.1.17) or exactly (Jensen, 1994), solving numerically three non-linear algebraic equations (for the solution of a_i in terms of the four lowest moments, please refer to Jensen, 1994).

The standardized moment process can be written in terms of the coefficients a_i as:

$$\frac{M - \mu}{\sigma} = k\,U\left[1 + \frac{a_2}{a_1 + 3a_3}\frac{(U^2 - 1)}{U} + \frac{a_3}{a_1 + 3a_3}\left(U^2 - 3\right)\right] \tag{2.1.19}$$

The probability distributions of the response process $M(t)$, it peaks and its extreme peak in time duration T can be thus determined from the transformation given by eqn. (2.1.13) and the fact that $U(t)$ is the standard normal process (see Mansour, 1991). From the probability distribution of the extreme peak in time duration T one may determine the most probable

extreme value (MPEV) as well as other extreme values (characteristic values) associated with certain probability levels in a formal way.

A simpler procedure that produces the same result is to insert the MPEV of $U(t)$ in the right hand side of Eqn. (2.1.19) in order to determine the MPEV of $M(t)$. The MPEV of $U(t)$ is:

$$\text{MPEV of U(T)} = \sqrt{2 \ln v_0 T} \tag{2.1.20}$$

Inserting eqn. (2.1.20) in (2.1.19) and using eqn. (2.1.15), (2.1.16) and (2.1.17) to obtain the coefficients a_i in terms of the skewness α and the kurtosis β, the MPEV of $M(t)$, denoted f, can be cast in the form:

$$f = \delta \sigma \sqrt{2 \ln v_0 T} \tag{2.1.21}$$

where the mean μ was taken to be zero (without loss of generality) and δ is a "non-linearity" parameter defined by:

$$\delta = k \left\{ 1 + \frac{\alpha(2 \ln v_0 T - 1)}{(6 + 2\gamma)\sqrt{2 \ln v_0 T}} + \frac{\gamma}{18}(2 \ln v_0 T - 3) \right\} \tag{2.1.22}$$

and

$$\gamma = \left[1 + 1.5(\beta - 3) \right]^{1/2} - 1$$

$$k = \left[1 + \frac{1}{2} \left(\frac{\alpha}{\gamma + 3} \right)^2 + \frac{\gamma^2}{54} \right]^{1/2} \tag{2.1.23}$$

Equation (2.1.21) is similar to eqn. (2.1.11) of the linear case except for the non-linearity parameter δ. It can be easily verified that eqn. (2.1.21) converges to eqn. (2.1.11) when the skewness α is zero and kurtosis β is 3, i.e., the linear case.

The second order strip theory for ships (see Jensen and Pedersen, 1979) has shown that the difference between hogging and sagging moments manifests itself in the sign of the skewness α, i.e., α is positive for sagging and has the same value but with a negative sign for hogging. This will influence the non-linearity parameter δ given by eqn. (2.1.22) since the second term will be positive for sagging and negative for hogging, with end result of a larger extreme sagging moment than a hogging moment (eqn. (2.1.21)).

An improvement of eqn. (2.1.22) for the non-linearity parameter δ can be made. A comparison of computation of an extreme value f_η associated with probability η, normalized by the standard deviation σ versus η is shown in Figure 2.1.3. The solid curve shows the

results for f_η/σ based on the second order strip theory using exact relations between the coefficients a_i and the 4 lowest statistical moments. The ship analyzed is the same as in Jensen and Dogliani (1993). The "line/dot" curve is based on eqn. (2.1.22) which uses Winterstein (1988) approximate values for the coefficients c_3 and c_4. As can be seen, the error due to the approximate relations (2.1.15)-(2.1.16) increases from about 3% at the MPEV ($\eta = 0.632$) to about 12% at a probability level $\eta = 0.0005$.
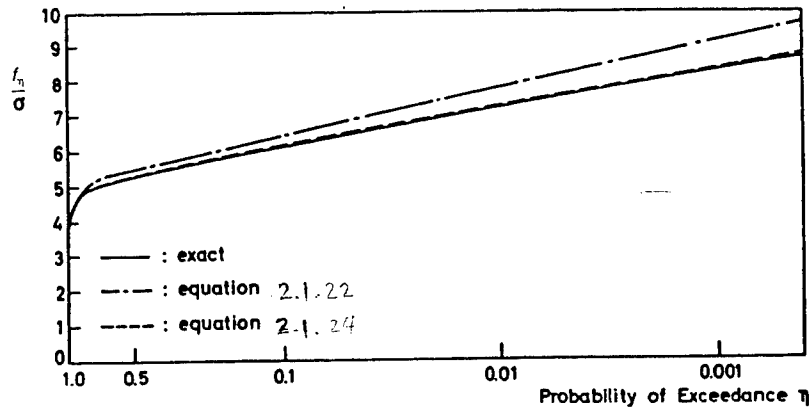
Figure 2.1.3 Exceedance probability of an extreme value.

A better approximation can be made by modifying Winterstein (1988) determined coefficients c_3 and c_4. By matching the Hermite Series coefficients with the exact, numerically computed results, the following modified coefficients were determined:

$$c_3 = \frac{\alpha}{5.8 + 2\gamma} \quad \text{and} \quad c_4 = \frac{\gamma}{30}$$

Using these coefficients, one obtains for the non-linearity parameter δ:

$$\delta = k \left\{ 1 + \frac{\alpha \left(2 \ln (v_0 T) - 1\right)}{(5.8 + 2\gamma) \sqrt{2 \ln(v_0 T)}} + \frac{\gamma}{30} \left(2 \ln (v_0 T) - 3\right) \right\} \tag{2.1.24}$$

where k and γ are given by eqn. (2.1.23). The dashed curve in Figure 2.1.3 is based on the modified non-linearity parameter given by eqn. (2.1.24). It is seen that it gives much better results than the original δ given by eqn. (2.1.22) in the present case, and therefore, will be used in the following analysis.

Figure 2.1.4 shows the effect of the skewness on the non-linearity parameter δ given by eqn. (2.1.24). δ_s designates the non-linearity parameter associated with sagging (positive α and δ_h is that associated with hogging (negative α). The two other parameters (β and $v_0 T$) were assumed fixed. Similarly, Figures 2.1.5 and 2.1.6 show the effects of the kurtosis β and the number of peaks $v_0 T$ on the non-linearity parameter, respectively. It is seen that

increasing any of these parameters will increase δ, but the impact of the skewness is pronounced.
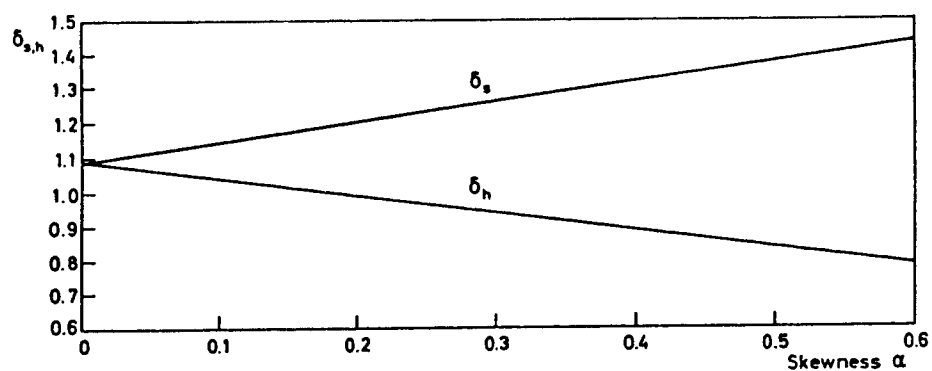
Figure 2.1.4 Effect of skewness on the non-linearity parameters for hogging and sagging moments.
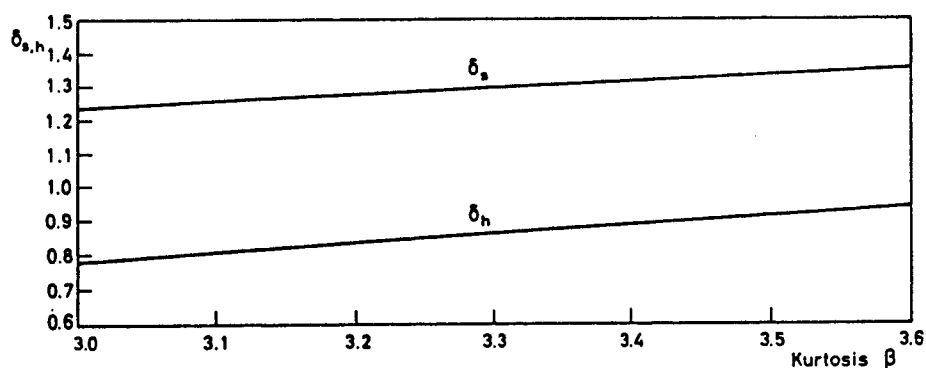
Figure 2.1.5 Effect of kurtosis on the non-linearity parameters for hogging and sagging moments.
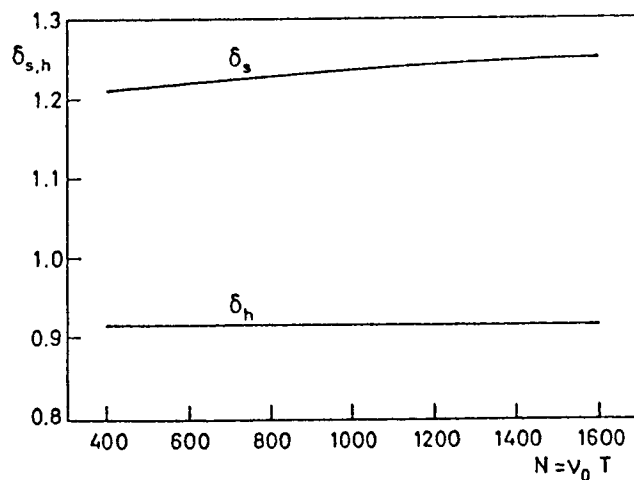
Figure 2.1.6 Effect of number of peaks on the non-linearity parameters for hogging and sagging moments.

Other characteristic values, besides the MPEV can be also approximately determined using an equation similar to eqn. (2.1.21) (or eqn. (2.1.11) for the linear case). An extreme value f_η associated with exceedance probability η can be determined by replacing v_0 by $v_{0\eta}$, i.e.,

$$f_\eta = \delta\, \sigma \sqrt{2 \ln v_{0\eta}\, T}$$ (2.1.25)

where

$$v_{0_\eta} \simeq \frac{v_0}{\ln\left[(1-\eta)^{-1}\right]}$$ (2.1.26)

The MPEV is associated with an exceedance probability $\eta = 1 - 1/e = 0.6321$. It is easy to verify that, in this special case $v_{0\eta} = v_0$ and eqn. (2.1.25) reduces to eqn. (2.1.21) for the most probable extreme value. The logarithms in the above equations have the Naplerean base "e".

The above equations apply to narrow-band and relatively narrow-band response spectra. An approximation for the wide-band case is possible for the MPEV if one uses in eqn. (2.1.21) (see Cartwright and Longuet-Higgins, 1956):

$$v_0 T \simeq \sqrt{(1-\varepsilon^2)}\, N$$ (2.1.27)

N is the number of peaks and ε is a spectrum broadness parameter given by:

$$\varepsilon^2 = 1 - \frac{m_2^2}{m_0 m_4} \;\; ; \;\; m_n = \int_0^\infty \omega^n\, S(\omega)\, d\omega \;\; ; \;\; n = 0, 2, 4$$ (2.1.28)

where $S(\omega)$ is the one-sided response spectrum and ω is frequency.

According to Silveria and Brillinger (1978), an extreme value associated with probability η becomes independent of ε as η approaches zero, and therefore, eqn. (2.1.25) may be used to approximately estimate f_η with $v_0 T = N =$ number of peaks of the wide-band process, for small values of η.

Estimation of slightly non-linear extreme loads:

As can be seen from eqn. (2.1.21), estimation of the MPEV can be made if the non-linearity parameter δ given by eqn. (2.1.24) is known. Eqn. (2.1.24) indicates that the non-linearity parameter δ depends on the skewness α, kurtosis β and $v_0 T$, i.e.,

$$\delta = \delta(\alpha, \beta, v_0 T)$$ (2.1.29)

Results of the second order strip theory have shown (see Jensen and Dogliani, 1993) that α and β depend on the significant wave height H_s, the zero crossing period of waves T_z, ship geometry, ship speed V and heading angle φ, i.e.,

$$\alpha = \alpha \ (H_s, \ T_z, \text{ship geometry}, \ V, \ \varphi) \qquad (2.1.30)$$

and

$$\beta = \beta \ (H_s, \ T_z, \text{ship geometry}, \ V, \ \varphi) \qquad (2.1.31)$$

Besides the dependence on α, β and $v_0 T$, the MPEV depends also on the "non-linear" standard deviation σ as can be seen from eqn. (2.1.21). In addition, the mean value for the non-linear extreme response, is non-zero and, in principle, should be added to the extreme value given by eqn. (2.1.21) or (2.1.25). The results by Jensen and Dogliani (1993) have shown, however, that the mean value is small, of the order of 2% of the MPEV, and can be neglected. In addition, the same reference indicated that the standard deviation calculated by the second order strip theory is only 2% different from the linear standard deviation. It is therefore suggested that the standard deviation computed by a linear strip theory program can be used in eqn. (2.1.21) or (2.1.25).

The skewness α and kurtosis β can be calculated only using a non-linear procedure like a second order strip theory program. A complete parametric study to determine design charts for α and β when varying the parameters indicated by eqns. (2.1.30) and (2.1.31) can be valuable in this regard and will be given in the next section of the report. An estimate can be thus made of α and β and therefore of the non-linearity parameter and the extreme response.

With reference to eqns. (2.1.30) and (2.1.31), the most important parameter related to ship geometry is, according to the second order strip theory, the slope at the waterline, which reflects ship flare. It is rather unfortunate that the second order strip theory limits the description of the entire changes in volume below and above the waterline to one parameter, the slope of the hull with respect to a vertical line at each station along the ship. It should be mentioned that it is this change in buoyancy above and below the waterline that contributes most to the difference between the linear and second order theories.

A flare coefficient c_f that describes "ship geometry" can be written in terms of the difference between the deck area A_{DK} and the waterplane area at the waterline A_{WP} divided by the vertical distance z_f between them and by the ship length L, i.e.,

$$c_f = \frac{A_{DK} - A_{WP}}{L \ z_f} \qquad (2.1.32)$$

Furthermore, from the cumulant $\overline{K_i}$ dependence on the significant wave height H_s given by

$$\overline{K}_i = d_i \, H_s^{2i-2} + e_i \, H_s^{2i} \qquad i = 2, 3, \ldots$$

one can infer that the skewness α is approximately linearly dependent on H_s and the kurtosis β is proportional to the square of H_s (d_i and e_i are constants). The results given by Jensen and Dogliani (1993) for a containership indeed supports this contention. Therefore, one may write

$$\frac{\alpha}{H_s} \simeq f_1 \, (c_f, T_z, V, \varphi) \qquad\qquad (2.1.33)$$

and

$$\frac{\beta}{H_s^2} \simeq f_2 \, (c_f, T_z, V, \varphi) \qquad\qquad (2.1.34)$$

These two equations provide the basis for the parametric study leading to design charts for α and β shown in the next section. Some practical information regarding α and β and the ratio of sagging to hogging moments are provided next.

Six ships have been analyzed using the second order strip theory. These are: a tanker, a frigate, a bulkcarrier, a floating production vessel, a feeder container ship and a Panmax containership. The results of the calculations in a sea state characterized by significant wave height $H_s = 15$ meters and average zero crossing period of 12 seconds are shown in Table 2.1.1. In all cases, except for the floating production vessel, which is designed for head sea and zero speed, vessels speed and heading angle are 2 m/sec and 135°, respectively. The shown hogging and sagging moments are extreme values associated with exceedence probability $\eta = 0.5$ during a time duration of 10^4 seconds. The flare coefficient c_f given by eqn. (2.1.32) has also been calculated and is shown in Table 2.1.1. The table shows the computed mean μ, linear standard deviation σ_i, non-linear standard deviation σ, skewness α and kurtosis β. These results are plotted in Figures 2.1.7, 2.1.8 and 2.1.9. These figures, in general, show the variation in the degree of non-linearity with the flare coefficient c_f. Figure 2.1.7 shows the increasing trend of the skewness and kurtosis data with c_f together with least square fit lines. Figure 2.1.8 shows the increasing trend of the sagging to hogging moments ratio as c_f increases. Figure 2.1.9 shows the ratios of the sagging to linear and hogging to linear moments and their variation with c_f. These figures indicate clearly that as c_f increases the non-linearities as modeled by α and β increase, and the sagging to hogging moment ratio increases. It should be mentioned that the service speed V of the vessels do not enter the results as all calculations are performed in a severe sea state in which only a minimum (2 m/sec) steering speed is applied.

	Tanker	Frigate	OBO	Floating production vessel	Feeder container ship	Container ship
Ship length L [m]	233	110	310	194	120	270
Block coefficient c_b	0.85	0.47	0.78	0.80	0.63	0.59
Flare coefficient c_f	0.03	0.06	0.09	0.20	0.27	0.30
M_{sag} [10^9 Nm]	3.70	0.246	10.90	3.04	0.325	4.9
M_{hog} [10^9 Nm]	3.66	0.198	8.19	2.18	0.218	2.8
M_{sag}/M_{hog}	1.01	1.24	1.33	1.39	1.49	1.75
μ/σ_ℓ	0.052	0.083	0.075	0.059	0.136	0.221
σ/σ_ℓ	1.016	1.024	1.018	1.006	1.056	1.038
skewness α	-0.017	0.147	0.226	0.140	0.326	0.489
kurtosis β	3.076	3.099	3.172	3.061	3.394	3.393
σ_ℓ [10^9 Nm]	0.922	0.053	2.374	0.722	0.059	0.901
M_{linear} [10^9 Nm]	3.50	0.209	8.95	2.72	0.229	3.45

Table 2.1.1 Extreme bending moments with 50% exceedance probability for six ships in sea state $H_s = 15$ m, $T_z = 12$ s during 10^4 s.
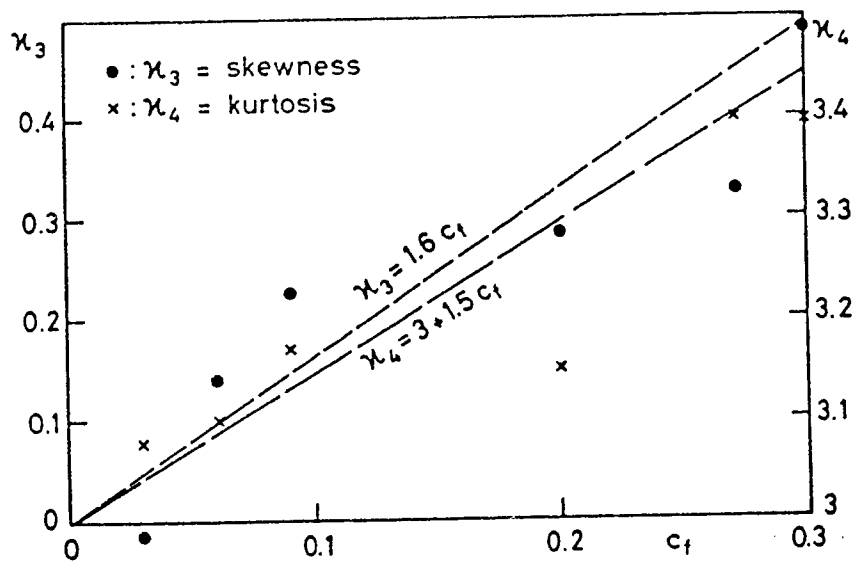
Figure 2.1.7 Variation of skewness and kurtosis with the flare coefficient c_f for six ships and best-fit-lines. Results are for the midship sagging bending moment. For hog and sign of the skewness should be changed.
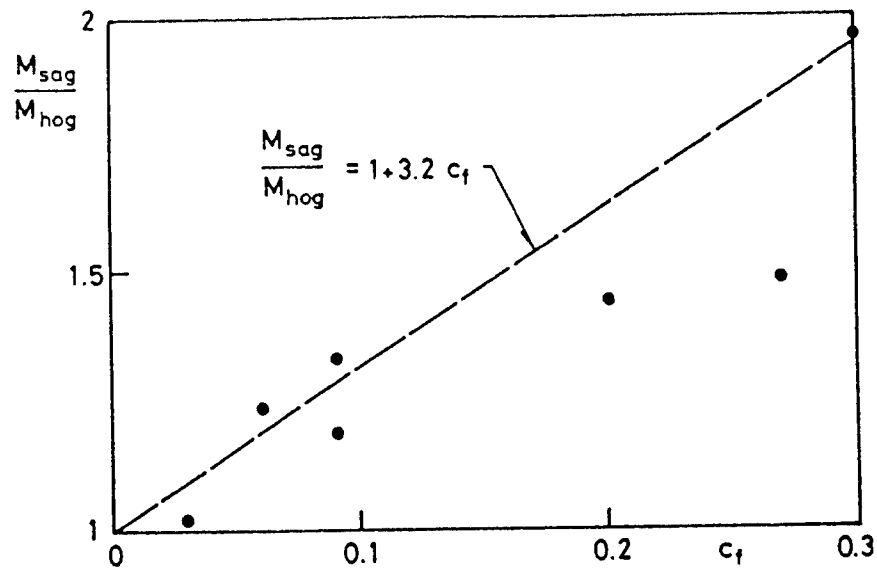
Figure 2.1.8 Variation of the ratio of sagging to hogging moments with the flare coefficient c_f for six ships and best-fit-line.
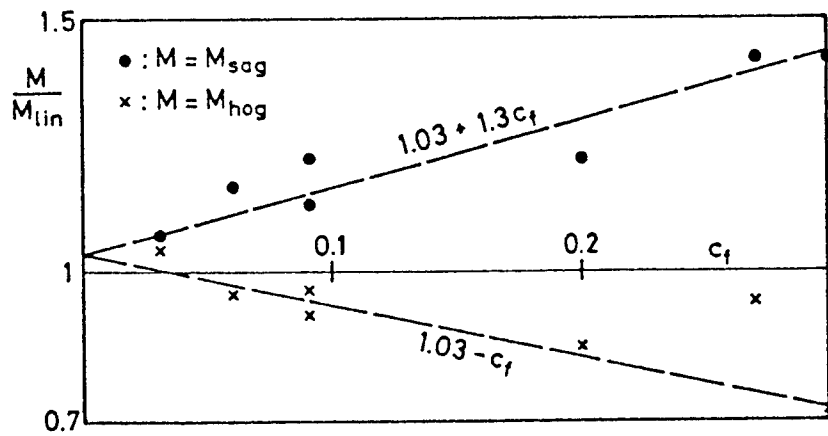
Figure 2.1.9 Variation of the ratio of hogging and sagging moments to the linear moment with the flare coefficient c_f for six ships and best-fit-lines.

Approximate combination of extreme loads

Approximate combination of slightly non-linear extreme load (e.g., hogging and sagging moments) with a linear load (e.g., horizontal moment) can be obtained using a procedure similar to that developed by Mansour (1994). The procedure, which is described in detail in that reference, ends up with the simple formula given by eqn. (2.1.7) for the combined load f_c:

$$f_c = f_1 + K f_2 \qquad\qquad f_1 > f_2 \qquad\qquad (2.1.7)$$

where the load combination factor K is given by eqn. (2.1.8):

$$K = \frac{m_r}{r}\left[m_c \left(1 + r^2 + 2\rho_{12} r\right)^{\frac{1}{2}} - 1 \right] \qquad\qquad (2.1.8)$$

and the individual extreme load components f_i, $i = 1,2$ are given by Eqn. (2.1.21):

$$f_i = \delta_i \, \sigma_i \, \sqrt{2 \ln v_{0i} T} \qquad\qquad (2.1.22)$$

If one of the two loads is linear, e.g., f_2, then its non-linearity parameter δ_2 reduces to unity. The non-linearity parameter is defined by eqn. (2.1.24). The coefficients m_r and m_c now reflect the slight non-linearity of the loads and are given by (refer to eqns. (2.1.9) and (2.1.10):

$$m_r = \frac{\delta_1}{\delta_2} \sqrt{\frac{\ln v_{01} T}{\ln v_{02} T}} \qquad\qquad (2.1.35)$$

$$m_c = \frac{\delta_c}{\delta_1} \sqrt{\frac{\ln v_{0c} T}{\ln v_{01} T}} \qquad\qquad (2.1.36)$$

The correlation coefficient at the standard deviation level, ρ_{12} can be approximately determined from:

$$\rho_{12} \simeq \frac{1}{\sigma_1 \sigma_2} \int_0^\infty Re\left\{ H_1(\omega) \, H_2^*(\omega) \right\} S_x(\omega) \, d\omega \qquad\qquad (2.1.37)$$

where $H_i(\omega)$ are the transfer functions of the loads (wave to load) and the superscript $*$ indicates the complex conjugate of the transfer function. $Re\{.\}$ indicates the real part of $\{.\}$ and $S_x(\omega)$ is the wave spectrum.

The load combination factor K is thus a function of

$$K = K\left(r, \rho_{12}, \alpha_1, \beta_1, v_{01}T, \alpha_2, \beta_2, v_{02}T, \alpha_c, \beta_c, v_{0c}T\right) \qquad (2.1.38)$$

where α_c, β_c and v_{0c} are the combined load skewness, kurtosis and rate of zero crossing, respectively. These three parameters appear in the non-linearity parameter of the combined response δ_c which appears in m_c given by eqn. (2.1.36). The non-linearity parameter δ_c is defined by eqn. (2.1.24) with $\alpha = \alpha_c$, $\beta = \beta_c$ and $v_0 = v_{0c}$.

In order to estimate K (see eqn. (2.1.38)) easily, it is clear that α_c, β_c and v_{0c} must be determined from the corresponding quantities for the individual load components, i.e., from α_i, β_i and v_{0i} where $i = 1$ or 2. It is also clear that further simplification is necessary, particularly for the case of interest, i.e., slightly non-linear vertical moment responses combined with linear horizontal moment response.

The skewness and kurtosis of the combined response may be estimated from individual component skewness and kurtosis by forming the cumulants and assuming independence in higher order expectations (see Appendix B). This leads to the approximate equations for zero mean random variables

$$\alpha_c \simeq \frac{1}{\sigma_c^3}\left[\alpha_1\,\sigma_1^3 + \alpha_2\,\sigma_2^3\right] \qquad (2.1.39)$$

and

$$\beta_c \simeq \frac{1}{\sigma_c^4}\left[(\beta_1 - 1)\,\sigma_1^4 + (\beta_2 - 3)\,\sigma_2^4 + 6\,\sigma_1^2\,\sigma_2^2\right] + 3 \qquad (2.1.40)$$

where

$$\sigma_c^2 = \sigma_1^2 + \sigma_2^2 + 2\,\rho_{12}\,\sigma_1\,\sigma_2 \qquad (2.1.41)$$

If one of the load responses is Gaussian then its corresponding μ, α and β are $\mu = \alpha = 0$ and $\beta = 3$ and the above equations are further simplified. It should be mentioned that for slightly non-linear load response (e.g., the vertical bending moment) μ can be taken as zero and σ can be taken as the linear standard deviation. The skewness and kurtosis, however, must be estimated either from a complete parametric study design chart (next section) or from the second order strip theory.

The combined response zero upcrossing rate v_{0c} may be estimated approximately from (see Appendix B):

$$v_{0c}^2 \simeq \left(\frac{1}{2\pi}\right)^2 \frac{\sum_i m_{2,i}}{\sum_i m_{0,i}} \qquad (2.1.42)$$

$$= \frac{\sigma_1^2 \, v_{01}^2 + \sigma_2^2 \, v_{02}^2}{\sigma_1^2 + \sigma_2^2}$$

where the summation index i is over all individual components and $m0,i$ and $m_{2,i}$ indicate the zero and second moments, respectively, of component i respfonse spectrum. It should be mentioned that springing response of ships cannot be considered "slightly" non-linear response since the quadratic terms are relatively large.

Further simplification and reduction of the parameters upon which the load combination factor K depends (see eqn. (2.1.38)) is possible for the special case of combining vertical and horizontal moment responses if the latter is considered linear. In this case, the spectral densities of the individual components as well as the combined spectral density overlap on a frequency scale (see, e.g., Friis Hansen, 1994). As a result of this overlap, the coefficients m_c and m_r appearing in eqn. (2.1.8) for K can be simplified:

$$m_c = \frac{\delta_c}{\delta_1} \sqrt{\frac{\ln v_{0c}T}{\ln v_{01}T}} \simeq \frac{\delta_c}{\delta_1} \qquad (2.1.43)$$

and

$$m_r = \delta_1 \sqrt{\frac{\ln v_{01}T}{\ln v_{02}T}} \simeq \delta_1 \qquad (2.1.44)$$

where δ_i, $i = 1, 2, c$ are given by eqn. (2.1.24). Thus the dependency of K on the variables given by eqn. (2.1.38) is reduced to

$$K = K \, (r, \rho_{12}, \alpha_1, \beta_1, v_{01}, \alpha_c, \beta_c, v_{0c}) \qquad (2.1.45)$$

where α_c, β_c and v_{0c} can be calculated from eqns. (2.1.39), (2.1.40) and (2.1.42), respectively.

Application examples

In the following, two application examples will be provided to show the use of the equations and analyses discussed earlier. The first example is concerned with estimating the non-linear vertical sagging and hogging moments assuming that only the linear vertical moment is known. The second example is concerned with combining the responses (stresses) due to vertical bending moment considered slightly non-linear and the horizontal moment considered linear.

2-21

Example 1

It is required to estimate for preliminary analysis the vertical sagging and hogging moments of a bulkcarrier in a sea state characterized by significant wave height $H_s = 15$ m and zero crossing period $T_z = 12$ s.

The ship is to operate in this storm condition for a period of 10^4 seconds (approximately 2.8 hours); and it is desired to estimate the extreme hogging and sagging moments during this period with exceedance probability $\eta = 0.5$. From ship line drawings the flare coefficient given by eqn. (2.1.32) was calculated to be $c_f = 0.1$; and the results of a linear strip theory ship motion program provided the standard deviation of the vertical bending moment in the sea state under consideration to be $\sigma_\ell = 2.4 \cdot 10^9$ Nm for ship heading and Froude number identical to those used in Figure 2.1.7 ($\phi = 135°$ and $Fr = 0.03$). Notice that these numbers are those of the OBO ship shown in Table 2.1.1. This is done purposely in order to compare the results of the approximate equations provided in this report with the more accurate results of the second order strip theory given in Table 2.1.1 for this ship.

In order to estimate the hogging and sagging moments, one must estimate first the skewness α and the kurtosis β. From Figure 2.1.7 these are given as a function of c_f in the form

$$\alpha = 1.6 \, c_f = 0.16$$

and

$$\beta = 3 + 1.5 \, c_f = 3.15$$

Next, one must estimate the non-linearity parameter for sagging, δ_s, and hogging δ_h, moments, respectively, given by eqn. (2.1.24). This equation shows that δ is a function of the coefficients γ and k. From eqn. (2.1.23), γ and k were computed to be:

$$\gamma = 0.107 \quad \text{and} \quad k = 1.001$$

In addition, eqn. (2.1.24), which provides the non-linearity parameter associated with the most probable extreme value, is a function of $v_0 T$. To determine the non-linearity parameter associated with exceedance probability $\eta = 0.5$ one must, as discussed earlier, replace v_0 by $v_{0\eta}$, eqn. (2.1.26). In the absence of better information on v_0 appearing in eqn. (2.1.26) for the vertical bending moment, it will be assumed that this value is equal to that of the waves. Since the waves have a zero crossing period $T_z = 12$ s, v_0 is assumed to be $v_0 = 0.083$ 1/s.

Although a more accurate v_0 for the vertical bending moment may be calculated from the spectral moments of the bending moment spectrum obtained from a linear strip theory program, this assumption is usually very satisfactory as a very low forward speed is used in the severe design sea state. In addition, v_0 always appears in all equations either as $\ln v_0 T$ or

$\sqrt{\ln v_0 T}$, and therefore, the error is minimal. $v_{0\eta}$ can be then determined from eqn. (2.1.26) as

$$v_{0\eta} = \frac{0.083}{\ln(0.5)^{-1}} = 0.1201 / \text{s} \quad \text{and} \quad v_{0\eta}T = 1200$$

Substituting the values of γ, k and $v_{0\eta}T$ in eqn. (2.1.24), and using positive skewness α to determine the non-linearity parameter for sagging δ_s and negative α for hogging, δ_h, one obtains:

$$\delta_s = 1.134 \quad \text{and} \quad \delta_h = 0.948$$

The corresponding extreme sagging and hogging moments associated with exceedance probability $\eta = 0.5$ can be calculated from eqn. (2.1.25):

$$f_s = 10.25 \cdot 10^9 \text{ Nm}$$

and

$$f_h = 8.57 \cdot 10^9 \text{ Nm}$$

The extreme sagging moment f_s is to be compared with $10.90 \cdot 10^9$ Nm shown in Table 2.1.1 as provided by the second order strip theory. The error is 6.0%. The extreme hogging moment given in Table 2.1.1 is $8.19 \cdot 10^9$ Nm and the resulting error in f_h is 4.6%.

Although similar results for f_s and f_h may have been obtained, in this case, using Figure 2.1.9, it is recommended to use the above outlined procedure. This procedure shows the dependence on the various important parameters and more importantly provides the flexibility of determining extreme values associated with different probability levels η and different number of encounters $v_0 T$ as can be seen from eqns. (2.1.24), (2.1.25) and (2.1.26).

Example 2

For preliminary purposes, it is required to determine the combined extreme longitudinal stress due to vertical sagging and horizontal bending moments associated with exceedance probability $\eta = 0.5$, at a location in the deck of a tanker in a stationary sea state characterized by $H_s = 15$ m and $T_z = 12$ s of duration $T = 10^4$ s. From a linear strip theory computer program, it was determined that the vertical bending stress standard deviation σ in this sea state is $\sigma_1 = 30$ N/mm^2. The standard deviation of the horizontal moment bending stress at the same location and in the same direction is $\sigma_2 = 14$ N/mm^2. The ISSC (1973) recommended value for the correlation coefficient between the two moments (or stresses) is $\rho_{12} = 0.32$. See Stiansen and Mansour (1975) and Mansour (1981) for calculation of ρ_{12} using eqn. (2.1.37). The ISSC recommended value will be used in this example. The flare coefficient calculated from the line drawing of this ship is $c_f = 0.15$.

First, the non-linear vertical sagging stress will be estimated using the procedure outlined in Example 1. Then the combined stress will be estimated using eqn. (2.1.7) with load combination factor K determined from eqn. (2.1.8).

These values are:

$$\alpha_1 = 0.240 \; ; \; \beta_1 = 3.225 \; ; \; \gamma_1 = 0.157 \quad \text{and} \quad k_1 = 1.002$$

$v_{0\eta}$ is calculated next using eqn. (2.1.26) with $v_0 = 0.083$ l/s. The resulting value is:

$$v_{0\eta} = 0.120 \text{ l/s} \quad \text{and} \quad v_{0\eta}T = 1200$$

The non-linearity parameter δ_1 associated with the sagging stress calculated from eqn. (2.1.24) is $\delta_1 = 1.198$. The corresponding extreme sagging stress at this probability level ($\eta = 0.5$) is calculated next from eqn. (2.1.25) as

$$f_1 = 1.198 \cdot 30\sqrt{2 \ln 1200} = 135.3 \text{ N} / \text{mm}^2$$

The horizontal bending stress will be considered linear (Gaussian response); therefore, the corresponding skewness $\alpha_2 = 0$ and kurtosis $\beta_2 = 3$. Substituting these values in eqns. (2.1.23) and (2.1.24) yield $\gamma_2 = 0$; $k_2 = 1$ and $\delta_2 = 1$. Thus eqn. (2.1.25) for the extreme value reduces to eqn. (2.1.11) for the linear case, and for exceedence probability $\eta = 0.5$, the extreme value of the horizontal stress is

$$f_2 = 14\sqrt{2 \ln 1200} = 52.7 \text{ N} / \text{mm}^2$$

In order to calculate the combined stress using eqn. (2.1.7), the load combination factor K must be calculated first from eqn. (2.1.8) with (see eqns. (2.1.43) and (2.1.44)):

$$m_r \simeq \delta_1 = 1.198 \quad \text{and} \quad m_c \simeq \frac{\delta_c}{\delta_1}$$

The calculation of m_c requires estimation of δ_c. Using eqns. (2.1.39), (2.1.40) and (2.1.41) one gets:

$$\alpha_c = 0.129 \; ; \; \beta_c = 3.666 \quad \text{and} \quad v_{0c} = 0.083 \text{ l/s}$$

Therefore, from eqn. (2.1.33) and from eqn. (2.1.24) with $v_{0c,\eta} = 0.120$ l/s (for $\eta = 0.5$), one gets

$$\gamma_c = 0.414 \; ; \; k_c = 1.002 \quad \text{and} \quad \delta_c = 1.225$$

and hence

$$m_c = \frac{\delta_c}{\delta_1} = 1.023$$

For $r = \sigma_2/\sigma_1 = 0.467$ and the above values for m_r, m_c and ρ_{12}, eqn. (2.1.8) yields a load combination factor $K = 0.667$. The combined extreme stress is thus, from eqn. (2.1.7),

$$f_c = f_1 + Kf_2 = 135.3 + 0.667 \cdot 52.7 = 170.5 \text{ N/mm}^2$$

This value is consistent with the value of fc determined from:

$$f_c = \delta_c \sigma_c \sqrt{2 \ln v_{0c,\eta} T} = 170.4 \text{ N} / \text{mm}^2$$

with σ_c determined from eqn. (2.1.41).

It should be noted that, if linear theory is used in both determining the extreme sagging stress and the load combination factor K_i, one would obtain:

$$f_1 = 30\sqrt{2 \ln 1200} = 113.0 \text{ N} / \text{mm}^2 \; ;$$

i.e., 20% less than the value based on non-linear analysis, and K_i (with $m_r = m_c = 1$):

$$f_c = 113.0 + 0.5 \cdot 52.7 = 139.4 \text{ N} / \text{mm}^2$$

that is, 22% smaller than that obtained by the approximate non-linear analysis.

It should also be noted that the correlation coefficient ρ is not constant; it depends on the probability level η. At the standard deviation level $\rho_{12} = 0.32$ while at a probability level η, an indication of the correlation can be calculated from:

$$\rho = \frac{f_c^2 - \left(f_1^2 + f_2^2 \right)}{2f_1 f_2} = 0.56$$

This increasing trend of ρ with the probability level is confirmed by Naess and Ness (1992).

In conclusion, a simple equation suitable for preliminary estimation of the extreme value of a slightly non-linear response was presented. The equation contains a newly defined non-linearity parameter which is a function of the response process skewness and kurtosis. The equation is consistent with the linear theory of extremes, and in fact, reduces to the linear theory prediction as a special case when the non-linearity parameter is equal to one. The equation is suitable for application to extreme values of vertical hogging and sagging bending moments acting on a ship. Unlike the linear theory, the present non-linear analysis can predict the difference between sagging and hogging moments. Parametric study is performed

in the next section in order to determine accurately the non-linearity parameter as a function of the parameters upon which it depends.

A simple formula for preliminary estimate of the combined response of a linear and a slightly non-linear response is also proposed. The formula contains a load combination factor which is a function of the ratio of the standard deviations of the individual responses, the correlation coefficient and the non-linearity parameter.

Nomenclature — Sections 2.1.2 and 2.1.3

a_i	coefficients, polynomial series
A_{DK}	deck plan area
A_{WP}	waterplane area
c_b	block coefficient
c_f	flare coefficient
c_i	coefficients, Hermite series
$E[.]$	expected value
f_i	characteristic value of response (stress or deflection) to load component i
f_c	combined response (stress or deflection)
f_η	extreme value associated with exceedence probability η
$H_i(\omega)$	frequency response function for load component i (transfer function)
$H_i^*(\omega)$	conjugate complex of $H_i(\omega)$
H_s	significant wave height
k	scaling factor
K	load combination factor for two correlated load responses
$\overline{K}$	cumulant
L	ship length
m_r	ratio defined by eqn. (2.1.9) or (2.1.35)
m_c	ratio defined by eqn. (2.1.10) or (2.1.36)
$m_{n,i}$	n'th spectral moment of component i response
$M(t)$	bending moment process
$M_0(t)$	normalized bending moment process
N_i	number of peaks associated with load component i
r	stress ratio $= \sigma_2/\sigma_1$
$Re(.)$	real part of a complex function
$S_x(\omega), S_c(\omega)$	wave and combined response spectra, respectively
T	time of exposure
T_z	zero upcrossing period of waves
$U(t)$	standard Gaussian process
V	ship speed

z_f	vertical distance between A_{DK} and A_{WP}
α	skewness
β	kurtosis
γ	parameter defined in eqn. (2.1.23) (subscript s for sag, h for hog)
δ	non-linearity parameter
ε	band width parameter
σ_i	standard deviation
μ	mean value
ν_{0i}	rate of zero upcrossing of load process i
ρ_{ij}	correlation coefficient between to response components i and j
σ	non-linear standard deviation
σ_c	standard deviation of the combined response
σ_l	linear standard deviation
φ	ship heading angle
ω	frequency

2.1.3 Design Charts for Estimating Non-linear Hogging and Sagging Bending Moments:

This section presents charts for preliminary estimates of the non-linearities associated with wave bending moments acting on a ship moving in a stationary sea. Deviation of the actual hull shape above the water line from "vertical wall" is characterized by a flare coefficient. The charts show the influence of the flare coefficient, among other parameters, on the non-linearity parameter discussed in section 2.1.2. Three application examples are given at the end of the section to illustrate how the charts can be used in conjunction with linear strip theory results in order to estimate slightly non-linear hogging and sagging moments. A list of nomenclature for this section is given at the end of section 2.1.2.

The principal results derived in the proceeding section (section 2.1.2) will be recalled next. In the case of two extreme linear loads, the resulting combined load was cast in the form (Mansour, 1995):

$$f_c = f_1 + K f_2 \qquad f_1 > f_2 \qquad (2.1.46)$$

where f_i are the individual extreme loads and K is a load combination factor defined by:

$$K = \frac{m_r}{r} \left[m_c \left(1 + r^2 + 2\rho_{12} r \right)^{\frac{1}{2}} - 1 \right] \qquad (2.1.47)$$

where : $r = \dfrac{\sigma_2}{\sigma_1} =$ ratio of the standard deviations of the loads

$$m_r = \sqrt{\frac{\ln v_{01} T}{\ln v_{02} T}} \qquad (2.1.48)$$

$$m_c = \sqrt{\frac{\ln v_{0c} T}{\ln v_{01} T}} \qquad (2.1.49)$$

A formulation for calculating the correlation coefficient ρ_{12} is given in Appendix A (see also Mansour, 1993). The factors m_r and m_c are close to unity in the case of combining two low frequency loads resulting from rigid body motion of a ship, such as vertical and horizontal moments.

In linear theory, the most probable extreme value of a load peak depends only on the first two moments of the underlying process probability distribution. The mean can be set to zero, without loss of generality, therefore the most probable extreme value depends only on the standard deviation of the process. For ocean wave loads with Rayleigh distributed peaks, the most probable extreme value is given by

$$f_i = \sigma_i \sqrt{2 \ln v_{0i} T} \qquad (2.1.50)$$

We now introduce a slight non-linearity in the load process. Section 2.1.2 principal results (see also Mansour and Jensen, 1995) is to introduce a "non-linearity" parameter δ defined as follows. For a slightly non-linear load, eqn. (2.1.50) becomes:

$$f_i = \delta_i \sigma_i \sqrt{2 \ln v_{0i} T} \qquad (2.1.51)$$

where the non-linearity parameter is defined by:

$$\delta_i = k_i \left[1 + \frac{\alpha_i \left(2 \ln v_{0i} T - 1 \right)}{\left(5.8 + 2\gamma_i \right) \sqrt{2 \ln v_{0i} T}} + \frac{\gamma_i}{30} \left(2 \ln v_{0i} T - 3 \right) \right] \qquad (2.1.52)$$

$$\gamma_i = \sqrt{1 + 1.5 \left(\beta_i - 3 \right)} - 1 \qquad (2.1.53)$$

$$k_i = \sqrt{1 + \frac{1}{2} \left(\frac{\alpha_i}{\gamma_i + 3} \right)^2 + \frac{\gamma_i^2}{54}} \qquad (2.1.54)$$

We note that for the linear case corresponding to a Gaussian distribution of loads, the skewness α_i and kurtosis β_i reduce to zero and three, respectively, and the non-linearity parameter δ_i becomes unity. In this case, eqn. (2.1.51) reduces to eqn. (2.1.50).

The difference between sagging and hogging moments manifests itself in the sign of the skewness α, i.e., α is positive for sagging and has the same value but with a negative sign for hogging. We see from eqns. (2.1.51) and (2.1.52) that the result is a larger extreme sagging bending moment than hogging bending moment. This is consistent with observations and measurements recorded on ships at sea.

Other characteristic values, besides the most probable extreme value can be also approximately determined using an equation similar to (2.1.51). An extreme value of a load f_η associated with exceedance probability η can be determined by replacing v_0 by $v_{0\eta}$, i.e.,

$$f_\eta = \delta \sigma \sqrt{2 \ln v_{0\eta} T} \qquad (2.1.55)$$

where

$$v_{0\eta} \approx \frac{v_0}{\ln \left(1 - \eta \right)^{-1}} \qquad (2.1.56)$$

The most probable extreme value is associated with an exceedance probability $\eta = 1 - 1/e = 0.6321$.

2.1.3.1 *Parametric study*

From eqn. (2.1.51), it is seen that estimation of the most probable extreme value of a slightly non-linear load can be made after evaluating the non-linearity parameter δ. Evaluating δ means determination of the skewness α and kurtosis β. Both of these moments were shown (Mansour and Jensen, 1995) to depend on the significant wave height H_S, the zero upcrossing period of waves T_z,[1] ship geometry, ship speed V and heading angle ϕ, i.e.,

$$\alpha = \alpha \ (H_S, \ T_z, \ \text{ship geometry}, \ V, \ \phi)) \tag{2.1.57}$$

and
$$\beta = \beta \ (H_S, \ T_z, \ \text{ship geometry}, \ V, \ \phi) \tag{2.1.58}$$

Furthermore, the skewness and kurtosis have been shown to be proportional to H_S and the square of H_S, respectively. Therefore :

$$\frac{\alpha}{H_s} = f \ (T_z, \ \text{ship geometry}, \ V, \ \phi) \tag{2.1.59}$$

and
$$\frac{\beta - 3}{H_s^2} = g \ (T_z, \ \text{ship geometry}, \ V, \ \phi) \tag{2.1.60}$$

This section will provide some insight on how the skewness and kurtosis depend on the last four parameters. It will also provide design charts for estimating short term hogging and sagging moments that can be used in the preliminary stage of a ship design. The software developed by Jensen (1993) based on a second order strip theory by Jensen and Pedersen (1974) was used in order to develop the design charts.

It should be noted that, while the quadratic theory is a major improvement over the linear strip theory the excitation and response in extreme (very high) sea states is highly non-linear and the quadratic theory results cease to be accurate.

The difficulty is inherent in the assumption of linear variation of sectional breadth with draft. A problem arises when the ship motion in very high seas exceeds the ship draft or free board (green water on deck or bow emergence). In these cases, adjustment of the vertical slope at the waterline is necessary, and the appropriate slope to use is not an obvious issue.

---

[1] In terms of the sea spectral moments m_0 and m_2, the zero upcrossing period T_z is defined by $T_z = 2\pi \sqrt{\dfrac{m_0}{m_2}}$.

The reader should refer to the paper by Jensen, Banke and Dogliani (1995) for additional information on this subject.

Environmental parameters H_s and T_z:

The units used for the significant wave height H_s throughout this section are meters. This is important since the quantities α/H_s and $(\beta - 3)/H_s^2$ plotted on the charts are dimensional (α and β are both non-dimensional). Plotting the results in this manner reduces the number of variables, and therefore, the number of charts, considerably. T_z, the zero upcrossing period, is expressed in seconds. Charts of the skewness and kurtosis as a function of each parameter are shown in Figures 2.1.11 to 2.1.36. But since H_s and T_z are generally not independent, see for instance the one parameter ITTC spectrum:

$$T_z = 11.12\sqrt{\frac{H_s}{g}} \qquad (2.1.61)$$

a set of charts for various sea state matching the above relation has also been produced in Figures 2.1.38 to 2.1.41, named charts for frequently occurring pairs of (H_s, T_z).

Ship speed and heading:

The heading angle takes values of 180° (head sea), 135° and 90°. The speed varies from 4 to 30 knots approximately. On the charts for frequently occurring pairs of (H_s, T_z), the speed is reduced in higher sea states in order to reflect realistic operating conditions.

Ship geometry:

The principal source of non-linearity in computing the extreme bending moment of a ship is the flare of the hull, i.e., the fact that the ship is not wall-sided. In linear strip-theory, the ship is assumed wall-sided and, if this assumption seems reasonable for a large tanker, it is not for a fast container ship or a naval vessel. The second order strip theory and the associated software used in this report take into account the slope of the hull at the waterline, and not the actual shape of the hull. This may lead to overestimation of the non-linearity if the hull shows a significant tumble-home, and vice-versa.

Given this limitation, a flare coefficient, C_f, was defined in order to quantify the flare. A ship with a large flare coefficient will show larger non-linearity than a ship with a smaller flare coefficient.

$$C_f = \frac{A_{dk} - A_{wp}}{L.z_f} \qquad (2.1.62)$$

The ship characteristics selected to input the program are those of a fast-container ship. Its main dimensions are shown below. From the body plan of the ship (Figure 2.1.10), the flare coefficient C_f was determined to be 0.48, using the trapezoidal integration rule to compute A_{dk} and A_{wp}.

Length between perpendicular (L)	270 m
Breadth amidships	32.2 m
Draft, even keel	10.85 m
Block coefficient	0.598
LCG aft of midship	10.12 m
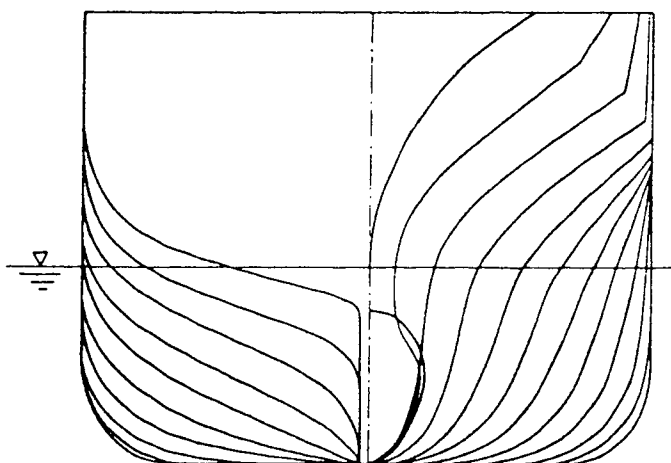
Figure 2.1.10 Body plan of a container ship (Flokstra, 1974).

2.1.3.2 Design charts

All charts shown in Figures 2.1.11 to 2.1.41 were plotted by configuring the input file, where the environmental parameters, ship speed and heading are stored. Each chart required typically 6 to 7 cases to compute, taking an average time of about 2 minutes on an IBM 486 DX2 66. The output file was then transferred to a spreadsheet and the charts were drawn.

Effect of significant wave height H_s:

This effect is clearly illustrated in Figures 2.1.11 and 2.1.12. The linear dependence of the skewness α on H_s is almost perfect, so is the dependence of β - 3 on H_s^2. Therefore,

the quantities α/H_s and $(\beta - 3)/H_s^2$ will be plotted versus the remaining parameters thereafter. As was stated before, one must pay attention to the units of those parameters, because they are dimensional.

Effect of wave zero upcrossing period T_z:

The effect of zero upcrossing period T_z (Figures 2.1.13 to 2.1.18) is not as clear as the effect of H_s. One notes a general increasing trend of α and β for both heading angles 180° and 135°, up to a maximum corresponding to about $T_z = 7$ seconds for low Froude numbers and, about 10 seconds for high Froude numbers (see Figures 2.1.13 to 2.1.18). The value of this maxima increases with the speed up to a certain point then it starts to decrease. Finally, it may be of interest to point out that, in beam seas, all curves are more clumped together, i.e., the influence of Froude Number is no longer important.

Effect of ship speed V and heading angle ϕ:

Figures 2.1.19 and 2.1.20 corroborate the above observation, that is, the existence of a maxima for skewness and kurtosis at a given speed, and the small dependence of α and β on speed in beam seas. However, as the heading angle decreases from 180° (head sea) to 90° (beam sea), both skewness and kurtosis increase.

Effect of the flare coefficient C_f:

All charts describing skewness and kurtosis as a function of C_f (Figures 2.1.21 to 2.1.36) show the same general trend: the skewness is linearly dependent on C_f and the kurtosis behaves like a higher order function of C_f. Regarding the kurtosis, its minimum value corresponds in most cases to $C_f = 0.2$. For low C_f, the skewness may take negative values. These charts (Figures 2.1.21 to 2.1.36) may be used for preliminary estimates of the non-linearity parameter δ and the difference between hogging and sagging moments for fine form ships.

The non-linearity parameter δ is plotted in Figure 2.1.37 versus C_f for a selected "design" sea state, $H_s = 15.5$ m and $T_z = 14$ sec. In order to represent realistic operating conditions, the ship speed was taken 4 knots, corresponding to a Froude number $Fr^{[1]} = 0.04$. The figure shows that δ varies rapidly with C_f indicating its importance. It also shows that there are non-linearities present even if $C_f = 0$.

---

[1] $Fr = V/\sqrt{gL}$

2-34

Charts for frequently occurring pairs of (H_s, T_z):

Figures 2.1.38 to 3.1.41 show the skewness and kurtosis for pairs of (H_s, T_z) that correspond to the ITTC one parameter spectrum (see eqn. (2.1.61)) and estimated maximum operating speeds. These values are shown in Table 2.1.2 below:

H_s (m)	4	6	8	10	12
T_z (s)	7.1	8.7	10	11.2	12.3
V (m/s)	10	8	6	4	4

**Table 2.1.2 — Frequently Occurring Pairs of (H_s, T_z) and
Corresponding Operating Speeds**

As stated before, these charts reflect realistic operating conditions, and may be used for estimating the maximum non-linearity parameter for a fine form ship with a given flare coefficient (see application example number 1).

2.1.3.3 *Application examples*

Example 1

    a. High flare coefficient

Consider the fast container ship ($C_f = 0.48$) that was used in the input file, cruising in moderate to severe sea ($H_s = 6$ m, $T_z = 8.7$ s) at 15.5 knots, its maximum speed in this sea state. From Figures 2.1.38 and 2.1.39, we get:

$$\frac{\alpha}{H_s} = 0.053 \quad \text{and} \quad \frac{\beta - 3}{H_s^2} = 0.0054$$

therefore: $\qquad\qquad \alpha = 0.318 \text{ and } \beta = 3.194$

From any linear strip-theory program, one can calculate the standard deviation σ of the vertical bending moment. This value was computed to be $\sigma = 5.02 \ 10^8$ Nm and the corresponding $\nu_0 = 0.1244 \text{ sec}^{-1}$. If one considers a time of exposure $T = 3$ hours (10800 s), then using eqns. (2.1.52), (2.1.53) and (2.1.54):

$$\gamma = 0.136$$

$$k = 1.0027$$

$$\delta = 1.240$$

hence, from eqns. (2.1.50) and (2.1.51), the most probable extreme values for the sagging bending moments are :

$$M_{sag} = 1.905 \ 10^9 \ \text{Nm} \qquad \text{(linear case)}$$

$$M_{sag} = 2.363 \ 10^9 \ \text{Nm} \qquad \text{(non-linear case)}$$

One may also compute an extreme value associated with exceedance probability 5%. From (2.1.56), v_{05} is computed as:

$$v_{05} = 2.4253 \ \text{sec}^{-1}$$

therefore, from (2.1.55), the extreme sagging bending moment with exceedance probability 5% is:

$$M_{sag}05 = 2.808 \ 10^9 \ \text{Nm} \qquad \text{(non-linear case)}$$

One may also compute the extreme hogging bending moment by switching the sign of α :

$$\alpha = -0.318 \quad \text{and} \quad \beta = 3.194$$

$$\gamma = 0.136$$

$$k = 1.0027$$

$$\delta = 0.869$$

Therefore : $\qquad M_{hog} = 1.905 \ 10^9 \ \text{Nm} \qquad \text{(linear case)}$

$$M_{hog} = 1.656 \ 10^9 \ \text{Nm} \qquad \text{(non-linear case)}$$

and,

$$M_{hog}05 = 1.968 \ 10^9 \ \text{Nm} \qquad \text{(non-linear case)}$$

b. Low flare coefficient

We now repeat the procedure described above, with an identical sea state ($H_S = 6$ m, $T_z = 8.7$ s) and the same speed of 15.5 knots, but for a ship with a low flare coefficient, $C_f = 0.2$.

From the charts (Figures 2.1.38 and 2.1.39), we get :

$$\frac{\alpha}{H_s} = 0.024 \quad \text{and} \quad \frac{\beta - 3}{H_s^2} = 0.0015$$

therefore:
$$\alpha = 0.144 \quad \text{and} \quad \beta = 3.054$$

From a linear strip-theory, we get :

$$\sigma = 5.00 \ 10^8 \ \text{Nm and} \ \nu_0 = 0.1240 \ \text{sec}^{-1}$$

hence:
$$\gamma = 0.040$$

$$k = 1.00058$$

$$\delta = 1.102 \text{ with } \alpha > 0 \text{ and } \delta = 0.929 \text{ with } \alpha < 0$$

Therefore, from eqns. (2.1.50) and (2.1.51):

$$M_{sag} = M_{hog} = 1.897 \ 10^9 \ \text{Nm} \qquad \text{(linear case)}$$

$$M_{sag} = 2.090 \ 10^9 \ \text{Nm} \qquad \text{(non-linear case)}$$

$$M_{hog} = 1.762 \ 10^9 \ \text{Nm} \qquad \text{(non-linear case)}$$

and, from (2.1.55) and (2.1.56):

$$M_{sag05} = 2.485 \ 10^9 \ \text{Nm} \qquad \text{(non-linear case)}$$

$$M_{hog05} = 2.095 \ 10^9 \ \text{Nm} \qquad \text{(non-linear case)}$$

c. <u>A design sea state</u>

A design sea state of $H_s = 10$ m, $T_z = 11.2$ sec. is selected next. The ship speed is assumed to be 4 m/sec and the heading angle is 180°. For a flare coefficient, $C_f = 0.4$ and $T = 3$ hours, one can obtain from Figures 2.1.38 and 2.1.39:

$$\alpha = 0.25 \quad \text{and} \quad \beta = 3.14$$

From eqns. (2.1.52) to (2.1.54) one obtains:

$$\delta = 1.1185 \text{ for sagging condition } (\alpha > 0)$$
$$= 0.891 \text{ for hogging condition } (\alpha < 0)$$

This results in a ratio of sag to hog moments of $1.185 \div 0.891 = 1.33$. For comparison, the ratio of the sag to hog moments was calculated from the American Bureau of Shipping Rules for Steel Vessels (1994, part 3) to be 1.26 for a ship of length = 270 m, B = 32.2 m and block coefficient = 0.598 (see Figure 2.1.10).

Example 2

The influence of the wave zero upcrossing period T_z will be investigated next. The fast container ship, $C_f = 0.48$, is assumed to be cruising at 27 knots in head sea ($\phi = 180°$) of significant wave height $H_s = 4$ m and zero upcrossing rate $T_z = 7$ s or $T_z = 10$ s, corresponding to short and long waves, respectively.

   a. Short waves

From Figures 2.1.13 and 2.1.14, we get:

$$\frac{\alpha}{H_s} = 0.02 \quad \text{and} \quad \frac{\beta - 3}{H_s^2} = 0.0014$$

therefore, $\qquad \alpha = 0.08$ and $\beta = 3.0224$

For $\sigma = 1.227 \ 10^8$ Nm, $\nu = 0.1707 \ \text{sec}^{-1}$ and for $T = 3$ hours, one obtains from eqns. (2.1.51) to (2.1.54):

$$\gamma = 0.016$$

$$k = 1.00018$$

$$\delta = 1.056 \text{ with } \alpha > 0 \quad \text{and} \quad \delta = 0.957 \text{ with } \alpha < 0$$

and, from (2.1.50) and (2.1.51) (see procedure details in Example 1):

$$M_{sag} = M_{hog} = 4.758 \ 10^8 \ \text{Nm} \qquad \text{(linear case)}$$

$$M_{sag} = 5.024 \ 10^8 \ \text{Nm} \qquad \text{(non-linear case)}$$

$$M_{hog} = 4.553 \ 10^8 \ \text{Nm} \qquad \text{(non-linear case)}$$

b. <u>Long waves</u>

We repeat the same process with $T_z = 10$ s. From Figures 2.1.13 and 2.1.14:

$$\frac{\alpha}{H_s} = 0.07 \quad \text{and} \quad \frac{\beta - 3}{H_s^2} = 0.0016$$

$$\alpha = 0.28 \quad \text{and} \quad \beta = 3.256$$

With $\sigma = 1.758 \ 10^8$ Nm and $v_0 = 0.1423$ sec^{-1}, one gets:

$$\gamma = 0.176$$

$$k = 1.0022$$

$$\delta = 1.234 \text{ with } \alpha > 0 \quad \text{and} \quad \delta = 0.908 \text{ with } \alpha < 0$$

Therefore,

$$M_{sag} = M_{hog} = 6.734 \ 10^8 \text{ Nm} \qquad \text{(linear case)}$$

$$M_{sag} = 8.310 \ 10^8 \text{ Nm} \qquad \text{(non-linear case)}$$

$$M_{hog} = 6.115 \ 10^8 \text{ Nm} \qquad \text{(non-linear case)}$$

It should be pointed out that the change in the non-linearity parameter for sagging from short to long waves (1.056 to 1.234) represents the maximum range of change according to Figures 2.1.13 and 2.1.14. The large increase in the sagging moment in the case of long waves is to be noted. The increase, however, is not all due to increase in the non-linearity parameter δ. In longer waves, the standard deviation has increased by about 43% whereas the non-linearity parameter has increased by 17%.

Example 3

The influence of the ship speed will be investigated in this example. The container ship is assumed to be cruising in moderate sea state of significant wave height $H_s = 5$ m and a corresponding zero upcrossing rate $T_z = 8$ s, determined from eqn. (2.1.61). The ship speed will be increased from 11.5 knots (6 m/s) to 19.5 knots (10 m/s) and the heading angle $\phi = 135°$.

a. <u>Low speed</u>

For the charts in Figures 2.1.27 and 2.1.28, we get:

$$\frac{\alpha}{H_s} = 0.067 \quad \text{and} \quad \frac{\beta - 3}{H_s^2} = 0.0085$$

therefore,
$$\alpha = 0.335 \quad \text{and} \quad \beta = 3.213$$

For $\sigma = 1.461\ 10^8$ Nm, $\nu_0 = 0.1242$ sec^{-1} and T = 3 hours, one computes from eqns. (2.1.51) to (2.1.54) :

$$\gamma = 0.1487$$

$$k = 1.003$$

$$\delta = 1.254 \text{ with } \alpha > 0 \quad \text{and} \quad \delta = 0.865 \text{ with } \alpha < 0$$

Therefore, from (2.1.50) and (2.1.51) one obtains:

$$M_{sag} = M_{hog} = 5.545\ 10^8 \text{ Nm} \qquad \text{(linear case)}$$

$$M_{sag} = 6.953\ 10^8 \text{ Nm} \qquad \text{(non-linear case)}$$

$$M_{hog} = 4.796\ 10^8 \text{ Nm} \qquad \text{(non-linear case)}$$

b. <u>High speed</u>

We repeat the same process with $V = 19.5$ knots, corresponding to the charts in Figures 2.1.31 and 2.1.32:

$$\frac{\alpha}{H_s} = 0.053 \quad \text{and} \quad \frac{\beta - 3}{H_s^2} = 0.009$$

therefore,
$$\alpha = 0.365 \quad \text{and} \quad \beta = 3.225$$

For $\sigma = 1.450\ 10^8$ Nm, $\nu_0 = 0.1426$ sec^{-1} and $T = 3$ hours, one computes from eqns. (2.1.51) to (2.1.54) :

$$\gamma = 0.1565$$

$$k = 1.0036$$

$$\delta = 1.279 \text{ with } \alpha > 0 \quad \text{and} \quad \delta = 0.851 \text{ with } \alpha < 0$$

Therefore, from (2.1.50) and (2.1.51) one obtains:

$$M_{sag} = M_{hog} = 5.555 \ 10^8 \ \text{Nm} \qquad \text{(linear case)}$$

$$M_{sag} = 7.105 \ 10^8 \ \text{Nm} \qquad \text{(non-linear case)}$$

$$M_{hog} = 4.728 \ 10^8 \ \text{Nm} \qquad \text{(non-linear case)}$$

The modest increase in the non-linearity parameter (2 %) with the ship speed indicates that speed is not an important factor. Figures 2.1.21 to 2.1.36 show, however, that the influence of the heading angle is more important.

In summary, several charts have been developed based on the quadratic theory. These charts, which can be used to estimate the non-linearity parameter in moderate to high sea states, are developed by varying the flare coefficient, sea state, ship speed and heading. The results indicate that the flare coefficient and sea state have important impact on the non-linearity parameter, whereas ship speed and heading seem to be less important. The limitation of the quadratic theory in extreme (very high) seas is also discussed.

A linear strip theory program may be used together with the presented charts in order to estimate slightly non-linear hogging and sagging wave moments. The use of the charts has been illustrated by three application examples given at the end of the section.
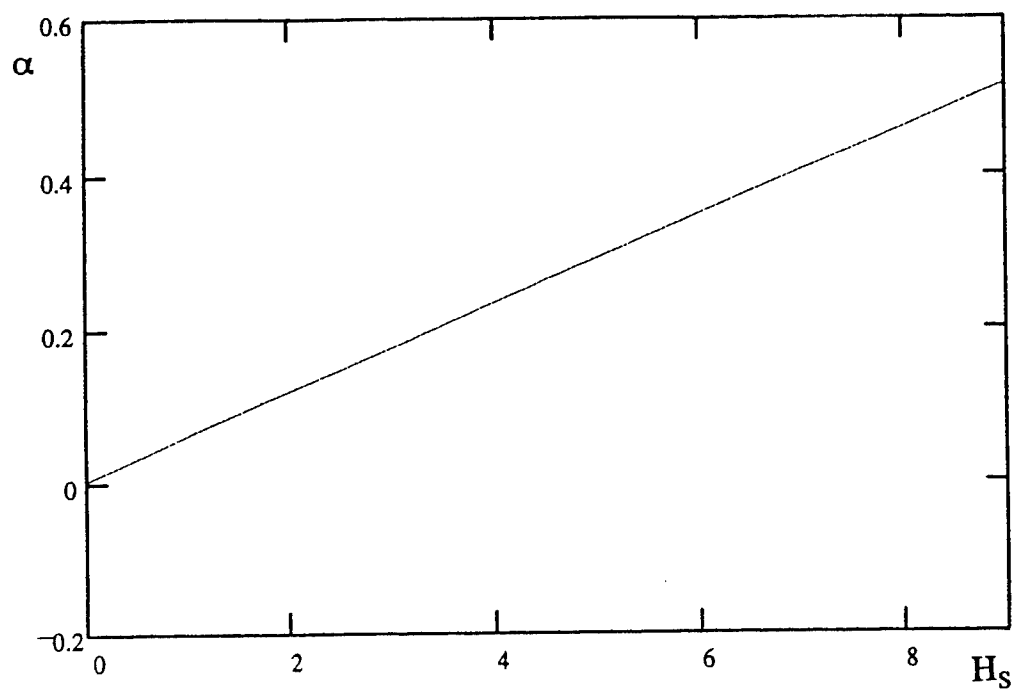
Figure 2.1.11 Skewness α versus H_s ($T_z = 9$ s, $V = 5$ m/s, $\phi = 180°$).
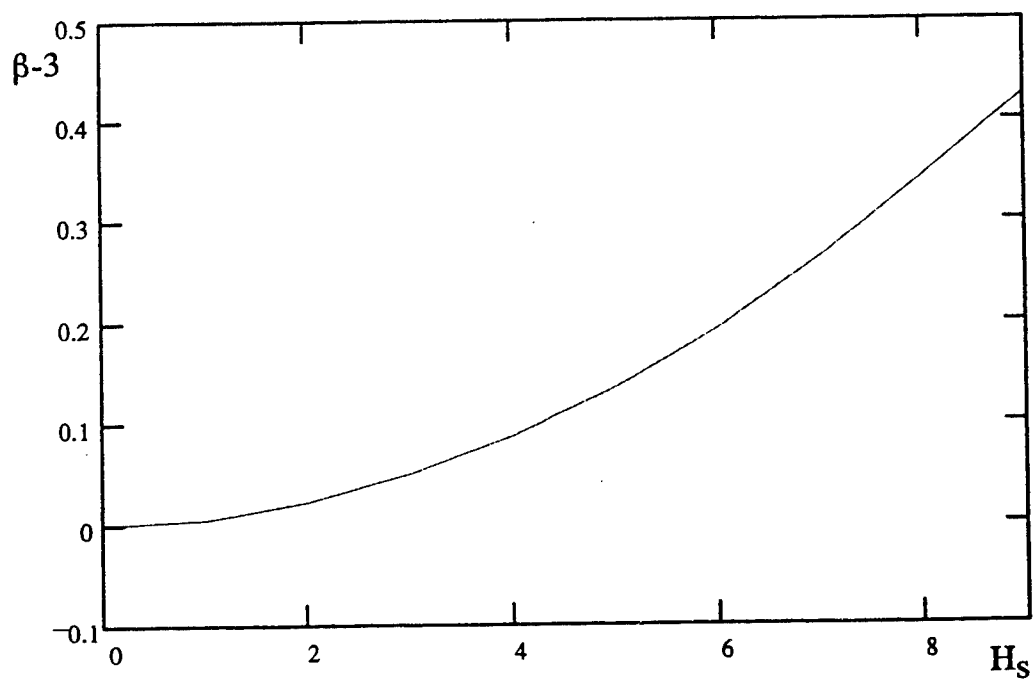
Figure 2.1.12 Kurtosis β - 3 versus H_s ($T_z = 9$s, $V = 5$ m/s, $\phi = 180°$).
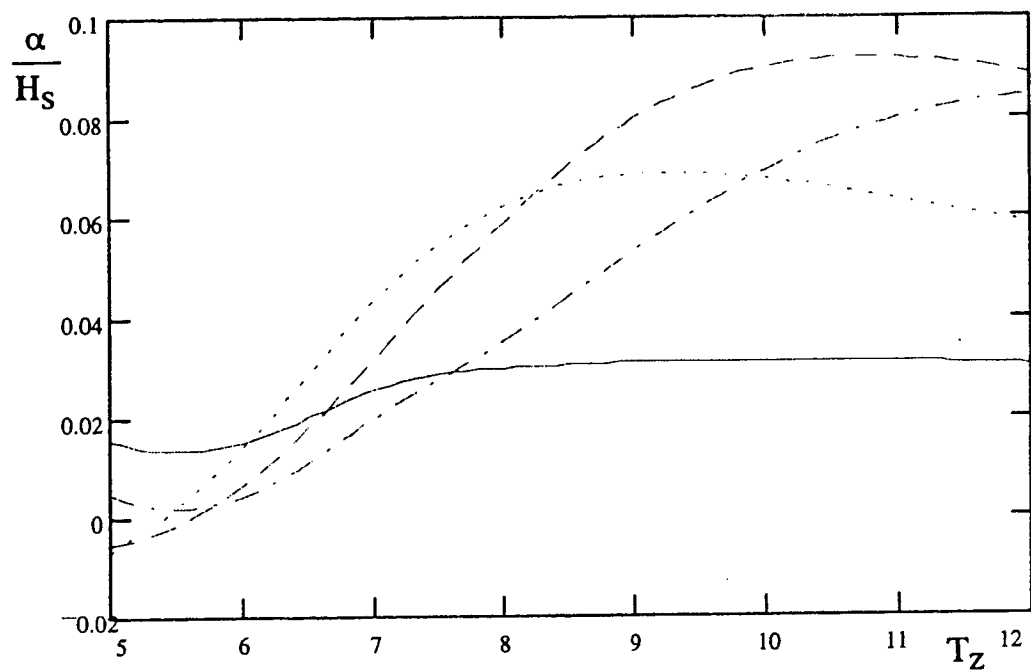
Figure 2.1.13 α/H_s versus T_z for different speeds and $\phi = 180°$.

——— $V = 2$ m/s,   ------- $V = 6$ m/s,   — — $V = .0$ m/s,   — — — $V = 14$ m/s
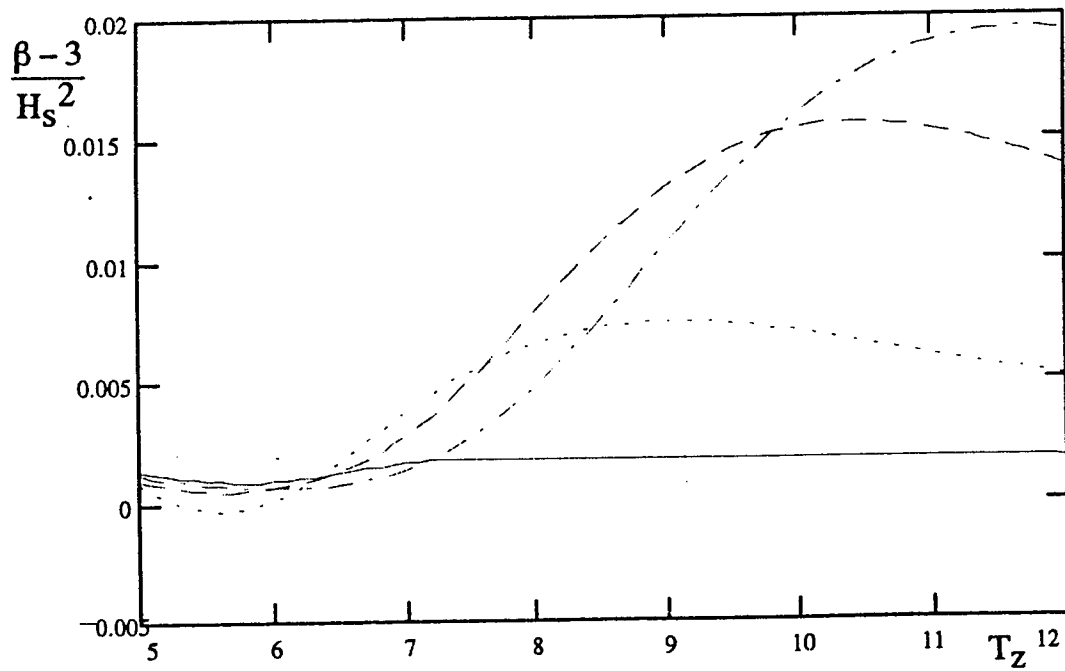
Figure 2.1.14 $(\beta - 3)/H_s^2$ versus T_z for different speeds and $\phi = 180°$.
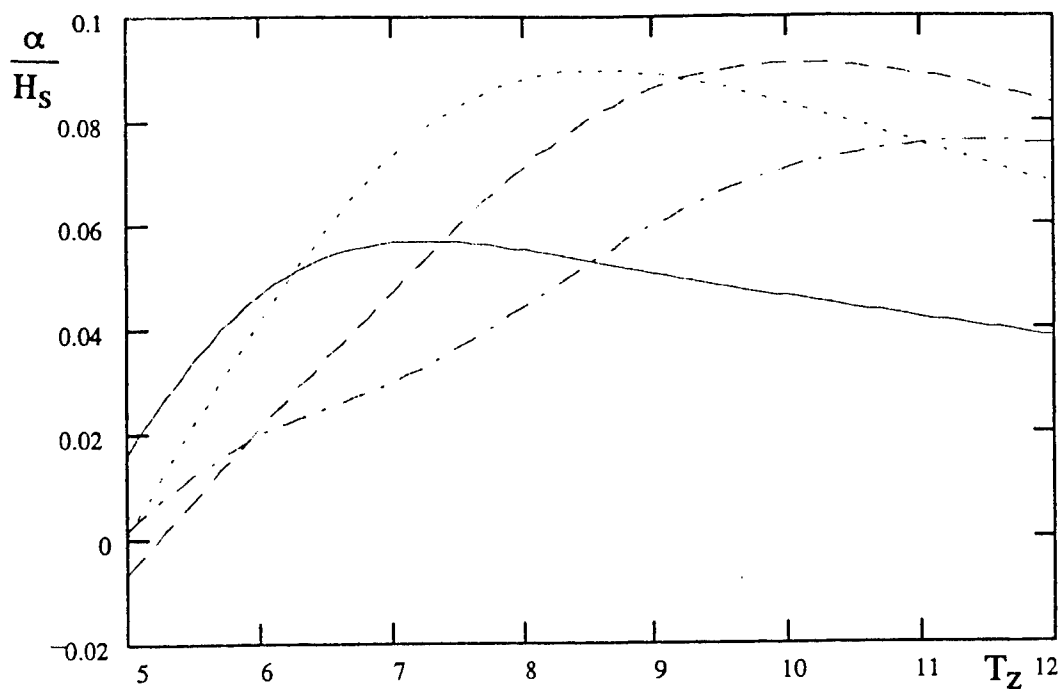
Figure 2.1.15 α/H_s versus T_z for different speeds and $\phi = 135°$.

—————— $V = 2$ m/s, ------- $V = 6$ m/s, — — $V = 10$ m/s, —‑—‑— $V = 14$ m/s
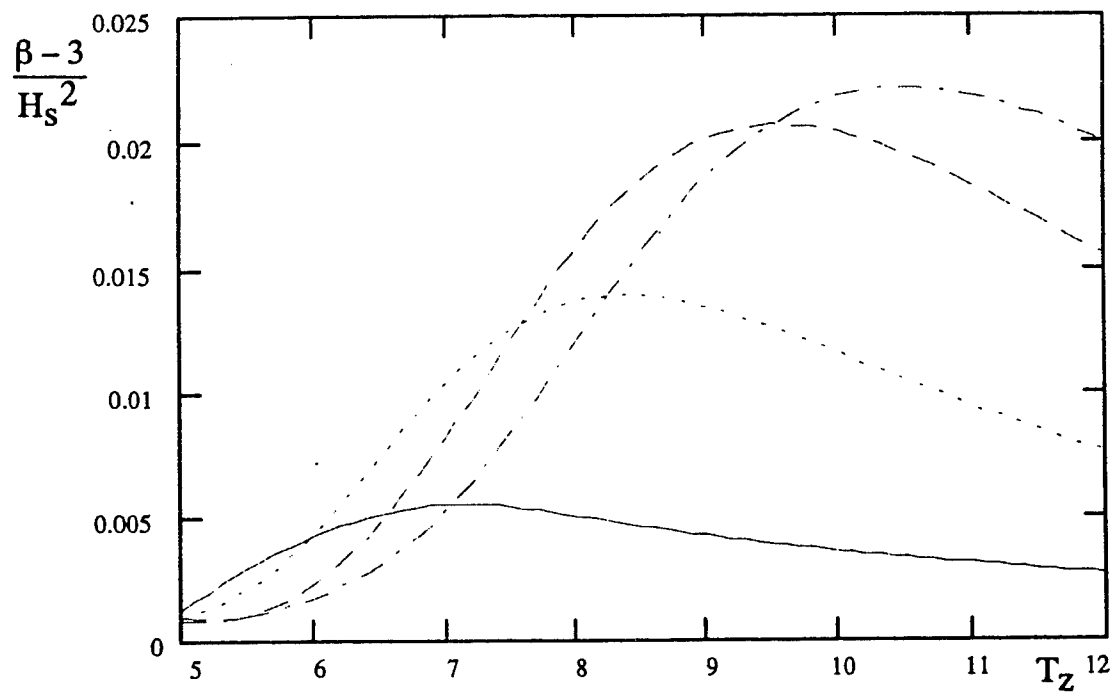
Figure 2.1.16 $(\beta - 3)/H_s^2$ versus T_z for different speeds and $\phi = 135°$.
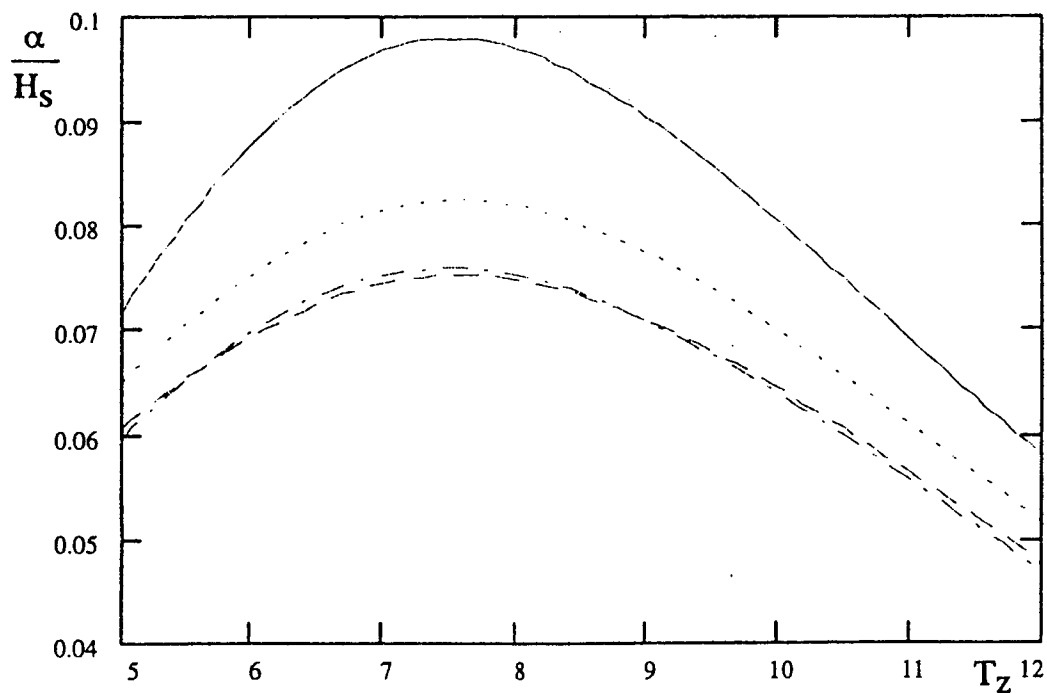
Figure 2.1.17 α/H_s versus T_z for different speeds and $\phi = 90°$.

——— $V = 2$ m/s,   ------- $V = 6$ m/s,   — — $V = 10$ m/s,   — — — $V = 14$ m/s
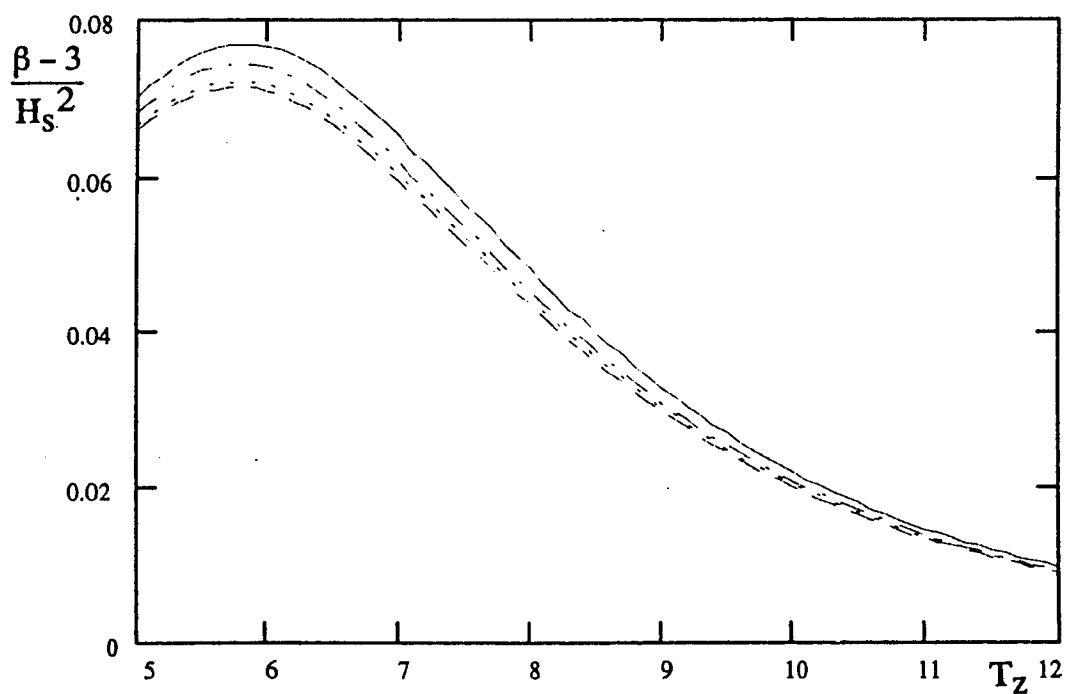
Figure 2.1.18 $(\beta - 3)/H_s^2$ versus T_z for different speeds and $\phi = 90°$.
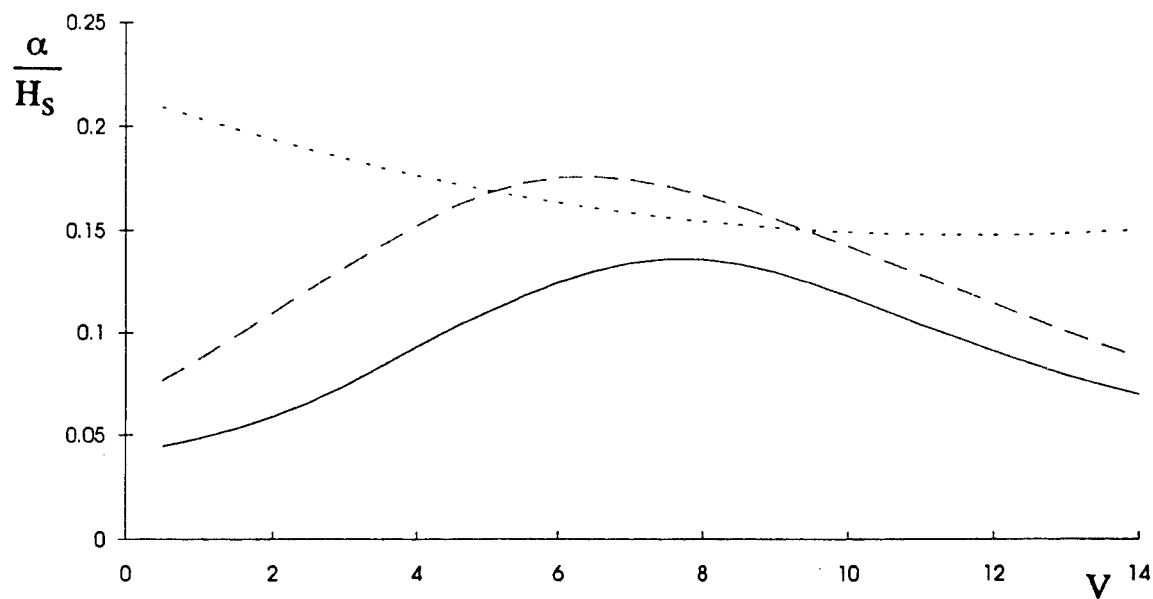
Figure 2.1.19 α/H_s versus V for different heading angles ($T_z = 8$ s).

———— $\phi = 180°$,   — — $\phi = 135°$,   — — — $\phi = 90°$
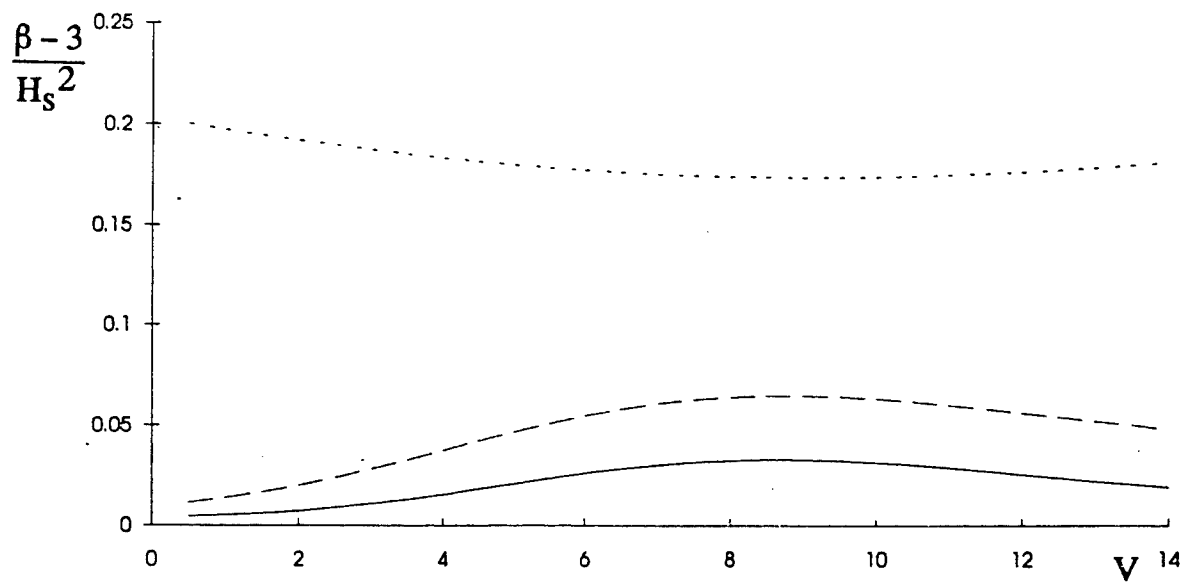
Figure 2.1.20 $(\beta - 3)/H_s^2$ versus V for different heading angles ($T_z = 8$ s).
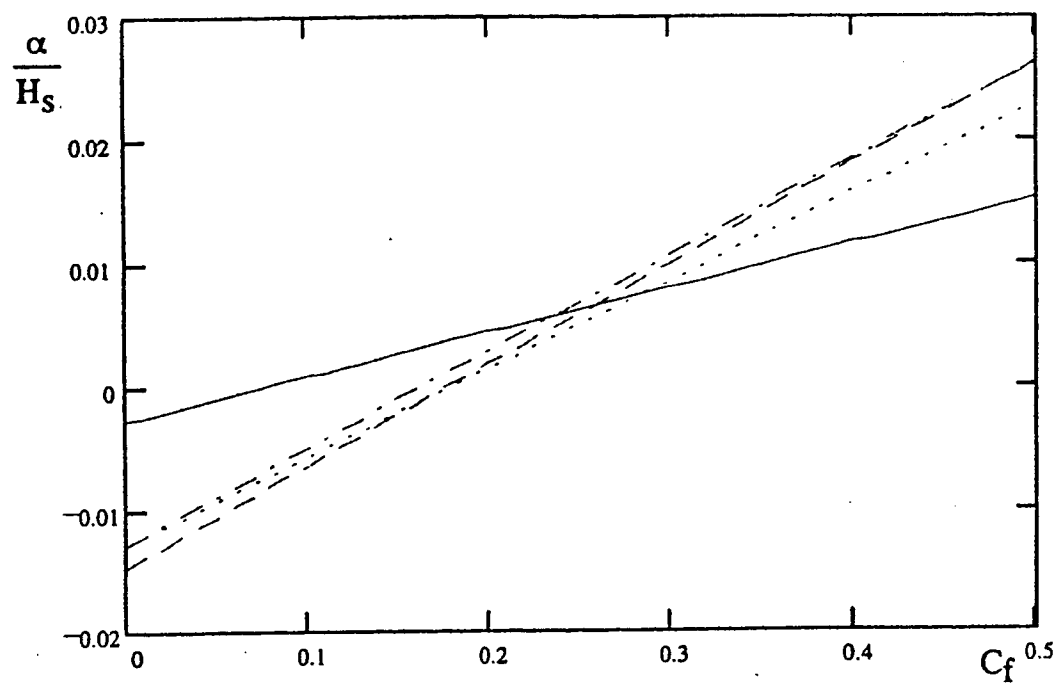
Figure 2.1.21 α/H_s versus C_f for $Fr = 0.039$ and $\phi = 180°$.

—————— $T_z = 8$ s, ------- $T_z = 10$ s, — — $T_z = 12$ s, — — — $T_z = 14$ s
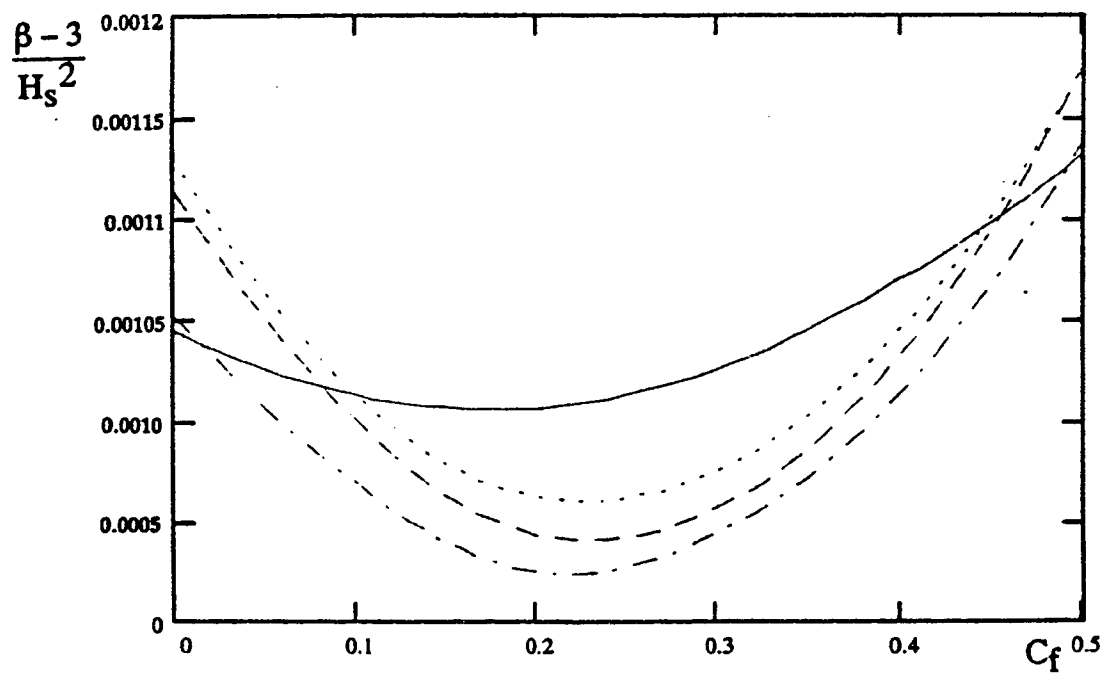
Figure 2.1.22 $(\beta - 3)/H_s^2$ versus C_f for $Fr = 0.039$ and $\phi = 180°$.
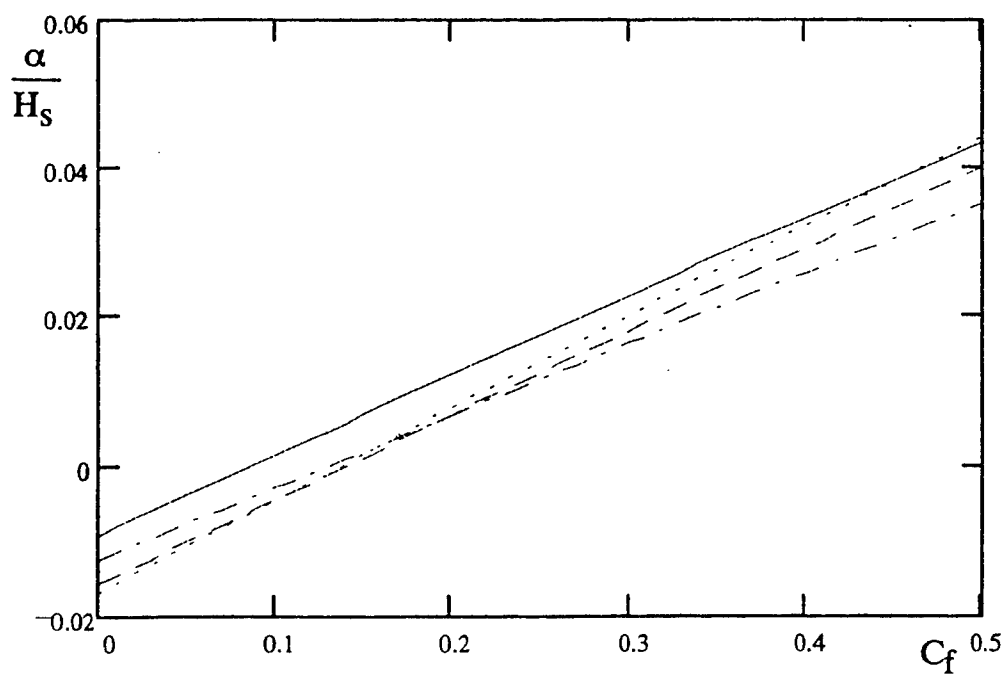
Figure 2.1.23 α/H_s versus C_f for $Fr = 0.039$ and $\phi = 135°$.

——— $T_z = 8$ s,   ------- $T_z = 10$ s,   — — $T_z = 12$ s,   —·—· $T_z = 14$ s
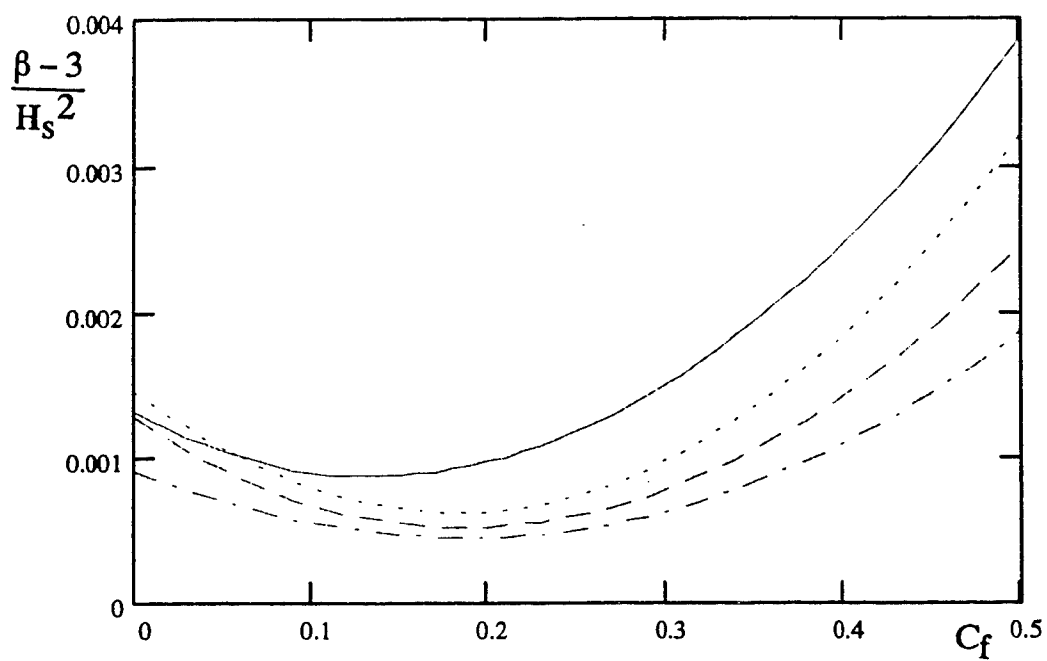
Figure 2.1.24 $(\beta - 3)/H_s^2$ versus C_f for $Fr = 0.039$ and $\phi = 135°$.
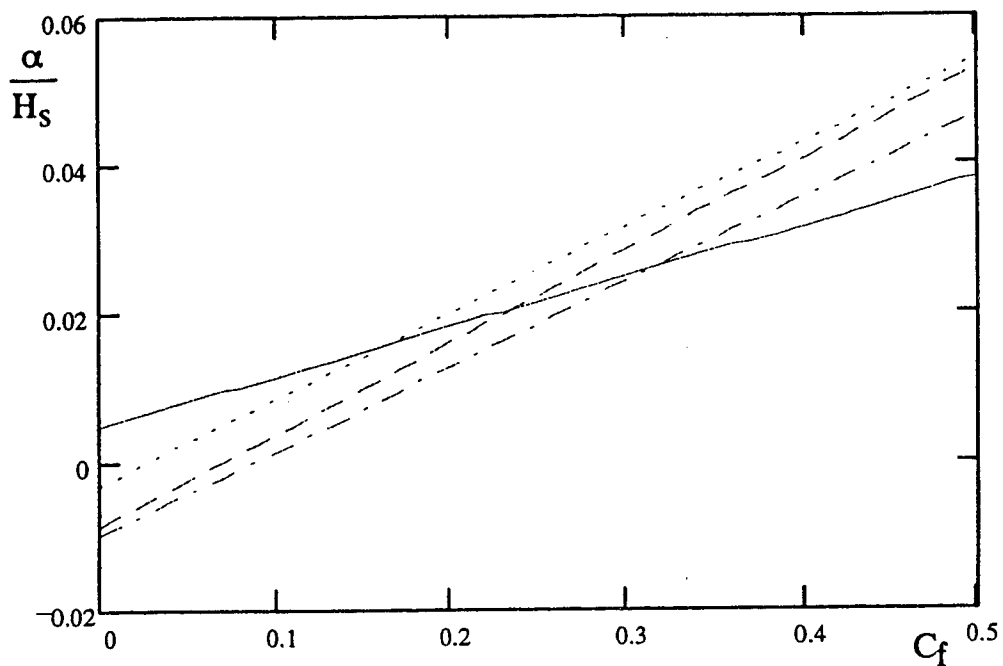
Figure 2.1.25 α/H_s versus C_f for $Fr = 0.117$ and $\phi = 180°$.

———— $T_z = 8$ s,   ---------- $T_z = 10$ s,   — — $T_z = 12$ s,   — · · — $T_z = 14$ s
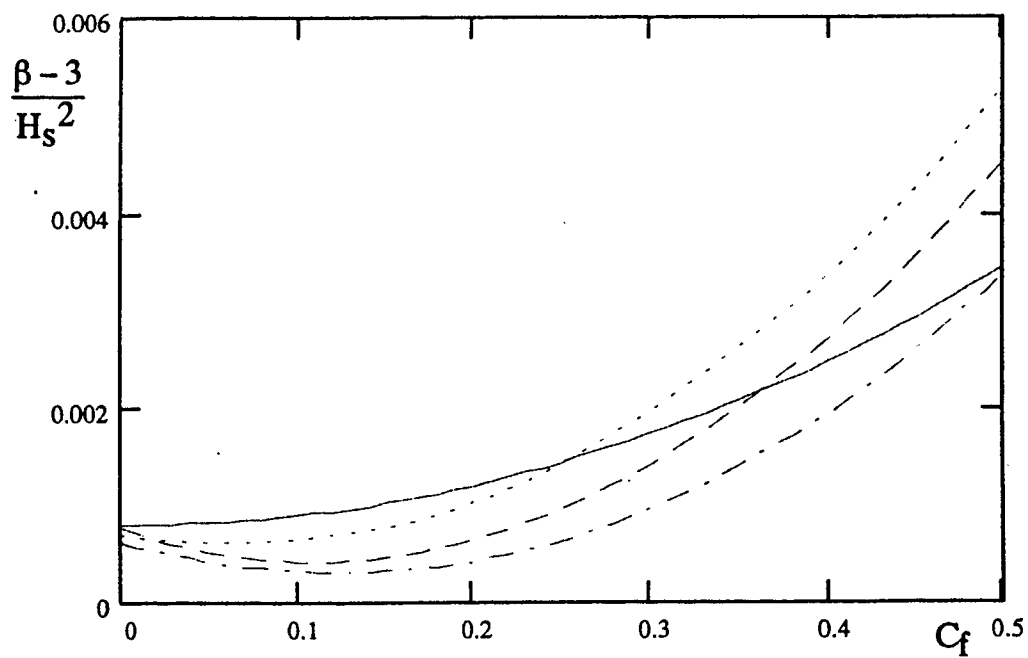
Figure 2.1.26 $(\beta - 3)/H_s^2$ versus C_f for $Fr = 0.117$ and $\phi = 180°$.

2-49
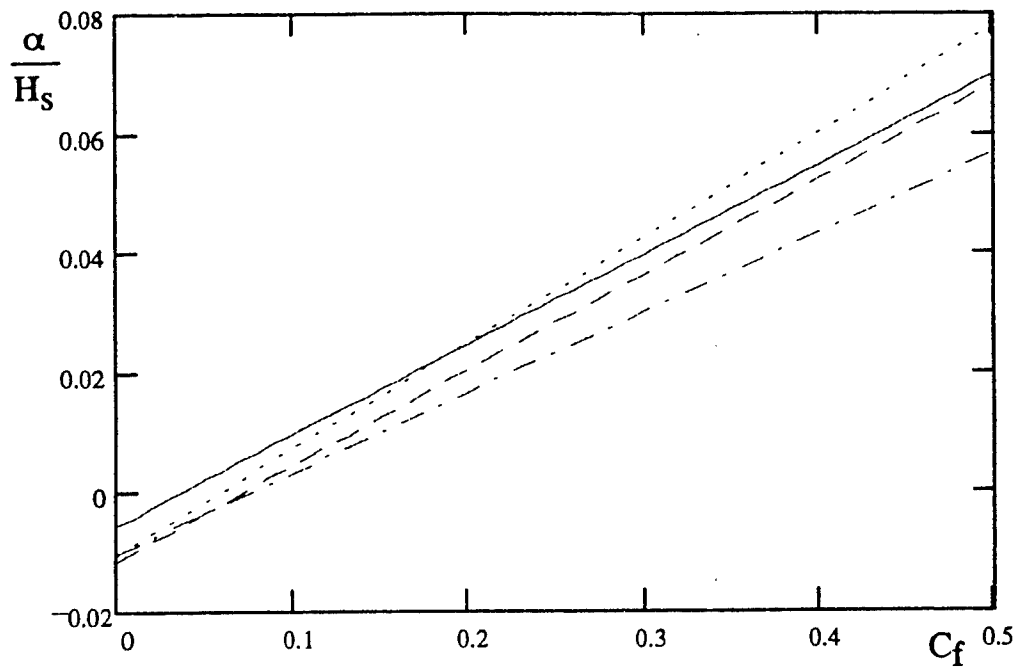
Figure 2.1.27 α/H_s versus C_f for $Fr = 0.117$ and $\phi = 135°$.

——— $T_z = 8$ s,   ------- $T_z = 10$ s,   — — $T_z = 12$ s,   — - — $T_z = 14$ s
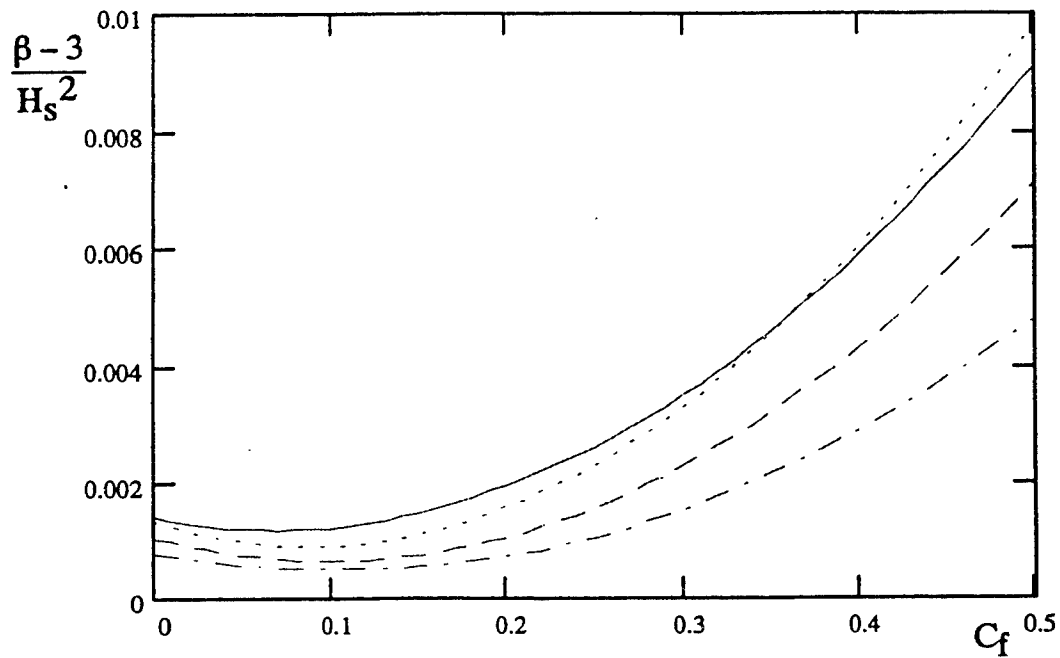
Figure 2.1.28 $(\beta - 3)/H_s^2$ versus C_f for $Fr = 0.117$ and $\phi = 135°$.
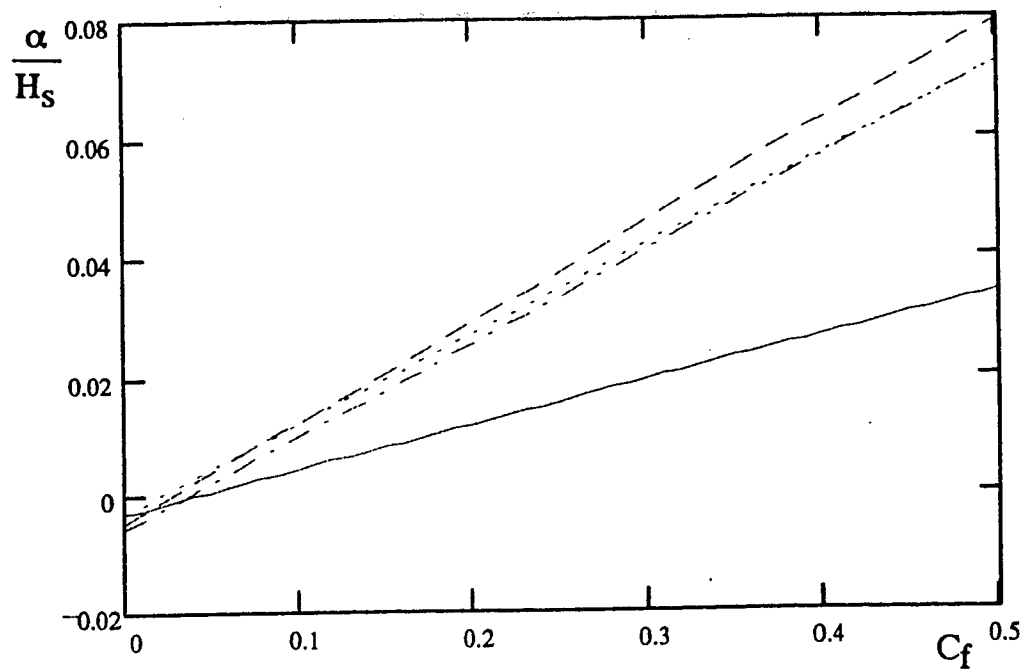
Figure 2.1.29 α/H_s versus C_f for $Fr = 0.194$ and $\phi = 180°$.

—— $T_z = 8$ s, ------- $T_z = 10$ s, — — $T_z = 12$ s, — — — $T_z = 14$ s
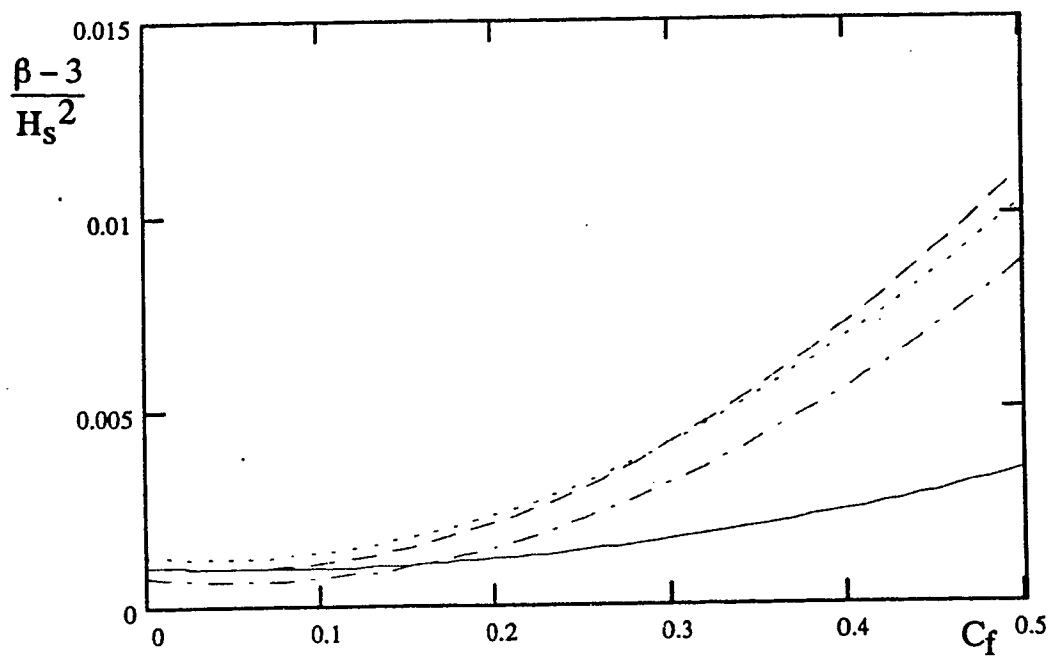
Figure 2.1.30 $(\beta - 3)/H_s^2$ versus C_f for $Fr = 0.194$ and $\phi = 180°$.
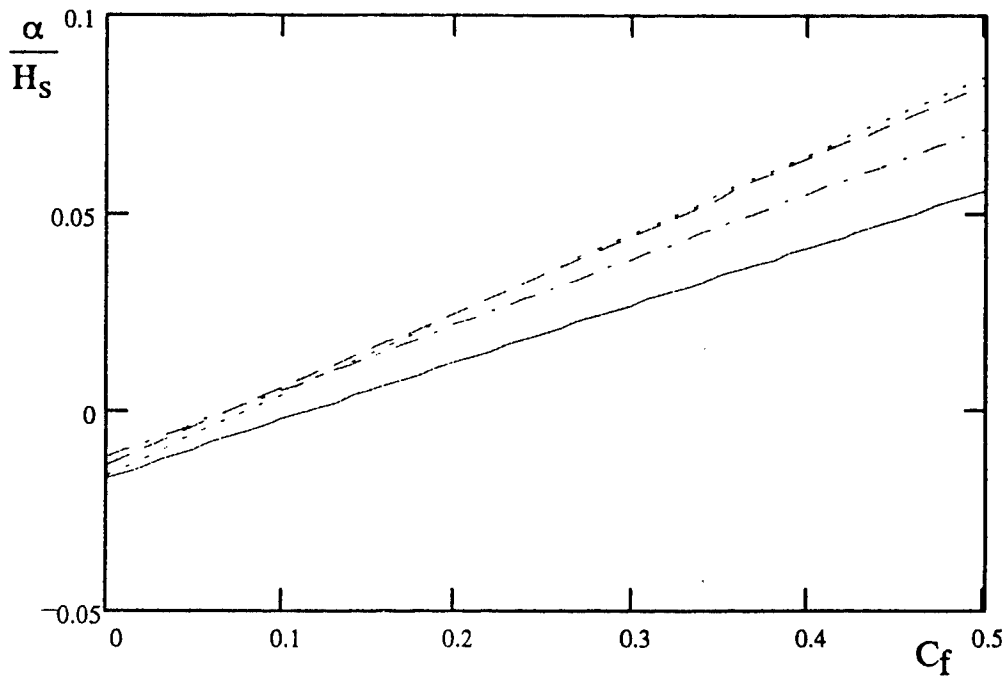
Figure 2.1.31 α/H_s versus C_f for $Fr = 0.194$ and $\phi = 135°$.

——— $T_z = 8$ s, ------- $T_z = 10$ s, — — $T_z = 12$ s, — — — $T_z = 14$ s
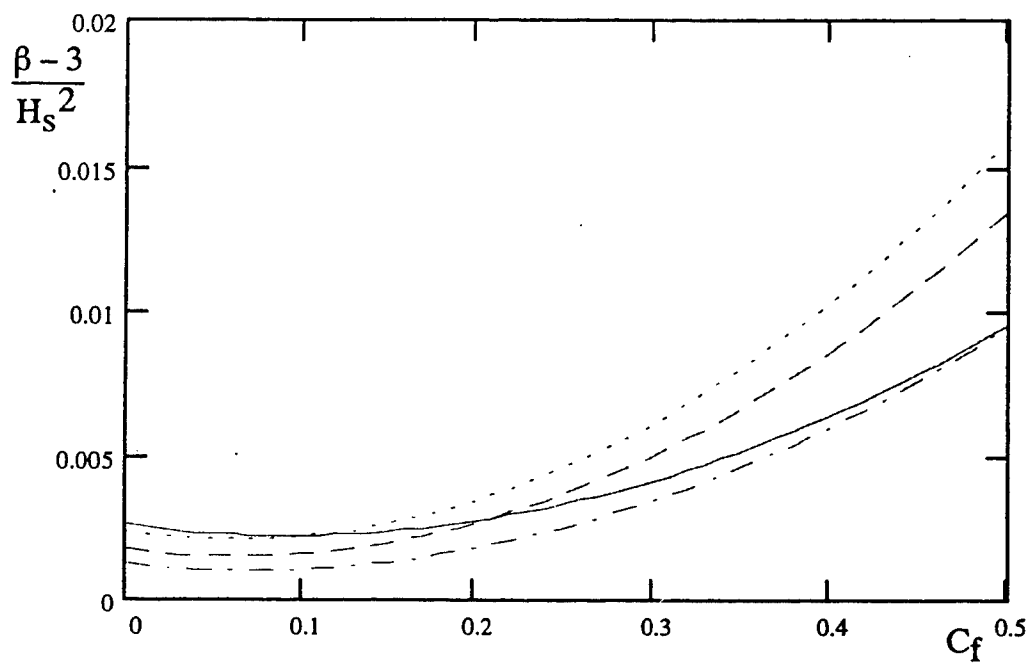
Figure 2.1.32 $(\beta - 3)/H_s^2$ versus C_f for $Fr = 0.194$ and $\phi = 135°$.
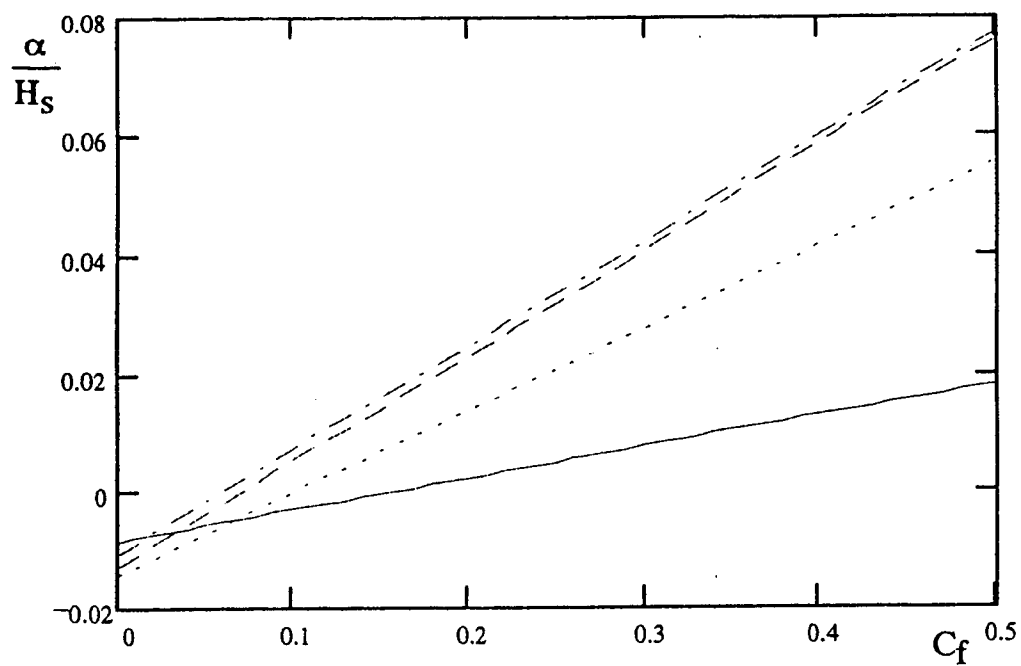
Figure 2.1.33 α/H_s versus C_f for $Fr = 0.272$ and $\phi = 180°$.

——— $T_z = 8$ s,   ------- $T_z = 10$ s,   — — $T_z = 12$ s,   —·—·— $T_z = 14$ s
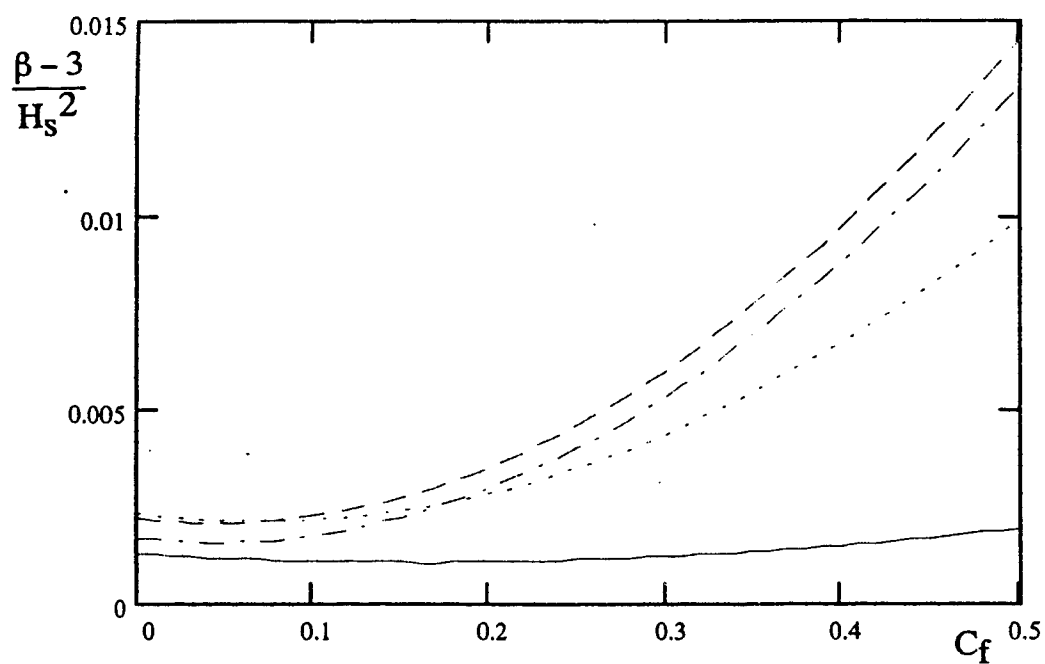
Figure 2.1.34 $(\beta - 3)/H_s^2$ versus C_f for $Fr = 0.272$ and $\phi = 180°$.

2-53
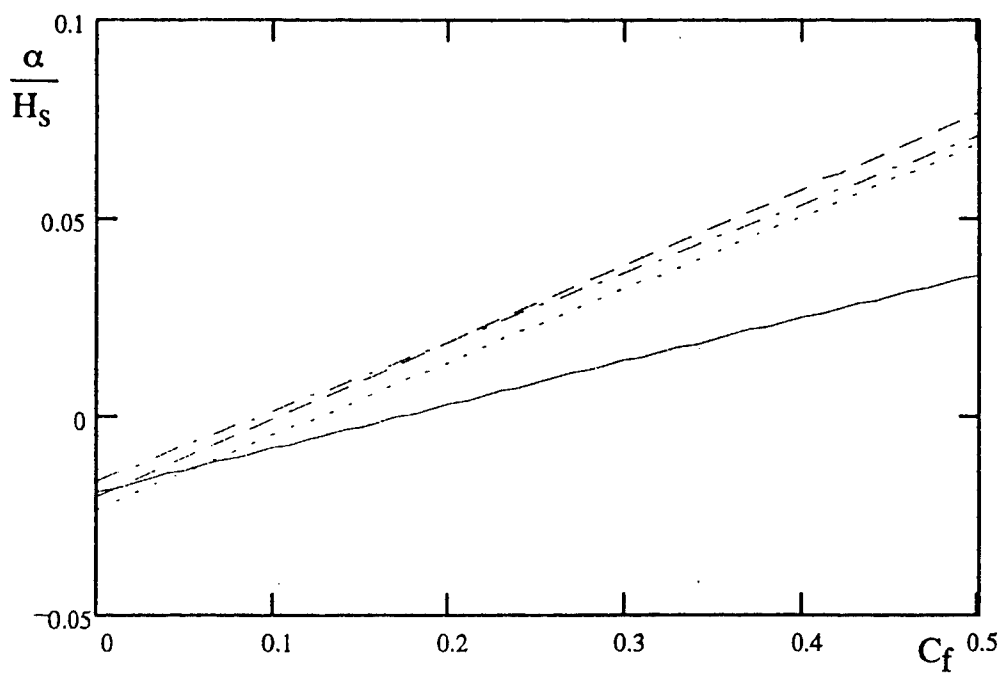
Figure 2.1.35 α/H_s versus C_f for $Fr = 0.272$ and $\phi = 135°$.

—————— $T_z = 8$ s, -------- $T_z = 10$ s, — — $T_z = 12$ s, — - — $T_z = 14$ s
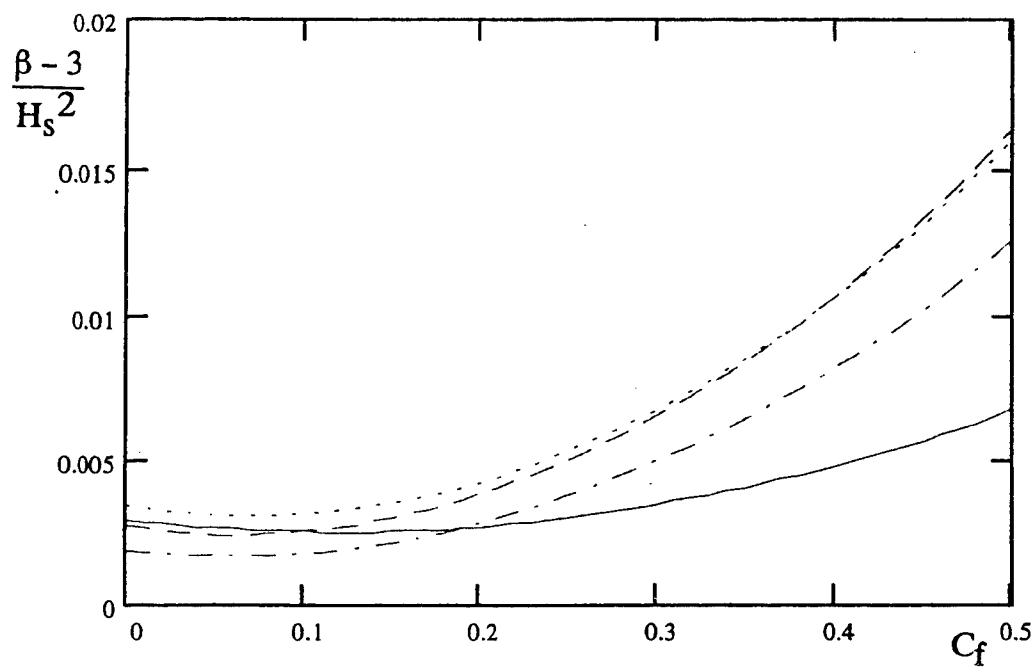
Figure 2.1.36 $(\beta - 3)/H_s^2$ versus C_f for $Fr = 0.272$ and $\phi = 135°$.
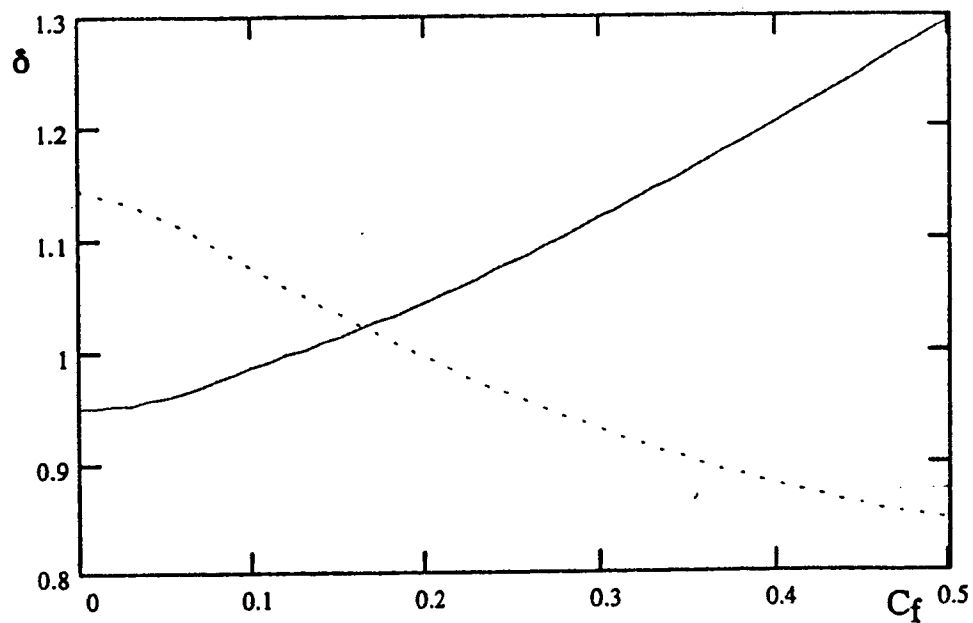
Figure 2.1.37 Non-linearity Parameter δ versus C_f

——— sagging ($\alpha > 0$)   ------ hogging ($\alpha < 0$)
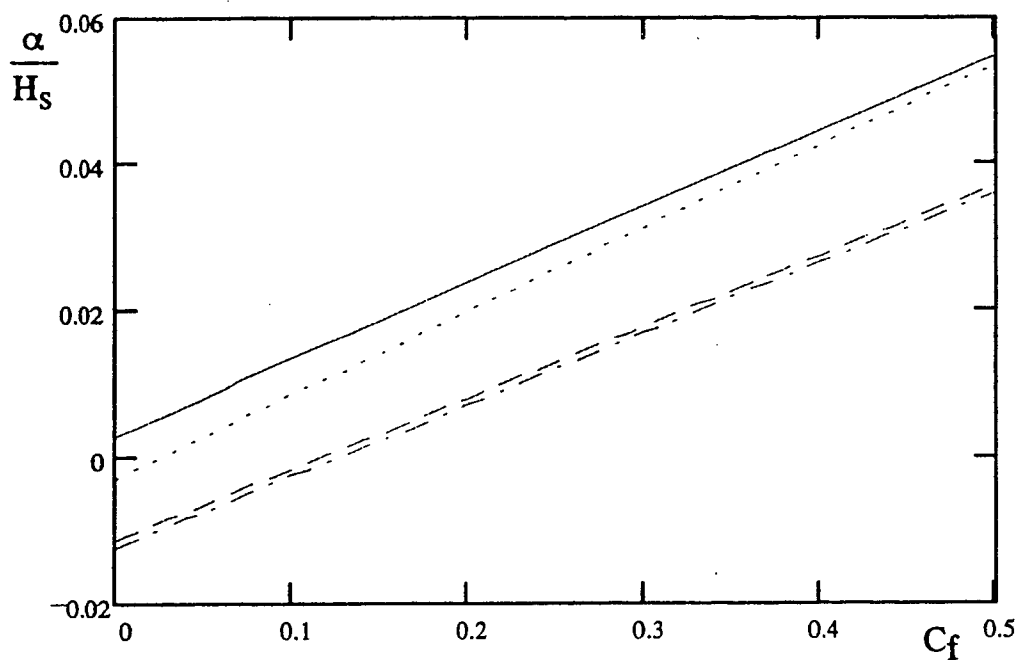
Figure 2.1.38 α/H_s versus C_f for frequently occurring pairs of (H_s, T_z), $\phi = 180°$.

——— $H_s = 6$ m, $T_z = 8.7$ s, $V = 8$ m/s,   — — $H_s = 10$ m, $T_z = 11.2$ s, $V = 4$ m/s

- - - - $H_s = 8$ m, $T_z = 10$ s, $V = 6$ m/s,   — — — $H_s = 12$ m, $T_z = 12.3$ s, $V = 4$ m/s

2-55
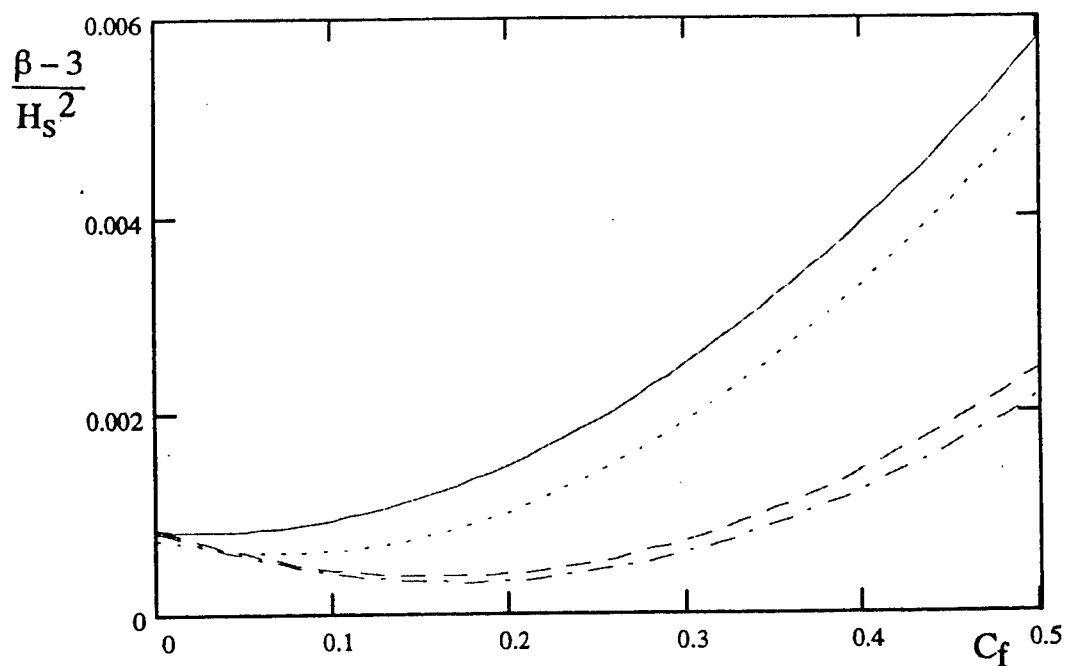
Figure 2.1.39 $(\beta - 3)/H_s^2$ versus C_f for frequently occurring pairs of (H_s, T_z), $\phi = 180°$.
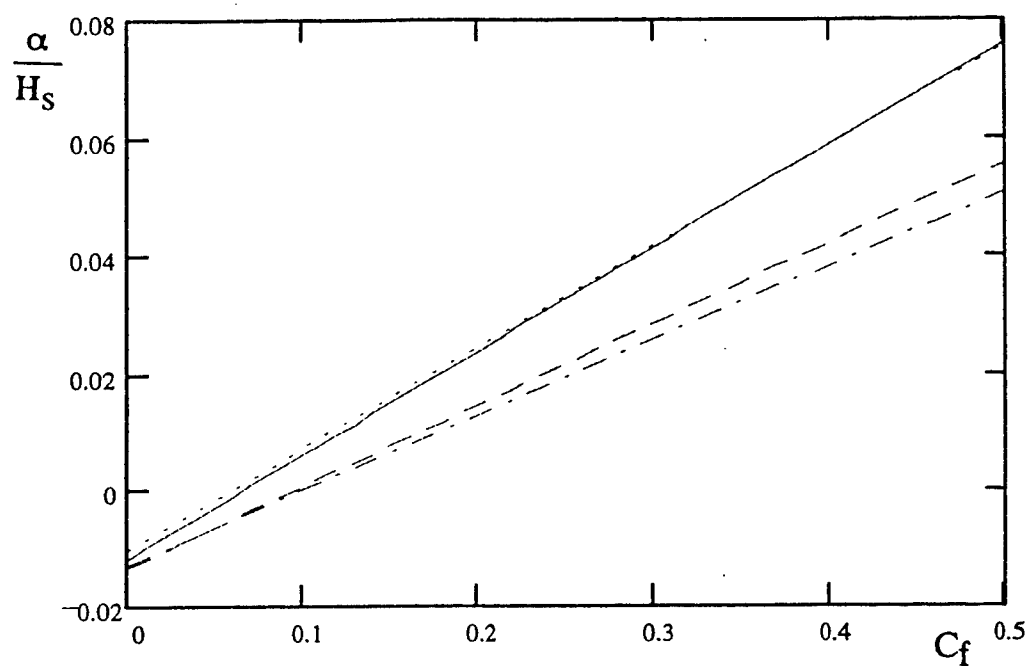
Figure 2.1.40 α/H_s versus C_f for frequently occurring pairs of (H_s, T_z), $\phi = 135°$.

——— $H_s = 6$ m, $T_z = 8.7$ s, $V = 8$ m/s,   — — $H_s = 10$ m, $T_z = 11.2$ s, $V = 4$ m/s

- - - - $H_s = 8$ m, $T_z = 10$ s, $V = 6$ m/s,   — — — $H_s = 12$ m, $T_z = 12.3$ s, $V = 4$ m/s
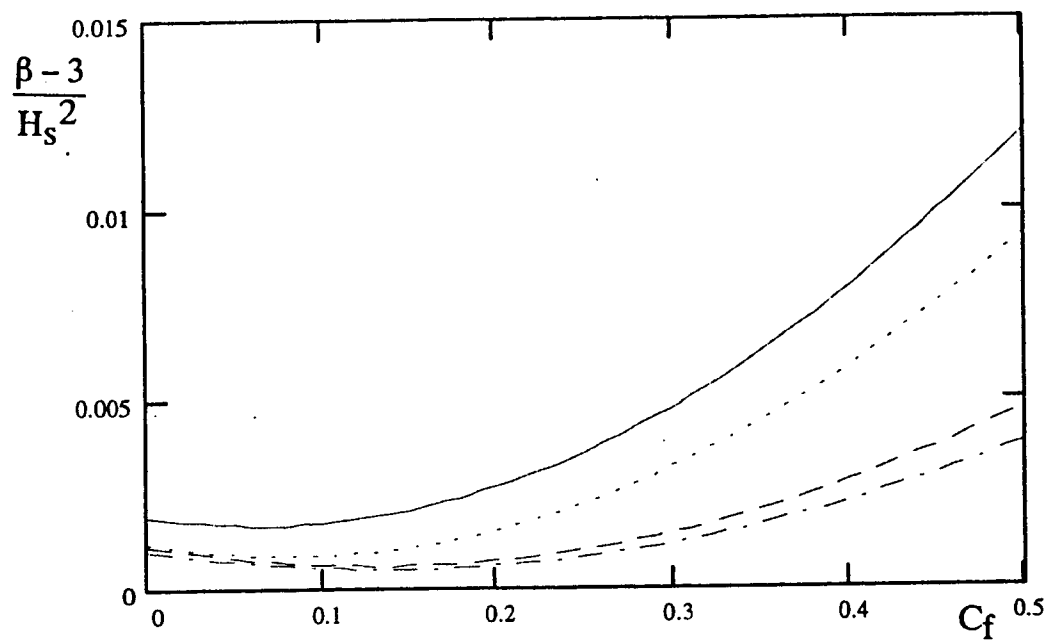
Figure 2.1.41 $(\beta - 3)/H_s^2$ versus C_f for frequently occurring pairs of (H_s, T_z), $\phi = 135°$.

2.1.4   Slamming Loads:

Slamming loads are significant in many types of oceangoing vessels, e.g. those with fine form, low draft, and high speed. The calculation of slam effects (stresses) requires the consideration of hull flexibility. The maximum slam loads do not typically occur when the wave induced loads are the largest, and such lack of perfect correlation needs to be considered in the calculation of combined load effects. Another characteristic one should mention is the marked nonlinearity of slam loads with respect to the wave height, resulting in the hull girder response being significantly different for the hogging and sagging parts of the wave cycle.

The treatment of slamming in ships is semi-empirical, relying on insights gained from in-service data and measurements, and contains large uncertainties related to the methods themselves (e.g. momentum versus impact slamming), effect of operational factors (i.e. discretionary changes in vessel heading and speed), and load combinations.

2.1.4.1   *The computer program SLAM — background*

An integrated package for ship hull global extreme loads and stresses arising from the combined effects of slamming and wave induced loads was developed by Friis-Hansen (1993). The load combination procedure is suitable for use in the presence of significant non-linearities. Phasing of slamming occurrence with regard to the wave induced load peak is implicitly obtained in the method from consideration of the basic physics of the problem, rather than input to it. The method accounts for the clustering of slam events using an envelope approach.

The primary output from the method is the probability distribution function of the combined extreme load effects arising from wave induced and slamming hull girder loads in a given sea state. The procedure requires as input the vessel motion transfer functions from linear ship motion theory, and wave induced load transfer functions from any appropriate theory, e.g., linear strip theory, quadratic strip theory, or fully nonlinear theory. Slam loads and their effects are internally calculated.

Generally, the term slamming refers to the impact generated when the ship bottom hits the water surface after a series of large heave and pitch motions have forced a part of the ship's bottom to emerge and therefore to reenter the water. Only this impact slamming is considered here. Full-scale measurements have shown that the slamming induced stresses at midship can be of the same order magnitude as the bending induced stresses (Ochi and Motter, 1973). Therefore, slamming stresses must be carefully evaluated in the design phase, and suitably be combined with the low-frequency wave-induced bending stresses. According to Ochi and Motter (1973), the necessary and sufficient conditions leading to slamming impact are:

- relative motion must exceed sectional draft (bottom emergence), and

- relative velocity at instant of reentry must exceed a certain magnitude, called the threshold velocity.

Ochi and Motter (1973) suggest a truncated exponential probability distribution of the impact pressure, and proposed a Poisson process model for slamming interarrival time by fitting experimental data. Further, they derived statistical properties for the slamming pressure. They proposed to calculate the slamming moment from the dynamic analysis of a hull girder under the impact forces conservatively using the extreme slamming pressure at each point. Moreover, they suggested to combine this extreme upper bound on the slamming moment with the extreme wave moment using a suitable (unspecified) phase angle. A more rigorous approach to obtain the statistical properties has been presented by Mansour and Lozow (1982). They assumed that slamming impact follows a Poisson pulse process with independent amplitudes and interarrival times.

Nikolaidis and Kaplan (1992) performed a Monte-Carlo simulation study to estimate the uncertainty in combining low-frequency wave bending moments and slamming bending moments in ships. They concluded that Turkstra's rule (1970) underestimates the mean value of the combined moment, and that the design load, estimated by Turkstra's rule, had a larger variability than the actual load. However, Nikolaidis and Kaplan did not include the effect of correlation. Turkstra's rule requires the maximum value of one of the processes to be combined with the corresponding value in time of the other process. For uncorrelated processes the corresponding value in time is easily obtained, whereas it is more involved for correlated processes.

Inaccuracies in the Poisson model may arise from (Nikolaidis and Kaplan, 1992):

- The times of occurrence of slamming impacts are not independent because of the periodic nature of the ship motions and waves.

- The times of occurrence of the slamming and the wave induced stress peaks are highly correlated. As has been reported by Ochi and Motter, a slamming impact usually generates the first peak of a compressive (sagging) in the deck as the wave induced stress passes from hogging to sagging.

- When the wave induced stress is high, it is very likely that the slamming induced stress is also high. Therefore, from a probabilistic point of view, the slamming and the waves stress intensities are positively correlated.

So far, no general mathematical method has been developed to calculate the probabilistic structure of the slamming and low-frequency stresses, although Ferro and Mansour (1985) proposed to apply Turkstra's rule. Ferro and Mansour based their work on earlier work by Mansour and Lozow (1982), which as mentioned assumed the slamming impact to follow a Poisson pulse process. However, the slamming process is not exactly a Poissson process, but approaches a Poisson process in the limit. This is because the narrow-band character of the process of the relative motion tends to concentrate the slamming

impacts into clumps, and thereby violating the assumption of mutual independence of the individual slamming impacts.

Friis-Hansen (1993) used a probabilistic model which takes the non-Poissonian character of slamming impact into account - more specifically the clumping effect. Further, the probabilistic model gives a combination rule for the low frequency wave induced bending moment and the high frequency slamming induced bending moment.

Assumptions embedded in the model are:

- The ship motions are sufficiently described by linear wave theory, and not influenced by the slamming impacts.

- The spectrum of the relative motion is narrow banded.

- The dynamic transients are small, and evolve slowly, so that the structure responds directly on the local wave sinusoid without significant effect of transients from previous waves.

The basic idea in Friis-Hansen's approach is to model the joint density function of the wave amplitude and the frequency for those waves that give local maximum wave induced slamming response within a clump of slamming impacts. The procedure to be followed is to consider an envelope process for the process of relative motion at the bow section in order to take the clumping effect into account. For a regular sinusoidal wave with fixed values of amplitude and frequency, the maximum/minimum value of the combined moment response is calculated. Given the joint density function for the wave amplitude and the frequency, this density can be used to weigh the calculated combined response, so that the response statistics (the first four moments) are obtained. Thus the analysis is quasistationary. Finally, the extreme value distribution is found based on the theory for first-passage time distributions in Poisson pulse processes. The mean interarrival times of the pulse is approximated by the use of the upcrossing rate of the envelope process, modified for so-called "empty" envelope excursions. A complete description of this process is given in the paper by Friis-Hansen (1993)

A computer code "SLAM" has been developed by Friis-Hansen based on the above procedure. The program will be used, among other methods, to analyze the four ships under consideration.

2.1.4.2 *Data entry — SLAM code*

The program provides several data input screens which ask for all necessary information: ship sections, loading, transfer function, sea state, and analysis. All of the required data is able to be input into the program manually. The ship sections and mass distribution, however, can also be imported from an outside source.

Ship Sections

The ship sections screen asks for the offsets, stiffness, shear modulus, station number, and location of the station from the forward perpendicular. The units and a brief description are as follows:

Input	Units
offsets, y and z coordinates	m
stiffness, EIz	MNm^2
$\quad$ E is Young's Modulus	MN/m
$\quad$ Iz is the moment of inertia around the	m^3
z-axis	
shear modulus, GkA	MN
$\quad$ G is the shear modulus	MN/m
$\quad$ k is the effective shear area factor	dimensionless
$\quad$ A is the area of the cross section	m^2
x-location, distance from the forward perpendicular	m

Ship Loading

The ship geometry can be input manually by opening the "Ship Sections" sheet and typing in the y and z coordinates, stiffnesses, and location for the given station. This process may then be repeated for as many stations as desired.

The position of the stations must be input starting from the bow. the corresponding mass at that station may be in any loading condition desired, if applicable.

The units of these inputs are as follows:

Input	Units
position (x coordinate) of station	m
mass	kg
radius of gyration	m

Transfer Functions

The transfer function sheet consists of the following fields:

- number of frequencies
  This tells the program how many frequencies should be run in the range specified in the following fields.

- low frequency (radians/second)

  This tells the program the frequency at which to begin calculation.
- high frequency (radians/second)

  This tells the program the frequency at which to stop calculation.

- integration points

  This tells the program how many longitudinal points along the vessel are to be used for the numerical methods calculations.

Sea State

The sea state sheet consists of the following fields:

- significant wave height, H_s (meters)

  Significant wave height is defined as the average of the highest 1/3 waves to be encountered.

- zero crossing period, T_z (seconds)

  Zero crossing period is the period of the wave and can be calculated by

$$T_z = 11.12 \sqrt{\frac{H_s}{g}} \quad \text{where g is the acceleration of gravity}$$

Analysis

The analysis sheet consists of the following fields:

- number of modes

  Defines the number of modes used when the dynamic response due to the slamming impact is calculated. Two modes are usually sufficient as higher modes produce insignificant changes in the results.

- number of simulations

  The statistics of the response moments are calculated by simulations.

- x-bow (meters)

  This is the longitudinal position at which slamming impact takes place. For this analysis, the position of slamming impact was taken as the location of damage which was determined using Figure (2.1.42) from SNAME Technical and Research Bulletin 2-30. The percent of total length read from the chart may be taken as the mean value for a given block coefficient. As will be shown later, the position of slamming impact will greatly influence the calculated slamming induced bending moments.

- x-midship (meters)

  This is the longitudinal position along the vessel at which the response is to be calculated.

- damping ratio

    This is a structural coefficient in the dynamic equations of motion. In the application analysis, a damping ratio of 0.0017 was used.
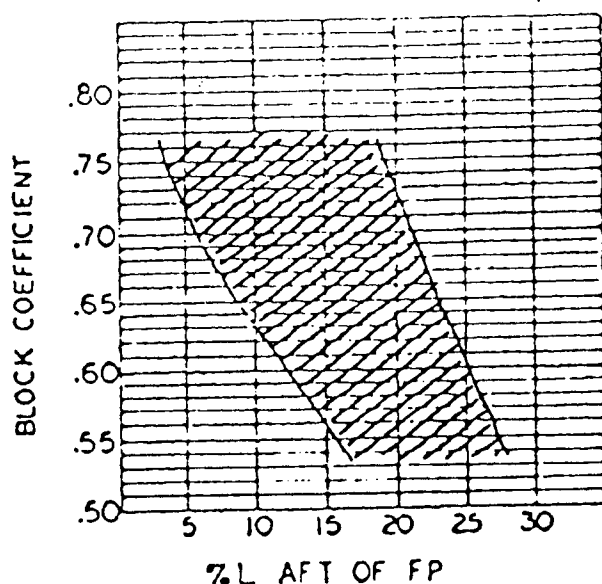
Figure 2.1.42 Longitudinal Location of Damage (SNAME T. & R. 2-30).

- heading angle (degrees)

    This is the angle of the vessel relative to the encountered waves where 0° signifies following seas and 180° signifies head seas.

- velocity (meters/second)

    The speed of the vessel corresponding to the particular sea state.

2.1.4.3 Other slamming load prediction methods

Some problems with the application of the SLAM code lead to a review of other tools which might be used to predict slamming loads and to combine them with wave induced loads.

Sikora has developed an empirical algorithm for estimating the maximum lifetime extreme loads on ships, including slamming loads. Major points from this procedure are described in Sikora and Beach (1989). Empirical response amplitude operators for various speeds and headings are combined with sea spectra to produce wave loads. A lifetime operational profile is developed and is discretized to form a grid of operational conditions, each condition having an associated probability. The response for each condition is then weighted by its probability of occurrence, and the sum of all conditions represent the lifetime extreme load including slamming. This method has shown good agreement with

experimental results. More details on this method are given in the application section of the report (section 3).

Another simplified approach is given in the Ship Structure Committee Report SSC 373, Loads and Load Combinations. This approach is described briefly as follows.

In obtaining combined wave bending and slam effects, the phasing between wave induced and slamming load effects is important. An explanatory sketch in this regard is shown in Figure 2.1.43 obtained from Ochi and Motter (1973). The illustration is for the hull girder midship deck stress. As the wave induced stress cycle changes from hogging to sagging, the slam impact results in a compressive (sagging) stress peak on the deck. The next hogging stress is termed the "initial slam stress", and subsequent stress peaks are termed "whipping stresses". This terminology is a matter of convenience and is not unique.
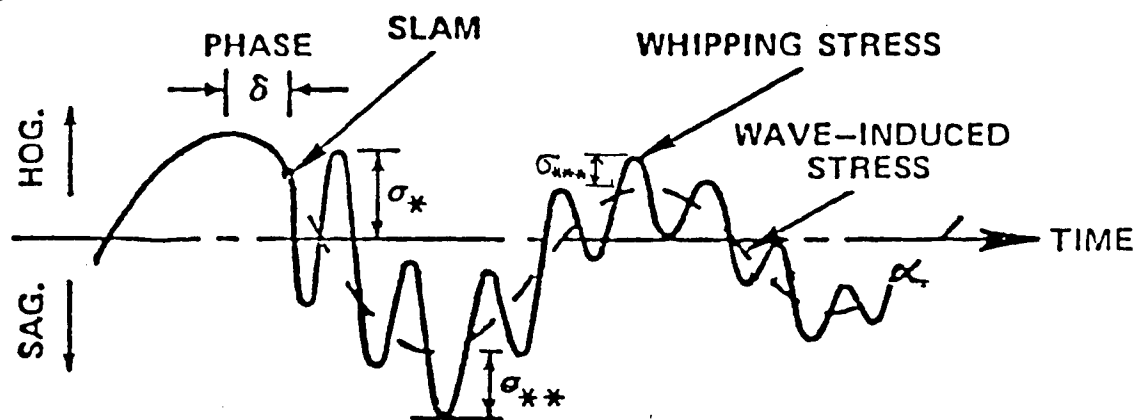
Figure 2.1.43 Stress Time History Including Slamming.

The phase angle between the hogging wave induced stress peak and the start of the slam transient, δ, is a random variable, which typically lies between 0 and 50 degrees, as may be seen from Figure 2.1.44 obtained from Lewis et al. (1973). It is possible for the second peak of the whipping stress, σ_* to exceed the wave induced hogging stress, if the phase lag δ is small enough. The whipping stress σ_{**} that follows a slam will, with certainty, increase the next peak sagging stress, and may also increase the subsequent peak hogging stress, the magnitude of the increase depending on the phase angle, the slam stress amplitude, and rate of decay. Usually, the slam transient increases the sagging part of the wave induced stress amidships, but at forward stations, there can also be an increase in the hogging stresses. Apart from bending stresses, shear stresses are also increased by slamming.

There are two established methods of obtaining slam pressures and loads, one due to Stavovy and Chuang (1977), and another due to Ochi and Motter (1973). The Stavovy and Chuang (SC) theory is typically preferred for high speed fine form vessels, while the Ochi and Motter (OM) theory works well for the fuller form, slower merchant ships. Both theories primarily treat impact slamming. A procedure for calculating forces due to flare entry has been developed by Kaplan (1972). The method is based on the linear shipmotion computer program SCORES, and uses a wave elevation time history simulation procedure. A probabilistic approach to obtaining slam related bending moments using the Timoshenko beam theory has been developed by Mansour and Lozow (1982), using the Ochi and Motter method to determine individual local slamming loads. An approach that considers the ship hull to be a set of nonuniform beams, with the response solved for using a normal mode method has been developed by Antonides (1972).

The case of bottom slamming in ships was considered by Ochi to depend on bow emergence and a relative velocity threshold being exceeded, based on experimental observations. The number of slams per unit time, λ_0, was obtained from the following expression, which combines the probability of bow emergence and the probability of a certain relative threshold velocity being exceeded:

$$\lambda_0 = \frac{1}{2\pi}\left(\frac{\sigma_{\dot{r}}}{\sigma_r}\right)\exp\left[-\left\{\frac{d^2}{2\sigma_r^2}+\frac{v_t^2}{2\sigma_{\dot{r}}^2}\right\}\right] \tag{2.1.63}$$

where the $\sigma_r^2, \sigma_{\dot{r}}^2$ are the variances of the relative motion and relative velocity (with respect to the wave) at the hull cross section, d is the section draft, and v_t is the threshold velocity. A typical value for the threshold velocity is 12 ft per second for a 520 ft long vessel, with Froude scaling applicable for other lengths. Relative velocities for slam events can vary depending on slam severity. For the Wolverine State (Wheaton, 1976), velocities in the range of 13 to 36 ft per second were reported, with average values about 22 for the more severe slam events. A conventional ship motion program is used to determine the relative motion and velocity. The variances of motion and velocity, and the number of slams per unit time, can then be calculated. For bow flare slamming, with momentum effects considered, the bow emergence condition is not necessary.

Slamming does not occur with every wave encountered. The incidences of slamming are dependent on vessel speed, heading, and rough weather countermeasures. The master of the vessel will take measures to limit the incidences of slamming, particularly so in smaller vessels where the effect of slamming is more felt. When action is taken, the effect will be significant as slamming is very speed dependent. Operational limitations on speed (Ochi and Motter, 1973) based on the probability of slam impact at a forward station reaching 0.03, or the significant amplitude of vertical bow acceleration reaching 0.5 g with a specified probability have been suggested. Speed can also be limited by a criterion considering local bottom damage.

The following is a time domain based approach for obtaining extreme values of the combined wave induced and whipping stress in slam events assuming both exist and can be calculated. A probabilistic method to combine the resulting transient stress history with the hull girder wave induced stress was developed in SSC 373.

A fundamental feature of the combination procedure is that the slam event occurs at a phase lag δ with respect to the hogging peak of the wave bending moment. The phase lag is measured from the hogging peak to the start of the slam transient.
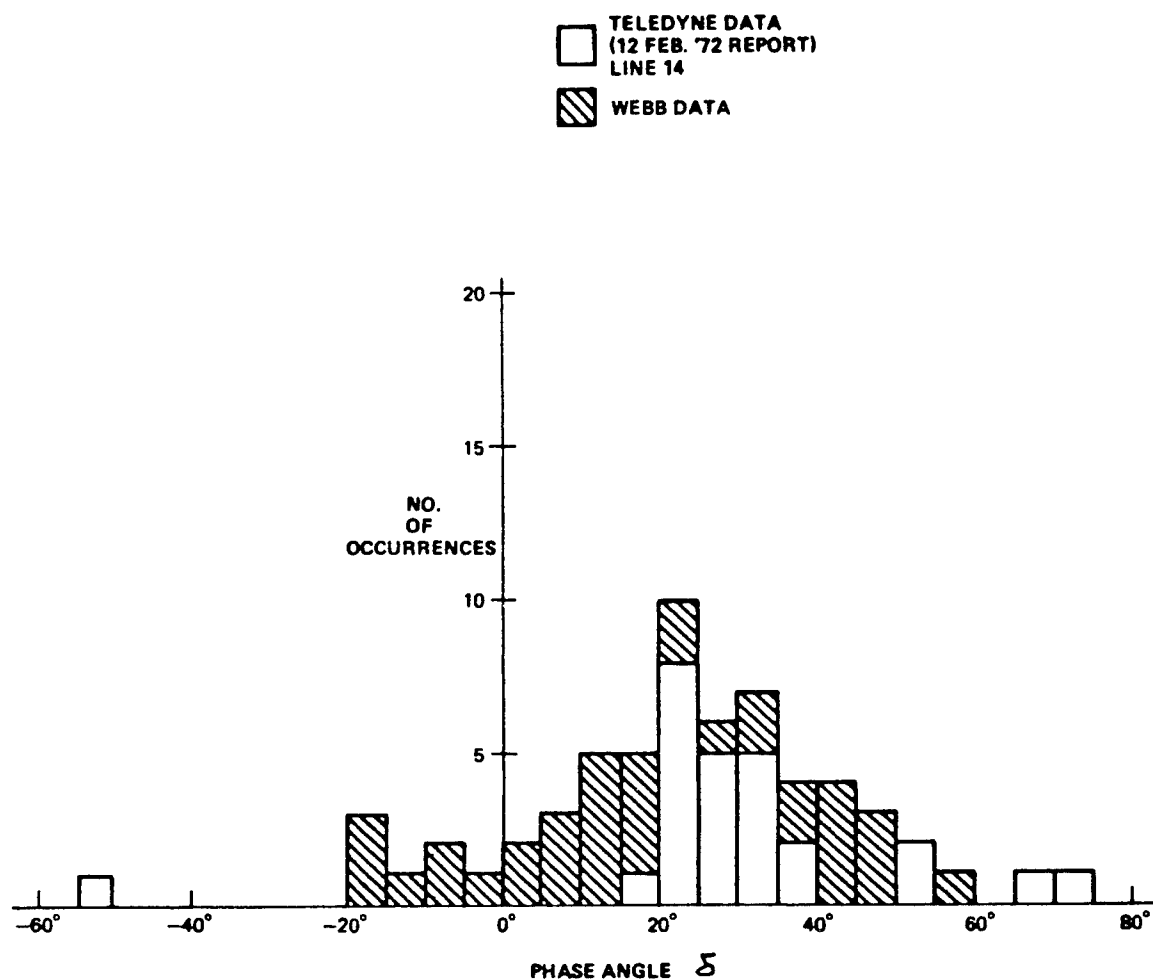
Figure 2.1.44 Distribution of Slam Phase Angle, Wolverine State.

2-66
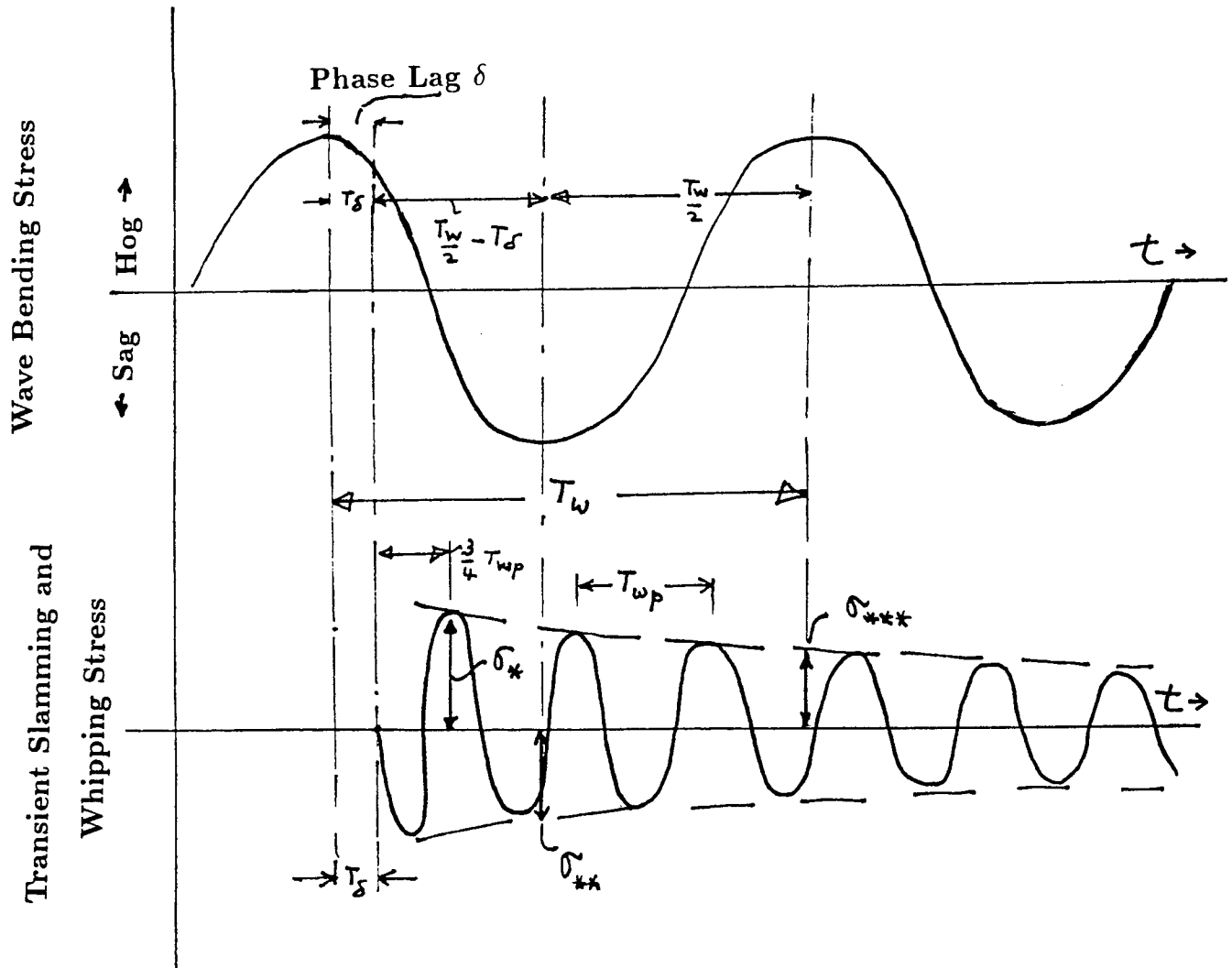
Figure 2.1.45 Combination of Slam Transient with Wave Induced Stress.

Consider the combination of wave induced bending and slam effects *at deck*, as depicted in Figure 2.1.45. The portion of the second peak of the slam transient that is additive to the low frequency hogging wave induced stress is denoted the initial slam stress amplitude σ_*. The whipping stress that follows a slam will add to the next wave induced sagging stress peak, and the subsequent hogging stress peak. The whipping stress, additive to the sagging peak of the low frequency wave induced load cycle, is denoted σ_{**}. The whipping stress, additive to the next hogging wave induced peak, is denoted σ_{***}. Note that σ_{**} and σ_{***} do not necessarily correspond to peaks of the slam transient, but are point in time values, calculated on the decay envelope of the slam transient stress time history. The notation used is that of Ochi and Motter (1973). In this slam stress envelope addition procedure, σ denotes a stress, not its r.m.s. value.

2-67

The magnitude of the addition to the wave induced stress will depend on the phase angle δ, the initial slam stress amplitude, and rate of decay. The additive whipping stresses referred to above are given approximately by

$$\sigma_{**} = \sigma_* \, \exp\left\{ -\lambda\left(\frac{T_w}{2} - T_\delta - \frac{3}{4} T_{wp} \right) \right\} \qquad (2.1.64)$$

$$\sigma_{***} = \sigma_* \, \exp\left\{ -\lambda\left(T_w - T_\delta - \frac{3}{4} T_{wp} \right) \right\} \qquad (2.1.65)$$

Here, T_δ is the time interval from the hogging peak to the slam initiation, which depends on the phase δ with respect to the hogging peak, and T_w is the period of the low frequency wave induced stress. The period of the slam transient is denoted T_{wp}. The values of $(T_w/2) - T_\delta - \frac{3}{4}T_{wp}$ and $T_w - T_\delta - \frac{3}{4}T_{wp}$ need to be positive. Also, $T_{wp} \ll T_w$. The variable λ is the logarithmic decrement representing the decay of the slam transient.

The total stress amplitude at the time of the first hogging slam stress peak is given approximately by

$$X_{s,1} = \sigma_* + A\cos\left(\delta + \frac{2\pi}{T_w} \frac{3}{4} T_{wp} \right) \cdot X_{hs} \qquad (2.1.66)$$

where A is the wave induced stress amplitude calculated on the basis of line on ship motion analysis.

The combined stress at the time of the sagging peak of the wave induced stress after the slam event is given approximately by

$$X_{s,2} = \sigma_{**} + A \cdot X_{hs} \qquad (2.1.67)$$

Similarly, the combined stress at the second hogging wave induced stress peak is given approximately by the following:

$$X_{s,3} = \sigma_{***} + A \cdot X_{hs} \qquad (2.1.68)$$

where σ_{**} and σ_{***} are determined from eqns. (2.1.64) and (2.1.65), respectively.

In the above equations, all variables are considered positive. The variable X_{hs} is a correction applied to account for hog-sag non-linearities.

Simplified Approach to Combined Slam and Wave Induced Loads

The previously discussed detailed approach to combined slam and wave induced stress extreme values is based on a time domain approach. In the following, a simplified approach is presented, that is also consistent with a frequency domain approach to the load combination problem involving two random processes.

In the case of two zero mean Gaussian stress processes i and j, the variance of the combined stress σ_c^2 is obtained from Appendix A:

$$\sigma_c^2 = \sigma_i^2 + \sigma_j^2 + 2\rho_{ij}\,\sigma_i\,\sigma_j$$

where σ_i^2 and σ_j^2 are the individual process variances, and ρ_{ij} is the correlation coefficient for the two processes. Since the extreme value of combined and individual stress processes, denoted f_c, f_i, and f_j, will typically satisfy

$$f_c \simeq c_c \sigma_c$$
$$f_i \simeq c_i \sigma_i$$
$$f_j \simeq c_j \sigma_j \quad ,$$

where c's are constants. Assuming $c_c = c_i = c_j$, it can be shown that

$$f_c^2 \cong f_i^2 + f_j^2 + 2\rho_{ij}\,f_i\,f_j$$

In addition, if the stress processes i and j are well separated on the frequency scale, $\rho_{ij} \simeq 0$, and we have the so-called Square Root of Sum of Squares rule for load combination:

$$f_c \cong \sqrt{f_i^2 + f_j^2}$$

Although derived above for Gaussian load processes, which are stationary by definition, the SRSS rule is known in practice to apply to cases involving non-stationary processes.

In the case of slamming and wave induced stresses, the combined stress extreme value f_c for a seastate, heading, and speed, is given on the basis of the SRSS rule, by

$$f_c = \sqrt{f_w^2 + f_{s\ell}^2}$$

where f_w and $f_{s\ell}$ are the individual (wave and slam related) extreme stresses, with the two processes assumed uncorrelated (in terms of frequency, not intensity) because of their typical frequency separation.

Nikolaides and Kaplan (1991) provide evidence through simulations that the SRSS method may indeed be applicable to the above load combination problem. Data on combined and individual (wave and slam) bending moments provided by Mansour and Ferro (1985) support the same conclusion. Recent work by Friis Hansen (1993) also indicates that the correlation coefficient between wave induced stress peaks and associated point in time slam stresses to be very small (-0.12 to -0.15 for a 270 m containership), thus again providing indirect support for the SRSS rule. However, further research is needed in this area to reach a final conclusion.

2.2 Methodology for Constructing Statistical Models for Nonlinear Hull Strength

In this section, the strength side of reliability analysis is considered. Hull failure modes are discussed briefly, followed by a description of the computer code ALPS/ISUM, which is suitable for estimating hull primary, secondary and tertiary strength. In the final subsections, simple formulations have been developed to estimate the hull strength (primary, secondary, and tertiary) to be used instead of the computer program ALPS/ISUM, in case an approximate estimate is sufficient. Interaction relations are provided in the last subsection.

2.2.1 Failure Modes:

Three types of behavior are usually considered in the analysis of ship structures; primary, secondary and tertiary. The primary behavior is associated with the ship as a whole. The ship is usually considered as a beam subjected to its own weight (including cargo) and supported by buoyancy distributed along its length. Acceleration effects and inertia loads are included by applying the equations of motions of the ship.

The secondary behavior is associated with a stiffened panel between bulkheads or webframes. Orthotropic or stiffened plate theory is used to determine deflections and stresses in the panel. The panel is usually subjected to inplane loads resulting from the overall bending of the hull.

The tertiary behavior is associated with plates between stiffeners considered as isotropic plates. These also are subjected to in-plane loads and, therefore, buckling becomes an important consideration.

Fatigue of ship details is an important concern in ship design. Separate analysis is usually conducted to ensure adequate fatigue life of typical details.

Each of the four levels of structural analysis discussed above (primary, secondary, tertiary and fatigue) may lead to one or several failure modes. In this study, all the above failure modes have been considered.

Primary (also called global or hull) failure modes consist of the fully plastic moment mode, the initial yield moment mode, and the instability collapse moment mode. The last includes buckling and post-buckling strength of the hull and is always the governing mode of failure. The fully plastic mode gives an upper bound on the ultimate moment. It is never attained in a hull of normal proportions. The initial yield mode assumes that buckling does not occur prior to yielding and is considered here only since it is a function of the standard elastic section modulus of the ship and the yield strength of the material, both normally used in current design practice. This mode provides a point of reference relative to current practice. It should be noted, however, that the initial yield moment is higher than the true instability collapse moment.

The secondary mode of failure relates to failure of a stiffened panel of the hull. Two main modes of failure are possible, stiffener-induced or plate-induced failure (see Hughes, 1983).

The tertiary mode of failure is associated with failure of a plate between stiffeners.

2.2.2 Computer Codes for Evaluating Ship Structural Strength:

In this study, the code ALPS/ISUM is used (A Computer program for nonlinear analysis of Large Plated Structures using the Idealized Structural Unit Method). The program was developed by Jeom Paik (1993) and is based on the idealized structural unit method. A brief description of the program and the underlying theory is given next.

The Idealized Structural Unit Method (ISUM), which was developed by Prof. Y. Ueda and Dr. S.M.H. Rashed in the mid 70's, is an effective tool for nonlinear analysis of large size structures. In this method, the structure is modeled as the combination of various large-size structural units (components), whose geometric and material nonlinear behaviors are idealized. As a result, the total number of elements and nodal points in ISUM modeling are much smaller than the Finite Element Method (FEM).

For analysis of a certain type of structure using ISUM, various kinds of the idealized structural unit should be formulated in advance. Four ISUM units have been developed. They are:

- The ISUM Beam-Column Unit
- The ISUM Rectangular (Unstiffened) Plate Unit
- The ISUM Stiffened Plate Unit
- The Hard Unit

In ship structures, heavy longitudinal girders or transverse frames supporting the stiffened plate panels which have quite large bending stiffness are modeled as the ISUM beam-column unit. This unit is formulated by taking into account lateral buckling, post-buckling behavior, tensile yielding, necking and ductile fracture behavior. The boundary of the unit is assumed to be simply-supported.

Unstiffened plates supported by heavy supporting members are modelled as the ISUM rectangular plate unit, as shown in Figure 2.2.1. Its edges are assumed to remain straight after deformation. This unit has four nodal points located at the four corners and the edge condition is assumed to be simply-supported.
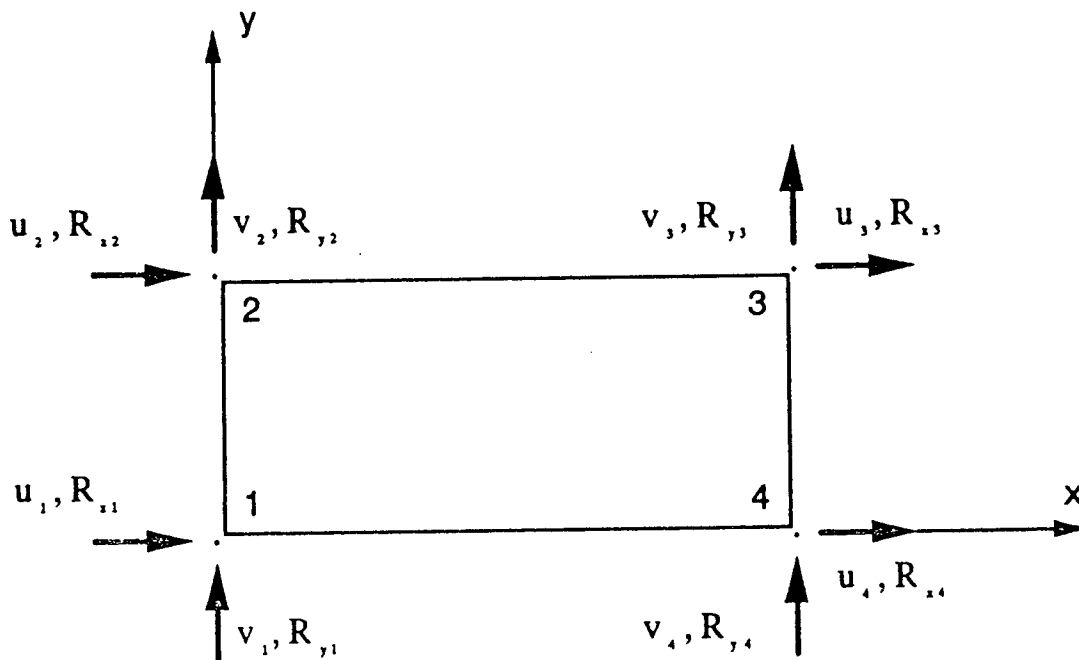
Figure 2.2.1 The ISUM Rectangular (Unstiffened) Plate Unit

The behavior of the plate is investigated based on fundamental theories, refined theoretical analysis such as the finite element method, and experimental results. The behavior is then idealized and conditions are formulated for the possible or expected failures of the plate, such as buckling and yielding. Stiffness matrices are derived in each of the respective states, i.e., before any failure and after different combinations of failures.

The deflected plate is replaced by an equivalent flat plate unit with reduced structural effectiveness. The following structural behavior is considered in this idealized plate unit (unstiffened):

- Elastic large deflection behavior

- Collapse and post-collapse behavior

- Tensile yielding, necking and ductile fracture behavior

- Initial deflection and welding residual stress

The behavior of the rectangular plate element, when subjected to an increasing load, is illustrated in Figure 2.2.2.
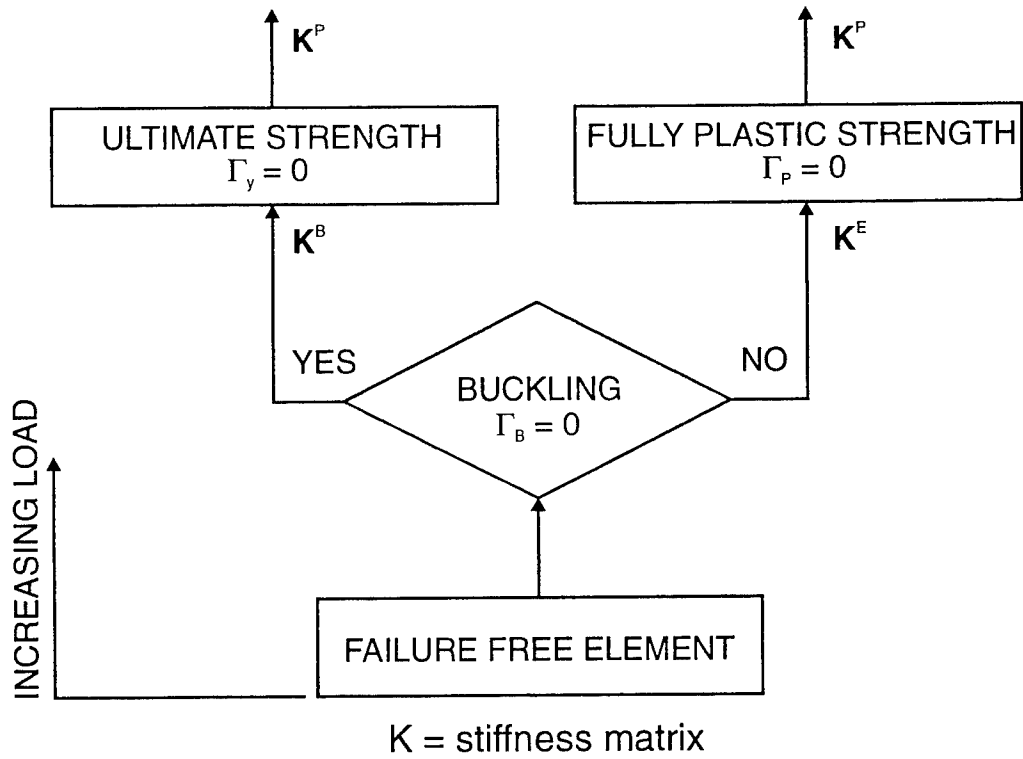
Figure 2.2.2   Behavior of the Rectangular Plate Unit

Before any failure occurs, the relation between an increment $\Delta\mathbf{R}$ of the nodal force vector $\mathbf{R}$ and an increment $\Delta\mathbf{U}$ of the nodal displacement vector $\mathbf{U}$ may be expressed in terms of an elastic stiffness matrix $\mathbf{K}^E$ as follows,

$$\Delta\mathbf{R} = \mathbf{K}^E \, \Delta \mathbf{U}$$

As the nodal forces increase at each loading step, the plate may buckle when a buckling condition is satisfied.

$$\Gamma_B = 0$$

where Γ_B is the buckling function.

After buckling, the relation between $\Delta\mathbf{R}$ and $\Delta\mathbf{U}$ may be expressed in terms of a post-buckling stiffness matrix $\mathbf{K}^B$, taking account of post-buckling effects, as follows,

$$\Delta\mathbf{R} = \mathbf{K}^B \, \Delta \mathbf{U}$$

If the element continues to carry further load until yielding starts, it would cause the element to reach its ultimate strength. The condition for yielding, Γ_Y, is given by

$$\Gamma_Y = 0$$

After yielding starts, the relation between $\Delta\mathbf{R}$ and $\Delta\mathbf{U}$ may be expressed in terms of an elastic-plastic stiffness matrix, $\mathbf{K}^P$, as follows

$$\Delta\mathbf{R} = \mathbf{K}^P \Delta\mathbf{U}$$

- Failure-Free Stiffness Matrix $\mathbf{K}^E$

Before any local failure (such as buckling) occurs, the membrane strains are assumed to be linearly distributed. The relation between the increment of the strain, $\Delta\varepsilon$, and the increment of the nodal displacement, $\Delta\mathbf{U}$, can be expressed as follows

$$\Delta\varepsilon = \mathbf{B}\Delta\mathbf{U}$$

where $\mathbf{B}$ is the strain-displacement matrix.

The relation between the increment of the stress, $\Delta\sigma$, and the increment of the strain, $\Delta\varepsilon$, can be expressed as follows,

$$\Delta\sigma = \mathbf{D}^E \Delta\varepsilon$$

where $\mathbf{D}^E$ is the stress-strain matrix in the elastic range,

$$D^E = \frac{E}{1-v^2}\begin{bmatrix} 1 & v & 0 \\ v & 1 & 0 \\ 0 & 0 & \frac{(1-v)}{2} \end{bmatrix}$$

Hence, the elastic failure-free stiffness matrix $\mathbf{K}^E$ may be derived as,

$$K^E = \int_v B^T D^E B dV$$

- Buckling Function Γ_B

When the plate encounters an in-plane compressive load, buckling may occur. Based on an analytical-numerical solution, the buckling condition Γ_B of the rectangular plate element may be written in terms of the average normal stresses σ_{xav} in the x-direction, and σ_{yav} in the y-direction, and a uniform shearing stress τ_{xy} as follows,

(i) when σ_{xav} is tensile and σ_{yav} is compressive

$$\Gamma_B = \frac{(m^2+\Omega^2)^2\,\sigma_{xav}}{m^2\,(1+\Omega^2)^2\,\sigma_{xcr}} + \frac{\sigma_{yav}}{\sigma_{ycr}} + \left(\frac{\tau_{xy}}{\tau_{xycr}}\right)^2 - 1$$

(ii) when σ_{xav} is compresive and σ_{yav} is tensile

$$\Gamma_B = \frac{(1+\Omega^2)^2\,\sigma_{yav}}{(m^2+\Omega^2)^2\,\sigma_{ycr}} + \frac{\sigma_{xav}}{\sigma_{xcr}} + \left(\frac{\tau_{xy}}{\tau_{xycr}}\right)^2 - 1$$

(iii) when σ_{xav} is compressive and σ_{yav} is compressive

$$\Gamma_B = \left[\frac{(\sigma_{xav}/\sigma_{xcr})}{1-(\tau_{xy}/\tau_{xycr})^2}\right]^{\alpha_1} + \left[\frac{(\sigma_{yav}/\sigma_{ycr})}{1-(\tau_{xy}/\tau_{xycr})^2}\right]^{\alpha_2} - 1$$

where

Ω = a/b (aspect ratio of the plate)

m = number of half-waves when the plate buckles.

When Γ_B is smaller than zero, it indicates that the plate has not buckled. As Γ_B is greater or equal to zero, the plate buckles.

• Post-Buckling Behavior and Stiffness Matrix $\mathbf{K}^B$

After the plate buckles, the stiffness of the plate will reduce. An imaginary plate is introduced in order to derive the post buckling stiffness. As a result, the post buckling stiffness can be shown as,

$$K^B = \int_v B^T\,D^B\,B dV$$

where $\mathbf{D}^B$ is the relation between an increment of stress and an increment of strain of the imaginary plate.

• Ultimate Strength Condition Γ_Y

Yielding is assumed to start at any of the checking points where the yield condition is satisfied,

$$\Gamma_y = \sigma_x^2 - \sigma_x\sigma_y + \sigma_y^2 + 3\tau_{xy}^2 - \sigma_0^2 = 0$$

Ultimate strength will be reached after yielding has occurred at a sufficient number of locations.

• Post-Ultimate Strength and Elastic-Plastic Stiffness Matrix $\mathbf{K}^P$

Starting from the evaluation of the elastic-plastic stress-strain relationship, we can obtain an equivalent elastic-plastic stiffness matrix as follows,

$$\mathbf{K}^P = \mathbf{K}^B - \mathbf{K}^B \, \Phi_i \Phi_j^T \, \mathbf{K}^B \, / \, S_{pi}$$

This is an unsymmetric matrix which is capable of representing the decrease of the carrying capacity at the post-ultimate strength state.

• The ISUM Stiffened Plate Unit

Stiffened plates supported by heavy supporting members are modeled as the ISUM stiffened plate unit. In this unit, a number of one-sided stiffeners are usually attached to the panel in the longitudinal and/or transverse directions.

The nonlinear behavior of the unit under combined in-plane loads and lateral pressure is idealized by taking into account ductile collapse, post-collapse behavior, tensile yielding, necking and ductile fracture behavior. The effects of initial imperfections are also considered in this unit.

• The Hard Unit

The hard unit is idealized to behave in a geometrically linear pattern (i.e., buckling will never occur), but it will possibly yield in tensile or compressive loads. It is useful, for example, to model bilge corners of ships which may develop high stresses.

Other computer programs are available for determining the ultimate strength of ships. The USN program "ULTSTR" developed by Adamchak (1989) is a good example of a nonlinear program that can be used to determine the hull ultimate capacity.

In addition to the ALPS/ISUM code, the computer program SANDY has been investigated in this study. SANDY, which was developed by Yong Bai (1990) is an efficient nonlinear finite element program. The application of SANDY to one of the ships under consideration produced good results. However, ALPS/ISUM was easier and faster to use, and, therefore, was used in this study to determine the primary, secondary, and tertiary strength of the four ships.

2.2.3   A Simple Formulation for Estimating Global Hull Strength:

The aim of this part of the study is to derive a simple analytical formula for predicting the ultimate collapse strength of a ship under a vertical bending moment, and also to characterize the accuracy and applicability of earlier approximate formulations. It is known that a ship hull will reach the overall collapse state if both collapse of the compression flange and yielding of the tension flange occur. Side shells in the vicinity of the compression and the tension flanges will often fail also, but the material around the final neutral axis will remain in the elastic state. Based on this observation, a credible distribution of longitudinal stresses around the hull section at the overall collapse state is assumed, and an explicit analytical

equation for calculating the hull ultimate strength is obtained. A comparison between the derived formula and existing expressions is made for large-scale box girder models, a one-third-scale frigate hull model, and full-scale ship hulls. A list of nomenclature for this section is provided at the end of the section.

Background:

As applied loads increase, structural members of the hull will buckle in compression and yield in tension. The hull can normally carry further loading beyond the onset of member buckling or yielding, but the structural effectiveness of failed members decreases or can even become negative and their internal stress will be redistributed to adjacent intact members. The most highly compressed member will collapse first and the stiffness of the overall hull decreases gradually. Buckling and collapse of structural members will occur progressively until the ultimate limit state is reached. When the structural safety of a ship's hull is considered, the ultimtae overall hull strength should be evaluated. It is also necessary to derive a simple expression for calculation of the hull ultimate strength so that it can be used as a design equation or failure function in reliability analysis (Moan *et al.*, 1994).

Classification societies provide design criteria for structural scantlings, which are usually based on first yielding and elastic buckling with a simple correction for plasticity. These expressions may not be the true ultimate limit state. To obtain an acceptable margin of safety against overall hull collapse, the hull ultimate strength provides a more reasonable criterion than the conventional elastic buckling or first yield criteria.

Previous studies on the development of a simple formula for the hull ultimate strength prediction may be classified into three approaches. The first is an analytical approach based on an assumed stress distribution over the hull section, from which the moment of resistance of the hull is theoretically calculated taking into account buckling in the compression flange and yielding in the tension flange. The second is an empirical approach where an expression is derived on the basis of experimental or numerical data from scaled hull models. The third is a linear approach where the behavior of the hull up to collapse of the compression flange is assumed to be linear, and the ultimate moment capacity of the hull is basically expressed as the ultimate strength of the compression flange multiplied by the elastic section modulus with a simple correction for buckling and yielding. The third approach is quite simple, but its accuracy may not be good because after buckling of the compression flange, the behavior of the hull is no longer linear and the neutral axis changes position. Empirical formulas (the second approach) may provide reasonable solutions for conventional hulls, but one has to be careful in using empirical formulas for new or general-type hulls since usually they are derived on the basis of limited data. On the other hand, analytical formulations (the first approach) can be applied to new or general hulls because they include section effects more precisely. The present formulation is based on the analytical approach.

Existing Formulations:

In this section, earlier approximate formulations for predicting ultimate strength of ships under vertical bending moment are reviewed. Only explicit expressions which do not require an iterative process are surveyed.

In discussing the results obtained from full-scale ship tests, Vasta (1958) assumed that the ship hull would reach the ultimate limit state when the compression flange, i.e., the upper deck in the sagging condition or the bottom plating in the hogging condition, collapses, and that relationship between the bending moment and curvature is linear. On the basis of these assumptions, he suggested the following expression for the hull ultimate strength prediction:

$$M_u = Z\sigma_u \qquad\qquad (2.2.1)$$

The analytical derivation of a hull ultimate strength formula taking into account buckling in compression and yielding in tension was first proposed by Caldwell (1965). The ship hull cross-section was idealized as an equivalent section with uniform plate thicknesses in deck, bottom, or sides, as shown in Figure 2.2.3. A distribution of longitudinal stresses of the equivalent single-hull section was made, assuming that all structural members have the same yield strength. The entire material in compression was assumed to have reached its ultimate buckling strength, while full yielding was assumed for the material in tension. The ultimate strength of the compression flange is not necessarily the same as that of the sides. The change of the neutral axis position was taken into account. The ultimate moment capacity of the hull was then analytically calculated by integration of the moment resulting from the stresses with respect to the neutral axis.
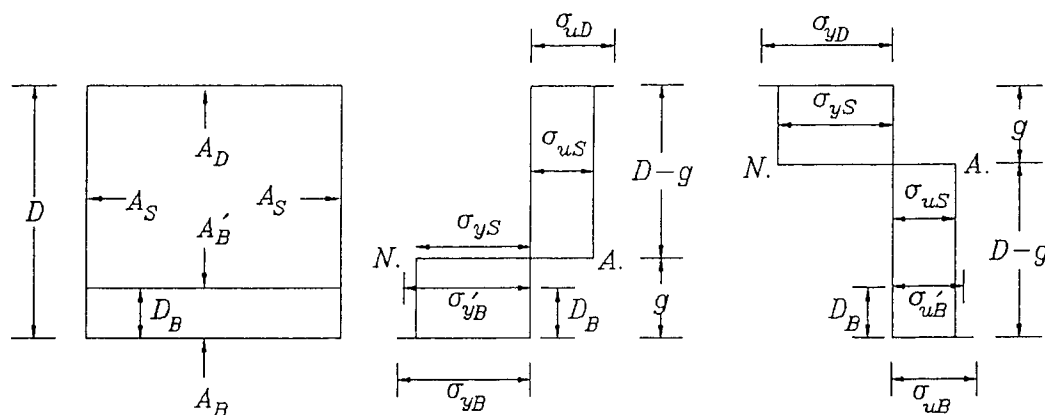
Figure 2.2.3   Modification of Caldwell's method to include composite hull materials and a double-hull configuration. Left—the equivalent double-hull configuration; center—the stress distribution for sagging; and right—the stress distribution for hogging.

Originally, Caldwell assumed the yield strength of all structural members to be the same, whether they are in the deck, side, or bottom. Modern ships, however, are often constructed from different materials such as mild steel and high-tensile steel. Also, Caldwell's original formula cannot be directly applied to the double-hull cross-section. In this study, Caldwell's original formula has been modified by including the effects of different materials and double-hull cross-sections, to allow its use in the subsequent comparisons.

The Caldwell procedure is modified as follows: The stress distribution of the hull section is indicated in Figure 2.2.3, allowing for the case where the yield strengths of the tension flange and side material under tension are not necessarily the same. Similarly, the ultimate buckling strength of the compression flange is not necessarily the same as the side shell buckling strength. The procedure is also modified to include a double-hull arrangement. From the condition that no axial force exists on the hull girder, the neutral axis height from the base line for a double-hull section can be determined in the sagging condition as

$$g = D \frac{A_D \sigma_{uD} + 2A_s \sigma_{uS} - A_B \sigma_{yB} - A_B' \sigma_{yB}'}{2A_S (\sigma_{uS} + \sigma_{yS})}$$
(2.2.2a)

where the yield strength of the inner bottom may be different from that of the outer bottom. Also, when $A_B' = 0$, the resulting neutral axis corresponds to that of a single-bottom section.

Similarly, in the hogging condition, the distance between the neutral axis and the deck is given by

$$g = D \frac{A_B \sigma_{uB} + A_B' \sigma_{uB}' + 2A_s \sigma_{uS} - A_D \sigma_{yD}}{2A_S (\sigma_{uS} + \sigma_{yS})}$$
(2.2.2b)

where the ultimate buckling strength of the inner bottom can be different from that of the outer bottom.

The ultimate moment capacity of the hull section in sagging condition is then derived as:

$$
\begin{aligned}
M_{us} &= A_D (-\sigma_{uD})(D-g) + 2\frac{D-g}{D} A_S (-\sigma_{uS})\frac{D-g}{2} \\
&\quad -2\frac{g}{D} A_S \sigma_{yS} \frac{g}{2} - A_B \sigma_{yB} g - A_B' \sigma_{yB}' (g-D_B) \\
&= -A_D (D-g)\sigma_{uD} - A_B g\sigma_{yB} \\
&\quad - A_B' (g-D_B)\sigma_{yB}' \\
&\quad - \frac{A_S}{D}\left[(D-g)^2 \sigma_{uS} + g^2 \sigma_{yS}\right]
\end{aligned}
$$
(2.2.3a)

where the sagging moment is taken as negative.

Similarly, in the hogging condition

$$M_{uh} = A_{D_g}\, \sigma_{yD} + A_B\, (D-g)\sigma_{uB}$$
$$+ A'_B\, (D-g-D_B)\sigma'_{uB} \qquad\qquad (2.2.3b)$$
$$+ \frac{A_S}{D}\left[(D-g)^2\, \sigma_{uS} + g^2\, \sigma_{yS} \right]$$

where the hogging moment is taken as positive.

For simplicity, it was assumed that the ultimate strength ratio of sides, σ_{uS}/σ_{yS} is equal to that of the compression flange, i.e., $\sigma_{uS}/\sigma_{yS} \cong \sigma_{uD}/\sigma_{yD}$ in the sagging condition and $\sigma_{uS}/\sigma_{yS} \cong \sigma_{uB}/\sigma_{yB}$ in the hogging condition.

The 1970 ISSC proceedings reintroduced Vasta's formula (eqn. 2.2.1), but Mansour and Faulkner (1973) criticized the formulation's assumptions because the location of the neutral axis will shift after buckling of the compression flange. They suggested a slightly modified formula given by

$$M_u = Z\sigma_u\,(1 + k) \qquad\qquad (2.2.4)$$

where k is a function of the ratio of the areas of one side shell to the compression flange. For a frigate, they calculated the value of k to be about 0.1.

Viner (1986) assumed that elastic behavior is maintained up to the point where the longitudinals of the compression flange reach the collapse state and that this brings about immediate hull collapse. On the basis of these assumptions, he suggested that

$$M_u = aZ\sigma_u \qquad\qquad (2.2.5)$$

where a is normal in the range of 0.92-1.05 (mean, 0.985).

By taking into account systematic errors associated with the yield strength, ultimate compressive strength, and section effects, Faulkner and Sadden (1979) suggested the following empirical formula

$$M_u = 1.15\, Z\sigma_y\, [-0.1 + 1.4465\sigma_u/\sigma_y - 0.3465\, (\sigma_u/\sigma_y)^2] \qquad (2.2.6)$$

On the basis of elastoplastic large deformation finite-element solutions for large-scale box girders and full-scale ship hulls, Valsgaard and Steen (1991) found that hull sections have strength reserve beyond the onset of collapse of the compression flange. For this reason, they introduced the concept of hull section strength margin, and suggested the formula

$$M_u = B_c\, Z\sigma_u \qquad\qquad (2.2.7)$$

where B_c varies with the actual shape of the hull cross-section. For the single-hull VLCC *Energy Concentration*, which collapsed in 1980, they calculated the mean value of B_c in the hogging condition to be 1.127.

The ultimate collapse strength of a ship's hull under a vertical bending moment closely correlates with the ultimate strength of the compression flange. In this regard, Frieze and Lin (1991) expressed a normalized ultimate moment capacity of the hull as a function of a normalized ultimate strength of the compression flange using the quadratic equation

$$M_u/M_p = d_1 + d_2\, \sigma_u/\sigma_y + d_3\, (\sigma_u/\sigma_y)^2 \tag{2.2.8}$$

where M_p is the fully plastic bending moment. On the basis of experimental and numerical results of scaled hull models, they determined the constants d_i of eqn. (2.2.8) by applying the least-squares method to the data in sagging and hogging conditions separately

$$d_1 = -0.172, \quad d_2 = 1.548, \quad d_3 = -0.368 \qquad \text{for sagging} \tag{2.2.9a}$$

$$d_1 = 0.003, \quad d_2 = 1.459, \quad d_3 = -0.461 \qquad \text{for hogging} \tag{2.2.9b}$$

Derivation of an Analytical Expression:

The overall collapse of a ship's hull under a vertical bending moment is governed by collapse of the compression flange. Also, according to the numerical studies of full-scale ships, there is still some reserve strength beyond collapse of the compression flange (Valsgaard, 1991; Rutherford, 1990; and Paik, 1993). This is because after buckling of the compression flange, the neutral axis of the hull cross-section moves toward the tension flange and a further increase of the applied bending moment is sustained until the tension flange yields. At later stages of this process, side shells around the compression and the tension flanges will also fail. However, in the immediate vicinity of the final neutral axis, the side shells will often remain in the elastic state up to the overall collapse of the hull girder. Depending on the geometric and material properties of the hull section, these parts may also fail, which corresponds to Caldwell's assumption.

Figure 2.2.4 shows a credible distribution of longitudinal stresses of the hull cross-section at the overall collapse state. The neutral axis has moved toward the tension flange from its initial position in the intact hull section. In the compressed parts of the section, the flange and a part of sides have reached their ultimate compressive limit state. The ultimate compressive strength of the flange may be different from that of the sides. In the parts of the section subjected to tension, the full yield strength in tension will have developed in the flange, but it is assumed that the sides remain in the elastic state. The yield strength of the tension flange may be different from that of the sides. The stress distribution in the vicinity of the neutral axis is assumed to be linear.

If th x-y coordinates are taken as shown in Figure 2.2.4, the stress distribution can be expressed by:

In sagging condition (see Figure 2.2.4):

$$\sigma_x = \sigma_{yB} \qquad \text{at } y = 0$$

$$= -\frac{1}{H}\left[(\sigma_{uS} + \sigma_{yS})y - H\sigma_{yS}\right] \qquad 0 < y < H$$

$$= \sigma'_B$$

$$(2.2.10a)$$

$$= -\frac{1}{H}\left[(\sigma_{uS} + \sigma_{yS})D_B - H\sigma_{yS}\right] \qquad \text{at } y = D_B$$

$$= -\sigma_{uS} \qquad H \le y < D$$

$$= -\sigma_{uD} \qquad \text{at } y = D$$
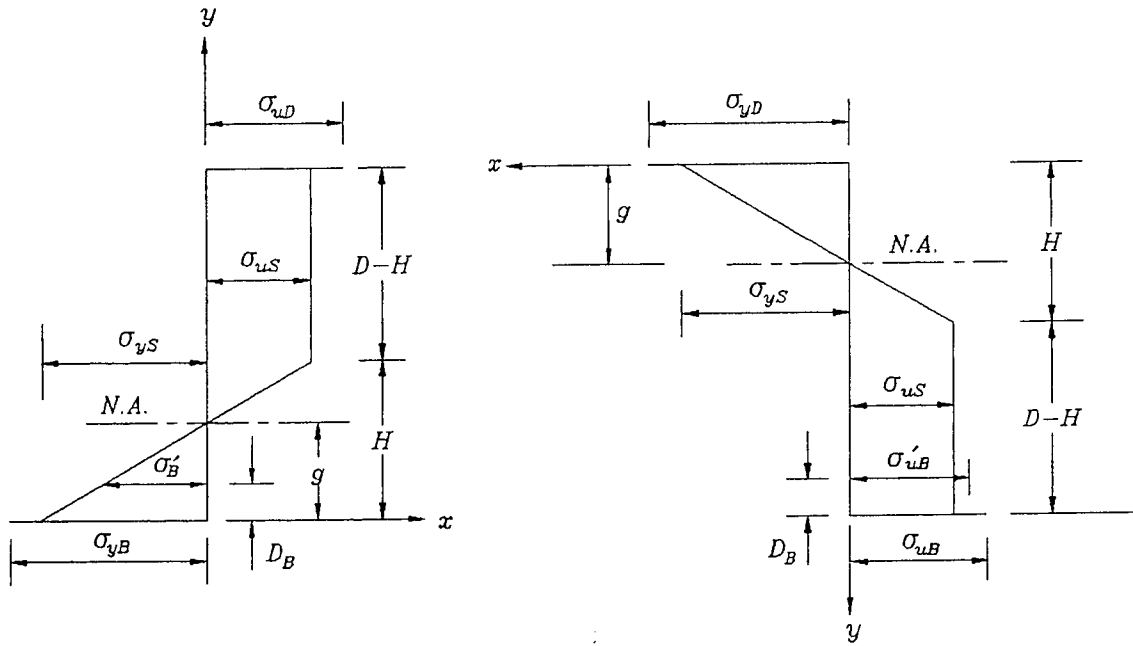
Figure 2.2.4   Assumed distribution of longitudinal stresses in a hull cross-section at the overall collapse state. The sagging condition is shown on the left, and hogging is shown on the right.

where compressive stress is negative and tensile stress is positive.

Similarly, in hogging condition (see Figure 2.2.4):

$$\sigma_x = \sigma_{yD} \qquad \text{at } y = 0$$

$$= -\frac{1}{H}\left[(\sigma_{uS} + \sigma_{yS})y - H\sigma_{yS}\right] \qquad 0 < y < H$$

$$= -\sigma_{uS} \qquad H \le y < D$$

$$= -\sigma'_{uB} \qquad \text{at } y = D - D_B$$

$$= -\sigma_{uB} \qquad \text{at } y = D$$

$$(2.2.10b)$$

From the condition that no axial force acts on the hull girder, the depth of the collapsed sides $(D-H)$, can be calculated, if H is known, such that

$$\int \sigma_x \, dA = 0 \tag{2.2.11}$$

Therefore, in the sagging condition

$$A_D \, (-\sigma_{uD}) + \frac{2A_S}{D}(D-H)(-\sigma_{uS})$$

$$+ \frac{A'_B}{H}\left[-(\sigma_{uS} + \sigma_{yS})D_B + H\sigma_{yS}\right] + A_B \, \sigma_{yB} \tag{2.2.12a}$$

$$+ \frac{2A_S}{D}\cdot\frac{1}{H}\int_0^H\left[-(\sigma_{uS} + \sigma_{yS})y + H\sigma_{yS}\right]dy = 0$$

or, since H must take a positive value

$$H = \frac{C_1 D + \sqrt{C_1^2 D^2 + 4C_2 D}}{2} \tag{2.2.12b}$$

where

$$C_1 = \frac{A_D \, \sigma_{uD} + 2A_S \, \sigma_{uS} - A_B \, \sigma_{yB} - A'_B \, \sigma_{yS}}{A_S \, (\sigma_{uS} + \sigma_{yS})}$$

$$C_2 = \frac{A'_B \, D_B}{A_S}$$

The position of the neutral axis, where the longitudinal stress is zero, can be determined from the condition that the stress distribution is linear, namely

$$g = y|\sigma_{x=0} \tag{2.2.13}$$

Therefore, the location of the neutral axis above the base line in the sagging condition is obtained by substituting eqns. (2.2.10a) and (2.2.12b) into eqn. (2.2.13) as

$$g = \frac{\left(C_1 D + \sqrt{C_1^2 D^2 + 4C_2 D}\right)\sigma_{yS}}{2(\sigma_{uS} + \sigma_{yS})} \tag{2.2.14}$$

Similarly, in the hogging condition, the depth of the collapsed sides under compression, $(D-H)$, can be obtained from

$$A_B \, (-\sigma_{uB}) + \frac{2A_S}{D} \, (D-H)(-\sigma_{uS})$$

$$+ A'_B \, (-\sigma_{uB}) + A_D \, \sigma_{yD} \qquad\qquad (2.2.15a)$$

$$+ \frac{2A_S}{D} \cdot \frac{1}{H} \int_0^H \left[-(\sigma_{uS} + \sigma_{yS})y + H\sigma_{yS} \right] dy = 0$$

or

$$H = D \, \frac{A_B \sigma_{uB} + A'_B \sigma'_{uB} + 2A_s \sigma_{uS} - A_D \sigma_{yD}}{A_S \, (\sigma_{uS} + \sigma_{yS})} \qquad\qquad (2.2.15b)$$

The neutral axis below the deck in the hogging condition can also be obtained by substituting eqn. (2.2.15b) into eqn. (2.2.13)

$$g = D \, \frac{A_B \sigma_{uB} \, \sigma_{yS} + A'_B \sigma'_{uB} \, \sigma_{yS} + 2A_s \sigma_{uS} \, \sigma_{yS} - A_D \sigma_{yD} \, \sigma_{yS}}{A_S \, (\sigma_{uS} + \sigma_{yS})^2} \qquad (2.2.16)$$

The ultimate moment capacity of the hull under sagging bending moment is

$$M_{us} = A_D \, (D-g)(-\sigma_{uD})$$

$$+ \frac{2A_S}{D} \, (D-H) \frac{D+H-2g}{2} (-\sigma_{uS})$$

$$+ A_B \, (-g)\sigma_{yB} \qquad\qquad (2.2.17a)$$

$$+ \frac{A'_B}{H}(g - D_B)\left[(\sigma_{uS} + \sigma_{yS}) D_B - H\sigma_{yS} \right]$$

$$+ \frac{2A_S}{D} \cdot \frac{1}{H} \int_0^H \left[-(\sigma_{uS} + \sigma_{yS})y + H\sigma_{yS} \right] (y-g)dy$$

or

$$M_{us} = -A_D \, (D-g)\sigma_{uD}$$

$$- \frac{A_S}{D} \, (D-H)(D+H-2g)\sigma_{uS} - A_B g\sigma_{yB}$$

$$+ \frac{A'_B}{H}(g - D_B)\left[D_B \, \sigma_{uS} - (H - D_B)\sigma_{yS} \right] \qquad (2.2.17b)$$

$$- \frac{A_S H}{3D}\left[(2H - 3g)\sigma_{uS} - (H - 3g)\sigma_{yS} \right]$$

with H and g defined by eqns. (2.2.12b) and (2.2.14), respectively.

Similarly, in the hogging condition, the ultimate moment capacity of the hull is given by

$$M_{uh} = A_B (D-g) \sigma_{uB} + \frac{2A_S}{D} (D-H) \frac{D+H-2g}{2} \sigma_{uS}$$

$$+ A_B' (D-g-D_B) \sigma_{uB}' + A_D g \sigma_{yD} \qquad (2.2.18a)$$

$$-\frac{2A_S}{D} \cdot \frac{1}{H} \int_0^H \left[-(\sigma_{uS} + \sigma_{yS}) y + H\sigma_{yS} \right] (y-g) dy$$

or

$$M_{uh} = A_D g\sigma_{yD} + A_B (D-g)\sigma_{uB}$$

$$+ A_B' (D-g-D_B)\sigma_{uB}'$$

$$+ \frac{A_S}{D} (D-H)(D+H-2g)\sigma_{uS} \qquad (2.2.18b)$$

$$+ \frac{A_S H}{3D} \left[(2H-3g)\sigma_{uS} - (H-3g)\sigma_{yS} \right]$$

with H and g defined by eqns. (2.2.15b) and (2.2.16), respectively.

To calculate the ultimate moment capacity of the hull using eqns. (2.2.17b) or (2.2.18b), the ultimate strength of the compression flange and the sides in the vicinity of the compression flange, which are usually stiffened panels, must be known. Theoretically, the possible failure modes of a stiffened panel under compressive loads can be divided into three classes (Smith, 1977):

1. Local collapse of plate between stiffeners

2. Overall collapse of plate with longitudinal and transverse stiffeners

3. Torsional/flexural buckling of stiffener with effective plating

The collapse of a stiffened panel will occur at the lowest value of the ultimate load calculated from 2 and 3 of the above three collapse patterns (Mansour, 1980, 1986; Ueda, 1995). Calculation of the ultimate strength considering all possible modes is not an easy task. For practical purposes, therefore, a number of simple formulas have been suggested. One promising formula is recommended. On the basis of existing and new collapse test results for a total number of 130 stiffened panels with appropriate values of initial imperfections, Paik and Lee (1995) derived an empirical formula for the ultimate compressive strength of a stiffened panel as a function of the plate slenderness ratio β and the column (stiffened) slenderness ratio λ, namely

$$\sigma_u/\sigma_y = (0.995 + 0.936\ \lambda^2 + 0.170\ \beta^2 + 0.188\ \lambda^2\ \beta^2 - 0.067\ \lambda^4)^{-0.5} \qquad (2.2.19)$$

where the terms including λ should be removed, i.e., $\lambda = 0$, for application to unstiffened plates.

Comparisons and Discussions:

In this section, a comparison is made between earlier approximate formulas of hull ultimate strength and the formula proposed in this study (eqns. (2.2.17b) or (2.2.18b)). Comparisons are also made with experimental and numerical results when possible.

Six large-scale box girder test models under pure vertical bending moment, as shown in Figures 2.2.5 to 2.2.7, were selected for this comparison. Originally, Dowling's models (1976) were tested in the sagging condition, but since the compression flanges were heavier than the tension flanges, the actual situation corresponds to a hogging condition if the model is turned over. Dowling, et al. (1976) provided experimental data
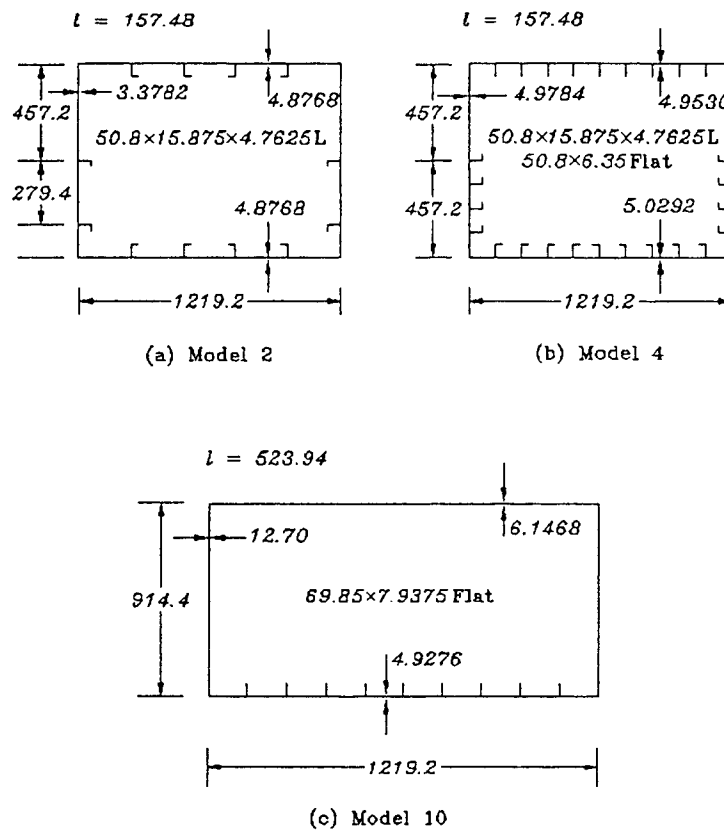
Figure 2.2.5a-c Midship sections of Dowling's box girder models, tested in hogging condition (mm).
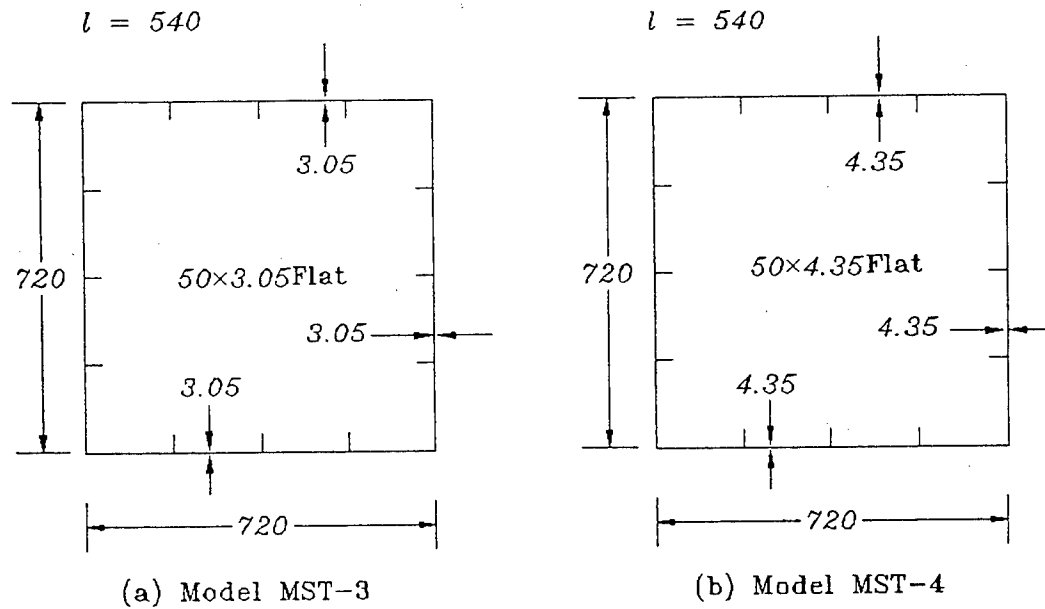
Figure 2.2.6a,b   Midship sections of Nishihara's box girder models, tested in sagging condition (mm).
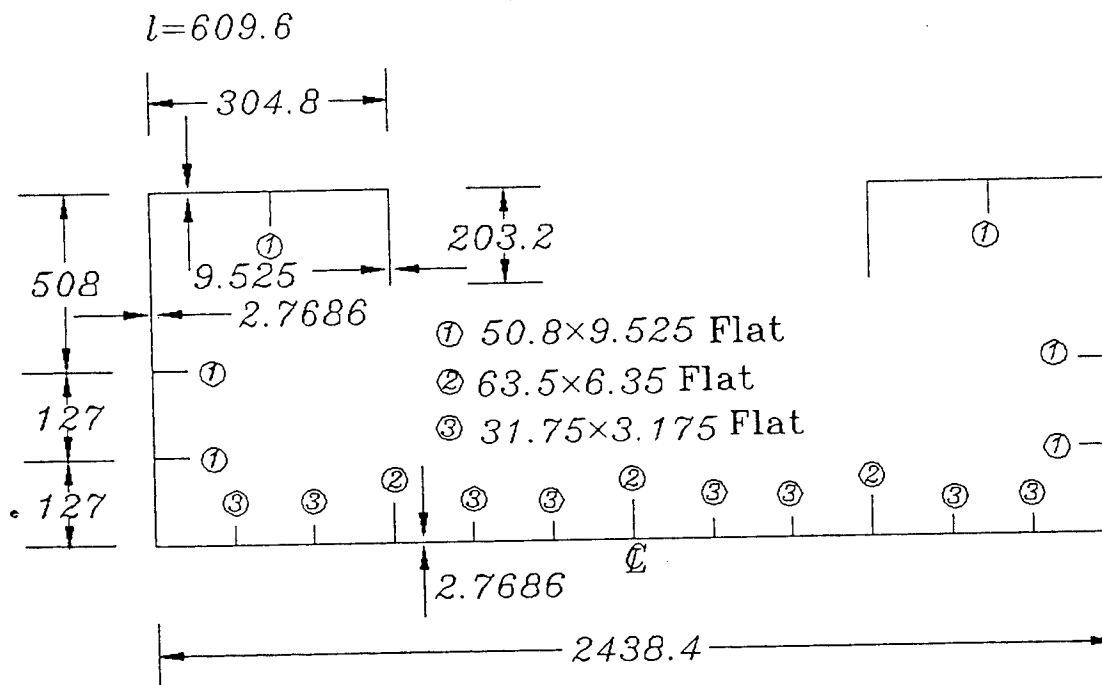
Figure 2.2.7   Midship section of Mansour's box girder model II, tested in hogging condition (mm).

of the ultimate strength of the compression flanges as well as of the overall hull. In Mansour's (1990) test model II, under the hogging condition, the bending moment was generated using air pressure cells (positive or negative pressure) located below the model, idealizing bottom pressure and load distribution on actual ship hulls. The other models were all loaded by a four-point bending mechanism.

To check the validity of a simplified method like the one presented here, experimental data for a larger model that can reduce scaling effects is preferable. In this regard, Dow (1991) tested a one-third-scale frigate hull model in the sagging condition (see Figure 2.2.8). In the 1994 ISSC proceedings, Jensen, et al. (1994) analyzed Dow's model using several methods, including the computer program for nonlinear analysis of large plated structures using the idealized structural unit method (ALPS/ISUM), developed by Paik (1993), and the results were compared.
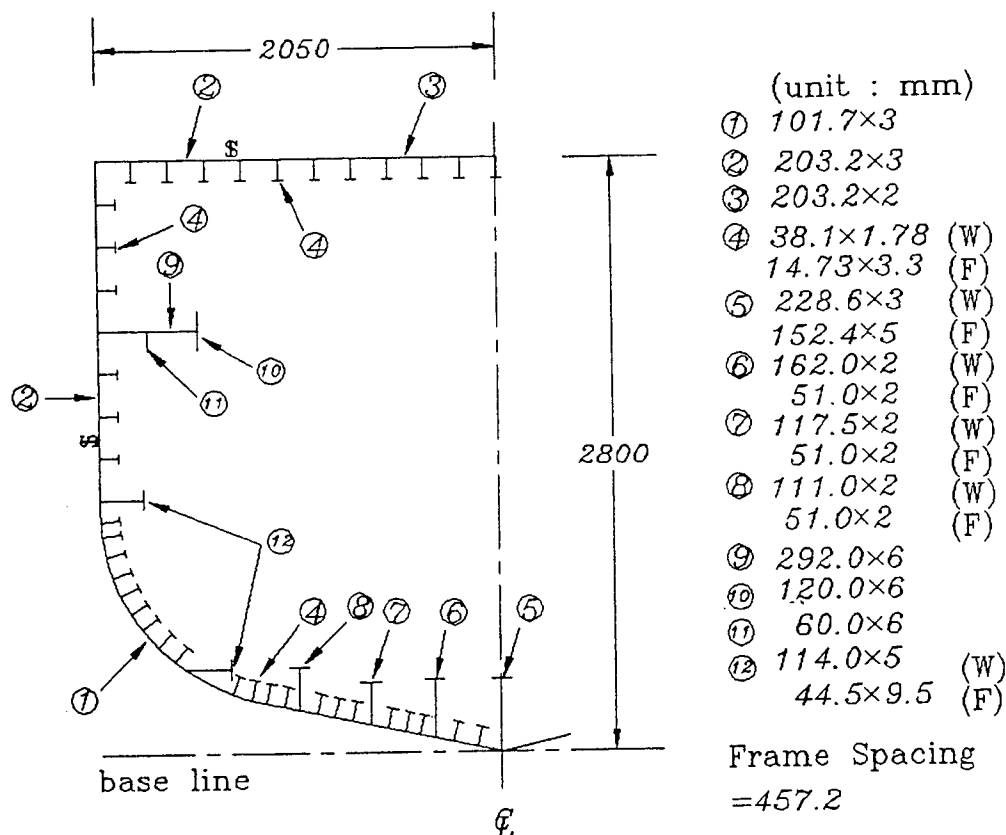
Figure 2.2.8   Midship section of one-third-scale frigate hull model, tested in sagging condition (mm).

It is extremely difficult to test the ultimate collapse behavior of a full-scale ship. Instead, simplified numerical methods that have been verified by comparisons with experimental results from relative large test models can be used for the analysis of actual full-scale ship hulls. The VLCC *Energy Concentration*, which collapsed in Europort on July 22, 1980 (see Figure 2.2.9), is a good example. (To investigate the cause of this failure, several

ultimate strength analyses of the ship have been performed (Rutherford, 1990; Valsgaard, 1991; and Paik, 1993.) Recently, the tanker industry adopted double-hull arrangements or the IMO regulations for prevention of oil pollution. Mansour, et al. (1995) have analyzed the ultimate strength of a double-hull tanker of 34 700 dwt using the ALPS/ISUM code (see Figure 2.2.10).

Figure 2.2.9   Midship section of the single-hull VLCC *Energy Concentration*, analyzed in both sagging and hogging conditions (mm).
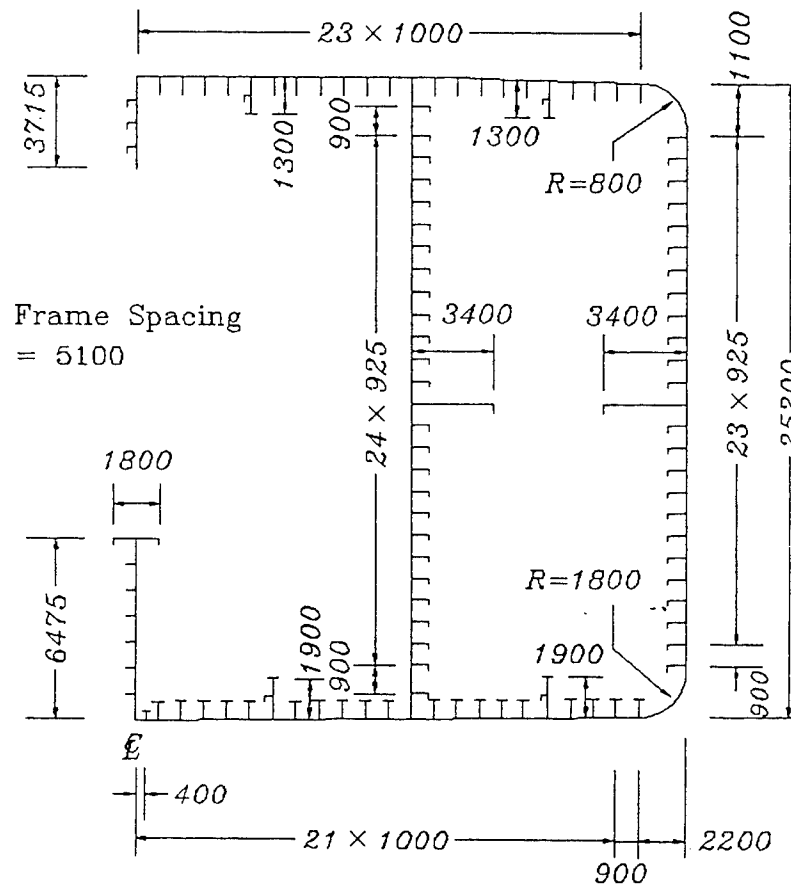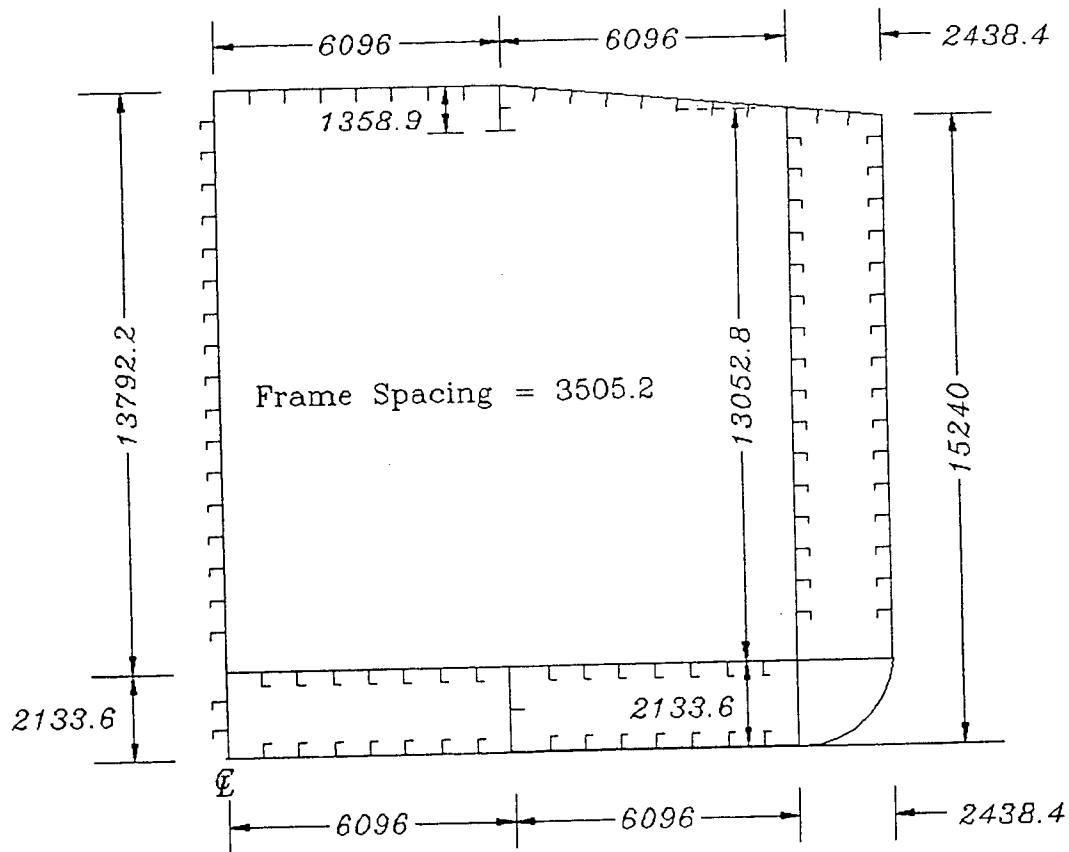
Figure 2.2.10 Midship section of a double-hull tanker of 34 700 dwt, analyzed in both sagging and hogging conditions (mm).

The ALPS/ISUM solutions of all test models described above have also been obtained (Paik, 1992). These analyses show that the ALPS/ISUM code provides a reasonable solution for progressive collapse analysis of a ship's hull.

In this section, comparisons between the earlier and present formulations of the hull ultimate strength are made. The results are also compared with the scaled test models and results from the ALPS/ISUM program for the two full-scale tanker hulls, the VLCC *Energy Concentration* and the 34 700 dwt double-hull tanker.

For calculation of the hull ultimate strength using eqns. (2.2.17b) or (2.2.18b), a designer needs to know in advance the ultimate strengths of the compression flange, as well as the sides in the vicinity of the compression flange. These ultimate strengths were estimatd using the empirical formula given by Paik and Lee (1995) in eqn. (2.2.19). These were then used in all hull ultimate strength formulations except for Dowling's models, where experimental results for the compression flange strength were used. The ultimate strengths of the compression flange for all hull sections (including Dowling's models) as estimated by eqn. (2.2.19) are shown in Table 2.2.1. By comparison with the results of Dowling's models, it was found that eqn. (2.2.19) provides a reasonable solution with an error of 15% in the worst case.

Model	D (mm)	D_B (mm)	A_D (mm²)	A_S (mm²)	A_B (mm²)	$A_B{}'$ (mm²)	Z_D (cm²)	Z_B (cm²)	σ_{yD} (Mpa)	σ_{yB} (Mpa)	σ_{yS} (Mpa)	σ_u/σ_y C.F.	σ_u/σ_y S.S.	M_p (ton-m)
Dowling 2	914.4	0.0	7216.0	3724.1	7216.0	0.0	7733.4	7733.4	293.2	293.2	208.1	0.690* / 0.789	0.450	233.57
Dowling 4	914.4	0.0	8941.9	5822.4	8989.5	0.0	9965.4	9997.5	217.3	217.3	276.5	0.856* / 0.964	0.856	256.89
Dowling 10	914.4	0.0	14988.4	11612.9	17005.4	0.0	17855	19209	329.6	334.2	273.4	0.763* / 0.745	0.610	641.72
Nishihara MST-3	720.0	0.0	2653.5	2653.5	2653.5	0.0	2547.4	2547.4	287.1	287.1	287.1	0.672	0.672	83.96
Nishihara MST-4	720.0	0.0	3784.6	3784.6	3784.6	0.0	3633.1	3633.1	263.6	263.6	263.6	0.785	0.785	109.94
Mansour II	762.0	0.0	8206.7	3077.4	8767.1	0.0	7126.3	7480.2	282.5	282.5	282.5	0.445	0.756	219.94
Dow's Frigate	2800.0	0.0	11905.0	13567.1	13567.1	0.0	51831	64569	245.0	245.0	245.0	0.537	0.537	1502.0
S/H Tanker	25800	0.0	2038183.5	1647087.3	2079042.0	0.0	67137000	67881000	315.0	315.0	315.0	S 0.785 / H 0.837	0.785	2216500
D/H Tanker	15240	2133.6	667733.5	826769.6	880324.4	603990	16512000	23283000	313.6	234.2	234.2	S 0.595 / H 0.877 / 0.792**	0.794	533700

Note : S = Sagging, H = Hogging

   C.F. = Compression Flange, S.S. = Side Shells

   * Obtained by the experiment

   ** Ultimate strength ratio of inner bottom

Table 2.2.1 Properties of Equivalent Hull Cross-Sections

Table 2.2.2 shows comparisons of eight ultimate strength formulas, including the present formula. The formulas of Caldwell (1965) and the current authors were derived using analytical approaches, and the formulas of Faulkner and Sadden (1979) and Frieze and Lin (1991) were obtained empirically, while the remaining formulas were all based on the linear approach. Instead of Caldwell's original expression, the modified formula (eqn. (2.2.3a) or (2.2.3b)), which includes the effects of different materials and double-bottom arrangements, was used in the comparison.

Model	Cond.	M_u/M_p										Error(%)		
		Exp.	ALPS/ISUM	Vasta	① Modified Caldwell	Mansour & Faulkner	Viner	Faulkner & Sadden	Valsgaard & Steen	② Frieze & Lin	③ Paik & Mansour	①	②	③
Dowling 2	H	0.684	0.723	0.684	0.723	0.752	0.673	0.835	0.770	0.721	0.722	+5.7	+5.4	+5.3
Dowling 4	H	0.844	0.856	0.739	0.920	0.813	0.728	0.878	0.832	0.914	0.858	+9.0	+8.3	+1.6
Dowling 10	H	0.736	0.755	0.779	0.836	0.857	0.767	0.941	0.878	0.848	0.810	+13.6	+15.2	+9.1
Nishihara MST-3	S	0.715	0.691	0.597	0.793	0.657	0.588	0.731	0.673	0.702	0.759	+10.9	-1.8	+5.8
Nishihara MST-4	S	0.805	0.747	0.698	0.875	0.768	0.687	0.840	0.786	0.816	0.818	+8.7	+13.7	+1.6
Mansour II	H	0.632	0.618	0.436	0.621	0.480	0.430	0.536	0.492	0.561	0.621	-1.7	-11.2	-1.7
Dow's Frigate	S	0.644	0.652	0.463	0.633	0.510	0.456	0.572	0.522	0.553	0.632	-4.7	-16.7	-1.9
S/H Tanker	S	-	0.775	0.764	0.887	0.870	0.753	0.920	0.861	0.816	0.840	+12.3	+5.3	+7.7
S/H Tanker	H	-	0.834	0.824	0.914	0.898	0.812	0.983	0.929	0.901	0.861	+7.7	+8.0	+3.1
D/H Tanker	S	-	0.715	0.589	0.738	0.648	0.580	0.726	0.664	0.619	0.712	+3.2	-13.4	-0.4
D/H Tanker	H	-	0.830	0.914	0.935	1.0	0.901	1.0	1.0	0.928	0.828	+12.7	+11.8	-0.2

Note: S = Sagging, H = Hogging
(1) Equation (2.2.3)
(2) Equation (2.2.9)
(3) Equation (2.2.17) or (2.2.18)

**Table 2.2.2 Comparison of Ultimate Strength Formulations
with Test Models and Tanker Hull Results**

There are significant differences in the results. The last three columns of Table 2.2.2 show the percentage error of three of the formulations (modified Caldwell, Frieze and Lin, and the work of the current authors), with respect to experimental results or ALPS/ISUM numerical solutions, when experimental results are not available. The Caldwell formula tends to overestimate the ultimate moment capacity. This is due to the stress distribution used by Caldwell, which assumed all material in tension reaches the yield strength (including the sides) and all material in compression reaches the ultimate buckling strength (including the sides).

The currently proposed formulation (eqn. (2.2.17b) or (2.2.18b)) gives lower ultimate moment values than Caldwell's approach. It shows closer agreement with the experimental and numerical results. The difference in the proposed formulation and Caldwell's modified (eqn. (2.2.3a) or (2.2.3b)) results from the difference in stress distribution in the sides. In the proposed formulation, the stresses are assumed to remain in the elastic range for the areas of the sides under compression in the immediate vicinity of the final neutral axis, as well as for the areas of the sides under tension.

It is clear from these comparisons that the proposed formulation (eqns. (2.2.17b) and (2.2.18b)) provides a quite reasonable solution and may be useful for preliminary design estimates of the ultimate strength of ships under a vertical bending moment.

Summary and Concluding Remarks:

In this part of the study, an anaytical expression for predicting the ultimate strength of single- and double-hull ships under vertical bending moments was derived. A credible distribution of longitudinal stresses over the hull section at the overall collapse state was assumed. It was postulated that parts of the compressed side shells, as well as the compression flange, will reach their ultimate limit state in compression. The tension flange will reach the yield strength of the material, while compressed side shells in the immediate vicinity of the final neutral axis, as well as all side shells under tension, are assumed to remain elastic and the stress distribution there is assumed to be linear. The neutral axis location, as well as the depth at which the stress distribution starts to become linear, can be determined from two conditions:

1. No axial force exists on the hull girder

2. The stress distribution is linear near the neutral axis

The ultimate strength moment of the hull was then calculated by integration of the assumed stress distribution with respect to the neutral axis. This resulted in explicit ultimte moment expressions for the sagging and hogging conditions. Using results from large-scale box girder models, a one-third-scale frigate hull model, and full-scale single- and double-hull tankers, a comparison between earlier formulations and the proposed formula was made. The results of the comparisons with experiments and numerical evaluations showed that this simplification was acceptable.

The following conclusions and suggestions can be drawn from this part of the study:

- The ultimate collapse strength of a ship's hull under a vertical bending moment correlates with the failure of the side shells, as well as of the compression/ tension flanges.

- There are significant differences in the ultimate moment results obtained from the different formulas used in the comparisons.

- The Caldwell formula, modified here to include the effects of different materials and double-hull arrangements, tends to overestimate the ultimate moment capacity of the hull sections.

- In design, the rules of classification societies specifying the requirements for the ship section modulus should be based on ultimate strength rather than initial yield, because, in some cases, initial yield does not reflect the true strength of the hull girder.

- The proposed formulae (eqns. (2.2.17b) and (2.2.18b)) provide quite reasonable results in comparison with experimental data and numerical results. Since the

proposed formula takes into account the geometric and material properties of the hull section more precisely, it may be applied to a general-type hull cross-section. The formula may be useful in preliminary design estimates of the ultimate strength of ships under a vertical bending moment.

- There is a lack of experimental data from large-scale steel models, and there is a need for further verification using such data. In particular, tests are needed using models of double-hull tankers.

List of Nomenclature for Section 2.2.3

A_B = total sectional area of outer bottom

A_B' = total sectional area of inner bottom

A_D = total sectional area of deck

A_S = half-sectional area of all sides (including longitudinal bulkheads and inner sides)

a_s = sectional area of a longitudinal stiffener with effective plating

b = breadth of plate between longitudinal stiffeners

D = hull depth

D_B = height of double bottom

E = Young's modulus

g = neutral axis position above the base line in the sagging condition or below the deck in the hogging condition

H = depth of hull section in linear elastic state

I_s = moment of inertia of a longitudinal stiffener with effective plating

I = length of a longitudinal stiffener between transverse beams

M_E = elastic bending moment

M_p = fully plastic bending moment of hull section

M_u = ultimate bending moment capacity of hull section

M_{uh}, M_{us} = ultimate bending moment on hogging or sagging conditions

r = radius of gyration of a longitudinal stiffener with effective plating $[= I_s/a_s)^{1/2}]$

t = plate thickness

Z = elastic section modulus at the compression flange

Z_B, Z_D = elastic section modulus at bottom or deck

β = slenderness ratio of plate between stiffeners $[= (b/t)(\sigma_y/E)^{1/2}]$

λ = slenderness ratio of a longitudinal stiffener with effective plating
$[= (\ell/\pi r)(\sigma_y/E)^{1/2}]$

σ_y = yield strength of the material

$\sigma_{yB}, \sigma'_{yB}$ = yield strength of outer bottom, inner bottom

σ_{yD}, σ_{yS} = yield strength of deck, side

σ_u = ultimate buckling strength of the compression flange

$\sigma_{uB}, \sigma'_{uB}$ = ultimate buckling strength of outer bottom, inner bottom

σ_{uD}, σ_{uS} = ultimate buckling strength of deck, side

2.2.4 A Simple Formulation for Estimating a Stiffened Panel Strength (Secondary Failure Mode):

The stiffened gross panel forms the backbone of most of a ship's structure. It is by far the most commonly used structural element in a ship; appearing in decks, bottoms, bulkheads, and side shell. The primary purpose of the panel is to absorb out of plane (or lateral) loads and distribute those loads to the ship's primary structure. It also serves to carry part of the longitudinal bending stress because of the orientation of the stiffeners. The amount of in-plane compression or tension experienced depends primarily on the location of the panel. Deck panels tend to experience large in-plane load and small lateral pressures, if any. Bottom panels experience large in-plane load, but usually with significant lateral pressures.

The definition of a stiffened gross panel, for this work, is a panel of plating which has stiffeners running in two orthogonal directions. This panel is bounded by other structure, which have significantly greater stiffness in the planes of the loads when compared to the panel and its stiffeners. These boundaries would be provided by structure, such as transverse bulkheads, longitudinal bulkheads, side shell, or large longitudinal girders (e.g., the CVK).

The collapse of a stiffened panel can be prevented by choosing the size of the transverse stiffeners so that they provide sufficient flexural rigidity to enforce nodes at the location of the transverse stiffeners. If the transverse stiffeners act as nodes, which is usually the case, then the collapse of the stiffened panel is controlled by the strength of the longitudinally-stiffened panel.

The strength of a longitudinally-stiffened panel is usually governed by the strength of its stiffness together with the effective plating. The effective plating is determined from buckling considerations if the plate is under edge compressive stress, or from shear lag analysis, if the stiffened plate is subjected to lateral load. Only ultimate strength limit state is considered since, when a column buckles, it reaches immediately its ultimate strength, in most cases.

The effective plating under edge compression can be determined from (see List of Nomenclature at the end of Section 2.2.5):

$$b_e = b \left(\frac{\sigma_{ul}}{\sigma_0} \right)$$

where (σ_{ul}/σ_0) is to be determined from:

a. For $a/b \geq 1.0$

$$\frac{\sigma_{ul}}{\sigma_0} = \begin{cases} = \left(\dfrac{\sigma_{cr}}{\sigma_0}\right)^{1/2} & \text{if } \beta \geq 3.5 \\[2mm] = \dfrac{2.25}{\beta} - \dfrac{1.25}{\beta^2} & \text{if } 1.0 \leq \beta < 3.5 \\[2mm] = 1.00 & \text{if } \beta < 1.0 \end{cases} \qquad (2.2.20)$$

where

$$\frac{\sigma_{cr}}{\sigma_0} = \frac{4\pi^2}{12(1-v^2)} \cdot \frac{1}{\beta^2} = \frac{3.612}{\beta^2}$$

b. For $a/b < 1.0$

$$\frac{\sigma_u}{\sigma_0} = \alpha\, C_u + 0.08(1-\alpha)\left(1 + \frac{1}{\beta^2}\right)^2 \leq 1.0$$

where

$$C_u = \begin{cases} = \left(\dfrac{4\pi^2}{12\left(1-v^2\right)} \cdot \dfrac{1}{\beta^2}\right)^{1/2} & \text{if } \beta \geq 3.5 \\[2mm] = \dfrac{2.25}{\beta} - \dfrac{1.25}{\beta^2} & \text{if } 1.0 \leq \beta < 3.5 \\[2mm] = 1.0 & \text{if } \beta < 1.0 \end{cases} \qquad (2.2.21)$$

For plates under lateral load, the effective plating can be determined from shear lag design curves such as those presented by Schade (1951) and Mansour (1970).

The strength of a longitudinal stiffened panel is governed by A, B, or C as follows (Mansour, 1985):

A. Column Buckling:

The strength in this mode is given by:

$$
\sigma_{cr} = \begin{cases} = \dfrac{\pi^2 E}{(\ell/r)^2} & \text{if } \sigma_{cr} \leq \sigma_p \\[20pt] = \sigma_0 - \dfrac{1}{C_s} & \text{if } \sigma_{cr} < \sigma_p \end{cases}
\tag{2.2.22}
$$

$$
C_s = \frac{\sigma_s}{\sigma_p\,(\sigma_0 - \sigma_p)} \qquad ; \qquad \sigma_s = \frac{\pi^2 E}{(\ell/r)^2}
$$

B. Beam-Column Buckling:

If a stiffener is subjected to axial stress s and lateral load that induces a moment M, the following relation provides the strength as a beam-column:

$$
\frac{\sigma}{\sigma_{cr}} + C\,\frac{M}{M_u} = 1
\tag{2.2.23}
$$

where M_u is the moment at which the flanges are fully plastic, and

$$
C = \frac{C_m}{1 - (\sigma/\sigma_{cr})} \geq 1.0
$$

$$
C_m = 0.6 + 0.4\,\frac{M_1}{M_2} \geq 0.4
$$

$M_1/M_2 > 0$ for single curvature bending, and $M_1/M_2 < 0$ for double curvature bending.

C. Torsional/Flexural Buckling:

a. Doubly-Symmetric Sections:

In this case, the shear center and the centroid of the section coincide. Therefore, the torsional and flexural modes are decoupled.

$$
\sigma_{ct} = \begin{cases} = \dfrac{1}{I_0}\left(GJ + \dfrac{\pi^2 E C_w}{l^2} \right) & \text{if } \sigma_{ct} \leq \sigma_p \\[20pt] = \sigma_0 \left[1 - \dfrac{\sigma_p\,(1 - \sigma_p/\sigma_0)}{\sigma_t} \right] & \text{if } \sigma_{ct} > \sigma_p \end{cases}
\tag{2.2.24}
$$

where

$$
\sigma_t = \frac{1}{I_0}\left(GJ + \frac{\pi^2 E C_w}{l^2} \right)
$$

b. Sections with a Single Plane of Symmetry:

In this case, the shear center and centroid of the section do not coincide and the ultimate limit state is governed by a combination of torsion and flexural buckling.

(i) Elastic range:

$$\sigma_{tfe} \leq \sigma_p$$

σ_{tfe} is the smallest root of the following equation:

$$\frac{I_c}{I_0} \sigma_{tfe}^2 - \sigma_{tfe} (\sigma_{cr} + \sigma_t) + \sigma_{cr} \sigma_t = 0 \tag{2.2.25}$$

(ii) Plastic range:

$$\sigma_{tfe} > \sigma_p$$

$$\sigma_{tfp} = \sigma_0 \left[1 - \frac{\sigma_p (1 - \sigma_p / \sigma_0)}{\sigma_{tfe}} \right] \tag{2.2.26}$$

2.2.5 A Simple Formulation for Estimating Unstiffened Panel Strength (Tertiary Failure Mode):

The strength of an unstiffened plate subjected to in-plane load acting on the "b" edge of the plate is given by (Mansour, 1986):

a. For $a/b \geq 1.0$

$$\frac{\sigma_{ul}}{\sigma_0} = \begin{cases} = \left(\dfrac{\sigma_{cr}}{\sigma_0} \right)^{1/2} & \text{if } \beta \geq 3.5 \\[2ex] = \dfrac{2.25}{\beta} - \dfrac{1.25}{\beta^2} & \text{if } 1.0 \leq \beta < 3.5 \\[2ex] = 1.00 & \text{if } \beta < 1.0 \end{cases} \tag{2.2.20}$$

where

$$\frac{\sigma_{cr}}{\sigma_0} = \frac{4\pi^2}{12(1 - v^2)} \cdot \frac{1}{\beta^2} = \frac{3.612}{\beta^2}$$

b. For $a/b < 1.0$

$$\frac{\sigma_u}{\sigma_0} = \alpha\, C_u + 0.08(1-\alpha)\left(1+\frac{1}{\beta^2}\right)^2 \le 1.0$$

where

$$C_u = \begin{cases} = \left(\dfrac{4\pi^2}{12\left(1-v^2\right)} \cdot \dfrac{1}{\beta^2}\right)^{1/2} & \text{if } \beta \ge 3.5 \\[2em] = \dfrac{2.25}{\beta} - \dfrac{1.25}{\beta^2} & \text{if } 1.0 \le \beta < 3.5 \\[2em] = 1.0 & \text{if } \beta < 1.0 \end{cases} \qquad (2.2.21)$$

List of Nomenclature

Material

E = modulus of elasticity

G = shear modulus

v = Poisson's ratio

σ_0 = average yield stress in compression

$\tau = \dfrac{\sigma_0}{\sqrt{3}}$; average yield stress in shear

σ_p = proportional (linear elastic) limit stress in compression; may be taken as 60% of σ_0

$y_p = \dfrac{\sigma_p}{\sigma_0}$; ratio indicating the start of non-linear behavior

Plate Between Stiffeners

a = plate length

b = plate width

t = plate thickness

α = a/b aspect ratio; can be smaller or larger than 1

β = $\dfrac{b}{t}\sqrt{\dfrac{\sigma}{E}}$; slenderness ratio

Stiffeners

A_c = cross-sectional area (including effective plating)

A_w = web area

b = spacing between stiffeners

b_e = effective width of plating

b_f = flange width

c_w = warping constant

d = web depth

I = moment of inertia (including effective plating)

I_c = polar moment of inertia about centroid

I_0 = polar moment of inertia about shear center

I_{fc} = moment of inertia of compression flange in lateral bending

I_{fe} = moment of inertia of tension flange in lateral bending

I_1 = moment of inertia in the plane of minimum stiffness

I_2 = moment of inertia in the plane of maximum stiffness

J = torsional constant

ℓ = stiffener's length between transverse girders

r = $\sqrt{1/A}$; radius of gyration

S = section modulus

t = plate thickness

t_f = flange thickness

t_w = web thickness

Applied Loads and Stresses

p = applied uniform pressure normal to plate

σ = normal stress

σ_x, σ_y = normal stress in the x and y directions

τ = applied edge shear stress

q = load per unit length

Critical and Ultimate Stresses

σ_{cr} = critical buckling compressive stress

σ_{ul} = ultimate compressive stress

τ_{ul} = ultimate shear stress (acting alone)

Bending Moments and Axial Loads

M = applied bending moment

M_0 = fully plastic bending moment

M_1 = smaller end moment in the plane of bending

M_2 = larger end moment in the plane of bending

M_{fy} = moment at which the flanges are fully plastic

M_y = moment at which yield first occurs

M_u = ultimate limit state

P = applied axial force

P_0 = fully plastic axial force = $\sigma_0 A_c$

2.2.6 Global Hull Strength Under Vertical and Horizontal Moments—Interaction Relations:

The ultimate moment capacity of a ship hull under combined moments may be investigated numerically, e.g., using ALPS/ISUM, by applying a fixed horizontal moment while the vertical moment is increased until the maximum hull capacity is reached. Conversely, a fixed vertical moment can be held constant while the horizontal moment is increased. In a third procedure, which is used in this study, both vertical and horizontal moments are increased at each time step until one of these moments reaches its maximum value (the collapse moment).

The work by Mansour and Thayamballi (1980) gives the following expression for the interaction relation between vertical and horizontal moments:

$$m_x + k \cdot m_y^2 = 1 \qquad \text{if} \quad |m_y| < |m_x| \qquad (2.2.27)$$

and

$$m_y + k \cdot m_x^2 = 1 \qquad \text{if} \quad |m_x| < |m_y| \qquad (2.2.28)$$

where

$$m_x = \frac{M_x}{M_{xu}}, \qquad m_y = \frac{M_y}{M_{yu}}$$

$$k = \frac{(A + 2A_S)^2}{16A_S(A - A_S) - 4(A_D - A_B)^2}$$

$$A = A_D + A_B + 2A_S$$

and

M_x = bending moment in vertical direction

M_y = bending moment in horizontal direction

M_{xu} = vertical ultimate collapse bending moment

M_{yu} = horizontal ultimate collapse bending moment

A_D = cross-sectional area of the deck including stiffeners

A_B = cross-sectional area of the bottom including stiffeners

A_S = cross-sectional area of one side including stiffeners

The above relation was originally derived for vertical and horizontal fully-plastic moments (see Mansour and Thayamballi, 1980). The applicability of this interaction relation has been tested, and was shown in Chapter 4 to be approximately valid when buckling is included. Chapter 4 provides more details on the strength under combined loading.

2.3   Methodology for Estimating Ship Failure Probabilities

2.3.1   Basic Concept in Reliability Technology:

In order to introduce the basic concept in the reliability analysis, the following example is given. Consider a simple beam subjected to a loading induced by the environment, e.g., wave load. Traditionally, in the design of such a beam, practitioners and designers have used fixed deterministic values for the load acting on the beam and for its strength. In reality, these values are not unique values, but rather have probability distributions that reflect many uncertainties in the load and the strength of the beam. Structural reliability theory deals mainly with the assessment of these uncertainties and the methods of quantifying and rationally including them in the design process. The load and the strength are thus modelled as random variables.

Figure 2.3.1 shows the probability density functions of the load and the strength of the beam in terms of applied bending moment and ultimate moment capacity of the beam, respectively. Both the load Z and the strength S are assumed in this example to follow the normal (Gaussian) probability distribution with mean values $\mu_z = 20,000$ ft-ton and $\mu_s = 30,000$ ft-ton, respectively, and standard deviations of $\sigma_z = 2,500$ ft-ton and $\sigma_s = 3,000$ ft-ton, respectively.
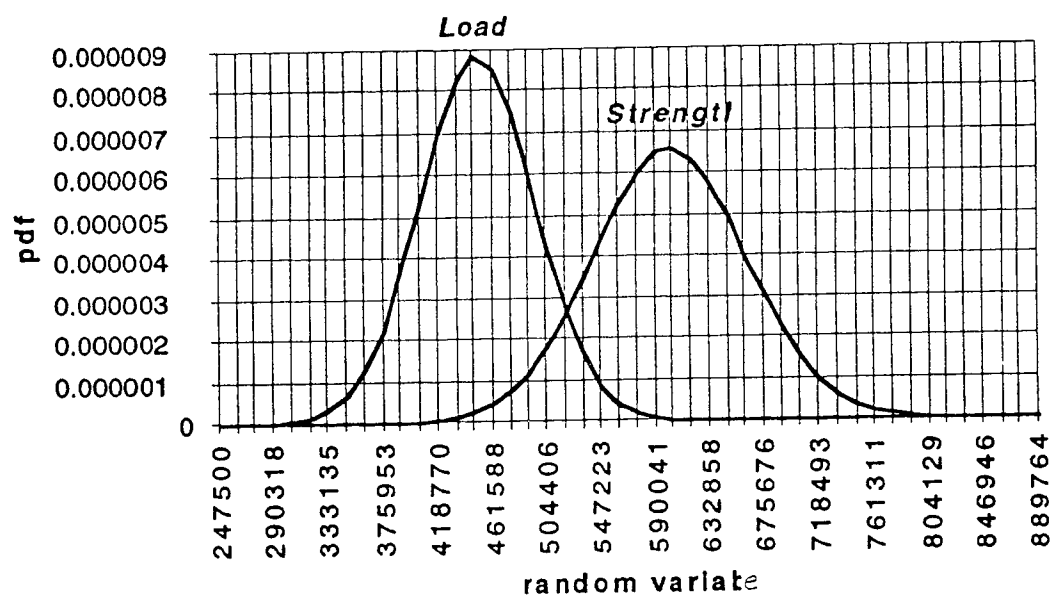
Figure 2.3.1   Load and Strength Probability Density Functions

We may now construct a simple function $g(s,z)$, called the limit state function, which describes the safety margin M between the strength of the beam and the load acting on it, i.e.,

$$M = g(s,z) = S\text{-}Z \tag{2.3.1}$$

Both S and Z are random variables and may assume several values. Therefore, the following events or conditions describe the possible states of the beam,

(i) $M = g(s,z) < 0$ represents a failure state since this means that the load Z exceeds the strength S.

(ii) $M = g(s,z) > 0$ represents a safe state

(iii) $M = g(s,z) = 0$ represents the limit state surface (line, in this case) or the border line between the safe and failure states

The probability of failure implied in (i) above can be computed from

$$p_f = P[M = g(s,z) \le 0] = \iint\limits_{g(s,z) \le 0} f_{S,Z}(s,z)\, ds\, dz \tag{2.3.2}$$

where $f_{s,z}(s,z)$ is the joint probability density function of S and Z and the domain of integration is over all values of s and z, where the margin M is not positive, i.e., not in the safe state. If the applied load on the beam is statistically independent from the beam strength, the above equation can be simplified and interpreted easily as:

$$p_f = \int_0^\infty F_S(z)\, f_Z(z)\, dz \tag{2.3.3}$$

where $F_s(\cdot)$ and $f_z(\cdot)$ are the cumulative distribution function of S and the probability density function of Z, respectively. Both, in this example, are Gaussian.

Equation (2.3.3) is the convolution integral with respect to z and can be interpreted with reference to Figure 2.3.1. If $Z = z$, the conditional probability of failure would be $F_s(z)$. But since $z < Z \le z + dz$ is associated with probability $f_z(z)dz$, integration of all values of z results in eqn. (2.3.3).

In our example, S and Z are both statistically independent and normally distributed. Equation (2.3.3) can be thus shown to reduce to:

$$p_f = \Phi(-\beta) \tag{2.3.4}$$

where $\Phi(\cdot)$ is the standard normal cumulative distribution function and β is called a safety index, defined as (see a plot of eqn. (2.3.4) in Figure 2.3.1A):

$$\beta = \frac{\mu_s - \mu_z}{\sqrt{\sigma_s^2 + \sigma_z^2}} \tag{2.3.5}$$

Notice that, as the safety index β increases, the probability of failure p_f as given by eqn. (2.3.4) decreases. The safety of the beam, as measured by the safety index β, can be thus increased (see eqn. (2.3.5)) by increasing the difference between the means $\mu_s - \mu_z$ or decreasing the standard deviations, σ_s and σ_z.
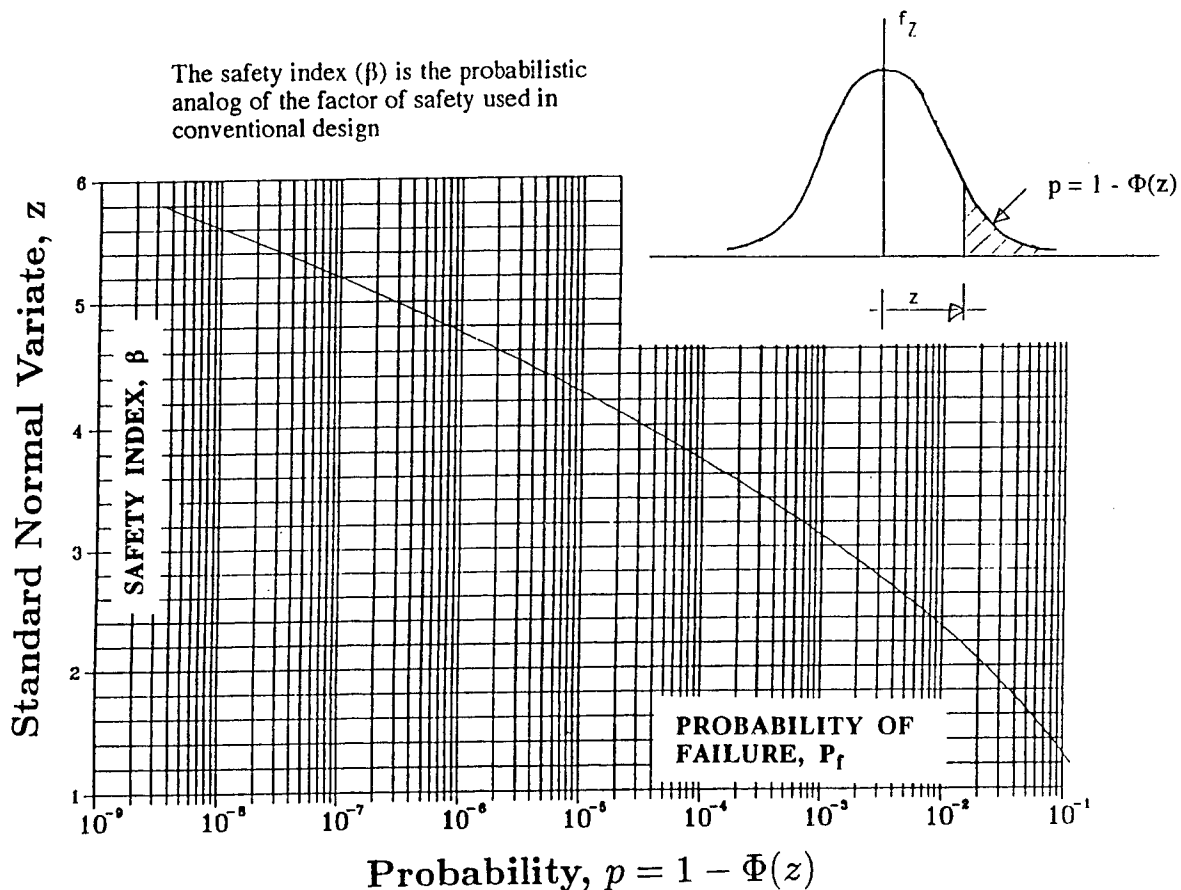
Figure 2.3.1A. Safety Index Versus Probability of Failure

Substituting in eqn. (2.3.5), the numerical values for μ_s, μ_z, σ_s and σ_z given in our simple beam example results in a safety index $\beta = 2.56$. Equation (2.3.4) can then be used in conjunction with tables of standard normal cumulative distribution functions to yield a probability of failure $= 5.23 \times 10^{-3}$.

The preceding example and Figure 2.3.1 indicate that certain specific load and strength information are necessary for performing reliability analysis of marine structures. It is mostly in this area that reliability analysis of marine structures differs from typical civil engineering structures. In this report, emhasis has been placed on developing the required load and strength information for marine structures.

Prior to estimating the loads acting on ships or marine structures, a statistical representation of the environment is necessary. This includes waves, wind, ice, seismic and current. The last four items are more important for fixed offshore structure than for floating vessels. The environmental information can then be used as input to determine the loads acting on the structure (see Section 2.1). Typically, an input/output spectral analysis procedure is used to determine the "short-term" loads in a specific sea condition (stationary condition). The required transfer function is determined from first- or second-order strip theory using the equations of motion of the vessel (see Sections 2.1.1 and 2.1.2), or from a

towing tank experiment. In offshore structures, Morison's equation is usually used to determine the wave load transfer function.

Prediction of the loads in a stationary sea condition (spectral analysis) is not sufficient for the reliability analysis. Extreme values and long-term (lifetime) prediction of loads and their statistics are more valuable. For this purpose, order statistics and statistics of extremes play a very important role. Gumbel's theory of asymptotic distributions is often used in this regard (Mansour, 1990). In the long-term prdiction, the fatigue loads, i.e., the cyclic repetitive loads which cause cumulative damage to the structure, must also be considered.

Methods of combining the loads, such as static and dynamic, including high- and low-frequency loads, have been considered in Section 2.1.2 and Appendix A. In nature, many of these loads act simultaneously, therefore, their combination must be evaluated for a meaningful reliability analysis.

In assessing the reliability of ship structures, two general loading situations may be used; short-term or long-term analysis. At the design stage, if one knows the route of the ship and if that route is more or less permanent, then the probability of failure can be predicted using long-term analysis. If, on the other hand, the route of the ship is not defined, then the short-term analysis can be used to obtain the probability of failure under one or more conditions that are considered to be the severest the ship may encounter during its lifetime.

The criterion usually used in the short-term analysis is to consider the single most severe sea condition (a sea condition with a specified return period, or more appropriately, a sea condition with a specified encounter probability) and subject the vessel to this condition for a specified period of time.

These two methods, short- and long-term analyses, will naturally produce different final results for the safety margins and, therefore, care must be taken when comparing safety margins of different ships, i.e., the method and criterion used in predicting the loads acting on the ship will have a considerable impact on the resulting safety index.

To further amplify on this point, the long-term distribution of the wave loads acting on a ship may be determined by tracing the expected route of the ship during its lifetime. Based on ocean wave statistics along that route, the long-term (lifetime) wave load probability distribution for the entire history may be determined. In the short-term analysis, a distribution of the extreme load is predicted on the basis of criteria such as one extreme sea storm of a specific encounter probability and duration, or a short-term operation in a specific location under severe sea conditions.

It should be noted that there is a fundamental difference between computed results based on these two avenues. In the short-term analysis, the computed probabilities of failure are conditional probabilities given the occurrence of an extreme wave load per a selected criterion. Care must be taken in this case in determining the response of the ship to this extreme load since non-linearities will play an important role. In the long-term analysis, however, the resulting probabilities of failure are associated with the entire history of the expected load acting on a ship during its lifetime, and is conditioned on the selected ship route. In the following sections, the short- and long-term procedures are described.

2.3.2   Short-Term Procedure:

2.3.2.1 *Description of the Short-Term Procedure*:

The following procedure may be applied in the short-term analysis.

a. From ship route (if known), ocean wave statistics, and a specified encounter probability (or return period) determine the design storm condition (see Section 2.3.2.2)

b. Calculate the rms value of the wave bending moment in the design sea condition using either second order strip theory (see Sections 2.1.1 to 2.1.3), or towing tank experiment. Calculate also the stillwater bending moment.

c. Estimate the strength parameters for each failure mode (see Section 2.2).

d. Calculate the probability of failure or the safety index for each failure mode (see Section 2.3.4).

The resulting probabilities are conditional probabilities. They are conditioned on encountering the design storm. The encounter probability can be estimated as described in the next section.

2.3.2.2 *Return Periods and Encounter Probabilities*:

Return periods and the associated wave heights are not sufficient by themselves to develop criteria to be used in the design of ships or fixed offshore structures. In addition, it is important to determine the *probability of the structure encountering* a design storm that has a specified return period. This probability of encounter will depend on the lifetime of the structure, i.e., on how long the structure will remain at the location where the return period and the associated wave height are calculated. If the structure life is long, the probability of encounter will be higher.

For fixed offshore platforms, the useful life of the structure can be estimated, and the corresponding encounter probability can be determined as outlined in the following sections. For ships, however, the estimation of the encounter probabilities is more complicated because of their mobility, and because of the fact that different regions (zones) in the oceans have different wave severity and wave statistics.

This part of the study presents a procedure for calculating ship/storm encounter probabilities which can be used as a better basis for establishing design criteria. The encounter probabilities can provide better and more meaningful criteria for design since they involve the life of the structure, as well as wave statistics, in the region of operation. Return periods involve wave statistics only, and do not involve the life of the structure. Therefore, return periods are less meaningful as a basis for developing design criteria. In the next section, the encounter probability in any ocean zone is developed as a function of the return period of a design wave and the life of the structure. A method of calculating return periods for specific wave heights is described as well. The method is based on extrapolating wave data at the site and depends on the probability distribution of wave heights at that location.

In the following section, the probability of a ship encountering a severe storm is developed as a "system probability" that depends on the ship route and wave statistics along that route. First-order bounds of the encounter probability are shown. In addition, a procedure is described to calculate the "exact" encounter probability for equally correlated waves in the different zones along the ship route. The developed procedures for calculating the bounds and the "exact" value are then applied to four ship routes, two in the Atlantic, and two in the Pacific Ocean. This section concludes with a discussion of the results obtained for the four ship routes and the impact of the routes on storm encounter probability. A list of nomenclature for this section is given at the end of this section.

Encounter Probability:

As mentioned earlier, the encounter probability of a specific wave height (or a sea state characterized by a significant wave height), not only depends on its return period R, but also on the life of the structure, L, in years. We will consider first any zone (location) i in the ocean, and in the next section, we will generalize the procedure to include all zones along a ship's route.

The probability that a wave height x will not be encountered during the portion of a structure's lifetime L_i spent in zone i will be called non-encounter probability P_{ne_i}. If the distribution function $F_{Y_i}(x)$ of the annual maximum wave heights is available, then from order statistics, the non-encounter probability is:

$$P_{ne_i} = P[\text{no exceedence of } x \text{ in life } L_i]$$
$$= P[Y_i \le x] = [F_{Y_i}(x)]^{L_i}$$

$$(2.3.6)$$

where

$\qquad Y_i \;=\;$ maximum wave height during time L_i

$\qquad L_i \;=\;$ time spent in zone i in years

$\qquad F_{Y_i}(x) \;=\;$ distribution function of the annual maximum in zone i

The distribution function of the annual maximum wave height can be written in terms of the distribution function of the individual wave heights $F_{X_i}(x)$, using, again, order statistics as:

$$F_{Y_i}(x) = [F_{X_i}(x)]^{k_i}$$

$$(2.3.7)$$

where k_i is the number of wave peaks (cycles) in zone i in one year. Thus, eqn. (2.3.6) can be written

$$P_{ne_i} = \left\{ [F_{X_i}(x)]^{k_i} \right\}^{L_i}$$

$$(2.3.8)$$

The return period of a wave height x is defined as the average length of time between exceedence. The waiting period w in years between exceedence in zone i has a probability law given by (Borgman):

$$P[W_i = w] = F_{Y_i}^{w-1}(x)[1 - F_{Y_i}(x)] \qquad (2.3.9)$$

and the average waiting period, i.e., the return period, is:

$$R_i = E[W_i] = [1 - F_{Y_i}(x)]^{-1} \qquad (2.3.10)$$

In terms of the distribution function of the wave heights, R_i is given by:

$$R_i = [1 - (F_{X_i}(x))^{k_i}]^{-1} \qquad (2.3.11)$$

The relationship between the non-encounter probability and the return period R_i can be obtained by eliminating $[F_{X_i}(x)]^{k_i}$ from eqns. (2.3.8) and (2.3.11), thus:

$$P_{ne_i} = (1 - R_i^{-1})^{L_i} \qquad (2.3.12)$$

and by definition:

$$P_{e_i} = 1 - (1 - R_i^{-1})^{L_i} \qquad (2.3.13)$$

where P_{e_i} is the probability of encounter. Equation (2.3.13) gives the basis for calculating the encounter probability of a wave height if its return period is known. Notice that if $R_i = L_i$, the non-encounter probability $\cong e^{-1}$ and the encounter probability $P_{e_i} = 1 - P_{ne_i} \cong 0.632$, that is, there is a high probability of a ship encountering a wave height with a return period L_i during the L_i years the ship operates in zone i. If the ship operates for five years in zone i ($L_i = 5$ years), the encounter probability is approximately 5% for $R_i = 100$ years, and 0.5% for $R_i = 1000$ years.

The return period R_i of a wave height x, in any zone i can be estimated from:

$$R_i = \frac{n_i}{n_0} y_0 \qquad (2.3.14)$$

and

$$n_i = [1 - F_{X_i}(x)]^{-1} \qquad (2.3.15)$$

where

n_0 = total number of wave data collected in zone i

y_0 = number of years of data collection in zone i

n_i = expected number of waves in zone i necessary to exceed wave height x

n_i can be calculated from eqn. (2.3.15) for any value of design wave x.

The procedure for determining the ship/storm encounter probability in any zone i can be summarized as follows:

a. Use wave data in zone i to determine the form and the parameters of the distribution function of wave heights $F_{X_i}(x)$, using any method of parameter estimation, e.g., method of moments, or regression analysis (see Figure 2.3.2 and the applications at the end of this section in which a three-parameter Weibull distribution was found to be adequate).

b. For the prescribed design wave height (or sea state characterized by a significant wave height) predict the number of waves necessary to exceed the design wave height using eqn. (2.3.15).

c. Use eqn. (2.3.14) to estimate the return period associated with the design wave height or significant wave height.

d. Determine the probability of encounter in zone i from eqn. (2.3.13) and information on how long the ship operates in zone i, i.e., L_i.

Notice that the non-encounter probability may also be computed independently from the return period using eqn. (2.3.8). Equation (2.3.8), however, does not show the dependence of the non-encounter probability on the return period.

Ship Routes and the Associated Encounter Probabilities:

Naturally, the probability of a ship encountering a severe storm (or the design sea state) will depend on the ship route and the wave statistics in the zones along the route. In the previous section, a procedure for calculating the encounter probability of a wave height in any zone i is described. Usually ships operate along routes that include several zones. Wave statistics in different zones of the oceans are available from sources such as *Global Wave Statistics* (Hogben *et al.*, 1986) and can be used to determine return periods and encounter probabilities in each zone, as described in the previous section. The operation time of the ship in each zone is important in order to determine L_i. The time the ship spends in harbor and in dry-dock should also be estimated, as these can be considered as a zone where the probability of encountering the design wave is equal to zero.

In order to determine the probability of encountering a wave height (or a specific sea state) along a ship route, we will consider the zones and the harbor as members in a series system. A series system is defined as a system in which a state of encounter occurs if an encounter occurs in any of its members. That is, for the system encounter probability to be realized, it is sufficient that the ship encounters the sea state (wave height) in any one zone. Similarly, the system non-encounter probability P_{ne} can be realized only if mutual non-encounter takes place in all zones, i.e.,

$$P_{ne} = P\left[\bigcap_{i=1}^{n} A_i\right] \qquad (2.3.16)$$

where A_i is the event of no encounter in zone i. That is, $P[A_i] = P_{ne_i}$ as determined in the previous section, and the symbol $\cap$ indicates the intersection or mutual occurrence of the events A_i. n is the total number of zones, including harbor. The system (overall) probability of encounter P_e is simply given by:

$$P_e = 1 - P_{ne} \qquad (2.3.17)$$

First-order bounds on the non-encounter probability given by eqn. (2.3.16) can be determined. Corresponding bounds can be also determined for the encounter probability given by (2.3.17). The upper and lower bounds on P_e are determined by assuming statistically independent or fully-correlated wave conditions in the zones along the ship route, respectively.

If A_i are assumed statistically independent, then:

$$P_{ne} = \prod_{i=1}^{n} P(A_i) = \prod_{i=1}^{n} P_{ne_i} \qquad (2.3.18)$$

and

$$P_e = 1 - \prod_{i=1}^{n} P_{ne_i} \qquad (2.3.19)$$

On the other hand, if A_i are assumed perfectly correlated, then:

$$P_e = \max_i [1 - P(A_i)] = 1 - \min_i P(A_i) = 1 - \min_i P_{ne_i} \qquad (2.3.20)$$

Thus, the bounds on the system encounter probability P_e are:

$$1 - \min_i (P_{ne_i}) \le P_e \le 1 - \prod_{i=1}^{n} P_{ne_i} \qquad (2.3.21)$$

These bounds are tight if the non-encounter probability in any of the zones is dominant. Although second-order bounds can be formulated, the first-order bounds were found to be sufficiently tight.

Instead of determining upper and lower bounds on P_e or P_{ne}, one can determine the "exact" value of either under certain assumptions. If the members of a series system are equally correlated, then an extension of the work by Stuart, summarized *in Structural Reliability and Its Applications* (Thoft-Christensen and Baker, 1982) leads to the following system probability of encounter:

$$P_e(\rho) = 1 - \int\limits_{-\infty}^{\infty} \prod_{i=1}^{n} \Phi\left[\frac{\beta_i + \sqrt{\rho}t}{\sqrt{1-\rho}}\right] \varphi(t)\, dt \qquad (2.3.22)$$

where β_i can be calculated from:

$$\beta_i = -\Phi^{-1}(P_{e_i}) = -\Phi^{-1}(1 - P_{ne_i}) \qquad (2.3.23)$$

Φ and φ denote the standard Gaussian cumulative distribution and density function, respectively, and ρ is the correlation coefficient. When $\rho = 0$, eqn. (2.3.22) converges to the upper bound of eqn. (2.3.21). Equation (2.3.22) will be used in the application given in the following section to determine the overall encounter probabilities for four ship routes as a function of an "average" correlation coefficient between the zones of each route. In addition, eqn. (2.3.21) will be used to determine the bounds.

The correlation coefficient ρ cannot be easily determined from currently available wave data. Fortunately, the encounter probability is rather insensitive to ρ, as will be seen in the next application example.

Applications: Storm Encounter Probabilities for Various Shipping Routes:

To illustrate the concepts presented earlier, the probability of encounter for various design wave heights, in four shipping routes, were calculated. The source for the data used in the analysis of all shiping routes is *Global Wave Statistics* (GWS) by Hogben, Dacunha, and Olliver (1986). Over 55 million visual observations of wind speed and direction, as well as wave height, period, and direction, obtained by the United Kingdom Meteorological Office marine data bank, were used to compile wave statistics for 104 zones covering most of the worlds' oceans. The observations come entirely from crews on merchant ships, so that the data is mostly from the shipping routes within the zones. This might present problems for locations away from major shipping lanes, but is all the more advantageous for the analysis presented in this section.*

The raw data was "enhanced" by the NMINET computer program, which uses the wind observations to improve the reliability of the wave statistics. For each zone, the wave statistics are presented for all directions, and on both an annual and seasonal basis. Although the total number of both wind and wave observations is listed for each zone, the statistics have been normalized to approximately 1,000 observations. Because the design lifetime for most marine structures is on the order of years, only the annual data from all directions was used in our analysis.

Pilot charts were obtained for both the North Atlantic and Pacific oceans. For each ocean, a northerly and southern route were chosen to contrast the effects of relative weather severity between routes. The time of operation in each zone was calculated in the following

---

* It may also be noted that most of the data were taken by ships, many of which are routed to avoid severe storms. The data thus may be biased in this regard, but may reflect wave statistics actually encountered by ships.

manner. The percentage of the route distance in each zone was measured from the pilot charts, after transferring the zone boundaries onto the chart itself. An average trip time, including time in port, was found by talking with representatives of shipping firms, or assuming an average speed. This approach may have a disadvantage of not accounting for the different relative speeds at which the ship moves over the duration of the trip. This would underestimate the time the ship spends in zones with severe weather conditions, as the vessel must reduce speed, increasing the time spent in that zone. A design life of 20 years was assumed for this analysis, and a period of one week a year was added to the port time for maintenance and inspection. Using all this information, the entire time spent in each zone L_i can be calculated. Table 2.3.1 shows the operation time in each zone, for all four routes, as well as the port/dry-dock time.

North Atlantic				North Pacific			
Northern Route		Southern Route		Northern Route		Southern Route	
Zone	Li	Zone	Li	Zone	Li	Zone	Li
8	5.9	23	7.72	13	7.15	21	1.08
9	5.9	24	7.0	14	0.55	22	1.08
10	2.9	25	1.86	20	7.0	29	1.85
11	2.9	Port	3.4	22	0.86	30	0.92
				29	0.86	31	1.95
				30	1.0	43	6.55
				Port	2.56	Port	3.51

**Table 2.3.1 Portion of Structure Design Life Spent in Each Zone,
Including Port, in Years**

In order to apply the equation described in the previous section, the cumulative distribution function $F_{X_i}(x)$ must be determined for each zone i. The wave data given GWS are in terms of significant wave heights. These significant wave heights are assumed to follow a three-parameter Weibull distribution given by:

$$F_{X_i} = 1 - e^{-(x-m_i/\bar{k}_i)^{l_i}} \tag{2.3.24}$$

and the corresponding density function $f_{X_i}(x)$ is:

$$f_{X_i}(x) = (l_i / \bar{k}_i)(x - m_i / \bar{k}_i)^{l_i - 1} e^{-(x-m_i/\bar{k}_i)^{l_i}} \qquad x \geq m_i \tag{2.3.25}$$

where m_i is the location parameter, $\bar{k}_i$ is the scale parameter, and l_i is the shape parameter of the Weibull distribution to be determined in each zone i. Taking the natural logarithm of both sides of eqn. (2.3.24) twice, it can be reduced to an equation of a straight line if plotted on *ln ln* versus *ln* scale (e.g., Mansour, 1990). The wave data for each zone is then plotted using standard statistics technique (Ang and Tang, 1984). The line that fits the data best is

drawn using linear regression analysis. This kind of analysis is easily accomplished with the use of a spread sheet. The parameter m_i is found by iteration, so that the standard error is minimized with a 95% confidence level. The parameters l_i and $\bar{k}_i$ are determined from the slope and intercept of the line (for complete details of determining the Weibull parameters, see W.M. Richardson, 1992).
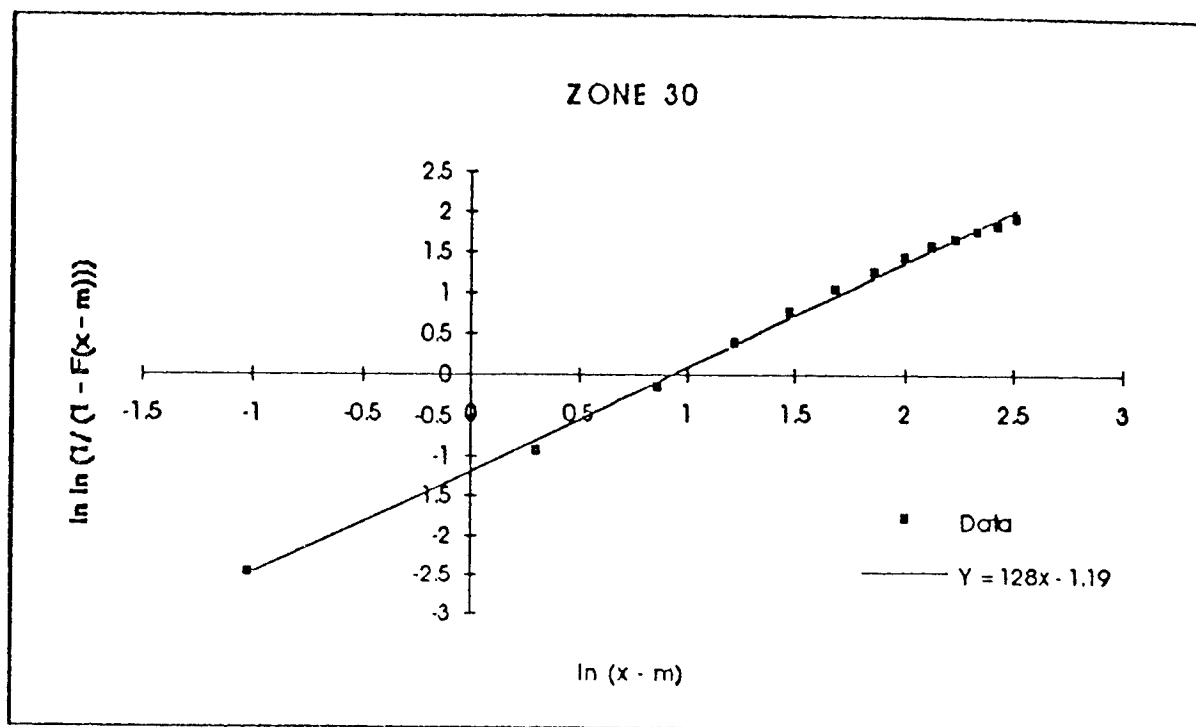
ZONE 30

Figure 2.3.2   Weibull Fit for Zone 30, Common to Both Pacific Routes

Figure 2.3.2 shows, graphically, examples of the procedure for determining the Weibull parameters, as well as the quality of fit to the Weibull distribution. Examples of the regression fit line with data in each zone are shown at the end of this section. In all cases, the fit is quite good in the region of lower wave heights, for which there are an abundant amount of observations. At the upper end, there is a slight divergence, possibly because of the fewer observations of waves of greater height, or alternatively, because the normalized wave statistics are given in discrete values when there was likely a fractional value given by the NMINET analysis (Hogben et al., 1986).

With the cumulative distribution function $F_{X_i}(x)$ determined for each zone, the procedure described earlier was used to determine the probabilities of encounter. That is, the expected number of waves necessary to exceed a design wave height was estimated from eqn. (2.3.15). Equation (2.3.14) was then used to determine the return period associated with that design wave height. The probability of encounter in each zone was determined from eqn. (2.3.13) using the information obtained on how long the ship operates in that zone, i.e., L_i. Finally, the bounds on the overall system probability of encounter are determined from eqn.

(2.3.21). The overall encounter probability was also determined as a function of the correlation between wave conditions in the various zones using eqns. (2.3.22) and (2.3.23). Correlation coefficients ρ = 0.0, 0.2, 0.4, 0.6, and 0.8 were assumed in the analysis. The integral in eqn. (2.3.22) was calculated numerically and a FORTRAN computer code was developed for the entire procedure.

For each of the four ship routes under consideration, five sea states (storm conditions) have been considered as examples. These are characterized by significant wave heights: $H_{1/3}$ = 16, 17, 18, 19, and 20 meters.

Since there is no available information on the exact period of time the data was collected in GWS, it was decided to perform the analysis based on the annual normalized data. The data given in GWS are the average data per year (i.e., y_0 = 1 year, and $n_0 \cong 1000$) and represent the total observed data.

Shipping Routes in the Atlantic:
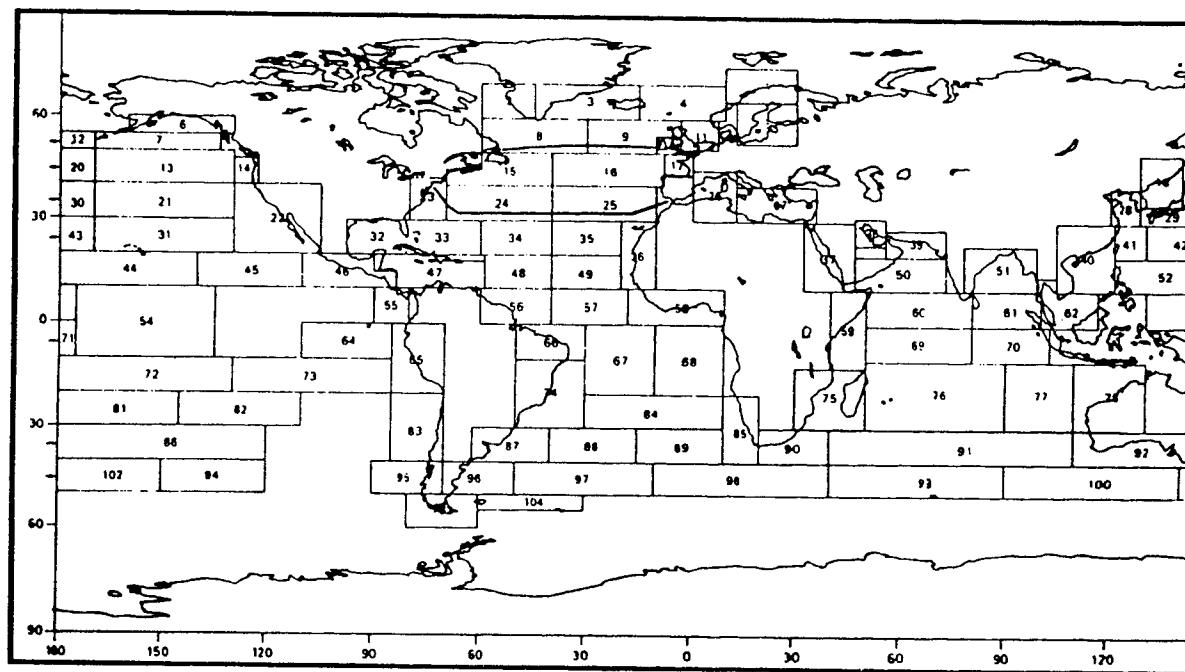
Figure 2.3.3   Northern and Southern Routes in the North Atlantic

As previously mentioned, two routes were chosen in the Atlantic ocean (Figure 2.3.3). For the route in the North Atlantic, which has some of the most extreme weather conditions in the world, probabilities of encounter are quite high (Table 2.3.2), ranging from about 65% for a 16m wave height, to 6% for 20m (ρ = 0.6). The Southern route is the "low powered"

shipping lane between Gibraltar and New York. As expected, the probability of encounters are very small, ranging between 26% and 1% (Table 2.3.3, $\rho = 0.6$).

$H_{1/3}$	Upper Bound	$\rho = 0.0$	$\rho = 0.2$	$\rho = 0.4$	$\rho = 0.6$	$\rho = 0.8$	Lower Bound
16	0.7953	0.79531	0.74602	0.69967	0.65415	0.60657	0.4399
17	0.5200	0.52005	0.48131	0.44276	0.40353	0.36179	0.2286
18	0.1808	0.18085	0.16906	0.15381	0.13524	0.11243	0.08267
19	0.09078	0.09069	0.08634	0.07024	0.05769	0.07956	0.03971
20	0.07348	0.07348	0.07063	0.06594	0.05421	0.05004	0.03771

Table 2.3.2 Probability of Encounter, with Bounds for Northern Route in North Atlantic

$H_{1/3}$	Upper Bound	$\rho = 0.0$	$\rho = 0.2$	$\rho = 0.4$	$\rho = 0.6$	$\rho = 0.8$	Lower Bound
16	0.2617	0.26171	0.25156	0.23947	0.22573	0.21076	0.2007
17	0.1280	0.12796	0.12427	0.11900	0.11209	0.10341	0.09574
18	0.0675	0.06755	0.06591	0.06313	0.05903	0.05348	0.04839
19	0.03049	0.03050	0.03002	0.02905	0.02736	0.02475	0.02177
20	0.01354	0.01355	0.01339	0.01299	0.01220	0.01078	0.00874

Table 2.3.3 Probability of Encounter, with Bounds for Southern Route in North Atlantic
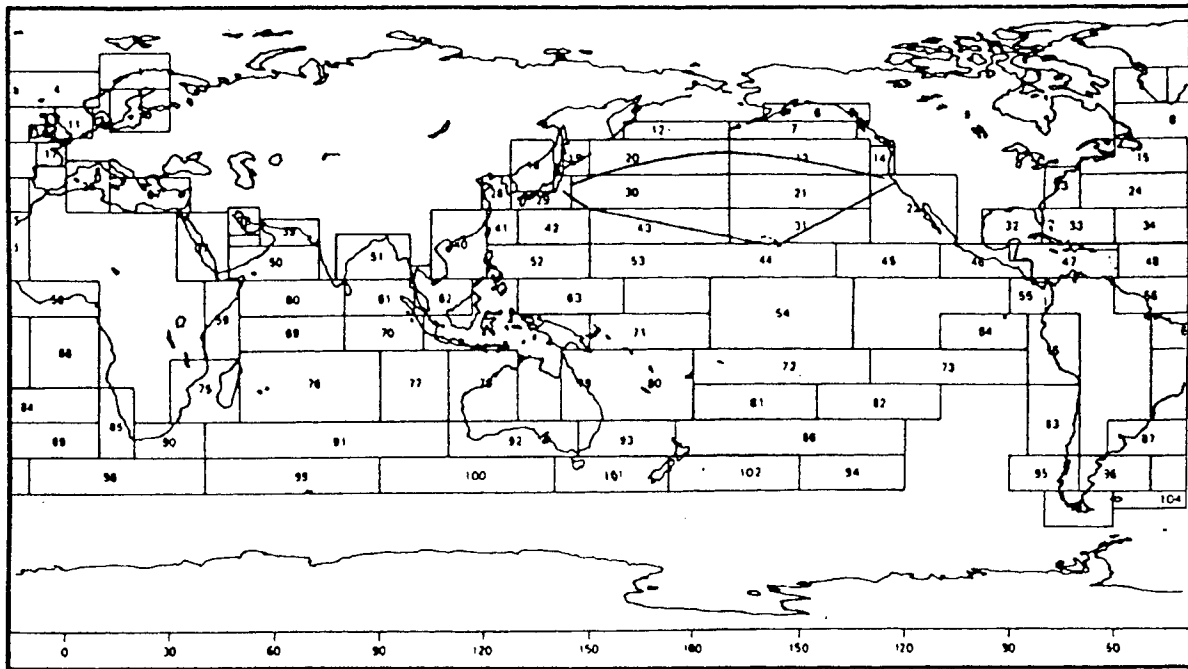
Figure 2.3.4 Northern and Southern Routes in North Pacific

In the Pacific, two main shipping routes were also examined; one is the great circle route between the San Francisco Bay and Yokohama, Japan, and the other, more Southerly route, going between the same locations by way of Honolulu, Hawaii. The encounter probabilities for these two routes are shown in Tables 2.3.4 and 2.3.5. Comparing the Northern route in the Pacific with its counterpart in the Atlantic, the probability of encounter is actually greater, 82% for a wave height of 16m (see Table 2.3.4, $\rho = 0.6$) versus 65% in the North Atlantic. This is because one zone in the Pacific, zone 20, has very severe weather conditions and, according to the assumed ship route, the ship spends seven years of its 20-year life in this zone. The overall P_e is strongly influenced by any single zone that has a high P_{e_i}. As an example, consider the upper bound given by eqn. (2.3.19). If P_{ne_i} in most zones approach one, and in a single zone it approaches 0.5, then multiplying these values together gives, from eqn. (2.3.19), an overall P_e close to 0.5.

For the Southern route, the P_e are again very low, ranging from 4% for $H_{1/3} = 16$m to 0.1% for $H_{1/3} = 20$m (Table 2.3.5, $\rho = 0.6$).

$H_{1/3}$	Upper Bound	$\rho = 0.0$	$\rho = 0.2$	$\rho = 0.4$	$\rho = 0.6$	$\rho = 0.8$	Lower Bound
16	0.8403	0.84034	0.83096	0.82559	0.82351	0.82323	0.8232
17	0.5994	0.59939	0.59685	0.59507	0.59422	0.59406	0.5941
18	0.3910	0.39104	0.38755	0.38433	0.38211	0.38134	0.3813
19	0.2347	0.23468	0.23269	0.23041	0.22849	0.2276	0.2276
20	0.1338	0.13382	0.13303	0.13192	0.13077	0.13009	0.1300

**Table 2.3.4 Probability of Encounter, with Bounds for
Northern Route in North Pacific**

$H_{1/3}$	Upper Bound	$\rho = 0.0$	$\rho = 0.2$	$\rho = 0.4$	$\rho = 0.6$	$\rho = 0.8$	Lower Bound
16	0.04603	0.04604	0.04474	0.04233	0.03854	0.03298	0.0242
17	0.01759	0.01760	0.01738	0.01686	0.01588	0.01417	0.01038
18	0.00749	0.00749	0.00743	0.00728	0.00693	0.00623	0.00297
19	0.00316	0.00317	0.00315	0.00310	0.00298	0.00270	0.00183
20	0.00133	0.00134	0.00132	0.00131	0.00127	0.00116	0.00076

**Table 2.3.5 Probability of Encounter, with Bounds for
Southern Route in North Pacific**

It is seen from Tables 2.3.2 to 2.3.5 that the effect of changes in the correlation coefficient has a relatively small impact on the encounter probabilities. It is also apparent that the upper and lower bounds on the probabilities of encounter are very close to the value obtained as a function of the correlation coefficient ρ, when $\rho = 0$ and $\rho = 0.8$, respectively.

Summary and Discussion:

A procedure has been developed for estimating ship/storm encounter probabilities which can be used as a basis for formulating design criteria. The encounter probabilities provide better and more meaningful criteria for design than wave return periods, since they involve the life of the structure as well as the wave statistics in the region of operation.

The encounter probabilities in any specific ocean zone were first determined as a function of the operation time in the zone, as well as the return period. The return period depends on the selected wave height. The overall encounter probability for a ship along any

given route was modeled as a "system probability" and first-order bounds were determined. In addition, the encounter probability as a function of the correlation coefficient of wave conditions in the different zones was determined assuming equal correlation coefficients between zones. The developed procedure has been applied to four ship routes, two in the Atlantic and two in the Pacific Ocean.

ENCOUNTER PROBABILITIES $\rho = 0.6$				
	North Atlantic		North Pacific	
H1/3	Northern Route	Southern Route	Northern Route	Southern Route
16	0.65415	0.22573	0.82351	0.03854
17	0.40353	0.11209	0.59422	0.01588
18	0.13524	0.05903	0.38211	0.00693
19	0.05769	0.02736	0.22849	0.00298
20	0.05921	0.01220	0.13077	0.00127

Table 2.3.6 Encounter Probabilities for All Routes and Design Waves

Table 2.3.6 shows the probabilities of a ship encountering sea states characterized by significant wave heights of 16, 17, 18, 19, and 20 meters for each of the four routes considered. It is interesting to note that if a probability of encounter not to exceed 0.059 is selected as a criterion to determine the "design" sea state, and if the ship is to operate a Northern route in the North Atlantic, then it is seen from Table 2.3.6 that a design significant wave height of 20 meters results. If the ship is to operate in a Southern route of the North Atlantic, the design significant wave height, as seen from the table, is 18 meters. In the Northern and Southern routes of the Pacific, the resulting design sea states that meet the encounter criterion are over 20 meters and slightly over 16 meters, respectively. The results in Table 2.3.6 pertain to a correlation coefficient equal to 0.6. The encounter probabilities presented in Tables 2.3.2 to 2.3.6 do not account for any attempt at avoiding bad weather conditions, either through weather forecasting, or maneuvering. The effects of such avoidance techniques would be to reduce the encounter probability in each zone P_{e_i} and hence, lower the overall encounter probability.

These results indicate a clear dependence of design sea state on the operation route of a ship as well as the ocean. The results also raise the question of whether or not classification societies should adopt different standards for different ship routes and oceans, assuming that the ship operation will not deviate from the "design route." A problem may arise, however, if a ship operator requires a different route where more severe weather is expected to be encountered. It may be, therefore, more prudent to base the rules on a route that results in the most severe weather condition for unrestricted service, and to change (increase) the allowable

stillwater bending moment if the ship operates along a route where the weather is expected to be less severe.

Nomenclature

A_i = Event of no encounter for zone i

$F_{X_i}(x)$ = Distribution function of individual wave heights in zone i

$F_{Y_i}(x)$ = Distribution for annual maximum in zone i

i = suffix used to denote any zone in the ocean

k_i = Annual number of wave peaks or cycles in zone i

L = Life of structure in years

L_i = Portion of structure life spent in zone i

n_i = Expected number of waves in zone i necessary to exceed wave height x

n_0 = Total number of wave data collected in zone i

n = Number of zones in a ship route

P_e = Probability of encounter

P_{e_i} = Probability of encounter of a certain design wave in a particular ocean zone i

P_{ne} = Probability of non-encounter

P_{ne_i} = Probability of non-encounter of a certain design wave in a particular ocean zone i

R_i = Return period, in years, for a wave in zone i

w = Waiting period, in years, between exceedence

y_0 = Number of years of data collection in zone i

x = Wave height

β = Safety index

ρ = Correlation coefficient

Φ = Standard Gaussian cumulative distribution function

φ = Standard Gaussian density function

2-122

(This page intentionally left blank)

Data and Linear Regression for North Atlantic

ZONE 8

$Y = 1.45x - 1.33$

ZONE 9

$Y = 1.28x - 1.35$

ZONE 10

ZONE 11

ZONE 23

ZONE 24

ZONE 25

Y-axis: ln ln (1/ (1 – F(x – m)))

X-axis: ln (x - m)

■ Data

—— Y = 1.28x -1.05
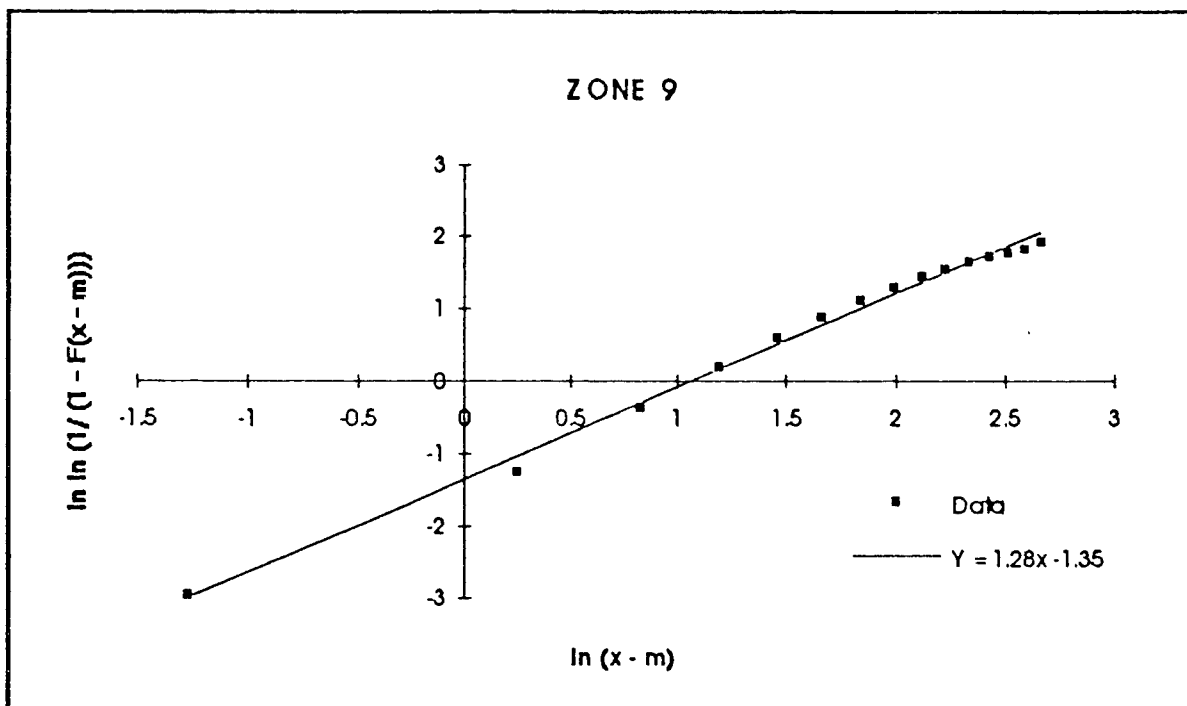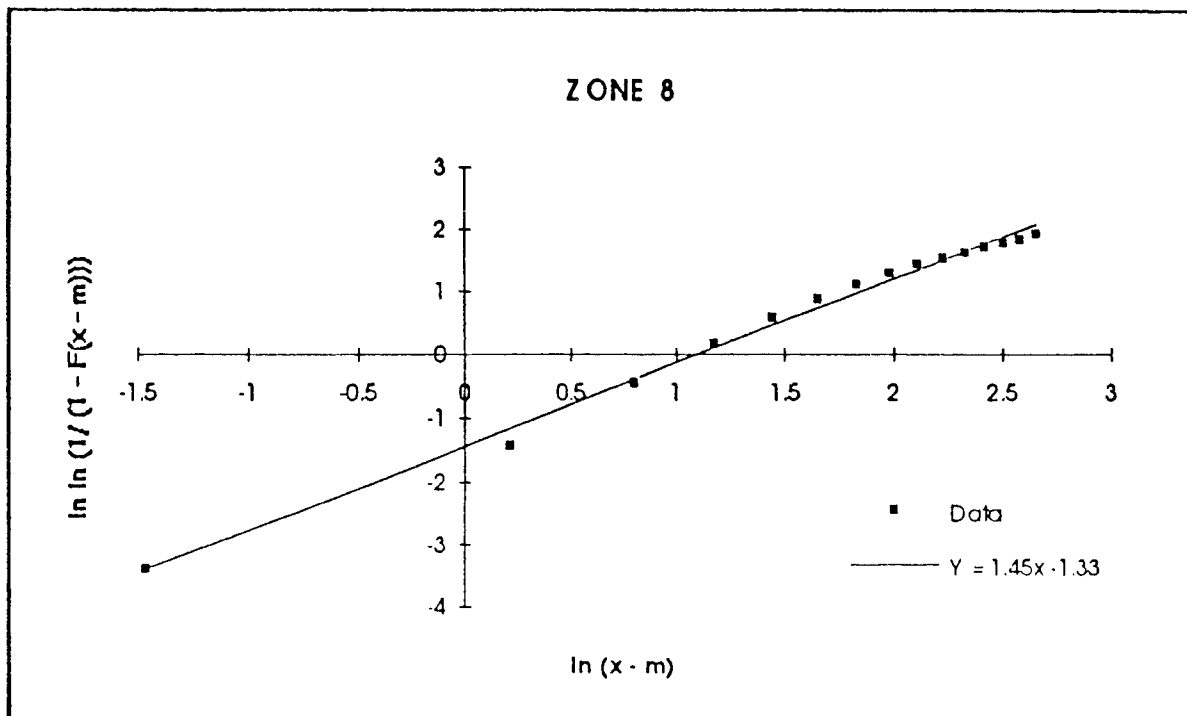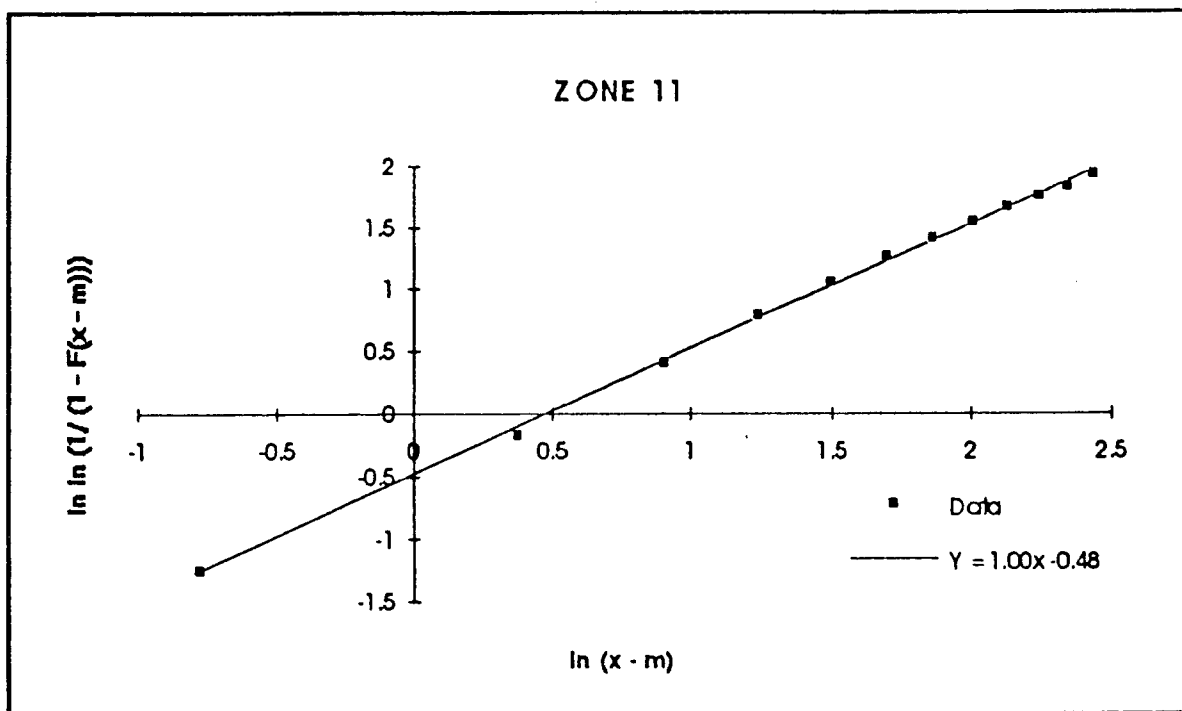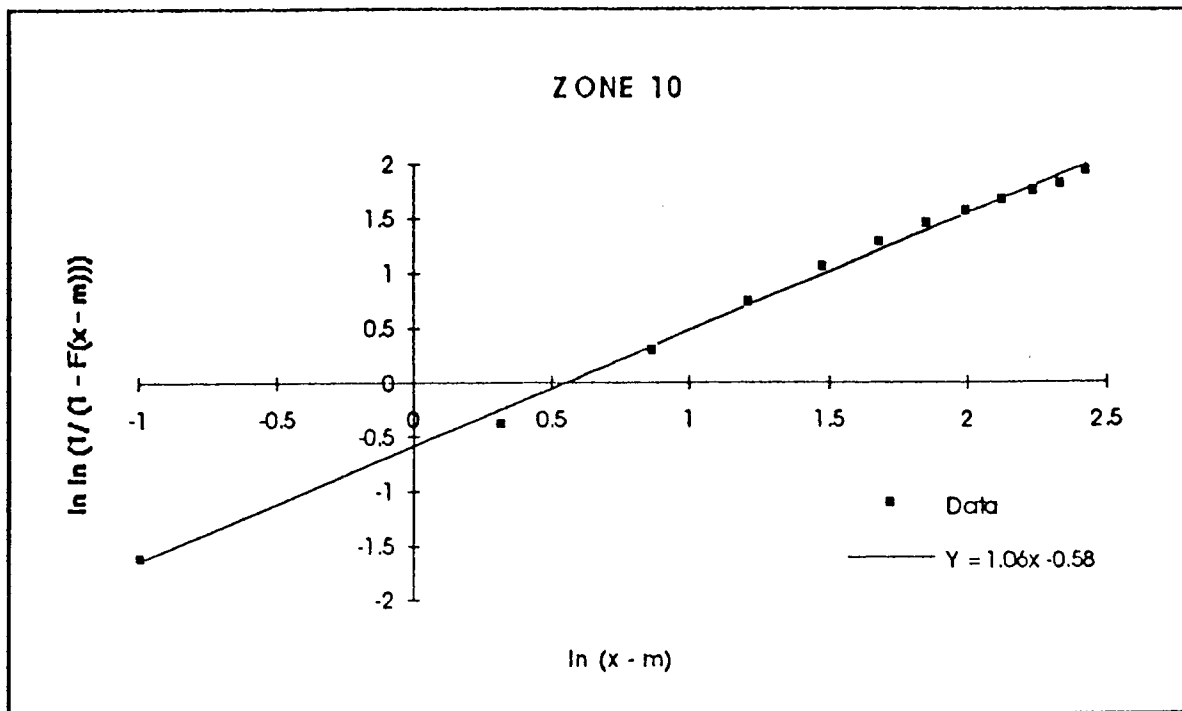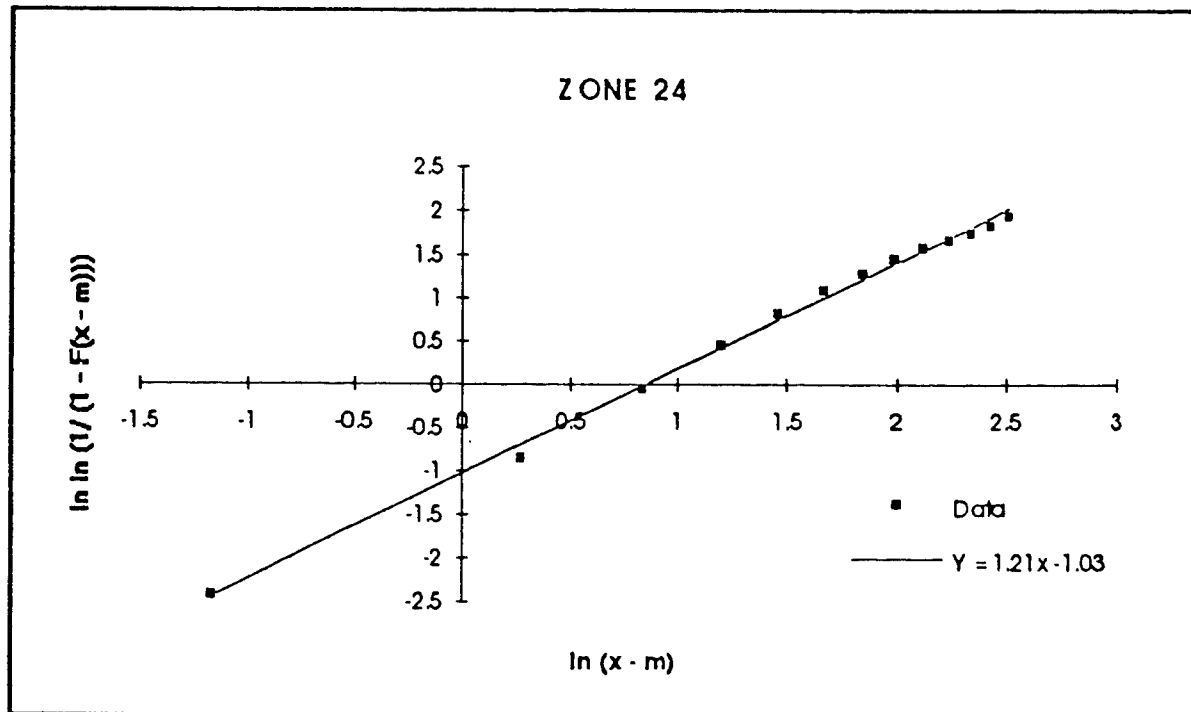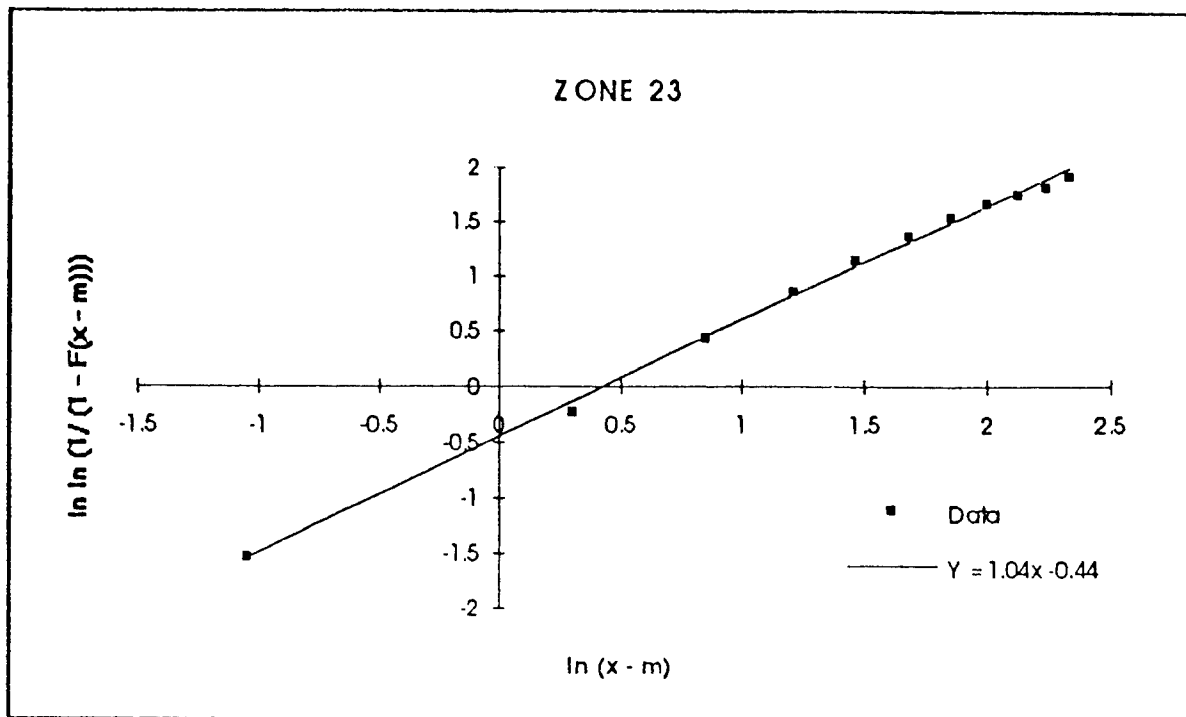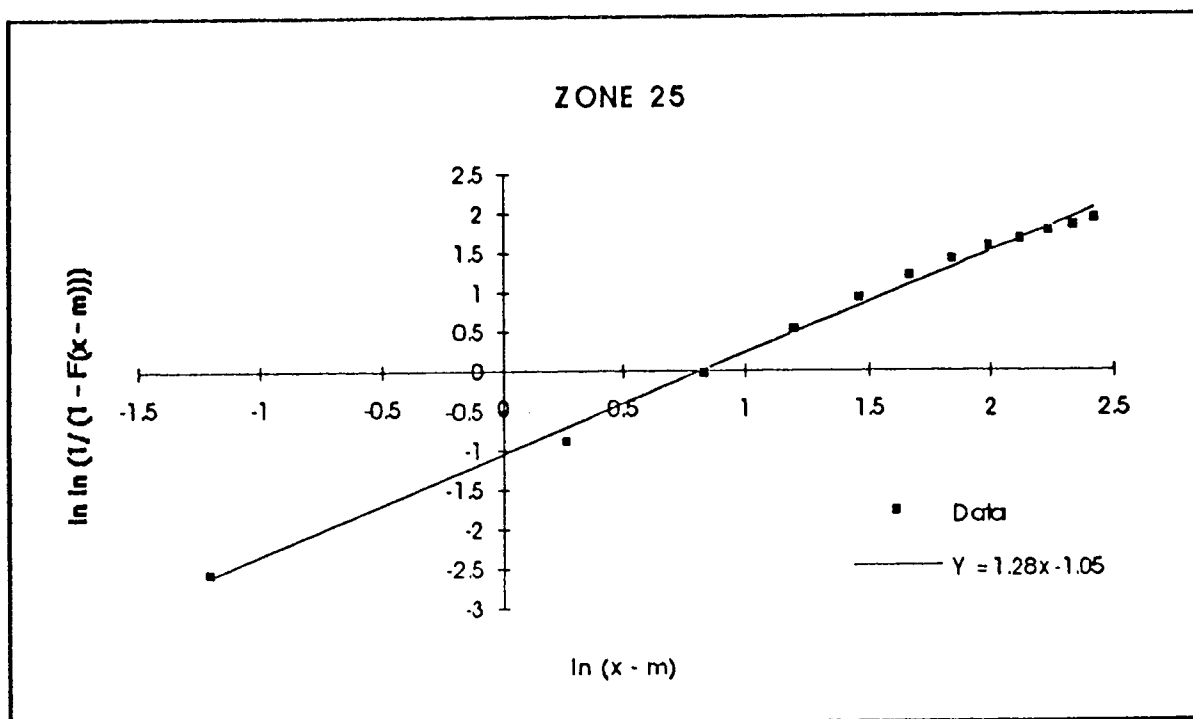
Data and Linear Regression for Zones in the Pacific

ZONE 13

ZONE 14

ZONE 20

ln ln (1 / (1 − F(x − m)))

ln (x − m)

Data

Y = 1.13x − 0.99

ZONE 21

ln ln (1 / (1 − F(x − m)))

ln (x − m)

Data

Y = 1.36x − 1.14

ZONE 22

Y = 1.20x - 0.05

ZONE 29

Y = 1.00x - 0.47

ZONE 30

Data

Y = 1.28x - 1.19

ZONE 31

Data

Y = 1.35x - 0.80

ZONE 43
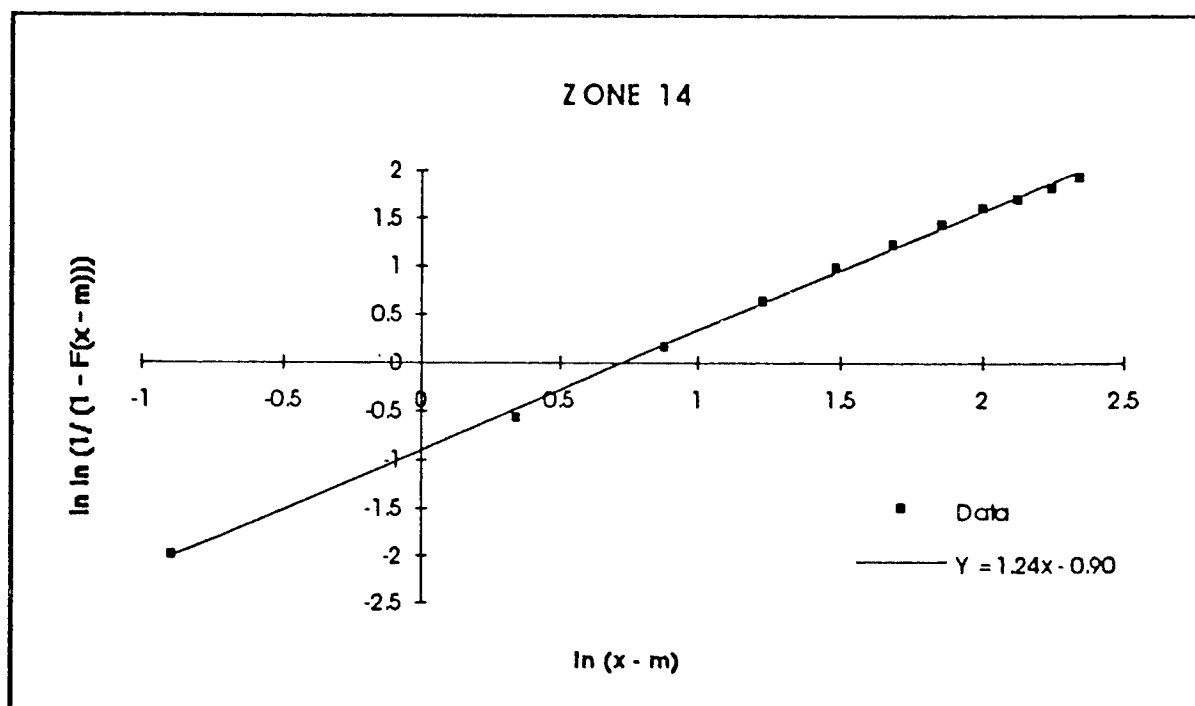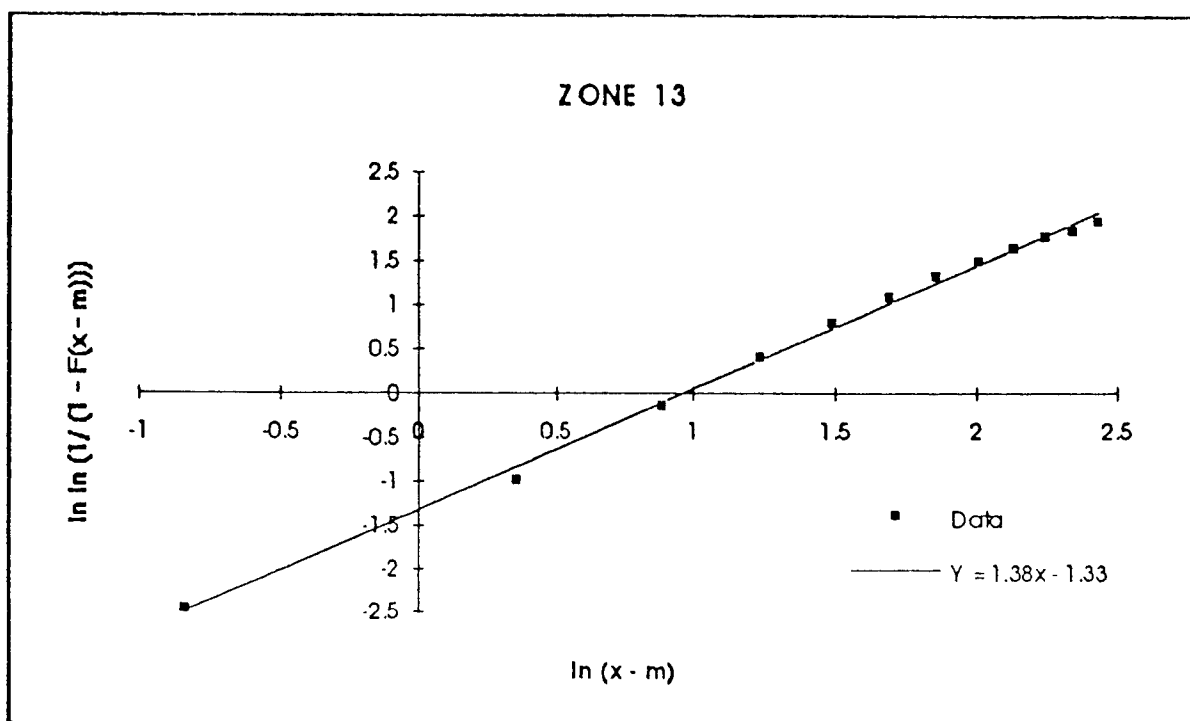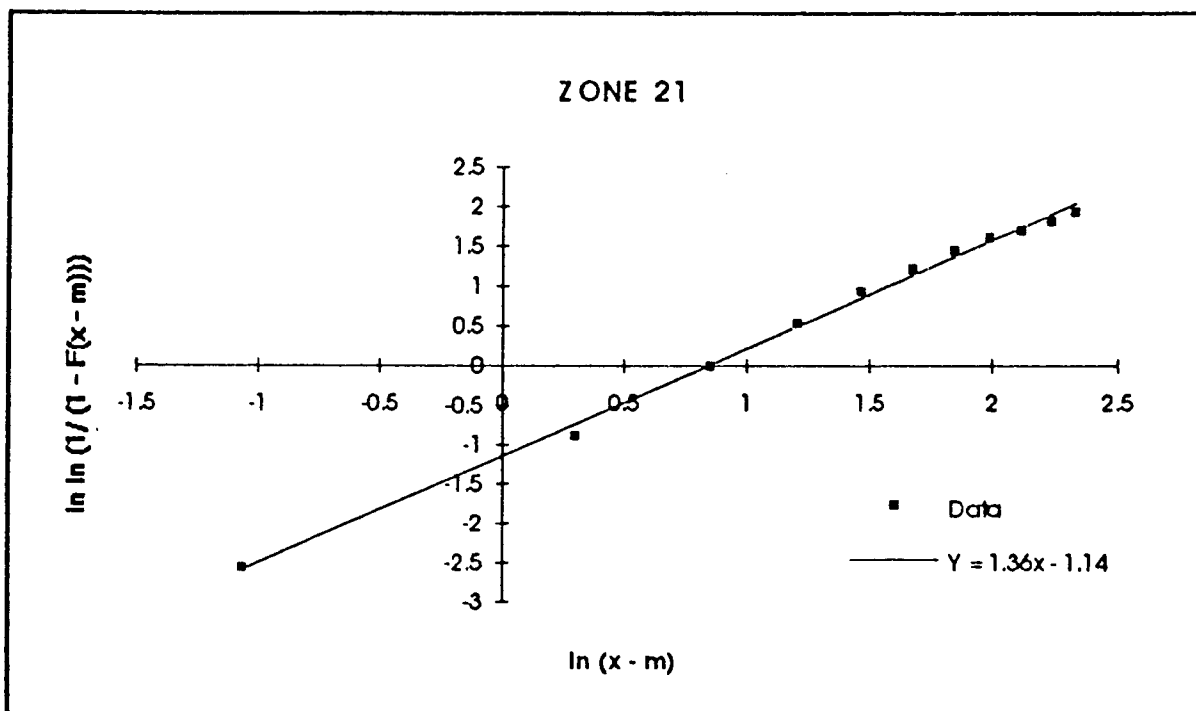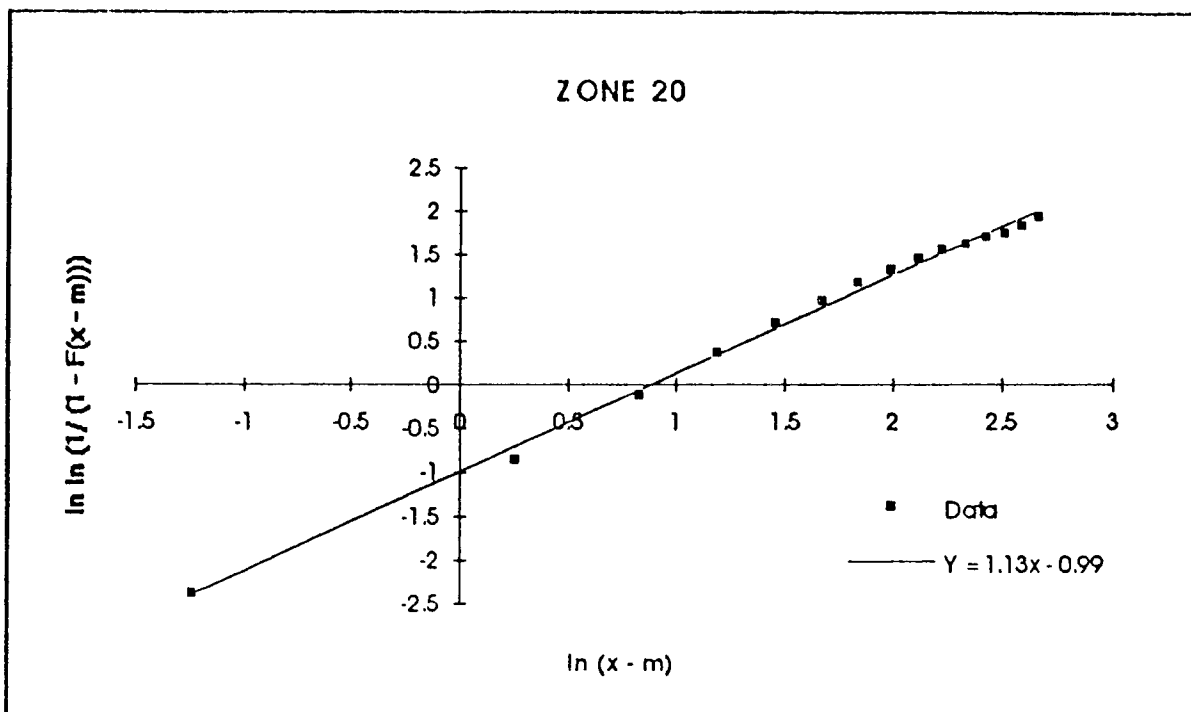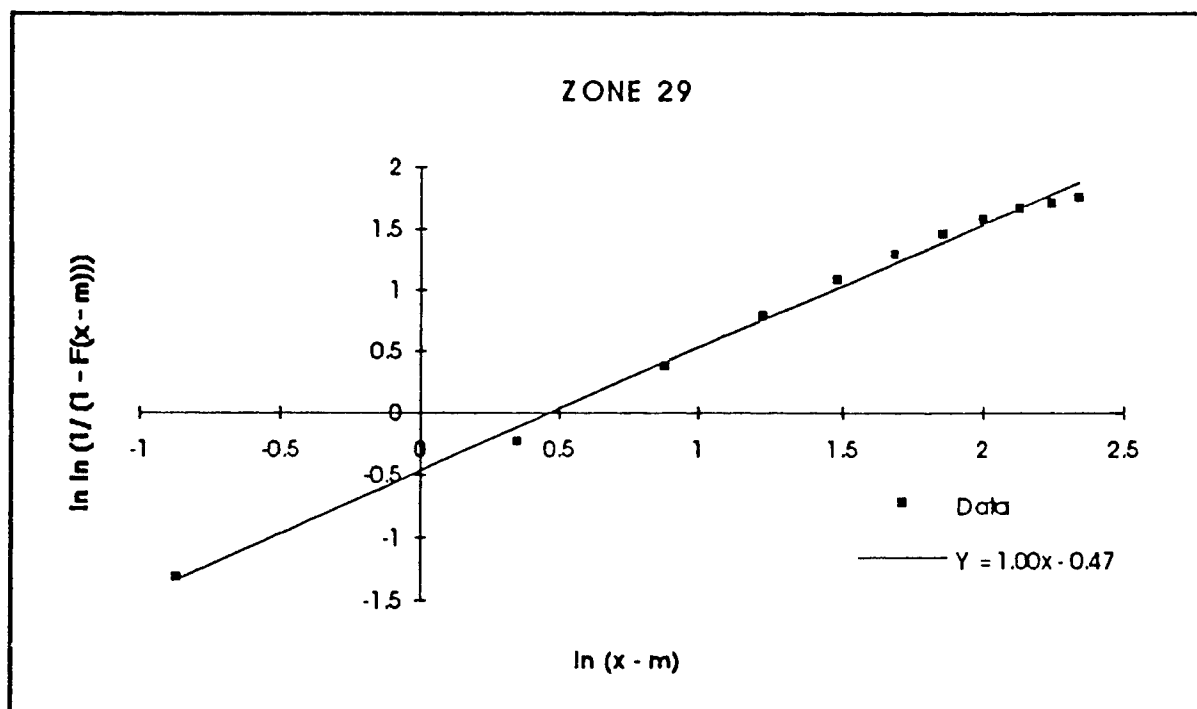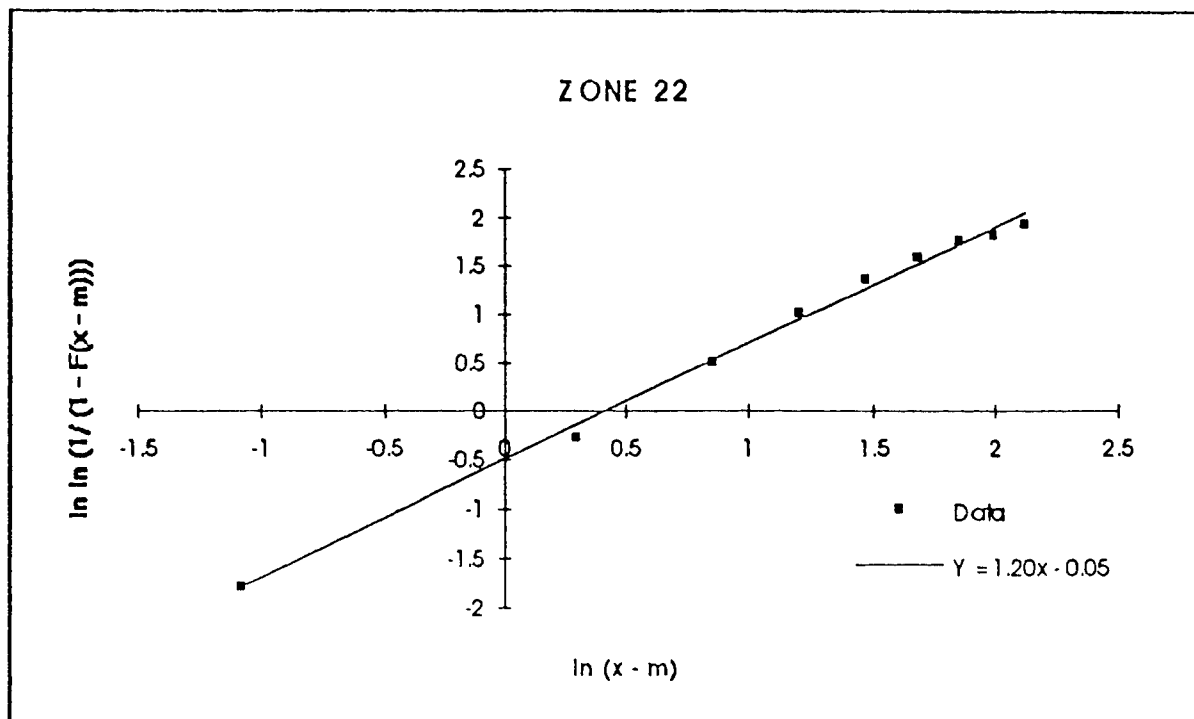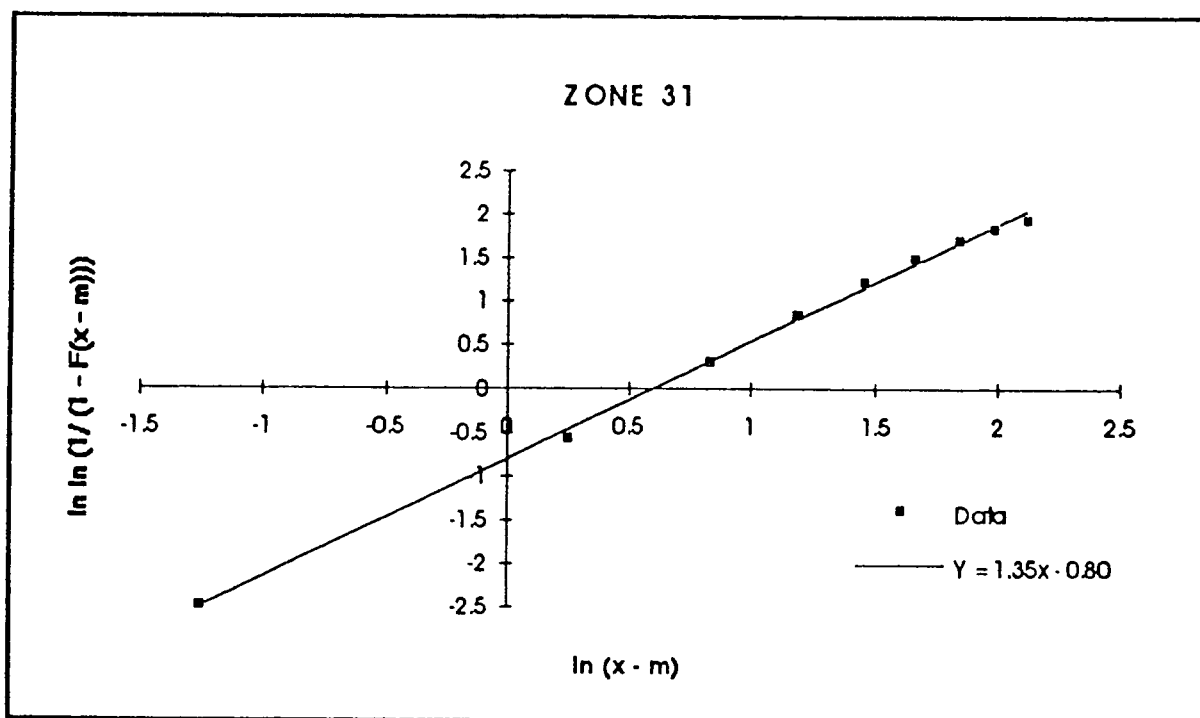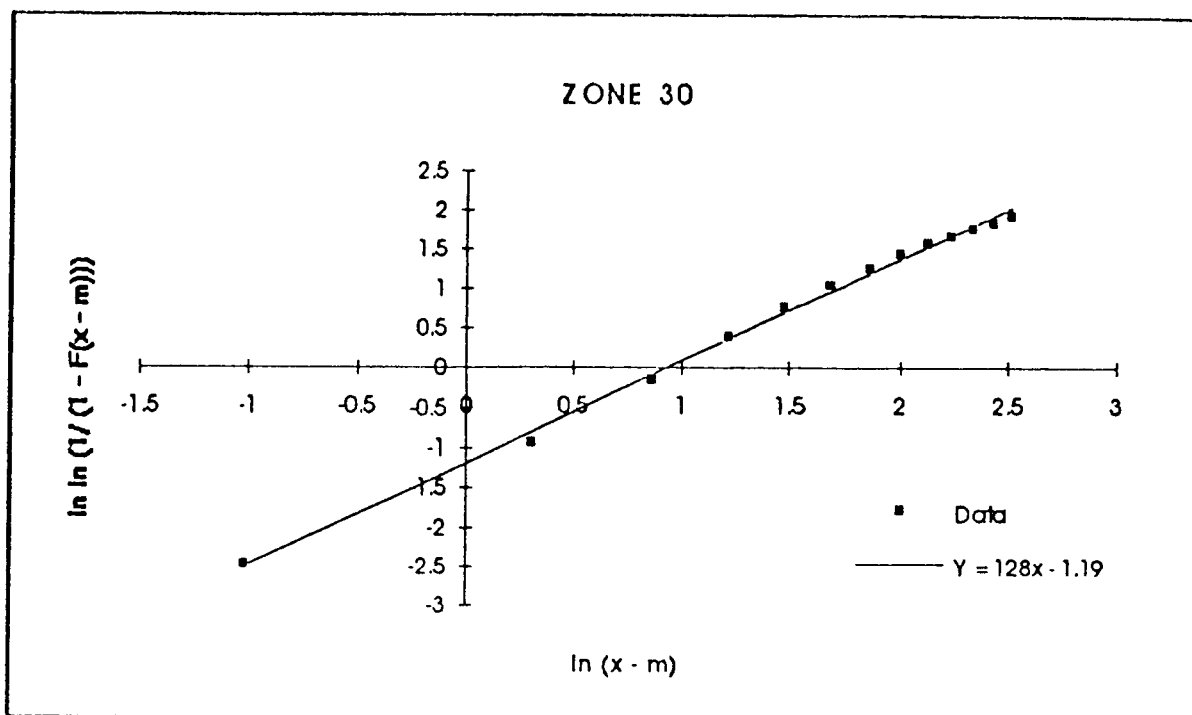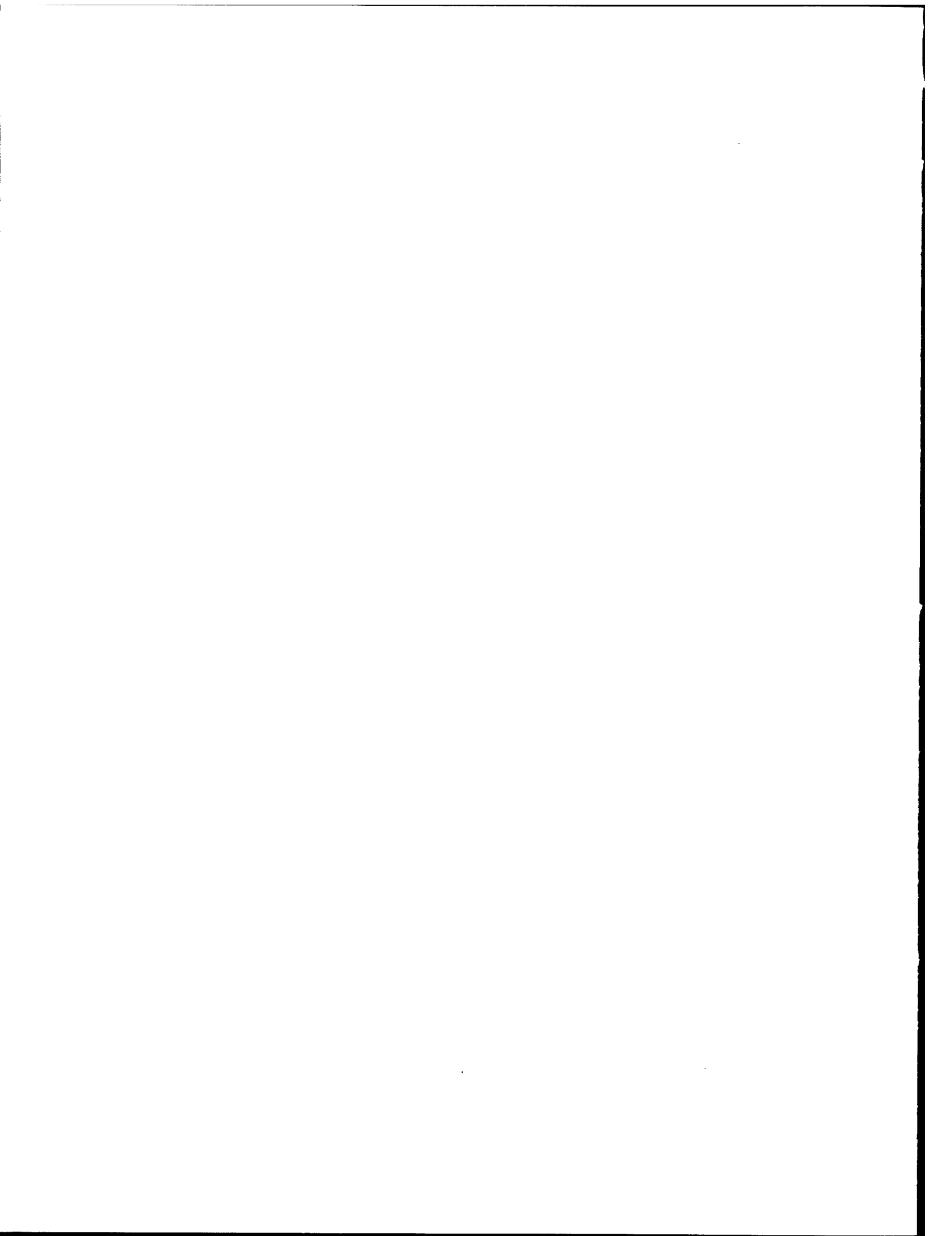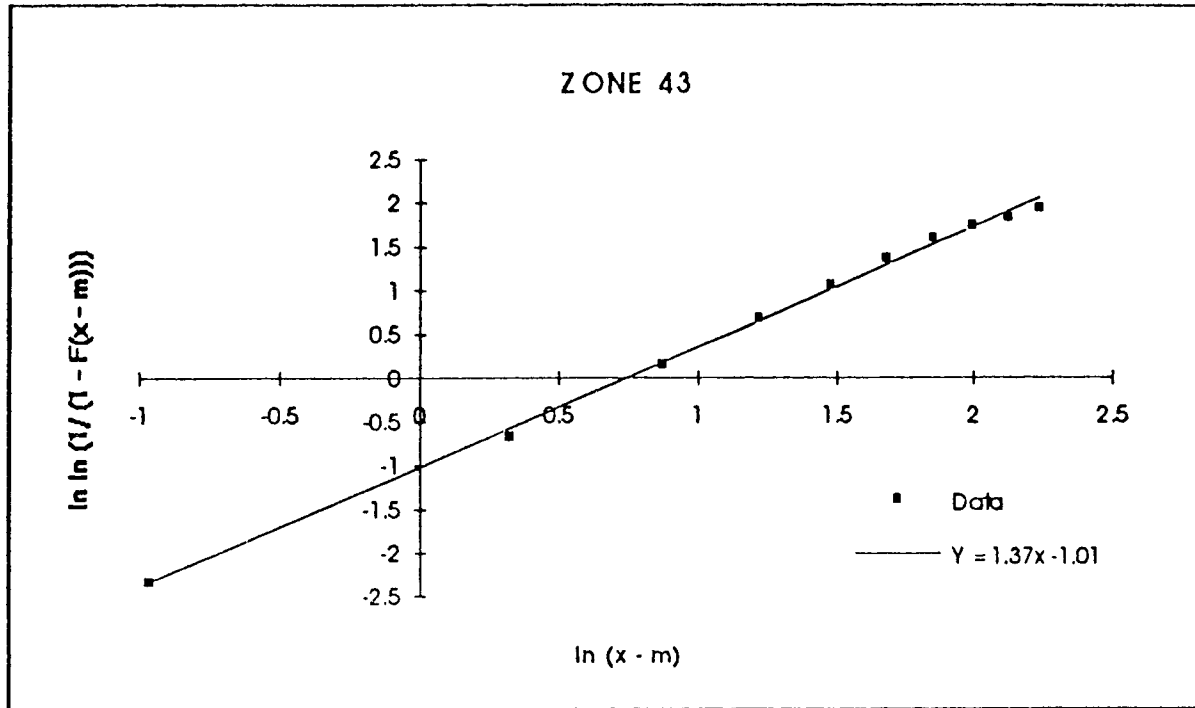
2.3.3 Long-Term Procedure:

In general, the long-term procedure entails the determination of the probability distribution of the maximum load during the lifetime of a ship taking into consideration the wave statistics along the ship route, loading conditions, speed, and heading. The procedure is particularly important for fatigue reliability analysis, where the entire history of loading should be determined. In that case (fatigue), the long-term distribution, instead of the maximum load distribution, is required and is usually assumed to be Weibull.

Several procedures have been proposed in the literature for determination of the lifetime maximum load distribution. Although their details may vary (sometimes depending on the ship type), most of them have common characteristics as follows:

1. Define the mission profile of the ship which includes

   a. Ship route

   b. Expected total years of service

   c. Number of days per year the ship is expected to be at port and underway

   d. Nominal cruising speed and maximum operating speed in each sea state, and the corresponding fraction of time during operation

   e. Distribution of ship headings

   f. Distribution of loading conditions

2. From the ship route and available wave statistics, obtain the frequency of occurrence of different sea conditions the ship will encounter in each of the geographic areas* (zones).

3. From Step 2 above and the mission profile of the ship, determine the frequency of encountering different sea conditions, loading conditions, speeds, and headings.

4. Determine the wave loads in each sea condition, loading condition, speed, and heading, using first- or second-order strip theory.

5. Use an extrapolation procedure to determine the distribution of the maximum load in a lifetime.

The details of two long-term procesures are described next.

A - Procedure Proposed in SR-1337 (SSC 373):

a - Long-Term Distribution of the Total Stress Including Stillwater Load:

The long-term distribution of the total stress (wave induced stress considering all wave peaks, and the long-term stillwater stress) is obtained as follows.

Consider that there are $i = 1,...,n_c$ loading conditions and $j = 1, ...,n_{SS}$ sea states during the vessel life. Also consider that the combined wave and slam stress amplitude for a sea state j, whose cumulative distribution function (CDF) is denoted F_{X_j}, is independent of the stillwater stress, which has a long-term density $F_{ST_i}(x)$ for the loading condition i. The probabilities of occurrence of the sea states and loading conditions are denoted P_{SS_j} and P_{ST_i}, respectively. The probabilities are such that

$$\sum_{j=1}^{n_{SS}} P_{SS_j} = 1$$

$$\sum_{i=1}^{n_c} P_{ST_i} = 1$$

The cumulative distribution function of the combined wave induced and slamming stress, considering all sea states, is given, for any loading condition, by

$$F_x'(r) = \sum_{j=1}^{n_{SS}} P_{SS_j} F_{X_j}(r) \tag{2.3.26}$$

---

* In almost all the main areas where ships operate, statistical data concerning wave heights and periods have been observed and tabulated. The surface of the earth is divided into a grid of ten-degree squares, known as Marsden squares. These squares are arranged into geographic areas over which wave conditions are fairly uniform. The areas are given a code number; see, for example, Hegben *et al.* (1986).

where the F_{X_j} are the individual CDFs of combined wave plus slam effects. For any particular loading condition, the CDF of the long-term total stress, consisting of the stillwater stress and the wave induced and slam effects, is then obtained by applying the convolution theorem:

$$F'_{T_i}(r) = \int_{-\infty}^{\infty} F'_X(r-x) \, f_{ST_i}(x) \, dx \qquad (2.3.27)$$

b - Extreme Value Distribution of the Total Stress:

The cumulative distribution function of the largest value of stress in a particular loading condition i can be obtained using the Ferry Borges and Castenhata model (1972), with pulse times representing voyages in that loading condition. The Ferry Borges process consists of pulses of uniform duration. In the present case, the duration of the pulses can be taken to be the average duration of a voyage in the loading condition i (e.g., laden or ballast). Knowing the average duration, t_i, one can obtain the number of pulses in the lifetime:

$$n_i = \frac{T_i}{t_i} \qquad (2.3.28)$$

where T_i is the total time spent in the loading condition i.

The cumulative distribution of the largest value of the total stress is then obtained as

$$F_{T_E}(r) = \sum_{i=1}^{n_c} \left[F'_{T_i}(r) \right]^{n_i} \cdot P_{ST_i} \qquad (2.3.29)$$

which assumes the likely total stress pulses in the individual voyages in a loading condition to be independent of one another. "r" represents the largest value of the total stress. The total number of loading conditions considered is n_c. Typically, n_c is a small number, e.g., 2, representing, say, laden and ballast conditions.

B - Long-Term Procedure Used in the SOST Code:

The long-term analysis is concerned with the probability distribution of the extreme peaks taken over a period of typically 10-20 years. The basic assumption in the analysis is that the process can be modelled as a sequence of stationary processes with independent peaks. Thereby, the probability of exceedence

$$Q(M_p(T)) = P(\max_T M_p > \zeta)$$

$$= 1 - \prod_{i=1}^{p} \exp(-v_i(\zeta)T_i)$$

$$= 1 - \prod_{i=1}^{p} \exp\left(-v_{0i} e^{-1/2 u_i^2(\zeta)} fs_i T\right)$$

$$= 1 - \exp\left(-T \sum_{i=1}^{p} v_{0i} \, fs_i e^{-1/2 u_i^2(\zeta)}\right)$$

where $Q(M_p(T))$ is the probability that individual peak values M_p of M exceed a level ζ during duration T, v_{0i} is the zero upcrossing rate, and $v_i(\zeta)$ is the upcrossing rate of level ζ. The number of different stationary conditions, characterized by fixed values of significant wave height H_s, zero crossing period T_z, forward speed V and heading angle ϕ, is denoted by p and the time spent in the ith stationary conditions by T_i. This period constitutes the fraction fs_i of the total time T. Thus, specification of

$$S_i \equiv \{H_s, T_z, V, \phi, fs\}_i \quad ; \quad i = 1,2,...,p$$

together with calculation of

$$v_{0i} \equiv v_0(S_i)$$
$$u_i(\zeta) = u(\zeta \mid S_i)$$

yields the long-term probability of exceedence (see Jensen and Dogliani, 1993 for more details).

The fraction fs of time spent in a specific stationary condition is taken as

$$fs = f_M(H_s, T_z) f_V(V \mid H_s) f_\phi(\phi)$$

where $f_M(H_s, T_z)$ is the joint density function of H_s and T_z and can be calculated from the operational profile covering a number n of Marsden zones,

$$f_M(H_s, T_z) = \sum_{j=1}^{n} P_j f_{Mj}(H_s, T_z)$$

The operational profile is thus characterized by the fraction P_j of time the ship is in Marsden zone j; $j = 1,2,...,n$. Directionality in the sea states as well as annual variations are not included in the above equation.

In severe sea-states, the ship's master usually reduces the speed in order to avoid excessive slamming and green water on deck. Therefore, the fraction f_V defining the use of the two forward speeds is made dependent on the significant wave heights H_s

$$f_v(V = V_{max} \mid H_s) = \begin{cases} f_{max} & \text{if } H_s \leq H_{s0} \\ 1 - f_{min} & \text{if } H_s > H_{s0} \end{cases}$$

$$f_v(V = V_{min} \mid H_s) = 1 - f_v(V = V_{max} \mid H_s)$$

where f_{max}, f_{min} and H_{s0} are to be specified. Finally, the fraction f_ϕ for the different headings are chosen as

$$f_\phi = \{p_0, p_{45}, p_{90}, p_{135}, p_{180}\}$$

with either

$$p_0 = p_{45} = p_{90} = p_{135} = p_{180}$$

or

$$p_0 = p_{45} = p_{90} = 3p_{135} = 3p_{180}$$

2.3.4   Estimation of Ship Failure Probabilities:

Literature on ship structure risk assessment is extensive and dates back to the early seventies (e.g., Mansour, *SNAME Trans.*, 1972, and *J. Ship Research*, 1972). There have been a number of investigations that were built on this earlier work. Particular mention may be made to Stiansen et al. (*The Naval Architect Journal*, *RINA*, 1980), Mansour and Faulkner (*Trans. RINA*, 1973), Faulkner and Sadden (*RINA*, 1979), and White and Ayyub (*Naval Eng. Journal*, 1985). The ship Structure Committee (SSC) has sponsored several projects related to this area, e.g., Kaplan *et al.* (1983), Daidola and Baser (1983), and Mansour (SR-1310, 1990). In addition, the SSC projects SR-1330 on "Probability-Based Ship Design Procedures: A Demonstration" and SR-1337 on "Loads and Load Combinations" have been completed and published in SSC 368 and SSC 373, respectively. A complete literature survey and summary of reliability methods for ship structures are included in SSC-351 "An Introduction to Structural Reliability Theory Directed at the Marine Industry."

Specific research in the area of code development has also been carried out by the American Bureau of Shipping (ABS) researchers, e.g., reported in *Trans. SNAME* (1984). An in-depth evaluation of uncertainties in hull strength prediction was conducted by Soares and Moan (1985), and application of first order second moment method to ship hull ultimate strength, including plastification, buckling, fatigue, and fracture, was undertaken by ABS (e.g., Thayamballi, et al., 1984, 1986, 1990). Wirsching and Chen (1988) applied reliability methods to marine structures. Some of the work is equally valid for ships, albeit with different values for the uncertainty parameters.

2.3.4.1 *Generalized Reliability Concept*:

The basic reliability concept demonstrated in Section 2.3.1 can be generalized to include several random variables instead of just two. In this case, eqn. (2.3.2) can be written in a general form as:

$$P_f = \int_F f_X(x)\,dx \qquad (2.3.30)$$

where

X = vector of random variables

$f_X(x)$ = joint probability density function

F = failure domain, defined by

$$F \equiv \{g(x) < 0\} \qquad (2.3.31)$$

where $g(\cdot)$ are limit state functions.

And, from the computed failure probability, the generalized safety index is defined by

$$\beta = \Phi^{-1}(1 - P_f) \qquad (2.3.32)$$

where $\Phi(\cdot)$ denotes the standard normal cumulative distribution function.

There are several reliability methods that can be used to solve the above equations. For example, there are four methods utilized by CALREL (Liu *et al.*, 1989) to compute the above quantities:

1. FORM: First-order reliability method. The limit state surfaces ($g(x) = 0$) are replaced by tangent hyperplanes at design points in a transformed standard normal space

2. SORM: Second-order reliability method. The limit state surfaces are replaced quadratic fitted at the design points in the standard normal space

3. Directional simulation method with exact or approximate surfaces

4. Monte Carlo simulation method

Reliability Methods:

Table 2.3.8 summarizes the different reliability methods that may be used for estimating the probability of failure. The following gives an historical review of some of these methods.

Mean Value First Order Second Moment Analysis:

The first serious attempt to apply probabilistic methods to the develoment of a design code was made by Allin Cornell. In 1969, he proposed the mean value first order second moment (MVFOSM) concept. Limit state functions that are "complicated" can be represented by the first terms of a Taylor's series expansion. The mean and standard deviation of the limit state function can be approximated, and the safety index is defined as the quotient of these two terms.

Analytical Methods
1. Mean Value First Order Second Moment (MVFOSM)
2. Hasofer-Lind generalized safety index
3. First Order Reliability Methods (FORM
a. Limit states represented by tangent hyperplanes at design points in transformed standard normal space
b. Rackwitz-Fiessler algorithm
4. Second Order Reliability Methods (SORM)
a. Limit states represented by hyperparaboloids at design points in transformed standard normal space
b. Wu/FPI
5. Advanced Mean Value (AMV) method

Monte Carlo Simulation
1. Direct Monte Carlo
2. Importance Sampling
3. Domain Restricted Sampling
4. Adaptive Sampling
5. Directional Sampling

Table 2.3.8 A Summary of Reliability Methods

While the concepts were employed to derive probability-based design requirements for the code of the American Concrete Institute, it was discovered that reliability estimates depended upon the mechanical formulation of the limit state function. This "mathematical" difficulty was later overcome by the Hasofer-Lind generalized safety index.

MVFOSM continues to be useful in providing "quick and dirty" estimates of the safety index for components.

The Generalized Safety Index:

In 1973, the lack of invariance problem associated with MVFOSM analysis was solved in a paper by Hasofer and Lind (1974). The scheme was to transform all of the basic variables to reduced variables having zero mean and standard deviation of unity (by subtracting from the variable its mean then dividing by its standard deviation). The safety index is then defined as the minimum distance from the origin of the reduced coordinates to the limit state function in reduced coordinates. This measure of reliability was proved to be

independent of the mechanical formulation of the subsequent development of structural reliability estimates for components. All of the other methods of fast probability integration described in the following essentially are refinements of the Hasofer-Lind safety index concept.

First Order Reliability Methods (FORM):

The Hasofer-Lind analysis requires that only the mean and standard deviation of each variable be considered and, therefore, ignores distributional information, even if it is available. A method proposed by Paloheimo and Hannus (1974) suggests that non-normal distributions be transformed into standard normals (by requiring that the distribution functions of the basic variable and the standard normal variate be equal). Then the generalized safety concept is applied in the space of standard normal variates. A decent estimate of the probability of failure can be made by the inverse standard normal distribution function of the safety index.

Later, the Rackwitz-Fiessler algorithm was proposed as an efficient computational method for FORM (1978). And, and additional refinement of this procesure, the Chen-Lind algorithm, was proposed (1983). But both schemes produce errors in probability of failure estimates in some (uncommon) problems. And, it is difficult to predict *a priori* the expected errors in probability estimates. This problem has led to the development of second order reliability analysis.

Second Order Reliability Analysis (SORM):

It was found that FORM produces errors whose magnitudes are difficult to predict in advance. This observation led to the development of SORM methods. A number of SORM algorithms have been proposed by Ditlevsen (1979), Fiessler, Neumann, and Rackwitz (1979), Tvedt (1983), and Breitung (1984). These methods rely on the FORM transformation into standard normal space. Wu (1984) has proposed a method (called the Wu/FPI algorithm) that, it is argued, is more robust and accurate because it avoids some of the mathematical pitfalls associated with transformation to standard normal space. It has been demonstrated that Wu/FPI can consistently produce point probability estimates with 5% of the exact value.

Advanced Mean Value (AMV) Method:

A practical limitation on FORM and SORM, as described above, is that the limit state function must have an explicit closed form. But there are many cases where a reliability analysis is required and the variables are related only through a numerical algorithm, e.g., finite element analysis. A very efficient numerical algorithm has been developed, also by Wu (1990), for dealing with these complex problems. The AMV method is the "heart" of a probabilistic finite element code (NESSUS) developed for NASA to solve complicated design problems associated with space propulsion systems.

Efficient Monte Carlo Simulation:

As computer capabilities have increased and computer costs have decreased, Monte Carlo simulation for structural reliability analysis has gained new respectability. It has also helped that efficient methods, principally importance sampling, have been developed. The importance sampling concept has been discussed by Shinozuka (1983). Variations on the basic importance sampling concept have been proposed. These include domain restricted sampling by Harbitz (1986), directional sampling by Bjerager (1990), and adaptive sampling by Bucher (1988). In summary, these methods can produce probability of failure estimates having narrow confidence intervals for small sample sizes. The bad news is that (a) all require an estimate of the probability of failure, and (b) their efficiency sharply decreases as the number of variables increase.

2.3.4.2 *Computer Codes for Probability of Failure Calculations:*

The literature search identified algorithms, of various levels of sophistication, that would be appropriate for ship structure reliability analysis. These are:

CALREL

This is a general purpose structural reliability analysis program. Its capabilities include: (a) probability of failure estimates for components, (b) probability of failure estimates for systems, (c) FORM and SORM analysis, (d) direct Monte Carlo analysis and directional simulation, and (e) sensitivity analysis (see Appendix C for detail).

COMPASS

This code is developed, maintained, and marketed by Martec Limited, Canada. It is a general-purpose software reliability analysis program.

PROBAN

PROBAN, developed and marketed by Det norske Veritas, is a general structural reliability analysis code. It is more sophisticated than CALREL, and it is also much more expensive (see Appendix C).

RELACS

RELACS was developed and is distributed by Risk Engineering, Inc., of Golden, CO. This program, also sophisticated and expensive, is intended to be a competitor to PROBAN.

University of Arizona Software

There are a number of small programs that are likely to be useful in performing reliability analysis. These include: (a) DISTS; determines which of several competing statistical distributions best fits a set of data; (b) POFAIL; produces exact probability of failure calculations for a limit state with only two random variables; (c) RACA; computes

safety index and probability of failure using the Hasofer-Lind, Chen-Lind, or Rackwitz-Fiessler algorithms, and (d) Wu/FPI; computes the safety index and probability of failure using second order reliability analysis. The Wu/FPI can be conveniently combined with a limit state analysis program (e.g., finite element program) to execute the Advanced Mean Value Method.

ABS

This is a general-purpose structural reliability program. Its capabilities include computation of probabilities of failure for components based on first order reliability method (FORM).

NESSUS

The NESSUS code was developed at Southwest Research Institute under contract with NASA/Lewis to produce a probabilistic structural analysis code having both nonlinear structural behavior and dynamic response capabilities. This code, having all of the reliability features of CALREL, is linked to a structural analysis (finite element) program. The "heart" of the NESSUS code is the Advanced Mean Value (AMV) reliability algorithm that allows fast reliability analysis of complicated structural systems. It has a simulation capability using adaptive sampling (see Appendix C).

CALREL and the University of Arizona software have been used for the advanced reliability analysis required in this project.

Capabilities of CALREL (Liu, et al., 1989):

- The capabilities of CALREL include:

1. First order reliability analysis (FORM)

2. Second order reliability analysis (SORM)

3. Monte Carlo simulation

4. Directional simulation (efficient Monte Carlo)

5. Computes sensitivity factors

6. Performs system reliability analysis using the failure mode approach

7. CALREL can be used to implement the advanced mean value (AMV) when a computer code is needed to relate the design variables.

- Features of CALREL include:

1. Cheap relative to its capabilities

2. Efficient

3. Easy to use

4. Runs on a PC

The manual of CALREL (see Liu, et al., 1989) indicates that FORM and SORM are applicable to component reliability analysis. FORM is applicable to series system reliability, directional simulation in conjunction with FORM or SORM is applicable to component or system reliability analysis, and Monte Carlo simulation is applicable to all classes of problems. CALREL has a modular structure with each group of analysis routines contained in a separate module. To run CALREL, it is necessary to compile the user-defined subroutines UGFUN, UDGX and UDD, and link them with the object modules of CALREL.

CALREL has a large library of probability distributions (see Liu *et al.*, 1989) that can be used for independent as well as dependent random variables. Table 2.3.9 lists the probability distributions that are currently available. These distributions can be used both as marginal and conditional. Additional distributions can be included through a user-defined subroutine, UDD.

1. normal	2. log normal	3. gamma	4. uniform	5 beta	
6. shifted exponential	7. shifted Rayleigh	8. type I largest value	9. type I smallest value	10. type II largest value	11. type II smallest value

Table 2.3.9 CALREL Probability Distribution Library

CALREL has been developed on a virtual-memory computer, MicroVAX, in FORTRAN-77 language. It is also available on IBM-PC and compatible computers with at least 640K RAM. For implementation on a PC, the procedure is provided on the floppy diskette containing the object code of CALREL.

2.3.4.3 Two Simple Formulations for Estimating Failure Probabilities:

A - Closed Form Method

a - Approximate Formula:

This closed-form approximation was developed by Mansour (1972). It is a simplified model to calculate the probability of failure by formulas with certain random and deterministic variables. The reference gives more details on the method. The following shows the final results for the probability of failure for the cases of deterministic and random stillwater bending moments.

Deterministic stillwater bending moment (primary hull failure mode):

a. Short term

$$P_f|_{n=1} = \left[1 - \Phi\left(\frac{\mu - m_0}{\sigma}\right)\right] + \frac{1}{\sqrt{2(\sigma/\sqrt{E})^2 + 1}}$$

$$\cdot e^{\frac{[(\mu - m_0)/\sqrt{E}]^2}{\sqrt{2(\sigma/\sqrt{E})^2 + 1}}} \cdot \varphi\left[\frac{\mu - m_0}{\sigma\sqrt{2(\sigma/\sqrt{E})^2 + 1}}\right] \qquad (2.3.33)$$

$$= P_f^{st} + P_f^{w} \approx P_f^{w}$$

b. Long term

$$P_f|_{n=1} = \left[1 - \Phi\left(\frac{\mu - m_0}{\sigma}\right)\right] + e^{\frac{\mu - m_0}{\lambda} + \frac{\sigma^2}{2\lambda^2}} \cdot \varphi\left[\frac{\mu - m_0}{\sigma} - \frac{\sigma}{\lambda}\right] \qquad (2.3.34)$$

$$= P_f^{st} + P_f^{w} \approx P_f^{w}$$

Random stillwater bending moment (primary hull failure mode):

a. Short term

$$P_f|_{n=1} = (1/\sigma_s)\sqrt{2/\pi E} \int_0^\infty \int_0^\infty \Phi[(z - \mu)/\sigma] \cdot (y/\sqrt{E})$$

$$\qquad (2.3.35)$$

$$\cdot e^{-(y/\sqrt{E})^2 - \frac{1}{2}\left(\frac{z - y - m}{\sigma_s}\right)^2} dy\, dz$$

b. Long term

$$P_f|_{n=1} \approx \Phi\left[\frac{\mu - m}{\sigma} - \frac{\sigma}{\lambda}\right] \cdot e^{(\sigma_s^2 + 2\lambda m + \sigma^2)/2\lambda^2 - (\mu/\lambda)} \qquad (2.3.36)$$

In the process of developing these equations, the wave bending moment in short term was assumed to follow a Rayleigh distribution and long term to follow the Exponential distribution. In this report, eqn. (2.3.33) is used to calculate the short-term probabilities of failure for four ships and a comparison was made with the CALREL results.

b - Integration Formula:

The integration formula (Mansour, 1972) for short term is (primary):

$$P_f = 1 - \frac{1}{\sigma\sqrt{2\pi}} \int_{m_0}^\infty [1 - e^{-(z - m_0/k)^l}]^n \cdot e^{-\frac{1}{2}\left(\frac{z - \mu}{\sigma}\right)^2} dz \qquad (2.3.37)$$

where

μ = mean of strength

σ = standard deviation of strength

m_0 = value of stillwater bending moment if considered to be deterministic

n = number of encounters

B - Mean Value First Order Second Moment Method

The safety index β according to the Mean Value First Order Second Moment Method is defined as the mean of the limit state function divided by its standard deviation.

As examples, the limit state function g and safety index β for different failure modes are:

a. For hull primary failure:

$$g = M_u - [M_s + k_w (M_w + k_d M_d)] \tag{2.3.38}$$

$$\beta = \frac{\mu_g}{\sigma_g}$$

where

$$\mu_g = \mu_{M_u} - \left[\mu_{M_s} + k_w (\mu_{M_w} + k_d \mu_{M_d})\right]$$

$$\sigma_g = \sqrt{\sigma_{M_u}^2 + \sigma_{M_s}^2 + k_w^2 \sigma_{M_d}^2 + k_w^2 k_d^2 \sigma_{M_d}^2 + 2\rho_{M_w M_d} k_w k_d \sigma_{M_w} \sigma_{M_d}}$$

where

M_u = ultimate strength

M_s = stillwater bending moment

M_w = wave bending moment

M_d = dynamic bending moment

k_w = load combination factor for stillwater and wave/dynamic moments

k_d = load combination factor for wave and dynamic moments

μ_i = mean of component i (e.g., μ_{M_u} is the mean of ultimate strength)

σ_i = standard deviation of component i

b. For secondary and tertiary failure modes:

$$g = f_u SM - [M_s + k_w (M_w + k_d M_d)]$$ (2.3.39)

$$\beta = \frac{\mu_g}{\sigma_g}$$

where

$$\mu_g = \mu_u \, \mu_{SM} - \left[\mu_{M_s} + k_w (\mu_{M_w} + k_d \, \mu_{k_d}) \right]$$

$$\sigma_g = \sqrt{(\sigma_u^2 \sigma_{SM}^2 + \sigma_u^2 \mu_{SM}^2 + \sigma_{SM}^2 \mu_u^2) + \sigma_{M_s}^2 + k_w^2 \sigma_{M_d}^2 + k_w^2 k_d^2 \sigma_{M_d}^2 + 2\rho_{M_w M_d} k_w k_d \sigma_{M_w} \sigma_{M_d}}$$

where

SM = section modulus

f_u = ultimate stress

M_s = stillwater bending moment

M_w = wave bending moment

M_d = dynamic bending moment

k_w = load combination factor for stillwater and wave/dynamic moments

k_d = load combination factor for wave and dynamic moments

μ_i = mean of component i

σ_i = standard deviation of component i

3. DATA BASE ON LOADS FOR FOUR SHIPS

In this Chapter, a data base on loads was developed for four selected ships used in this report as application examples. This data base on loads together with the data base on strength which is developed in Chapter 4, constitute the two basic components necessary to perform the reliability analysis under extreme loads given in Chapter 5. Chapter 6 discusses the sensitivity factors that influence the reliability of the four ships and Chapter 7 describes the fatigue reliability procedure and shows the results of application to the four ships.

3.1 Characteristics of the Selected Ships

Four ships have been selected after consultation with the Project Technical Committee (PTC). The four ships cover a wide range of current interest. The selected ships will be referred to as: Cruiser No. 1, Cruiser No. 2, Double Hull Tanker and SL-7 ships. The general characteristics of the four ships are given in Tables 3.1.1 to 3.1.3. Additional general information on these ships are given in Appendix D. Many structural drawings, longitudinal strength calculations, offsets, line drawings and other data have been obtained but not included in this report.

	Cruiser No. 1	Cruiser No. 2
Ship Length, Lpp (feet	529.0	529.0
Ship Beam (molded) (feet)	55.0	55.0
Draft Amidships (molded) (feet)	22.44	19.8
Displacement (LT salt water)	9,400	7,996
Trim by stern (inches)	-5.0	-1.83
GMT (corrected (feet)	2.75	2.56
LCG aft of midships (feet)	12.63	7.37
VCG above molded BL (feet)	23.0	23.28
Roll Gyradius in air (feet)	22.38	22.78
Pitch Gyradius in air (feet)	133.36	133.36
Yaw Gyradius in air (feet)	132.63	132.63

Table 3.1.1 General Characteristics of Cruisers No. 1 and No. 2

Length Between Perpendiculars, LBP	640 ft
Beam Molded	96 ft
Depth	50 ft
Design Load Draft	34 ft
Displacement	44,596 L.tons
Deadweight	34,700 L.tons
Web Frame Spacing	11.5 ft
Tank Length, Typical	57.5 ft

Table 3.1.2 General Characteristics of a Double Hull Tanker

Length, Overall	946′ 7″
Length, Between Perpendiculars	880′ 6″
Beam, Molded	105′ 6″
Depth to Main Deck	51′ 11″
Draft, Design	36′ 8″
Draft, Scantling	39′ 0″
Displacement (34′ 0″ draft) – Long Tons	47,760

Table 3.1.3 General Characteristics of an SL-7 Ship

3.3   Collected Load Data for Four Ships

This section is concerned with data collected on loads and developing load models for each of the four ships. A considerable part of the data has been obtained for the four ships from SSC sponsoring organizations and open literature on the subject.

The sought load data and information include, whenever possible, stillwater loads, low frequency wave induced loads, high frequency slamming loads and fatigue stress ranges. The required load data can be based on analytical methods, model experiments and/or full scale sea trials. Important loads that are not available will be estimated either analytically using a ship motion program or empirically based on existing data on similar ships. Cracks and buckling data are also sought from ship records and operating experience.

The load information obtained varied from a fairly complete set for Cruiser No. 1 to a partial set for the double hull tanker. Cruiser No. 1 load data obtained include stillwater loads, linear transfer functions for wave induced loads, slamming loads and extreme loads and load combinations. The data are based on analytical methods, model experiments and sea trials. Less data is available on Cruiser No. 2. The SL-7 data obtained include ship loading conditions, stillwater loads and hull offsets. Wave load linear transfer function and some data on slamming loads are also available on the SL-7 (primarily from Ship Structure Committee reports). The available information on the double hull tanker is limited to stillwater loads and hull offsets. Because of the lack of complete information on wave induced loads, it was decided to use a second order strip theory to determine these loads for all four ships (see section 3.4). An estimate will be made of slamming loads either analytically using a specialized slamming program (see section 3.6) or empirically from available data.

Appendix E gives some of the collected results of the loads on Cruisers No. 1 and No. 2 as well as the double hull tanker and the SL-7 ship.

As mentioned earlier, a second order frequency domain computer program (SOST) will be used to determine the non-linear wave loads. The advantages of using a frequency domain analysis over performing non-linear time domain load simulations are:

1. Non-linear time domain load simulation is not within the current state of the art (see Dalzell, 1991).

2. Load simulation cannot be used realistically in sensitivity analysis, particularly when many variables are involved in a design.

3. Most likely, practitioners will not use reliability methodology if it hinges on running a lengthy non-linear time domain load simulation program before running a reliability computer program.

4. Standard frequency domain linear ship motion programs and the associated spectral analysis are capabilities that are available in many design offices and government agencies. They can be easily used together with a provided set of non-linearity coefficients and design charts (see sections 2.1.2 and 2.1.3) to estimate the non-linear loads in high sea states.

Some linear frequency domain analyses were also performed in Phase I of the project.

As an example, the linear ship motion program (SCORES) has been used to develop response spectra and the associated statistics for Cruiser No. 2 for vertical, horizontal and torsional moments. The results are shown in Figures 3.3.1 to 3.3.9. Tables given additional values of moment response for different headings and speeds are given in Appendix E.
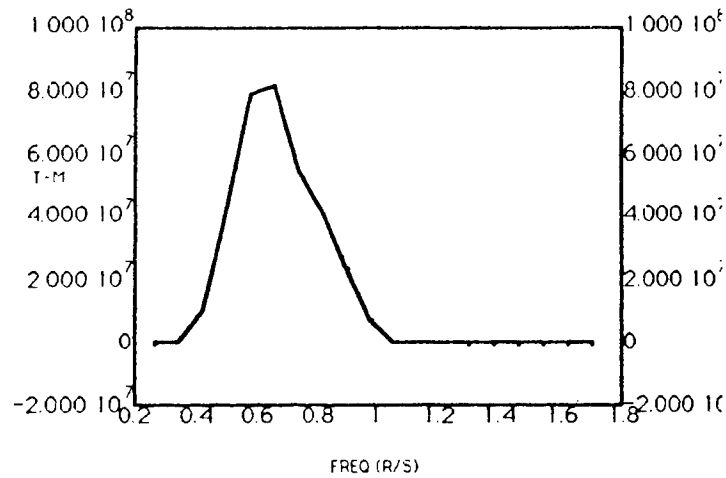
Figure 3.3.1 Vertical Moment — Sea State 6, Heading 45 deg., Speed 15 KTS
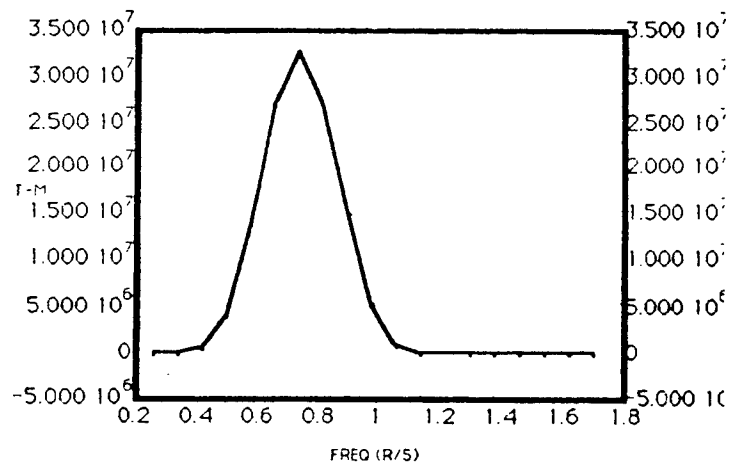
Figure 3.3.2 Horizontal Moment — Sea State 6, Heading 45 deg., Speed 15 KTS
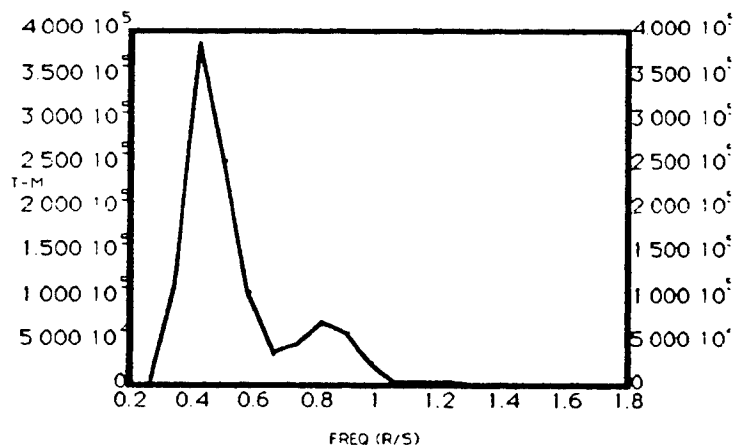
Figure 3.3.3 Torsional Moment —Sea State 6, Heading 45 deg., Speed 15 KTS

3-4
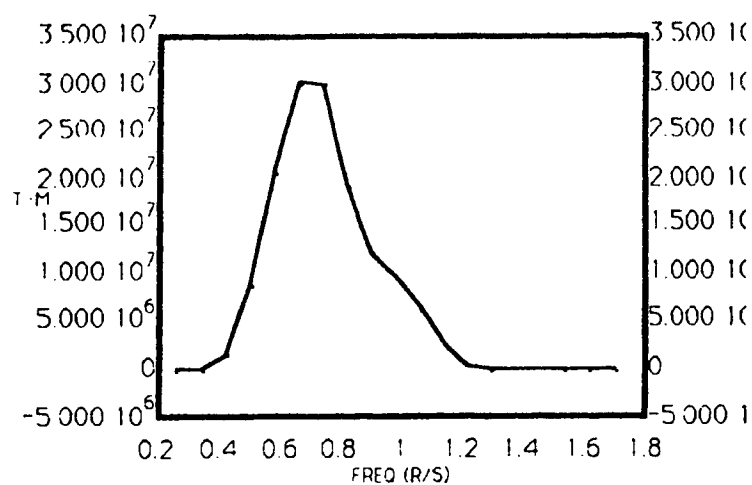
Figure 3.3.4 Vertical Moment — Sea State 6, Heading 60 deg., Speed 10 KTS
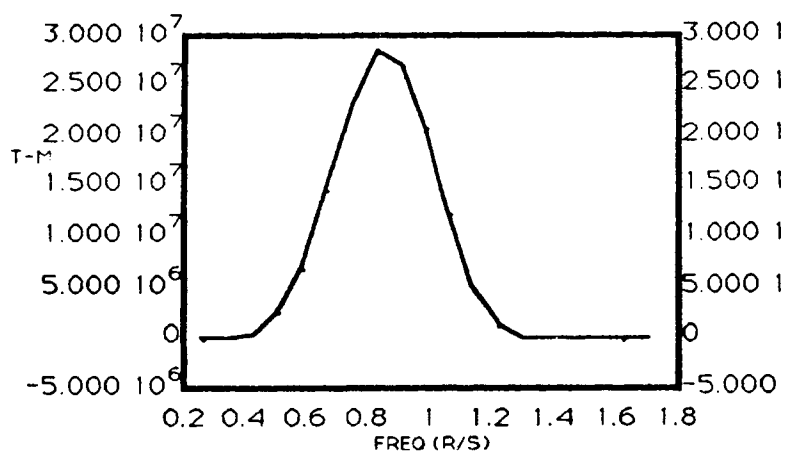
Figure 3.3.5 Horizontal Moment — Sea State 6, Heading 60 deg., Speed 10 KTS
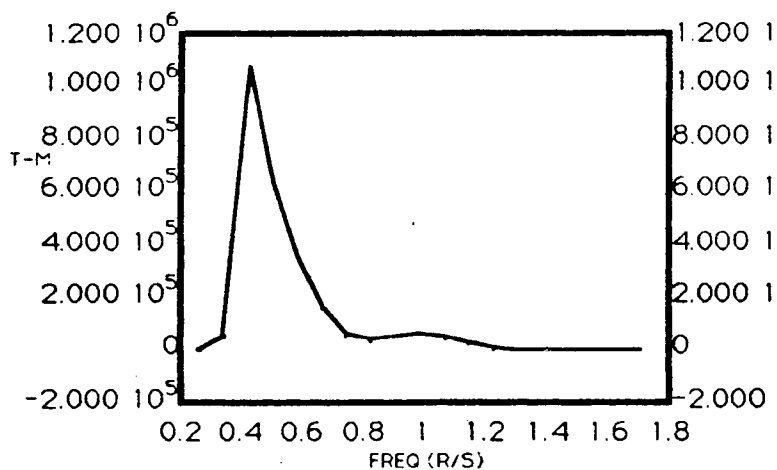
Figure 3.3.6 Torsional Moment — Sea State 6, Heading 60 deg., Speed 10 KTS
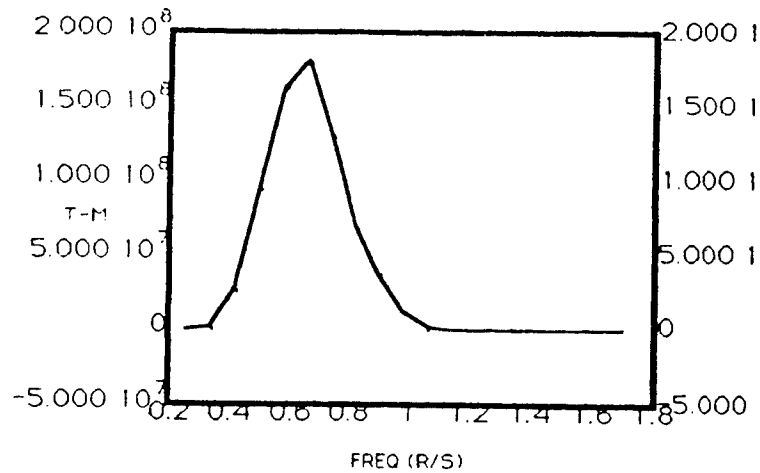
Figure 3.3.7 Vertical Moment — Sea State 7, Heading 45 deg., Speed 10 KTS
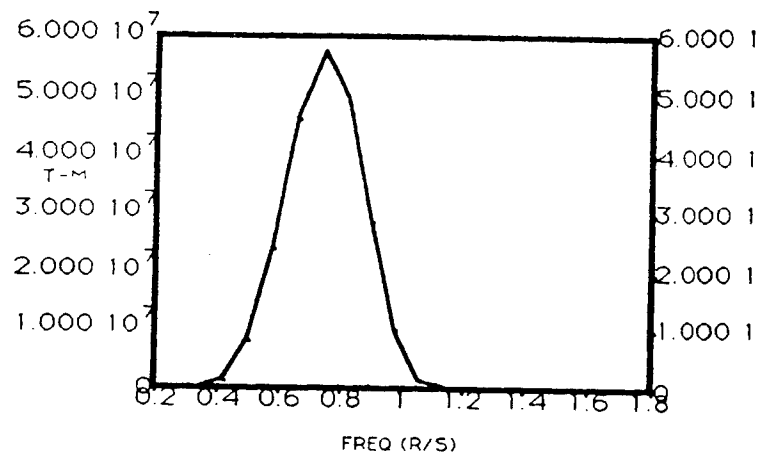
Figure 3.3.8 Horizontal Moment — Sea State 7, Heading 45 deg., Speed 10 KTS
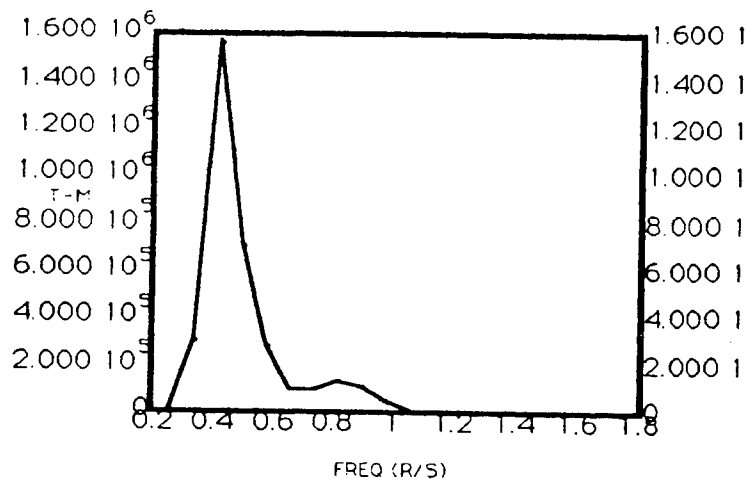
Figure 3.3.9 Torsional Moment — Sea State 7, Heading 45 deg., Speed 10 KTS

3-6

3.4 Short and Long Term Non-linear Wave Bending Moment

A second order strip theory procedure is applied to the four ships of interest, in both short-term extreme conditions and in long-term operating conditions. The results obtained using this procedure are compared to results obtained using various empirical or quasi-empirical methods. The results show that while the second order strip theory is a marked improvement over traditional linear strip theory and can produce good results, it has its limitations. Though some problems with the second order strip theory exist, it is believed that the second order strip theory can provide insight into the extreme loading problem, particularly the difference between sagging and hogging bending moment. Used in conjunction with empirical or semi-empirical methods, the second order strip theory can help provide a more insightful estimate of extreme (design) loads than can be obtained using an empirical method alone.

Second Order Strip Theory (SOST) Code — Short Term Results:

The SOST code was used to analyze the four ships: two cruisers, denoted as Cruiser 1 and Cruiser 2, a double hulled tanker, and a high speed containership (the SL-7). Characteristics of interest for the four ships are listed in Table 3.4.1.

Ship	LBP (feet)	Beam (feet)	Δ (LT)	LCG (ft. aft FP)	Still Water BM [Lt-ft (10^3)]
Cruiser 1	529.0	55.0	9400	275.5	+76.8
Cruiser 2	529.0	55.0	7996	270.17	+64.5
SL-7	880.5	105.5	47760	478.1	+599.1
Tanker	640.0	96.0	44596	304.0	-97.9
+ bending moment is hogging					

Table 3.4.1

Each ship was analyzed in a short term extreme sea state at two headings (head and bow seas). Table 3.4.2 summarizes the parameters associated with this sea state.

Short Term Analysis Parameters	
Significant Wave Height (ft)	45.0
Upcrossing Period (s)	14.0
Ship Speed (kts)	6.0

Table 3.4.2

Figure 3.4.1 illustrates the vertical bending moment response spectrum at amidship for Cruiser 1 in the head seas case. Though the quadratic terms are more than one order of magnitude smaller than the linear terms, their contribution to the probability of exceedence levels is not negligible. Figures 3.4.2 to 3.4.9 show plots of the bending moment magnitude versus probability of exceedence for all four ships in both headings; head seas (180°) and bow seas (135°).
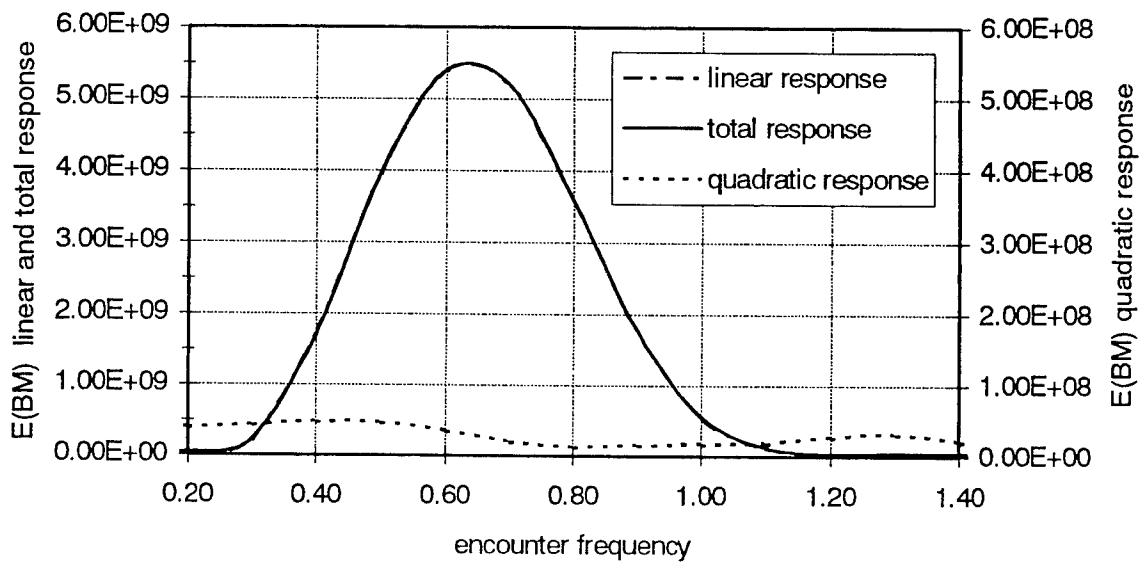
Figure 3.4.1 Linear and Total Response — Cruiser 1
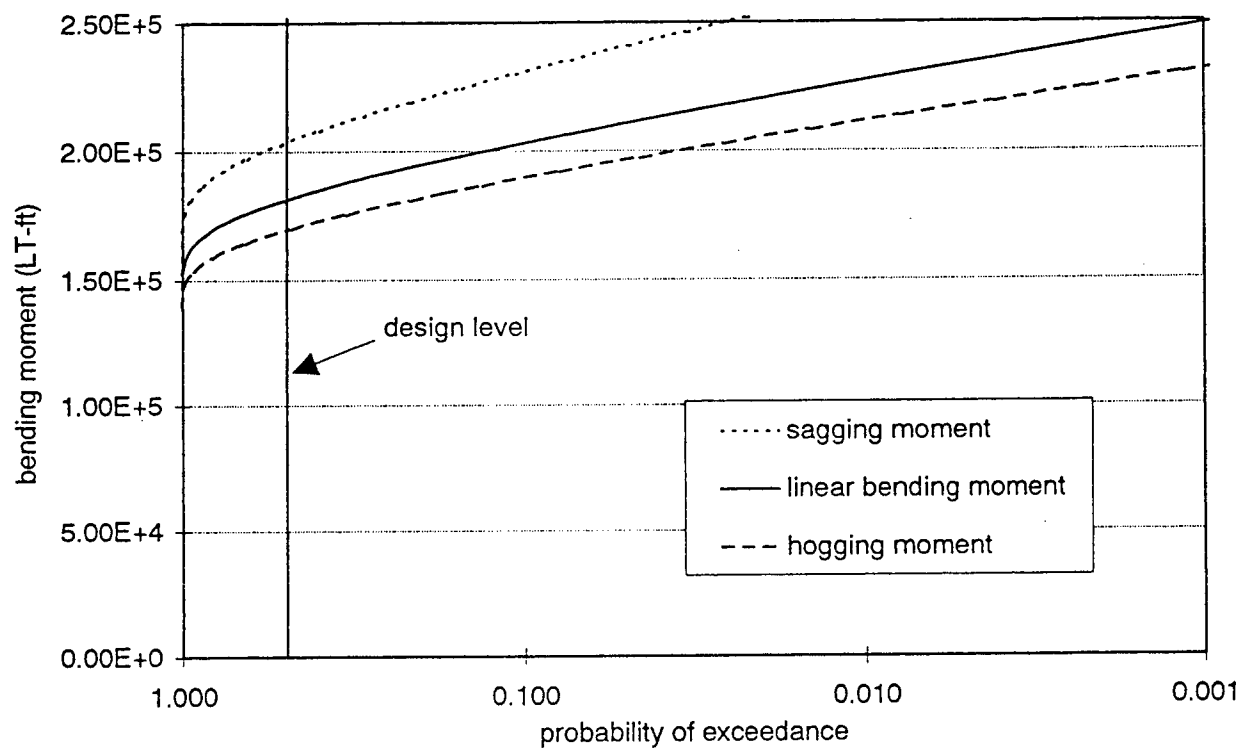
Figure 3.4.2 Cruiser 1 — Short Term Probability of Exceedence – Heading = 180
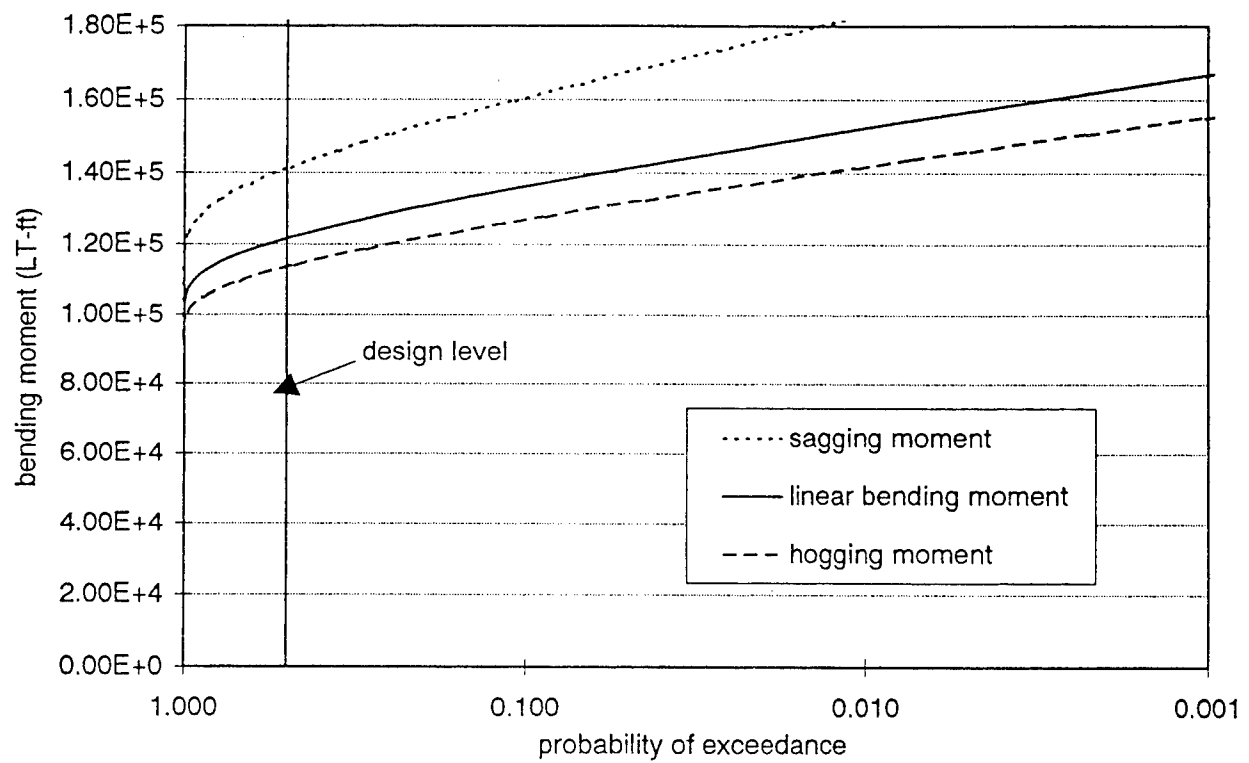
Figure 3.4.3 Cruiser 1 — Short Term Probability of Exceedence – Heading = 135
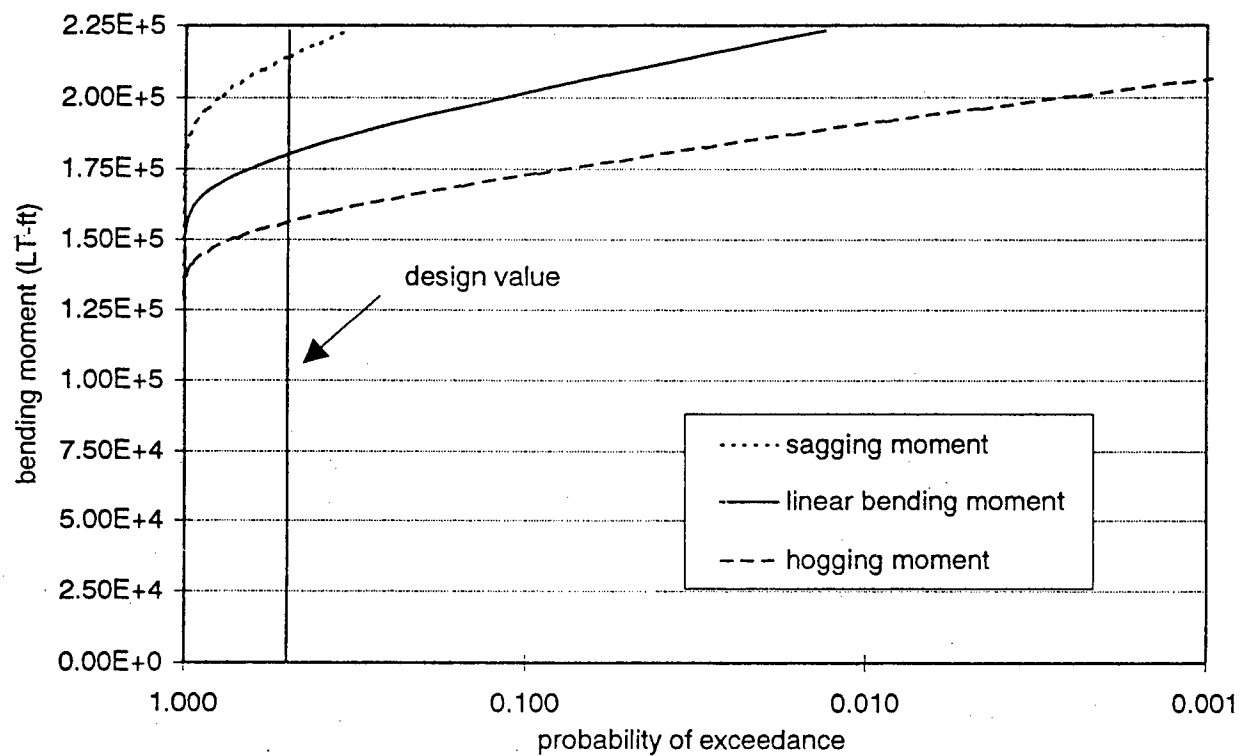
Figure 3.4.4 Cruiser 2 — Short Term Probability of Exceedence – Heading = 180
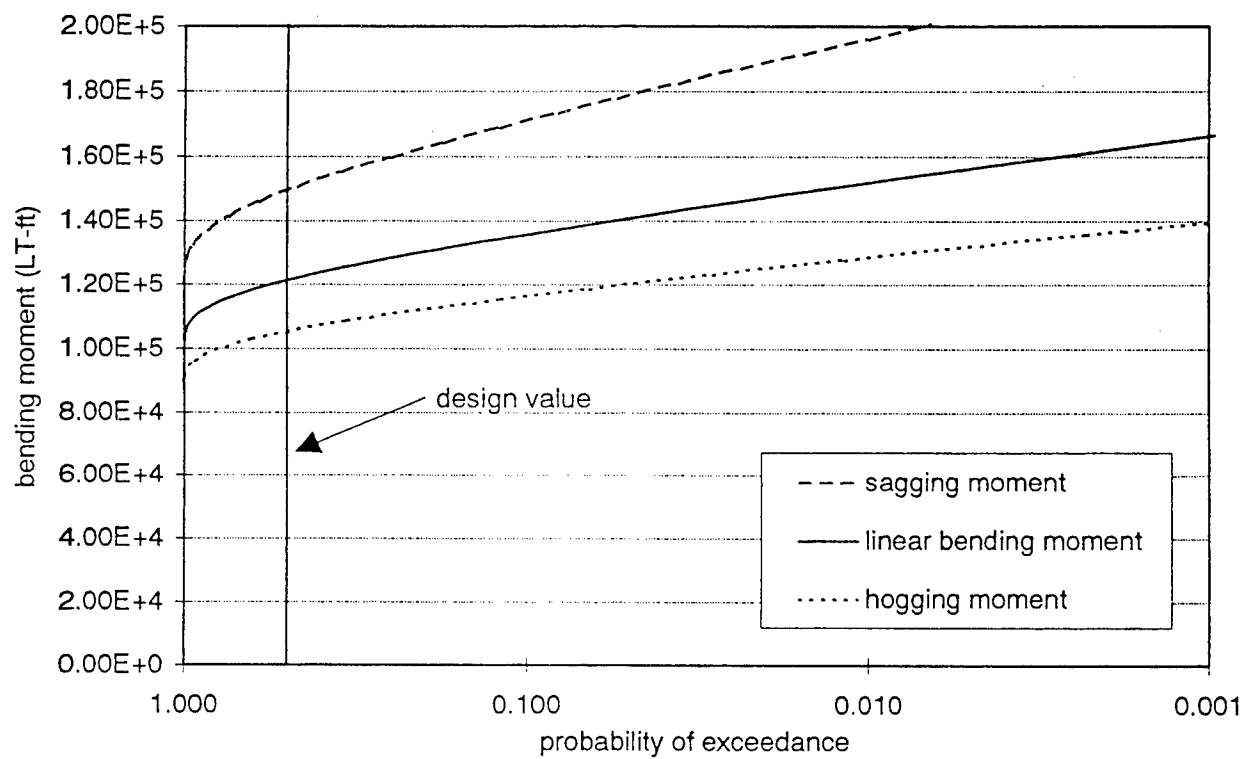
Figure 3.4.5 Cruiser 2 — Short Term Probability of Exceedence – Heading = 135
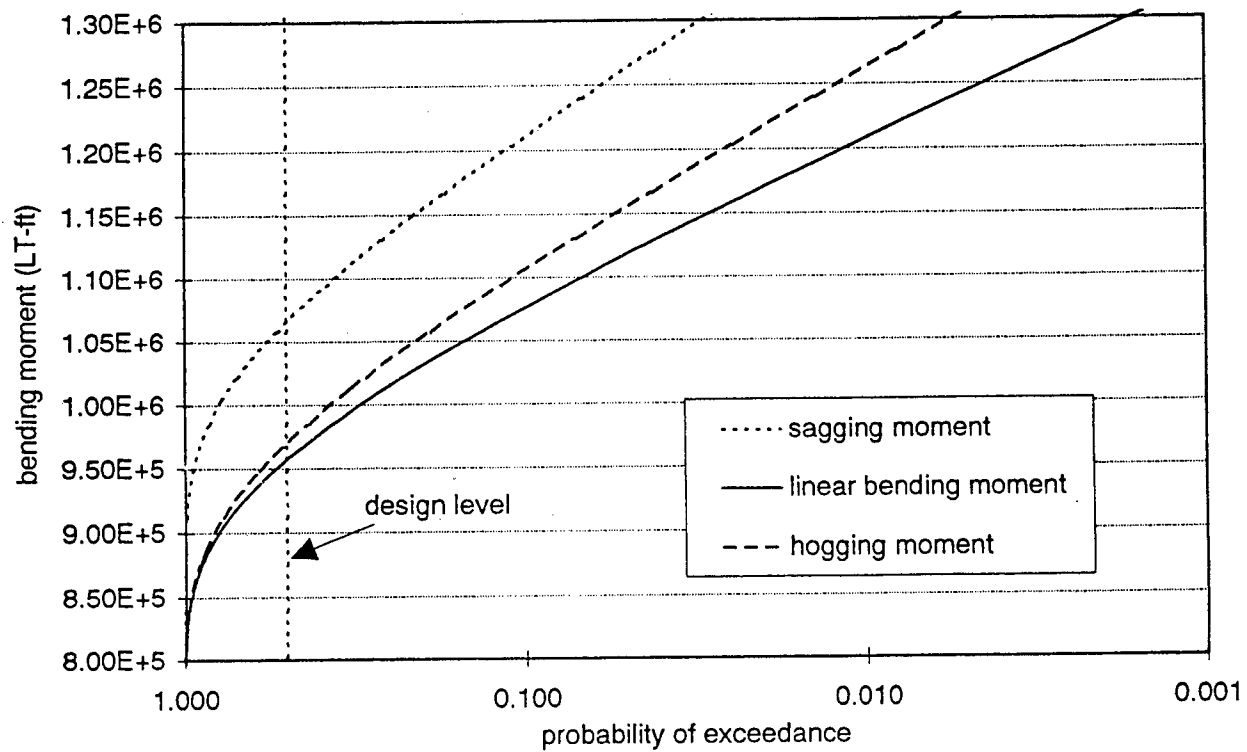
Figure 3.4.6 SL-7 — Short Term Probability of Exceedence – Heading = 180
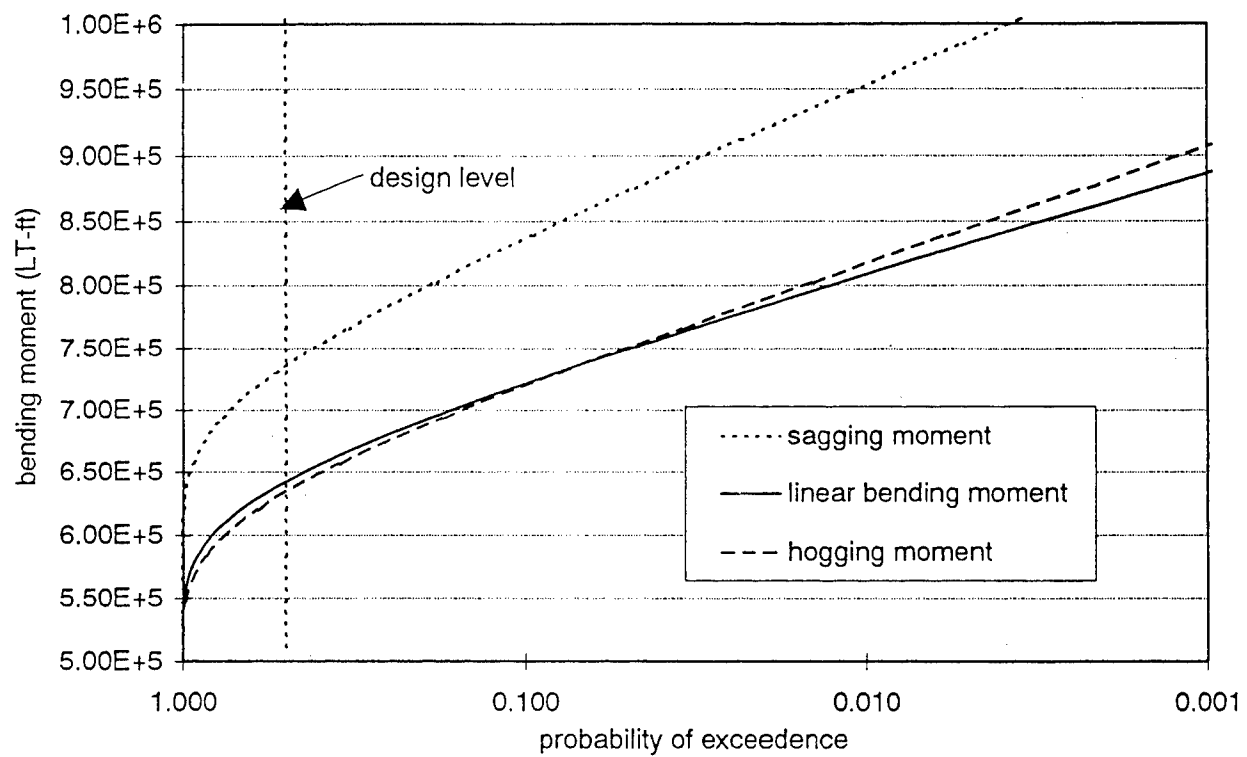
Figure 3.4.7 SL-7 — Short Term Probability of Exceedence – Heading = 135
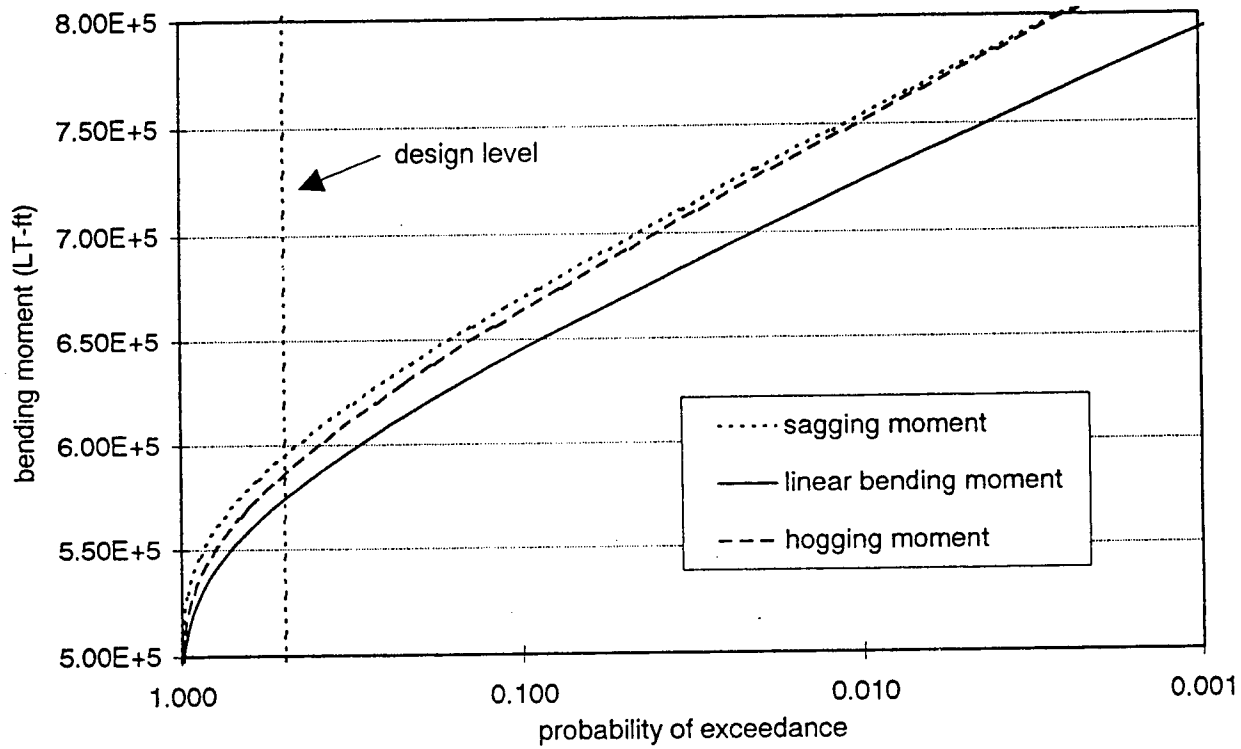
Figure 3.4.8 Tanker — Short Term Probability of Exceedence – Heading = 180
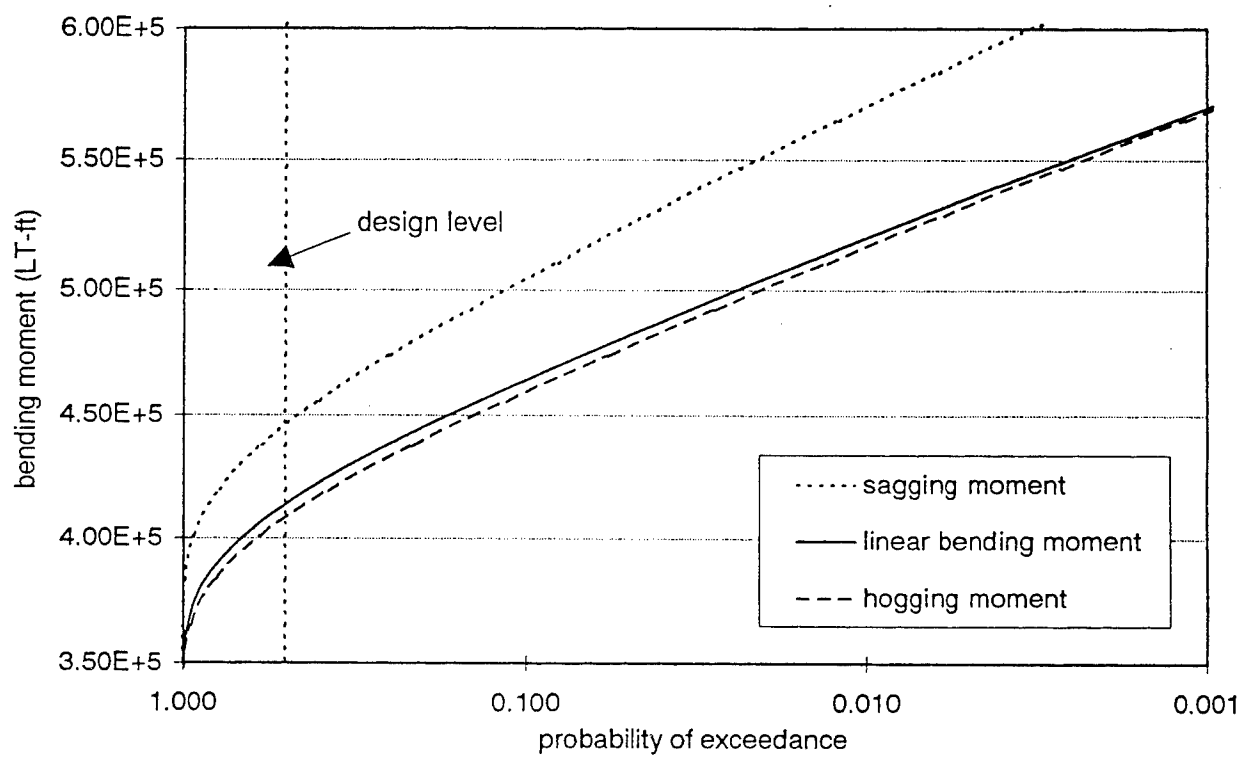
Figure 3.4.9 Tanker — Short Term Probability of Exceedence – Heading = 135

Discussion:

One of the most important input parameters in the SOST procedure is the derivative of the beam at the waterline with respect to a vertical coordinate. This is the parameter which seems to exert the most influence upon the sag-hog ratio, which is a measure of the non-linearity associated with the response. In very high seas, the quadratic strip theory will have difficulties similar to those experienced by linear strip theory when relative motions are greater than the freeboard or less than the draft. In an attempt to apply SOST to extreme seas and circumvent this problem, Jensen et al. (1993) have proposed the following procedure.

If the amplitude of the relative motion $(z - z_0)$ becomes larger than the freeboard F or the draft T, then the following equations should be used to estimate the appropriate input slope, B_1:

$$B_1 = \begin{cases} B_1^+ = 2\dfrac{A_s - A_0 - B_0\left(z - z_0\right)}{\left(z - z_0\right)^2}; \ z - z_0 \geq F \\[4mm] B_1^- = 2\dfrac{-A_0 - B_0\left(z - z_0\right)}{\left(z - z_0\right)} \quad ; z - z_0 \leq -T \end{cases} \tag{3.4.1}$$

where A_0 = section area to the waterline
        B_0 = beam at the waterline
        A_s = total section area to uppermost deck

This insures that $0 \leq A(x,z) \leq A_s(x)$ for all values of x and z. The calculations show that the sectional slopes, B_1, at the bow give the main contribution to differences between the sagging and hogging bending moments. As the two values generated in eqn. (3.4.1) might be different, the slope input into the SOST program is taken to be the average of the two:

$$B_1 = \frac{1}{2}\left(B_1^+ + B_1^-\right) \tag{3.4.2}$$

It is also in the bow where we might expect relative motions to exceed the freeboard or draft. With this in mind, eqn. (3.4.1) is used to adjust the slopes of the forward part of the ship only. In this work, the forward 20% of the ship was adjusted using eqn. (3.4.1). This was done several different ways. Table 3.4.3 summarizes the results of the 50% level (mean values) of the short term predictions for the four ships, comparing the results obtained using the actual slopes at the waterline and the results obtained using the adjusted slopes which ensures no excess buoyancy. All ships were analyzed in the head seas condition, and results are in thousands of long ton-feet. The slopes were adjusted using relative motion output from the same operating condition.

Ship	Slope	Sagging Moment	Linear Moment	Hogging Moment	Sag/Hog
Cruiser 1	actual	224.9	181.1	147.0	1.52
	adjusted	198.8	181.1	169.1	1.18
Cruiser 2	actual	223.2	180.0	145.1	1.54
	adjusted	213.9	180.1	155.9	1.37
SL-7	actual	1473.6	956.2	728.5	2.02
	adjusted	1065.0	957.8	969.6	1.10
Tanker	actual	698.1	574.3	500.6	1.38
	adjusted	594.8	574.5	586.1	1.01

Table 3.4.3 Wave Bending Moment, Short Term, 50% Probability Level

As can be seen in Table 3.4.3, the section slope in the bow region is of major importance in predicting the non-linearities in the response. In light of this, Cruiser 1 was used as a test case for various adjusted slope techniques. The program was run with Cruiser 1 in a variety of sea states, all with a ship speed of 10 knots and heading of 180 (head seas). This was done three times, once using actual slopes, once using adjusted slopes as described above, and once using B^+ from eqn. (3.4.1) to generate the sagging moment results and B^- to generate the hogging moment results. The resulting sag to hog ratio is shown for all three cases as shown in Figure 3.4.10. As the figure indicates, using actual slopes leads to unreasonably high non-linearities in extreme sea states because the relative motion exceeds the freeboard or the draft. Both methods of adjusted slope provide similar results and seem to be more reasonable. They both eliminate the buoyancy that does not exist when the relative motion exceeds the freeboard or the draft. The results shown in Figures 3.4.2 to 3.4.9 for the four ships are all based on the average adjusted slope.
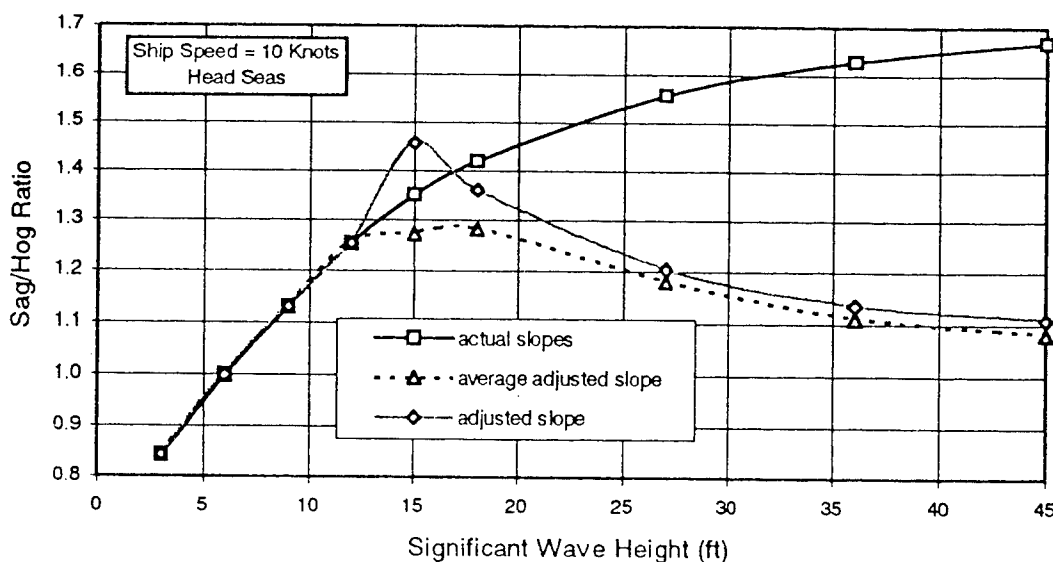
Figure 3.4.10 Sag/Hog Ratio versus Significant Wave Height — Cruiser 1

Long Term Analysis — SOST Code Results:

The long-term procedure has been applied to the four ships under consideration. The mission profile selected for all ships was identical in order to provide the same basis for comparison. The route selected was mostly North Atlantic with a small portion in the Mediterranean (see Figure 3.4.11). Information on fraction of time spent in each zone along the route, speeds and headings are shown in Table 3.4.4.

Figures 3.4.12 to 3.4.15 show the long-term non-linear hog and sag bending moments versus probability of exceedence for all four ships using SOST long-term procedure. At the 50% probability level, the values are higher than the corresponding results of the short term procedure. It should be noted that the slopes used in the long term analysis were average adjusted slopes, calculated using relative motions associated with the short term sea states presented previously.
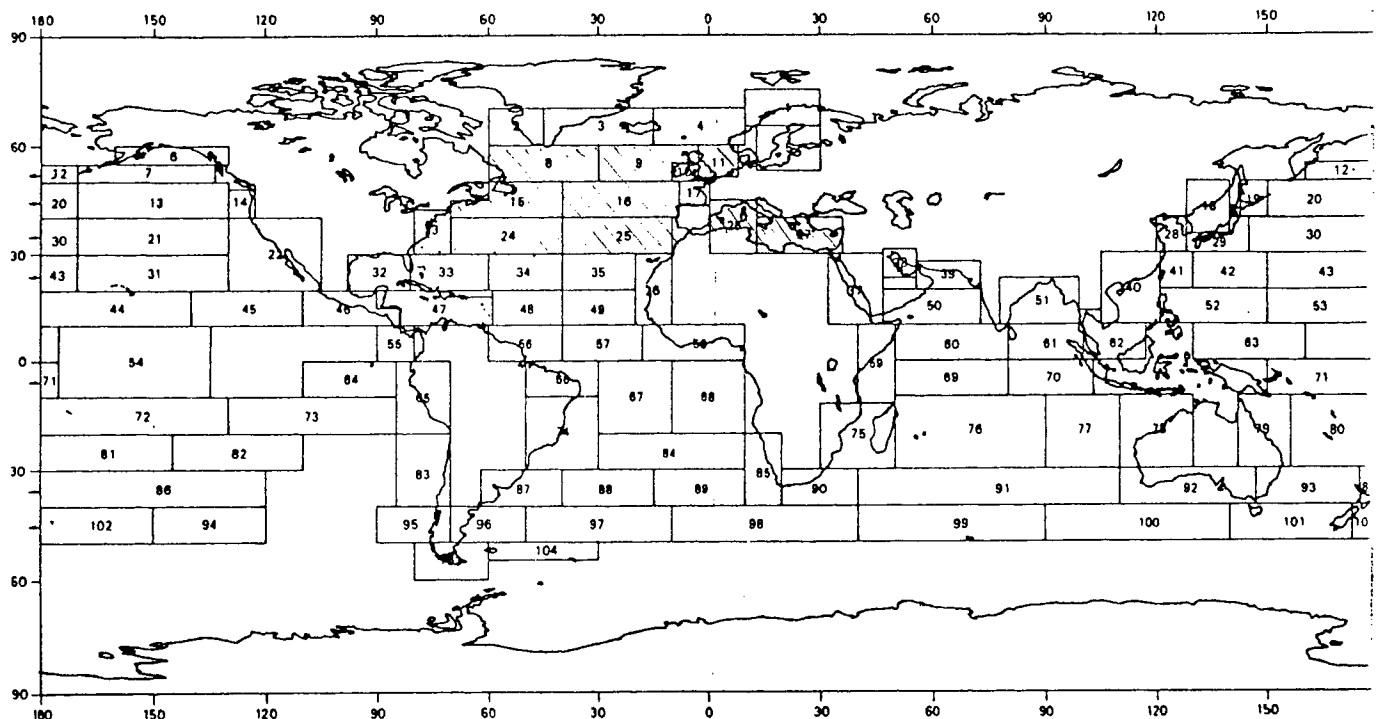
Figure 3.4.11 Operational Routes of Four Ships

3-19

	Fraction of Time
Marsden area No. 8	.059
Marsden area No. 9	.059
Marsden area No. 10	.059
Marsden area No. 11	.059
Marsden area No. 15	.118
Marsden area No. 16	.118
Marsden area No. 17	.059
Marsden area No. 23	.118
Marsden area No. 24	.118
Marsden area No. 25	.118
Marsden area No. 26	.059
Marsden area No. 27	.059

Total Period (years)	15.000

Hs1 = practical Hs limit for service speed	16.500
Fraction of time with service speed when Hs < Hs1	.800
Fraction of time with minimum speed when Hs > Hs1	1.000
Service Speed >=	30.500

Fraction of time with heading 0 det (following)	.111
Fraction of time with heading 45 deg	.222
Fraction of time with heading 90 deg	.222
Fraction of time with heading 135 deg	.333
Fraction of time with heading 180 deg (head)	.111

Table 3.4.4 Summary of Long Term Operational Profile
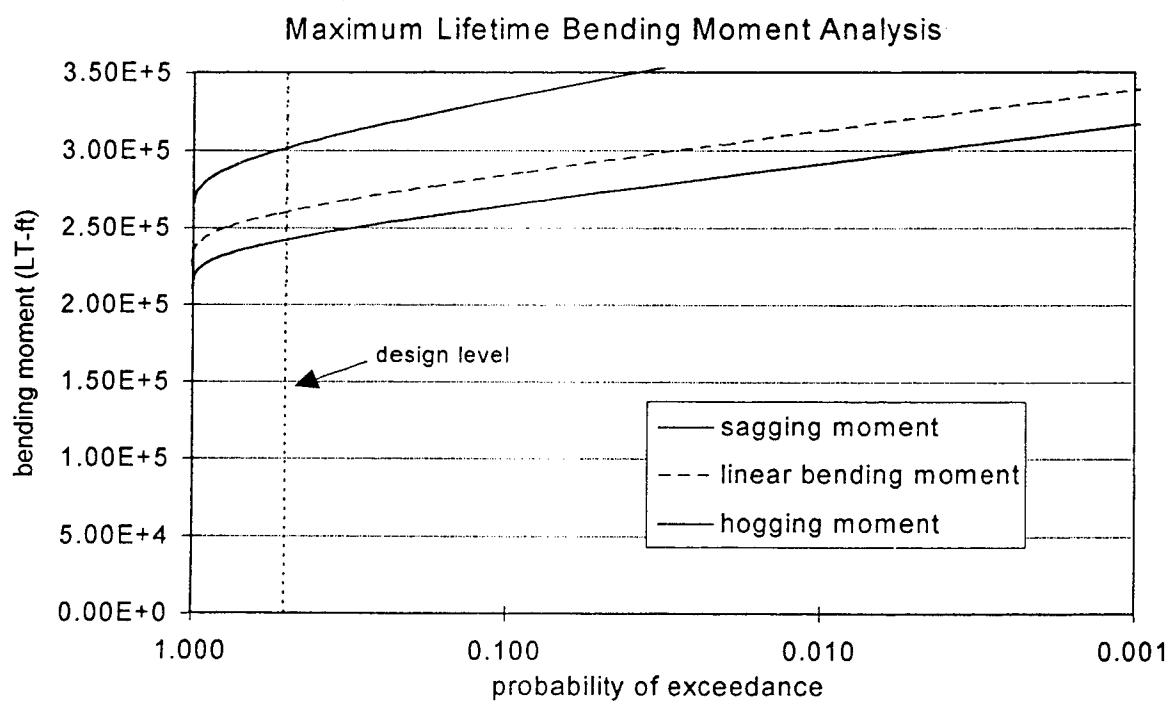
Figure 3.4.12 SOST Long Term Analysis

Cruiser 1 Vertical Bending Moment
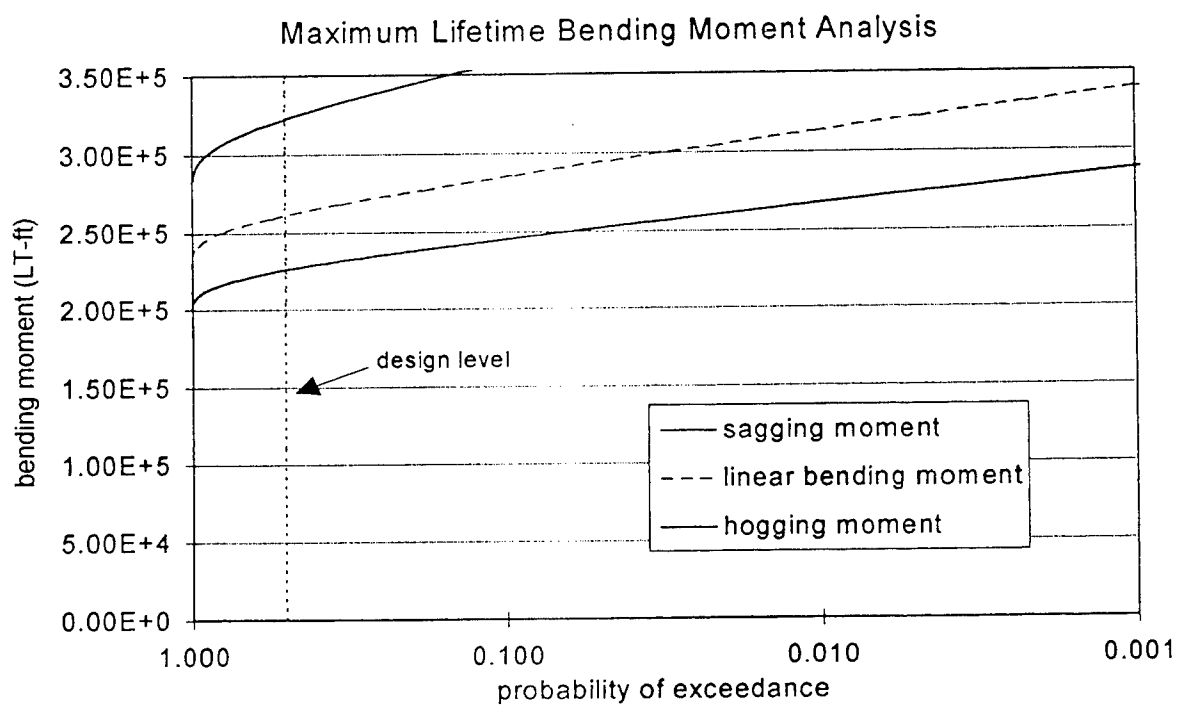
Figure 3.4.13 SOST Long Term Analysis

Cruiser 2 Vertical Bending Moment
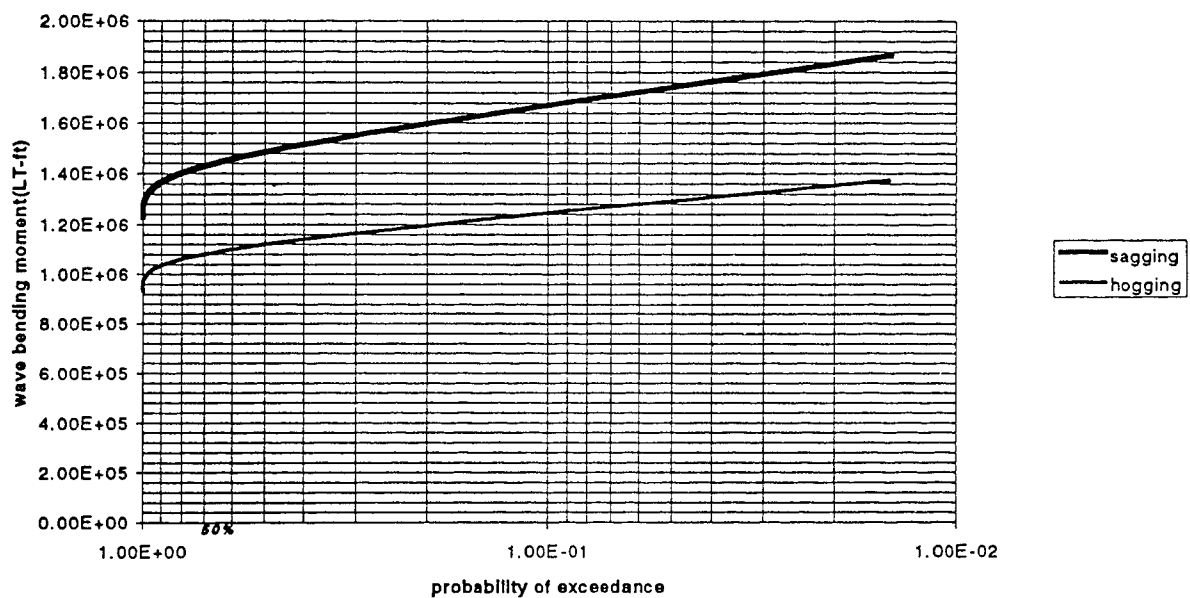
Figure 3.4.14 SOST Long Term Analysis
SL-7 Vertical Bending Moment
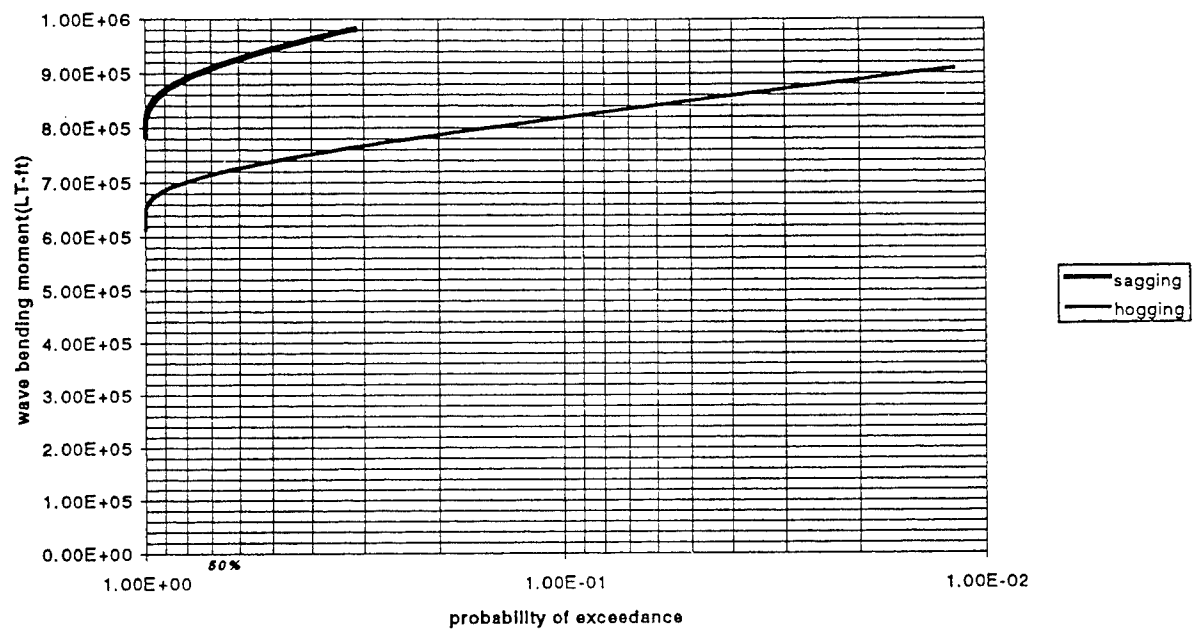
Figure 3.4.15 SOST Long Term Analysis

Tanker Vertical Bending Moment

Other Load Prediction Methods:

A review has been conducted of other tools which might be used to predict a design extreme vertical bending moment for the four ships. Two such procedures will be discussed here; both procedures are empirical in nature.

Sikora has developed algorithms for estimating the maximum lifetime extreme loads on ships. Major points from this procedure, described in Sikora (1989), will be highlighted here. Empirical response amplitude operators for various speeds and headings are combined with sea spectra to produce wave loads. A lifetime operational profile is developed and is discretized to form a grid of operational conditions, each condition having an associated probability. The response for each condition is then weighted by its probability of occurrence, and the sum of all conditions represents the lifetime extreme load. This method has shown good agreement with experimental results.

The empirical RAOs used in this procedure were developed from model test and sea trial data. Nondimensional RAO is presented in Sikora's work in tabular form; Table 3.4.5 is a copy of this.

Normalized Wave Frequency $F_3\Omega$	Normalized Bending Moment $\sqrt{RAO}/\rho g L^2 B F_1 F_2$
0.4	0.0000
0.6	0.0045
0.8	0.0114
0.9	0.0151
0.95	0.0170
1.0	0.0180
1.05	0.0177
1.1	0.0167
1.2	0.0143
1.4	0.0100
1.6	0.0064
1.8	0.0042
2.0	0.0036

Table 3.4.5 Normalized Response Amplitude Operator

The scaling factors listed in Table 3.4.5 are defined as follows:

$$F_1 = \left| \sqrt[3]{\cos\theta} \right|$$
$$F_2 = 1.1\tanh(1.5 + v/g) + 0.03(v/g)^2 \qquad (3.4.3)$$
$$F_3 = \sqrt{\cos\theta}$$

where v and θ are the ship speed and healing, respectively. These empirical RAOs, coupled with appropriate sea spectra and operational profiles can be used to predict lifetime extreme bending moments. The operational profile grid mentioned previously is defined by two parameters, frequency of occurrence of a particular significant wave height, and the probability of occurrence of a speed/heading combination in that wave height. These numbers are reproduced in Tables 3.4.6 and 3.4.7.

Significant Wave	Frequency of Occurrence		
Height (meter)	Area A	Area B	Area C
<1	0.0503	0.3692	0.2254
1-2	0.2665	0.3303	0.3849
2-3	0.2603	0.1480	0.2305
3-4	0.1757	0.0723	0.0945
4-5	0.1014	0.0355	0.03033
5-6	0.0589	0.0181	0.01735
6-7	0.0346	0.0110	0.00675
7-8	0.0209	0.0066	0.00390
8-9	0.0120	0.0036	0.00312
9-10	0.0079	0.00247	0.00177
10-11	0.0054	0.00138	0.00058
11-12	0.0029	0.00074	0.00031
12-13	0.0016	0.00040	0.00031
13-14	0.00074	0.00019	0.00010
14-15	0.00045	0.00012	0.00001
>15	0.00041	0.00010	0.0
Area A – North Atlantic			
Area B – Combined Atlantic, Mediterranean, and Caribbean			
Area C – Combined Pacific			

Table 3.4.6 Frequency of Occurrence of Sea States

Frigates and Small Ships (Displacement <10,000 LT)				
		Significant Wave Height (m)		
Speed (Kts)	Heading	0-5	6-10	>10
5	Head	0.013	0.025	0.0
	Bow	0.025	0.375	0.808
	Quartering	0.025	0.050	0.042
	Following	0.013	0.025	0.0
15	Head	0.088	0.023	0.0
	Bow	0.175	0.338	0.142
	Quartering	0.175	0.045	0.008
	Following	0.088	0.023	0.0
25	Head	0.025	0.0025	0.0
	Bow	0.050	0.038	0.0
	Quartering	0.050	0.005	0.0
	Following	0.025	0.0025	0.0
High Speed Cargo Ships				
5	Head	0.010	0.125	0.175
	Bow	0.020	0.125	0.175
	Quartering	0.020	0.125	0.175
	Following	0.010	0.063	0.088
15	Head	0.096	0.115	0.075
	Bow	0.193	0.115	0.075
	Quartering	0.193	0.115	0.075
	Following	0.096	0.058	0.038
25	Head	0.019	0.010	0.0
	Bow	0.038	0.010	0.0
	Quartering	0.038	0.010	0.0
	Following	0.019	0.005	0.0
Commercial Cargo Ships				
5	Head	0.010	0.125	.175
	Bow	0.020	0.125	.175
	Quartering	0.020	0.125	.175
	Following	0.010	0.063	0.88
15	Head	0.115	0.125	.075
	Bow	0.231	0.125	.075
	Quartering	0.231	0.125	.075
	Following	0.115	0.063	.038

Table 3.4.7 Frequency of Occurrence of Heading Speed Combinations

Using a representative sea spectrum, the empirical RAO information, and the probability of exceedence information from Tables 3.4.6 and 3.4.7, one can predict the lifetime extreme bending moment. Having done this procedure for a number of ships, Sikora suggests the following equation for maximum lifetime response:

$$BM_{max}[\text{ft} - \text{tn}] = SW + CL^{2\frac{1}{2}}B \qquad (3.4.4)$$

where SW is the stillwater bending moment, L and B are in feet, and C is defined as follows. For ships which can be expected to exhibit whipping, such as flat bottomed commercial ships:

$$\text{Hog: } C = 6.6(10^{-4})$$

$$\text{Sag: } C = 9.0(10^{-4}) \qquad (3.4.5)$$

For fine bow ships which are less subject to whipping, such as naval vessel or fast containerships:

$$\text{Hog: } C = 5.8(10^{-4})$$

$$\text{Sag: } C = 7.9(10^{-4}) \qquad (3.4.6)$$

Another 'approximate method' for generating appropriate design values for maximum bending moments is provided in the ABS rules.

$$M_{ws}[\text{lt} - \text{ft}] = -k_1 C_1 L^2 B(C_b + 0.7) \times 10^{-3}$$
$$M_{wh}[\text{lt} - \text{ft}] = +k_2 C_1 L^2 B C_b \times 10^{-3} \qquad (3.4.7)$$

where
$$k_1 = 1.026$$
$$k_2 = 1.772$$
$$C_1 = 10.75 - \left(\frac{984 - L}{328}\right)^{1.5}$$
$$L = \text{length of vessel}$$
$$B = \text{breadth of vessel}$$
$$C_b = \text{block coefficient}$$

Both Sikora's method (eqns. (3.4.4) to (3.4.6)) and the ABS equation were applied to the four ships of interest in order to compare empirical predictions of the sagging moment to hogging moment ratio with results obtained using SOST in the long term analysis. This comparison is summarized in Table 3.4.8. The rules provided by DnV for the determination of wave induced loading were also used for the four ships. The resulting ratios were identical to those obtained using the ABS rules.

Ship	ABS (and DnV) Sag/Hog	Sikora Sag/Hog	SOST Long Term Sag/Hog
Cruiser 1	1.37	1.36	1.25
Cruiser 2	1.42	1.36	1.43
SL-7	1.31	1.36	1.33
Tanker	1.12	1.36	1.28

Table 3.4.8 Comparison of Sag/Hog Ratios

The results generated using the quadratic theory in a long term analysis show reasonable agreement with the results obtained using the class society rules.

While more work should be done to further investigate the performance of the quadratic theory, it seems reasonable to make several conclusions at this point. Long-term analysis using the quadratic theory can produce reasonable results. Using adjusted slopes which were calculated using relative motions generated from an extreme short term sea state seems to produce believable results. For the purpose of design, it appears that the application of the quadratic theory in this way, coupled with approximate methods, should produce results which are more rational than straightforward application of purely empirical formulations.

3.5 Slamming Loads — SLAM Code Results

The midship slamming bending moments for the four ships have been determined using the software SLAM discussed in section 2.1.4. The program which was developed by P. Friis-Hansen (1993) requires inputs of ship geometry, stiffeners, mass distribution, parameters for calculating the transfer functions, location of slamming impact, sea state speed and heading. The program runs modeled simulations of the vessel and gives outputs of extreme value distributions of slamming bending moment, wave bending moment and combined wave and slamming bending moments.

These bending moments have been determined for the four ships under consideration and the corresponding stresses (compressive) were calculated at the deck and bottom of each ship. The position of slamming impact (input) was taken as the location of damage in ships based on data analyzed in a report by SNAME Panel HS-2: Notes on Ship Slamming, Technical and Research Bulletin 2-30, SNAME, 1993. Figure 3.5.1 is reproduced from that publication and shows the longitudinal location of damage as a percentage of length aft of the forward perpendicular. Figures 3.5.2 to 3.5.9 and Tables 3.5.1 to 3.5.4 show some of the input data and bending moment and stress results. The stress results are plotted versus significant wave height, and the total stress (wave, slamming and stillwater) was compared with the yield strength of the material for each ship. All values above the dotted line in Tables 3.5.1 to 3.5.4 are inputs and the values below it are the results.

For all vessels analyzed, total stresses in the deck remained well below the yield strength of the material and the ultimate strength even in the most severe sea state. The results indicate superior stress characteristics of the two cruisers compared to the commercial ships. The cruisers use high strength steel more extensively. The spacing of the intercostals and other longitudinals in the bottom of the cruisers is closer than that of the tanker or the SL-7 ship.

The total stress in the bottom of the cruisers is also well below the yield and ultimate strength. For the Tanker and the SL-7, however, the total bottom stress is below the yield strength of the material, but exceeds the ultimate strength for a sea state characterized by a significant wave height of 15.5 m. This method seems to overestimate the load. Other slamming estimation methods are discussed and applied to the four ships in section 3.4 (see Eqns. (3.4.4) to (3.4.7)).
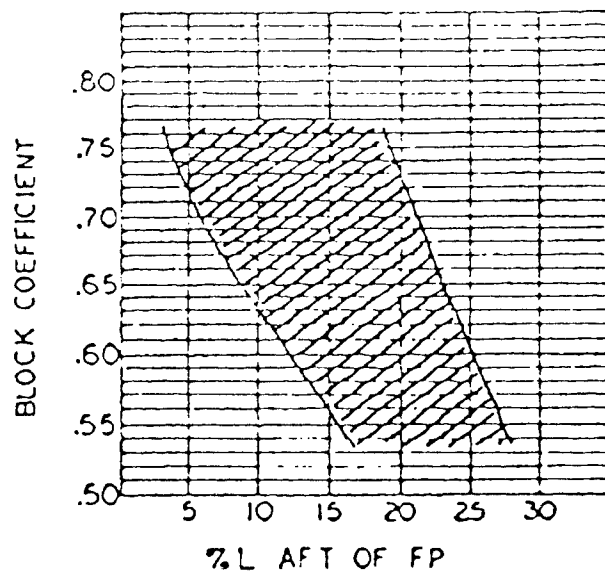
Figure 3.5.1 Longitudinal Location of Damage (SNAME T and R 2-30)

File   Data   Calculate   View   Window   Help

CRUISER1.SHP

Length between perpendiculars: 161.240 [m]   Breadth: 16.764 [m]

For Help press F1   NUM

Slamming - CRUISER1.SHP

File   Data   Calculate   View   Window   Help

Loading

	x-location	mass	radii
1	0.	37000	3.162
2	8.23	45000	3.162
3	15.39	52000	3.162
4	23.82	60000	3.162
5	32.25	62000	3.162
6	40.31	63000	3.162
7	48.37	67000	3.162
8	56.43	72000	3.162
9	64.5	74700	3.162
10	72.56	84000	3.162
11	80.62	92400	3.162
12	88.68	68800	3.162
13	96.74	76700	3.162
14	104.8	68800	3.162
15	112.87	65000	3.162

Mass distribution

Draught at midship 6.813 [m]   OK

Trim (Dap - Dfp) 0.066 [m]   Cancel

Length between perpendiculars: 161.240 [m]   Breadth: 16.764 [m]

For Help, press F1   NUM

Figure 3.5.2 Cruiser 1 Input Data

Ship Name	Cruiser 1	Cruiser 1	Cruiser 1	Cruiser 1	Cruiser 1	Cruiser 1
Sig Wave Hieght (m)	4	6	8	10	12	15.5
Wave Period (s)	7.1	8.7	10	11.2	12.3	14
Ship Speed (m/s)	15	12	9	6	6	4
Heading Angle (deg)	180	180	180	180	180	180
Number of Modes	2	2	2	2	2	2
Number of Simulations	250	250	250	250	250	250
Number of Frequencies	160	160	160	160	160	160
Number of Integration Points	41	41	41	41	41	41
Low Frequency (rad/sec)	0	0	0	0	0	0
High Frequency (rad/sec)	8	8	8	8	8	8
Slam Impact Position (m)	122.54	122.54	122.54	122.54	122.54	122.54
B.M. Calculation Position (m)	80.62	80.62	80.62	80.62	80.62	80.62
Upcrossing Rate (1/sec)	1.29E-05	2.14E-03	1.95E-03	2.47E-04	4.35E-04	4.87E-05
Bending Moments (MNm)						
Mean Slam - Sag (Std Dev)	-1.54 (1)	-3.29 (2)	-1.66 (2)	-3.02 (2)	-2.84 (2)	-2.15 (1)
Mean Slam - Hog (Std Dev)	1.89 (2)	3.98 (3)	2.22 (3)	4.52 (3)	4.36 (3)	3.64 (2)
Mean Wave - Sag (Std Dev)	-300.29 (66)	-267.20 (25)	-408.26 (50)	-584.90 (44)	-609.40 (46)	-713.95 (32)
Mean Wave - Hog (Std Dev)	300.29 (66)	267.20 (25)	408.26 (50)	584.90 (44)	609.40 (46)	713.95 (32)
Mean Combined - Sag (Std Dev)	-300.58 (66)	-265.70 (25)	-407.70 (50)	-583.14 (44)	-608.00 (47)	-713.33 (33)
Mean Combined - Hog (Std Dev)	301.03 (65)	271.01 (25)	409.66 (51)	586.50 (45)	611.15 (47)	714.83 (32)
Extreme Combined Sag	-495	-383	-554	-730	-765	-842
Extreme Combined Hog	495	385	564	736	760	841
Section Modulus at Midship (m^3)						
Deck	4.48	4.48	4.48	4.48	4.48	4.48
Bottom	5.05	5.05	5.05	5.05	5.05	5.05
Stresses & Strengths at Midship (MN/m^2)						
Deck						
Stillwater Stress	43.18	43.18	43.18	43.18	43.18	43.18
Slamming & Wave Stress	110.38	85.41	123.54	162.78	170.59	187.76
Total Induced Stress	67.20	42.23	80.36	119.60	127.41	144.58
Yield Strength	563.84	563.84	563.84	563.84	563.84	563.84
Ultimate Strength	349.96	349.96	349.96	349.96	349.96	349.96
Bottom						
Stillwater Stress	43.18	43.18	43.18	43.18	43.18	43.18
Slamming & Wave Stress	98.07	76.28	111.74	145.82	150.58	166.62
Total Induced Stress	141.25	119.46	154.92	189.00	193.75	209.80
Yield Strength	547.22	547.22	547.22	547.22	547.22	547.22
Ultimate Strength	314.00	314.00	314.00	314.00	314.00	314.00

Table 3.5.1 Cruiser 1 Slamming Effects for Various Sea State
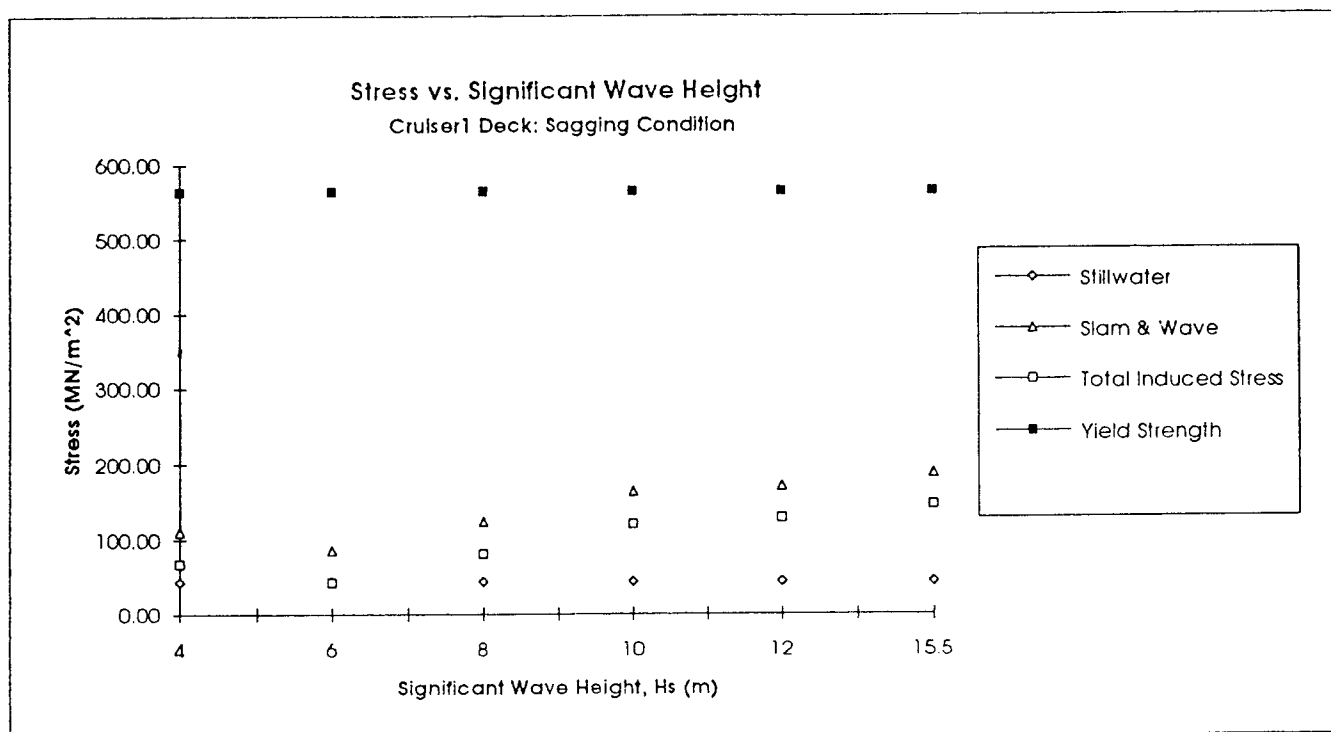
Figure 3.5.3 Comparison of Stresses and Yield Strength for Cruiser 1

File   Data   Calculate   View   Window   Help

Length between perpendiculars: 161.240 [m]   Breadth: 16.764 [m]

For Help, press F1   NUM

Slamming - CRUISER2.SHP

File   Data   Calculate   View   Window   Help

	x-location	mass	radii
1	0	41000	3.162
2	8.23	47000	3.162
3	15.39	49000	3.162
4	23.82	53000	3.162
5	32.25	52000	3.162
6	40.31	54000	3.162
7	48.37	59000	3.162
8	56.43	69000	3.162
9	64.5	81000	3.162
10	72.56	78000	3.162
11	80.62	75000	3.162
12	88.68	74000	3.162
13	96.74	77000	3.162
14	104.8	75000	3.162
15	112.87	56000	3.162

Mass distribution

Draught at midship 6.547 [m]

Trim (Dap - Dfp) 0.019 [m]

OK

Cancel

Length between perpendiculars: 161.240 [m]   Breadth: 16.764 [m]

For Help, press F1   NUM

Figurte 3.5.4 Cruiser 2 Input Data

Ship Name	Cruiser 2	Cruiser 2	Cruiser 2	Cruiser 2	Cruiser 2	Cruiser 2
Sig Wave Hieght (m)	4	6	8	10	12	15.5
Wave Period (s)	7.1	8.7	10	11.2	12.3	14
Ship Speed (m/s)	15	12	9	6	6	4
Heading Angle (deg)	180	180	180	180	180	180
Number of Modes	2	2	2	2	2	2
Number of Simulations	250	250	250	250	250	250
Number of Frequencies	160	160	160	160	160	160
Number of Integration Points	41	41	41	41	41	41
Low Frequency (rad/sec)	0	0	0	0	0	0
High Frequency (rad/sec)	8	8	8	8	8	8
Slam Impact Position (m)	117.7	117.7	117.7	117.7	117.7	117.7
B.M. Calculation Position (m)	80.62	80.62	80.62	80.62	80.62	80.62
Upcrossing Rate (1/sec)	1.29E-05	1.73E-03	1.24E-03	7.05E-05	1.33E-04	4.76E-06
Bending Moments (MNm)						
Mean Slam - Sag (Std Dev)	-1.63 (2)	-3.83 (2)	-3.86 (2)	-3.96 (2)	-3.87 (2)	-3.28 (2)
Mean Slam - Hog (Std Dev)	1.95 (2)	4.52 (3)	5.03 (3)	5.58 (3)	5.50 (3)	5.05 (3)
Mean Wave - Sag (Std Dev)	-276.47 (75)	-225.97 (21)	-353.67 (53)	-555.25 (54)	-582.58 (58)	-736.53 (48)
Mean Wave - Hog (Std Dev)	276.47 (75)	225.97 (21)	353.67 (53)	555.25 (54)	582.58 (58)	736.53 (48)
Mean Combined - Sag (Std Dev)	-276.56 (75)	-224.65 (22)	-351.77 (53)	-554.71 (52)	-581.16 (57)	-735.58 (47)
Mean Combined - Hog (Std Dev)	276.95 (74)	230.29 (22)	357.93 (53)	557.20 (55)	584.38 (59)	737.89 (48)
Extreme Combined Sag	-494	-336	-513	-722	-762	-902
Extreme Combined Hog	494	339	514	746	774	899
Section Modulus at Midship (m^3)						
Deck	4.80	4.80	4.80	4.80	4.80	4.80
Bottom	5.23	5.23	5.23	5.23	5.23	5.23
Stresses & Strengths at Midship (MN/m^2)						
Deck						
Stillwater Stress	33.55	33.55	33.55	33.55	33.55	33.55
Slamming & Wave Stress	102.88	69.97	106.83	150.36	158.69	187.84
Total Induced Stress	69.33	36.42	73.28	116.81	125.14	154.29
Yield Strength	330.84	330.84	330.84	330.84	330.84	330.84
Ultimate Strength	287.07	287.07	287.07	287.07	287.07	287.07
Bottom						
Stillwater Stress	33.55	33.55	33.55	33.55	33.55	33.55
Slamming & Wave Stress	94.51	64.86	98.34	142.72	148.08	171.99
Total Induced Stress	128.06	98.40	131.88	176.27	181.63	205.54
Yield Strength	334.99	334.99	334.99	334.99	334.99	334.99
Ultimate Strength	253.75	253.75	253.75	253.75	253.75	253.75

Table 3.5.2 Cruiser 2 Slamming Effects for Various Sea States
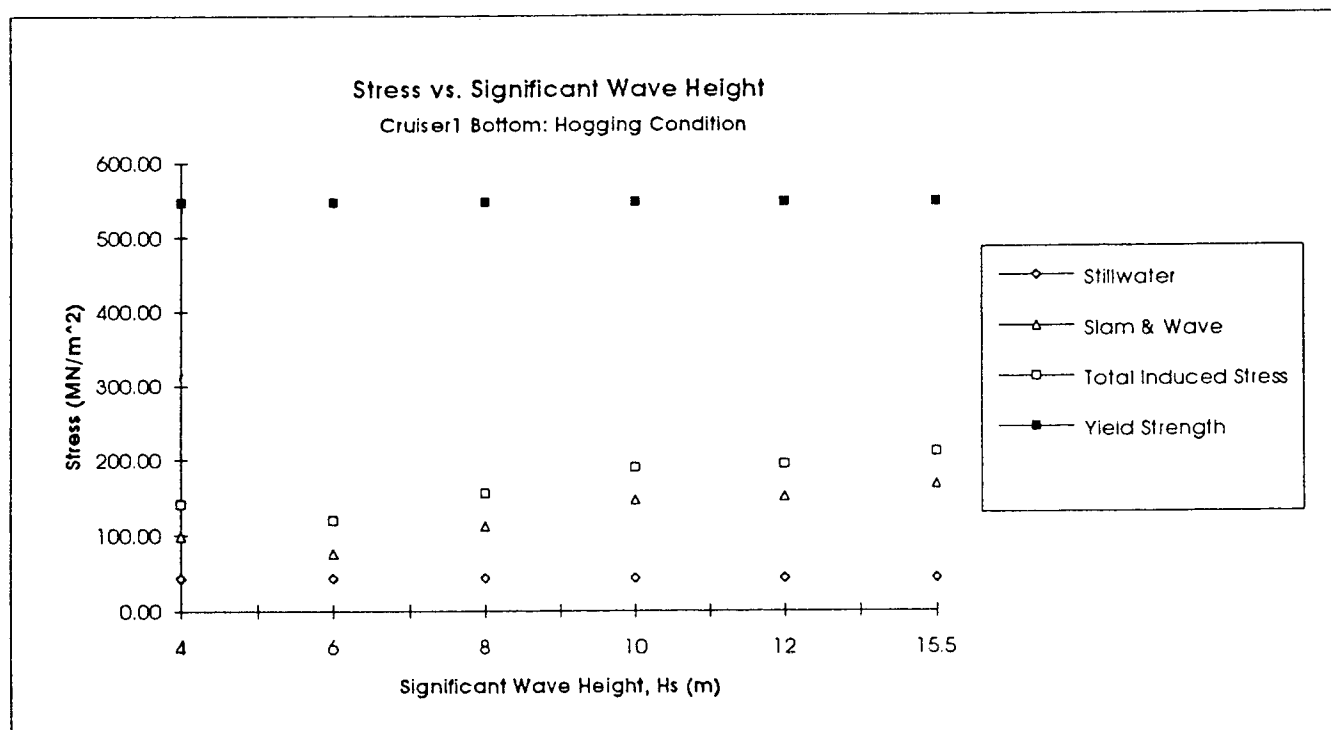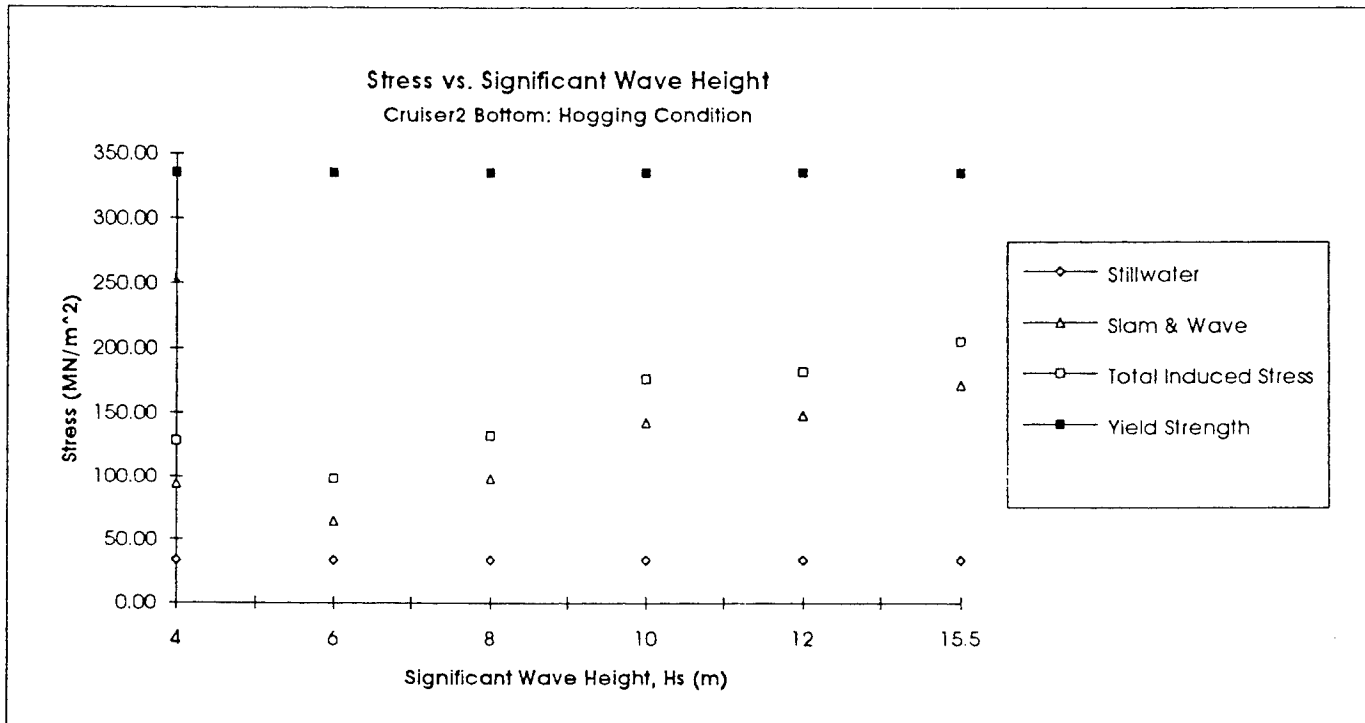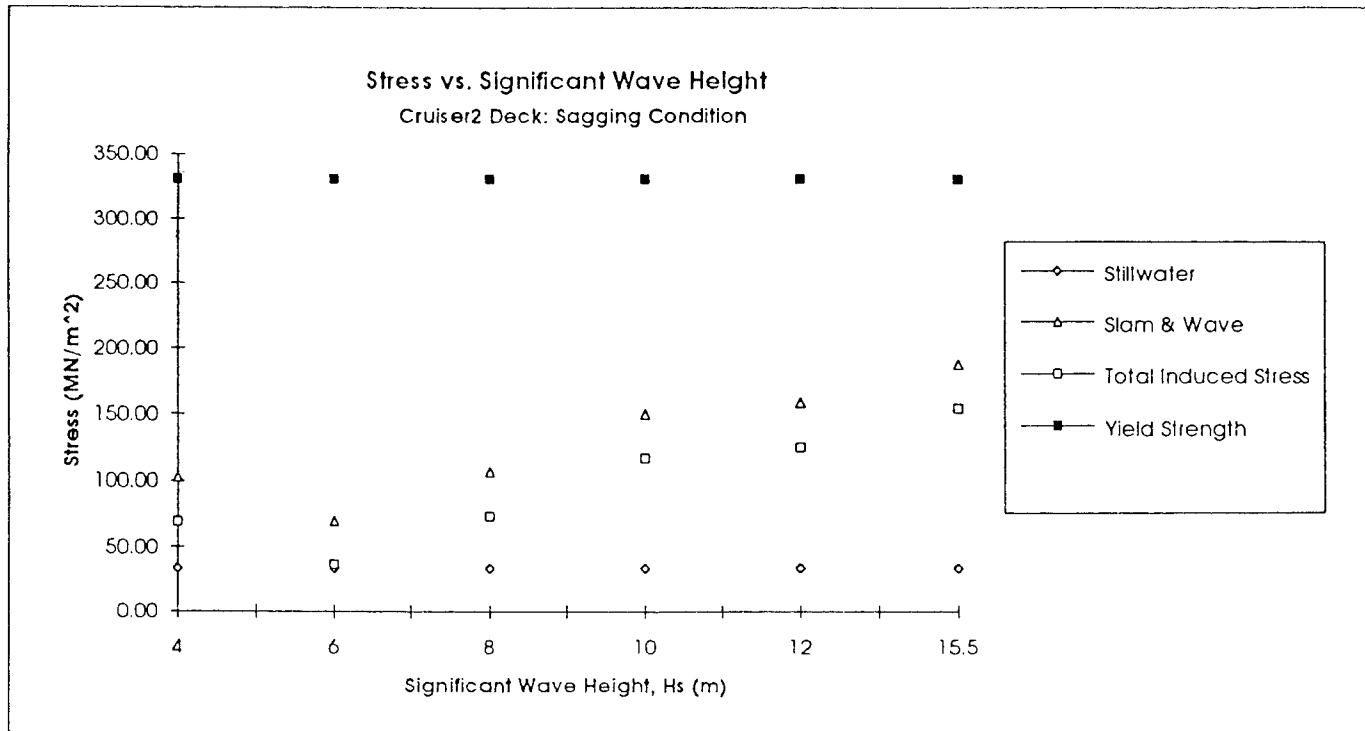
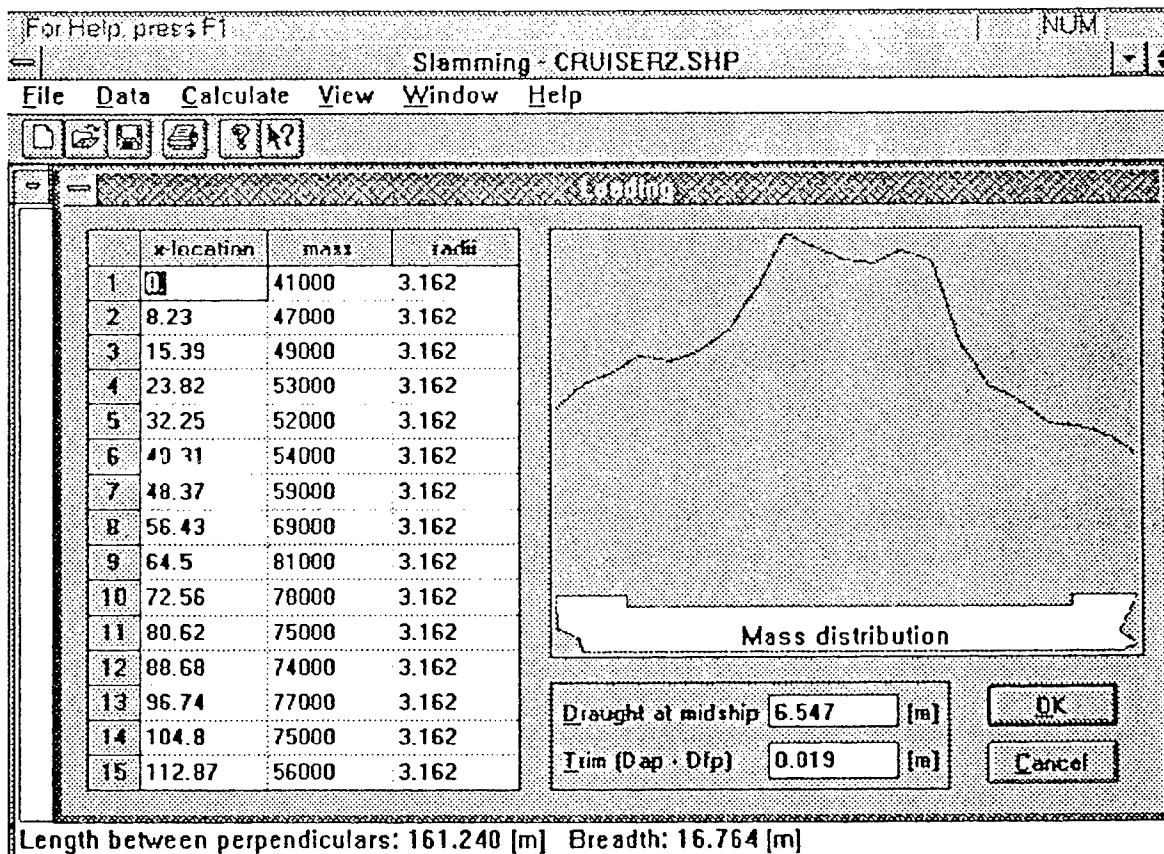Figure 3.5.5 Comparison of Stresses and Yield Strength for Cruiser 2
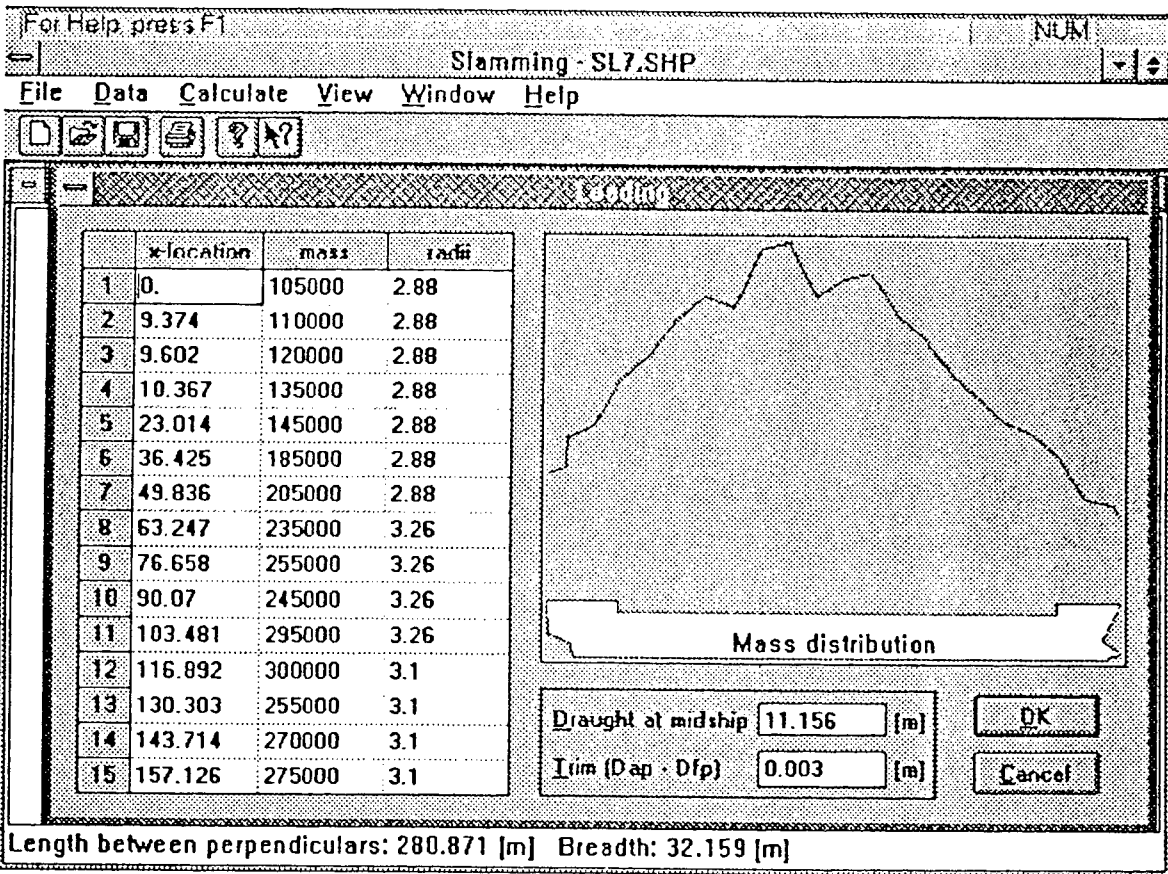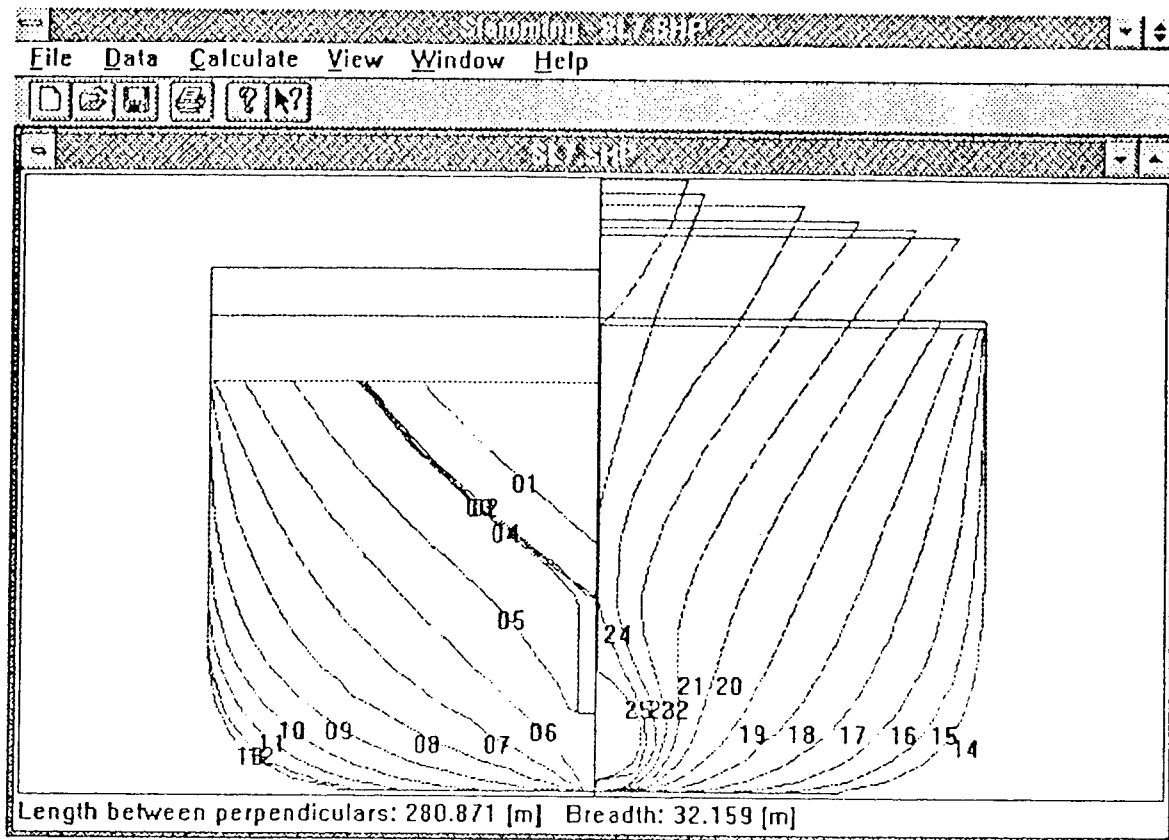
Figure 3.5.6 SL-7 Input Data

Ship Name	SL-7	SL-7	SL-7	SL-7	SL-7	SL-7
Sig Wave Height (m)	4	6	8	10	12	15.5
Wave Period (s)	7.1	8.7	10	11.2	12.3	14
Ship Speed (m/s)	10	8	6	4	4	3
Heading Angle (deg)	180	180	180	180	180	180
Number of Modes	2	2	2	2	2	2
Number of Simulations	250	250	250	250	250	250
Number of Frequencies	160	160	160	160	160	160
Number of Integration Points	41	41	41	41	41	41
Low Frequency (rad/sec)	0	0	0	0	0	0
High Frequency (rad/sec)	8	8	8	8	8	8
Slam Impact Position (m)	222	222	222	222	222	222
B.M. Calculation Position (m)	140.435	140.435	140.435	140.435	140.435	140.435
Upcrossing Rate (1/sec)	5.45E-25	2.17E-08	1.81E-06	2.10E-06	1.50E-05	2.71E-05
Bending Moments (MNm)						
Mean Slam - Sag (Std Dev)	-0.42 (2)	-2.19 (3)	-7.12 (4)	-3.00 (2)	-2.75 (2)	-3.65 (2)
Mean Slam - Hog (Std Dev)	0.44 (2)	2.28 (4)	13.29 (8)	9.65 (5)	8.99 (6)	9.79 (6)
Mean Wave - Sag (Std Dev)	-3551.50 (333)	-2727.94 (70)	-3381.13 (116)	-4193.22 (112)	-4349.39 (100)	-4726.03 (79)
Mean Wave - Hog (Std Dev)	3551.50 (333)	2727.94 (70)	3381.13 (116)	4193.22 (112)	4349.39 (100)	4726.03 (79)
Mean Combined - Sag (Std Dev)	-3551.27 (334)	-2728.51 (69)	-3375.76 (117)	-4191.19 (112)	-4347.44 (100)	-4722.94 (78)
Mean Combined - Hog (Std Dev)	3551.82 (333)	2729.78 (69)	3384.27 (114)	4193.28 (112)	4349.43 (100)	4727.60 (81)
Extreme Sag	-4128	-2964	-3719	-4524	-4657	-5018
Extreme Hog	4174	2976	3730	4531	4667	5030
Section Modulus at Midship (m^3)						
Bottom	35.16	35.16	35.16	35.16	35.16	35.16
Stresses & Strengths at Midship (MN/m^2)						
Bottom						
Stillwater Stress	46.95	46.95	46.95	46.95	46.95	46.95
Slamming & Wave Stress	118.71	84.64	106.08	128.86	132.73	143.05
Total Induced Stress	165.66	131.59	153.03	175.81	179.68	190.00
Yield Strength	205.44	205.44	205.44	205.44	205.44	205.44
Ultimate Strength	163.57	163.57	163.57	163.57	163.57	163.57

Table 3.5.3 SL-7 Slamming Effects for Various Sea States
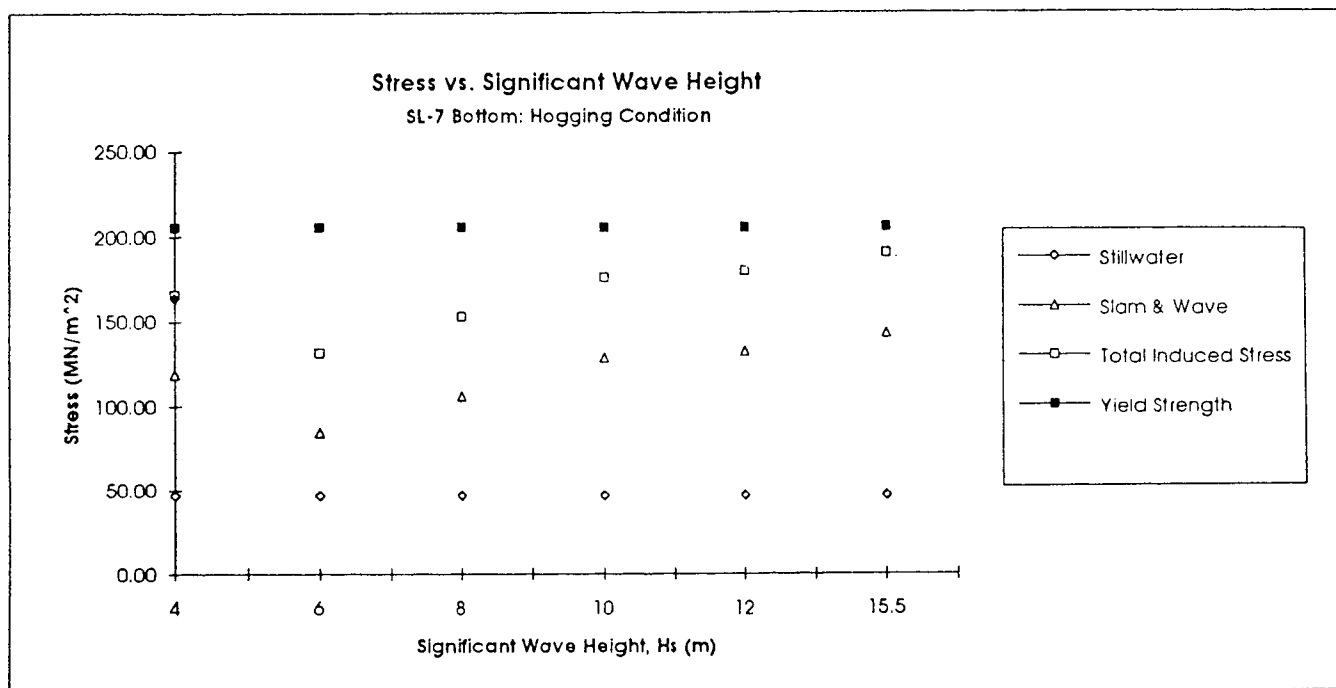
Figure 3.5.7 Comparison of Stresses and Yield Strength for SL-7

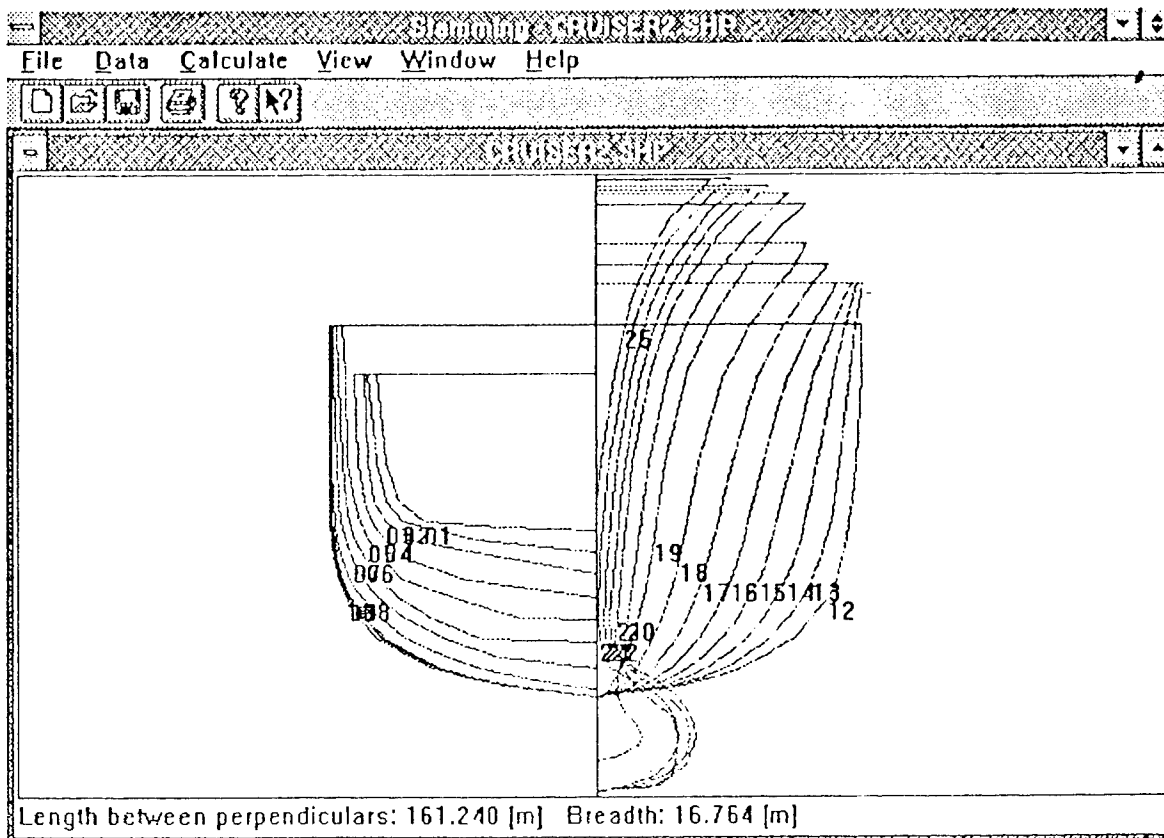3-39
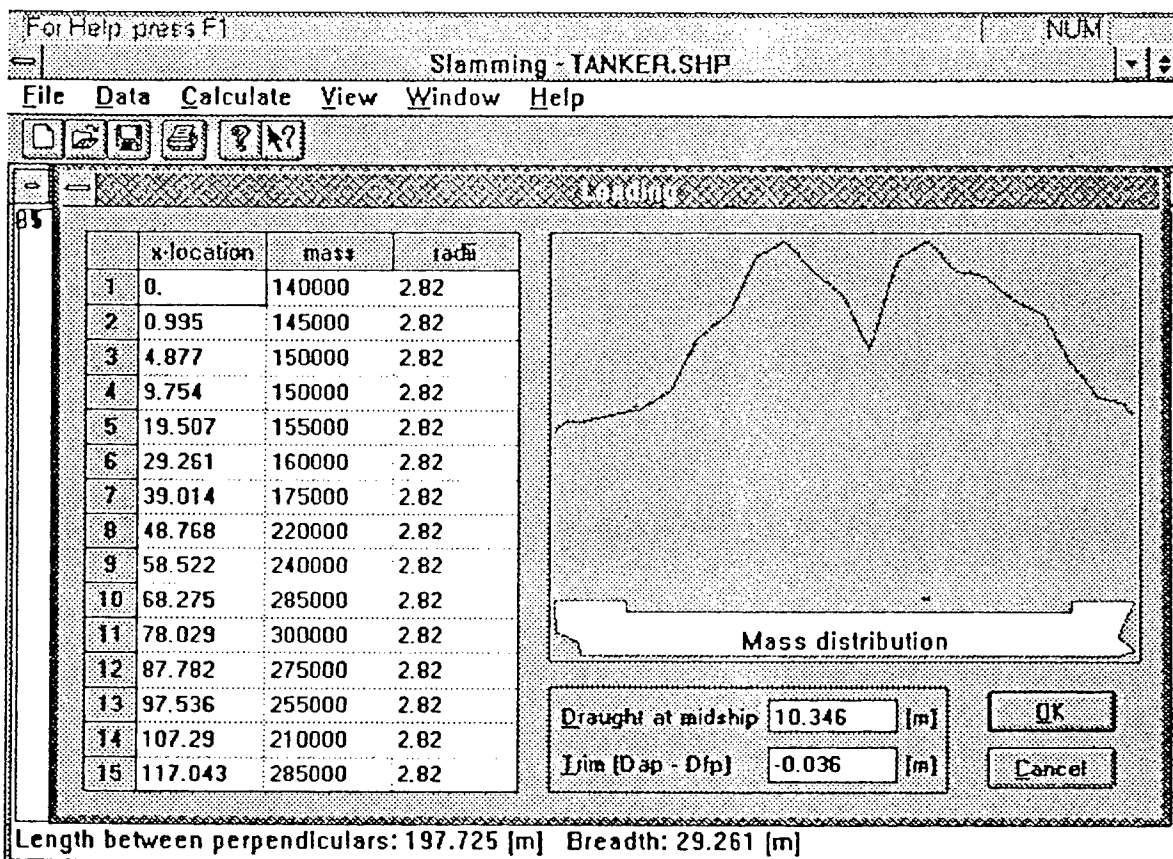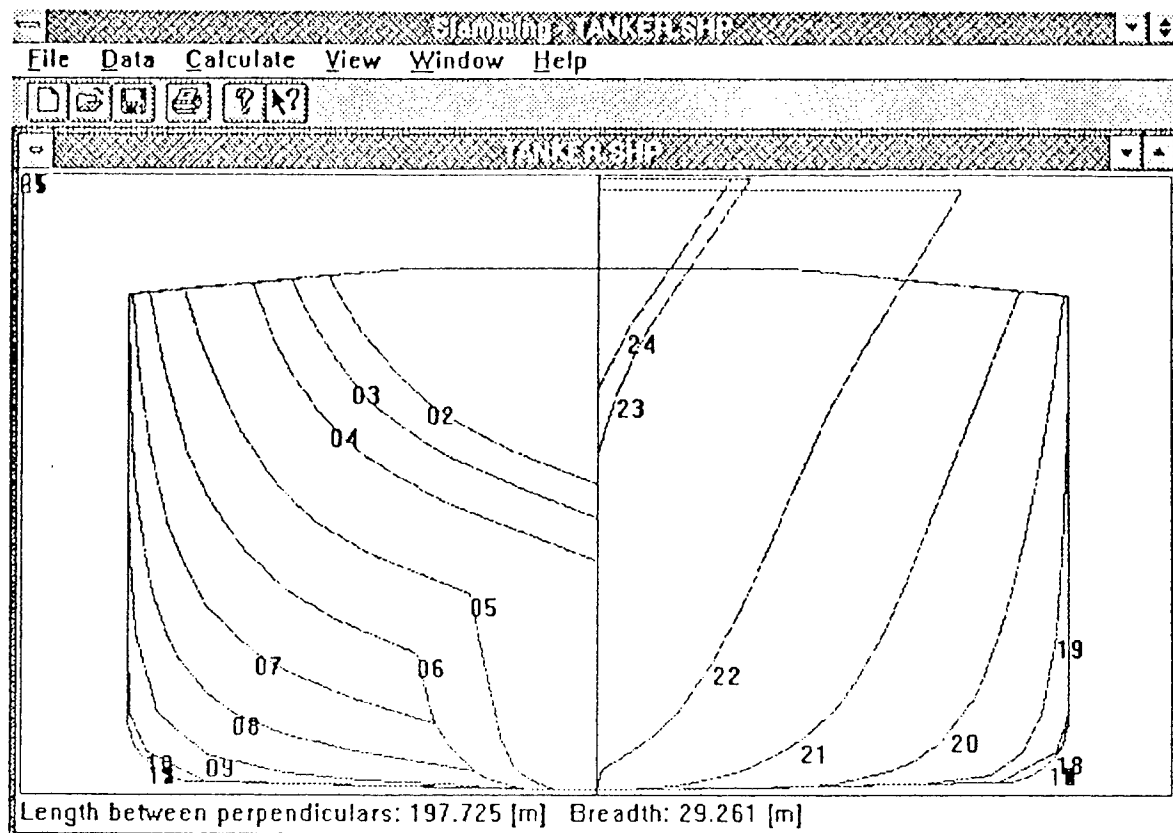
Figure 3.5.8 Tanker Input Data

Ship Name	Tanker	Tanker	Tanker	Tanker	Tanker	Tanker
Sig Wave Height (m)	4	6	8	10	12	15.5
Wave Period (s)	7.1	8.7	10	11.2	12.3	14
Ship Speed (m/s)	10	8	6	4	4	3
Heading Angle (deg)	180	180	180	180	180	180
Number of Modes	2	2	2	2	2	2
Number of Simulations	250	250	250	250	250	250
Number of Frequencies	160	160	160	160	160	160
Number of Integration Points	41	41	41	41	41	41
Low Frequency (rad/sec)	0	0	0	0	0	0
High Frequency (rad/sec)	8	8	8	8	8	8
Slam Impact Position (m)	176.5	176.5	176.5	176.5	176.5	176.5
B.M. Calculation Position (m)	98.863	98.863	98.863	98.863	98.863	98.863
Upcrossing Rate (1/sec)	2.04E-20	5.95E-07	2.89E-05	3.83E-05	1.31E-04	1.64E-04
Bending Moments (MNm)						
Mean Slam - Sag (Std Dev)	-1.02 (3)	-19.10 (12)	-19.53 (11)	-17.25 (10)	-16.03 (9)	-6.41 (7)
Mean Slam - Hog (Std Dev)	1.08 (4)	19.78 (12)	19.93 (11)	17.54 (10)	16.07 (10)	6.74 (7)
Mean Wave - Sag (Std Dev)	-2132.87 (226)	-1505.41 (26)	-1674.86 (45)	-1947.99 (45)	-2006.16 (50)	-2172.63 (41)
Mean Wave - Hog (Std Dev)	2132.87 (226)	1505.41 (26)	1674.86 (45)	1947.99 (45)	2006.16 (50)	2172.63 (41)
Mean Combined - Sag (Std Dev)	-2133.03 (226)	-1497.41 (29)	-1664.91 (51)	-1945.27 (53)	-2012.59 (57)	-2176.14 (45)
Mean Combined - Hog (Std Dev)	2133.24 (226)	1516.52 (28)	1679.08 (50)	1958.54 (46)	2011.07 (47)	2177.80 (45)
Extreme Combined Sag	-2506	-1599	-1860	-2147	-2216	-2343
Extreme Combined Hog	2506	1646	1899	2112	2185	2336
Section Modulus at Midship (m^3)						
Deck	15.91	15.91	15.91	15.91	15.91	15.91
Bottom	19.92	19.92	19.92	19.92	19.92	19.92
Stresses & Strengths at Midship (MN/m^2)						
Deck						
Stillwater Stress	41.33	41.33	41.33	41.33	41.33	41.33
Slamming & Wave Stress	157.52	100.51	116.92	134.96	139.29	147.28
Total Induced Stress	116.19	59.18	75.59	93.63	97.96	105.95
Yield Strength	313.81	313.81	313.81	313.81	313.81	313.81
Ultimate Strength	199.97	199.97	199.97	199.97	199.97	199.97
Bottom						
Stillwater Stress	64.13	64.13	64.13	64.13	64.13	64.13
Slamming & Wave Stress	125.78	82.62	95.31	106.01	109.67	117.25
Total Induced Stress	189.91	146.74	159.44	170.13	173.80	181.38
Yield Strength	234.50	234.50	234.50	234.50	234.50	234.50
Ultimate Strength	170.06	170.06	170.06	170.06	170.06	170.06

Table 3.5.4 Tanker Slamming Effects for Various Sea States
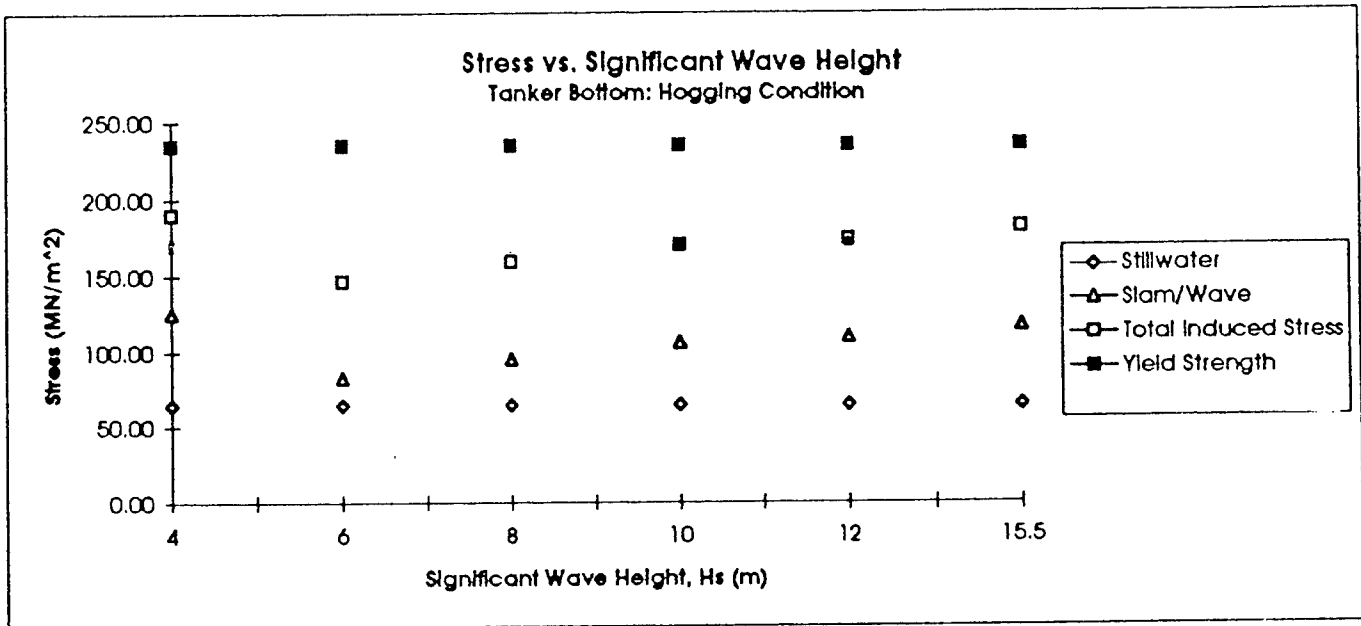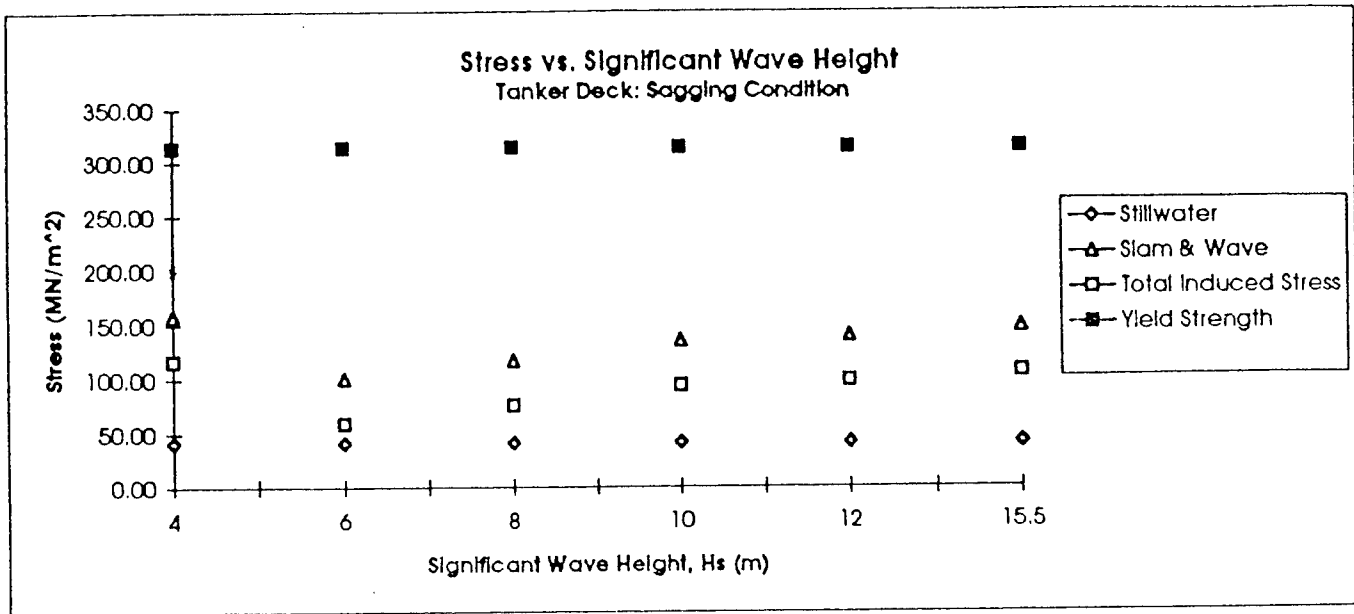
Figure 3.5.9 Comparison of Stresses and Yield Strength for Tanker

# 4. DATA BASE ON STRUCTURAL STRENGTH FOR FOUR SHIPS

In this chapter, the strength component of the reliability analysis is considered for the four ships. First, the global hull strength (primary failure mode) was estimated under vertical bending moment and under combined vertical and horizontal moments. Next, the strength of stiffened and unstiffened panels (secondary and tertiary failure modes) were determined for panels in the deck and in the bottom of all four ships. In all cases (primary, secondary and tertiary), the ALPS/ISUM computer program (see section 2.2.2) was used to determine the strength. A set of strength results were also obtained using the simple formulation discussed in section 2.2.5.

4.1 Hull Ultimate Strength — ALPS/ISUM Code Results

4.1.1 Hull Strength Under Vertical Moment:

The four ships under consideration, two cruisers, an SL-7 ship and a tanker were analyzed to determine their hull strength in hogging and sagging modes. The midship sections of Cruiser 1, the SL-7 and the Tanker are shown in Figures 4.1.1 to 4.1.3. Cruiser 2 midship section is similar to Cruiser 1. Prior to conducting the analysis, it was important to investigate the impact of residual stresses and initial deformations on the hull strength. The SL-7 ship and the Tanker were selected for this investigation.

A. Impact of Residual Stresses on Ultimate Strength:

The effect of residual stresses on the ultimate strength of the SL-7 containership was investigated using ALPS/ISUM (see section 2.2.2). The vertical bending moment-curvature relation for the ship referenced to the fully plastic moment is shown in Figure 4.1.4. Several values of the residual stress coefficient Cr are shown in the figure. Cr is defined as

$$Cr = \sigma_r/\sigma_o = \text{ratio of residual stress to yield strength} \qquad (4.1.1)$$

It can be seen from Figure 4.1.4 that increasing the residual stress will decrease the ultimate moment capacity. In particular, changing Cr from 0.2 to 0.4 decreases considerably the moment capacity of the ship. Figures 4.1.5 and 4.1.6 show results for sagging and hogging moments referenced to the initial yield moment and the horizontal moment.

Based on the study performed by Mansour et al. (1990), the magnitude of the residual stress coefficient Cr will be taken as 0.1 in the following analysis for all four ships.

4-1
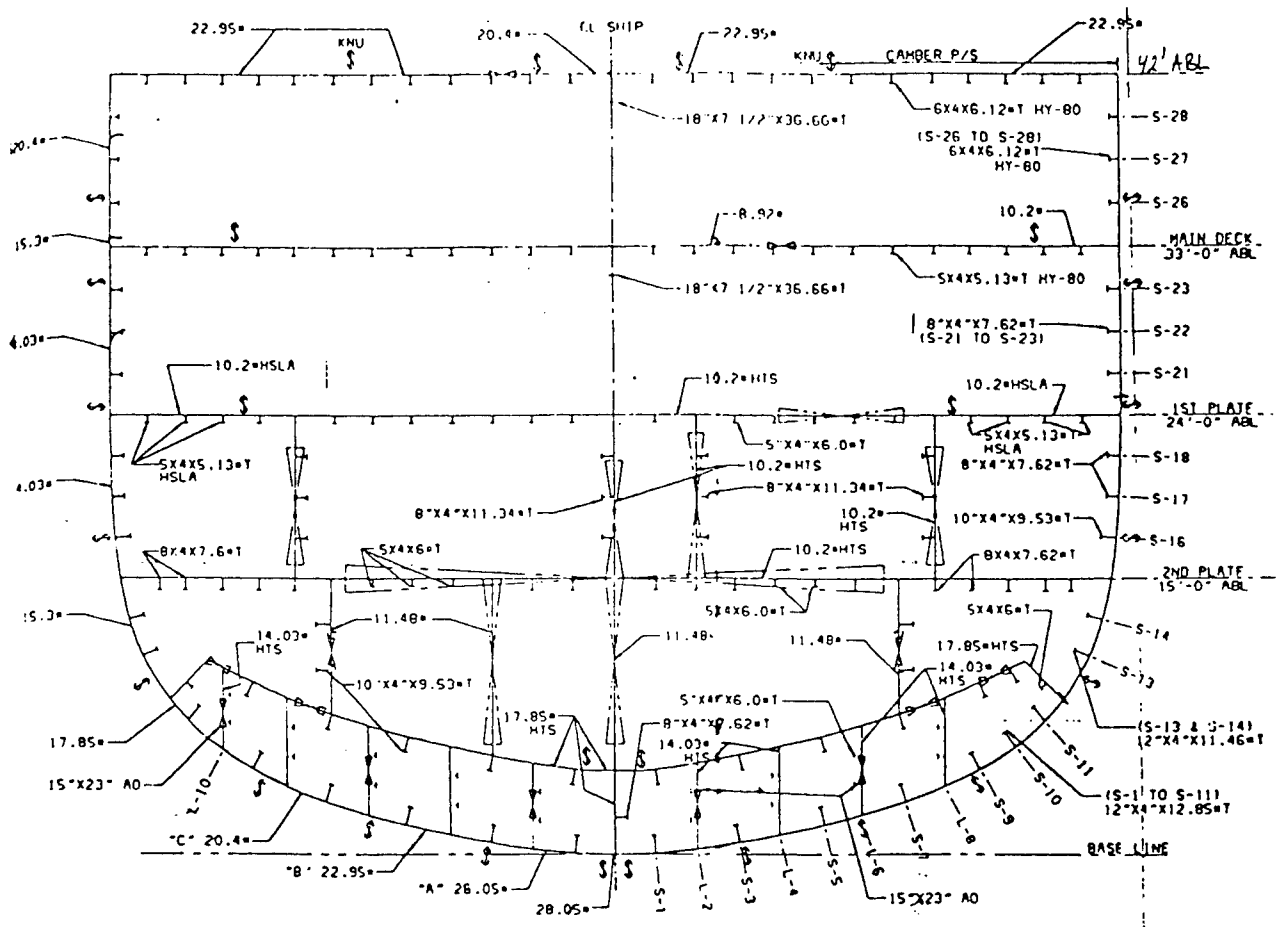
Figure 4.1.1 Station No. 10 — Cruiser 1
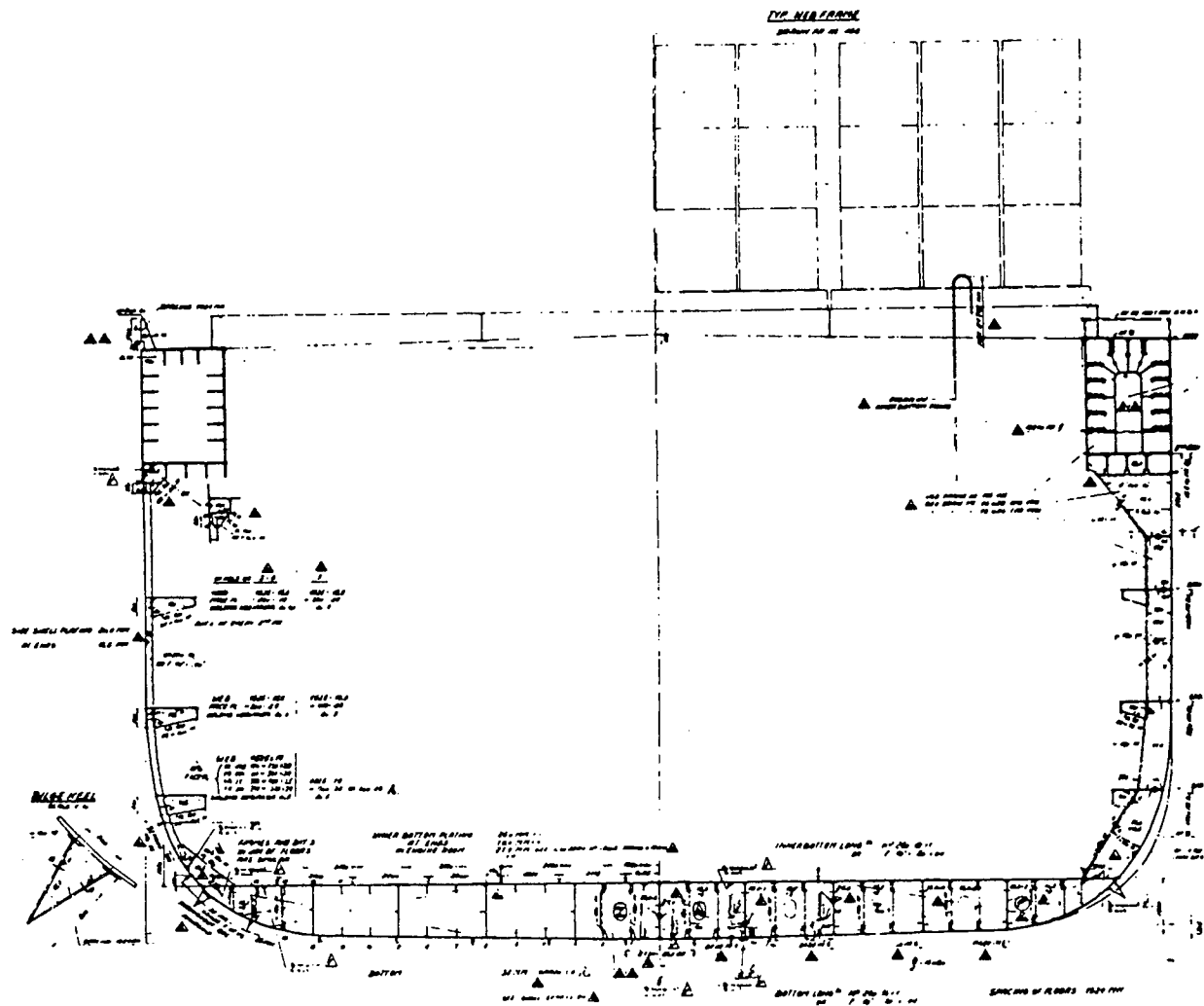
Figure 4.1.2 Midship Section of SL-7 Container Ship
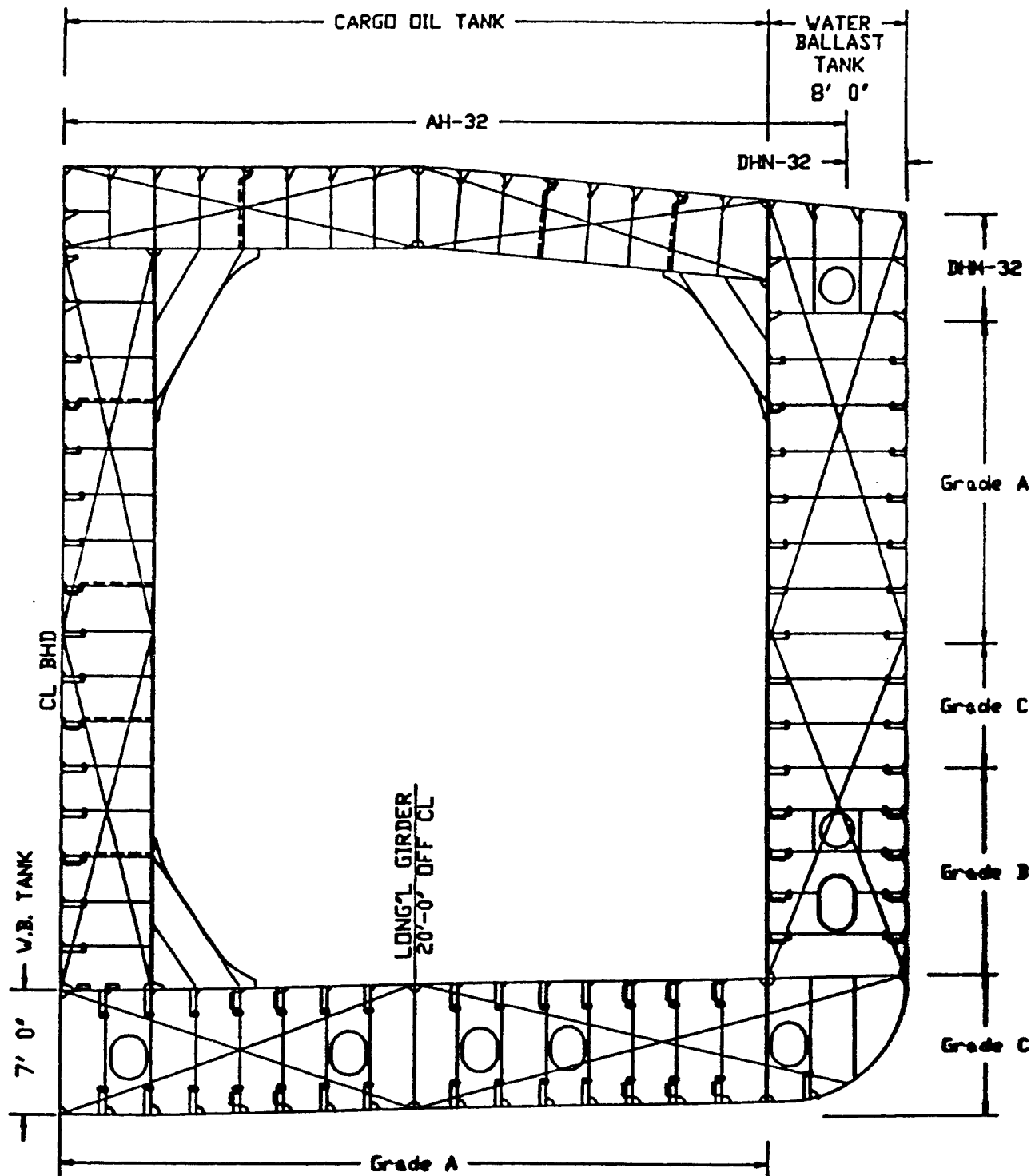
Figure 4.1.3 Midship Section of Tanker
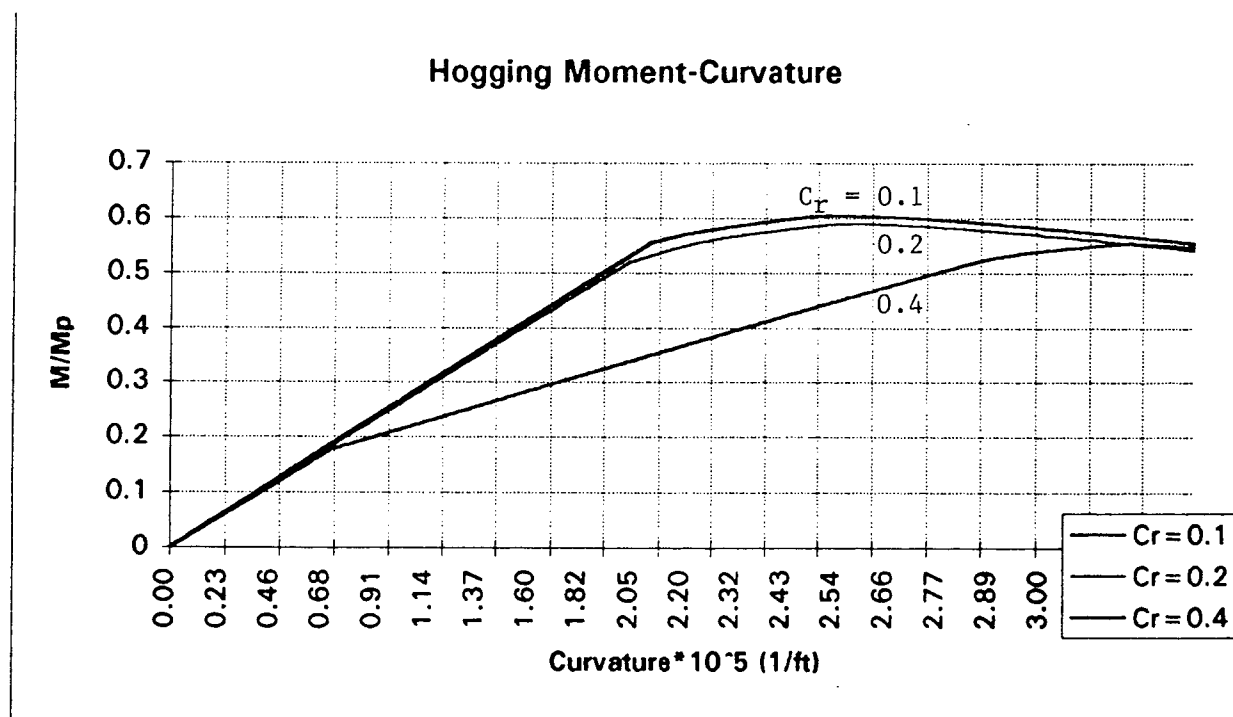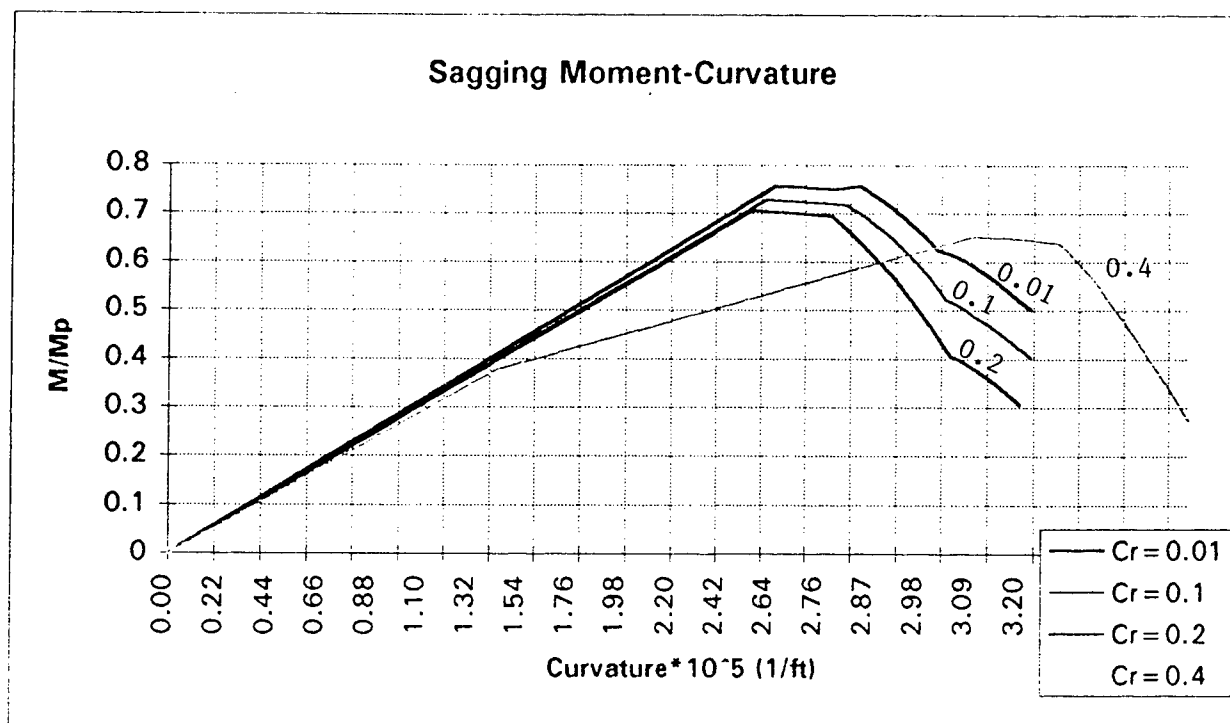
Figure 4.1.4 SL-7 Vertical Bending Moment-Curvature Relation
(Referenced to Fully Plastic Moment)
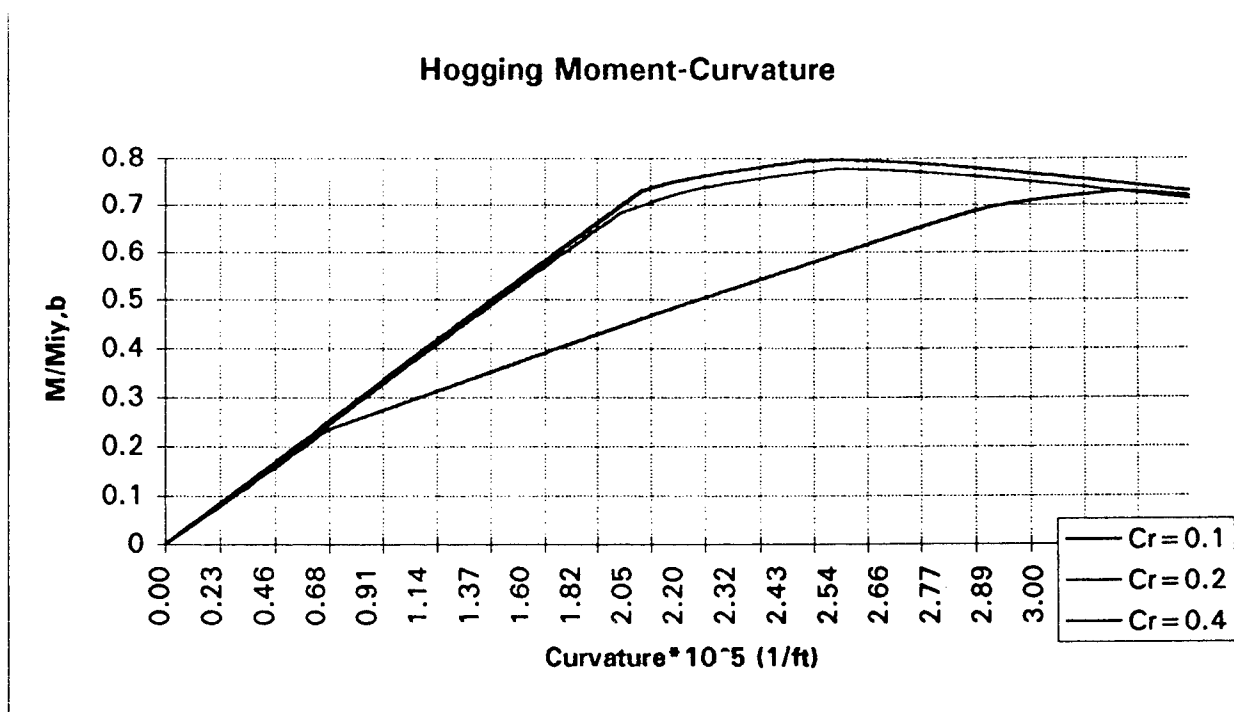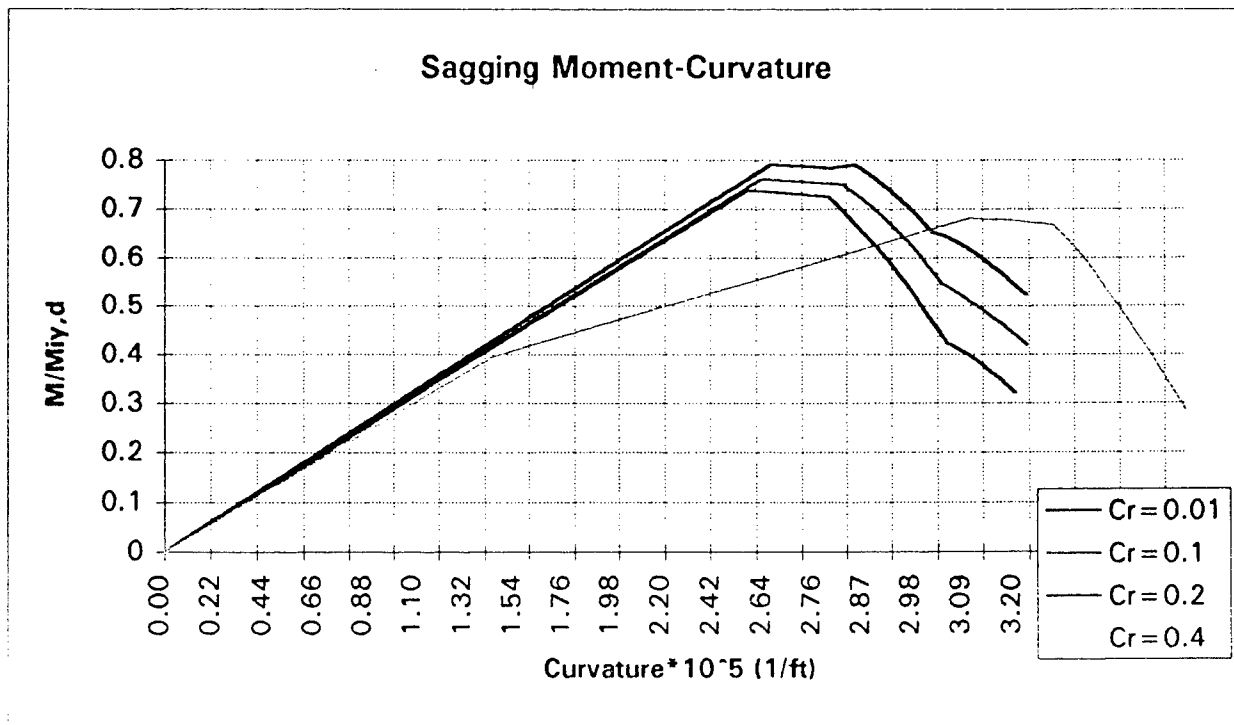
Figure 4.1.5 SL-7 Vertical Bending Moment-Curvature Relation
(Referenced to Initial Yield Moment)

Horizontal Moment-Curvature Relationship

Horizontal Moment-Curvature Relationship
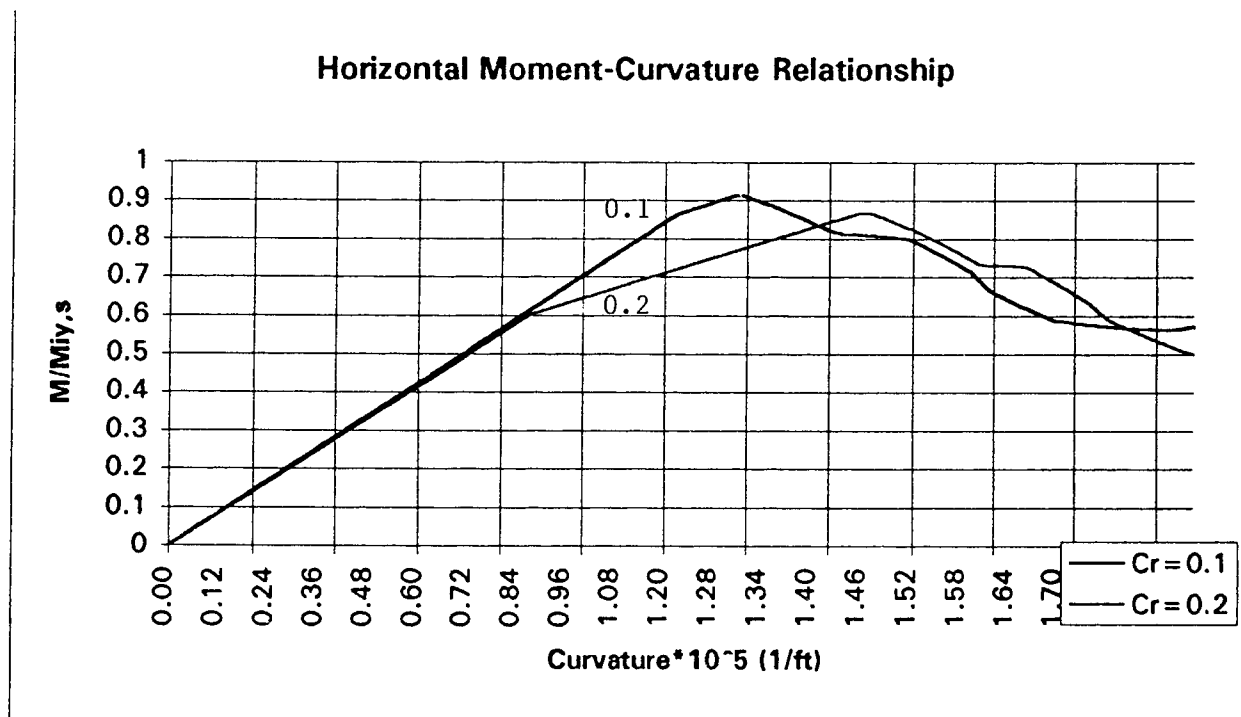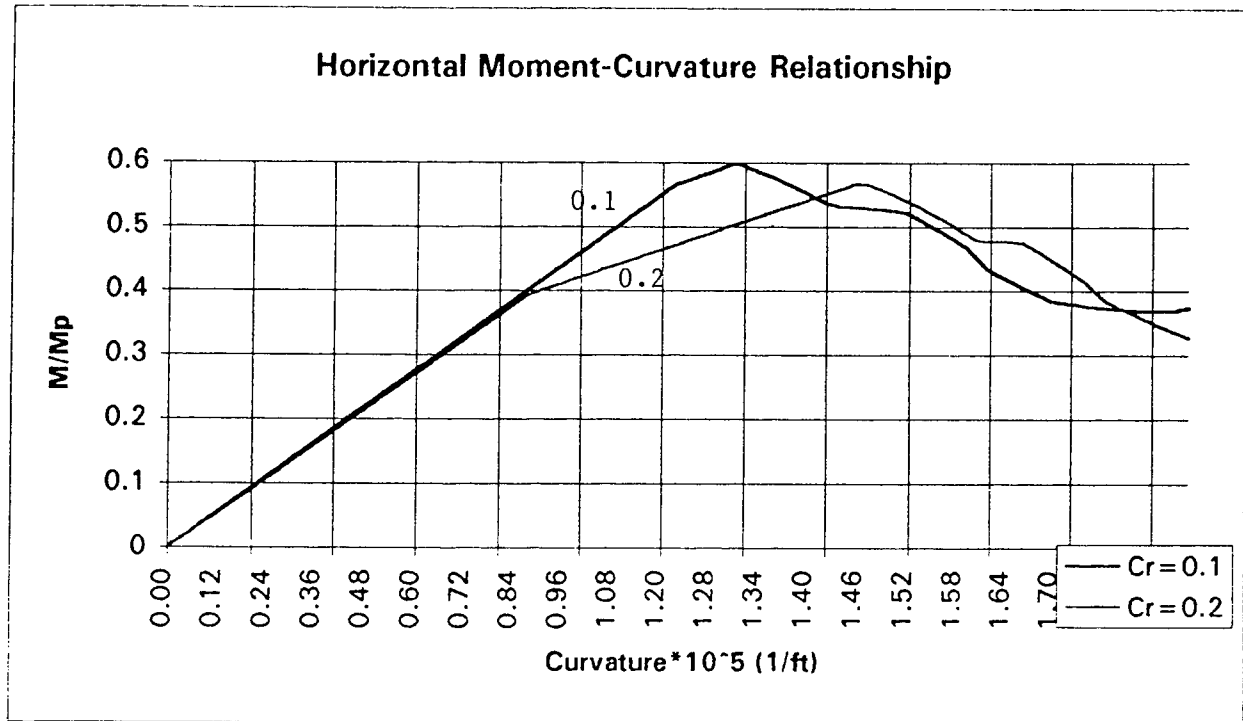
Figure 4.1.6 SL-7 Horizontal Bending Moment-Curvature Relation

B. Impact of Initial Deformation on Ultimate Strength:

The influence of initial deformation on ultimate strength was also studied using ALPS/ISUM. Figure 4.1.7 shows the vertical sagging moment-curvature relation for the double hull tanker for several values of initial deformation.

It can be seen that the impact of the initial deformation on the collapse moment is not small and careful consideration should be given in assigning a value for it. Based on the study conducted by Mansour *et al.* (1990), an initial deformation coefficient of 0.5 will be used for all four ships in the following study. This coefficient is defined as the maximum initial deflection divided by the plate thickness, i.e., A_{om}/t.

C. The Moment Curvature Relations for the Four Ships:

Figures 4.1.4 and 4.1.5 show the sagging and hogging collapse moments for the SL-7 ship, referenced to the fully plastic moment and to the initial yield moment, respectively. Figure 4.1.6 shows the horizontal collapse bending moment versus curvature, referenced to both fully plastic and initial yield moments. Similar results for the vertical and horizontal collapse moments for the remaining ships are shown in Figures 4.1.7 to 4.1.15. These results will be discussed in section 4.1.3.

4.1.2 Hull Strength Under Combined Vertical and Horizontal Moments — Interaction Relations:

The ultimate moment capacity of a ship hull under combined moments may be investigated numerically by applying a fixed horizontal moment while the vertical moment is increased until the maximum hull capacity is reached. Conversely, a fixed vertical moment can be held constant while the horizontal moment is increased. In a third procedure, which is used in this study, both vertical and horizontal moments are increased at each time step until one of these moments reaches its maximum value (the collapse moment).

Figure 4.1.16 shows the SL-7 containership sagging moment-curvature relation and the horizontal moment-curvature relation when applied simultaneously. Figure 4.1.17 shows the interaction relation resulting from repeating the procedure at different ratios of vertical to horizontal moments.

Figures 4.1.18 to 4.1.20 show similar results for the remaining three ships.

4.1.2.1 *Approximate analytical moment interaction relation:*

The study by Mansour and Thayamballi (1980) gives the following expression for the interaction relation between vertical and horizontal moments:

$$m_x + k \cdot m_y^2 = 1 \qquad \text{if} \qquad |m_y| < |m_x| \qquad (4.1.2)$$

and $\qquad m_y + k \cdot m_x^2 = 1 \qquad \text{if} \qquad |m_x| < |m_y|$

where

$$m_x = \frac{M_x}{M_{xu}}, \quad m_y = \frac{M_y}{M_{yu}}$$

$$k = \frac{(A + 2A_S)^2}{16A_S(A - A_S) - 4(A_D - A_B)^2} \qquad (4.1.3)$$

$$A = A_D + A_B + 2A_S$$

and
M_x = bending moment in vertical direction
M_y = bending moment in horizontal direction
M_{xu} = vertical ultimate collapse bending moment
M_{yu} = horizontal ultimate collapse bending moment
A_D = cross-sectional area of the deck including stiffeners
A_B = cross-sectional area of the bottom including stiffeners
A_S = cross-sectional area of one side including stiffeners

The above relation was originally derived for vertical and horizontal fully plastic moments (see Mansour and Thayamballi, 1980). The applicability of this interaction relation has been tested for the four ships under consideration to examine if it is still valid when the vertical and horizontal moments are ultimate collapse moments instead of fully plastic moments, i.e., when buckling is included.

The results are shown in Figures 4.1.21 to 4.1.24. The shown curves, which fit the numerical data best, are all based on eqn. (4.1.2) with $k = 0.8$. In Mansour and Thayamballi's report (1980), a value of $k = 0.78$ was calculated for a Tanker according to eqn. (4.1.3). The interaction relation (4.1.2) for the SL-7 containership shown in Figure 4.1.21 does not fit the numerical results as well as the other ships (Figures 4.1.22 to 4.1.24). The reason may be attributed to lack of deck in the containership.

4.1.3   Discussion of the Results:

Table 4.1.1 shows, for each of the four ships, the elastic section modulus at deck and at bottom, the vertical and horizontal moments of inertia, the vertical and horizontal fully plastic moments M_{pv} and M_{ph}, the initial yield moments at deck, bottom and side, the ultimate hogging and sagging moments and the ultimate horizontal moment. From Table 4.1.1, it can be seen that, although the elastic section moduli of the two cruisers are not very different, the initial yield moments at deck and bottom for Cruiser 1 are much larger than the

corresponding values for Cruiser 2. The reason for this is that more high strength steel is used in the construction of Cruiser 1 than in 2.

Ship	Cruiser 1	Cruiser 2	Tanker	SL-7
SM_d (in^2-ft)	23,384	25,021	74,093	143,340
SM_b (in^2-ft)	26,730	27,578	104,056	177,935
I_v (ft^4)	3,638	3,826	15,703	35,288
I_h (ft^4)	4,538	4,921	41,842	88,341
M_{pv} (LT-ft)	969,085	763,456	1,803,259	3,140,267
M_{ph} (LT-ft)	1,043,903	854,581	2,652,318	4,964,418
$M_{iy,d}$ (LT-ft)	834,496	524,309	1,505,536	3,003,612
$M_{iy,b}$ (LT-ft)	911,543	577,880	1,579,159	2,384,012
$M_{iy,s}$ (LT-ft)	847,187	539,970	1,905,008	3,230,715
M_u (LT-ft), hogging	523,050	437,737	1,118,237	1,898,130
M_u (LT-ft), sagging	517,948	454,948	1,049,942	2,285,396
M_u (LT-ft), horizontal	469,576	504,030	1,689,045	2,963,184

Table 4.1.1 Ultimate Strength Analysis of the Four Ships

The initial yield and fully plastic moments for the double hull tanker and the SL-7 ship are considerably higher than those for the cruisers. The elastic section moduli and cross sectional areas for these ships are much larger than those of the cruisers.

Table 4.1.2 shows the ratios of the hogging, sagging and horizontal ultimate moments for each ship to the fully plastic and initial yield moments. The ratio of the ultimate moment to the initial yield moment may be taken as an approximate measure of the efficiency of utilizing the material strength and the efficiency of the stiffening system against buckling. However, fatigue considerations which become more important for high strength steel limit the utilization of such a measure as a true indicator of the efficiency.

Returning to Table 4.1.2, one can see that extensive use of high strength steel in Cruiser 1 led to large discrepancy between the ratios of the ultimate moments to the initial yield moments when compared to those of Cruiser 2. These ratios, 0.574 in hogging and 0.621 in sagging for Cruiser 1, are much smaller than the corresponding values, 0.758 and 0.868 for Cruiser 2. The same trend is true for the ratios of the ultimate moment to the fully plastic moment. In general, the ratios of the ultimate moments to the initial yield and to the fully plastic moments are higher for the two commercial vessels than for Cruiser 1. The commercial vessels are constructed from lower strength steel.

	Ship	Cruiser 1	Cruiser 2	Tanker	SL-7
hogging	M_u (LT-ft)	523,050	437,737	1,118,237	1,898,130
	M_u/M_p	0.540	0.573	0.620	0.604
	$M_u/M_{iy,b}$	0.574	0.758	0.708	0.796
sagging	M_u (LT-ft)	517,948	454,948	1,049,942	2,285,396
	M_u/M_p	0.535	0.596	0.582	0.728
	$M_u/M_{iy,d}$	0.621	0.868	0.697	0.761
horizontal	M_u (LT-ft)	469,576	504,030	1,689,045	2,963,184
	M_u/M_p	0.450	0.590	0.637	0.600
	$M_u/M_{iy,s}$	0.554	0.933	0.887	0.917

Table 4.1.2 Ultimate Strength Ratios

It should be noted that the interaction relation given by eqn. (4.1.2) or Figures 4.1.21 to 4.1.24 can be used in two ways:

(a)   to determine the ultimate vertical bending moment for a given value of the horizontal moment, or

(b)   to determine the safe region (the region inside the curves) when a combination of vertical and horizontal moments occurs on a ship.
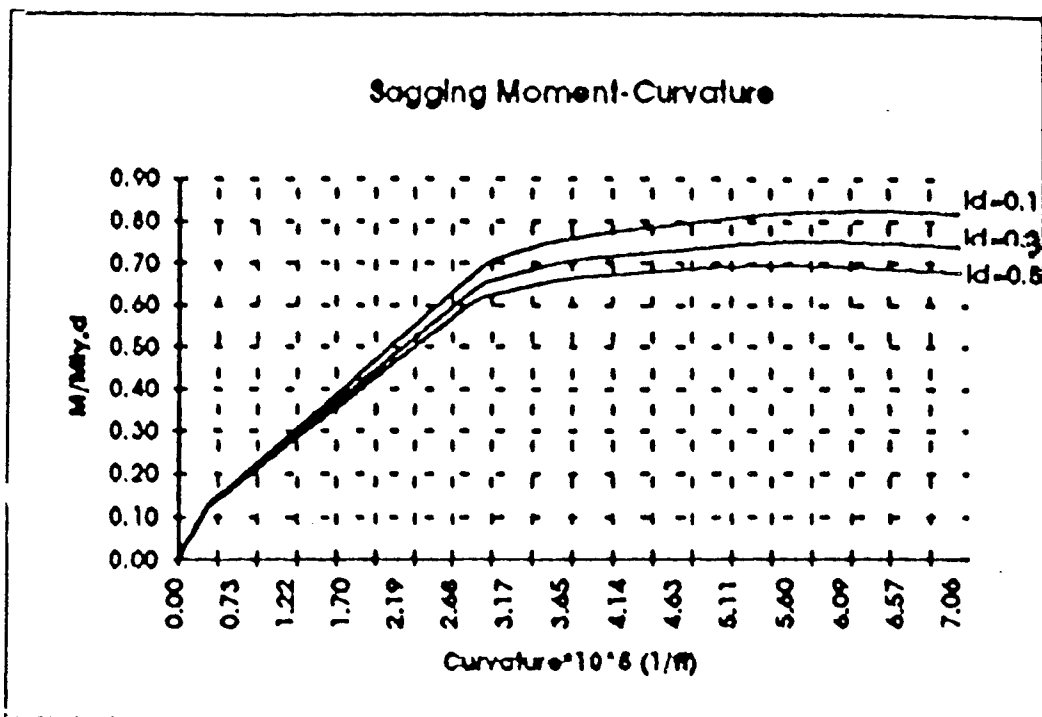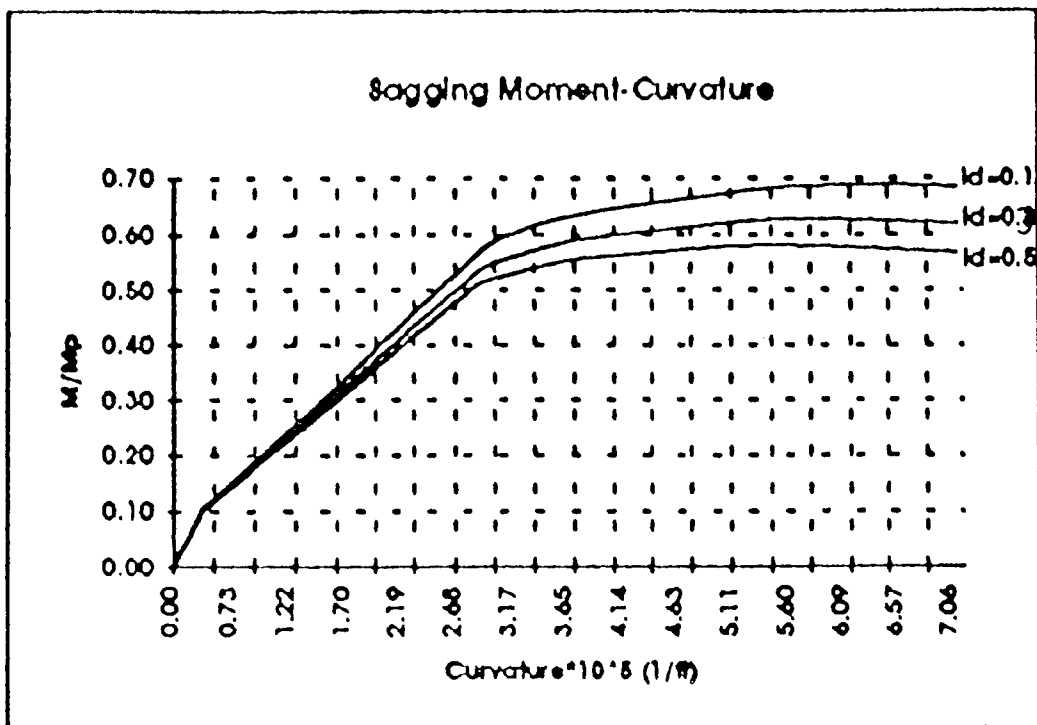
Figure 4.1.7 Tanker Vertical Bending Moment-Curvature Relation
(Referenced to Fully Plastic Moment)

4-12
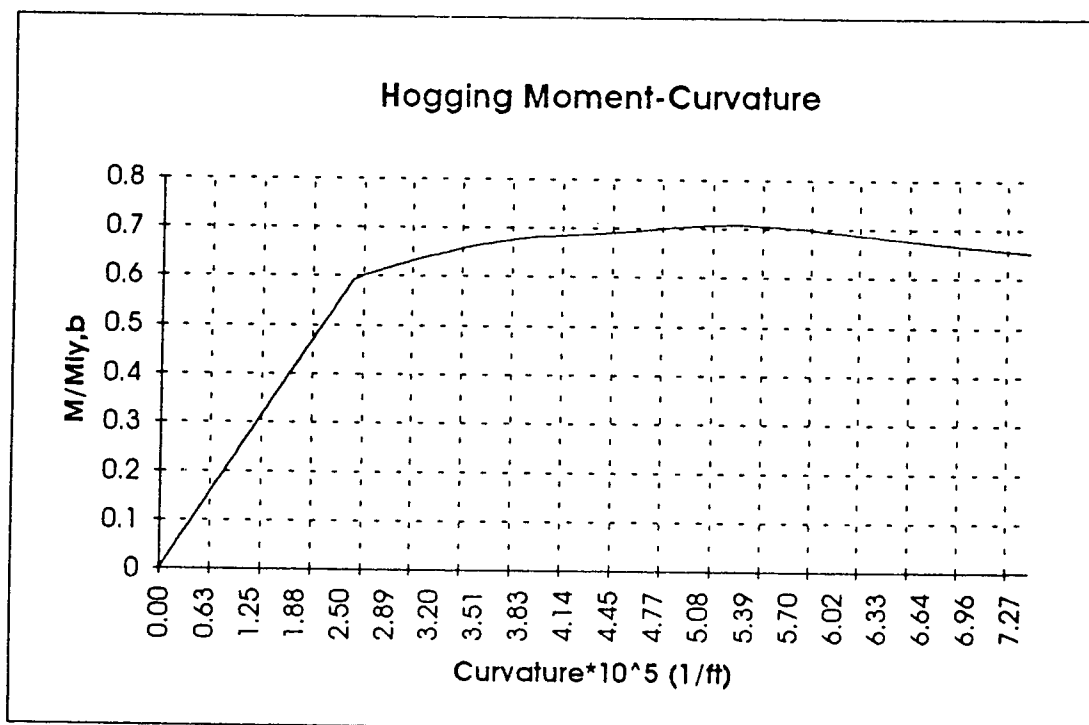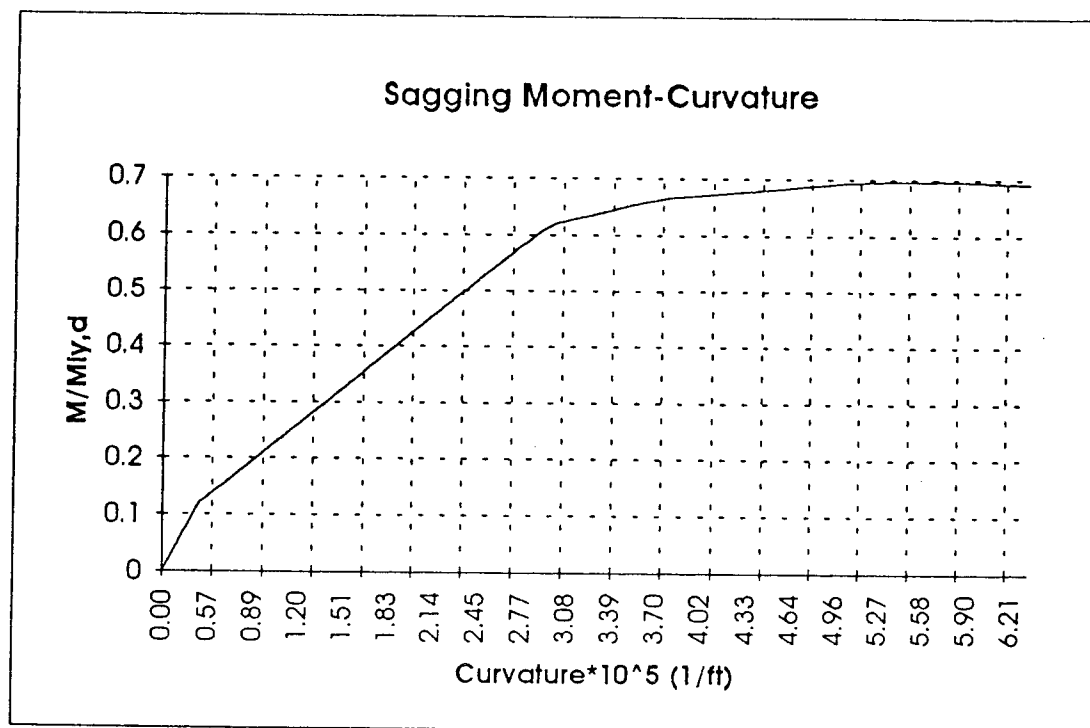
Figure 4.1.8 Tanker Vertical Bending Moment-Curvature Relation
(Referenced to Initial Yield Moment)
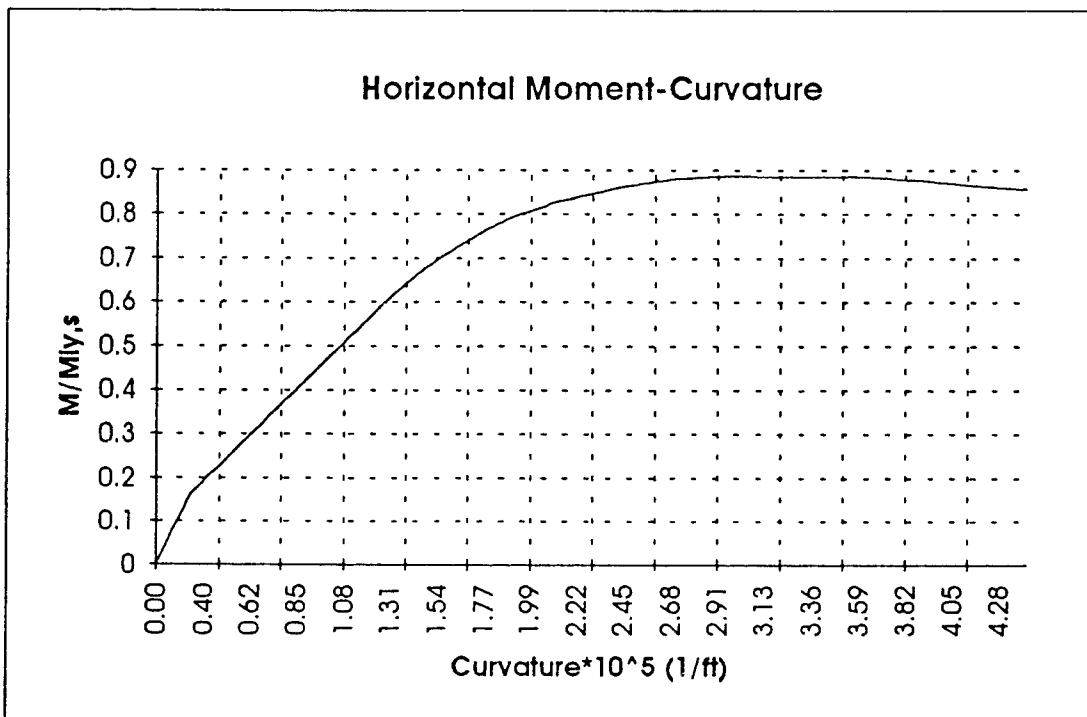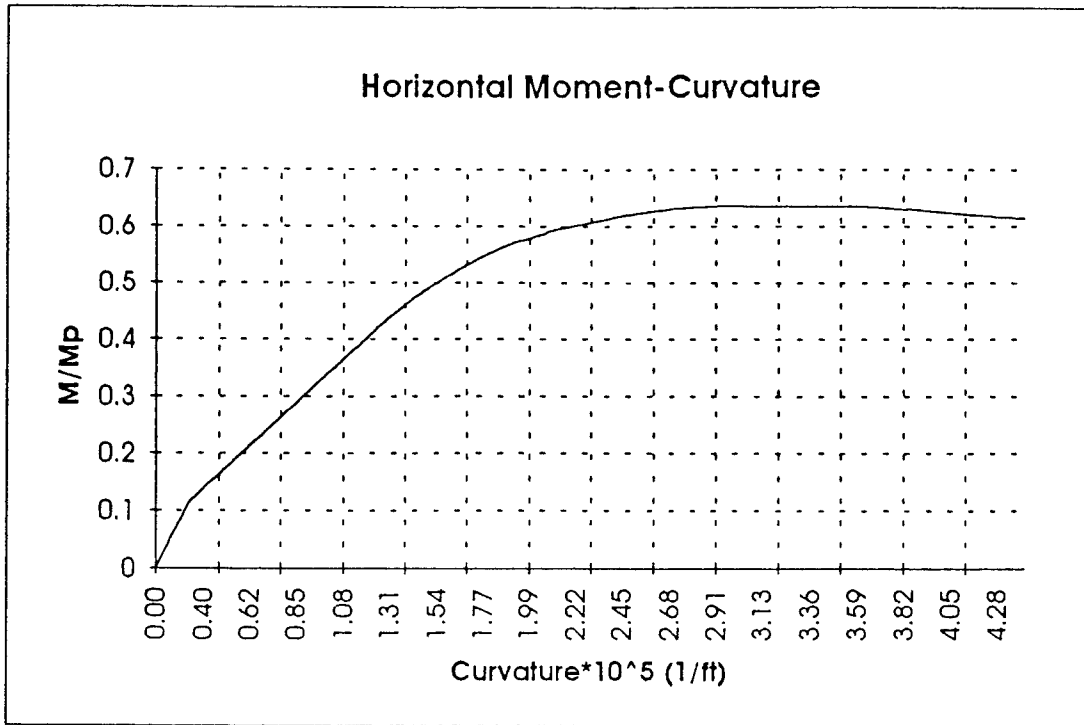
Figure 4.1.9 Tanker Horizontal Bending Moment-Curvature Relation
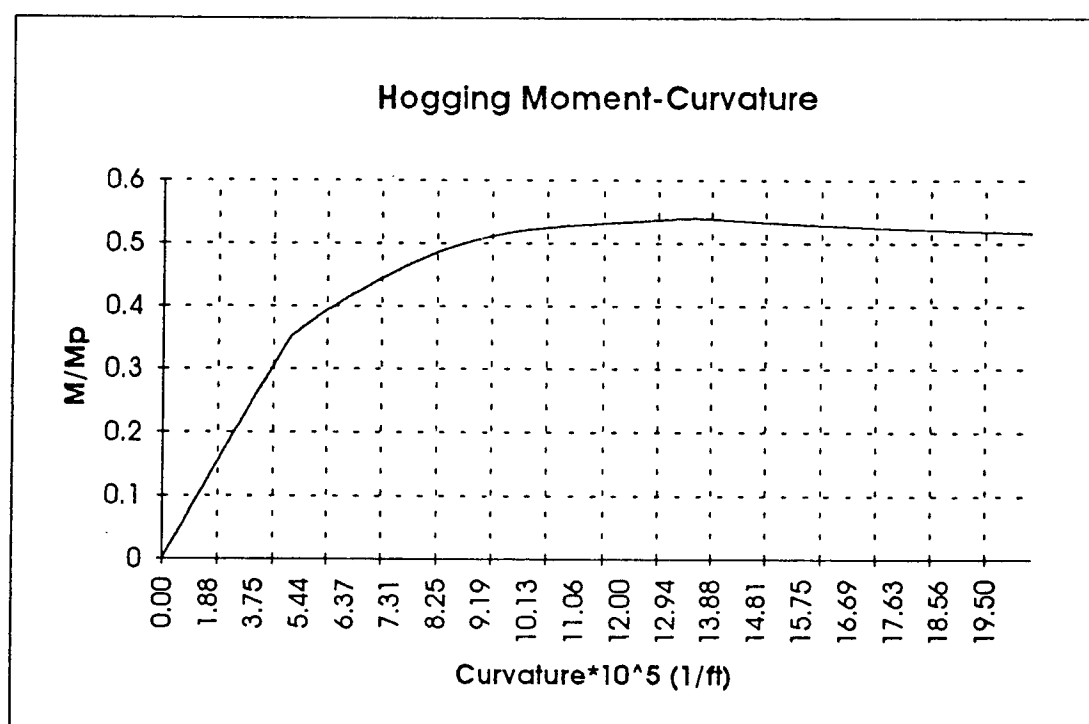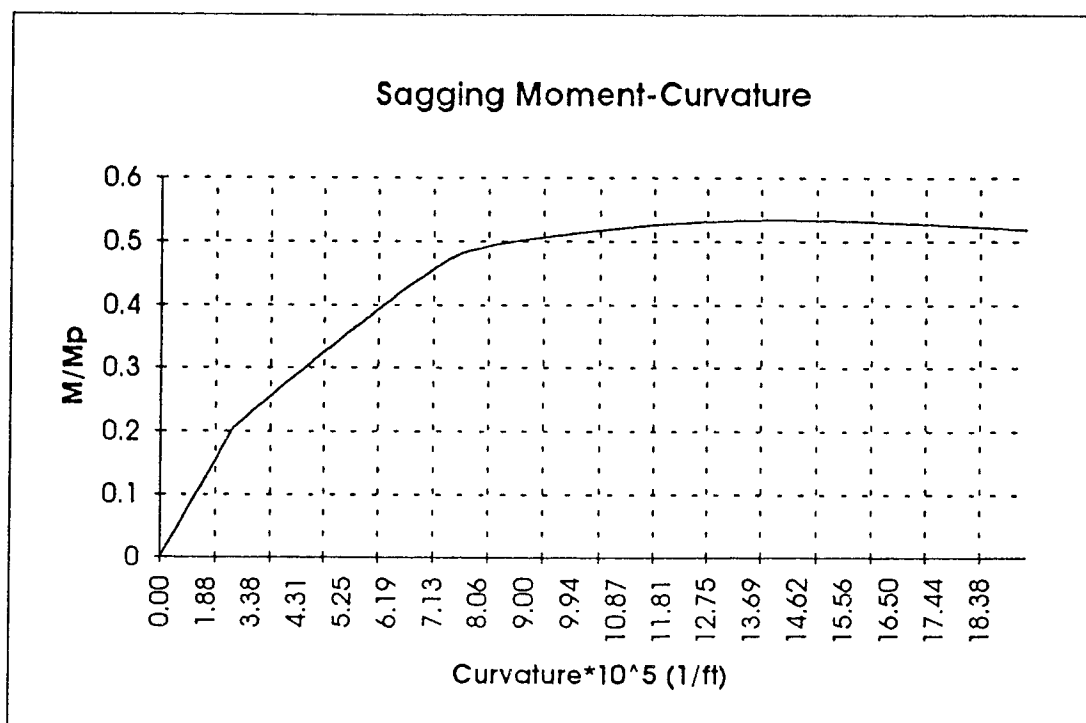
Figure 4.1.10 Cruiser 1 Vertical Bending Moment-Curvature Relation
(Referenced to Fully Plastic Moment)
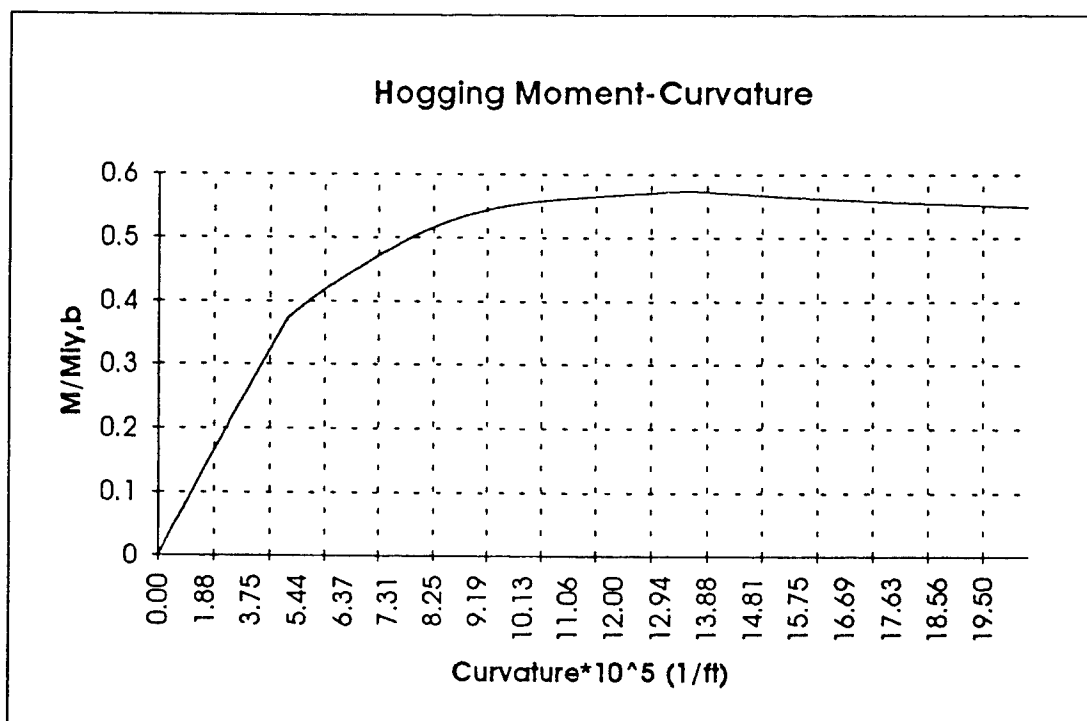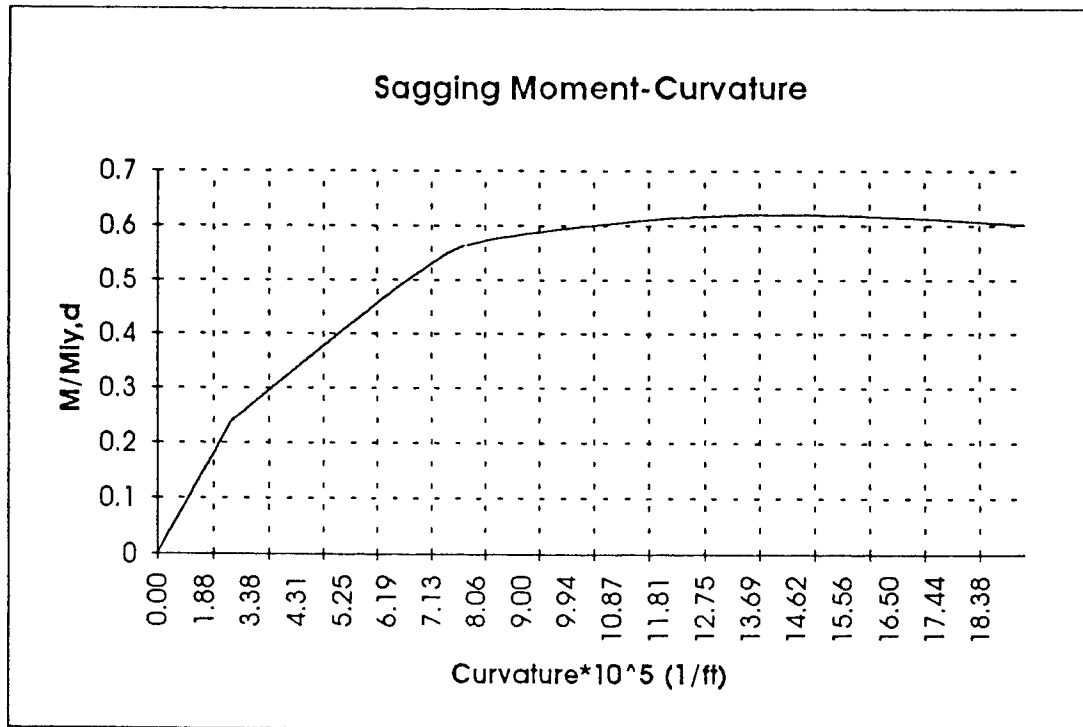
Figure 4.1.11 Cruiser 1 Vertical Bending Moment-Curvature Relation
(Referenced to Initial Yield Moment)
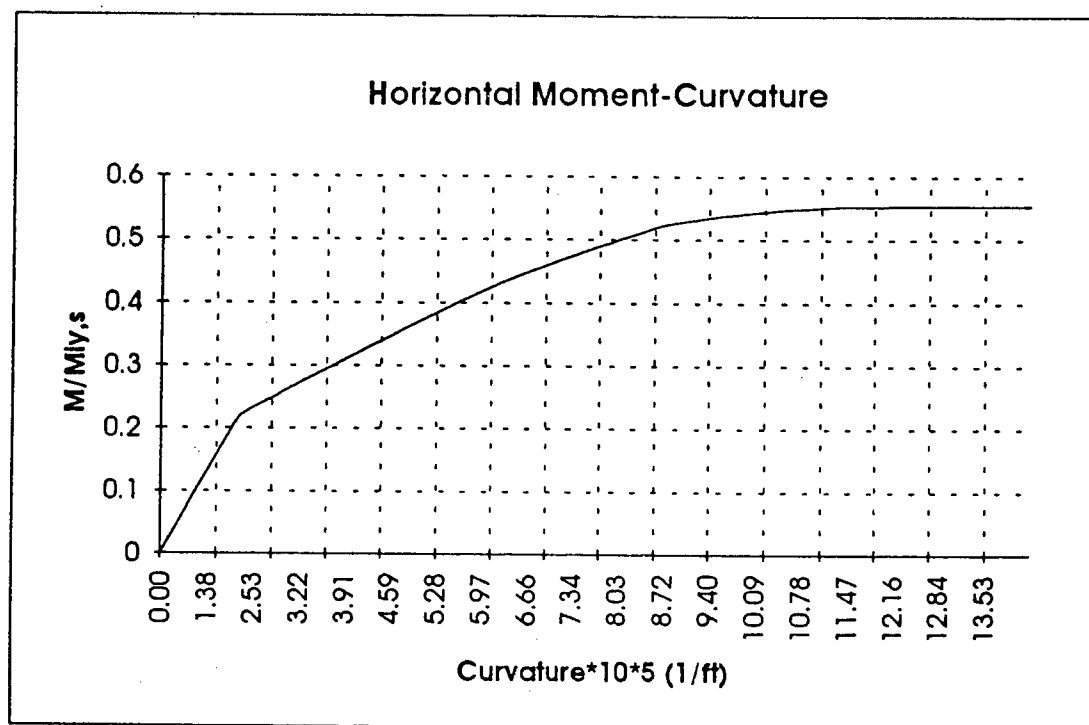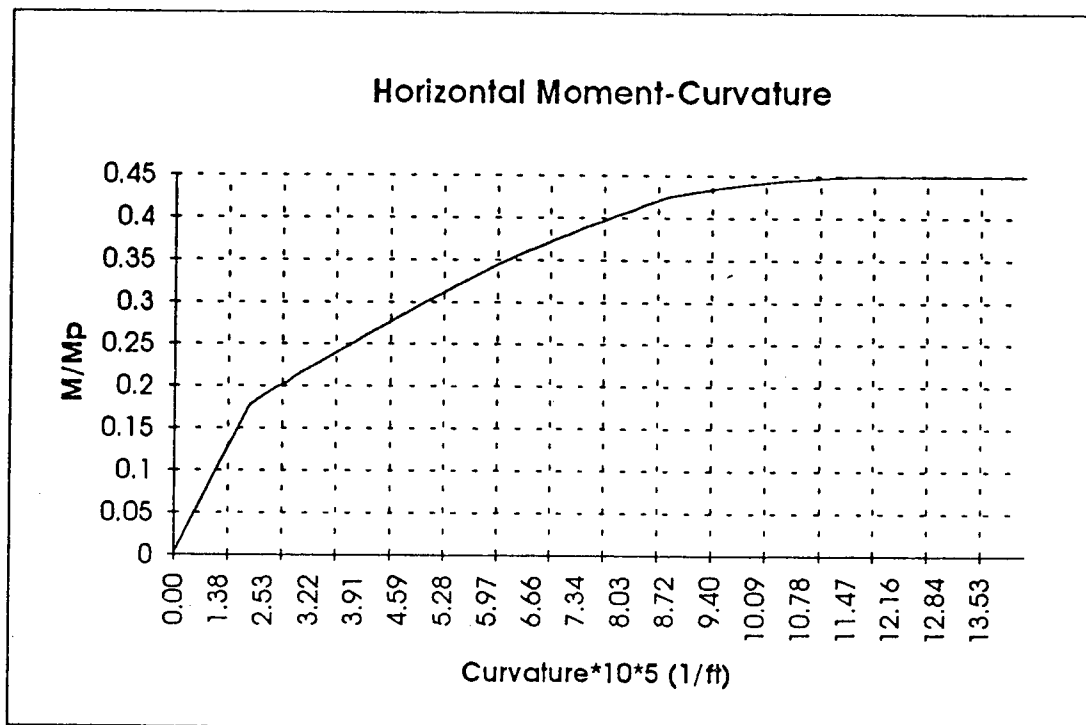
Figure 4.1.12 Cruiser 1 Horizontal Bending Moment-Curvature Relation
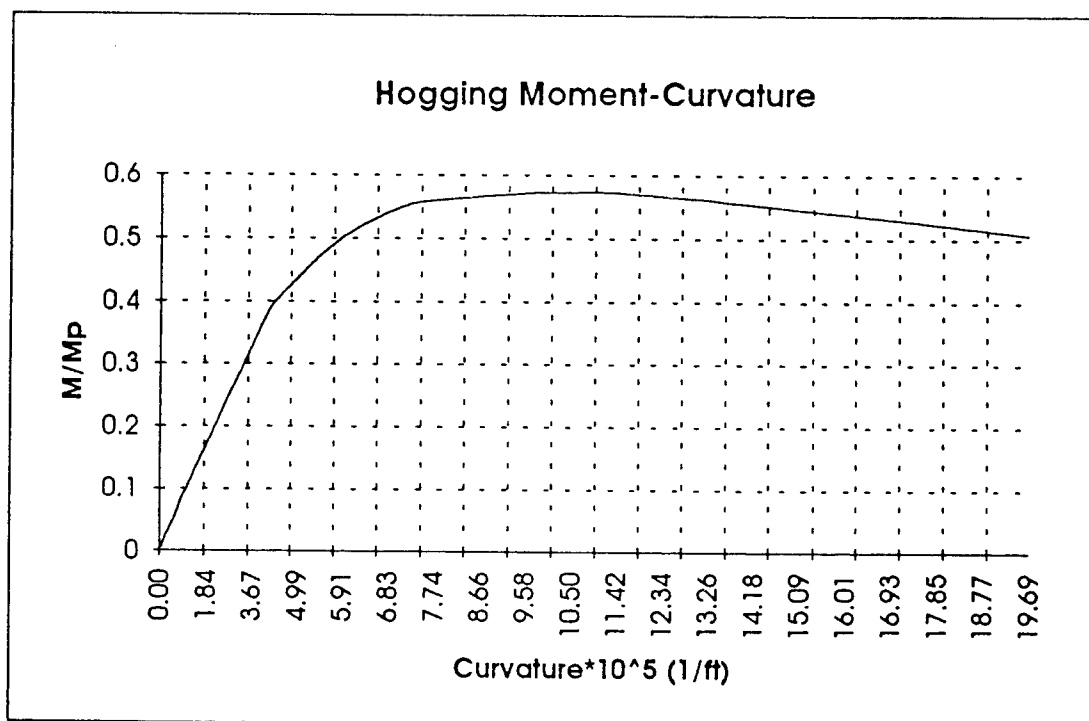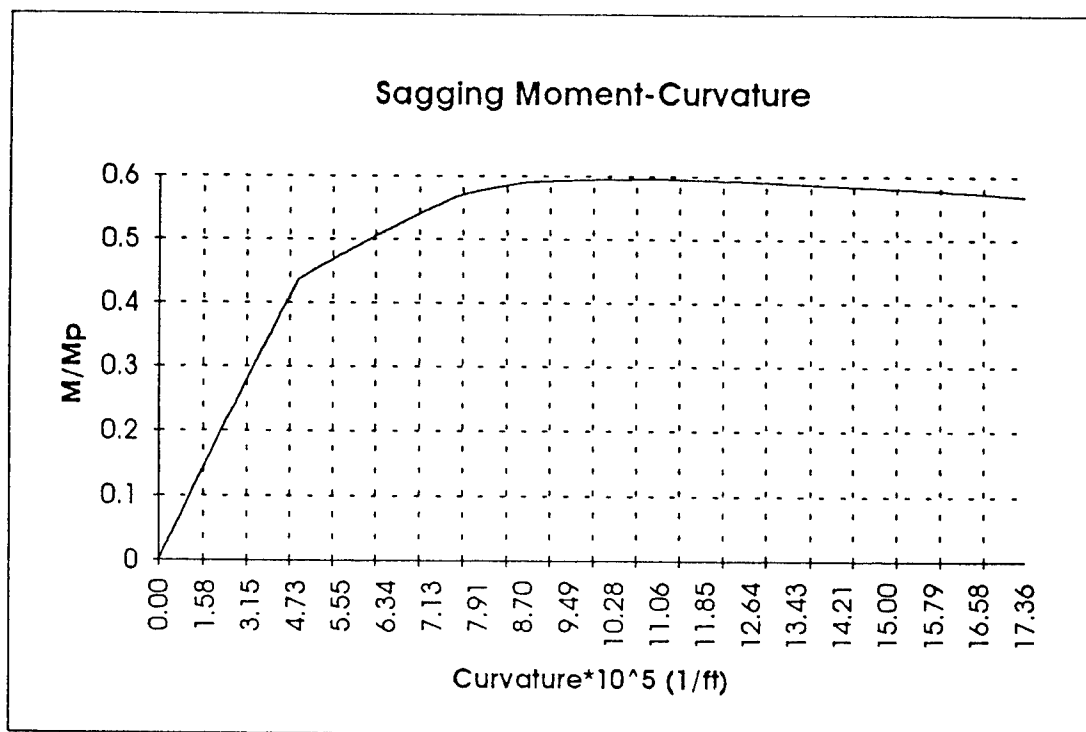
Figure 4.1.13 Cruiser 2 Vertical Bending Moment-Curvature Relation
(Referenced to Fully Plastic Moment)
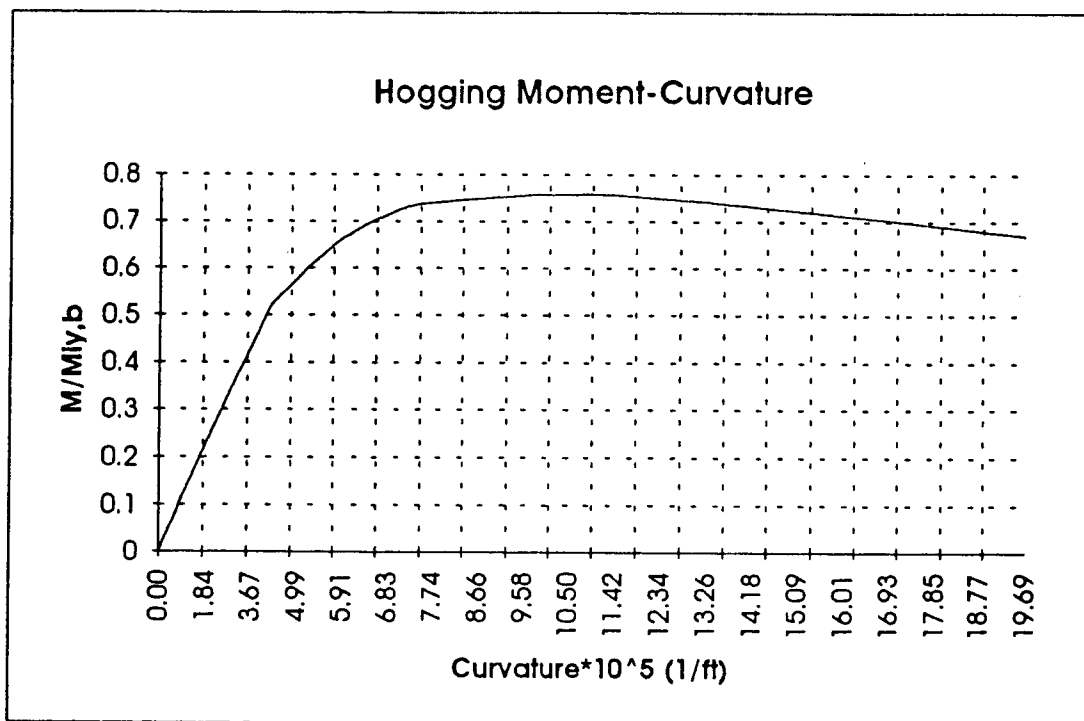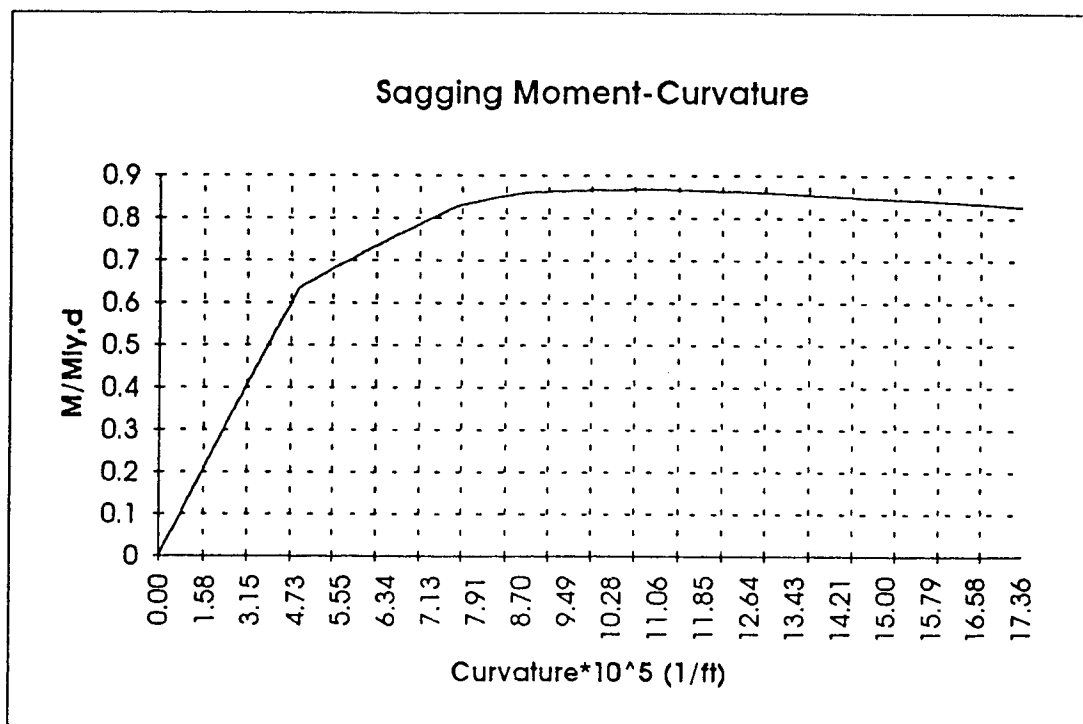
Figure 4.1.14 Cruiser 2 Vertical Bending Moment-Curvature Relation
(Referenced to Initial Yield Moment)

Horizontal Moment-Curvature

Horizontal Moment-Curvature
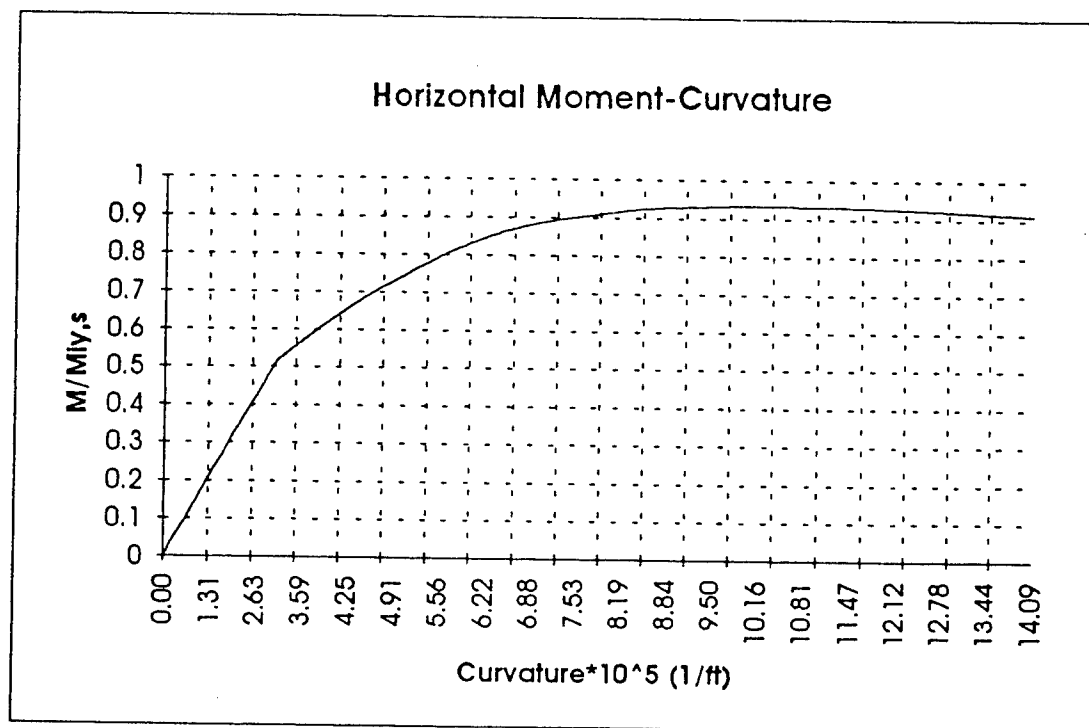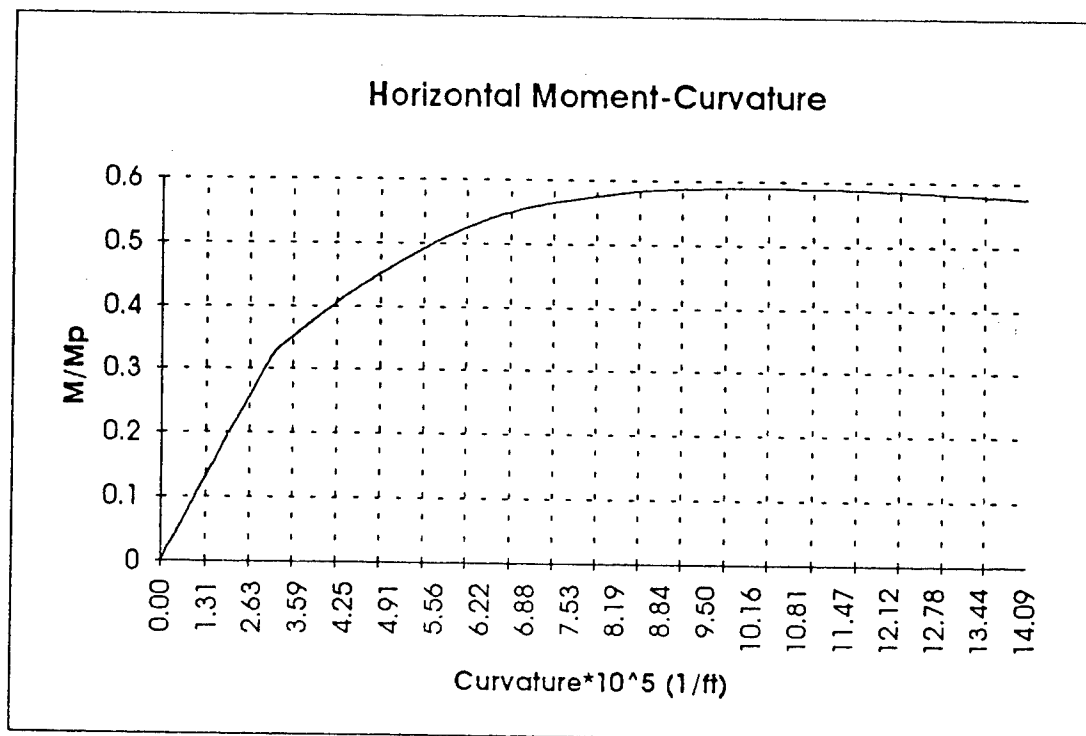
Figure 4.1.15 Cruiser 2 Horizontal Bending Moment-Curvature Relation

Sagging Moment-Curvature (Cr=0.1)

Horizontal Moment-Curvature (Cr=0.1)
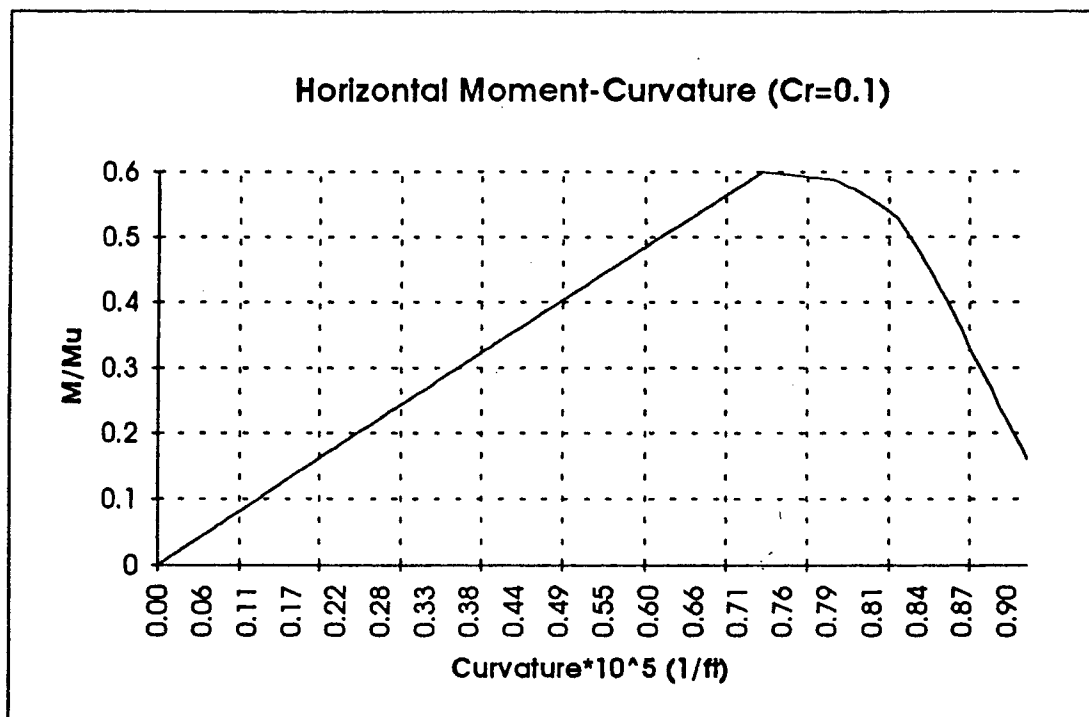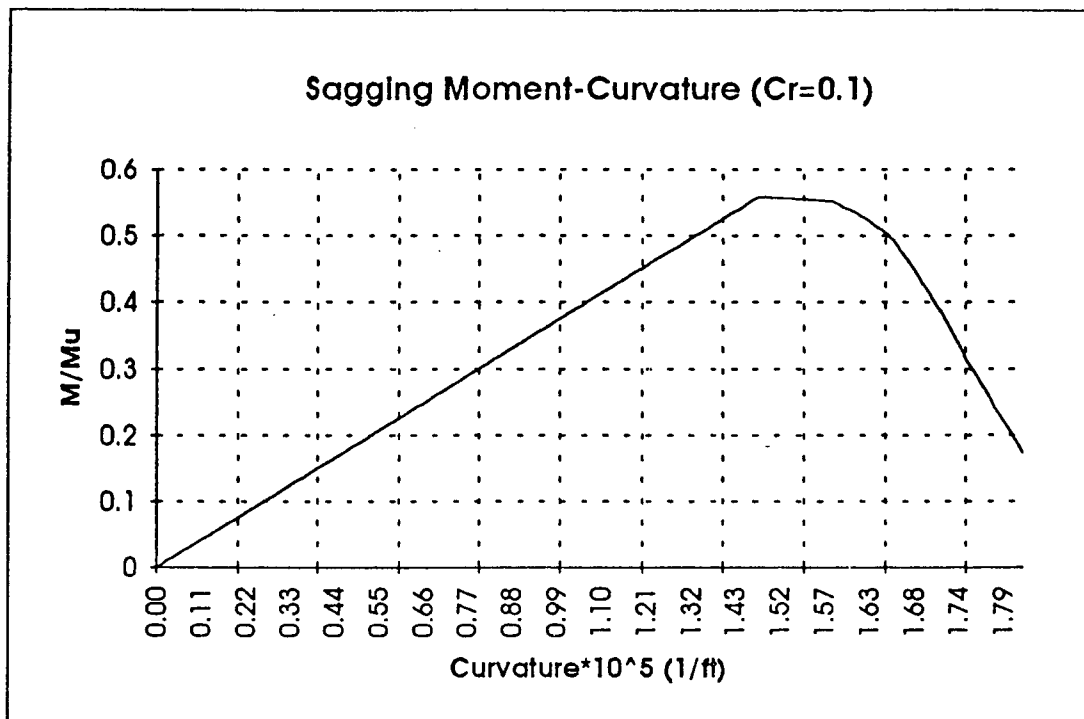
Figure 4.1.16 SL-7 Procedure of Combining Vertical and Horizontal Moments
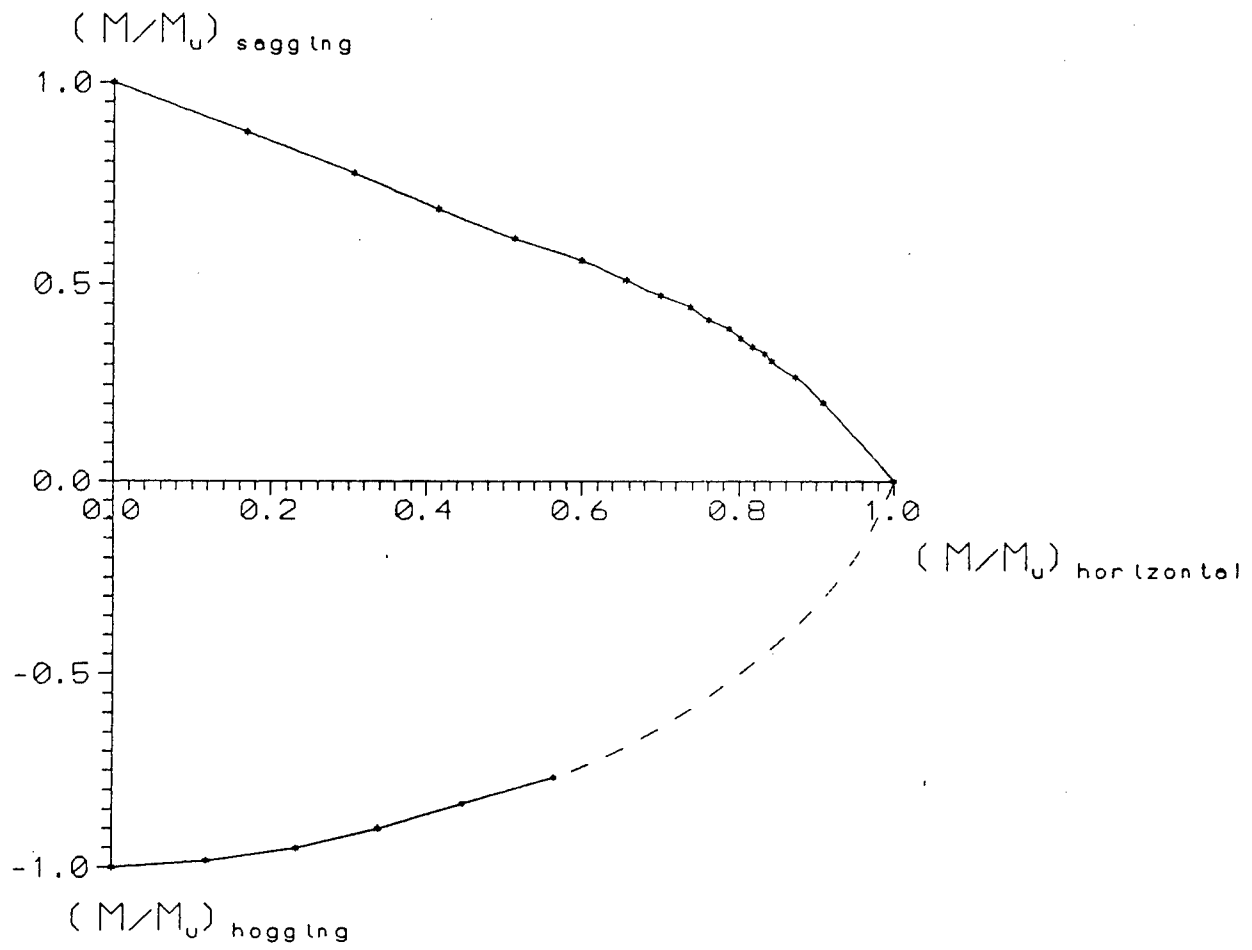
Figure 4.1.17 SL-7 Interaction Curve
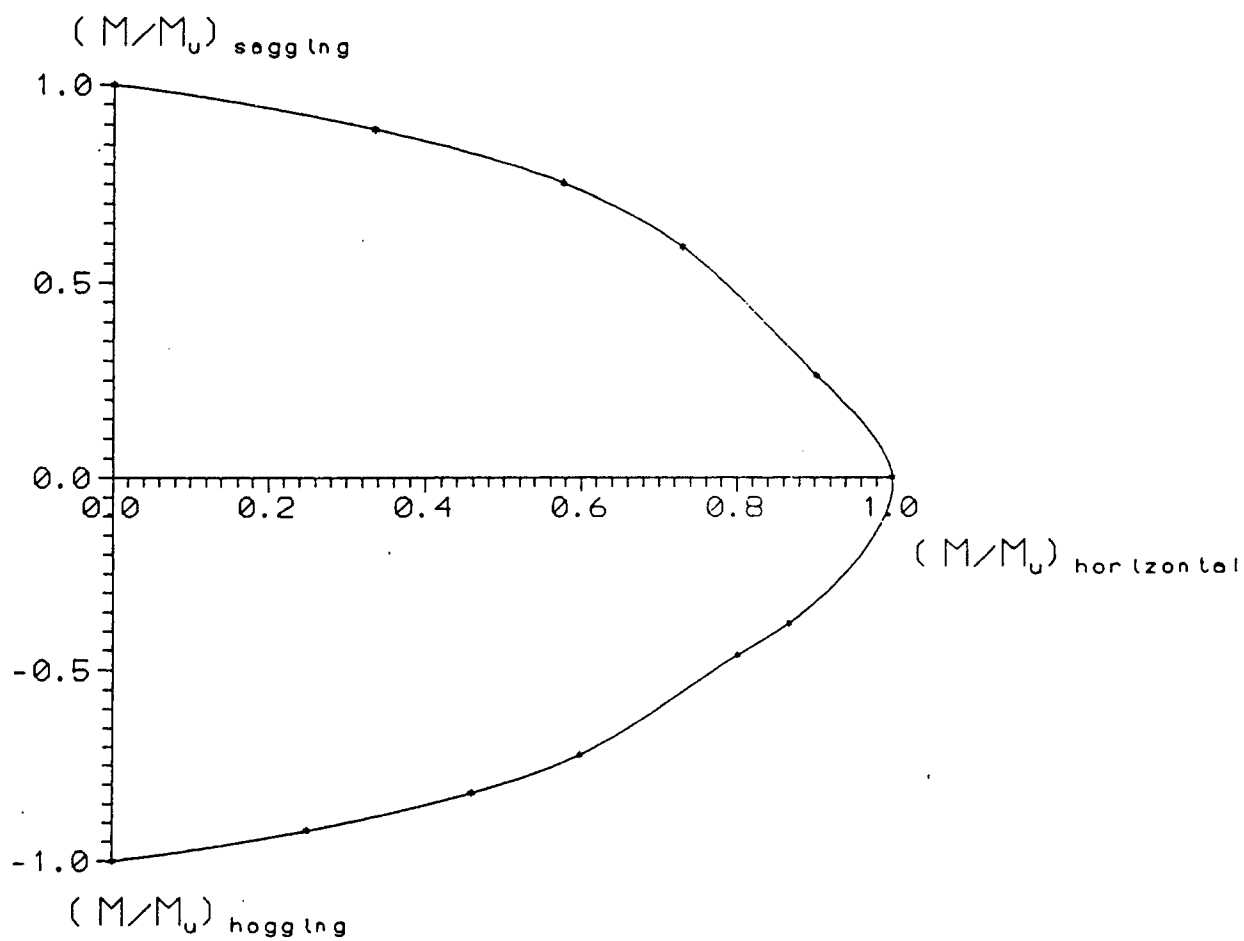
Figure 4.1.18 Tanker Interaction Curve
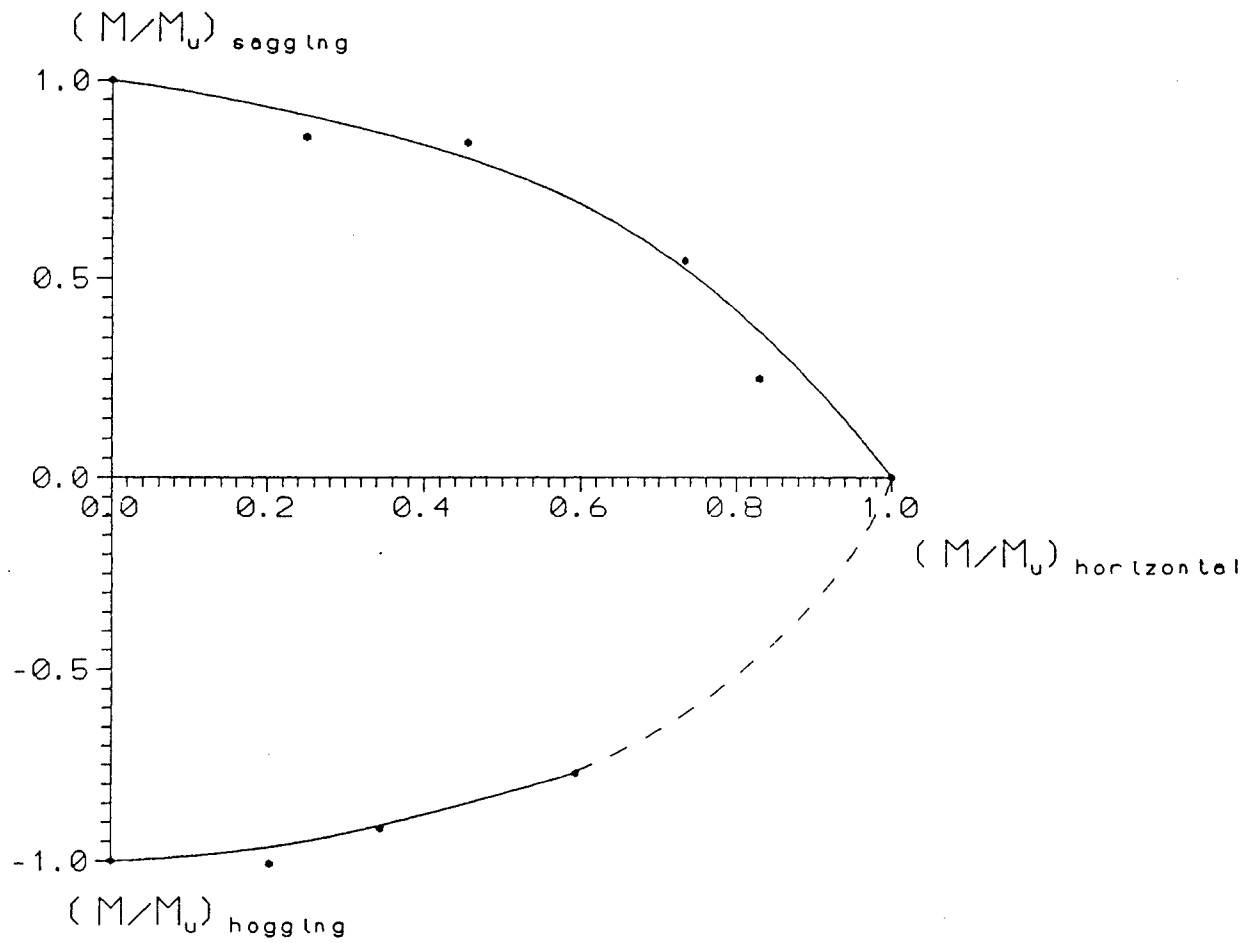
Figure 4.1.19 Cruiser 1 Interaction Curve
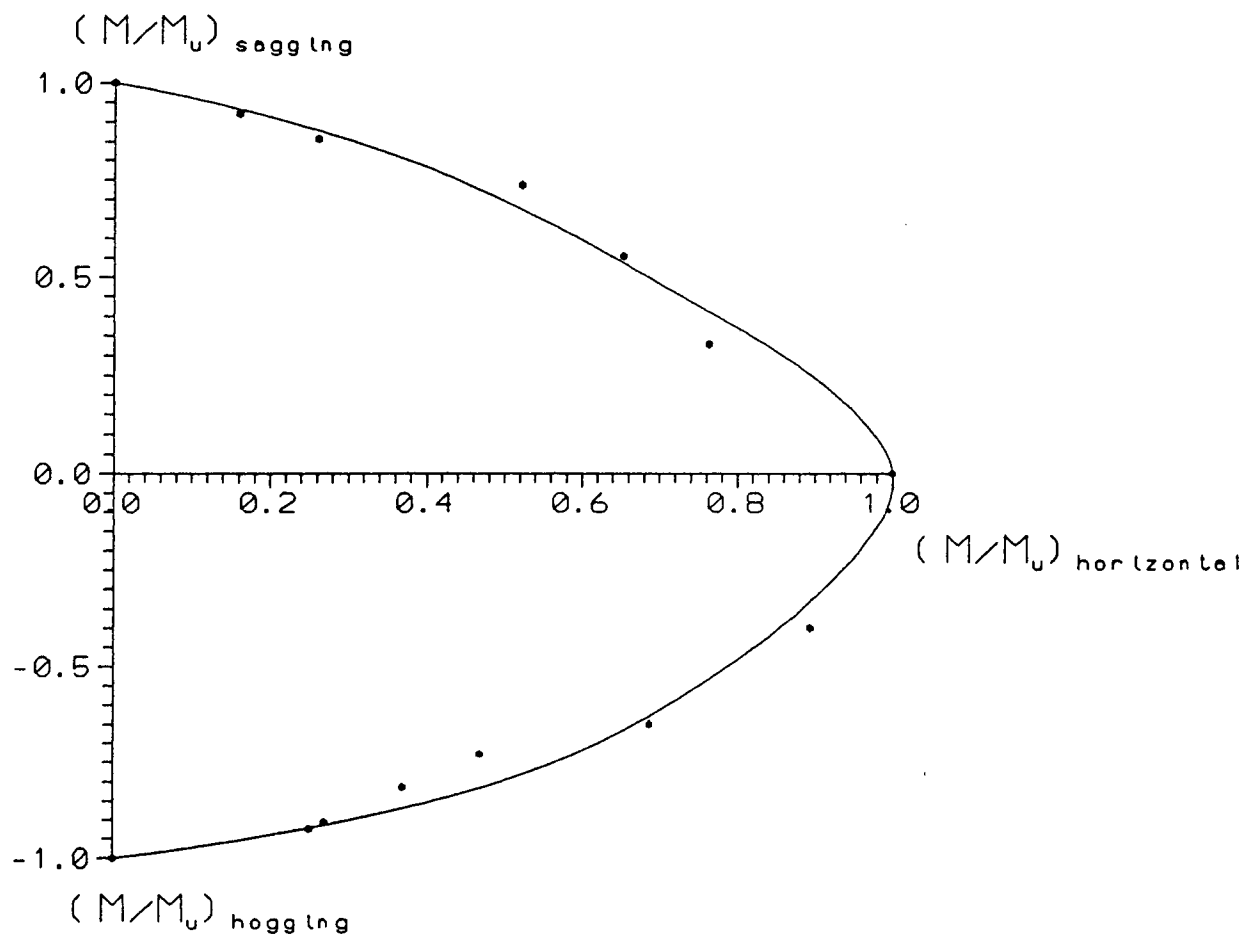
Figure 4.1.20 Cruiser 2 Interaction Curve
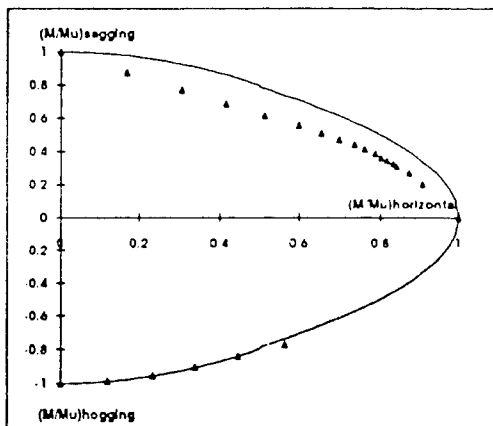
Figure 4.1.21 SL-7 Interaction Relation,
Equation (4.1.2)
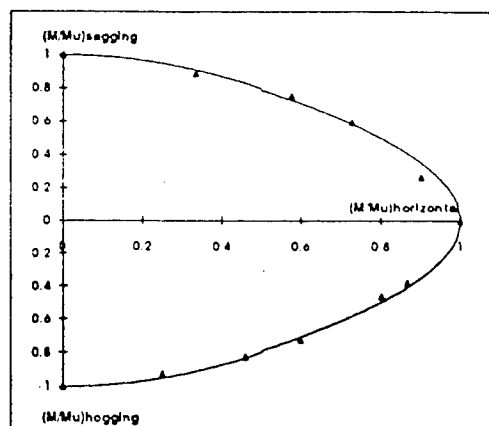
Figure 4.1.22 Tanker Interaction Relation,
Equation (4.1.2)
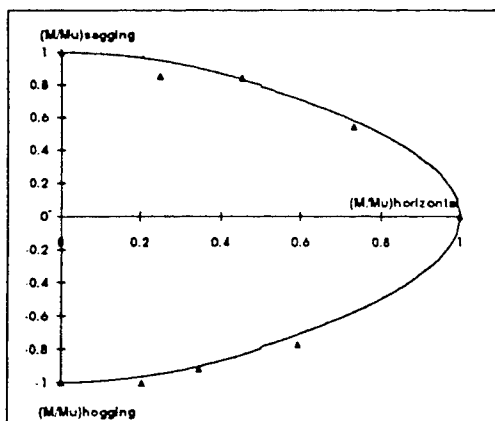
Figure 4.1.23 Cruiser 1 Interaction Relation,
Equation (4.1.2)
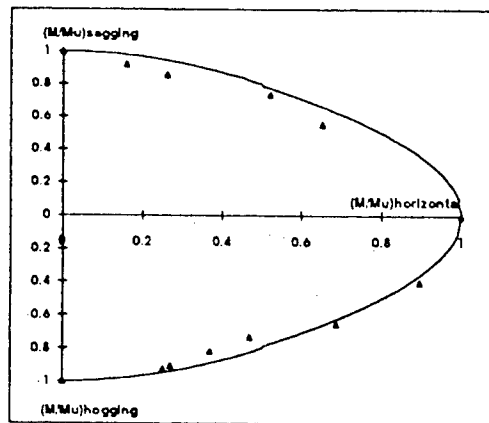
Figure 4.1.24 Cruiser 2 Interaction Relation,
Equation (4.1.2)

4.2 Ultimate Strength in Secondary and Tertiary Modes

The ultimate strength in secondary and tertiary modes for the four ships can be computed using ISUM stiffened and unstiffened plate units. Plates at deck and bottom are considered separately under compressive loads. The lateral water pressure acting at the bottom is also considered. The magnitude of the water pressure is the same as the static pressure having a height equals to depth at the midship section.

The residual stress coefficient Cr is taken as 0.1 and the initial deformation parameter is taken as 0.2 for all cases.

Tables 4.2.1 and 4.2.2 show the results of secondary and tertiary modes.

	Ship	Cruiser 1	Cruiser 2	Tanker	SL-7
Deck	σ_u (ksi)	46.2	32.8	30.6	**
	σ_y (ksi)	80.0	47.0	45.5	**
	σ_u/σ_y	0.578	0.698	0.673	**
Bottom	σ_u (ksi)	45.3	29.7	17.7	22.2
	σ_y (ksi)	77.8	47.0	34.0	30.0
	σ_u/σ_y	0.582	0.632	0.521	0.740

Table 4.2.1 Secondary Mode (Stiffened Plates)

	Ship	Cruiser 1	Cruiser 2	Tanker	SL-7
Deck	σ_u (ksi)	45.9	36.7	38.3	**
	σ_y (ksi)	80.0	47.0	45.5	**
	σ_u/σ_y	0.574	0.781	0.842	**
Bottom	σ_u (ksi)	55.6	35.3	28.4	28.0
	σ_y (ksi)	80.0	47.0	34.0	30.0
	σ_u/σ_y	0.695	0.751	0.835	0.933
σ_u = average ultimate stress					
σ_y = yield strength of the material					

Table 4.2.2 Tertiary Mode (Unstiffened Plates)

Finally, a comparison was made between ALPS/ISUM results and the approximate formulation presented in section 2.2.5 for the tertiary mode. the results are shown in Table 4.2.3. The table shows that the ultimate strength using the approximate formulation is always higher than the ALP/ISUM results. Most likely, this is because the approximate formulation does not account for lateral pressure, residual stress or initial deflection, at least not in an explit manner for the latter two.

	Ship	Cruiser 1	Cruiser 2	Tanker	SL-7
Deck	σ_u/σ_y (ALPS)	0.574	0.781	0.842	**
	σ_u/σ_y (formula)	0.676	0.868	0.929	**
Bottom	σ_u/σ_y (ALPS)	0.695	0.751	0.835	0.933
	σ_u/σ_y (formula)	0.836	0.916	1.000	1.000

**Table 4.2.3 Comparison of Tertiary Mode Between ALPS/ISUM
and Approximate Formula**

Note:
1. Plates at bottom are subjected to water pressure.
2. Residual stress parameter $(\sigma_{rx}/\sigma_o) = 0.1$.
3. Initial deflection parameter $(A_{om}/t) = 0.2$.
4. The approximate formulas do not consider lateral pressure, residual stress, or initial deflection.

5. RELIABILITY ANALYSIS AND FAILURE PROBABILITIES

A great deal of work has gone into developing estimates of the structural strengths of the four ships (Chapter 4) as well as computing various ocean-induced forces on the ships (Chapter 3), both in a short-term and over each ship's lifetime. (Note that this part of the study deals only with ultimate strengths — fatigue failure is covered in Chapter 7.) Armed with all of these data together with four earlier studies conducted in Ship Structure Committee projects (SR-1310, 1330, 1337 and 1345), it is possible to conduct a comprehensive reliability analysis. The results of the reliability analysis can be conceptually divided into two main sections. First, the "level of safety" can be estimated for a wide variety of loading conditions for each of the ships. This "level of safety" is quantified as either a safety index (β) or, equivalently, a probability of failure. Second, information can be gathered on the sensitivity of the safety index (or probability of failure) to changes in the input variables. These variables include the strength of the structure, the various loadings imposed on the structure, and load combination factors (accounting for the correlations between different loadings). This sensitivity analysis is presented in Chapter 6.

Throughout the analysis of the results, an important thread is that of comparison. Since the exact same procedures produce the results for all cases and all ships, comparing the *relative* values of various outputs should yield valid conclusions. This is true despite inevitable inaccuracies in the analysis. Comparisons will be drawn between military-designed versus commercially-designed ships, between the use of high-strength versus mild steel in construction, between failure modes, and between loading conditions. The object of such comparisons will be to discern some sort of pattern in the data. These patterns can then be assessed and some generalizations and conclusions drawn. The particulars of the ships are repeated in Table 5.1.

	Cruiser 1	Cruiser 2	SL-7	Tanker
Length, BP (ft)	529.0	529.0	880.5	625.0
Beam (ft)	55.0	55.0	105.5	96.0
Draft (ft)	22.4	19.8	30.0	34.0
Displacement (LT)	9680	7996	47760	44513

Table 5.1 Particulars for the Four Ships

5.1 Theoretical Considerations

The starting point of a reliability analysis is the definition of failure. In the most general sense, a structure fails when the applied load exceeds the structure's ability to carry that load. This relationship is expressed mathematically in a "limit state" equation. There are a number of common forms of limit state equations, each equally valid. If the load applied to the structure is defined as L and the resistance of the structure to that load as S, then the failure event can be defined in any of the following ways (even more are possible):

$$L \geq S \qquad \frac{L}{S} \geq 1 \qquad L - S \geq 0 \qquad S - L \leq 0$$

For the purposes of this analysis, we have selected the fourth equation as the basic form that we will employ. The limit state equation is then defined as $G = S - L$; and the probability of failure is the probability that $G \leq 0$. Symbolically, $P_f = P[G \leq 0]$.

In reliability analysis, both the strength and the load are considered to be random variables. Each of the variables is characterized by a distribution and several parameters, usually the mean and some measure of the variation (coefficient of variation or standard deviation). For this analysis, three different distributions are used often: normal (Gaussian), lognormal, and extreme value. Table 5.1.1 summarizes the equations for each of the distributions used. In the table, ζ and λ are the parameters of the lognormal distribution.

Distribution	Normal	Lognormal	Extreme Value
Probability Density Function	$f_x(x) = \dfrac{1}{\sqrt{2\pi}\sigma} e^{-\frac{1}{2}\left(\frac{x-\mu}{\sigma}\right)^2}$	$f_x(x) = \dfrac{1}{\sqrt{2\pi}\zeta x} e^{-\frac{1}{2}\left(\frac{\ln x - \lambda}{\zeta}\right)^2}$	$f_x(x) = F_x(x)\dfrac{b}{a} x e^{-\frac{x^2}{2a}}$ $a = \dfrac{\mu\sigma\sqrt{6}}{\pi} - \dfrac{6\sigma^2(0.5772)}{\pi^2}$ $b = e^{\left(\frac{\pi\mu}{2\sigma\sqrt{6}} - 0.5772\right)}$
Cumulative Distribution Function	$F_x(x) = \Phi\left(\dfrac{x-\mu}{\sigma}\right)$	$F_x = \Phi\left(\dfrac{\ln x - \lambda}{\zeta}\right)$	$F_x(x) = e^{-be^{-\frac{x^2}{2a}}}$
Mean	μ	$e^{\left(\lambda + \frac{\zeta^2}{2}\right)}$	μ
Standard Deviation	σ	$e^{\left(\lambda + \frac{\zeta^2}{2}\right)}\sqrt{e^{\zeta^2} - 1}$	σ

Table 5.1.1 Equations for the Statistical Distributions

When dealing with a ship, the load term is usually broken down into several component parts. This introduces the necessity of dealing with the correlations between the various load terms, adding a bit more complexity to the limit state equations. A simple, yet effective, method of accounting for these correlations is the use of load combination factors. Section 2.1.2 and Appendix A cover the theoretical development of this method in great detail. Essentially, this method assumes that the total combined load can be written as the sum of the component loads, with all but one (the largest) of the loads being modified by a coefficient to account for the correlations between the loads, i.e., $f_c = f_1 + K_2 f_2 + K_3 f_3$, where f_c

is the total combined load, f_i is the ith component load, and K_i is the ith load combination factor.

Once a limit state equation has been formulated for the desired problem, appropriate distributions and statistical characteristics assigned to each of the variables, and any load combination factors determined, the next step is to use this information to calculate the probability of failure (or safety index) for the system. For this project, the software program CALREL (CALifornia RELiability) was utilized to perform this calculation (Liu *et al.*, 1989). CALREL is a FORTRAN-based program developed at the University of California, Berkeley, and designed to be used in a wide variety of component- and system-level structural reliability analyses. For our purposes, the inputs that CALREL requires consist of

1. a limit state equation;

2. a distribution and its associated parameters, forming a complete statistical description of the variable, for each random variable in the analysis;

3. the values of any constants used in the limit state equation.

After all of these inputs have been determined, CALREL can calculate a variety of useful information about the reliability of the ship. Of interest in this case are the probability of failure, safety index and a variety of sensitivity measures.

(*Note: The following description of the theory behind CALREL is summarized from the CALREL User's Manual*, Liu *et al.*, 1989.) Computation of the probability of failure is accomplished by evaluating the following integral:

$$P_f = \int_F f_X(x)dx$$

In this integral, X is a vector consisting of the random variables in the analysis, $f_X(x)$ is the joint probability density function of the random variables, and $F \equiv \{G(x) < 0\}$ is the domain of failure. Closed-form evaluation of this integral is, in general, not possible when many variables and non-Gaussian distributions are used. Therefore, some simplification is necessary to perform this calculation. CALREL is capable of employing several methods for simplifying this integral and then numerically estimating the probability of failure. The two methods used for this project were the first- and second-order reliability methods (FORM and SORM). FORM involves approximating the higher-order failure surface $G(x) = 0$ by using hyperplanes that are tangent to the failure surface at specified design points in a transformed standard normal space. SORM takes this idea one step further by fitting hyperparaboloids near the design points, providing for a more accurate approximation of the failure surface. The design point (the most-likely-failure point) is found by an interative method and the integral is then evaluated numerically. The *CALREL User's Manual* provides additional references for a more detailed treatment of both of these methods.

5.2   Inputs (Random Variables)

Reliability analysis requires a statistical description for each of the input variables. This means that, for each variable, it is necessary to choose an appropriate distribution and then determine the mean value and variability (coefficient of variation or standard deviation). There are a total of six variables for each ship that represent that ship's strength in various loading conditions. Each ship also is subjected to up to three different loads (three for the sagging condition and two for the hogging condition), varying with the different load cases. Additionally, there are up to two load combination factors (one less than the number of laods). Thus, each has as many as elevent variables.

Strengths:

The strength variables are defined by the geometry and the materials that make up the structure of the ship. Since the ship's ability to withstand loads is different for different types of loadings, there is a different strength variable for each different type of load.

For the primary failure mode, two different strengths are used. The first of these is M_{IY}, the initial-yield moment. This is defined as the global hull bending moment that, if applied to the ship, would cause the stress in the partial-section of the ship in tension (the deck for hogging loads and the bottom for sagging loads) to just reach the yield strength of the material. This is found by multiplying the appropriate section modulus by the yield strength of the material.

$$M_{IY} = SM_i \times \sigma_y \quad i = \{\text{deck, bottom}\}$$

Determination of the section modulus for the deck and bottom are fairly straightforward geometric calculations and the yield strength is a known value. Although the initial yield moment is generally <u>not indicative of the true resistance of the ship's structure</u>, it is included in the analysis because it is a common design criterion. It is thus possible to make some comparisons between this value and a more accurate estimation of the ship's ultimate strength.

This ultimate moment is the second of the two strengths used in the primary failure mode analysis. The ultimate moments used in this analysis are based on computations performed in Chapter 4 using ALPS/ISUM, a structural analysis program by Paik (1993). The ultimate moment is determined by using ALPS to generate a moment-curvature diagram for the hull section (Mansour *et al.*, 1995). In essence, ALPS applies a known amount of curvature to the section and then calculates the bending moment that would be required to generate that curvature. This computation is repeated, increasing the curvature each time, for a user-selected range of curvatures. The resulting moment-curvature data pairs are then plotted. The ultimate moment of the section is then estimated by reading the value off of the curve where it "levels out". In other words, this is when a small increase in applied moment yields a very large increase in curvature. Figure 5.2.1 is a sample moment-curvature diagram

for a ship (one not included in this study) that has the ultimate moment indicated on the plot. A more detailed treatment of this method is contained in Chapter 4.
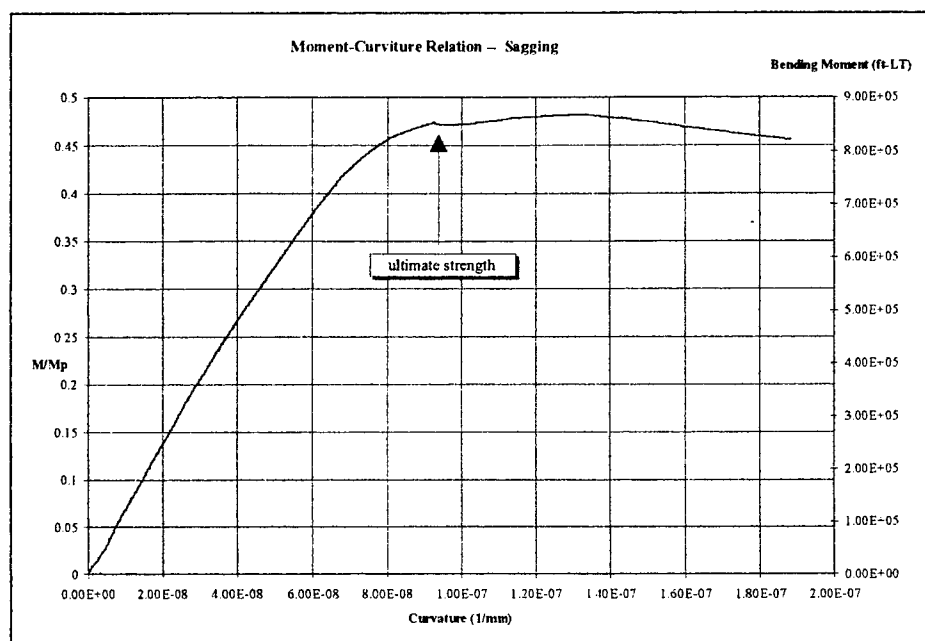
Figure 5.2.1 Sample Moment-Curvature Diagram

The secondary failure mode examines gross panel buckling collapse in either the deck or the bottom of the ship due to compressive bending stresses. ALPS/ISUM is used to determine the stress level in failure, $S_{u,2}$. The determination of this strength includes residual stresses, initial deflections, and (for bottom panels) lateral pressure. In the reliability analysis, the secondary and tertiary ultimate strengths and the section moduli are taken as separate random variables.

Determination of the tertiary mode ultimate strength is accomplished in the same manner as the secondary mode. The only difference is that the structural unit in question is a single stiffened panel. Again, the tertiary mode ultimate strength, $S_{u,3}$, was calculated using ALPS/ISUM.

5-5

Once the base strengths are calculated, these values are used to determine appropriate values to use in the statistical description of the strength variables. All strengths are assumed to be lognormally distributed, while the section moduli are assumed to follow a normal distribution. In order to correct for inherent conservatism in the calculated strengths, the mean values analysis of all the strengths used in the reliability analysis are taken to be 15 percent larger than the calculated values (SSC-368). This bias is needed because all of these failure criteria have their basis in the minimum yield strength of the material (Galambos, 1989, and SSC-368). The calculated section modulus values are used, unchanged, as the mean values for those variables. The mean values of the strength variables used in the reliability analysis (as modified above) are shown in Table 5.2.1; and the assumed coefficients of variation for the strengths are shown in Table 5.2.2. Both military ships have a smaller coefficient of variation on strengths than the civilian ships to account for the generally better quality control and maintenance of the military ships. Also, a larger coefficient of variation is used for the primary ultimate moment than the initial yield moment to account for uncertainties in the modeling of the ultimate strength (Hughes *et al.*, 1994, and Mansour *et al.*, 1993).

It is important to note that there are no values given for the SL-7 for the secondary and tertiary failure modes in the sagging condition. This is due to the fact that the SL-7 has no deck structure for much of its length.

Variable	Units	Cruiser 1	Cruiser 2	SL-7	Tanker
M_{IY} (hogging)	ft-LT	959,670	602,955	3,454,154	1,731,366
M_{IY} (sagging)	ft-LT	1,048,274	664,562	2,741,614	1,816,033
M_U (hogging)	ft-LT	601,508	503,398	2,182,850	1,285,973
M_U (sagging)	ft-LT	595,640	523,190	2,628,205	1,207,433
$S_{u,2}$ (hogging)	LT/in^2	23.256	15.248	11.398	9.087
$S_{u,2}$ (sagging)	LT/in^2	23.719	16.839		15.710
$S_{u,3}$ (hogging)	LT/in^2	28.544	18.123	14.375	14.581
$S_{u,3}$ (sagging)	LT/in^2	23.565	18.842		19.663
SM_d	in^2-ft	23,384	25,021	74,093	143,340
SM_b	in^2-ft	26,730	27,578	104,056	177,935

Table 5.2.1 Mean Strengths (Adjusted)

Variable	Cruiser 1	Cruiser 2	SL-7	Tanker
M_{IY}	0.09	0.09	0.10	0.10
M_U	0.10	0.10	0.11	0.11
$S_{u,2}$	0.10	0.10	0.11	0.11
$S_{u,3}$	0.10	0.10	0.11	0.11
SM_d	0.04	0.04	0.04	0.04
SM_b	0.04	0.04	0.04	0.04

Table 5.2.2 Coefficients of Variation on Strengths

Loads:

Load variables come in two flavors. The first, stillwater bending moment (M_{sw}), is determined by the designer and the loading of the ship. Thus, it is subject to direct human control. The second flavor, the wave-induced and dynamic bending moments (M_w and M_d) are environmental and can only be influenced by humans indirectly (i.e., by route planning, etc.). As with the strength variables, we need to assign appropriate statistical descriptions to each of the load variables.

The stillwater bending moment for each ship is generally assumed to be the same for every case (exception: *Tanker*, see below). Reference values for stillwater bending moments are calculated for either full load or maximum allowable conditions, the mean values (for use in the reliability analysis) have to be reduced from the reference values. For the military ships, the mean value is assumed to be 80 percent of the full load calculated value. For the commercial ships, the mean value is assumed to be 60 percent of the calculated maximum allowable value (Mansour *et al.*, 1993, and SSC-373). The stillwater bending moment is assumed to follow a normal distribution with either a coefficient of variation of 0.15 for the military ships or a coefficient of variation of 0.25 for the commercial ships (see Mansour *et al.*, 1993). The differences between the two ship types account for the fact that the majority of the weights of a warship are relatively constant, while weights on commercial ships vary quite a bit (due to different cargo loading conditions). The stillwater bending moments for *Cruiser 1*, *Cruiser 2*, and *SL-7* are all hogging moments.

Tanker is a special case. In general, tankers spend about half of their operating life in a fully loaded condition and the other half in a ballast condition. Thus, there are two distinct stillwater bending moments: one for each condition. When in the fully loaded condition, the *Tanker* has a sagging stillwater bending moment. For the ballast condition, the *Tanker's* stillwater bending moment is a hogging moment. The means of the stillwater bending moments and the assumed coefficients of variation for all ships are shown in Table 5.2.3.

Variable	Cruiser 1 (hogging)	Cruiser 2 (hogging)	SL-7 (hogging)	Tanker (hogging)	Tanker (sagging)
M_{sw} (ft-LT)	61,400	51,600	359,500	256,700	100,000
COV	0.15	0.15	0.25	0.25	0.25

Table 5.2.3 Stillwater Bending Moment, Means and Coefficients of Variation

The mean values for the extreme wave-induced bending moment, M_w, are calculated using SOST, a computer program that utilizes second-order strip theory to calculate wave induced ship motions and loads (see section 2.1 and Chapter 3). For the short term time frame, an extreme sea condition is chosen based on a small encounter probability (see Table 5.2.4). The ship is also assumed to be traveling in head seas. From the SOST output, the 50 percent probability-of-exceedence value is taken as the mean for the reliability analysis. The extreme wave moment is assumed to follow the extreme value distribution (from Table 5.1.1) with a coefficient of variation of 0.10 (see SSC-373).

Short Term Sea Conditions	
Significant Wave Height (ft)	45.0
Upcrossing Period(s)	14.0
Ship Speed (kts)	6.0

Table 5.2.4 Short Term Sea Conditions

For the long-term time frame, a time-weighting method is used to calculate an operational profile. For the sake of continuity and comparability, the same profile is used for all four ships. First, the ships' at-sea lifetime is estimated to be fifteen years. Next, a group of Marsden areas in the north Atlantic are selected, and the fraction of the ships' life spent in each is estimated. Estimates are made as to the percentage of time that the ships will spend in each of five possible headings, relative to the direction of the seas (head, bow, beam, quartering and following). A service speed and a steerage speed are selected, and a wave height-based cutoff criteria for slowing to steerage speed is assumed (see Chapter 3). SOST is fed this information and generates an operational profile..

From this profile and repeated short-term analyses, SOST is able to generate probability-of-exceedence of extreme lifetime hogging and sagging bending moments for each ship. The value at the 50% exceedence probability is taken as the mean value for the extreme wave bending moment distribution. As with the short term, an extreme value distribution is used and a coefficient of variation of 0.10 is used (SSC-368). A summary of the extreme wave-induced bending moments is given in Table 5.2.5. (For a more detailed description of the SOST analysis, see section 2.1 and Chapter 3.)

Variable		Cruiser 1	Cruiser 2	SL-7	Tanker
Short Term	M_w, hogging (ft-LT)	169,100	155,900	969,600	586,100
	M_w, sagging (ft-LT)	198,900	213,900	1,065,000	594,800
Long Term	M_w, hogging (ft-LT)	275,300	270,400	1,110,000	752,000
	M_w, sagging (ft-LT)	278,100	290,700	1,480,000	943,000

Table 5.2.5 Mean Values of Extreme Wave-Induced Bending Moment

In order to model the effects of slamming, a dynamic moment (M_d) is introduced into the analysis. Since the slamming-induced moment is a sagging moment, it is included only when the sagging loading condition is considered. Based on work by Sikora and Beach (1989), the results of the SLAM program presented in Chapter 3 and SSC-373, the dynamic moment is taken to be a fraction of the extreme wave moment. For the fine-hulled warships, the mean extreme dynamic moment is assumed to be 40 percent of the mean extreme wave moment. For the fuller-formed commercial ships, this percentage is taken to be smaller; specifically, a value of 20 percent of M_w is used. The extreme dynamic moment is taken to follow the extreme value distribution (see Table 5.1.1). A coefficient of variation of 0.30 is used, due in part to the large uncertainty in modeling dynamic effects with this method (SSC-373). Table 5.2.6 shows, for each ship, the mean extreme dynamic moments used in the analysis.

Variable	Cruiser 1	Cruiser 2	SL-7	Tanker
M_d, short-term (ft-LT)	79,600	85,600	213,000	119,000
M_d, long-term (ft-LT)	111,200	116,300	296,000	188,600

Table 5.2.6 Mean Values for the Dynamic Bending Moment

Load Combination Factors:

As explained above, load combination factors are used in this analysis to account for the correlations between various loads. Two combination factors are needed: one to combine the wave-induced and dynamic moments (k_d), and a second to combine the wave-dynamic composite moments with the stillwater moment (k_w). Based on the work conducted in the Ship Structure Committee Project on "Loads and Load Combinations" (SSC-373) and of Mansour and Jensen (1995, nos. 1 and 2), values were selected for both load combination factors. Since these factors are semi-empirical, it is prudent to include each as a random variable rather than as deterministic constants. The normal distribution was chosen to model this uncertainty. Coefficient of variations were selected for each of the factors, with k_w having a coefficient of variation of 0.05, and k_d having a coefficient of variation of 0.15. The second of these is somewhat large because of the higher uncertainty in making a valid judgment about k_d's value. The mean load combination factors and their coefficients of variation are shown in Table 5.2.7.

Factor	Mean	COV
k_w	1.0	0.05
k_d	0.7	0.15

Table 5.2.7 Load Combination Factors

5.3   Limit State Equations

Now that all of the variables have been quantified, the next step in the analysis is the formulation of the limit state equations. In general, there are eight limit state equations for each ship. The same limit state equations are used for both the short-term and long-term time frames. Thus, for each failure mode, there is one equation for the hogging loading condition and one for the sagging condition. There are four failure modes — for a total of eight equations. These equations are shown in Table 5.3.1. (Note: Since SL-7 has no deck for most of its length, secondary and tertiary analyses are not performed for the sagging condition for this ship.)

Failure Mode	Hogging	Sagging
Primary (initial yield)	$G = M_{IY} - \left[M_{sw} + k_w M_w \right]$	$G = M_{IY} - \left[-M_{sw} + k_w \left(M_w + k_d M_d \right) \right]$
Primary (ultimate strength)	$G = M_U - \left[M_{sw} + k_w M_w \right]$	$G = M_U - \left[-M_{sw} + k_w \left(M_w + k_d M_d \right) \right]$
Secondary	$G = S_{u,2} - \dfrac{\left[M_{sw} + k_w M_w \right]}{SM_b}$	$G = S_{u,2} - \dfrac{\left[-M_{sw} + k_w \left(M_w + k_d M_d \right) \right]}{SM_b}$
Tertiary	$G = S_{u,3} - \dfrac{\left[M_{sw} + k_w M_w \right]}{SM_d}$	$G = S_{u,3} - \dfrac{\left[-M_{sw} + k_w \left(M_w + k_d M_d \right) \right]}{SM_d}$

Table 5.3.1 Limit State Equations

There are two important differences between the hogging and sagging equations. First, there is the addition of the dynamic moment (and the corresponding load combination factor). The dynamic moment's sign is such that it will add to a sagging wave moment (SSC-373). The second difference is due to the sign of the stillwater bending moment. Since the stillwater bending moment is a hogging moment, it combines additively with the hogging loads, but subtracts from the sagging loads. This sign change is accounted for in the limit state equation.

The exception to all of this is *Tanker*. Because there are two distinct stillwater bending moments, one hogging and one sagging, each must be accounted for separately. In the short-term time frame, this is not a major problem, as each operating condition is combined with the most detrimental stillwater bending moment to arrive as a worst-case

scenario. The full load (sagging) stillwater bending moment is added to sagging wave and dynamic loads, while the ballast (hogging) stillwater bending moment is added to the hogging wave loads. The real problem comes when the long-term analysis is conducted. Here it is necessary to consider that the ship actually spends part of its lifetime in each condition. To this end, four cases were considered for each failure mode. Specifically, the full load and ballast stillwater bending moments are each combined with both hogging and sagging wave loads. Because it is necessary to calculate each of these four sub-cases for each failure mode, there are a total of sixteen limit state equations needed for *Tanker*. The eight equations given in Table 5.3.1 are used for the ballast sub-cases, and the remaining eight equations (for use with the full load sub-cases) are given in Table 5.3.2. Note that the only difference is the change in the sign of the stillwater bending moment.

Failure Mode	Hogging	Sagging
Primary (initial yield)	$G = M_{IY} - \left[-M_{sw} + k_w M_w \right]$	$G = M_{IY} - \left[M_{sw} + k_w \left(M_w + k_d M_d \right) \right]$
Primary (ultimate strength)	$G = M_U - \left[-M_{sw} + k_w M_w \right]$	$G = M_U - \left[M_{sw} + k_w \left(M_w + k_d M_d \right) \right]$
Secondary	$G = S_{u,2} - \dfrac{\left[-M_{sw} + k_w M_w \right]}{SM_b}$	$G = S_{u,2} - \dfrac{\left[M_{sw} + k_w \left(M_w + k_d M_d \right) \right]}{SM_b}$
Tertiary	$G = S_{u,3} - \dfrac{\left[-M_{sw} + k_w M_w \right]}{SM_d}$	$G = S_{u,3} - \dfrac{\left[M_{sw} + k_w \left(M_w + k_d M_d \right) \right]}{SM_d}$

Table 5.3.2 Limit State Equations for *Tanker*, Full Load Condition

5.4 Failure Probabilities and Safety Indices for Four Ships — CALREL Code Results

With all the variables defined and the limit state equations formulated, the next step is to actually perform the reliability analysis by running CALREL. CALREL provides a variety of important information in its output. In the interest of brevity, not all of the outputs for each of the 68 separate CALREL cases are covered in detail. Instead, a single case is explained thoroughly and then a summary of the remaining cases is presented. The sample case chosen for illustration investigates primary (ultimate) hull girder failure of *Cruiser 1* caused by sagging wave loads experienced in a short-term extreme sea condition. The CALREL output file for this case is included as Appendix F, and will be referred to frequently.

The first part of the output file is an echo of the input data. This covers areas such as the number of random variables in the analysis, statistical information for those variables and a number of parameters controlling the numerical algorithms of the program. For our sample

case, there are six random variables. The statistical characteristics of these variables are shown in Table 5.4.1.

Variable	M_U	M_{sw}	M_w	M_d	k_w	k_d
Distribution	Lognormal	Normal	Ext. Value	Ext. Value	Normal	Normal
Mean	59.6	6.14	19.9	7.96	1.0	0.7
Std. Dev.	5.96	0.922	1.99	2.39	0.05	0.105
Note: All bending moment values are in units of 10^4 ft-LT						

Table 5.4.1 Statistics of the Input Variables for the Sample Case

The second portion of the output is the results of the FORM and SORM analyses. The FORM results are presented first. The most important information here is the safety index and its corresponding probability of failure. Also, as a part of the FORM output, CALREL provides the coordinates of the design point in both original (x^*) and standard normal (u^*) space and the corresponding value of the limit state function. Ideally, the value of the limit state function should be zero at the design point; however, due to the numerical approximations in the computer model, it will not be exactly zero.

In the SORM analysis, CALREL uses two different integration schemes to calculate the probability of failure. The two schemes used are the improved Breitung formula (1984) and Tvedt's exact integral (1990). For most cases, the probabilities of failure calculated using the different schemes were nearly the same, usually only differing by one or two percent at most. Table 5.4.2 summarizes all three estimations of the safety index and probability of failure for this case. When reporting results, the FORM results were taken as the result for that case and is rounded off to two decimal places. For example, the safety index for this case is reported as being 6.47.

Estimation Method	Safety Index (β)	Probability of Failure (P_f)
FORM	6.4746	4.752×10^{-11}
SORM (improved Breitung)	6.4669	5.001×10^{-11}
SORM (Tvedt's exact integral)	6.4670	4.999×10^{-11}

Table 5.4.2 Comparison of Different Reliability Methods (Sample Case)

The Tanker Problem:

Compiling results for *Tanker* posed some interesting problems. As stated before, the short term cases are straightforward applications of a "worst-case" scenario, combining the least favorable stillwater and wave bending moments. While this sort of simplification is justifiable in a short-term case, it is not possible to make the same sort of assumption over the

long term. Instead, it is necessary to combine each of the stillwater bending moments (full-load and ballast) with both types of wave loading (hogging and sagging).

Therefore, for each long-term failure mode, four cases are needed (as opposed to two cases per long-term failure mode for the other ships). A CALREL analysis is performed for each of these cases. In order to conform with the data from the other ships, it is necessary to combine the different operating conditions for each type of wave load into one combined answer (see Figure 5.4.1). It is assumed that *Tanker* spends half of its life spent in each operating condition. The probabilities of failure resulting from the CALREL analyses are combined for each loading condition (hogging and sagging wave loads) by weighting the probability of failure for each stillwater bending moment (full load and ballast) by the fraction of the ship's total life spent in either the full load or ballast condition. Mathematically,

$$P_f^i = t_{FL} P_{f,FL}^i + t_{BAL} P_{f,BAL}^i$$

where

- P_f^i is the total probability of failure in the ith case (e.g., secondary, sagging, short-term)
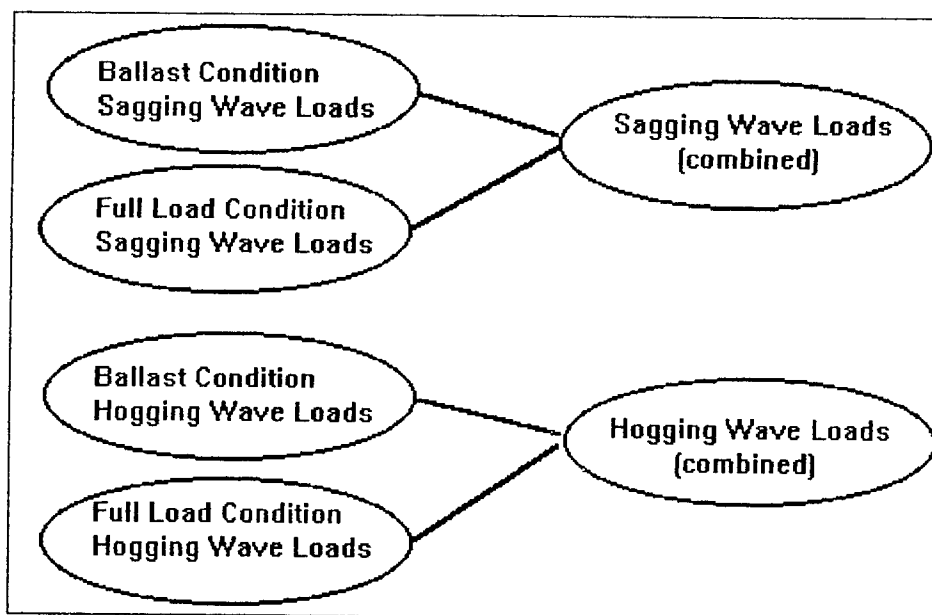
Figure 5.4.1 Combining Long Term Results for *Tanker*

5-13

- $P^i_{f,FL}$ and $P^i_{f,BAL}$ are the probabilities of failing in the ith case with the full load or ballast stillwater bending moments, respectively

- $t_{FL} = t_{BAL} = 0.5$ are the fractions of the ship's total life spent in the full load and ballast conditions, respectively.

Safety Assessment:

Table 5.4.3 contains the results for all of the different cases for each ship. Figure 5.4.2 shows also the same results. For each case, both the safety index and the accompanying probability of failure are given. For time frame and failure mode, the safety index for the more hazardous of the two loading conditions is shaded. These twenty-four values are the "critical β's" and are the governing cases for each ship (see Tables 5.4.4 and 5.4.5). These results can help to answer the key questions of this project: *"How do the relative reliabilities of the different ships compare? Can we rank them in terms of their safety?"*

In this section, an attempt is made to answer this question using the information gained in this study. The naval ships are discussed and compared first and the commercial ships second. The "critical β" cases are evaluated for each ship and some preliminary qualitative judgments are derived from the results. Attempts are made to derive correlations between the various directions (hogging and sagging) of failure and the properties of the ships. Differences between the ships are noted and their effects on the relative safety of the ships are investigated.

As a secondary point, the presence or absence of a proper failure chain is determined for each ship. When designing a structure, a common technique is to design it such that, if the structure is to fail, it will fail in a tertiary or a secondary mode. This is indicated by having safety factors such that $\beta_{primary} > \beta_{secondary} > \beta_{tertiary}$. If the ship is designed so that this inequality is satisfied, failure would most likely appear first in individual local panels, spread next to the gross panel, and finally encompass the entire hull girder. In this way, a warning of impending total failure is provided by localized failures that do not threaten the survival of the structure. The idea behind this is that if the ship's watch officer looks out and sees the deck plates buckling, he can order the ship to change course or slow to reduce the wave loadings before a more destructive failure can occur. By looking at the critical β's for each ship, it is possible to see if such a "failure chain" exists.

Graph 8 : Safety Index vs Ship Type (by CALREL Program)
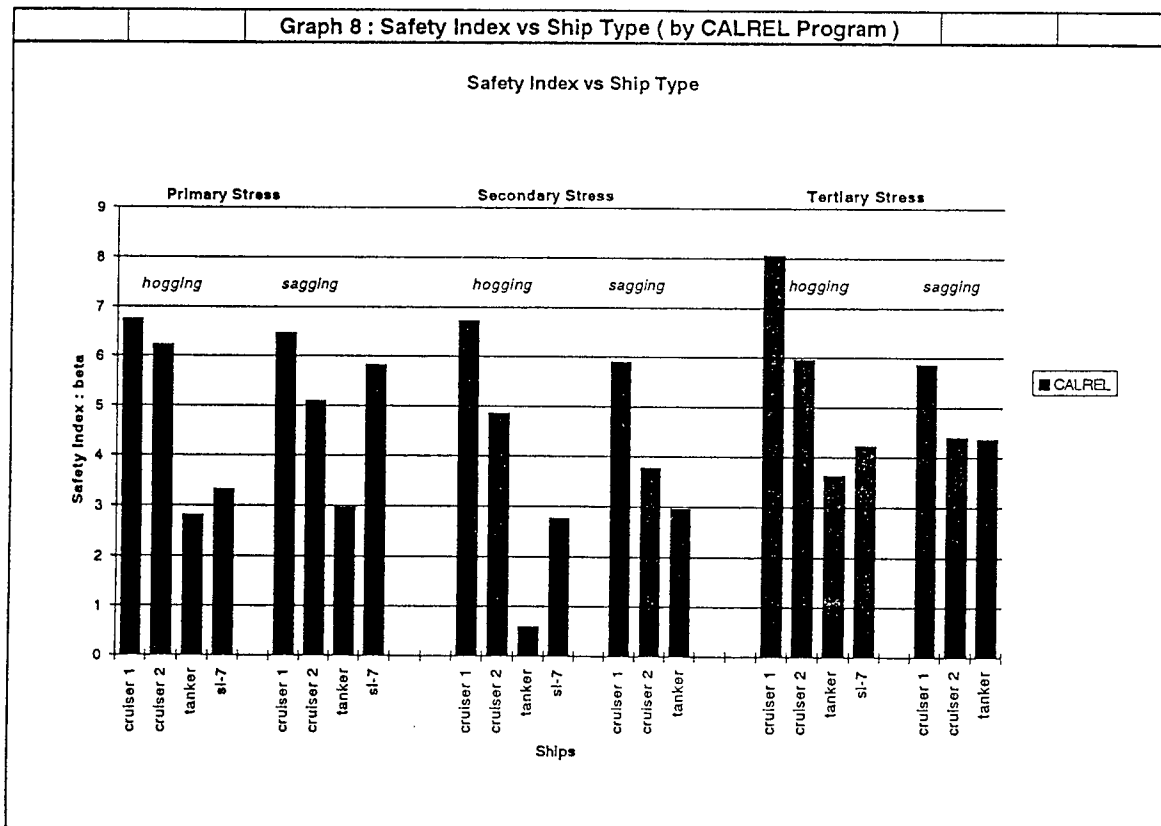
Figure 5.4.2

	Short Term				Long Term			
	Sagging		Hogging		Sagging		Hogging	
	β	P_f	β	P_f	β	P_f	β	P_f
Cruiser 1								
Primary (IY)	10.29	0.00E+00	10.45	0.00E+00	7.92	1.22E-15	7.40	6.86E-14
Primary (ULT)	6.47	4.92E-11	6.75	7.43E-12	4.27	9.78E-06	4.09	2.16E-05
Secondary	5.89	1.94E-09	6.74	7.96E-12	3.75	8.84E-05	4.16	1.59E-05
Tertiary	5.86	2.32E-09	8.06	3.33E-16	3.71	1.04E-04	5.43	2.82E-08
Cruiser 2								
Primary (IY)	6.75	7.43E-12	7.77	4.00E-15	4.67	1.51E-06	4.54	2.82E-06
Primary (ULT)	5.10	1.70E-07	6.22	2.50E-10	3.09	1.00E-03	3.18	7.36E-04
Secondary	3.74	9.20E-05	4.86	5.88E-07	1.73	4.18E-02	1.89	2.94E-02
Tertiary	4.38	5.94E-06	5.96	1.27E-09	2.39	8.42E-03	3.03	1.22E-03
SL-7								
Primary (IY)	6.26	1.93E-10	6.58	2.36E-11	4.20	1.34E-05	5.88	2.06E-09
Primary (ULT)	5.83	2.78E-09	3.32	4.50E-04	3.84	6.15E-05	2.67	3.79E-03
Secondary	#N/A	#N/A	2.74	3.07E-03	#N/A	#N/A	2.11	1.74E-02
Tertiary	#N/A`	#N/A	4.21	1.28E-05	#N/A	#N/A	3.58	1.72E-04
Tanker								
Primary (IY)	5.87	2.19E-09	5.01	2.73E-07	3.31	4.69E-04	4.03	2.81E-05
Primary (ULT)	3.02	1.26E-03	2.82	2.40E-03	0.81	2.08E-01	2.03	2.14E-02
Secondary	3.24	5.98E-04	0.57	2.84E-01	1.05	1.46E-01	0.04	4.83E-01
Tertiary	4.63	1.83E-06	3.61	1.53E-04	2.30	1.07E-02	2.77	2.78E-03

Table 5.4.3 Reliability Results for All Ships, All Cases

	Cruiser 1		*Cruiser 2*		*SL-7*		*Tanker*	
Primary (ULT)	6.47	S	5.10	S	3.32	H	2.82	H
Secondary	5.89	S	3.74	S	2.74	H	0.57	H
Tertiary	5.86	S	4.38	S	4.21	H	3.61	H

Table 5.4.4 Critical β's and Loading Conditions, Short Term

	Cruiser 1		*Cruiser 2*		*SL-7*		*Tanker*	
Primary (ULT)	4.09	H	3.09	S	2.67	H	0.81	S
Secondary	3.75	S	1.73	S	2.11	H	0.04	H
Tertiary	3.71	S	2.39	S	3.58	H	2.30	S

Table 5.4.5 Critical β's and Loading Conditions, Long Term

Naval Ships:

Cruiser 1 shows good results for both short-term extreme seas as well as over the long term, with a maximum lifetime probability of failure of approximately 10^{-4} ($\beta = 3.71$) on local failure and 10^{-5} ($\beta = 4.09$) on ultimate failure. *Cruiser 2* appears to be satisfactory as well, particularly in the short term. The long-term probability of secondary failure is a little less comforting, with a lifetime probability of approximately 4 percent ($\beta = 1.73$). This is still rather small and, given that a secondary failure is unlikely to be catastrophic, it is probably an acceptable risk.

Note that nearly all of the critical cases for the military ships involve failure in sagging waves. This can be attributed to the presence of the dynamic moment in the sagging condition and the nonlinearities in wave response that cause the sagging wave moments to be larger than the hogging wave moments. Even though the stillwater bending moment is a hogging moment, the dynamic moment in the sagging condition is large enough to more than offset the stillwater moment. Strengths are not substantially different for the two directions.

Cruiser 1 and *Cruiser 2* have the same hull form and structure, but *Cruiser 1* is about 15 percent heavier and uses more high-strength steel. The increase in displacement from *Cruiser 2* to *Cruiser 1* increases the stillwater moment (hogging) while decreasing the non-linearity of the wave-induced moments, increasing the hogging wave moment and decreasing the sagging wave moment. the substitution of high-strength steel in *Cruiser 1* increases the strength variables (M_u, $S_{u,2}$, and $S_{u,3}$) by between 14 and 48 percent (see Table 5.2.1). Overall, the combination of these various factors results in an increase of *Cruiser 1* safety index β by 32 percent. It should be noted, however, that this increase in safety does *not* include the (most likely detrimental) effects that the use of high-strength steels has on fatigue life. The fatigue aspects are presented in Chapter 7. It should be also noted that all safety indices are calculated at midship sections (no knuckles).

Cruiser 1 exhibits a proper chain of failures in both the long term and the short term for sagging loads. There is a steady progression from the tertiary mode (lowest safety index) to the primary mode (highest safety index). Hogging loads are another story, however. For the hogging loads, the failure chain is reversed, with the most likely first failure being global hull collapse. While this is not exactly desirable, it could be accepted because the hogging failure modes are much less likely than the sagging modes.

The failure chain for *Cruiser 2* is a little less ideal. While primary failure has the highest safety index, as it should, secondary failure is more likely to occur than tertiary failure. Therefore, there may be little or no warning before a gross panel collapse. Still, a gross panel collapse would probably still happen prior to a primary mode failure, providing some warning time. The failure chain for *Cruiser 2* is unchanged for the different time periods and wave load directions.

Commercial Ships:

The commercial ships seem to be somewhat riskier than their naval counterparts, probably reflecting the thinner margins to which they are designed. *SL-7* behaves tolerably well in short-term extreme seas, with its largest probability of failure being secondary failure at a likelihood of about 0.3 percent (β = 2.74). The long term analysis generates a little concern, with a lifetime probability of secondary failure of 1.74 percent (β = 2.67) being the largest. Results for *Tanker* are even more disconcerting. While the short-term probability of primary ultimate failure is a somewhat tolerable 0.24 percent (β = 2.82), the probability of experiencing a gross panel (secondary) failure in the bottom of the hull is about 28 percent (β = 0.57), much higher than would seem to be reasonable. Long term results are, predictably, worse. The lifetime probability of primary hull girder failure is a grim 21 percent (β = 0.81), and the probability of seeing a secondary failure over the ship's lifetime is an abysmal 48 percent (β = 0.04). It is important to note here that *Tanker* has been operating off the west coast (between Santa Barbara and San Diego) for many years without any failure problems; however, the sea conditions in its normal operating area are not nearly as severe as those that it is subjected to in this analysis (North Atlantic).

In short-term conditions, hogging waves are the controlling causes of failure for the commercial ships.[*] In the long-term analyses, this trend is less clear. Hogging waves dominate all of the critical failure cases for *SL-7*, due to a combination of several factors. The most important being the hogging stillwater bending moment interacts additively with the hogging wave loads to increase the total load on the ship in this condition. For the commercial ships, the reduced dynamic sagging moments are smaller than the hogging stillwater moments, resulting in larger total loads in the hogging condition.

As could be expected, the situation is more clouded for the long-term analysis of *Tanker*. In order to make some sense out of it, one must look to the component sub-cases that are combined for the long-term analysis as outlined in the previous sub-section. These results are shown in Table 5.4.6. It is clear that the combined probability of failure for each case is largely driven by whichever sub-case combined stillwater and wave loadings in the same direction. Primary mode failure for *Tanker* is controlled by the low β value for the full load, sagging waves sub-case. It is here that stillwater, wave and dynamic loads combined to produce the highest total combined load for any of the cases. This is aggravated by the fact that the ultimate strength of the hull is slightly lower in the sagging direction. Together, this results in a high probability of failure. The secondary failure mode is similar to the primary mode, with the only difference being the absence of the dynamic load. The secondary strength in the hogging direction is about 60 percent of the strength in the sagging direction. This combination produces the lowest safety index encountered in the study.[**] Tertiary mode results follow the lead of the other two, but do not indicate nearly as dangerous of a situation.

---

[*] Secondary and tertiary sagging are not investigated with *SL-7*.
[**] If the ship were to operate in this condition (full load) for its entire life.

The failure chain for the commercial ships is nearly identical to that of *Cruiser 2* in all important aspects. Both *Tanker* and *SL-7* would probably experience gross panel failure prior to global hull collapse, with local panel failure being initially unlikely. This failure chain is consistent across both the long term and short term for both ships.

| | Long Term – Full Load | | | | Long Term – Ballast | | | |
| | Sagging | | Hogging | | Sagging | | Hogging | |
	β	P_f	β	P_f	β	P_f	β	P_f
Primary (IY)	3.11	9.36E-04	5.77	3.98E-09	4.50	3.40E-06	3.86	5.67E-05
Primary (ULT)	0.25	4.01E-01	3.98	3.45E-05	2.17	1.50E-02	1.72	4.27E-02
Secondary	0.57	2.84E-01	0.61	2.71E-01	2.39	8.42E-03	-0.51	6.95E-01
Tertiary	2.03	2.12E-02	3.57	1.79E-04	3.56	1.85E-04	2.55	5.39E-03

Table 5.4.6 Results for Tanker Sub-Cases

The Primary, Initial Yield Moment, Cases:

By perusing the results in Table 5.4.3, one can see that the primary initial yield moment is a mediocre predictor of the true strength of the ship. Using the initial yield moment to assess the reliability of a ship's structure results in an *un*-conservative estimate. While this is to be expected, given the nature of stiffened panel buckling, it is generally hoped that the "factor of danger" would be consistent for any cases considered. However, the results of this study show that this is not true, and that the "factor of danger" varies from short term to long term, from ship to ship, and for different wave loading directions. Figure 5.4.3 shows how this "factor of danger" (equal to the safety index from the ultimate limit case divided by the safety index from the initial yield case) varies for different ships, wave loads, and time frames. If this factor were constant, all of the bars would be of about the same height. Clearly, they are not. The ultimate limit safety index varies from about 24 percent to 93 percent of the initial yield safety index (please refer to Figure 5.4.3 and Table 5.4.3). From these observations, it can be concluded that the initial yield moment cannot be used to rank the ships in terms of their safety. Designing a ship's structure based on yield strength criteria is unlikely to produce designs with a consistent level of reliability.
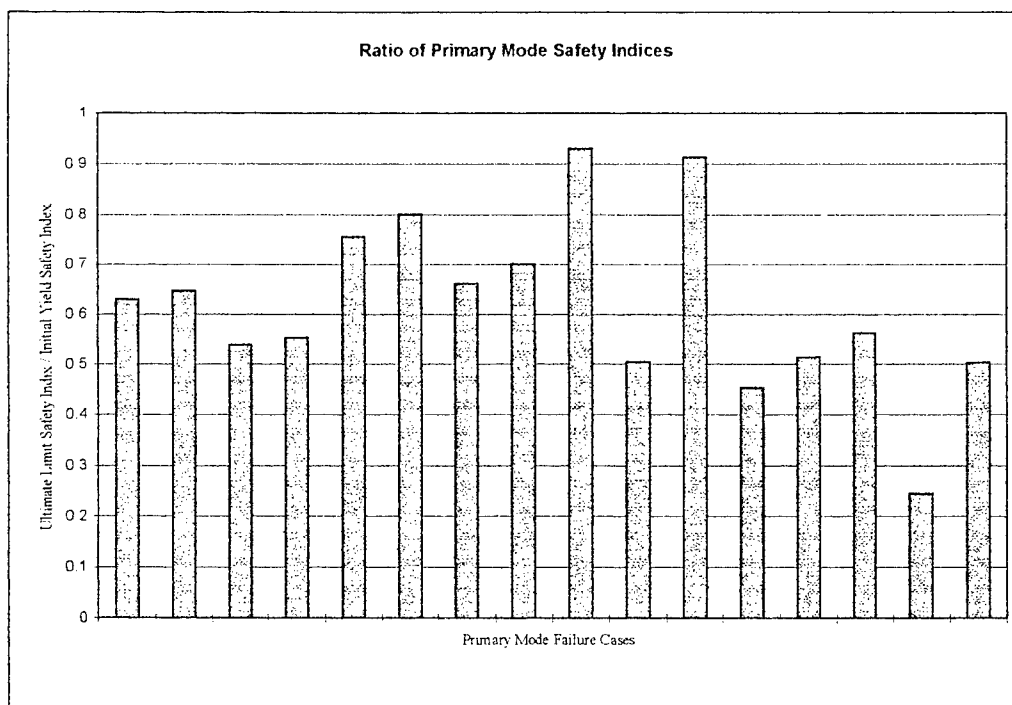
Figure 5.4.3 "Factor of Danger"

5.5   Parametric Study and Comparison with the Simple Formulation Results

In this section, we will focus our effort on the short-term reliability analysis for the four ships in hogging and sagging conditions and with consideration to primary, secondary, and tertiary stresses. Two different simple methods are available for analyzing ship structures which were presented in section 2.3.4.3. The purpose of this section is to apply these two methods to the four ships and to compare the results with those from CALREL. In addition, a parametric study was conducted in order to determine the relationship between *safety index* and certain design parameters.

The reliability methods are:

1) Numerical Method: CALREL program for structural analysis

2) Closed Form (approximate formula) presented in section 2.3.4.3

3) Mean Value First Order Second Moment Method presented in section 2.3.4.3

Identical mean values and coefficients of variation of the design variables have been used in all three methods. These values have been discussed and presented in sections 5.2 to 5.4.

Figure 5.5.1 and the accompanying table show the results of this comparison for primary, secondary and tertiary failure modes and for all four ships. In general, the approximate methods show the same general trend as CALREL results, but entail some errors. The percentage error is shown in Table 5.5.1. In most cases, CALREL gives larger safety indices than the other two methods, but there is no clear indication as to which of the simple formulas is more accurate.

		Ship Type vs Safety Index Using Three Methods							
				Ships	method 1	method 2	method 3		
		Primary	hogging	cruiser 1	6.76	5.56	5.87		
				cruiser 2	6.23	5.23	5.56		
				tanker	2.82	2.32	2.82		
				sl-7	3.32	2.69	3.11		
			sagging	cruiser 1	6.47	6.18	5.95		
				cruiser 2	5.10	5.07	4.83		
				tanker	2.96	2.43	2.72		
				sl-7	5.83	5.70	5.34		
		Secondary	hogging	cruiser 1	6.73	5.29	5.61		
				cruiser 2	4.86	4.01	4.39		
				tanker	0.60	0.33	0.85		
				sl-7	2.77	1.97	2.57		
			sagging	cruiser 1	5.91	5.61	5.33		
				cruiser 2	3.78	3.87	3.52		
				tanker	2.96	2.43	2.72		
				sl-7	N	N	N		
		Tertiary	hogging	cruiser 1	8.06	6.01	6.30		
				cruiser 2	5.96	4.77	5.16		
				tanker	3.63	3.03	3.46		
				sl-7	4.23	3.02	3.43		
			sagging	cruiser 1	5.87	5.59	5.31		
				cruiser 2	4.40	4.39	4.08		
				tanker	4.37	3.65	3.84		
				sl-7	N	N	N		
method 1: CALREL program			method 2: Closed Form Method		method 3: Mean Value First Order Second Moment Method				
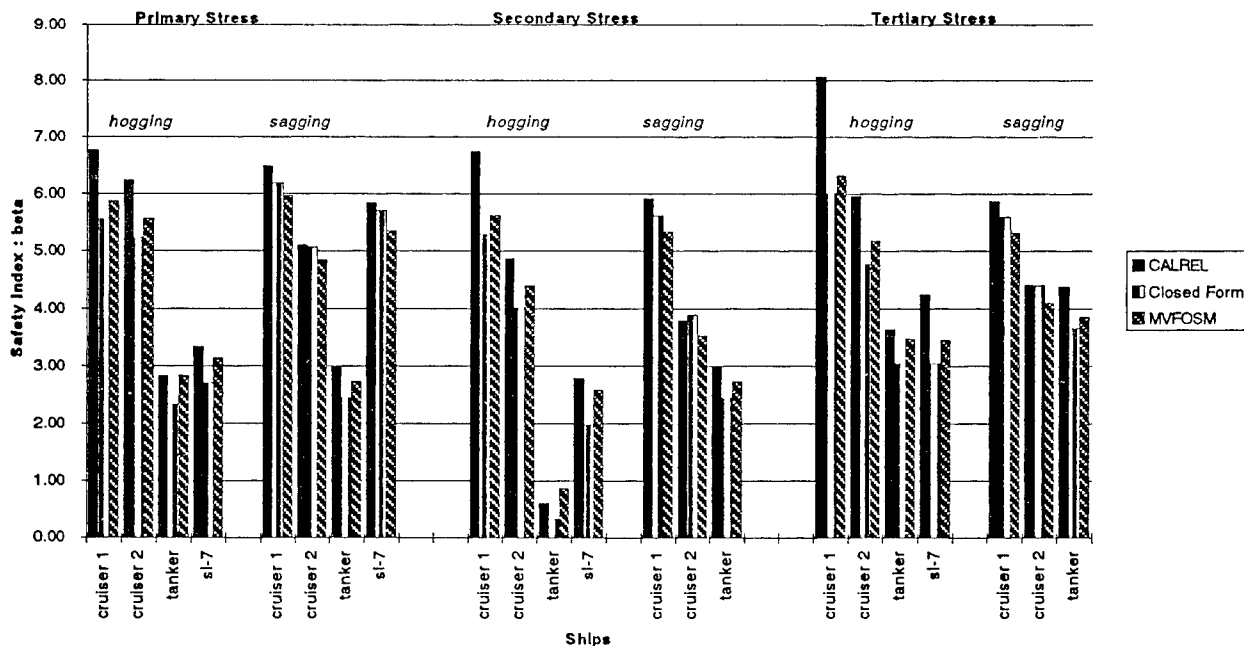
Figure 5.5.1 Comparison of Three Reliability Methods

Comparison of Three Methods				
	cruiser1		cruiser2	
	safety index	*safety index*	*safety index*	*safety index*
	method2	*method3*	*method2*	*method3*
hogging				
primary	-17.80%	-13.11%	-16.07%	-10.83%
secondary	-21.44%	-16.65%	-17.50%	-9.73%
tertiary	-25.48%	-21.77%	-19.99%	-13.35%
sagging				
primary	-4.51%	-7.97%	-0.67%	-5.26%
secondary	-5.01%	-9.77%	2.49%	-6.95%
tertiary	-4.77%	-9.59%	-0.20%	-7.18%
	tanker		sl-7	
	safety index	*safety index*	*safety index*	*safety index*
	method2	*method3*	*method2*	*method3*
hogging				
primary	-17.61%	-0.01%	-18.87%	-6.18%
secondary	-45.02%	41.38%	-29.02%	-7.18%
tertiary	-16.63%	-4.75%	-28.50%	-18.90%
sagging				
primary	-15.36%	-5.53%	-2.20%	-8.36%
secondary	-17.90%	-8.22%	N	N
tertiary	-16.56%	-12.17%	N	N

error = $[(\beta_{method2} \text{ or } \beta_{method3}) - \beta_{method1}]/\beta_{method1}$

"-" means the safety index is smaller than method 1

"+" means the safety index is greater than method 1

method 1 : CALREL Program

method 2 : Closed Form Method

method 3 : Mean Value First Order Second Moment Method

Table 5.5.1 Percentage Error – Three Reliability Methods

Next, a parametric study was conducted to see if there was any detectable trend of the safety index with respect to ship type or a design parameter. First, with respect to ship type, Figure 5.4.2 and the safety indices presented in the previous section indicate that the two naval vessels have higher safety level than the two commercial ships. This trend is consistent in almost all three failure modes (see Figure 5.4.2).

The safety index versus displacement was considered next. Figure 5.5.2 and the accompanying table show that there is no general trend of β with displacement. Figures 5.5.3 and 5.5.4 show the trend of the safety index with a safety factor based on initial yield (see Figure 5.5.3) and one based on the ultimate collapse moment (Figure 5.5.4). In general, the factor of safety based on the ultimate moment gives a better indication of the ship safety than the one based on initial yield moment since, in the former case, the safety index consistently increases with the factor of safety (Figure 5.5.4). Figure 5.5.5 shows moment ratio versus ship length. The moment ratio is defined as the value calculated from SOST at a probability of exceedence of 50 percent divided by the bending moment calculated according to ABS Rules. In almost all cases, SOST values, at that probability level, are higher than the ABS values.

Figures 5.5.6 to 5.5.8 show the safety index plotted versus mean margin defined as the strength mean minus the mean of the load. The scatter of the data shown in Figure 5.5.6 indicates the impact of standard deviation (and the distribution) as well as ship type on the safety index, whereas the scatter in the data shown in Figures 5.5.7 and 5.5.8 (less scatter) indicates the impact of only the standard deviation on the safety index. These figures indicate that the safety margin should not be used as a measure of safety instead of the safety index.

More detailed results of the comparison between the three reliability methods and of the parametric study is shown in Appendix G.

				Displacement vs Safety Index			
		Ships	Displacement	method 1	method 2	method 3	
Primary	hogging	cruiser 2	9.02E+03	6.23	5.23	5.56	
		cruiser 1	9.68E+03	6.76	5.56	5.87	
		tanker	4.46E+04	2.82	2.32	2.82	
		sl-7	4.78E+04	3.32	2.69	3.11	
	sagging	cruiser 2	9.02E+03	5.10	5.07	4.83	
		cruiser 1	9.68E+03	6.47	6.18	5.95	
		tanker	4.46E+04	2.96	2.43	2.72	
		sl-7	4.78E+04	5.83	5.70	5.34	
Secondary	hogging	cruiser 2	9.02E+03	4.86	4.01	4.39	
		cruiser 1	9.68E+03	6.73	5.29	5.61	
		tanker	4.46E+04	0.60	0.33	0.85	
		sl-7	4.78E+04	2.77	1.97	2.57	
	sagging	cruiser 2	9.02E+03	3.78	3.87	3.52	
		cruiser 1	9.68E+03	5.91	5.61	5.33	
		tanker	4.46E+04	2.96	2.43	2.72	
		sl-7	4.78E+04	N	N	N	
Tertiary	hogging	cruiser 2	9.02E+03	5.96	4.77	5.16	
		cruiser 1	9.68E+03	8.06	6.01	6.30	
		tanker	4.46E+04	3.63	3.03	3.46	
		sl-7	4.78E+04	4.23	3.02	3.43	
	sagging	cruiser 2	9.02E+03	4.40	4.39	4.08	
		cruiser 1	9.68E+03	5.87	5.59	5.31	
		tanker	4.46E+04	4.37	3.65	3.84	
		sl-7	4.78E+04	N	N	N	
method 1: CALREL program		method 2: Closed Form Method		method 3: Mean Value First Order Second Moment Method			
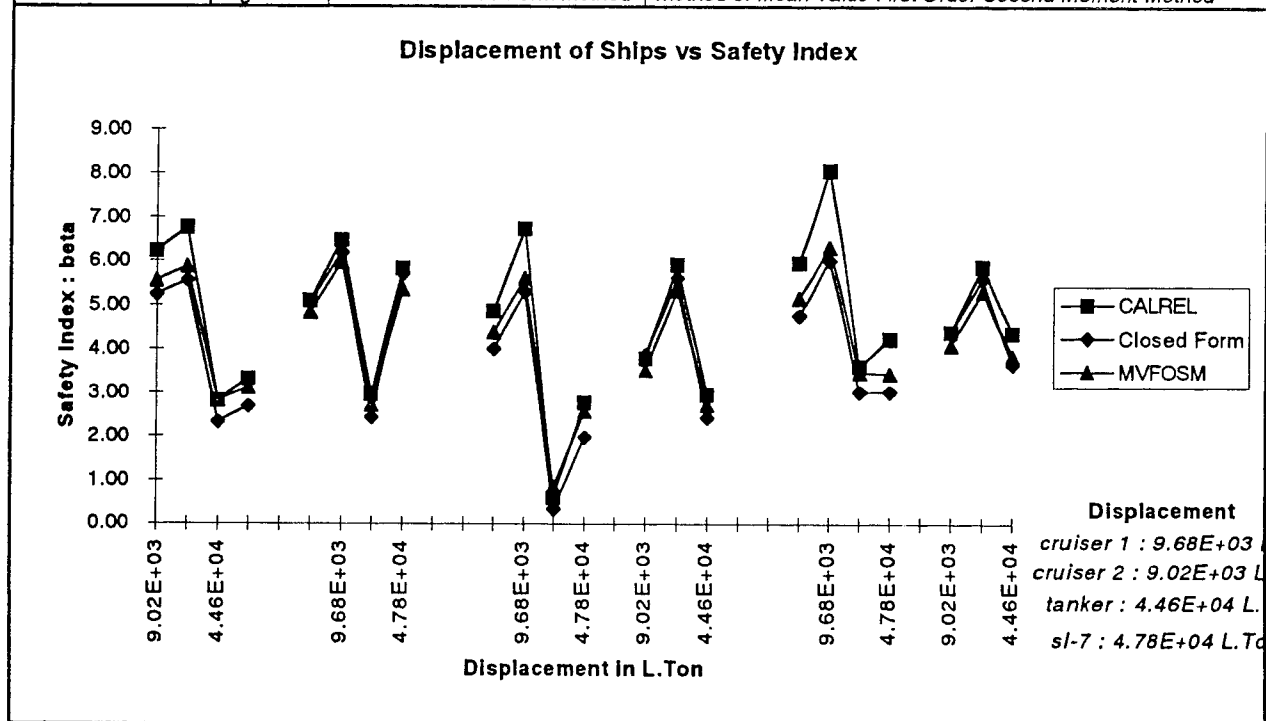
Figure 5.5.2 Safety Index versus Displacement

Factor of Safety vs Safety Index						
Primary Stress						
deck						
Ships	Initial yield moment	ABS moment	SFI	beta 1	beta 2	beta 3
sl-7	3.00E+06	1.80E+06	1.67E+00	3.32E+00	2.69E+00	3.11E+00
tanker	1.51E+06	8.80E+05	1.71E+00	2.82E+00	2.32E+00	2.82E+00
cruiser 2	5.24E+05	2.71E+05	1.93E+00	6.23E+00	5.23E+00	5.56E+00
cruiser 1	8.34E+05	2.74E+05	3.04E+00	6.76E+00	5.56E+00	5.87E+00
bottom						
Ships	Initial yield moment	ABS moment	SFI	beta 1	beta 2	beta 3
sl-7	2.38E+06	1.80E+06	1.33E+00	5.83E+00	5.70E+00	5.34E+00
tanker	1.58E+06	8.79E+05	1.80E+00	2.70E+00	2.29E+00	2.55E+00
cruiser 2	5.78E+05	2.71E+05	2.13E+00	5.10E+00	5.07E+00	4.83E+00
cruiser 1	9.12E+05	2.74E+05	3.32E+00	6.47E+00	6.18E+00	5.95E+00
method1 : CALREL structural program						
method2 : Closed Form (by approximation)						
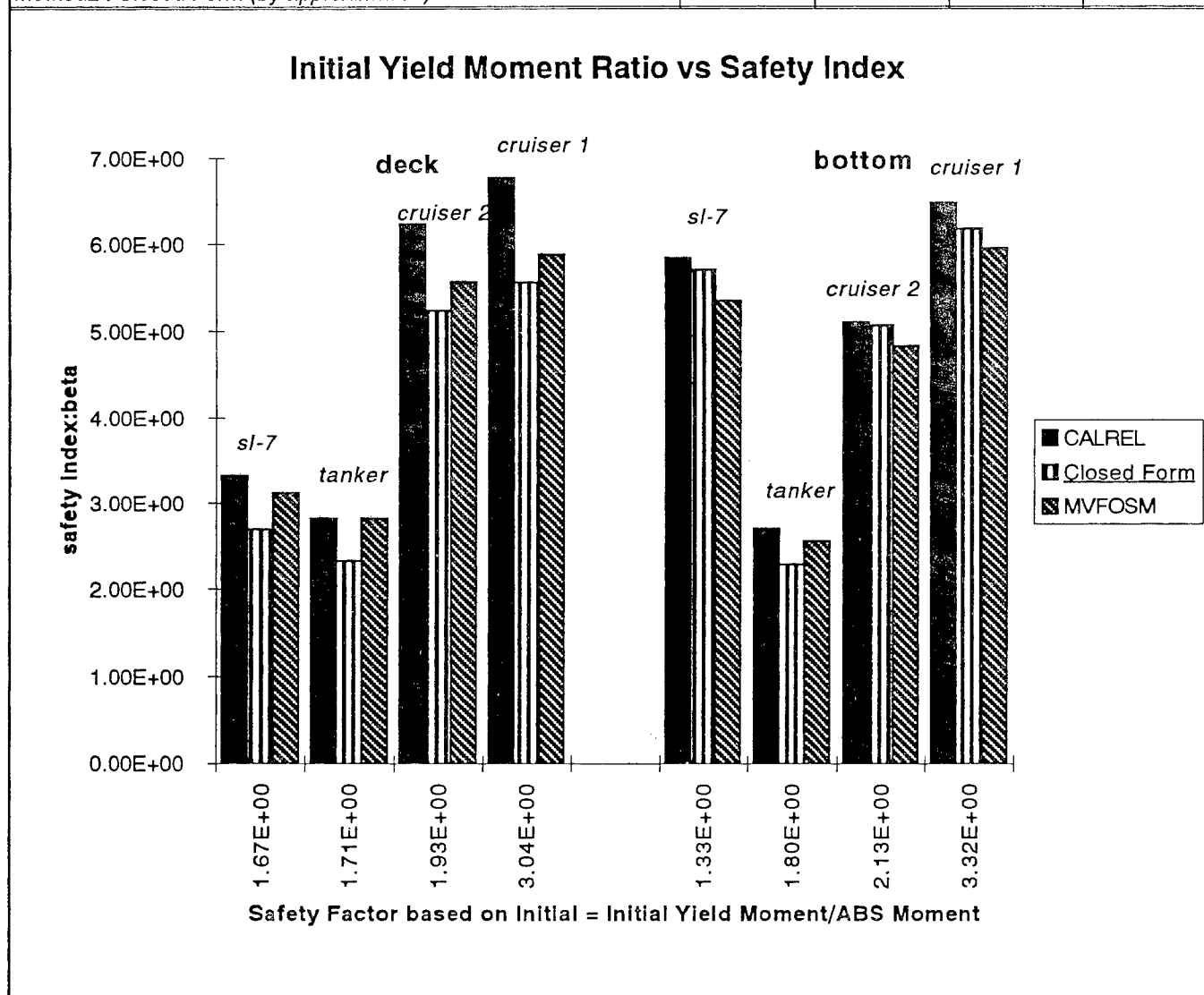
Figure 5.5.3 β versus Factor of Safety Based on Initial Yield

5-26

hogging						
Ships	Ultimate moment	Nonlinear moment	SFu	beta 1	beta 2	beta 3
tanker	1.12E+06	5.86E+05	1.91E+00	2.82E+00	2.32E+00	2.82E+00
sl-7	1.90E+06	9.70E+05	1.96E+00	3.32E+00	2.69E+00	3.11E+00
cruiser 2	4.38E+05	1.56E+05	2.81E+00	6.23E+00	5.23E+00	5.56E+00
cruiser 1	5.23E+05	1.69E+05	3.09E+00	6.76E+00	5.56E+00	5.87E+00
sagging						
Ships	Ultimate moment	Nonlinear moment	SFu	beta 1	beta 2	beta 3
tanker	1.05E+06	5.95E+05	1.77E+00	2.70E+00	2.29E+00	2.55E+00
cruiser 2	4.55E+05	2.14E+05	2.13E+00	5.10E+00	5.07E+00	4.83E+00
sl-7	2.29E+06	1.07E+06	2.15E+00	5.83E+00	5.70E+00	5.34E+00
cruiser 1	5.18E+05	1.99E+05	2.60E+00	6.47E+00	6.18E+00	5.95E+00
method1 : CALREL structural program						
method2 : Closed Form (by approximation)						
method3 : Mean Value First Order Second Moment						
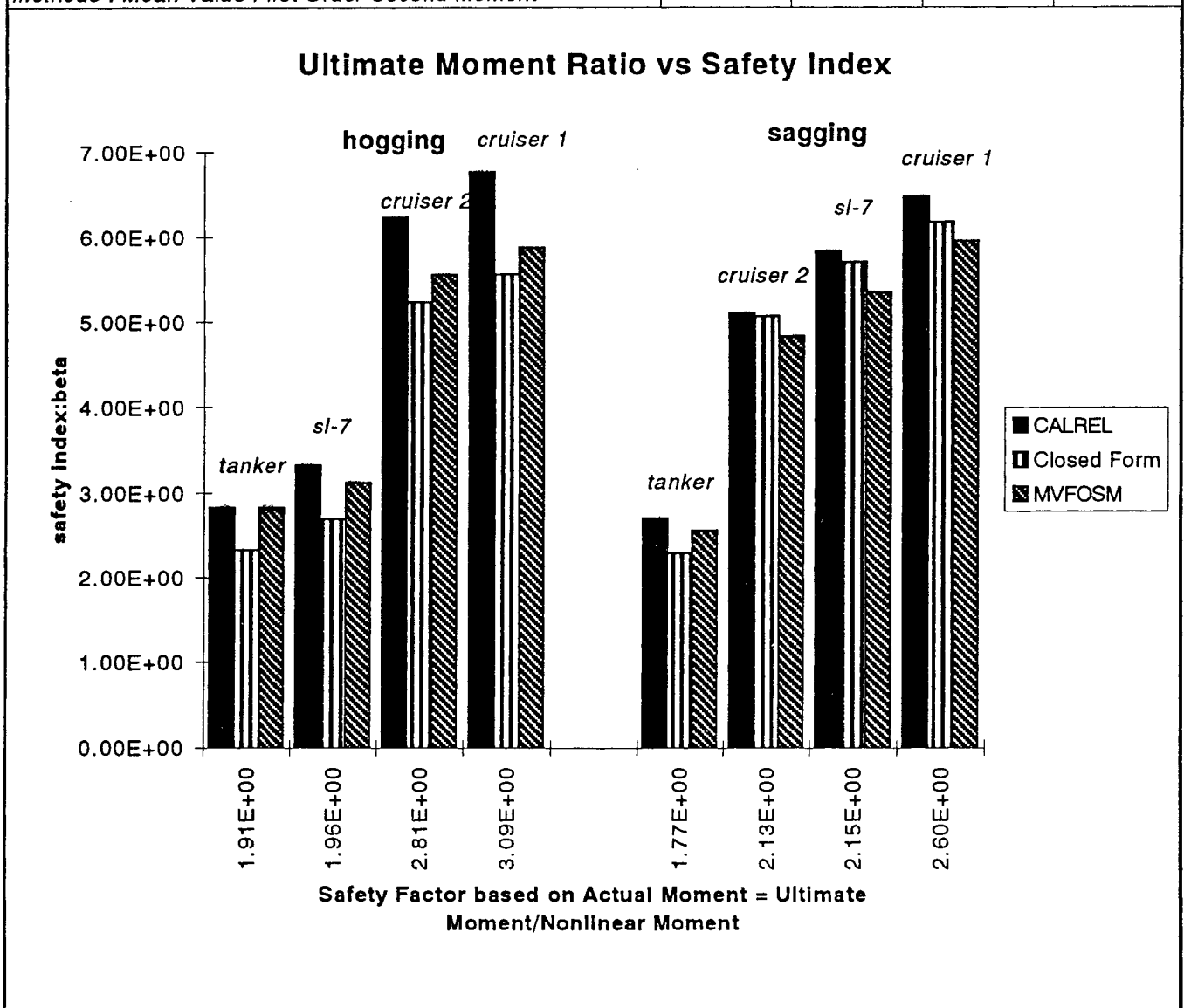
Figure 5.5.4 β versus Factor of Safety Based on Ultimate Moment

Ship Length vs Wave Bending Moment Ratio

		Ships	Length	Ratio(wave)		
Primary	hogging	cruiser 1	529.00	1.37E+00		
		cruiser 2	529.00	1.30E+00		
		tanker	640.00	1.21E+00		
		sl-7	880.50	1.10E+00		
	sagging	cruiser 2	529.00	1.26E+00		
		cruiser 1	529.00	1.15E+00		
		tanker	640.00	1.08E+00		
		sl-7	880.50	9.42E-01		
ps : Ratio(wave)=Wave Bending Moment(real)/Wave Bending Moment(ABS)						
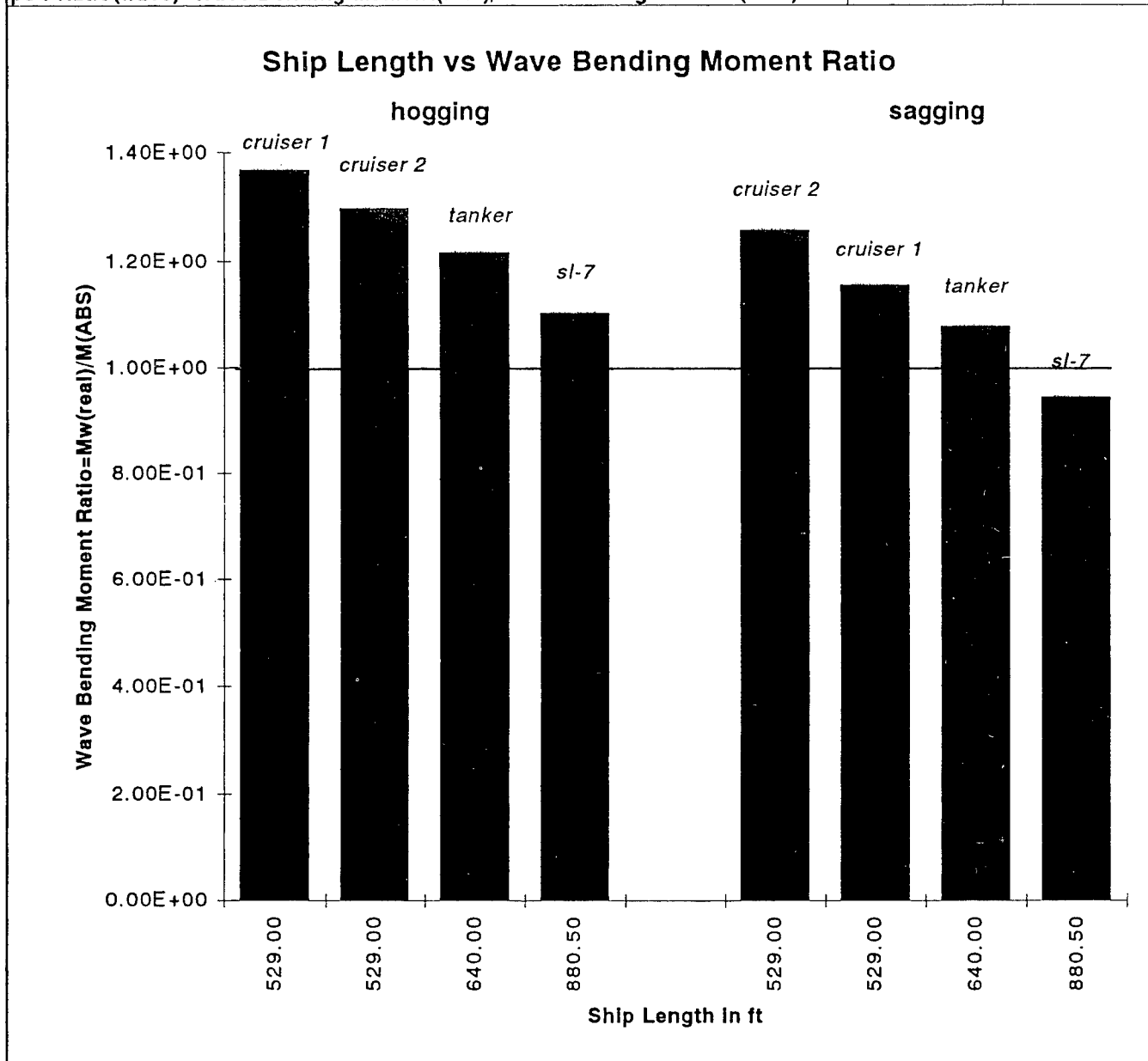
Figure 5.5.5 Moment Ratio versus Ship Length
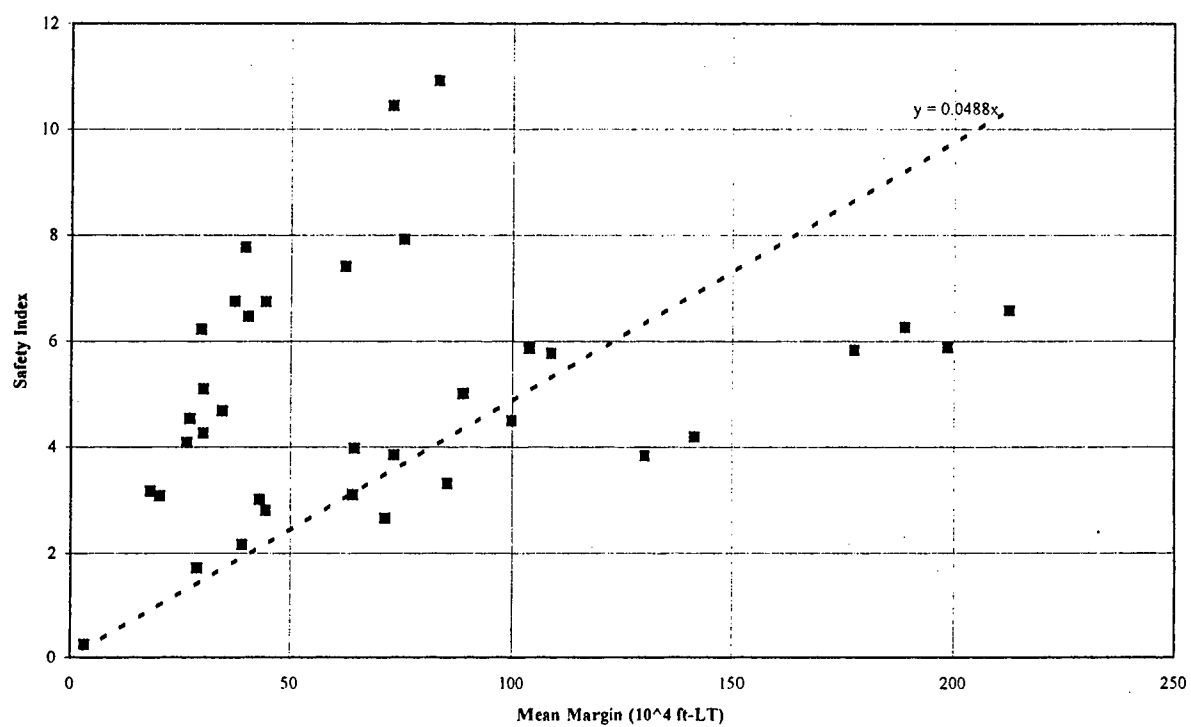
Figure 5.5.6 Safety Index versus Mean Margin — All Ships
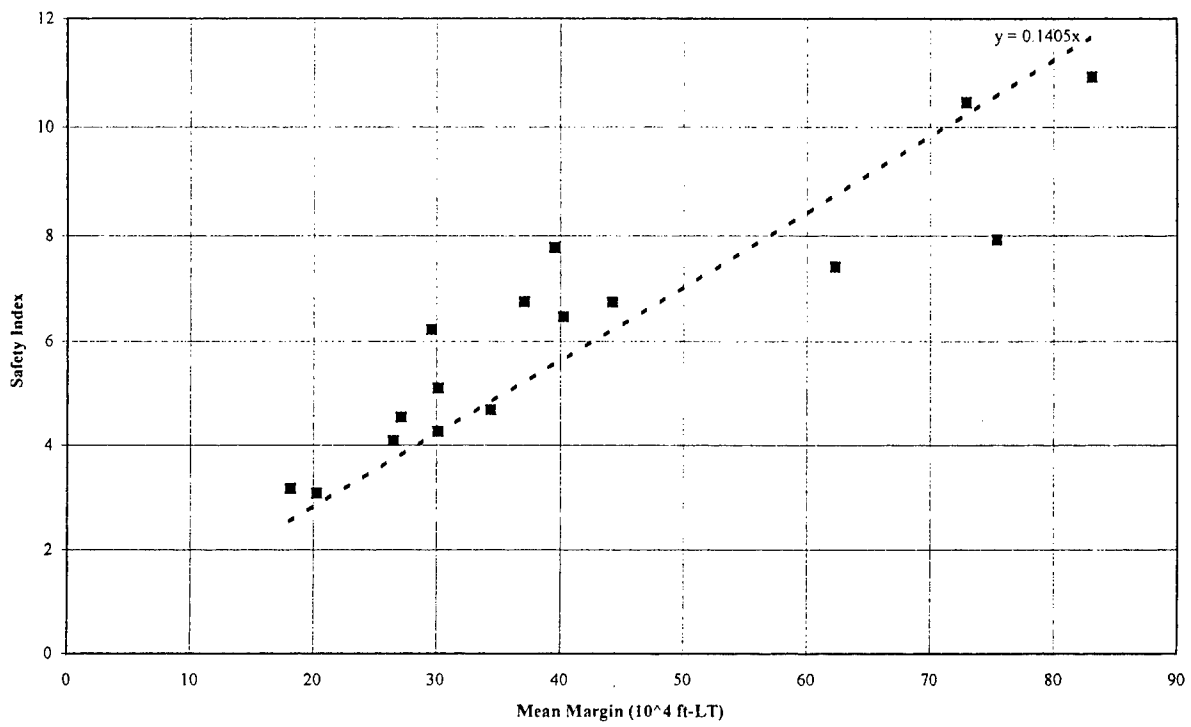
Figure 5.5.7 Safety Index versus Mean Margin — Naval Ships
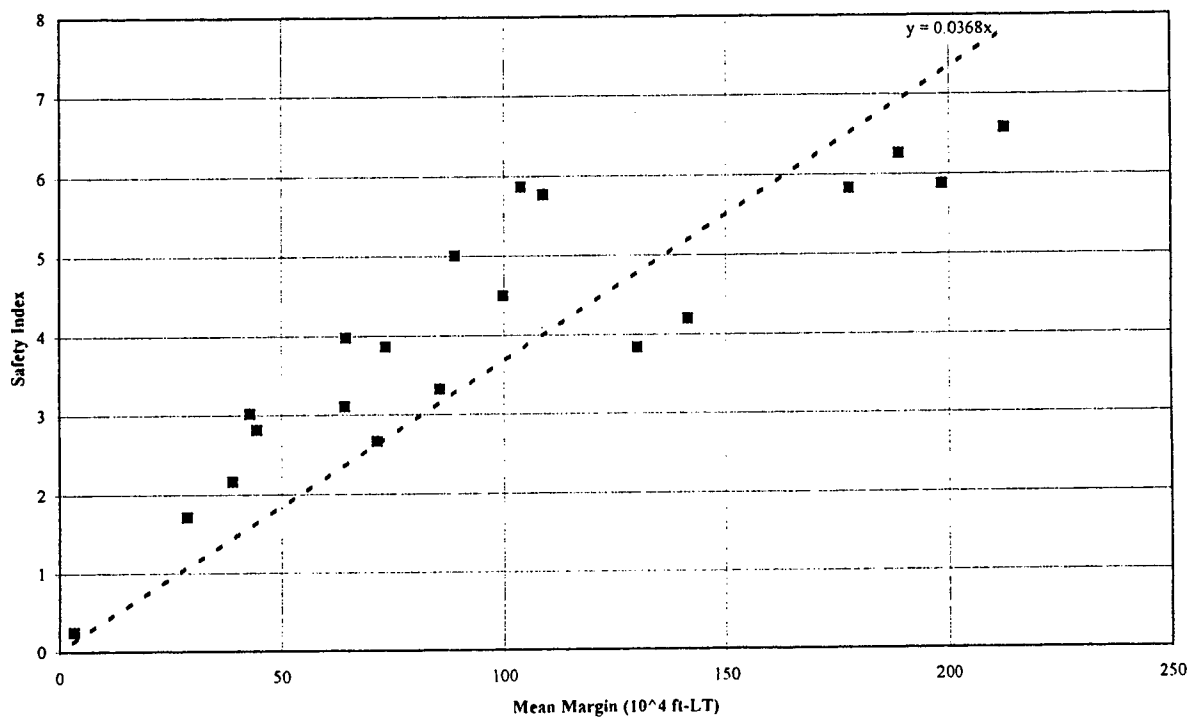
Figure 5.5.8 Safety Index versus Mean Margin — Commercial Ships

6. SENSITIVITY ANALYSIS

6.1. Sensitivity Parameters and Importance Factors

As mentioned in Chapter 5, CALREL provides four important sensitivity measures for each random variable defined in Table 6.1.1. In these equations, $\mathbf{x}^*$ and $\mathbf{u}^*$ are the coordinates of the design point in the original and standard-normal (transformed) spaces, respectively. Also, n_i is the value of the sensitivity parameter n for the ith random variable. These parameters are based on the FORM calculations and are thus only approximations that lose their accuracy as β deviates substantially from the baseline value. The first two parameters, α and γ, are known as "importance factors" and are a measure of the relative importance of each of the random variables, i.e., how much weight each has in the determination of the safety index. these two parameters are always numerically equal, so either one can be used for analysis. The second two parameters, δ and η, are measures of the sensitivity of the safety index to changes in the mean value and standard dseviation, respectively, of the random variable in question. A more in-depth treatment of sensitivity factors can be found in Mansour and Wirsching (1995) and in the Phase I final report of this project.

$\alpha_i = \dfrac{\partial\beta}{\partial u_i^*}$	$\gamma_i = \dfrac{\partial\beta}{\partial x_i^*}$	$\delta_i = \sigma_i \dfrac{\partial\beta}{\partial\mu_i}$	$\eta_i = \sigma_i \dfrac{\partial\beta}{\partial\sigma_i}$

Table 6.1.1 Sensitivity Factors

Sensitivity data is taken from two places in the CALREL output file. The FORM output includes a set of sensitivity factors. For the internally defined distributions (normal and lognormal in this analysis), all four sensitivity factors (α, γ, δ, and η) are tabulated for each variable. For user-defined distributions (extreme value in this analysis), only α and γ are provided here. In order to determine δ and η, it is necessary to instruct CALREL to perform a separate sensitivity analysis. The results of this analysis are in the final section of the output file. The table we are concerned with is the first one, i.e., the one that tabulates $\partial\beta/\partial$(parameter) for each of the variables. For the extreme value distribution, "par 1" is the mean value and "par 2" is the standard deviation. Thus, the final two sensitivity factors can be directly computed by multiplying the values given in this table by the appropriate standard deviation. Specifically, for the ith variable,

$$\delta_i = \sigma_i \frac{\partial\beta}{\partial(\text{par 1})_i} \quad \text{and} \quad \eta_i = \sigma_i \frac{\partial\beta}{\partial(\text{par 2})_i}$$

The coordinates of the design point and the sensitivity factors for a sample case are shown in Table 6.1.2. (Note: The units of $\mathbf{x}^*$ for the bending moments are 10^4 ft-LT.)

	x*	u*	α	γ	δ	η
Mu	40.77	-3.75	-0.5791	-0.5791	0.8024	-2.2182
Ms	5.36	-0.85	-0.1313	-0.1313	0.1313	-0.1116
Mw	31.42	4.06	0.6277	0.6277	-0.35104	-1.39957
Md	12.65	2.25	0.3474	0.3474	-0.37404	-0.41753
Kw	1.10	1.94	0.2994	0.2994	-0.2994	-0.5805
Kd	0.84	1.34	0.2075	0.2075	-0.2075	-0.2787

Table 6.1.2 Sensitivity Data for Sample Case

Looking at the absolute values of the importance factors (α) for each of the different variables provides some insight into the relative weight that each one has in determining the final reliability of the structure. For this sample case, the most critical variable is the wave bending moment, Mw, with an importance factor of 0.6277. Close behind this is the ultimate strength, Mu, of the section; the magnitude of its importance factor is 0.5791. It is clear that the remaining variables are much less important. Thus, one can determine that the strength and the wave loads will dominate this failure mode. This is the primary way that sensitivity data is used in this study.

Another way to look at the relative impact of the different variables is by examining the sensitivity to the coefficient of variation (η). If a variable has a small value of η, then assuming that it is a deterministic constant will have a small impact on the probability of failure estimate. Since the complexity of the mathematical reliability program is greatly influenced by the number of variables in the analysis, it is important to reduce the number of random variables in the system as much as is practical. By looking for variables with small values of η, one can determine which, if any, of the random variables in the system can be taken as deterministic. For example, in this case, the stillwater bending moment has a value of η that is an order of magnitude smaller than some of the other variables, implying that not much accuracy would be lost in assuming that it is a constant.

Dealing with the sensitivity factors for the Tanker is somewhat more complex than the other ships. This is because of the two sub-cases that must be considered; full load and ballast (see section 5.4). It is possible to generate estimates of some of the sensitivity factors semi-manually. For example, to calculate δ's for a particular case, first run both sub-cases in the base case through CALREL with the "normal" variables. The composite probability of failure can be calculated as described in section 5.4. Next, perturb the mean values of each variable, in turn, by a small amount and repeat the previous two steps. These two pairs of data points for the Tanker can then be used to estimate δ by dividing the change in the probability of failure by the change in the mean value of the variable in question and multiplying this value by the standard deviation of that variable. Obviously, this is a very time-consuming process and it yields only a rough two-point estimate of the local slope. If one wished to calculate the δ's for all variables for *one* case (e.g., tertiary failure, sagging waves) it would be necessary to run CALREL twenty-eight times! Calculating each of the

other three sensitivity factors for each of the variables would require a similar amount of work, resulting in over one hundred CALREL runs for a *single case*. This is obviously impractical and was not done.

Instead, the combination of sensitivity factors for the Tanker was approached in a more qualitative manner. In determining the relative importance of variables for a particular case, the variables are first ranked in order of importance for each sub-case. Next, these two lists are combined, taking into account the relative contribution of each sub-case to the combined probability of failure of the Tanker. In general, the probability of failure for one sub-case was substantially higher than for the other sub-case, and the combined probability of failure was generally very close to the larger one. Thus, more weight is given to the sensitivity factors for this more hazardous sub-case.

For example (primary-ultimate failure mode, sagging waves, long term), the three most important variables in the Tanker full load sub-case are ultimate moment, wave moment, and wave load combination factor (see Table 6.1.3). For the ballast sub-case, the most important variables are wave moment, ultimate moment, and stillwater moment. Since, in this case, the safety index for the full load case is substantially smaller than that of the ballast case, the ranking of important variables for the combined case is taken as that of the full load sub-case.

	Full Load (β = 0.25)	Ballast (β = 2.17)
M_u	0.7575	0.5859
M_{sw}	0.1473	0.3292
M_w	0.5054	0.6364
M_d	0.1942	0.1867
k_w	0.3142	0.3104
k_d	0.1126	0.1103

Table 6.1.3 Magnitude of Importance Factors (α) for a Sample Tanker Case

6.2 Results and Critical Variables

Complete sensitivity results for all cases are included in Appendix H. Since there is so much sensitivity data, it was decided that this part of the analysis would focus on the sensitivity results for the "critical β" cases. The sensitivity results for these cases are summarized in Tables 6.2.1 thru 6.2.8.

The primary goal of the sensitivity study is to rank the variables in their order of importance. To this end, summary tables of the importance factors (α's) for all four ships and each variable are compiled for all of the critical cases. Table 6.2.9 contains this data.

Primary (ULT)				$\beta =$	6.47		sagging
	x*	u*	α	γ	δ	η	
Mu	4.08E+01	-3.75E+00	-0.5791	-0.5791	0.8024	-2.2182	
Ms	5.36E+00	-8.50E-01	-0.1313	-0.1313	0.1313	-0.1116	
Mw	3.14E+01	4.06E+00	0.6277	0.6277	-0.35104	-1.39957	
Md	1.27E+01	2.25E+00	0.3474	0.3474	-0.37404	-0.41753	
Kw	1.10E+00	1.94E+00	0.2994	0.2994	-0.2994	-0.5805	
Kd	8.41E-01	1.34E+00	0.2075	0.2075	-0.2075	-0.2787	
Secondary				$\beta =$	5.89		sagging
	x*	u*	α	γ	δ	η	
Su	1.70E+01	-3.28E+00	-0.5556	-0.5556	0.7439	-1.8689	
SMd	2.22E+01	-1.32E+00	-0.2226	-0.2226	0.2347	-0.3013	
Ms	5.40E+01	-8.04E-01	-0.1361	-0.1361	0.1361	-0.1094	
Mw	2.98E+02	3.64E+00	0.6173	0.6173	-0.35203	-1.25788	
Md	1.20E+02	2.01E+00	0.3397	0.3397	-0.3671	-0.37021	
Kw	1.09E+00	1.73E+00	0.293	0.293	-0.293	-0.507	
Kd	8.26E-01	1.20E+00	0.2024	0.2024	-0.2024	-0.2421	
Tertiary				$\beta =$	5.86		sagging
	x*	u*	α	γ	δ	η	
Su	1.69E+01	-3.26E+00	-0.5551	-0.5551	0.7419	-1.8548	
SMd	2.22E+01	-1.31E+00	-0.2225	-0.2225	0.2345	-0.2991	
Ms	5.41E+01	-8.01E-01	-0.1365	-0.1365	0.1365	-0.1094	
Mw	2.97E+02	3.62E+00	0.6175	0.6175	-0.35263	-1.25251	
Md	1.20E+02	2.00E+00	0.3398	0.3398	-0.36734	-0.36854	
Kw	1.09E+00	1.72E+00	0.2931	0.2931	-0.2931	-0.5043	
Kd	8.25E-01	1.19E+00	0.2025	0.2025	-0.2025	-0.2408	

Table 6.2.1 Critical Sensitivity Factors, Cruiser 1, Short Term

Primary (ULT)			β =	4.09			hogging
	x*	u*	α	γ	δ	η	
Mu	4.61E+01	-2.63E+00	-0.6422	-0.6422	0.8182	-1.7434	
Ms	6.63E+00	5.28E-01	0.1289	0.1289	-0.1289	-0.068	
Mw	3.74E+01	2.90E+00	0.7089	0.7089	-0.43065	-1.2012	
Kw	1.05E+00	1.07E+00	0.2616	0.2616	-0.2616	-0.28	
Secondary			β =	3.75			sagging
	x*	u*	α	γ	δ	η	
Su	1.91E+01	-2.12E+00	-0.5625	-0.5625	0.6884	-1.2448	
SMd	2.26E+01	-8.51E-01	-0.2254	-0.2254	0.2335	-0.2007	
Ms	5.73E+01	-4.55E-01	-0.1205	-0.1205	0.1205	-0.0548	
Mw	3.49E+02	2.26E+00	0.5985	0.5985	-0.39865	-0.83039	
Md	1.45E+02	1.33E+00	0.3529	0.3529	-0.39245	-0.26272	
Kw	1.06E+00	1.14E+00	0.3021	0.3021	-0.3021	-0.3447	
Kd	7.83E-01	7.95E-01	0.2104	0.2104	-0.2104	-0.1672	
Tertiary			β =	3.71			sagging
	x*	u*	α	γ	δ	η	
Su	1.90E+01	-2.10E+00	-0.5625	-0.5625	0.6872	-1.2333	
SMd	2.26E+01	-8.43E-01	-0.2254	-0.2254	0.2335	-0.1989	
Ms	5.73E+01	-4.53E-01	-0.121	-0.121	0.121	-0.0548	
Mw	3.48E+02	2.24E+00	0.5978	0.5978	-0.39976	-0.82232	
Md	1.45E+02	1.32E+00	0.3534	0.3534	-0.39312	-0.26085	
Kw	1.06E+00	1.13E+00	0.3025	0.3025	-0.3025	-0.3422	
Kd	7.83E-01	7.88E-01	0.2107	0.2107	-0.2107	-0.166	

Table 6.2.2 Critical Sensitivity Factors, Cruiser 1, Long Term

Primary (ULT)			β =	5.10			sagging
	x*	u*	α	γ	δ	η	
Mu	3.88E+01	-2.95E+00	-0.5766	-0.5766	0.7532	-1.7516	
Ms	4.71E+00	-5.88E-01	-0.1148	-0.1148	0.1148	-0.0675	
Mw	3.04E+01	3.23E+00	0.6311	0.6311	-0.37086	-1.16609	
Md	1.23E+01	1.79E+00	0.3495	0.3495	-0.37985	-0.34412	
Kw	1.08E+00	1.54E+00	0.3009	0.3009	-0.3009	-0.4638	
Kd	8.12E-01	1.07E+00	0.2081	0.2081	-0.2081	-0.2218	
Secondary			β =	3.74			sagging
	x*	u*	α	γ	δ	η	
Su	1.36E+01	-2.11E+00	-0.5577	-0.5577	0.6815	-1.2237	
SMd	2.42E+01	-8.43E-01	-0.2233	-0.2233	0.2313	-0.1971	
Ms	4.78E+01	-4.98E-01	-0.1318	-0.1318	0.1318	-0.0656	
Mw	2.68E+02	2.27E+00	0.6003	0.6003	-0.39975	-0.83546	
Md	1.12E+02	1.34E+00	0.3538	0.3538	-0.39347	-0.26394	
Kw	1.06E+00	1.14E+00	0.3029	0.3029	-0.3029	-0.3463	
Kd	7.84E-01	7.96E-01	0.2109	0.2109	-0.2109	-0.1679	
Tertiary			β =	4.38			sagging
	x*	u*	α	γ	δ	η	
Su	1.47E+01	-2.46E+00	-0.5579	-0.5579	0.7011	-1.4191	
SMd	2.40E+01	-9.84E-01	-0.2234	-0.2234	0.2327	-0.2286	
Ms	4.74E+01	-5.41E-01	-0.1227	-0.1227	0.1227	-0.0663	
Mw	2.83E+02	2.69E+00	0.6101	0.6101	-0.38092	-0.97284	
Md	1.16E+02	1.53E+00	0.3468	0.3468	-0.38165	-0.29529	
Kw	1.07E+00	1.31E+00	0.2977	0.2977	-0.2977	-0.3904	
Kd	7.96E-01	9.10E-01	0.2066	0.2066	-0.2066	-0.1881	

Table 6.2.3 Critical Sensitivity Factors, Cruiser 2, Short Term

Primary (ULT)			β =	3.09			sagging
	x*	u*	α	γ	δ	η	
Mu	4.33E+01	-1.85E+00	-0.5917	-0.5917	0.7078	-1.1467	
Ms	4.91E+00	-3.30E-01	-0.1055	-0.1055	0.1055	-0.0348	
Mw	3.47E+01	1.86E+00	0.5968	0.5968	-0.42864	-0.70684	
Md	1.45E+01	1.15E+00	0.368	0.368	-0.41391	-0.23428	
Kw	1.05E+00	9.83E-01	0.3147	0.3147	-0.3147	-0.3094	
Kd	7.72E-01	6.86E-01	0.2194	0.2194	-0.2194	-0.1505	
Secondary			β =	1.73			sagging
	x*	u*	α	γ	δ	η	
Su	1.51E+01	-1.04E+00	-0.5884	-0.5884	0.6567	-0.6684	
SMd	2.46E+01	-4.17E-01	-0.2356	-0.2356	0.24	-0.1076	
Ms	4.99E+01	-2.18E-01	-0.123	-0.123	0.123	-0.0268	
Mw	3.13E+02	9.49E-01	0.5361	0.5361	-0.47899	-0.33378	
Md	1.30E+02	6.64E-01	0.3746	0.3746	-0.4366	-0.11772	
Kw	1.03E+00	5.76E-01	0.3252	0.3252	-0.3252	-0.1872	
Kd	7.41E-01	3.95E-01	0.2227	0.2227	-0.2227	-0.0879	
Tertiary			β =	2.39			sagging
	x*	u*	α	γ	δ	η	
Su	1.63E+01	-1.42E+00	-0.5824	-0.5824	0.6716	-0.878	
SMd	2.44E+01	-5.67E-01	-0.2333	-0.2333	0.239	-0.1414	
Ms	4.95E+01	-2.76E-01	-0.1136	-0.1136	0.1136	-0.0314	
Mw	3.27E+02	1.35E+00	0.5569	0.5569	-0.4493	-0.49703	
Md	1.37E+02	8.94E-01	0.3679	0.3679	-0.42159	-0.17467	
Kw	1.04E+00	7.68E-01	0.3161	0.3161	-0.3161	-0.2428	
Kd	7.56E-01	5.33E-01	0.2193	0.2193	-0.2193	-0.1169	

Table 6.2.4 Critical Sensitivity Factors, Cruiser 2, Long Term

Primary (ULT)				β =	3.32			hogging
	x*	u*	α	γ	δ	η		
Mu	1.67E+02	-2.39E+00	-0.7138	-0.7138	0.911	-1.7732		
Ms	4.65E+01	1.17E+00	0.3505	0.3505	-0.3505	-0.4112		
Mw	1.16E+02	1.88E+00	0.5626	0.5626	-0.40255	-0.67231		
Kw	1.04E+00	7.57E-01	0.2262	0.2262	-0.2262	-0.1713		
Secondary				β =	2.74			hogging
	x*	u*	α	γ	δ	η		
Su	9.16E+00	-1.94E+00	-0.6994	-0.6994	0.858	-1.4222		
SMb	1.73E+02	-7.06E-01	-0.2549	-0.2549	0.2626	-0.1899		
Ms	4.50E+02	1.00E+00	0.3618	0.3618	-0.3618	-0.3625		
Mw	1.10E+03	1.43E+00	0.5156	0.5156	-0.40856	-0.48296		
Kw	1.03E+00	6.13E-01	0.2215	0.2215	-0.2215	-0.1358		
Tertiary				β =	4.21			hogging
	x*	u*	α	γ	δ	η		
Su	1.04E+01	-2.89E+00	-0.6824	-0.6824	0.908	-2.0322		
SMb	1.71E+02	-1.05E+00	-0.2488	-0.2488	0.2598	-0.2716		
Ms	4.79E+02	1.33E+00	0.3151	0.3151	-0.3151	-0.42		
Mw	1.24E+03	2.41E+00	0.5709	0.5709	-0.37093	-0.83595		
Kw	1.05E+00	9.18E-01	0.2172	0.2172	-0.2172	-0.1995		

Table 6.2.5 Critical Sensitivity Factors, SL-7, Short Term

Primary (ULT)			$\beta =$	2.67			hogging
	x*	u*	α	γ	δ	η	
Mu	1.75E+02	-1.94E+00	-0.7186	-0.7186	0.8818	-1.464	
Ms	4.41E+01	9.07E-01	0.3359	0.3359	-0.3359	-0.3046	
Mw	1.27E+02	1.51E+00	0.5606	0.5606	-0.43512	-0.55378	
Kw	1.03E+00	6.41E-01	0.2376	0.2376	-0.2376	-0.1524	
Secondary			$\beta =$	2.11			hogging
	x*	u*	α	γ	δ	η	
Su	9.61E+00	-1.50E+00	-0.7045	-0.7045	0.831	-1.1303	
SMb	1.74E+02	-5.48E-01	-0.2568	-0.2568	0.2629	-0.151	
Ms	4.26E+02	7.38E-01	0.3454	0.3454	-0.3454	-0.2548	
Mw	1.22E+03	1.10E+00	0.5137	0.5137	-0.44145	-0.37241	
Kw	1.03E+00	4.99E-01	0.2335	0.2335	-0.2335	-0.1164	
Tertiary			$\beta =$	3.58			hogging
	x*	u*	α	γ	δ	η	
Su	1.09E+01	-2.46E+00	-0.6829	-0.6829	0.8769	-1.745	
SMb	1.72E+02	-8.97E-01	-0.249	-0.249	0.2584	-0.2332	
Ms	4.56E+02	1.08E+00	0.2991	0.2991	-0.2991	-0.3224	
Mw	1.36E+03	2.07E+00	0.5754	0.5754	-0.39649	-0.74459	
Kw	1.04E+00	8.15E-01	0.2262	0.2262	-0.2262	-0.1844	

Table 6.2.6 Critical Sensitivity Factors, SL-7, Long Term

Primary (ULT)				β =	2.82			hogging
	x*	u*	α	γ	δ	η		
Mu	1.02E+02	-2.07E+00	-0.7255	-0.7255	0.9002	-1.569		
Ms	3.33E+01	1.19E+00	0.4167	0.4167	-0.4167	-0.4946		
Mw	6.66E+01	1.43E+00	0.5034	0.5034	-0.39801	-0.47355		
Kw	1.03E+00	6.15E-01	0.2161	0.2161	-0.2161	-0.1329		
Secondary				β =	0.57			hogging
	x*	u*	α	γ	δ	η		
Su	8.63E+00	-4.21E-01	-0.7045	-0.7045	0.7475	-0.3717		
SMb	1.01E+02	-1.54E-01	-0.2567	-0.2567	0.2588	-0.0496		
Ms	2.75E+02	2.84E-01	0.4748	0.4748	-0.4748	-0.1348		
Mw	5.89E+02	2.43E-01	0.4061	0.4061	-0.43698	-0.0162		
Kw	1.01E+00	1.30E-01	0.2179	0.2179	-0.2179	-0.0284		
Tertiary				β =	3.61			hogging
	x*	u*	α	γ	δ	η		
Su	1.10E+01	-2.53E+00	-0.6958	-0.6958	0.8985	-1.8241		
SMb	9.76E+01	-9.22E-01	-0.2537	-0.2537	0.2635	-0.2437		
Ms	3.45E+02	1.38E+00	0.3798	0.3798	-0.3798	-0.5243		
Mw	7.00E+02	1.87E+00	0.5141	0.5141	-0.369	-0.61003		
Kw	1.04E+00	7.53E-01	0.2072	0.2072	-0.2072	-0.156		

Table 6.2.7 Critical Sensitivity Factors, Tanker, Short Term

Primary (ULT) — sagging — β = 0.25

	x*	u*	α	γ	δ	η
Mu	1.17E+02	-2.15E-01	-0.7575	-0.7575	0.7866	-0.2441
Ms	1.01E+01	4.17E-02	0.1473	0.1473	-0.1473	-0.0061
Mw	9.39E+01	1.43E-01	0.5054	0.5054	-0.55854	0.027979
Md	1.81E+01	5.50E-02	0.1942	0.1942	-0.23687	0.035403
Kw	1.00E+00	8.90E-02	0.3142	0.3142	-0.3142	-0.0279
Kd	7.03E-01	3.19E-02	0.1126	0.1126	-0.1126	-0.0036

Primary (ULT) — sagging — β = 2.17

	x*	u*	α	γ	δ	η
Mu	1.04E+02	########	-0.5859	-0.5859	0.6773	-0.8147
Ms	2.10E+01	-7.24E-01	-0.3292	-0.3292	0.3292	-0.2384
Mw	1.07E+02	1.40E+00	0.6364	0.6364	-0.50724	-0.58589
Md	1.98E+01	4.11E-01	0.1867	0.1867	-0.22182	-0.02268
Kw	1.03E+00	6.83E-01	0.3104	0.3104	-0.3104	-0.212
Kd	7.26E-01	2.43E-01	0.1103	0.1103	-0.1103	-0.0268

Secondary — hogging — β = 0.61

	x*	u*	α	γ	δ	η
Su	8.59E+00	-4.63E-01	-0.719	-0.719	0.7662	-0.4094
SMb	1.01E+02	-1.69E-01	-0.2621	-0.2621	0.2643	-0.0547
Ms	1.03E+02	1.22E-01	0.1898	0.1898	-0.1898	-0.0232
Mw	7.53E+02	3.51E-01	0.5446	0.5446	-0.56956	-0.07576
Kw	1.01E+00	1.84E-01	0.2859	0.2859	-0.2859	-0.0526

Secondary — hogging — β = -0.51

	x*	u*	α	γ	δ	η
Su	9.39E+00	3.51E-01	-0.7137	-0.7137	-0.7137	0.1714
SMb	1.02E+02	1.28E+02	-0.2601	-0.2601	-0.2601	0.0229
Ms	2.43E+02	-2.15E-01	0.4372	0.4372	0.4372	0.0941
Mw	7.17E+02	-2.04E-01	0.4151	0.4151	0.4151	0.171996
Kw	9.94E-01	-1.20E-01	0.244	0.244	0.244	0.0293

Tertiary — sagging — β = 2.03

	x*	u*	α	γ	δ	η
Su	1.67E+01	########	-0.6984	-0.6984	0.8191	-1.0782
SMd	7.92E+01	-5.26E-01	-0.2546	-0.2546	0.2605	-0.1441
Ms	1.06E+02	2.49E-01	0.1206	0.1206	-0.1206	-0.03
Mw	1.04E+03	1.15E+00	0.5584	0.5584	-0.47282	-0.42642
Md	1.96E+02	3.57E-01	0.1729	0.1729	-0.20619	-0.01352
Kw	1.03E+00	5.88E-01	0.2844	0.2844	-0.2844	-0.1672
Kd	7.22E-01	2.11E-01	0.1019	0.1019	-0.1019	-0.0215

Tertiary — sagging — β = 3.56

	x*	u*	α	γ	δ	η
Su	1.56E+01	########	-0.5673	-0.5673	0.7019	-1.2073
SMd	7.85E+01	-7.41E-01	-0.2068	-0.2068	0.2134	-0.1613
Ms	1.95E+02	-9.69E-01	-0.2705	-0.2705	0.2705	-0.2621
Mw	1.20E+03	2.39E+00	0.6675	0.6675	-0.4351	-0.9694
Md	2.06E+02	5.79E-01	0.1617	0.1617	-0.18961	-0.04068
Kw	1.05E+00	1.02E+00	0.2851	0.2851	-0.2851	-0.291
Kd	7.36E-01	3.44E-01	0.0959	0.0959	-0.0959	-0.033

Table 6.2.8   Critical Sensitivity Factors, Tanker, Long Term

Primary, Ultimate Limit, Short Term / **Primary, Ultimate Limit, Long Term**

Ship load	Cruiser 1 sagging	Cruiser 2 sagging	SL-7 hogging	Tanker hogging	Ship load	Cruiser 1 hogging	Cruiser 2 sagging	SL-7 hogging	Tanker sagging
β	6.47	5.1	3.32	2.82	β	4.09	3.09	2.67	0.81
Mu	-0.5791	-0.5766	-0.7138	-0.7255	Mu	-0.6422	-0.5917	-0.7186	-0.7575
Ms	-0.1313	-0.1148	0.3505	0.4167	Ms	0.1289	-0.1055	0.3359	0.1473
Mw	0.6277	0.6311	0.5626	0.5034	Mw	0.7089	0.5968	0.5606	0.5054
Md	0.3474	0.3495	#N/A	#N/A	Md	#N/A	0.3680	#N/A	0.1942
Kw	0.2294	0.3009	0.2262	0.2161	Kw	0.2616	0.3147	0.2376	0.3142
Kd	0.2075	0.2081	#N/A	#N/A	Kd	#N/A	0.2194	#N/A	0.1126

Secondary, Short Term / **Secondary, Long Term**

Ship load	Cruiser 1 sagging	Cruiser 2 sagging	SL-7 hogging	Tanker hogging	Ship load	Cruiser 1 sagging	Cruiser 2 sagging	SL-7 hogging	Tanker hogging
β	5.89	3.74	2.74	0.57	β	3.75	1.73	2.11	0.04
Su	-0.5556	-0.5577	-0.6994	-0.7045	Su	-0.5625	-0.5884	-0.7045	-0.7137
SMx	-0.2226	-0.2233	-0.2549	-0.2567	SMx	-0.2254	-0.2356	-0.2568	-0.2601
Ms	-0.1361	-0.1318	0.3618	0.4748	Ms	-0.1205	-0.1230	0.3454	0.4372
Mw	0.6173	0.6003	0.5156	0.4061	Mw	0.5985	0.5361	0.5137	0.4151
Md	0.3397	0.3538	#N/A	#N/A	Md	0.3529	0.3746	#N/A	#N/A
Kw	0.2930	0.3029	0.2215	0.2179	Kw	0.3021	0.3252	0.2335	0.2440
Kd	0.2024	0.2109	#N/A	#N/A	Kd	0.2104	0.2227	#N/A	#N/A

Tertiary, Short Term / **Tertiary, Long Term**

Ship load	Cruiser 1 sagging	Cruiser 2 sagging	SL-7 hogging	Tanker hogging	Ship load	Cruiser 1 sagging	Cruiser 2 sagging	SL-7 hogging	Tanker hogging
β	5.86	4.38	4.21	3.61	β	3.71	2.39	3.58	2.30
Su	-0.5551	-0.5579	-0.6825	-0.6958	Su	-0.5625	-0.5824	-0.6829	-0.6984
SMx	-0.2225	-0.2234	-0.2488	-0.2537	SMx	-0.2254	-0.2333	-0.2490	-0.2546
Ms	-0.1365	-0.1227	0.3151	0.3798	Ms	-0.1210	-0.1136	0.2291	0.1206
Mw	0.6175	0.6101	0.5709	0.5141	Mw	0.5978	0.5569	0.5754	0.5584
Md	0.3398	0.3468	#N/A	#N/A	Md	0.3534	0.3679	#N/A	#N/A
Kw	0.293	0.2977	0.2172	0.2072	Kw	0.3025	0.3161	0.2262	0.2844
Kd	0.2025	0.2066	#N/A	#N/A	Kd	0.2107	0.2193	#N/A	0.1019

Table 6.2.9 Importance Factors for Critical Cases

Inspection of the results for the warships indicates a fairly consistent pattern, with the wave bending moment being the most important, followed by the strength of the ship (whichever is appropriate to the case) and the dynamic bending moment. There are only two exceptions to this pattern in all of the critical cases. First, since the long term, primary critical case for Cruiser 1 is a hogging wave case, there is no dynamic moment, and the load combination factor (k_w) moves into third place. the second exception is the reversal of the wave bending moment and the strength variable for the long term secondary and tertiary critical cases of Cruiser 2. Still, in all cases, the difference between the importance of the strength and the wave moment is not very large. It appears that these are the two most critical variables, with the weight of the other variables being much less in all cases.

The situation for the commercial ships is a little different. Clearly, the most important variable here is the strength, winning out by a large margin in every critical case for both ships. For SL-7, this pattern continues with wave moment being the second most important and the stillwater moment showing up as third in all critical cases. This order is very definite, with substantial separation between the scores for the three. Typically, the determination of the second and third leading variables for Tanker are somewhat more confused. Wave bending moment is the second for two cases and third for two more. The wave load combination factor also makes an appearance in the top three, being third in two cases. It is interesting to note that, unlike the Cruiser 2 cases, k_w shows up for Tanker in sagging cases. Taking all of this into account, it appears that wave bending moment and stillwater moment are second and third for Tanker (after the strength), as they are for SL-7 (see Table 6.2.10).

	Cruiser 1 and Cruiser 2	*SL-7 and Tanker*
First	wave bending moment (M_w)	strength (M_U, $S_{u,2}$, or $S_{u,3}$)
Second	strength (M_U, $S_{u,2}$, or $S_{u,3}$)	wave bending moment (M_w)
Third	dynamic bending moment (M_d)	stillwater bending moment (M_{sw})

Table 6.2.10 Top Three Most Important Variables

A second important goal for the sensitivity analysis is to attempt to reduce the complexity of the reliability problem by determining if any of the variables could be assumed to be constant without appreciably degrading the accuracy of the analysis. To this end, it is necessary to examine the sensitivity results for the critical cases, Tables 6.2.1 to 6.2.8. The parameter of interest here is η, the sensitivity of the safety index to fractional changes in the standard deviation of the variable in question. If this value is very small, that means that the variability of that parameter does not have a major impact on the reliability results. Examining the twenty-seven critical case results shows that there is only really one possible candidate for conversion to a deterministic parameter: the stillwater bending moment.

For the stillwater bending moment, η is very small in all of the critical cases for Cruiser 1 and Cruiser 2. It is an order of magnitude smaller than the largest η's and about one third the size of the next largest η. Thus, it is probably safe to assume that replacing the random stillwater bending moment with a deterministic one would have little effect on the reliability results for the naval vessels. This sort of assumption is *not* justified for the commercial ships. In many of these cases, η for the stillwater bending moment is larger than some of the other η's, and even of the same order of magnitude as the largest η's in a few cases.

From the perspective of one who has performed quite a few computer-based reliability analyses of this type, the amount of effort saved in simplifying the analysis is not really worth the effort required to justify the assumptions of non-variability. Simplifications of this sort are important in reducing the complexity of a problem to a tractable degree if it is to be done by hand, but are not necessary when performing the reliability analysis on a

6-13

computer. It is a rather simple matter for the computer to deal with additional random variables. Assuming that a characteristic value of the variable in question is available (as would be needed anyway) and that some reasonable assumption can be made as to the variables distribution and variation, it is a relatively simple matter to modify an existing CALREL input file to accept the additional random variable. As far as computation is concerned, additional variables do not pose a noticeable problem here either. The running time of CALREL is only a few seconds (on a 486DX2-66 DOS PC), and there is no discernible change in running time based on the number of random variables included in the analysis.

7. FATIGUE RELIABILITY ASSESSMENT

7.1   Background

In ship structure, fatigue failures are expected to occur first at welded joints or at other points in the structure having "severe" stress concentrations. For this study, a fatigue reliability assessment was performed for the following detail:

a) Cruiser 1   Hatch opening before and after modifications

b) Cruiser 1   Deck house corner before and after modifications

c) Cruiser 2   Hatch opening

d) Cruiser 2   Deck house corner

e) Tanker   Stiffener welds parallel and perpendicular to the direction of loading

f) SL-7   Hatch opening corner before and after modifications

Reliability assessment at a given detail involves first the development of an expression for the cycles to fatigue failure, N. This expression would include the following:

a) the estimated long term stress distribution

b) modeling error associated with stress

c) the fatigue strength model

d) modeling error associated with strength

In general, each one of these terms possess uncertainty, and in a reliability model, in general all design factors would be considered as random variables.

Stress cycles to fatigue failure[*] can be written as:

$$N = N(\underset{\sim}{X}) \tag{7.1}$$

---

[*] A stress cycle is a component of an oscillating stress process consisting of a trough (of magnitude T) and accompanying peak (of magnitude P). For fatigue life estimation purposes, a cycle is quantified by: (1) the range, P-T, and (2) the mean value, (P+T)/2, or alternatively, the stress ratio, T/P. For welded joints, in the first approximation, it is assumed that fatigue life is independent of stress ratio, an assumption which is commonly made.

where X is a vector of random design factors. Therefore, N itself is a random variable.

The probability of fatigue failure of a detail is the probability that the cycles to failure N is less than the service life, N_T.

$$p_f = P(N < N_T) \qquad (7.2)$$

In general, p_f can be computed by any one of a number of methods (see Appendix I).

Each of the fatigue design factors are developed in the following sections.

7.2   Fatigue Strength

7.2.1   Constant Amplitude S-N Fatigue Strength:

The fatigue strength of a given component is typically determined by tests in which specimens are subject to constant amplitude stress. Cycles to failure are measured, and a curve is fit to the data.

$$N = N(S; \theta) \qquad (7.3)$$

where θ is a vector of parameters of the analytical model determined by a fit (e.g., least squares) to the data.

Typically, fatigue data plot as a straight line on log-log paper, implying the analytical form:

$$NS^m = A \qquad (7.4)$$

where, in this special case, $\theta = (m, A)$; m is the fatigue strength exponent, and A is the fatigue strength coefficient.

This will be the fundamental form used in this study. It will also be assumed that: (a) the equation is valid to $S = 0$, i.e., there is no endurance limit, and (b) Miner's rule is valid. The assumption of no endurance limit is made on the basis of general knowledge in the marine structure business that the endurance limit tends to disappear when stresses are random and there is the presence of a corrosive environment.

For reliability analysis, it is necessary to define m and A as random variables. A basic assumption is that the fatigue process is defined by the linear regression model. Taking the log of both sides of eqn. (7.4),

$$\log N = \log A - m \log S \qquad (7.5)$$

This is a linear form. Let,

$$X = \log S \quad Y = \log N$$
$$a = \log A \quad b = -m \tag{7.6}$$

So that the strength model can be written as,

$$Y = a + bX \tag{7.7}$$

Note that S (and therefore X) is the independent variable. Given S-N data, least squares analysis can be performed. The least squares model implies that: (a) the data (here in log-log space) follows a linear trend, and (b) the distribution of Y given X has a normal distribution with the mean given by eqn. (7.7) above and standard deviation, σ. Thus, it follows that cycle life N given stress S will be lognormal with a constant coefficient of variation.

S-N data (S_i, N_i) is transformed to $X_i = \log S_i$, $Y_i = \log N_i$. Least squares analysis is employed to compute $\hat{a}, \hat{b}$ and s, which are the estimators of a, b, and σ, the standard deviation of Y given X. Then using lognormal mathematics (see Appendix I), the parameters are:

$$m = -\hat{b} \tag{7.8}$$

The median of A is

$$\tilde{A} = 10^{\hat{a}} \tag{7.9}$$

The coefficient of variation of A is

$$C_A = \sqrt{10^{(s^2/.434)} - 1} \tag{7.10}$$

Given in Table 7.1 is a statistical summary of the data for various details given in British and Norwegian rules.

7.2.2 S-N Curves Used in This Study:

The S-N curves used in this study are all based on the linear form of eqn. (7.4). A statistical summary of the curves are presented in Table 7.2.

Fatigue strength for Case 1, the original hatch opening on Cruiser 1 is defined by the S-N curve for plain steel. Two cases are considered. In the first, S-N data on HY-80, provided by NSWC, was employed. This data and the least squares curve are shown on Figure 7.1. Also shown on this figure is the S-N curve for the UK Department of Energy B-curve also used for plain steel.

Table 7.1
Statistical Summaries of Fatigue Data and Design S-N Curves
used in British and Norwegian Rules

	STATISTICAL SUMMARY				DESIGN CURVE	
	Median $\tilde{A}$			COV of N	A_0	
Class[a]	m	MPa	ksi	(%)	MPa	ksi[b]
B	4.0	2.34 E15	1.04 E12	44	1.01 E15	4.47 E11
C	3.5	1.08 E15	1.25 E11	50	4.23 E13	4.91 E10
D	3.0	3.99 E12	1.21 E10	51	1.52 E12	4.64 E 9
E	3.0	3.29 E12	1.00 E10	63	1.04 E12	3.17 E 9
F	3.0	1.73 E12	5.28 E 9	54	6.30 E11	1.92 E 9
F2	3.0	1.23 E12	3.75 E 9	56	4.30 E11	1.31 E 9
G	3.0	5.66 E11	1.73 E 9	43	2.50 E11	7.63 E 8
W	3.0	3.68 E11	1.12 E 9	44	1.60 E11	2.88 E 8

Notes: (a) See BS 5400 (1980) and NS 3472 (1984) for detail of welded joints
(b) Median minus two standard deviations on a log basis

Table 7.2
A Statistical Summary of the S-N Curves Used in This Study

	m	$\widetilde{A}$ (ksi units)	C_A	Comments
HY-80	7.70	2.87E21	0.544	Based on tests on smooth and polished HY-80 plate.*
DEn B-Curve	4.0	1.04E12	0.44	Plain steel in the as-rolled condition with flame cut surfaces subsequently ground or machined to remove all visible signs of the drag lines.
DEn C-Curve	3.5	1.25E11	0.50	Welds parallel to the direction of applied stress. Butt or fillet welds with the welds made by an automatic submerged or an open arc process.
DEn F-Curve	3.0	5.28E9	0.54	Welded attachments on the surface of a stressed member. Attachment parallel to the direction of applied stress.
*Ref.: E. J. Czyryes, Naval Surface Warfare Center, Carderock Division, Annapolis, MD.				
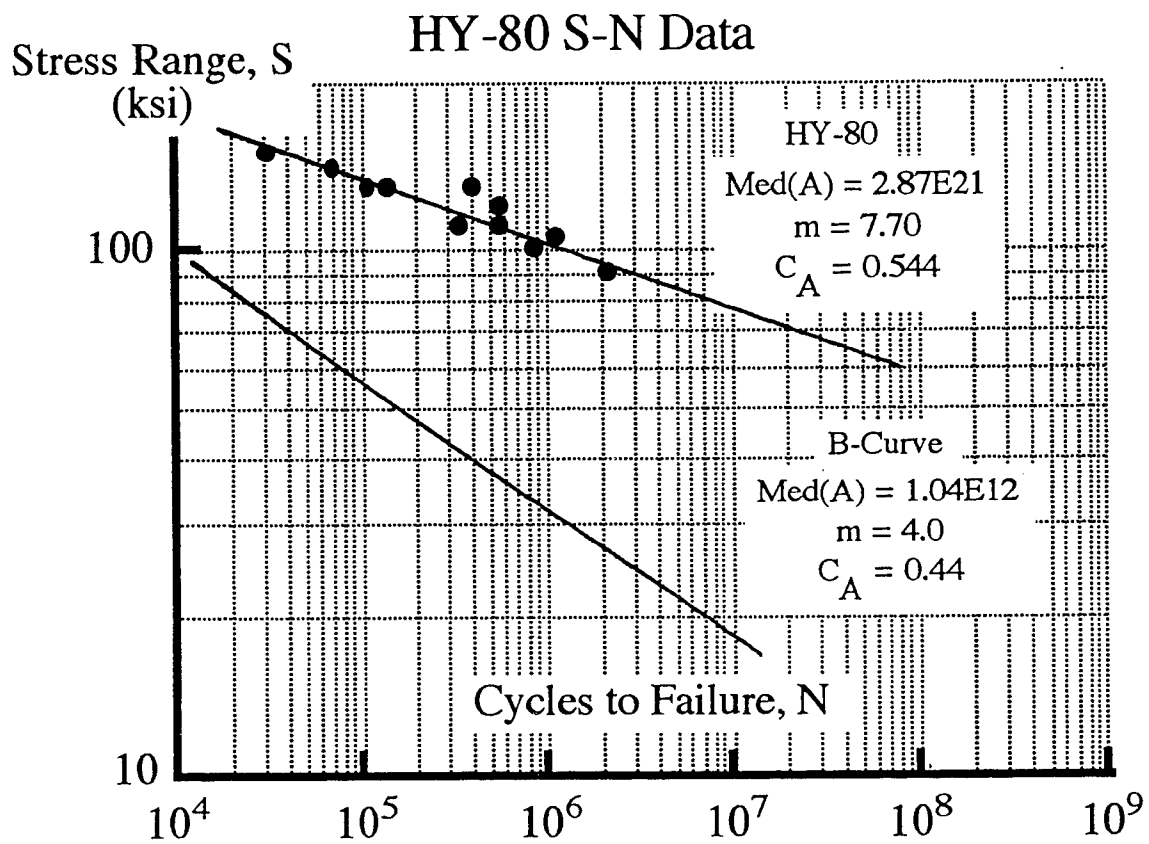
Figure 7.1 HY-80 and DEn B Fatigue Curves
(no endurance limit assumed)

Fatigue strength in welded joints is defined by the UK Department of Energy C and F curves. The statistics of these models are given in Tables 7.1 and 7.2, and the median curves are presented in Figure 7.2. Pictures of the details from UK documents are provided in Figure 7.3.

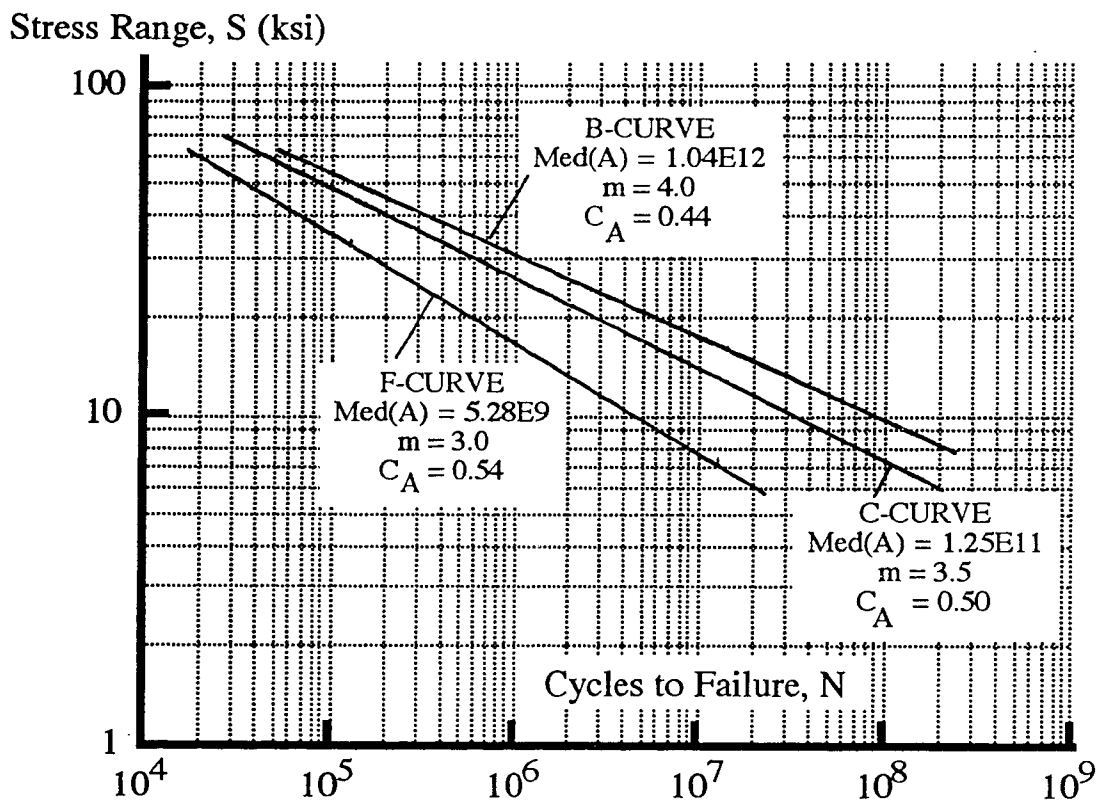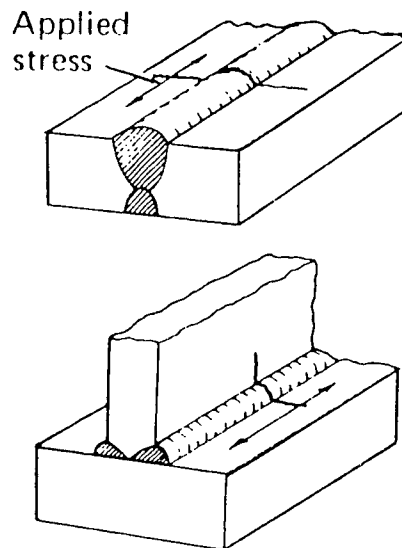## UK Department of Energy S-N Curves

Stress Range, S (ksi)

B-CURVE
Med(A) = 1.04E12
$m = 4.0$
$C_A = 0.44$

F-CURVE
Med(A) = 5.28E9
$m = 3.0$
$C_A = 0.54$

C-CURVE
Med(A) = 1.25E11
$m = 3.5$
$C_A = 0.50$

Cycles to Failure, N

Figure 7.2 DEn B, C, and F Curves
(no endurance limit assumed)

CONTINUOUS WELDS, PARALLEL TO THE DIRECTION OF APPLIED STRESS
Fatigue strength defined by the DEn C-curve

WELDED ATTACHMENTS ON THE SURFACE OF A STRESSED MEMBER
Fatigue strength defined by the DEn F-curve
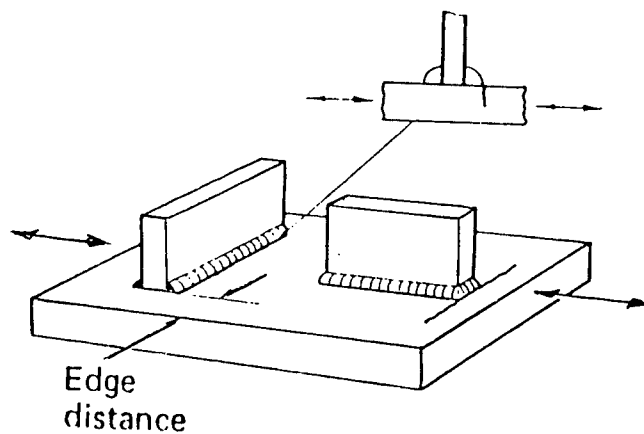
Figure 7.3 Illustrations of the Welded Detail Used for Definition of the S-N Curve.

7.2.3 Stress Endurance Limits:

Consider the presence of a stress endurance limit S_Q, a stress below which there is no fatigue damage. The fatigue strength is given as,

$$N(S) = \begin{bmatrix} AS^{-m} & S \geq S_Q \\ \infty & S < S_Q \end{bmatrix}$$

(7.11)

The stress endurance limits occur at 10^7 cycles in the DEn curves and have values as given in Table 7.3 and shown in Figure 7.4.

Table 7.3
Stress Endurance Limits

(occur at 10^7 cycles; based on median values)

	S_Q (ksi)
DEn B-curve	18.0
DEn C-curve	14.8
DEn F-curve	8.1
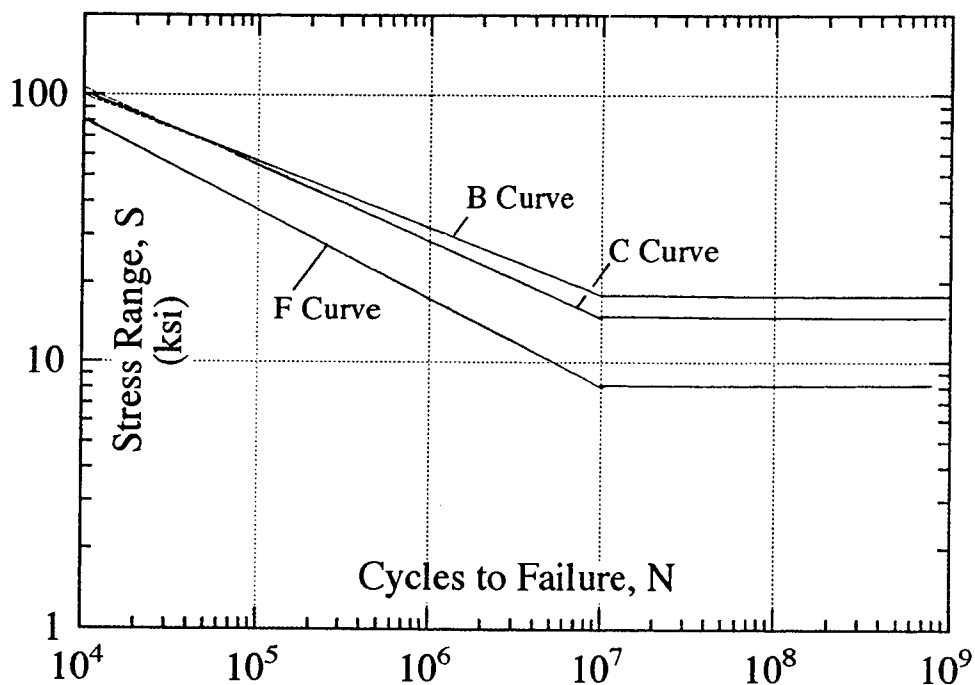
Figure 7.4 DEn B, C, and F Median Curves Showing Endurance Limits.

7.3   Fatigue Stress

7.3.1   Distribution of Stress Ranges: The Weibull Distribution:

Let S denote the stress range associated with one cycle. Over the service life of the ship, there will be a total of N_T cycles applied. Because the stress process is random in a marine structure, S will be a random variable. Numerous experiments measuring the long term distribution of stress ranges in ships have indicated that the Weibull generally provides a good fit to S (e.g., Munse *et al.* (1983)). The Weibull distribution will be used in this study to model S, i.e., the Weibull will represent the long term distribution of stress ranges.

Assuming that S has a Weibull distribution, the distribution and density functions are

$$F_S(s) = P(S \leq s) = 1 - \exp\left[-\left(\frac{s}{\delta}\right)^{\xi}\right] \tag{7.12}$$

$$f_S(s) = \frac{\xi}{\delta}\left(\frac{s}{\delta}\right)^{\xi-1} \exp\left[-\left(\frac{s}{\delta}\right)^{\xi}\right] \tag{7.13}$$

for $\xi > 0$ and $\delta > 0$

where ξ is the Weibull shape parameter and δ is the Weibull scale parameter. The mth moment of S is

$$E(S^m) = \delta^m \ \Gamma\left(\frac{m}{\xi}+1\right) \tag{7.14}$$

where $\Gamma(1)$ is the gamma function [$\Gamma(x + 1) = x!$; note, some HP calculators evaluate $x!$ for non integer values].

7.3.2   Probability Plotting:

A transformation can be made on F_S to plot it as a straight line. Taking the log of eqn. (7.12) twice, it can be shown that

$$\ln[-\ln(1-F)] = \xi \ln s - \xi \ln \delta \tag{7.15}$$

Letting

$$\begin{aligned} Y &= \ln[-\ln(1-F)] \\ X &= \ln s \end{aligned} \tag{7.16}$$

Eqn. (7.15) has a linear form in X and Y

$$Y = a + bx \qquad (7.17)$$

In terms of the distribution parameters,

$$a = -\xi \ln \delta \qquad (7.18)$$

$$b = \xi$$

7.3.3   A Special Form of the Weibull Distribution Useful for Marine Structures:

Define "design," or "once-in-a-lifetime" stress range, S_o

$$P(S > S_0) = \frac{1}{N_T} \qquad (7.19)$$

S_0 is the stress which S will exceed on the average, once every N_T times. Substituting eqn. (7.19) into eqn. (7.12):

$$S_0 = \left[\ln(N_T) \right]^{1/\xi} \delta \qquad (7.20)$$

Thus the basic distribution parameters can be considered as S_o, ξ, and N_T.

$$E(S^m) = S_o^m (\ln N_T)^{-m/\xi, xi} \Gamma\left(\frac{m}{\xi} + 1 \right) \qquad (7.21)$$

In section 7.4.2 it is shown that $S_e^m = E(S^m)$ where S_e is an equivalent constant amplitude fatigue stress.

7.3.4   Graphical Presentations of the Distribution of S:

It is common practice in the marine industry to represent the long term distribution of stress ranges in the form of Figure 7.5.
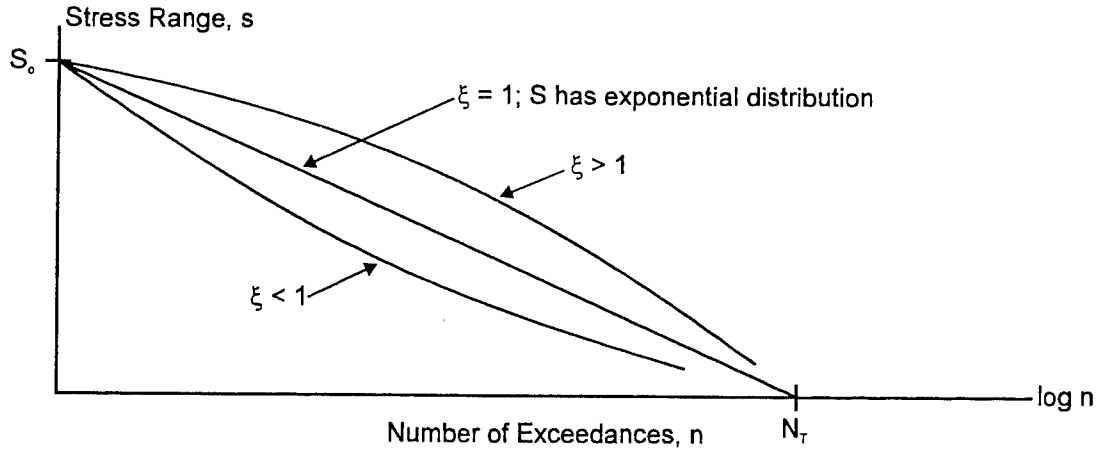
Figure 7.5 Graphical Form of the Long Term Distribution of Stress Ranges.

The equation of the curve of Figure 7.5 can be derived for the case when S is Weibull. Define n as the total number of exceedances of stress level s in the life of N_T. For any stress s:

$$P(S > s) = \frac{n}{N_T} \tag{7.22}$$

But this is by definition, 1 - F_S. Thus from eqn. (7.12),

$$\exp\left[-\left(\frac{s}{\delta}\right)^{\xi}\right] = \frac{n}{N_T} \tag{7.23}$$

and substituting for δ from eqn. (7.20),

$$\exp\left[-\ell n\ N_T\left(\frac{s}{S_o}\right)^{\xi}\right] = \frac{n}{N_T} \tag{7.24}$$

Thus given the parameters S_o, ξ, and N_T, a distribution function of the form of Figure 7.5 can be constructed.

7.3.5 The Long Term Distribution of Stress Ranges for the Four Ships:

Step 1. Using Program SOST, the distribution of the largest mid-ship stress in hog and in sag was constructed for each of the four ships. The results for Cruiser 1 is provided as an example in Table 7.4. Let N_T denote the sample size, in this case the number of stress

cycles experienced in the service life. Let Y denote the largest stress in a sample of size N_T. The distribution function for Y is given as F_Y; the values of $1 - F_Y$ are shown in Table 7.4.

It is assumed that each ship experiences the same route profile over its service life. It is also assumed that the service life is 15 years of continuous operation. The estimated total number of cycles for each ship is given in Table 7.5.

Table 7.5
Stress Cycles N_T During Service Life*

Cruiser 1	8.89E7
Cruiser 2	9.56E7
Tanker	5.99E7
SL-7	5.56E7

*15 years of continuous operation.

Step 2. Establish the distribution of individual mid-ship stresses in hog and sag. Note that stresses will be stress amplitudes, i.e., zero to peak. Let S denote the amplitude of a single stress cycle. From elementary extreme value theory, the distribution functions (cdf's) of Y and S are related by,

$$F_Y(s) = \left[F_S(s)\right]^{N_T} \tag{7.25}$$

and therefore the cdf of S is,

$$F_S(s) = \left[F_Y(s)\right]^{1/N_T} \tag{7.26}$$

The cdf of S was derived for each of the four ships using eqn. (7.26). Each was plotted on Weibull probability paper. The results are shown in Figures 7.6 through 7.13. Because of the limited values of Y provided, only a fraction of the cdf of S could be established. Nevertheless, on the basis of the information available, the assumption of a Weibull model for S seems reasonable.

Table 7.4
Distribution of the Maximum Hog and Sag Stress
Over the Service Life (Cruiser 1)

SAG						HOG					
Cruiser 1											
SMd =	1.07E+04	section modulus (ft-in²) at section #5 at deck									
sagging				1 - F_Y	Y	hogging				1 - F_Y	Y
BM (lb-ft)		prob		prob of exceed	stress(psi)	BM (lb-ft)		prob		prob of exceed	stress(psi)
0.00	0.00	1.00	0.00	1.0000	0.00E+00	0.00	0.00	1.00	0.00	1.0000	0.00E+00
2.00	7.00	1.00	0.00	1.0000	1.86E+03	2.00	7.00	1.00	0.00	1.0000	1.86E+03
4.00	7.00	1.00	0.00	1.0000	3.73E+03	4.00	7.00	1.00	0.00	1.0000	3.73E+03
6.00	7.00	1.00	0.00	1.0000	5.59E+03	6.00	7.00	1.00	0.00	1.0000	5.59E+03
8.00	7.00	1.00	0.00	1.0000	7.45E+03	8.00	7.00	1.00	0.00	1.0000	7.45E+03
1.00	8.00	1.00	0.00	1.0000	9.32E+03	1.00	8.00	1.00	0.00	1.0000	9.32E+03
1.20	8.00	1.00	0.00	1.00	1.12E+04	1.20	8.00	1.00	0.00	1.0000	1.12E+04
1.40	8.00	1.00	0.00	1.0000	1.30E+04	1.40	8.00	1.00	0.00	1.0000	1.30E+04
1.60	8.00	1.00	0.00	1.0000	1.49E+04	1.60	8.00	1.00	0.00	1.0000	1.49E+04
1.80	8.00	1.00	0.00	1.0000	1.68E+04	1.80	8.00	1.00	0.00	1.0000	1.68E+04
2.00	8.00	1.00	0.00	1.0000	1.86E+04	2.00	8.00	1.00	0.00	1.0000	1.86E+04
2.20	8.00	1.00	0.00	1.0000	2.05E+04	2.20	8.00	1.00	0.00	1.0000	2.05E+04
2.40	8.00	1.00	0.00	1.0000	2.24E+04	2.40	8.00	1.00	0.00	1.0000	2.24E+04
2.60	8.00	1.00	0.00	1.0000	2.43E+04	2.60	8.00	1.00	0.00	1.0000	2.42E+04
2.80	8.00	1.00	0.00	1.0000	2.61E+04	2.80	8.00	9.95	-1.00	0.9968	2.61E+04
3.00	8.00	1.00	0.00	1.0000	2.79E+04	3.00	8.00	8.54	-1.00	0.8544	2.79E+04
3.20	8.00	9.95	-1.00	0.9945	2.98E+04	3.20	8.00	4.69	-1.00	0.4694	2.98E+04
3.40	8.00	8.73	-1.00	0.8729	3.17E+04	3.40	8.00	1.86	-1.00	0.1863	3.17E+04
3.60	8.00	5.59	-1.00	0.5587	3.35E+04	3.60	8.00	6.42	-2.00	0.0642	3.35E+04
3.80	8.00	2.77	-1.00	0.2774	3.54E+04	3.80	8.00	2.10	-2.00	0.0210	3.54E+04
4.00	8.00	1.21	-1.00	0.1214	3.73E+04	4.00	8.00	6.72	-3.00	0.0067	3.73E+04
4.20	8.00	5.04	-2.00	0.0504	3.91E+04	4.20	8.00	2.13	-3.00	0.0021	3.91E+04
4.40	8.00	2.05	-2.00	0.0205	4.10E+04	4.40	8.00	6.76	-4.00	0.007	4.10E+04
4.60	8.00	8.31	-3.00	0.0083	4.29E+04	4.60	8.00	2.15	-4.00	0.0002	4.29E+04
4.80	8.00	3.37	-3.00	0.0034	4.47E+04	4.80	8.00	6.88	-5.00	0.0001	4.47E+04
5.00	8.00	1.38	-3.00	0.0014	4.66E+04	5.00	8.00	2.22	-5.00	0.0000	4.66E+04
5.20	8.00	5.65	-4.00	0.0006	4.84E+04	5.20	8.00	7.29	-6.00	0.0000	4.84E+04
5.40	8.00	2.33	-4.00	0.0002	5.03E+04	5.40	8.00	2.43	-6.00	0.0000	5.03E+04
5.60	8.00	9.71	-5.00	0.0001	5.22E+04	5.60	8.00	8.26	-7.00	0.0000	5.22E+04
5.80	8.00	4.07	-5.00	0.0000	5.40E+04	5.80	8.00	2.86	-7.00	0.0000	5.40E+04
6.00	8.00	1.72	-5.00	0.0000	5.59E+04	6.00	8.00	1.01	-7.00	0.0000	5.59E+04
6.20	8.00	7.34	-6.00	0.0000	5.78E+04	6.20	8.00	3.64	-8.00	0.0000	5.78E+04
6.40	8.00	3.15	-6.00	0.0000	5.96E+04	6.40	8.00	1.33	-8.00	0.0000	5.96E04
6.60	8.00	1.36	-6.00	0.0000	6.15E+04	6.60	8.00	4.95	-9.00	0.0000	6.15E+04
7.00	8.00	2.61	-7.00	0.0000	6.52E+04	6.80	8.00	7.11	-10.00	0.0000	6.52E+04
7.20	8.00	1.15	-7.00	0.0000	6.71E+04	7.20	8.00	2.74	-10.00	0.0000	6.71E+04
7.40	8.00	5.12	-8.00	0.0000	6.89E+04	7.40	8.00	1.07	-10.00	0.0000	6.89E+04
7.60	8.00	2.29	-8.00	0.0000	7.08E+04	7.60	8.00	4.17	-11.00	0.0000	7.08E+04
7.80	8.00	1.03	-8.00	0.0000	7.27E+04	7.80	8.00	1.65	-11.00	0.0000	7.27E+04
8.00	8.00	4.63	-9.00	0.0000	7.45E+04	8.00	8.00	6.53	-12.00	0.0000	7.45E+04

Figure 7.6 Stress Distribution Function; Cruiser 1, Hog

Cruiser 1   SAG

──── y = -0.24857 + 0.90152x R= 0.99993

$$Y = \ln[-\ln(1-F)]$$

WEIBULL

ln S
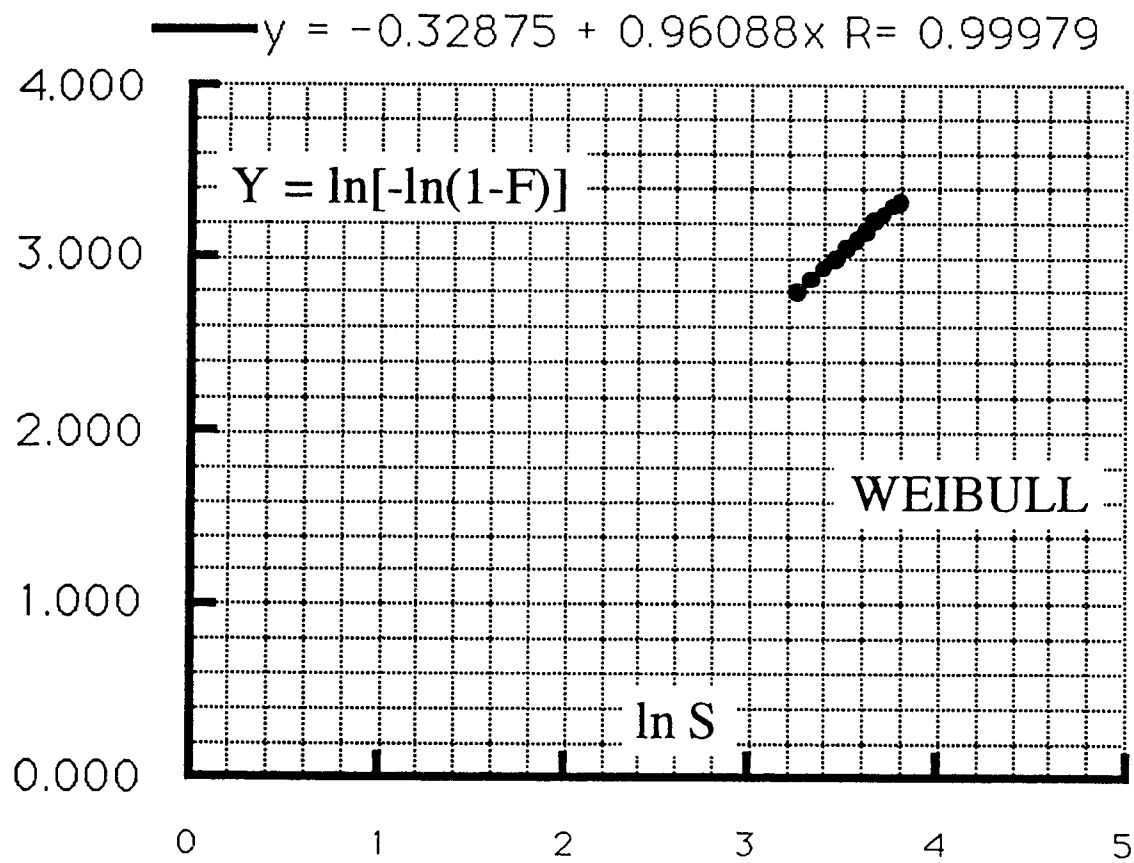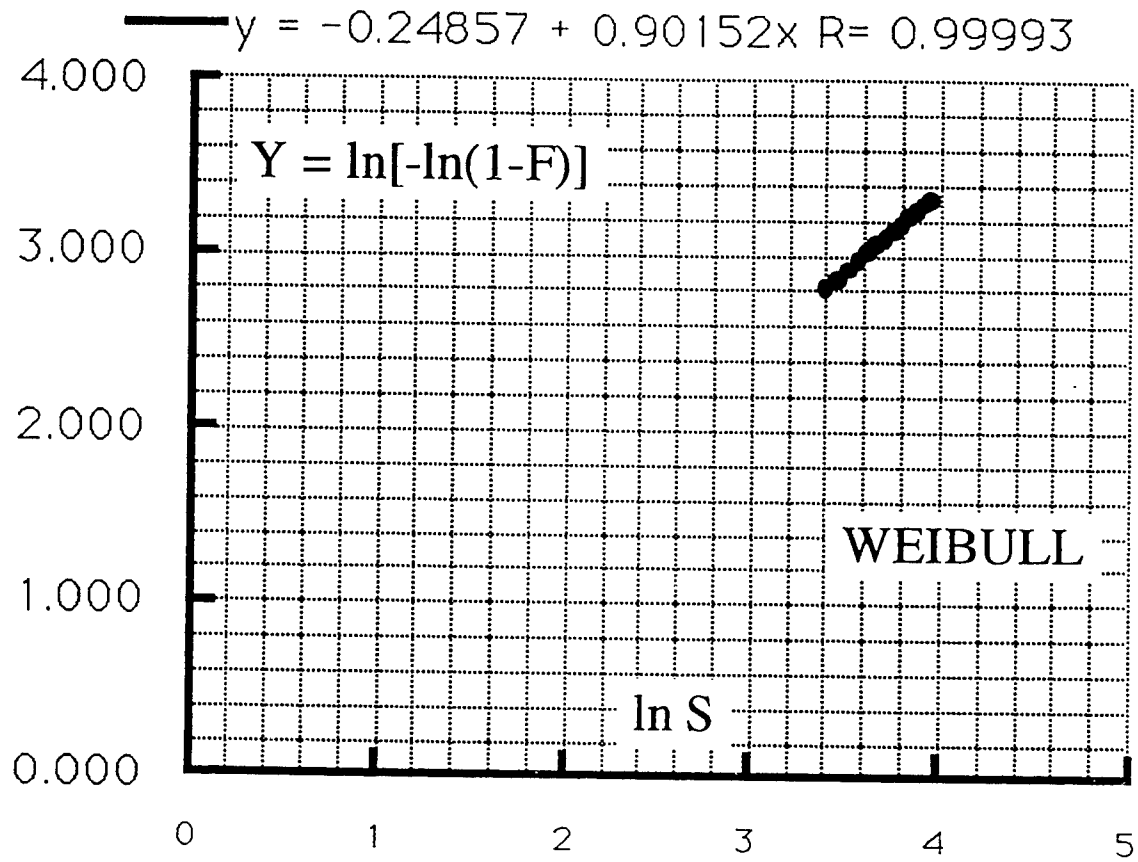
Figure 7.7 Stress Distribution Function; Cruiser 1, Sag
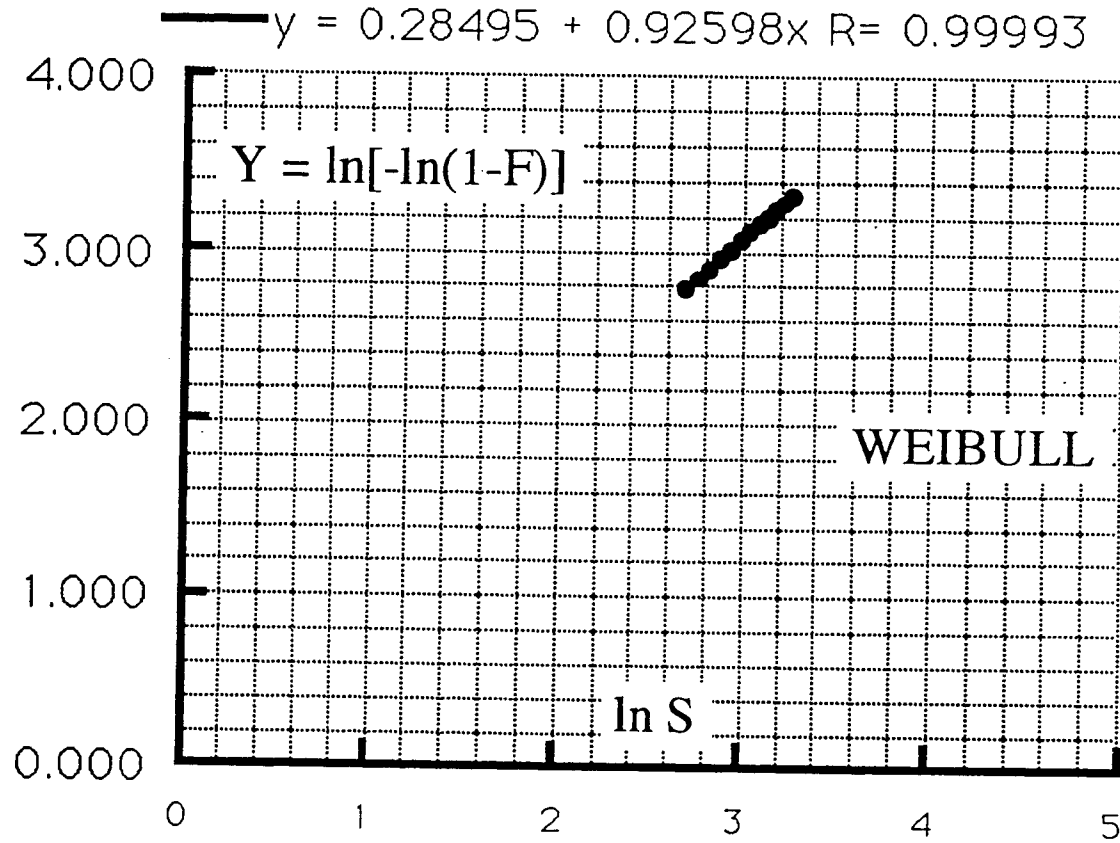
Figure 7.8 Stress Distribution Function; Cruiser 2, Hog
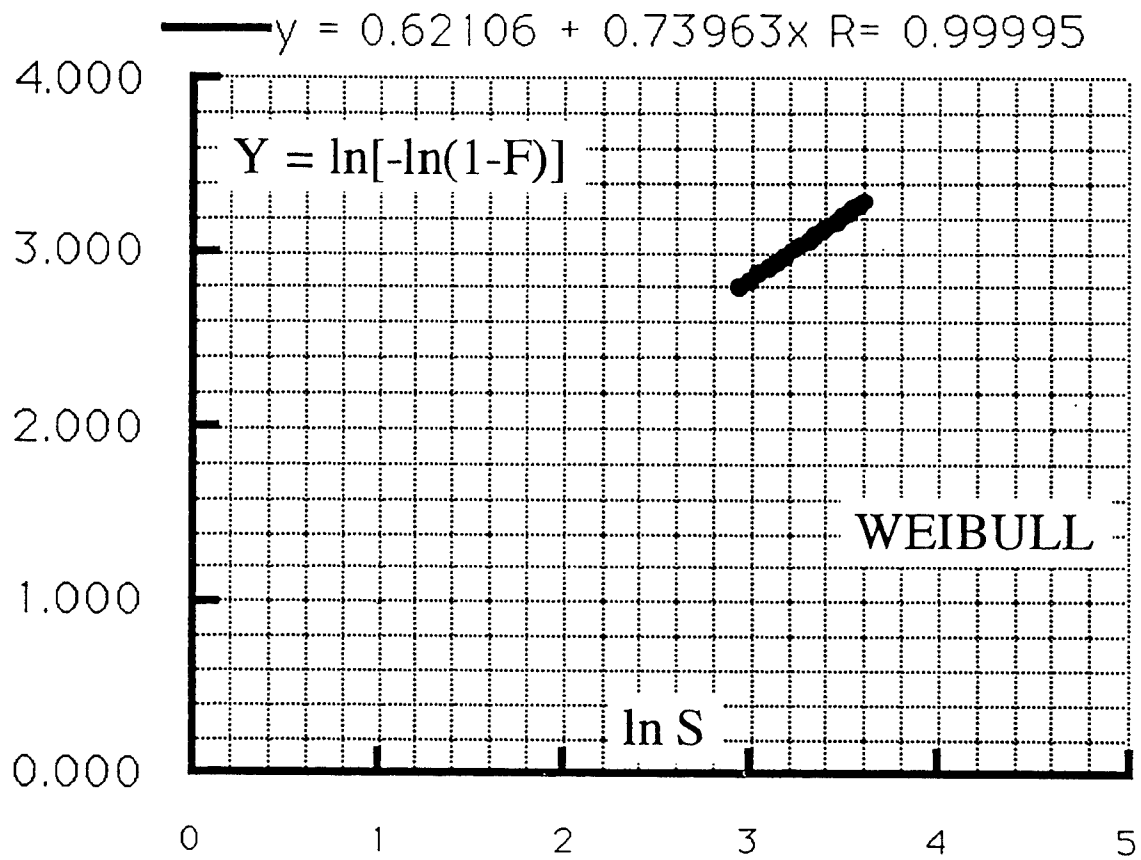
Figure 7.9 Stress Distribution Function; Cruiser 2, Sag

Tanker   HOG

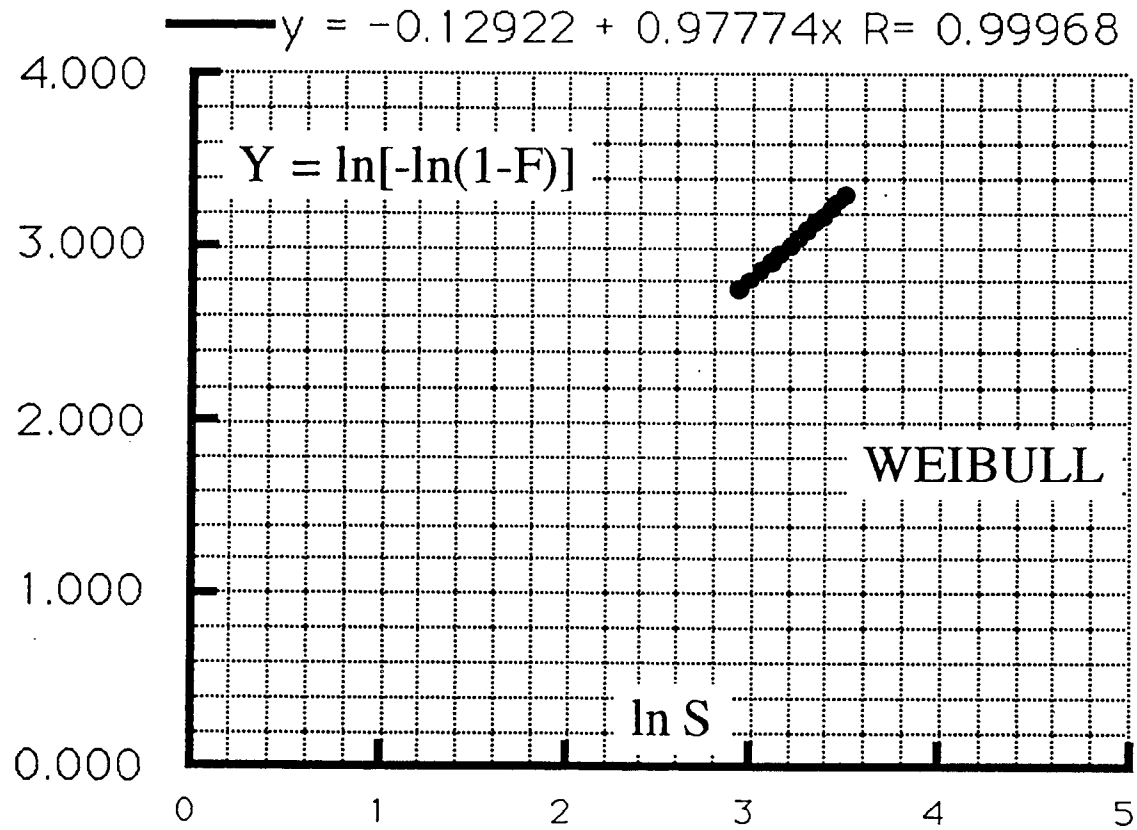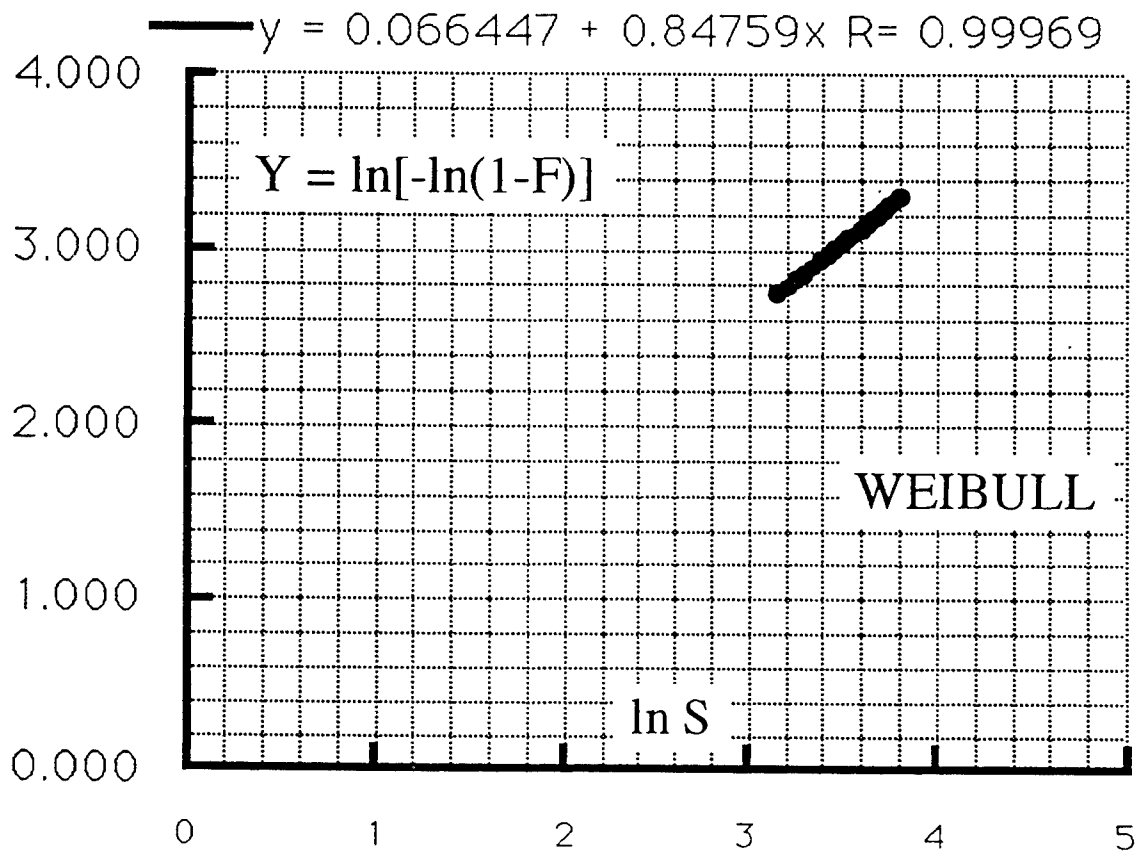$y = -0.12922 + 0.97774x$ R= 0.99968

$Y = \ln[-\ln(1-F)]$

WEIBULL

ln S

Figure 7.10 Stress Distribution Function; Tanker, Hog

Tanker   SAG

y = 0.066447 + 0.84759x R= 0.99969

$Y = \ln[-\ln(1-F)]$

WEIBULL

ln S

Figure 7.11 Stress Distribution Function; Tanker, Sag

SL-7   HOG
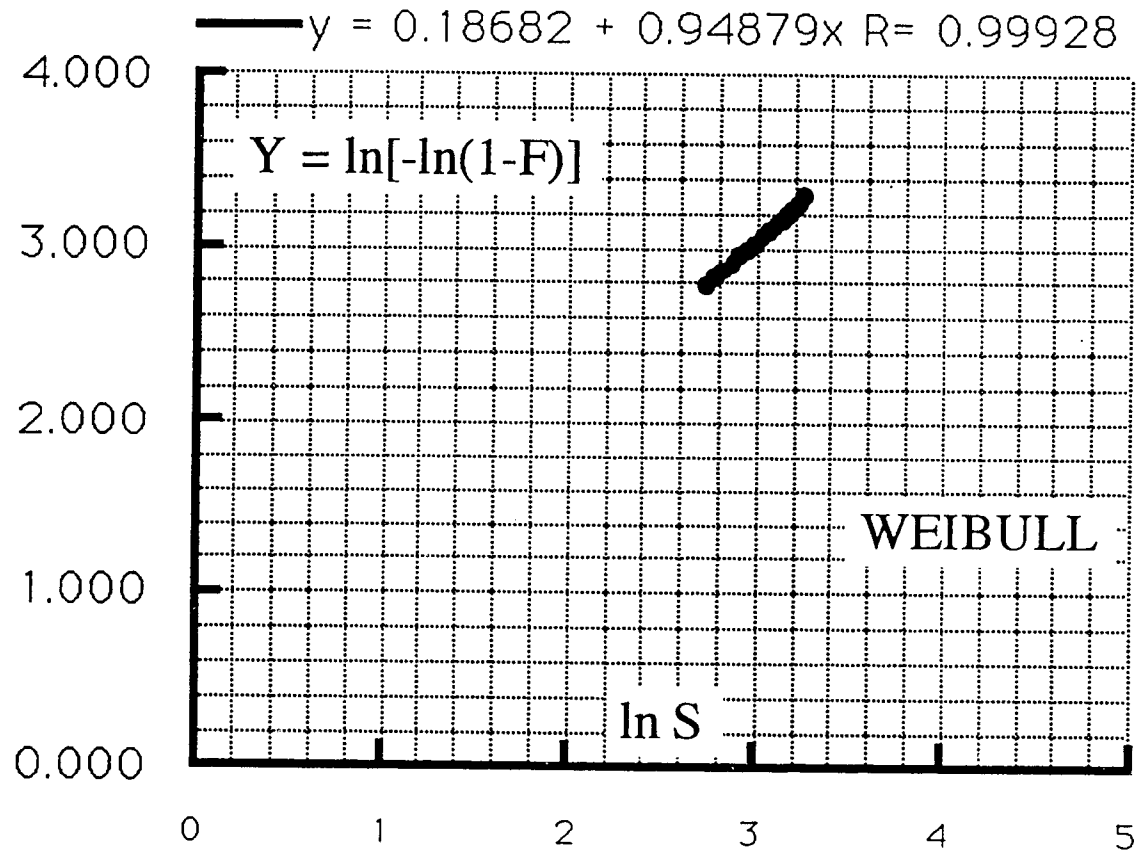
Figure 7.12 Stress Distribution Function; SL-7, Hog
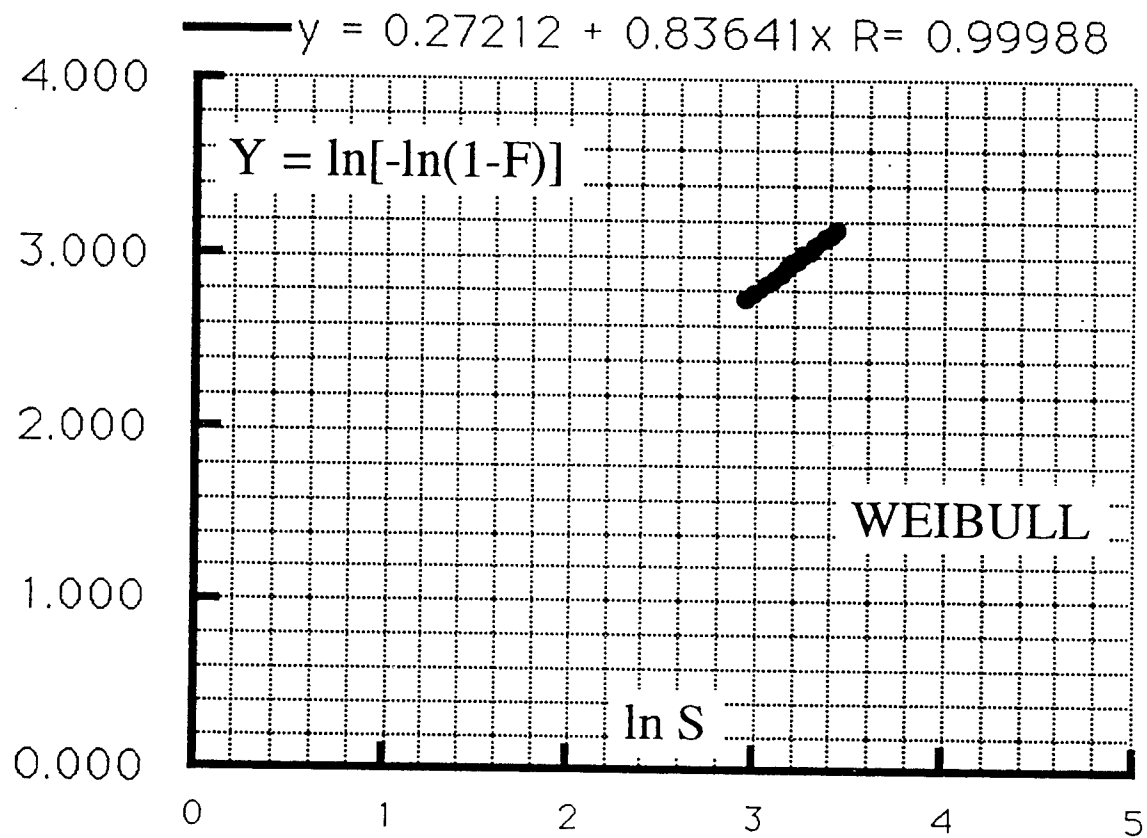
Figure 7.13 Stress Distribution Function; SL-7, Sag

The plotting routine used for Figures 7.6 through 7.13 automatically performs least squares analysis, and the results are shown on the figures. These parameters are directly translated into ξ and δ, the Weibull shape and scale parameters using eqns. 7.18. The parameters for hog and sag stresses are given in Table 7.6.

Table 7.6
Weibull Parameters for Hog and Sag Stresses

	Hog		Sag	
	ξ	δ (ksi)	ξ	δ (ksi)
Cruiser 1	0.961	1.41	0.901	1.310
Cruiser 2	0.926	0.736	0.739	0.432
Tanker	0.978	1.14	0.848	0.924
SL-7	0.948	0.821	0.836	0.722

Step 3. Stress ranges are derived. The cdf's of stresses in hog and sag are given separately. But fatigue stresses must be given as stress ranges. The hog and sag distributions are combined using the basic assumption that a hog stress having a probability level, p, would combine with a sag stress at the same value of p. The stress range at level p would then simply be the sum of the hog and sag stress. The operation is illustrated in Figure 7.14.[*]

It should be noted that the sum of two Weibull variates having the same ξ is also Weibull. But, if the two variates have different ξ, the sum will not be Weibull; as seen from Table 7.6, this will be the case for the distribution for each ship. However, the values of hog and sag ξ are close enough for each ship, that the Weibull sum would be a reasonable approximation.

As suggested in Figure 7.14, the addition is made at two values of the cdf of S, $Y = 2.91$ $(1 - F_S = 10^{-8})$, and $Y = 1.0$ $(F_S = 0.066)$. The stress range model is then assumed to be a straight line drawn between the two points.

The cdf of stress ranges S for each of the four ships is shown in Figures 7.15 through 7.18; the least squares estimators are included.

---

[*] Unlike the ultimate strength, the fatigue strength is a function of the stress range (hog to sag) rather than the hog and sag stresses individually. In the linear case, the stress range is simply the sum of the two stresses. The method developed for the above non-linear case is approximate, but is believed to be accurate.
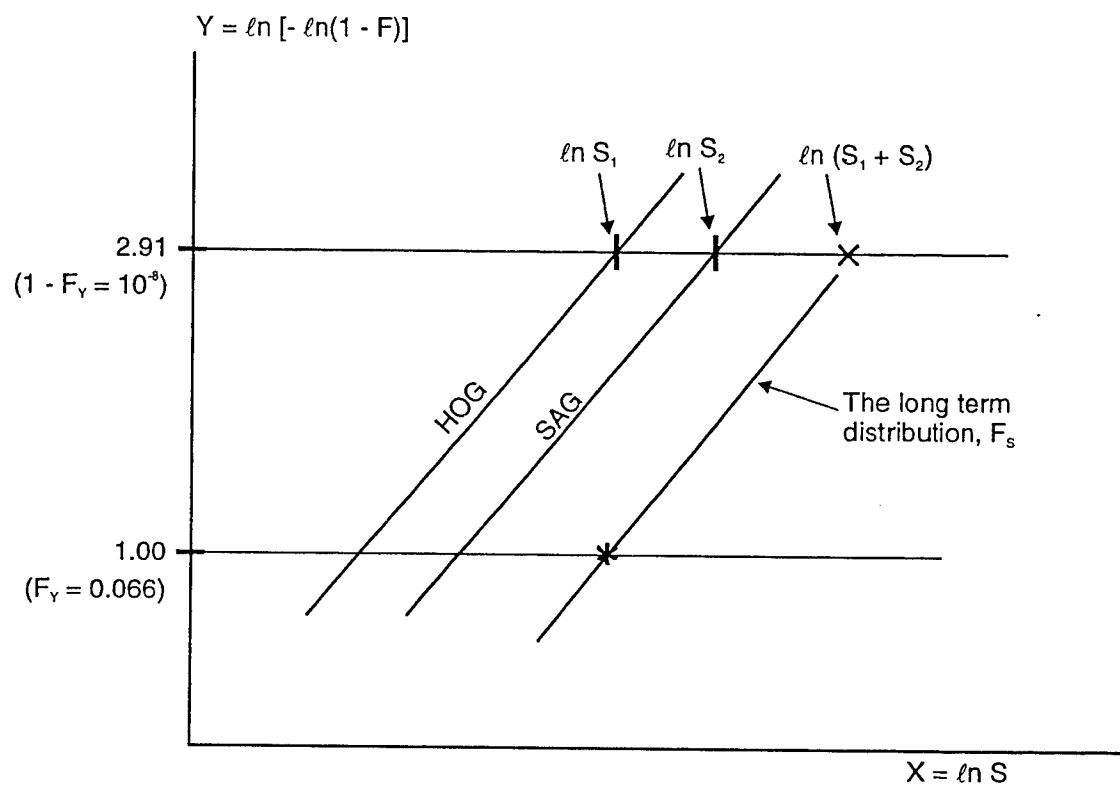
Figure 7.14 The Process of Adding Hog and Sag Stresses to Obtain Stress Range.
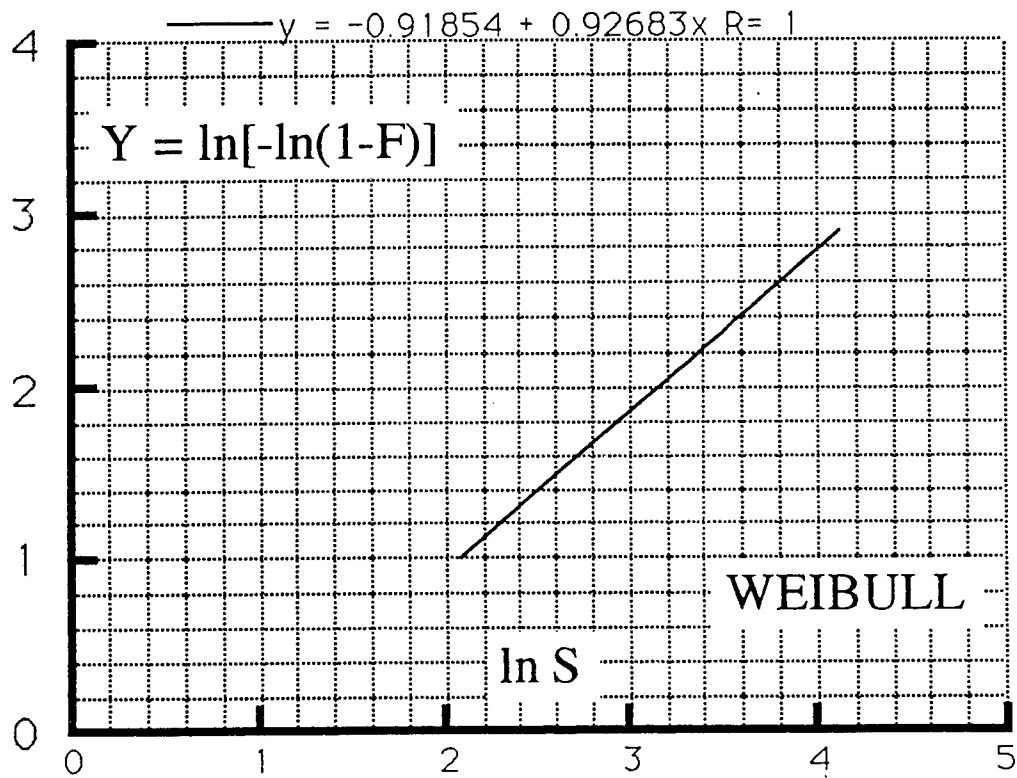
Cruiser 1   Long Term
Distribution of Stress Ranges

Figure 7.15 Long Term Distribution of Stress Ranges; Cruiser 1.
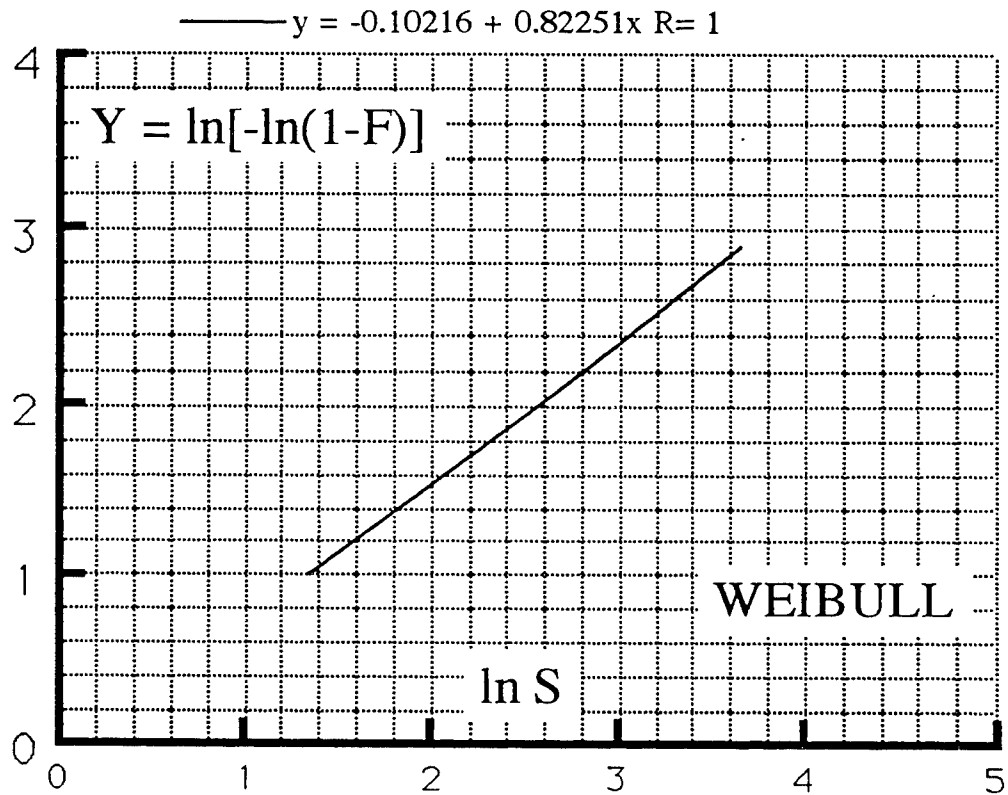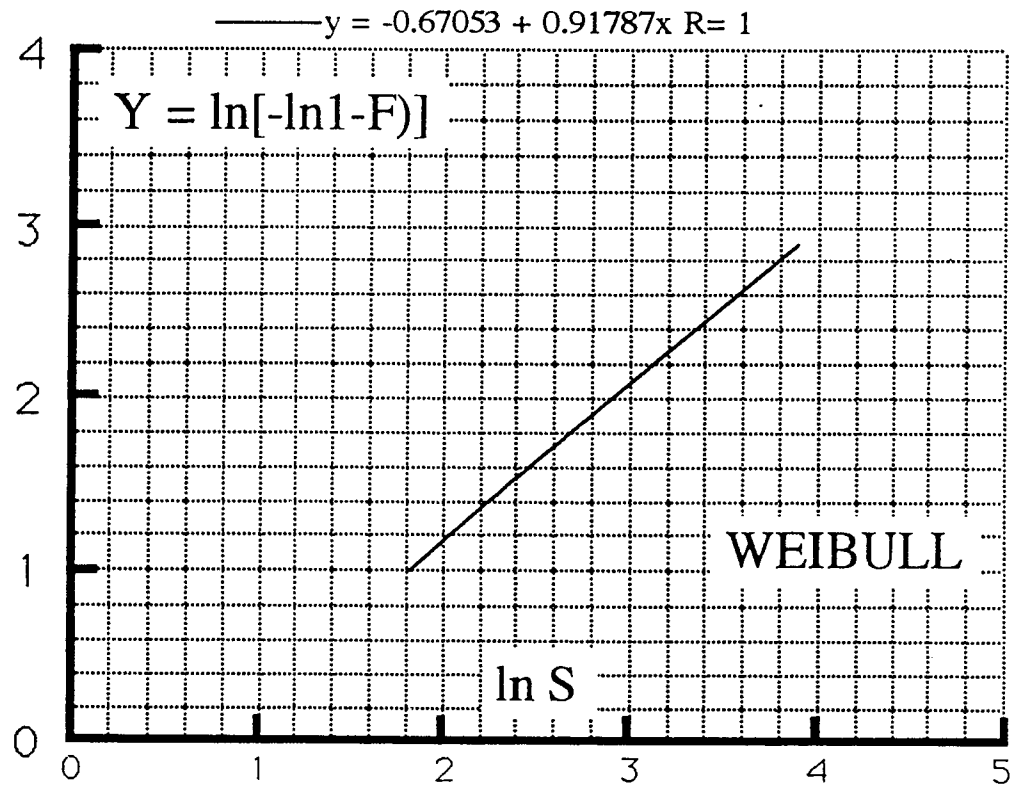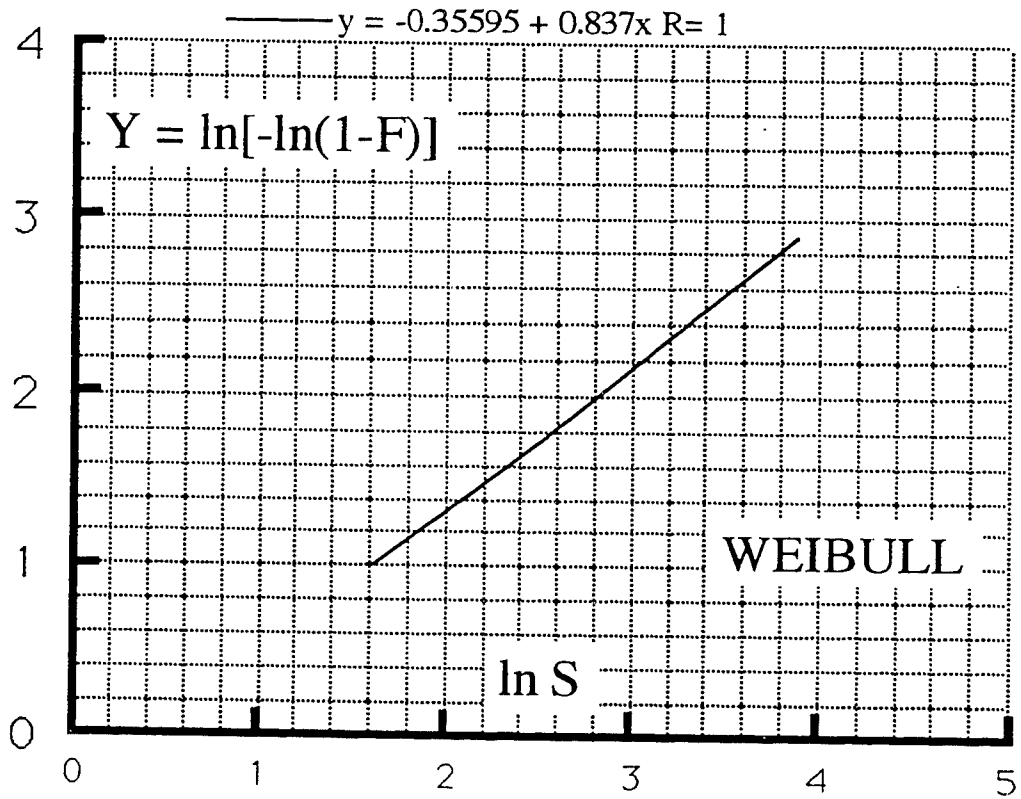
Cruiser 2   Long Term Distribution
of Stress Ranges

——— y = -0.10216 + 0.82251x R= 1

$Y = \ln[-\ln(1-F)]$

WEIBULL

ln S

Figure 7.16 Long Term Distribution of Stress Ranges; Cruiser 2.

Tanker   Long Term Distribution
of Stress Ranges

y = -0.67053 + 0.91787x R= 1

$Y = \ln[-\ln 1 - F)]$

WEIBULL

ln S

Figure 7.17 Long Term Distribution of Stress Ranges; Tanker.

SL-7   Long Term
Distribution of Stress Ranges

y = -0.35595 + 0.837x R= 1

Y = ln[-ln(1-F)]

WEIBULL

ln S

Figure 7.18 Long Term Distribution of Stress Ranges; SL-7.

Values of ξ and δ are computed from the least squares estimators (using eqn. (7.18)). Then the values of S_o are computed using eqn. (7.20).

The final result, ... the long term mid-ship stress range distribution for each ship is given in Table 7.7. The distributions of the stress ranges in terms of exceedances are given in Figures 7.19 through 7.22.

Cruiser 1   Long Term
Distribution of Stress Ranges

Stress Range, S (ksi)

$S_o = 61.9$ ksi

$\xi = 0.927$

$N_T = 8.89E7$

Number of Exceedances, N (cycles)

60

40

20

0

1   10^2 10^4 10^6 10^8
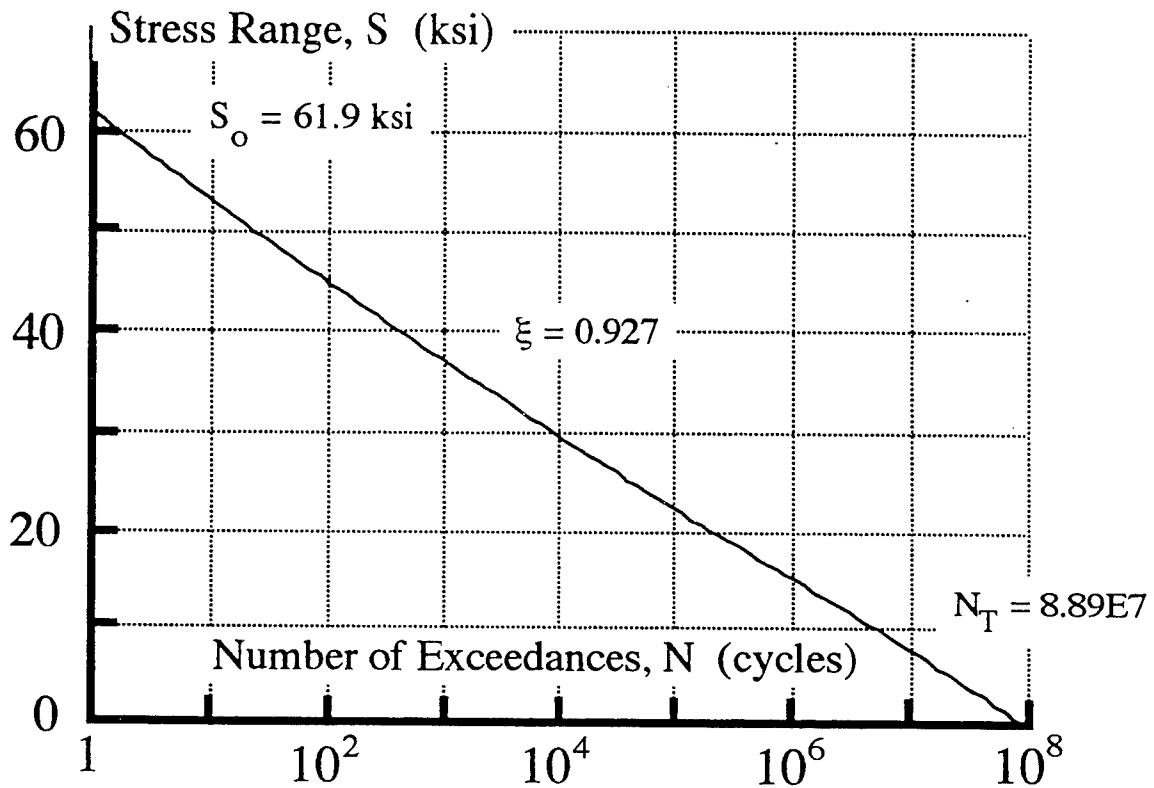
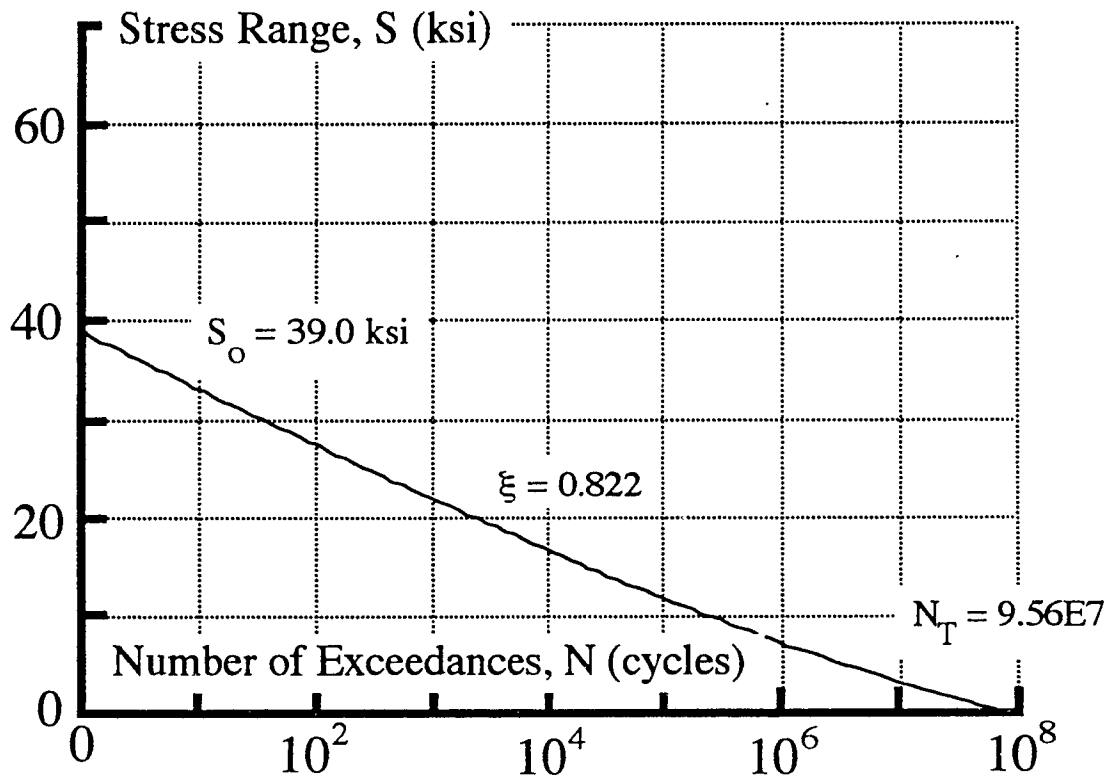Figure 7.19 Long Term Distribution of Stress Ranges; Cruiser 1.

Figure 7.20 Long Term Distribution of Stress Ranges; Cruiser 2.

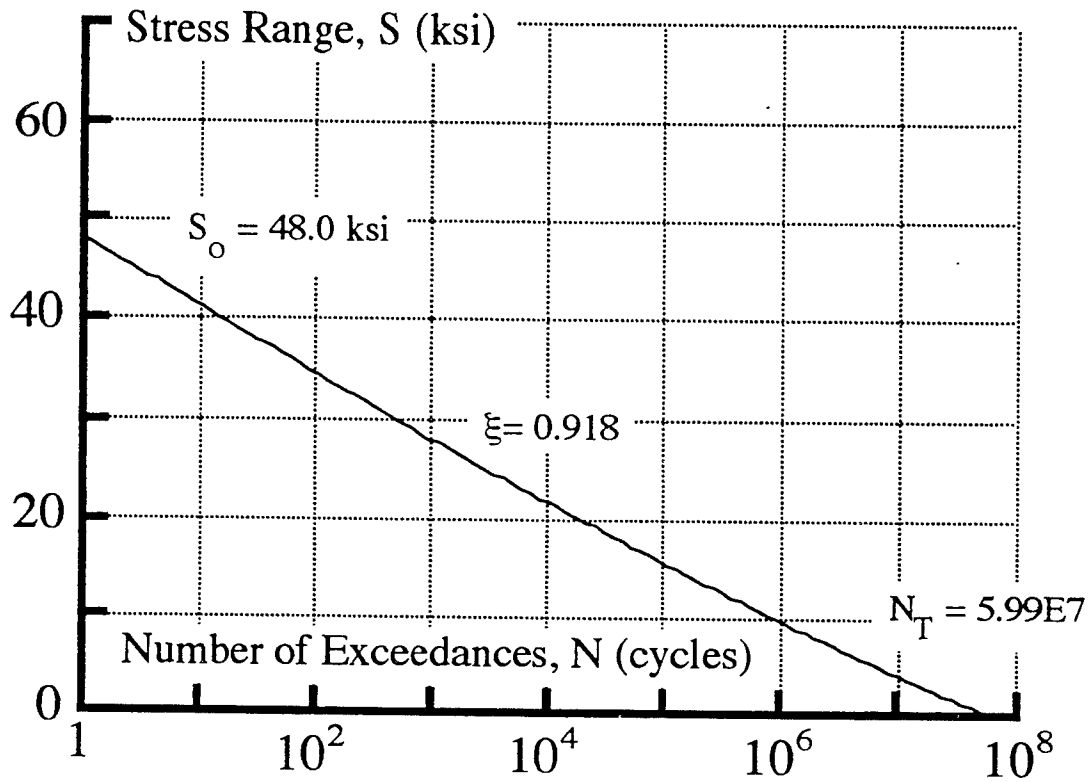# Tanker   Long Term
Distribution of Stress Ranges

Figure 7.21 Long Term Distribution of Stress Ranges; Tanker

SL-7   Long Term
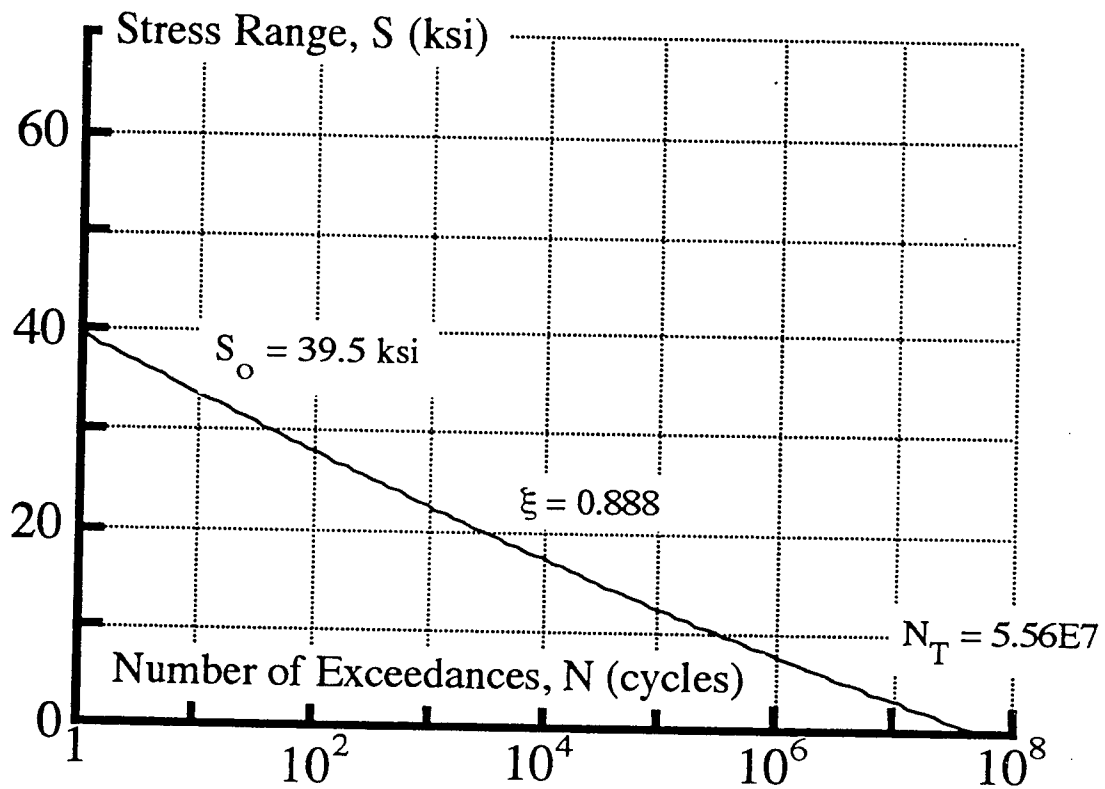## Distribution of Stress Ranges

Stress Range, S (ksi)

$S_o = 39.5$ ksi

$\xi = 0.888$

$N_T = 5.56E7$

Number of Exceedances, N (cycles)

60

40

20

0

10^2 10^4 10^6 10^8

1

Figure 7.22 Long Term Distribution of Stress Ranges; SL-7.

Table 7.7
Summary
Long Term Distribution of Stress Ranges

	Weibull Shape Parameter ξ	Weibull Scale Parameter δ (ksi)	S_o (ksi)	N_T (cycles)
Cruiser 1	0.927	2.69	61.9	8.89E7
Cruiser 2	0.822	1.13	39.0	9.56E7
Tanker	0.918	2.07	48.0	5.99E7
SL-7	0.888	1.54	39.5	5.56E7

7.3.6   Stress Modeling Error:

7.3.6.1   *General comments*

Assumptions made in the models and procedures used to compute fatigue stress produce errors. These errors must be accounted for explicitly when performing a reliability assessment.

Following the steps in performing a fatigue stress analysis, there is uncertainty in:

a) The model which is used to describe the environment (i.e., the long term distribution of wave heights).

b) The model which is used to translate the environment into loading on the structure (i.e., wave loads on ship).

c) Computer codes (or equations) used to determine dynamic response of ship.

d) Computer codes (or equations) used to determine nominal forces and stresses in structure (e.g., deck stresses).

e) Methods used to calculate stresses at the points of stress concentration (i.e., stress concentration factors).

In each step, there are assumptions in the models used for analysis, and therefore the error associated with each must be quantified.

An important component of modeling error which is not considered in this study is the uncertainty associated with operations. That is,

a) Changes in routes. For example, the reassignment of a TAPS tanker to the Gulf of Mexico.

b) Assignment of a warship to different global theaters.

c) Structural changes to the ship, e.g., the rework on the hatch openings in the SL-7's.

d) Changes in cargo and mission.

None of these uncertainties are explicitly accounted for in this study. It is assumed that each of the four ships travel the same route and are exposed to the same environment.

7.3.6.2 Error and the definition of bias

An error can be defined as the difference between a computed or estimated result and the actual value. Modeling errors can be:

a) Systematic. A systematic error is where the bulk of observed data lies above or below some predicted value, often described by the term "bias".

b) Random. Random errors have a distribution which might be described by a probability density function.

The relevant question — how does one quantify these errors?

In probabilistic design, stress modeling errors are described with bias, defined as:

$$\text{Bias} = \frac{\text{The real, or actual, load effect}}{\text{The estimated load effect by the best predictive model}} \tag{7.27}$$

But, the bias contains systematic and random errors. Therefore, in a reliability analysis, it could be treated as a random variable. Letting B be a random variable denoting bias, it is necessary to specify:

a) the median, $\tilde{B}$ (or mean)

b) the coefficient of variation, C_B

c) the distribution.

7.3.6.3 *Example*

Consider a simple example, Let S' be the "best estimate stress" a random variable; let B denote modeling error. Then the actual stress is,

$$S = BS' \qquad (7.28)$$

It is mathematically convenient to assume that B has a lognormal distribution. For example, if both B and S' have lognormal distributions, then S will also have an exact lognormal (see Appendix I), with median and coefficient of variation (COV).

$$\tilde{S} = \tilde{B}\ \tilde{S}'\ , \qquad (7.29)$$

$$C_S = \sqrt{\left(1 + C_B{}^2\right)\left(1 + C_{S'}{}^2\right) - 1} \qquad (7.30)$$

where the tildes indicate median values and C's denote COV's.

7.3.6.4 *Example: Several quantifiable sources of error*

As an extension, consider several sources of modeling error. Assume that the actual stress can be written as

$$S = BS' \qquad (7.31)$$

where

$$B = B_1 \cdot B_2 \cdots B_n = \prod_{i=1}^{n} B_i \qquad (7.32)$$

and where B_i is a random variable which quantifies the ith source of error.

If each B_i can be assumed to be lognormal, then the median ($\tilde{B}$) and COV (C_B) of B are (Ref.: Appendix I):

$$\tilde{B} = \prod_{i=1}^{n} \tilde{B}_i \qquad (7.33)$$

$$C_B \sqrt{\prod_{i=1}^{n}\left(1 + C_i^2\right) - 1}$$

$$\left(\text{or } C_B \approx \sqrt{\sum_{i=1}^{n} C_i^2} \quad \text{for small } C_i \right) \tag{7.34}$$

7.3.6.5 How to define B; an example

Ultimately modeling error should be quantified using expert testimony. Typically expert testimony provides tolerances, e.g., "I believe that our analysis predicts stress within ±10%". Translate this tolerance into a lognormally distributed random variable, B.

Assume that the median of B, $\tilde{B} = 1.0$. Assume that the tolerance translates into a 99% probability range. Thus $\ell n\, B$ is normally distributed with 99% of the population between ±2.57 $\sigma_{\ell nB}$. The range from the median, $B = 1.0$ to +10%, namely $B = 1.1$ is 2.57 standard deviations on a log basis. Thus,

$$\sigma_{\ell n\, B} = \frac{\ell n\, 1.1 - \ell n\, 1.0}{2.57} \tag{7.35}$$
$$= 0.037$$

And the coefficient of variation, (COV) of B is (see eqn. I.17)

$$C_B = \sqrt{\exp\left(\sigma_{\ell n\, B}^2\right) - 1} \tag{7.36}$$
$$= 0.037$$

Thus B is lognormal, with a median of $\tilde{B} = 1.0$, and a COV, $C_B = 0.037$.

7.3.6.6 Stress modeling error used in this fatigue analysis

Fatigue stress modeling error for this analysis is quantified in Table 7.8. The values are assumptions made by the authors of this study but based on other experiences. The overall uncertainty defined by the COV of B of 15.5% is very typical of other studies, and is assumed by the authors to be reasonable for this study.

For a COV of 15.5%, there is a probability of 99% that B will lie between 0.67 and 1.49. Thus it can be concluded, using this model for B, that the actual fatigue stress (Miner's stress) will lie within 67% and 149% of the best estimate.

Table 7.8
Fatigue Stress Modeling Error:
A Summary

	Uncertainty in ...	Median	COV
B_1	long term distribution of wave heights	1.0	0.10
B_2	wave loading	1.0	0.10
B_3	computer code used for dynamic response	1.0	0.037
B_4	computer code for stress analysis	1.0	0.037
B_5	stress concentration factor	1.0	0.037
B	overall	1.0	$0.155^{(b)}$

Notes:

    (a) ±10% error assumed. Assumed to translate to a 99% tolerance. See example in text.

    (b) Computed using eqn. (7.34).

7.4 Miner's Rule

7.4.1 Fatigue Damage:

Unfortunately, the fatigue strength defined above is based on constant amplitude fatigue tests. To predict fatigue under the variable amplitude stresses experienced in marine structures, using constant amplitude data, Miner's rule is employed. A summary of Miner's rule is presented in Figure 7.23. Note in this figure that n_1 is the number of applied cycles at stress S_1, N_1 is the number of cycles to failure under S_1. The concept of fractional damage and total damage D is defined in this figure.

Assume now that the long term distribution of the random variable S (stress ranges) is given by the probability density function shown in Figure 7.24.

Block loading to simulate a random process.
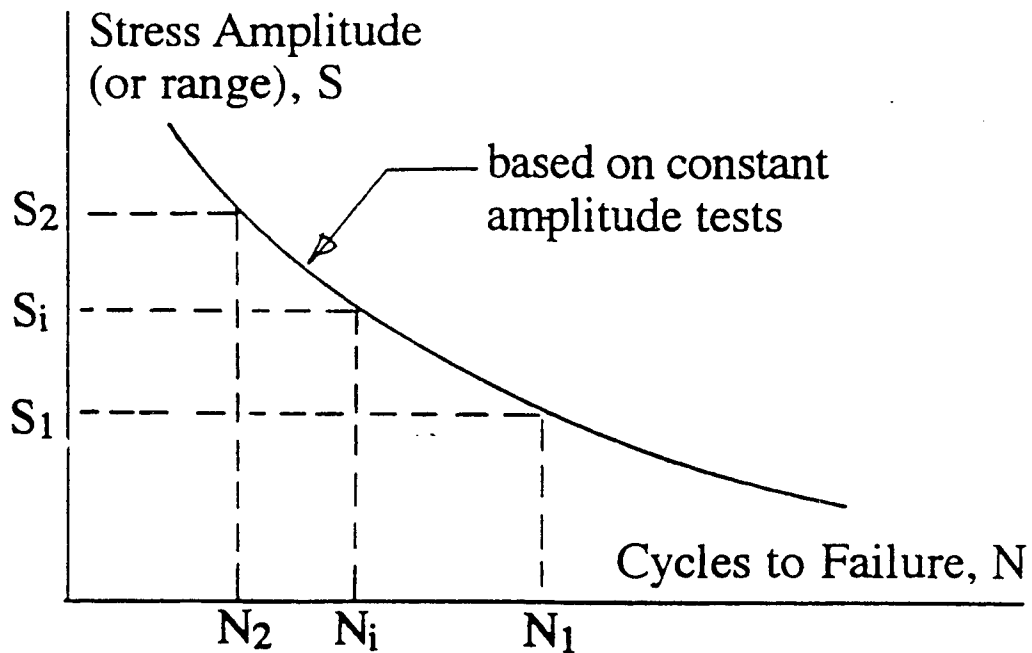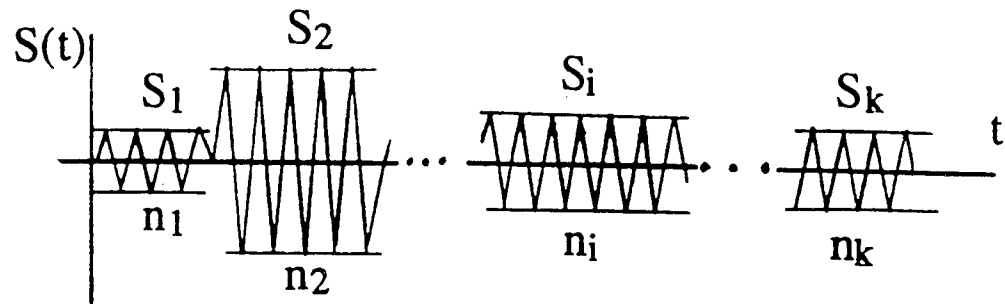
- Fractional damage at stress, $S_i = \dfrac{n_i}{N_i}$

- Total damage is a sum of fractional damages $\quad D = \displaystyle\sum_{i=1}^{k} \dfrac{n_i}{N_i}$

- Failure $\rightarrow$ $D \geq 1.0$
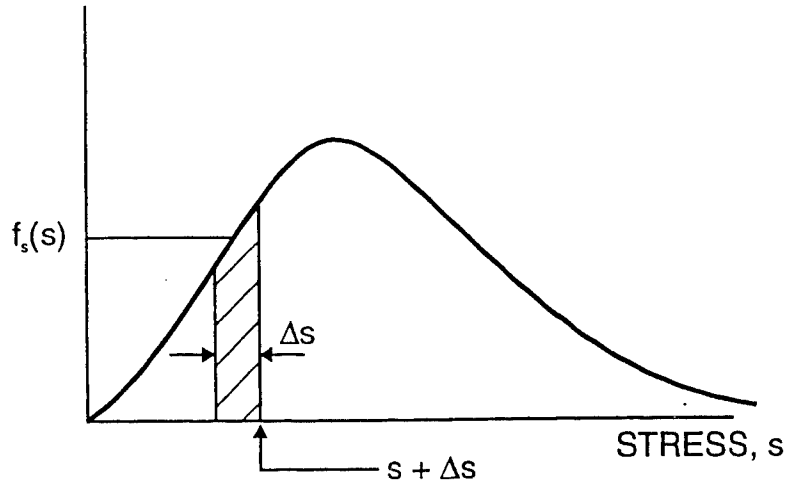
Figure 7.23 An illustration of Miner's Rule.

Figure 7.24 Probability density formation of S, stress range.

The fraction of stresses in $(s, s + \Delta s)$ is:

$$f_i \approx f_S(s)\, \Delta s \tag{7.37}$$

and the total number in $(s, s + \Delta s)$ is

$$n_i = n f_i \tag{7.38}$$

where n is the total number of stress cycles. Then

$$D = \sum \frac{n_i}{N_i} \tag{7.39}$$

and

$$D \approx n \sum_{i\text{-}1}^{k} \frac{f_S(s)\, ds}{N(s)} \tag{7.40}$$

As $\Delta s \to 0$

$$D = n \int_{0}^{\infty} \frac{f_S(s)\, ds}{N(s)} \tag{7.41}$$

If the S-N curve is given as $NS^m = A$, then

$$D = \frac{n}{A} \int_0^\infty s^m f_S(s) \, ds \qquad (7.42)$$

But by definition the integral is the expected value of S^m

$$E(S^m) = \int_0^\infty s^m f_S(s) \, ds \qquad (7.43)$$

Then, the total fatigue damage is

$$D = \frac{n}{A} E(S^m) \qquad (7.44)$$

7.4.2 Equivalent Constant Amplitude Stress:

If the stress is constant amplitude, then damage is

$$D = \frac{n}{A} S^m \qquad (7.45)$$

Comparing (7.44) and (7.45), an equivalent constant amplitude stress for a random process is

$$S_e = \left[E(S^m) \right]^{1/m} \qquad (7.46)$$

This stress is sometimes called "Miner's stress".

7.4.3 Miner's Stress when the S-N Cuve has an Endurance Limit:

When stress endurance limits are considered, the expression for $E(S^m)$ must be modified. The only stresses that "count" are those for which $S > S_Q$. The expression for $E(S^m)$ of eqn. (7.43) assumes that all $S > 0$ produce fatigue damage. The more general expression is

$$E\left(S^m\right) = \int_{S_Q}^\infty s^m f_s(s) \, ds \qquad (7.47)$$

But for a Weibull stress spectra, the density function of S is given by eqn. (7.13). Thus $E(S^m)$ becomes,

$$E\left(S^m\right) = \int_{S_Q}^{\infty} s^m \left(\frac{\xi}{\delta}\right)\left(\frac{s}{\delta}\right)^{\xi-1} \exp\left[-\left(\frac{s}{\delta}\right)^{\xi}\right] ds \qquad (7.48)$$

Let,

$$t = \left(\frac{s}{\delta}\right)^{\xi} \qquad (7.49)$$

Then the integral reduces to

$$E\left(S^m\right) = \delta^m \int_z^{\infty} t^{a-1} \exp(-t)\, dt \qquad (7.50)$$

$$a = \frac{m}{\xi} + 1$$

where, $\qquad\qquad\qquad\qquad\qquad\qquad\qquad\qquad\qquad\qquad$ (7.51)

$$z = \left(\frac{S_Q}{\delta}\right)^{\xi}$$

The integral of eqn. (7.50) has the form of an incomplete gamma function, $\Gamma(a,z)$. Using the value of δ from eqn. (7.20), it follows that Miner's stress can be written as,

$$S_e^m = E(S^m) = S_0^m \left[\ln\left(N_T\right)\right]^{-m/\xi} \Gamma(a,z) \qquad (7.52)$$

7.2.4 Strength Modeling Error: The Quality of Miner's Rule

Over the years, there have been numerous fatigue tests on welded joints in which the loading was a random stress process. The general conclusion was that, for welded joints and a reasonably narrow banded stress process typical of wave induced stresses, Miner's rule is valid in a first approximation.

In a fatigue test, damage D at failure, denoted as Δ, can be recorded for each specimen. When several specimens are tested, a random sample of Δ is obtained and statistical analyses can be performed. If Miner's rule works, the median Δ will be close to 1.0. A summary of observed statistics from a few investigators is presented in Table 7.2. There is no clear sharp conclusion. It appears that Miner's rule works reasonably well on the average; yet there is considerable uncertainty. Wirsching (1983) has plotted data from several investigators on lognormal probability paper and found that the lognormal fit all samples reasonably well.

Table 7.9
Some Test Results on Damage at Failure

	Damage at Failure, $\Delta*$	
	Median	Coefficient of Variation
Miner (1945); Miner's original work	0.95	0.26
Fatigue Under Complex Stress (1977); A syntheses of results of the SAE Fatigue Design and Evaluation Committee	1.09	0.90
Schütz (1979), crack initiation (a) 29 random sequence test series (b) Tests with large quasi-static mean load changes (c) significant plastic strains at notch	 1.05 0.60 0.37	 0.55 0.60 0.78
Schilling et al. (1974): tests on welded steel beams	1.15	0.48
Berge and Eide (1981): tests on welded sections; some stress relieved	1.06	0.40
Eide and Berge (1989): tests on welded sections; some stress relieved	0.78	0.19
Shin and Lukens (1983): extensive survey of random test data	0.90	0.67
Gurney (1983): test data on welded joints	0.85	0.28
Default value used in reliability analysis for welded joints, Wirsching (1984)	1.0	0.30

*Statistics based on a lognormal distribution of Δ.

A comprehensive study of Δ observed by investigators on welded joints was performed by Gurney (1988). He has provided a summary of the statistics of the sample mean of Δ. While the center of the distribution is at $\Delta = 1.0$, again a broad distribution is indicated.

The bottom entry in Table 7.9 has been suggested as a default value. It was approved as such by a panel of experts on an API project [Wirsching (1983)] and has been employed by others who have performed fatigue reliability on welded joints. Note that the default values are not out of line with other data on welded joints. It is this default value that will be used in this reliability study.

In summary, damage at failure will be modelled as a random variable,

$$\Delta \sim \text{lognormal} \qquad \text{Median, } \Delta = 1.0 \qquad \text{COV, } C_\Delta = 0.30 \qquad (7.53)$$

7.5   Fatigue Reliability Assessment Using the Lognormal Format

Miner's stress is evaluated using eqns. (7.43) or (7.47). This is the "best estimate" stress. The actual stress is given as,

$$S_e = B \, S_e'$$
(7.54)

where S_e' is the best estimate (deterministic) stress, and B is stress modeling error as described in Sec. 7.3.6.

The expression for damage for eqn. (7.44) becomes, with the introduction of B,

$$D = \frac{n}{A} B^m \, S_e'^m$$
(7.55)

where S_e^m is now the mth power of the best estimate Miner's stress.

At failure (the limit state)

$$D = \Delta, \quad \text{when} \quad n = N$$
(7.56)

where N is the total number of cycles to failure. The damage equation, solved for N, becomes,

$$N = \frac{A\Delta}{B^m \, S_e'^m}$$
(7.57)

Assume that Δ, A, and B are lognormally distributed random variables. Then N will have an exact lognormal distribution (see Appendix I). There will be a closed form solution for the probability of a fatigue failure prior to the end of the intended service life, N_T.

$$p_f = P(N \leq N_T)$$
(7.58)

But the analytical form follows the lognormal format. Thus

$$p_f = \Phi(-\beta)$$
(7.59)

where β is the safety index, defined for this limit state as

$$\beta = \frac{\ell n\left(\tilde{N}/N_T\right)}{\sigma_{\ell n \, N}}$$
(7.60)

where,

$$N = \frac{\tilde{A} \, \tilde{\Delta}}{\tilde{B}^m \, \tilde{S}_e^m}$$

(7.61)

and,

$$\sigma_{\ell n \, N} = \sqrt{\ell n \left\{ \left(1 + C_\Delta^2\right)\left(1 + C_A^2\right)\left(1 + C_B^2\right)^{m^2} \right\}}$$

(7.62)

7.6   Fatigue Reliability Analysis of the Four Ships

About the fatigue reliability analysis presented in the following sections ....

- **The Detail.** Fatigue reliability analyses were performed on the following detail:

  a) Cruiser 1. Hatch opening before and after modifications

  b) Cruiser 1. Deck house corner before and after modifications

  c) Cruiser 2. Hatch opening

  d) Cruiser 2. Deck house corner

  e) Tanker. Stiffener welds parallel and perpendicular to the direction of loading

  f) SL-7. Hatch opening corner

- **What the results mean.** In the context of this analysis, the probability of fatigue failure means the probability of the event development of a significant crack. In no way is the integrity of the ship structure immediately compromised. It should be noted, however, that the fracture mechanics fatigue equations predict relatively rapid crack growth once the crack has been initiated.

- **The Basic Analysis.** For the basic reliability analysis it is assumed that there is no stress endurance limit, i.e., the S-N curves are extrapolated into the high cycle range down to $S = 0$. Concern over what seemed to be inappropriately high failure probabilities motivated a closer look at the assumptions used.

- **Introduction of the Stress Endurance Limit.** The presence of a stress endurance limit "filters out" those smaller stress ranges in the spectrum that do not contribute to the damage. Estimated failure probabilities are predictably lower.

- **Reliability as a Function of Operating Time.** Reliability estimates cited above are based on the event of fatigue cracking be the *end* of the service life of the ship. But a probability of failure at any life N_0 can be estimated by replacing N_T by N_0 in eqn. (7.60). p as a function of time is estimated in the following analyses.

- **Using the Munse Data.** S-N models from the Munse data bank (Munse, 1983) were used to define fatigue strength. The Munse data (without stress endurance) produced generally higher reliabilities than the basic analysis.

- **Reliability Estimates as a Function of Stress.** The stress levels used for the analysis may be high relative to a typical operational profile. Reliability estimates as a function of stress for select detail are presented.

Case 1   Cruiser 1 Original Hatch Opening

Commentary:

The original design of a hatch opening just fore of the deck house of Cruiser 1 experienced the development of a significant fatigue crack. As a result, this detail was subsequently modified. A perspective of the original hatch opening is shown in Figure 7.24. Detail of the hatch opening is provided in Figure 7.25.

Two cases are considered in this analysis. In the first, HY-80 data provided by the NSWC was used. As presented in Section 7.2.2, these data define a statistical model which is quite different from that defined by the UK Department of Energy. Therefore, both curves are used in this analysis and the results compared.

- Case 1a   Cruiser 1, Original Hatch Opening: HY-80 Data

A stress analysis (using finite element methods) was employed to determine the stress concentrations. The results are shown in Figure 7.26. As shown in these figures, the peak stresses occur at the cutouts where the fatigue strength is defined by plain steel S-N curves (and not welded joint curves as is the case for most of the structure). The SCF (stress concentration factor) is 2.45.

Fatigue reliability analysis using the HY-80 data is summarized in Table 7.10.

- Case 1b   Cruiser 1, Original Hatch Opening: DEn B-Curve

Fatigue reliability analysis using the DEn B-curve is summarized in Table 7.11. Analysis is performed both for the case with and without a stress endurance limit.

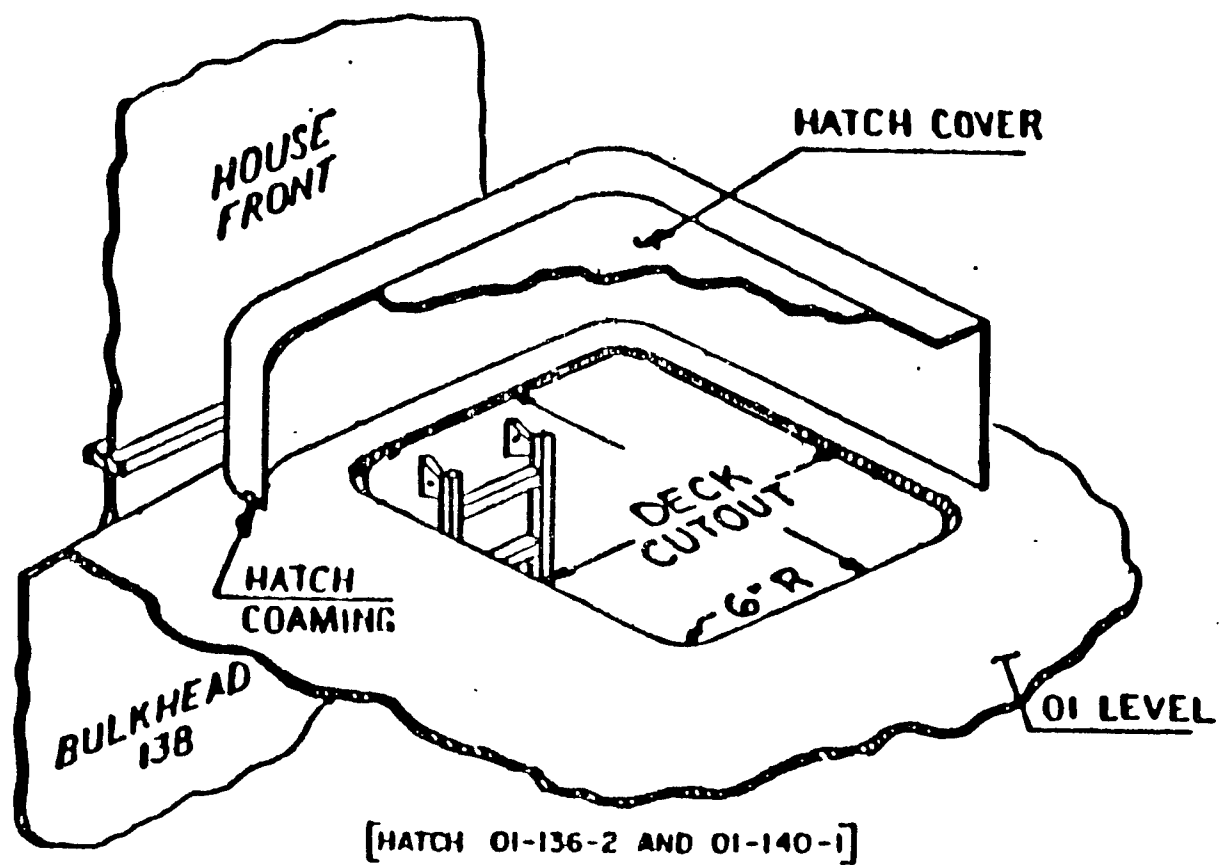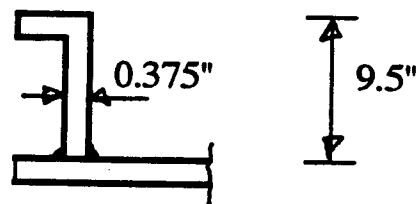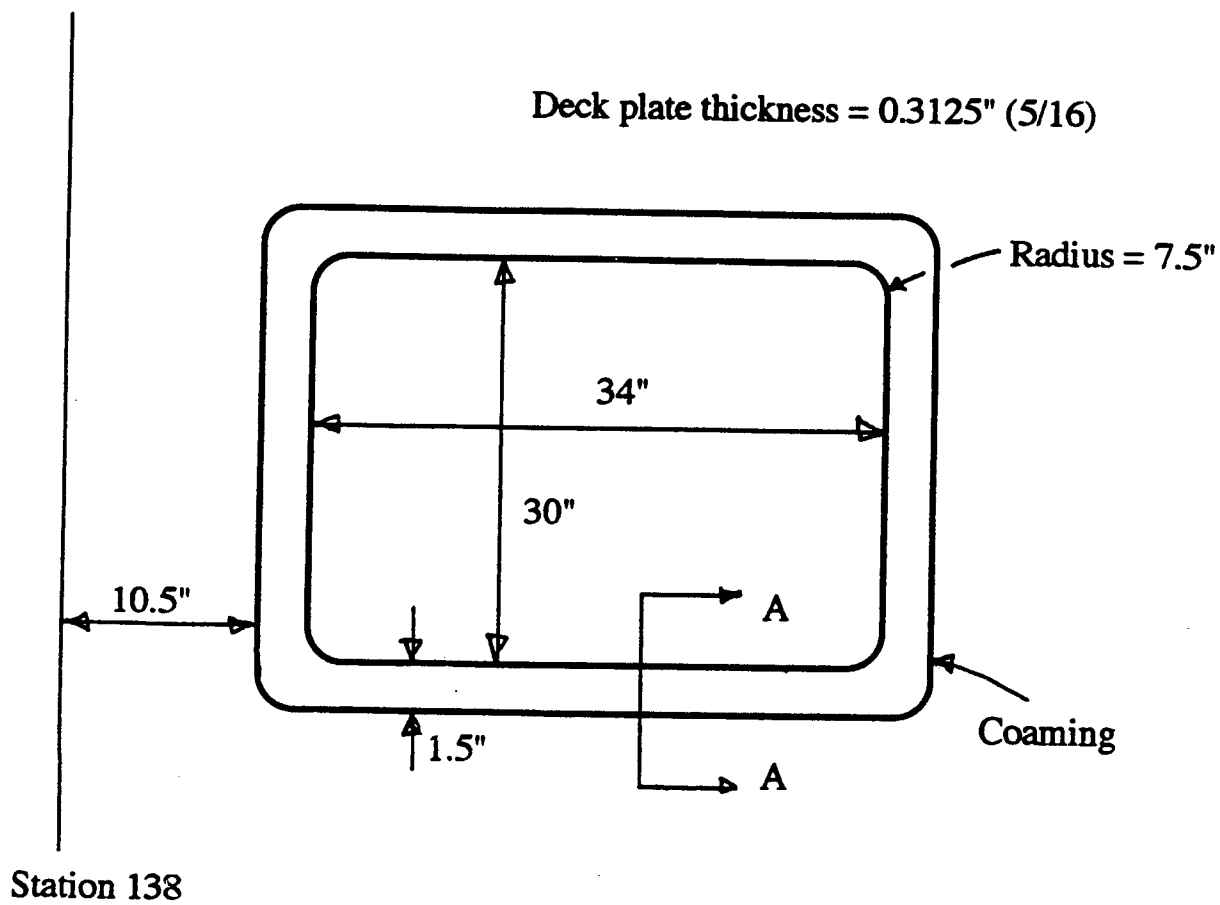The probability of fatigue cracking as a function of time is presented in Figure 7.27.

HOUSE FRONT

HATCH COVER

DECK CUTOUT

6" R

HATCH COAMING

BULKHEAD 138

01 LEVEL

[HATCH 01-136-2 AND 01-140-1]

Figure 7.24 Perspective of Original Hatch Opening of Cruiser 1.

Deck plate thickness = 0.3125" (5/16)

Radius = 7.5"

34"

30"

10.5"

A

Coaming

1.5"

A

Station 138

0.375"

9.5"

Section A-A

Figure 7.25 Original Hatch Opening of Cruiser 1.

ROM Engineering, Inc. P.O. Box 65170 (520) 299-4574
Tucson, AZ 85728 (520) 299-4574 fax
rome@azstarnet.com

ANSYS 5.2
DEC 28 1995
16:13:16
ELEMENT SOLUTION
STEP=1
SUB =1
TIME=1
SY   (NOAVG)
TOP
RSYS=0
DMX =.899E-05
SMN =-.715604
SMNB=-.81327
SMX =2.455
SMXB=3.005
      -.715604
      -.363354
      -.011103
      .341147
      .693398
      1.046
      1.398
      1.75
      2.102
      2.455
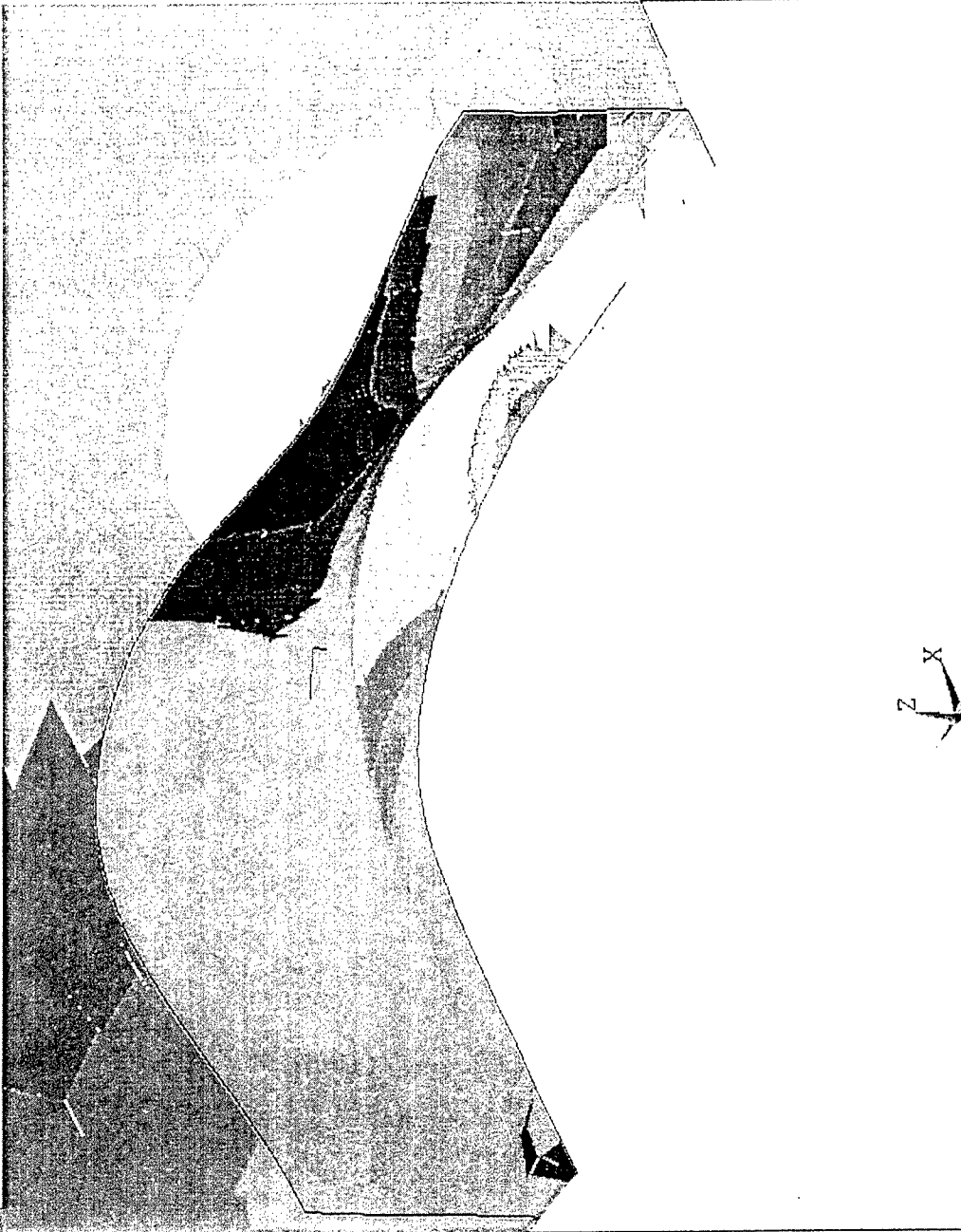
#1 Hatch Opening, Original Design

Figure 7.26 Cruiser 1. Stress Concentration at Hatch Opening

Table 7.10
Fatigue Reliability Assessment, Case 1a

SHIP	Cruiser 1		
Description of the detail:	Hatch opening (original)		
Long term distribution of stress ranges in the deck (see Table 7.7)		S_O (ksi) N_T ξ	61.9 8.89E7 0.923
SCF due to increased plate thickness			1.0
SCF due to detail			2.45
Miner's stress (see eqn. (7.21))		S_e (ksi)	29.5
Stress modeling error (see Table 7.8)		$\tilde{B}$ C_B	1.0 0.155
Strength modeling error (uncertainty in Miner's rule; see eqn. (7.53))		$\tilde{\Delta}$ C_Δ	1.0 0.3
Fatigue strength (smooth specimen fatigue data on HY-80; hatch opening is flame cut with no welded joint, i.e., faceplate)		m $\tilde{A}$ (ksi units) C_A	7.70 2.87E21 0.544
RELIABILITY ASSESSMENT	Safety Index, β		3.81
	Probability of Failure, p_f		6.8E-5

Table 7.11
Fatigue Reliability Assessment, Case 1b

SHIP	Cruiser 1		
Description of the detail:	Hatch opening (original)		
Long term distribution of stress ranges in the deck		S_O (ksi)	61.9
		N_T	8.89E7
		ξ	0.923
SCF due to increased plate thickness			1.0
SCF due to detail			2.45
Miner's stress		S_e (ksi)	17.0
Stress modeling error		$\tilde{B}$	1.0
		C_B	0.155
Strength modeling error (uncertainty in Miner's rule)		$\tilde{\Delta}$	1.0
		C_Δ	0.3
Fatigue strength (DEn B-curve for plain steel; hatch opening is flame cut with no welded joint, i.e., faceplate)		m	4
		$\tilde{A}$ (ksi units)	1.04E12
		C_A	0.44
RELIABILITY ASSESSMENT			
	Safety Index, β		-2.46
	Probability of Failure, p_f		≈ 1.0

RELIABILITY ASSESSMENT (including stress endurance limit)		
	Stress endurance limit, S_Q (ksi)	18.0
	Safety index, β	-1.19
	Probability of failure, p_f	0.88
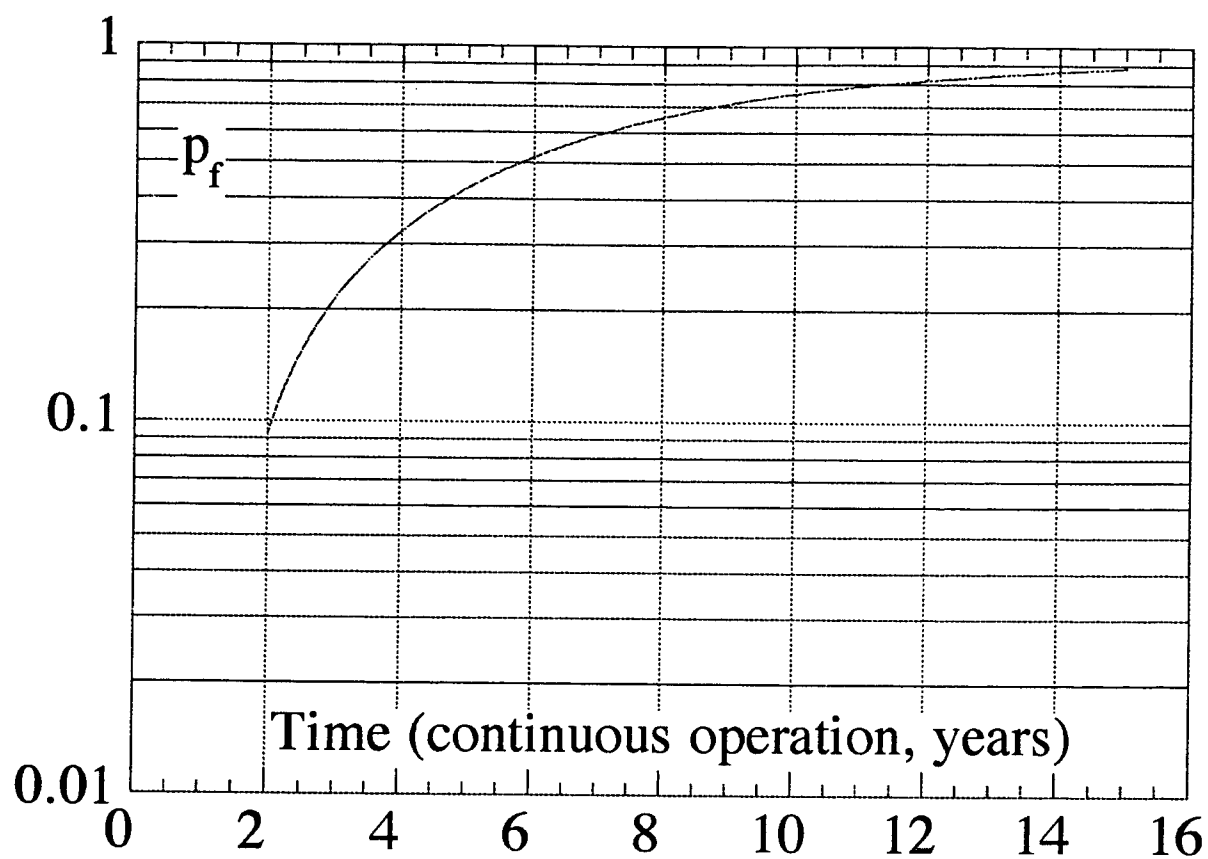
Figure 7.27 Probability of Fatigue Cracking as a Function of Time

Cruiser 1 Original hatch opening

Case 2   Cruiser 1 Modified Hatch Opening

Commentary:

As a result of fatigue problems with the original hatch opening design, a modification was required. A thicker deck plate insert surrounding the hatch opening was provided along with a plate welded to the face of the opening for reinforcement.

A perspective of the hatch opening is provided in Figure 7.28. The detail is provided in Figure 7.29. Finite element analysis results indicate an SCF of 1.88. The increase in plate thickness from 0.3125 to 0.50 suggests that an effective SCF of 0.625 be also applied to the deck stresses (based on 0.50 thickness), for a net effective SCF of 1.175.

Here the fatigue strength is devined by the welded joint, and DEn C-curve applies.

Fatigue reliability analysis both with and without a stress endurance limit, is summarized in Table 7.12.

The probability of fatigue cracking as a function of time is given in Figure 7.31.

4" x 1/2" FB COAMING
(CTRD) ALL AROUND

HATCH COVER

HOUSE FRONT

HATCH COAMING

DECK CUTOUT

6" R

BULKHEAD 138

OI LEVEL

[HATCH OI-136-2 AND OI-140-I]

20.4# INSERT
℞ (HY-80)
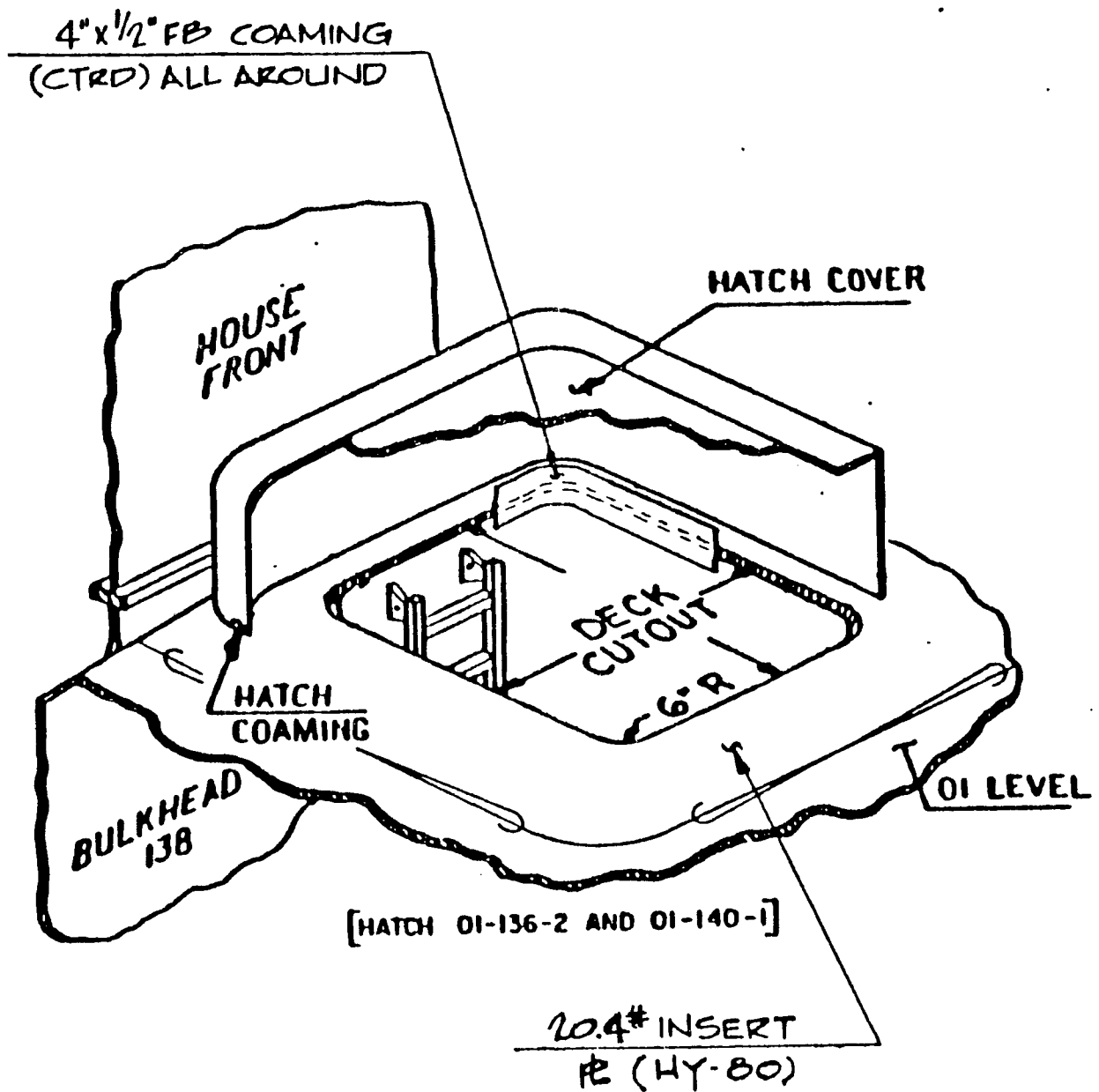
Figure 7.28 Perspective of Modified Hatch of Cruiser 1 Opening.

Figure 7.29 Modified Hatch Opening of Cruiser 1.
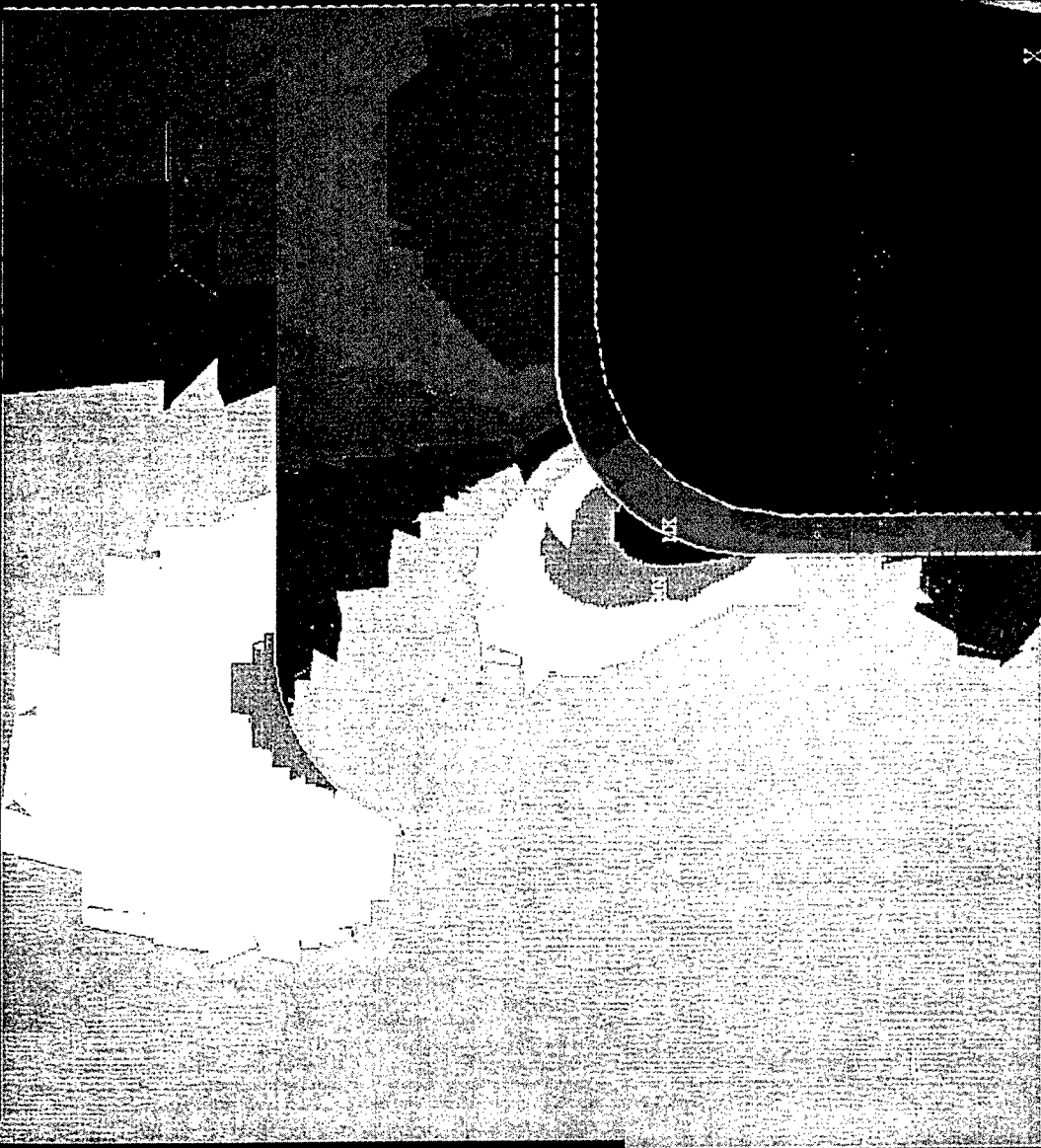
Figure 7.30 Cruiser 1. Stress Concentration at Hatch Opening

Table 7.12
Fatigue Reliability Assessment, Case 2

SHIP	Cruiser 1		
Description of the detail:	Hatch opening (modified)		
Long term distribution of stress ranges in the deck		S_O (ksi)	61.9
		N_T	8.89E7
		ξ	0.923
SCF due to increased plate thickness (plate insert increases t from 5/16 to 1/2)			0.625
SCF due to detail			1.88
Miner's stress		S_e (ksi)	7.08
Stress modeling error		$\tilde{B}$	1.0
		C_B	0.155
Strength modeling error (uncertainty in Miner's rule)		$\tilde{\Delta}$	1.0
		C_Δ	0.3
Fatigue strength (DEn C-curve for continuous welds parallel to the direction of applied stress; welded joint on the faceplate)		m	3.5
		$\tilde{A}$ (ksi units)	1.25E11
		C_A	0.50
RELIABILITY ASSESSMENT	Safety Index, β		0.514
	Probability of Failure, p_f		0.30

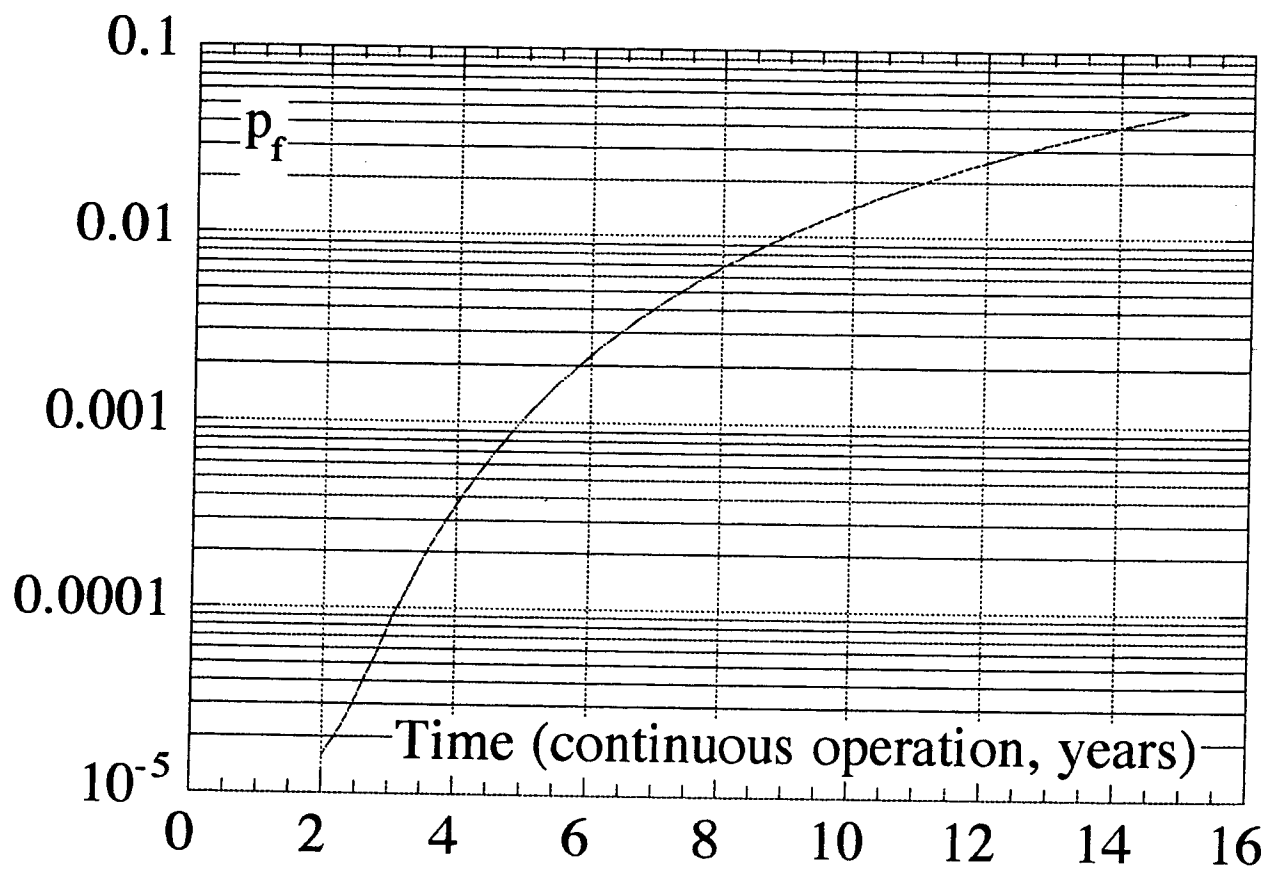| RELIABILITY ASSESSMENT (including stress endurance limit)		
	Stress endurance limit, S_Q (ksi)	14.8
	Safety index, β	1.65
	Probability of failure, p_f	0.049

Figure 7.31 Probability of Fatigue Cracking as a Function of Time

Cruiser 1 Modified hatch opening

Case 3   Cruiser 1 Original Deck House Corner

Commentary:

Fatigue cracks were developed at the deck house corner (region of confluence of the deck house, the deck, and the side shell). As a result, the detail was modified to improve the fatigue strength.

A perspective of the original detail is provided in Figure 7.32. Results of the finite element analysis is presented in Figure 7.33.

It was somewhat unclear as to where the peak stresses occurred, but it was assumed that the vulnerable spot was the toe of the weld between the deck and the deck house frame, with the stresses being orthogonal to the weld. Thus the DEn F-Curve would apply.

Fatigue reliability analysis, both with and without a stress endurance limit, is summarized in Table 7.13.

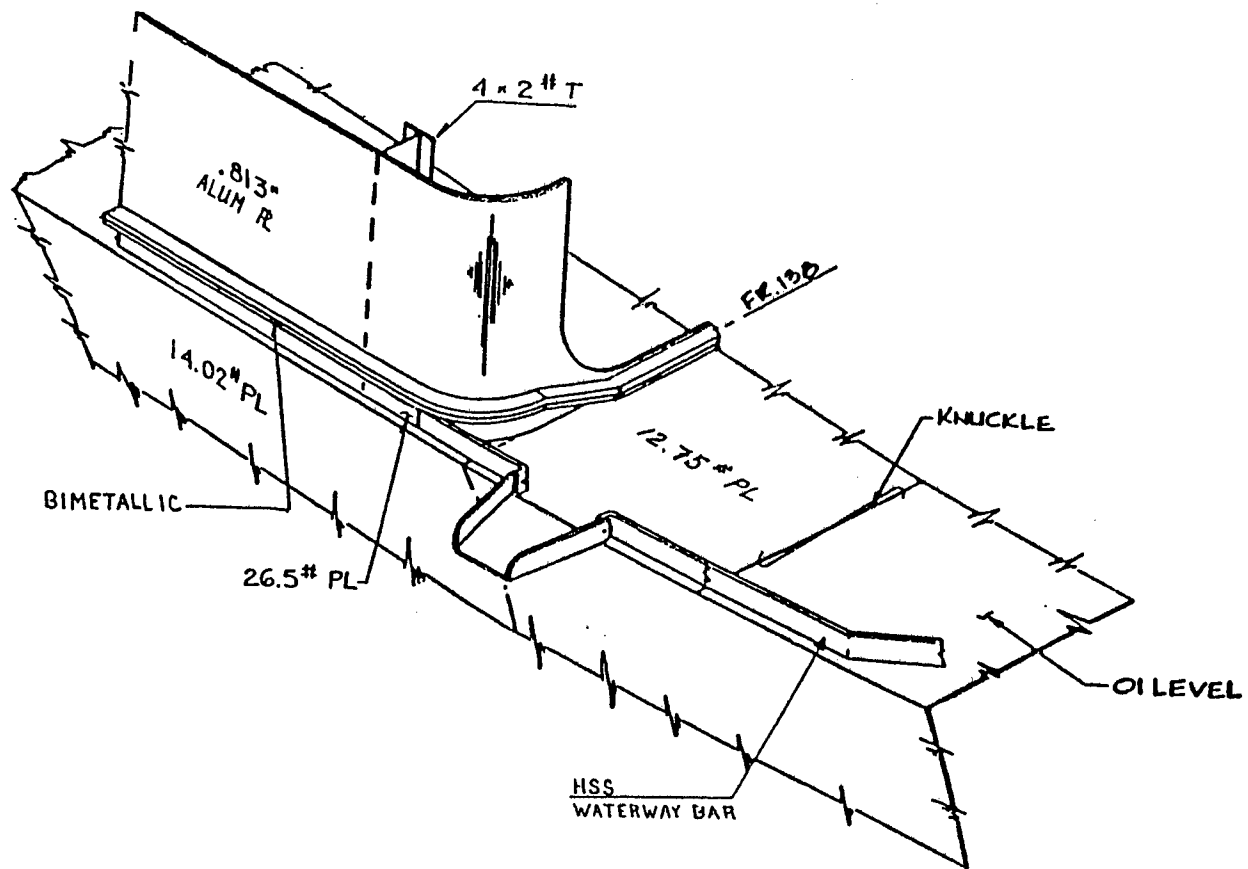The probability of fatigue cracking as a function of time is given in Figure 7.34.

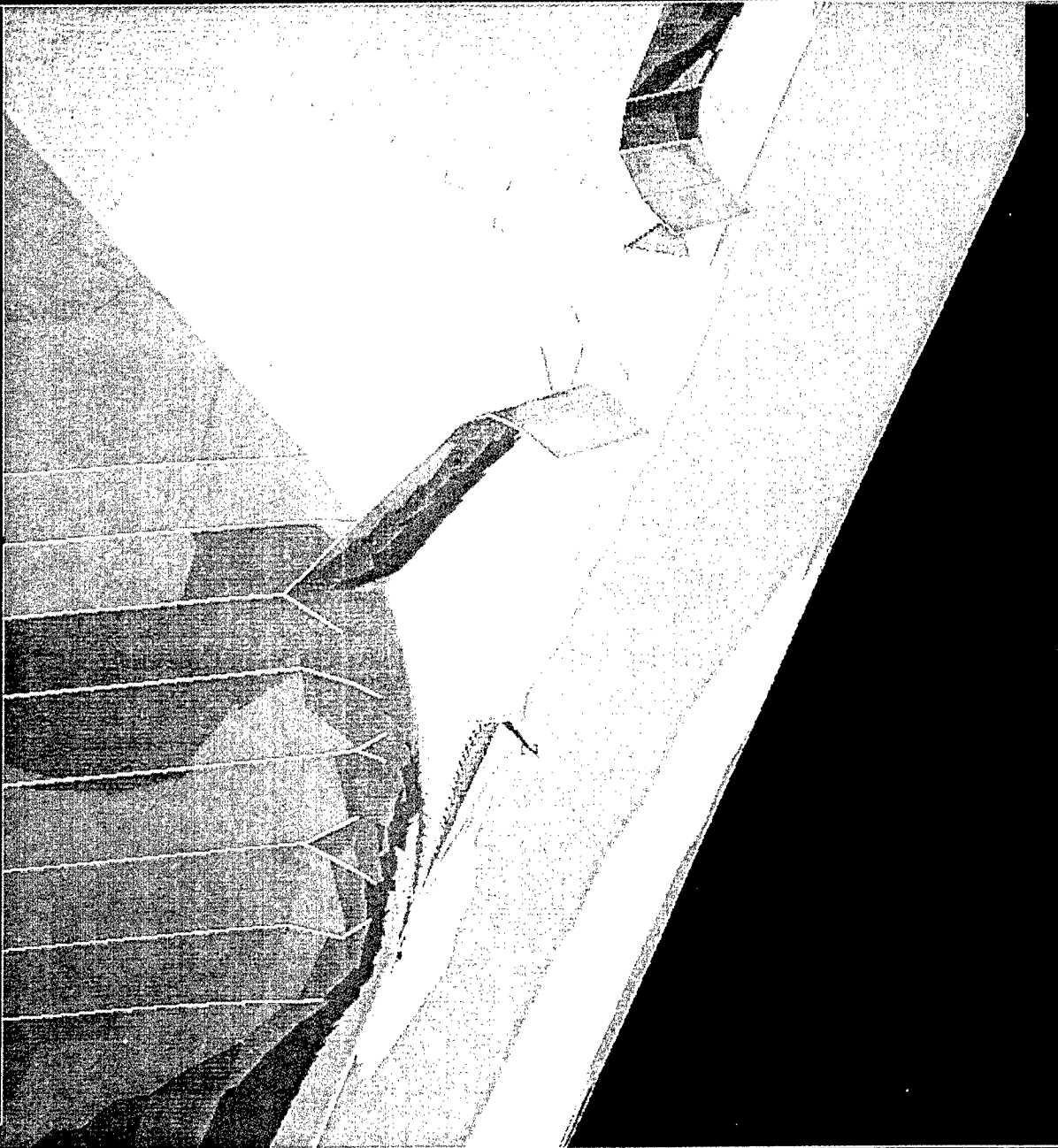Figure 7.32 Perspective of Original Deck House Corner of Cruiser 1.

Figure 7.33 Cruiser 1. Stress Analysis of Original Deck House Corner

Table 7.13
Fatigue Reliability Assessment, Case 3

SHIP	Cruiser 1		
Description of the detail:	Deck house corner (original)		
Long term distribution of stress ranges in the deck		S_O (ksi)	61.9
		N_T	8.89E7
		ξ	0.923
SCF due to increased plate thickness			1.0
SCF due to detail			.968
Miner's stress		S_e (ksi)	5.19
Stress modeling error		$\widetilde{B}$	1.0
		C_B	0.155
Strength modeling error (uncertainty in Miner's rule)		$\widetilde{\Delta}$	1.0
		C_Δ	0.3
Fatigue strength (DEn F-curve for weld attachments to plate; stress perpendicular to weld.)		m	3.0
		$\widetilde{A}$ (ksi units)	5.28E9
		C_A	0.54
RELIABILITY ASSESSMENT			
	Safety Index, β		-1.15
	Probability of Failure, p_f		0.87

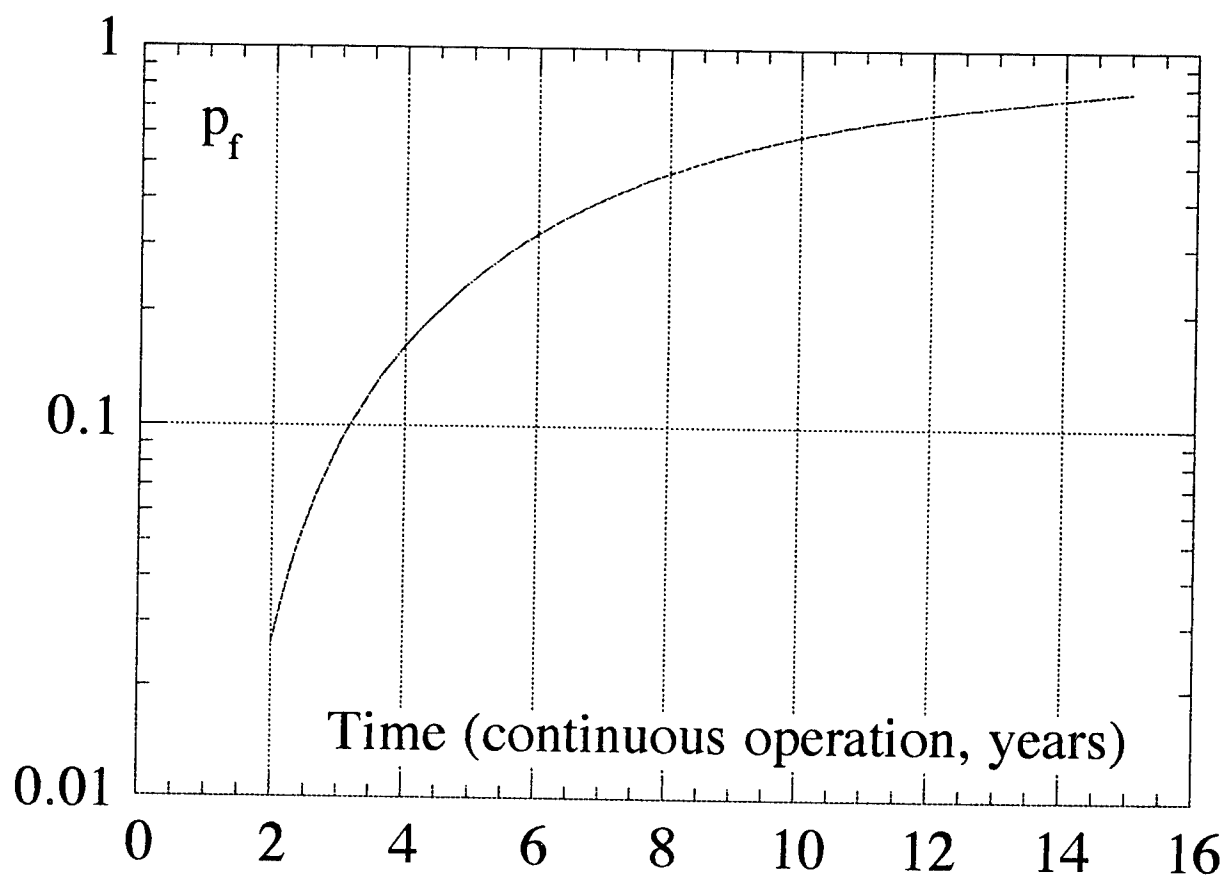| RELIABILITY ASSESSMENT (including stress endurance limit)		
	Stress endurance limit, S_Q (ksi)	8.1
	Safety Index, β	-0.78
	Probability of Failure, p_f	0.78

Figure 7.34 Probability of Faltigue Cracking as a Function of Time

Cruiser 1 Original deck house corner

Case 4   Cruiser 1, Modified Deck House Corner

Commentary:

Modifications were made to the deck house corner after fatigue problems were experienced with the original design. Inserts were provided to the deck to increase the thickness from 0.3125 to 0.75 inches, and the side shell to increase the thickness from 0.3436 to 0.75. There were also changes made to the detail at the node. A perspective of the detail is shown in Figure 7.35.

The effective SCF includes the product of the reduction in stress due to increased deck thickness of $0.3125/0.75 = 0.4167$ and the SCF $= 1.28$ due to the detail. It is assumed that the fatigue sensitive point is at the toe of the weld between the deck and the deck house frame. Finite element analysis results are shown in Figure 7.14.

Again the DEn F-Curve would apply.

Fatigue reliability analysis, both with and without a stress endurance limit, is summarized in Table 7.14.

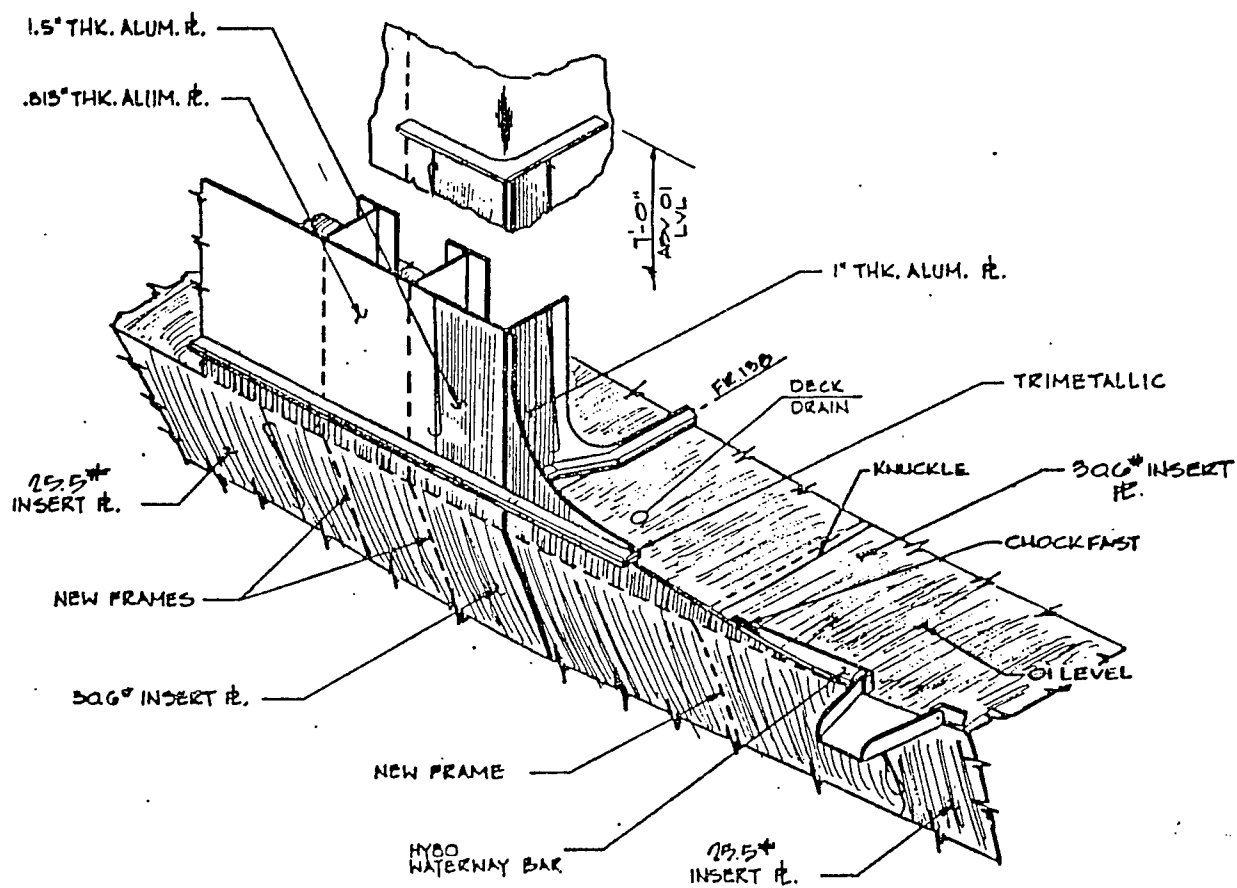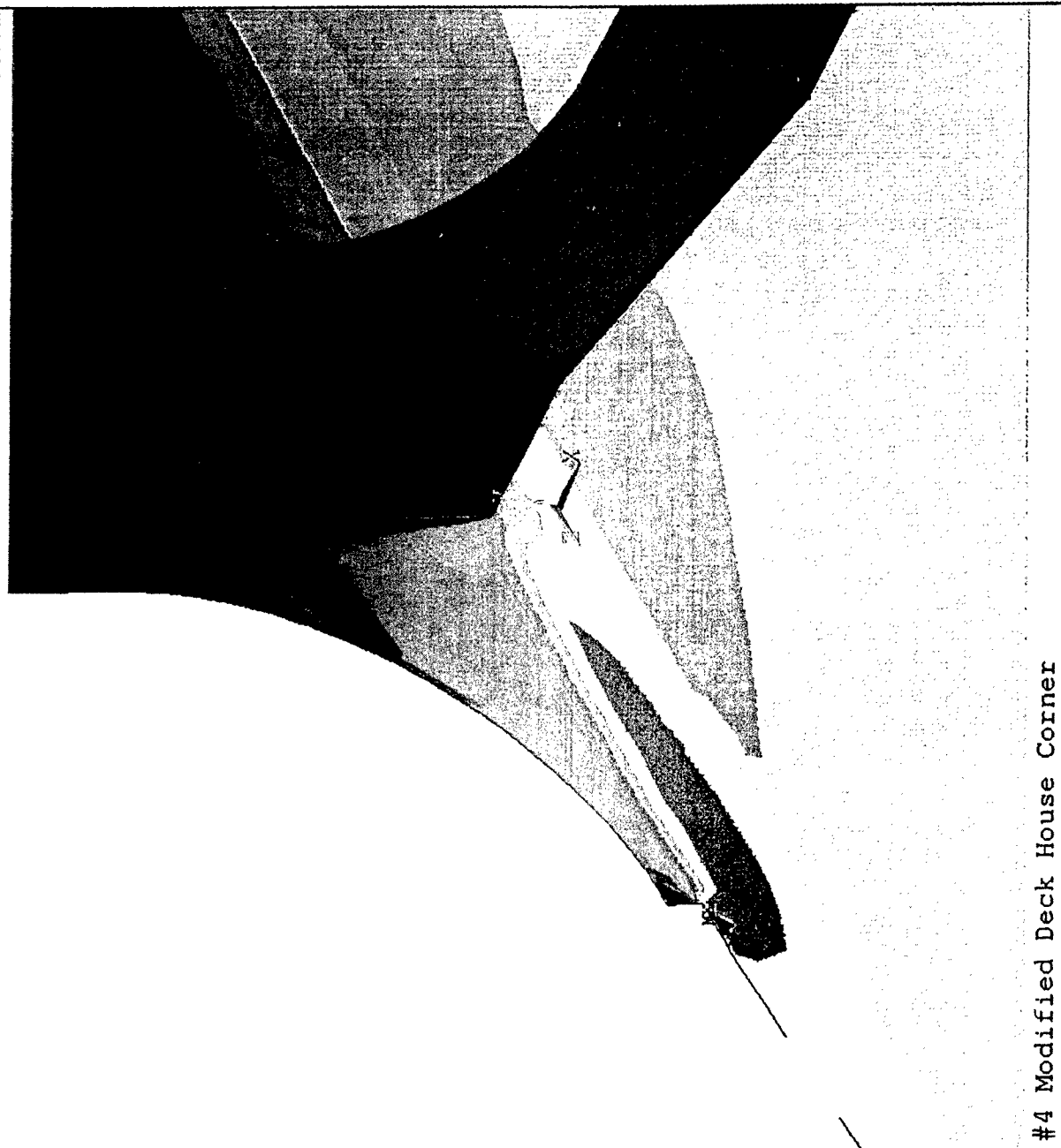The probability of fatigue cracking as a function of time is given in Figure 7.37.

Figure 7.35 Perspective of Modified Deck House Corner of Cruiser 1

Figure 7.36 Cruiser 1. Stress Analysis of Modified Deck House Corner

Table 7.14
Fatigue Reliability Assessment, Case 4

SHIP	Cruiser 1		
Description of the detail:	Deck house corner (modified)		
Long term distribution of stress ranges in the deck		S_O (ksi)	61.9
		N_T	8.89E7
		ξ	0.923
SCF due to increased plate thickness (insert increases t from 5/16 to 3/4)			0.417
SCF due to detail			1.28
Miner's stress		S_e (ksi)	2.87
Stress modeling error		$\tilde{B}$	1.0
		C_B	0.155
Strength modeling error (uncertainty in Miner's rule)		$\tilde{\Delta}$	1.0
		C_Δ	0.3
Fatigue strength (DEn F-curve for weld attachments to plate; stress perpendicular to weld.)		m	3.0
		$\tilde{A}$ (ksi units)	5.28E9
		C_A	0.54
RELIABILITY ASSESSMENT			
	Safety Index, β		0.73
	Probability of Failure, p_f		0.23

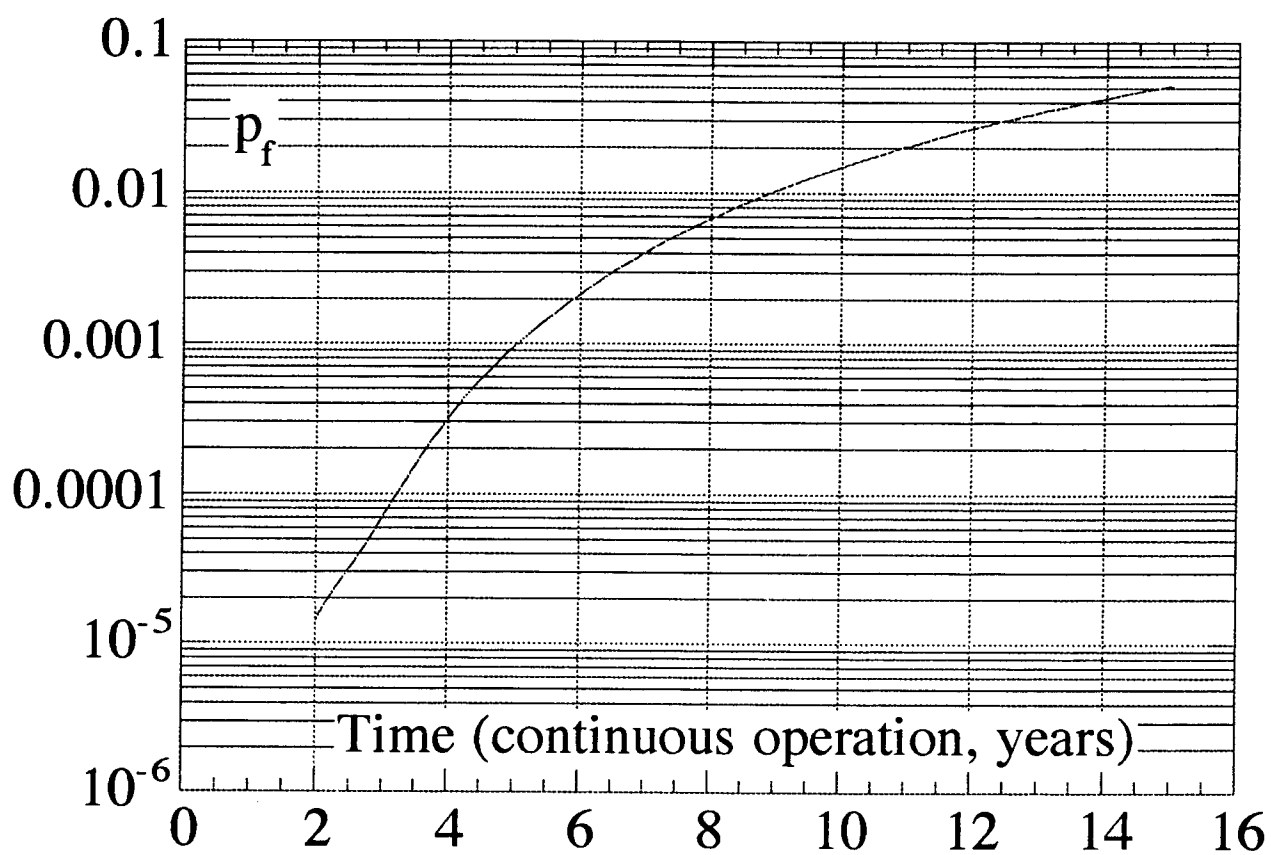| RELIABILITY ASSESSMENT (including stress endurance limit)		
	Stress endurance limit, S_Q (ksi)	8.1
	Safety index, β	1.62
	Probability of failure, p_f	0.05

Figure 7.37 Probability of Fatigue Cracking as a Function of Time

Cruiser 1. Modified deck house corner

Case 5   Cruiser 2 Deck House Corner

Commentary:

On the basis of experience with Cruiser 2, it is assumed that the deck house corner of Cruiser 2 is a point of fatigue vulnerability. This detail is similar to the Cruiser 1 original design with the following exceptions: (a) the deck house is set back to frame 142 (from 138 on the 52), (b) the deck house front is angled forward from the side shell at an angle of about 20°, (c) the deck plate thickness is 0.50 inches.

A top view sketch of the detail is given in Figure 7.38. Finite element analysis results are given in Figure 7.39.

Fatigue reliability analysis, both with and without a stress endurance limit, is summarized in Table 7.15.

The probability of fatigue cracking as a function of time is given in Figure 7.40.
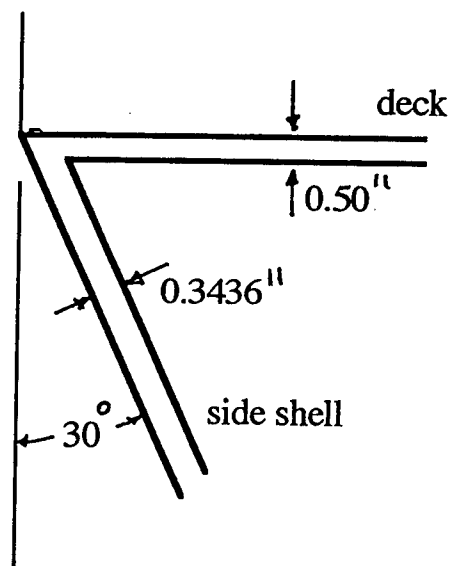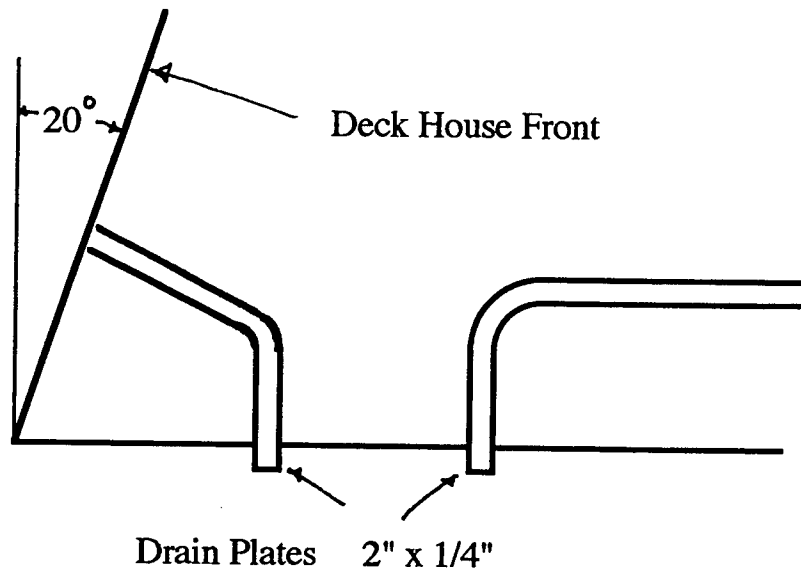
Deck Plate Thickness = 0.50"

Deck House Front

20°

Drain Plates   2" x 1/4"

deck

0.50"

0.3436"

side shell

30°

Figure 7.38 Sketch of Deck House Corner for Cruiser 2

ANSYS 5.2
DEC 29 1995
10:52:24
NODAL SOLUTION
STEP=1
SUB =1
TIME=1
SX   (AVG)
TOP
RSYS=0
DMX =.319E-05
SMN =.110774
SMNB=-1.329
SMX =3.492
SMXB=6.969

.110774
.486498
.862223
1.238
1.614
1.989
2.365
2.741
3.117
3.492

ROM Engineering, Inc. P.O. Box 65170 (520) 299-4574
                       Tucson, AZ 85728 (520) 299-4574 fax
                                        rome@azstarnet.com
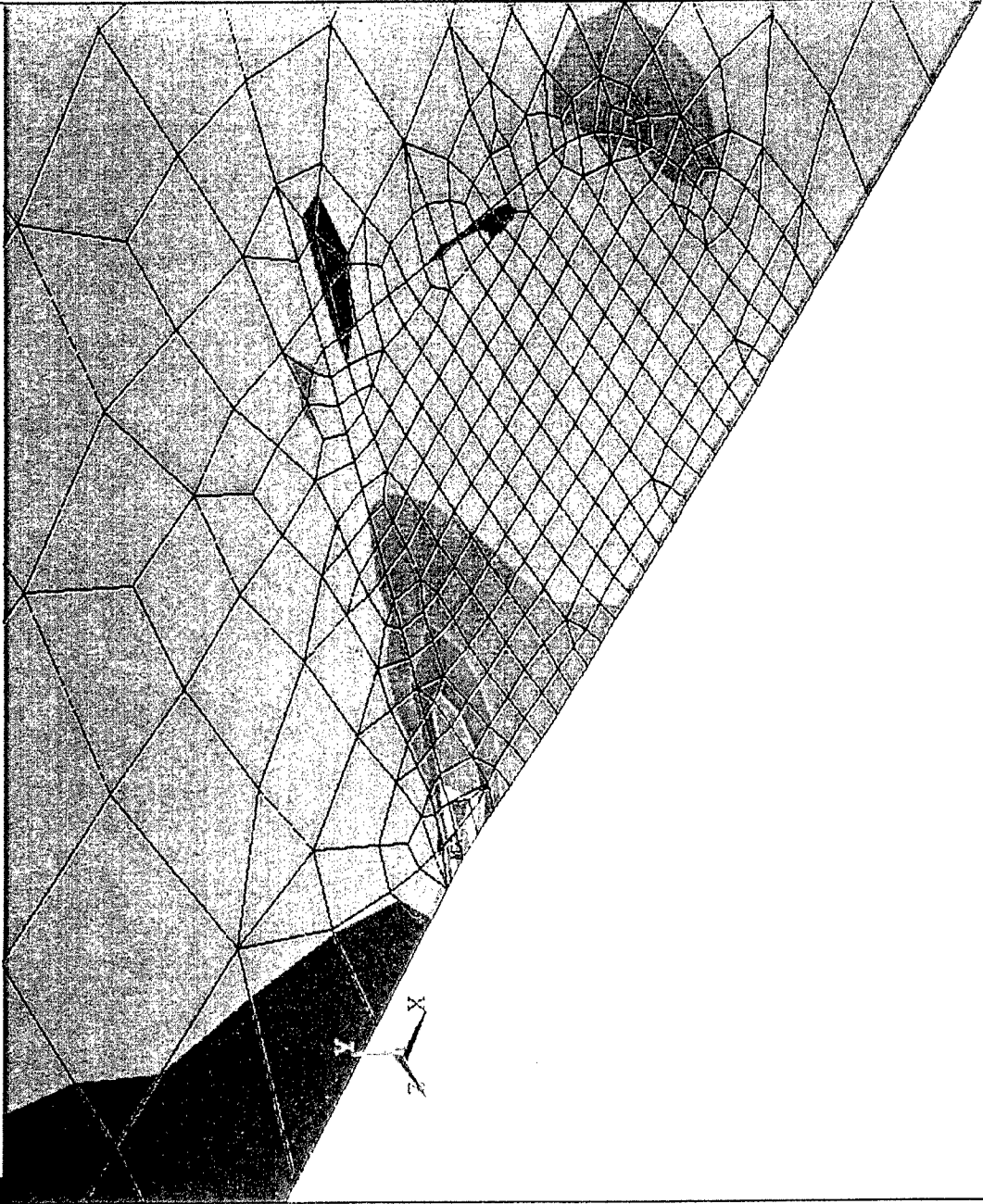
#5 Modified Deck House Corner 2, Nodal Stress Concentration in Deck

Figure 7.39 Cruiser 2. Stress Analysis of Deck House Corner

7-74

Table 7.15
Fatigue Reliability Assessment, Case 5

SHIP	Cruiser 2		
Description of the detail:	Deck house corner		
Long term distribution of stress ranges in the deck		S_O (ksi)	39.0
		N_T	9.56E7
		ξ	0.822
SCF due to increased plate thickness			1.00
SCF due to detail			2.00[*]
Miner's stress		S_e (ksi)	5.49
Stress modeling error		$\tilde{B}$	1.0
		C_B	0.155
Strength modeling error (uncertainty in Miner's rule)		$\tilde{\Delta}$	1.0
		C_Δ	0.3
Fatigue strength (DEn F-curve for weld attachments to plate; stress perpendicular to weld.)		m	3.0
		$\tilde{A}$ (ksi units)	5.28E9
		C_A	0.54
RELIABILITY ASSESSMENT			
	Safety Index, β		-1.47
	Probability of Failure, p_f		0.93

RELIABILITY ASSESSMENT (including stress endurance limit)		
	Stress endurance limit, S_Q (ksi)	8.1
	Safety index, β	-0.15
	Probability of failure, p_f	0.56

---

[*] The FEM analysis of Figure 7.39 suggests an "infinite" stress at the sharp notch in the model. It was assumed that a SCF = 2.0 was a more realistic description of the fatigue stresses in this case.
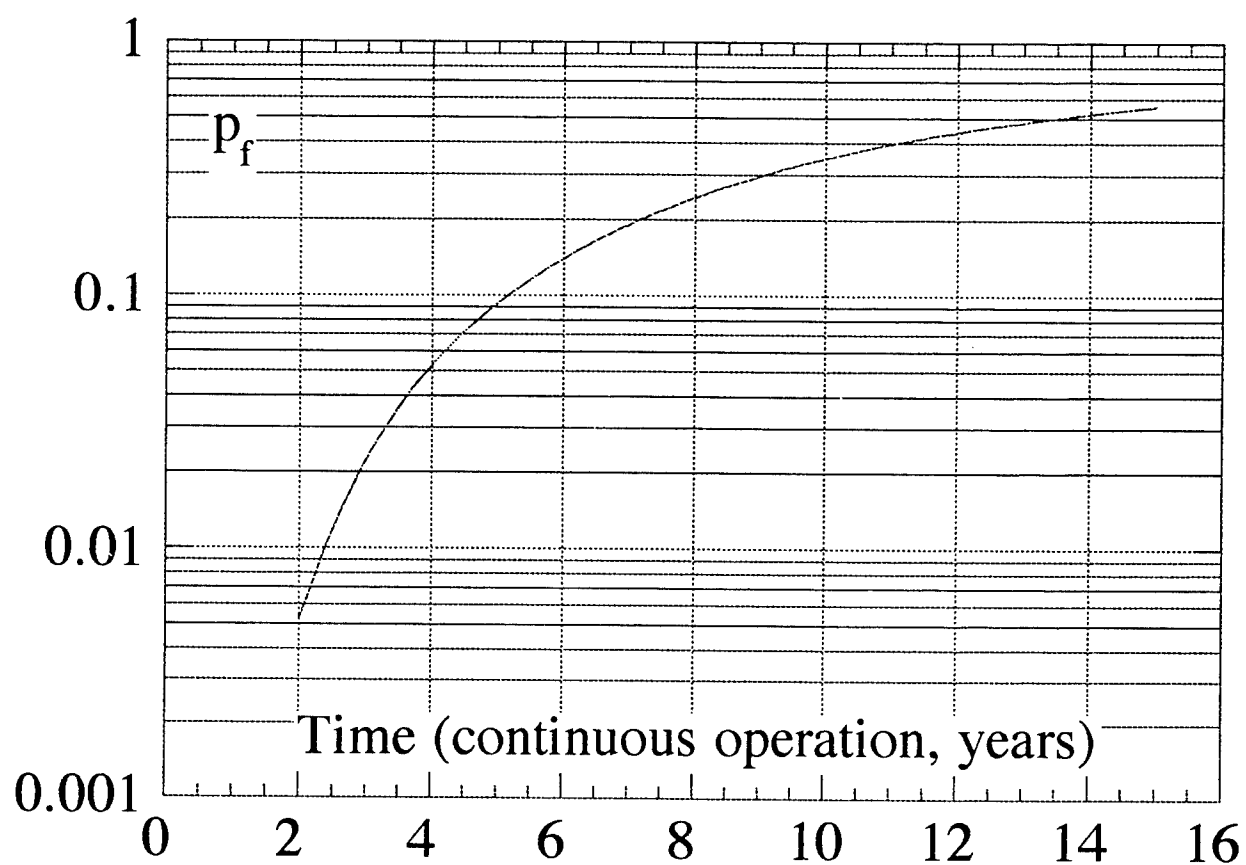
Figure 7.40 Probability of Fatigue Cracking as a Function of Time

Cruiser 2. Deck house corner

Case 6   Cruiser 2 Hatch Opening

Commentary:

Fatigue reliability analysis was performed on a hatch opening forward of the deck house. This is not a detail for which fatigue has been a problem.

A sketch of the detail is given in Figure 7.41. Results of the finite element analysis are given in Figure 7.42.

Because the welds are parallel to the direction of applied stresses, the DEn C-curve will be used.

Fatigue reliability analysis, both with and without a stress endurance limit, is summarized in Table 7.16.

The probability of fatigue cracking as a function of time is given in Figure 7.43.

Deck plate thickness = 0.50" (1/2)

Radius = 5.5"

32.75"

Faceplate

32.75"

A

A

Faceplate

0.3125"

6.5"

1"
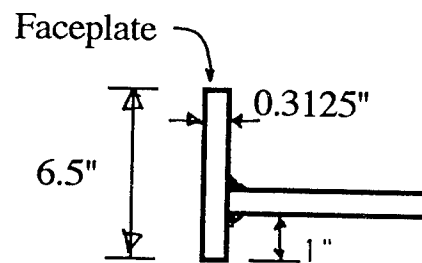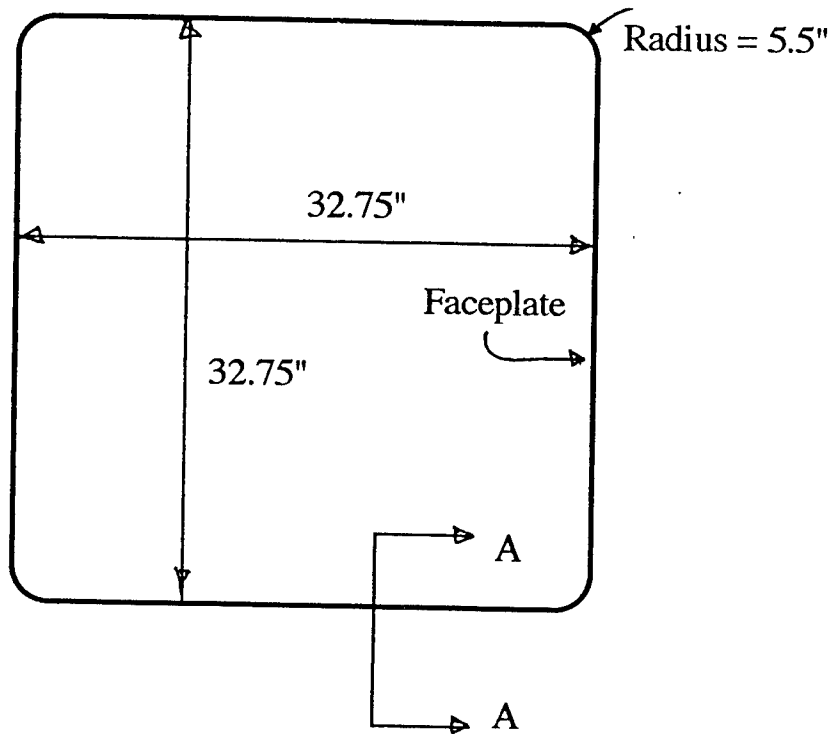
Section A-A

Figure 7.41 Hatch Opening of Cruiser 2

```
ANSYS 5.2
DEC 28 1995
14:03:16
NODAL SOLUTION
STEP=1
SUB =1
TIME=1
SY        (AVG)
TOP
RSYS=0
DMX =.114E-04
SMN =-.161426
SMNB=-.182935
SMX =2.56
SMXB=2.625
     -.161426
     .140992
     .443411
     .745829
     1.048
     1.351
     1.653
     1.956
     2.258
     2.56
```
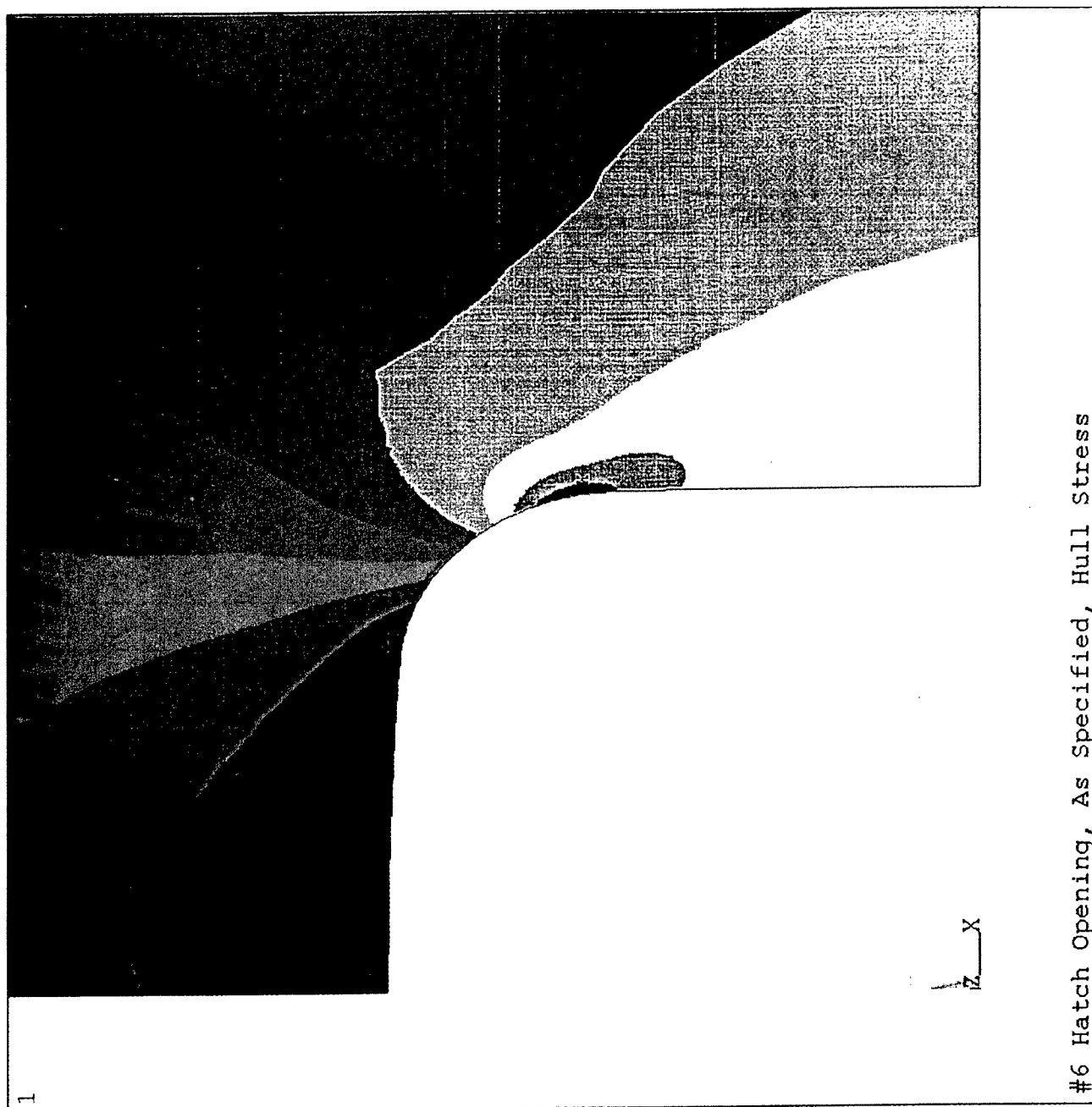
1

#6 Hatch Opening, As Specified, Hull Stress

Figure 7.42 Cruiser 2. Stress Concentration at Hatch Opening

Table 7.16
Fatigue Reliability Assessment, Case 6

SHIP	Cruiser 2		
Description of the detail: Hatch opening			
Long term distribution of stress ranges in the deck		S_O (ksi)	39.0
		N_T	9.56E7
		ξ	0.822
SCF due to increased plate thickness			1.0
SCF due to detail			2.56
Miner's stress		S_e (ksi)	8.03
Stress modeling error		$\tilde{B}$	1.0
		C_B	0.155
Strength modeling error (uncertainty in Miner's rule)		$\tilde{\Delta}$	1.0
		C_Δ	0.3
Fatigue strength (DEn C-curve for continuous welds parallel to the direction of applied stress.)		m	3.5
		$\tilde{A}$ (ksi units)	1.25E11
		C_A	0.50
RELIABILITY ASSESSMENT			
	Safety Index, β		-0.149
	Probability of Failure, p_f		0.56

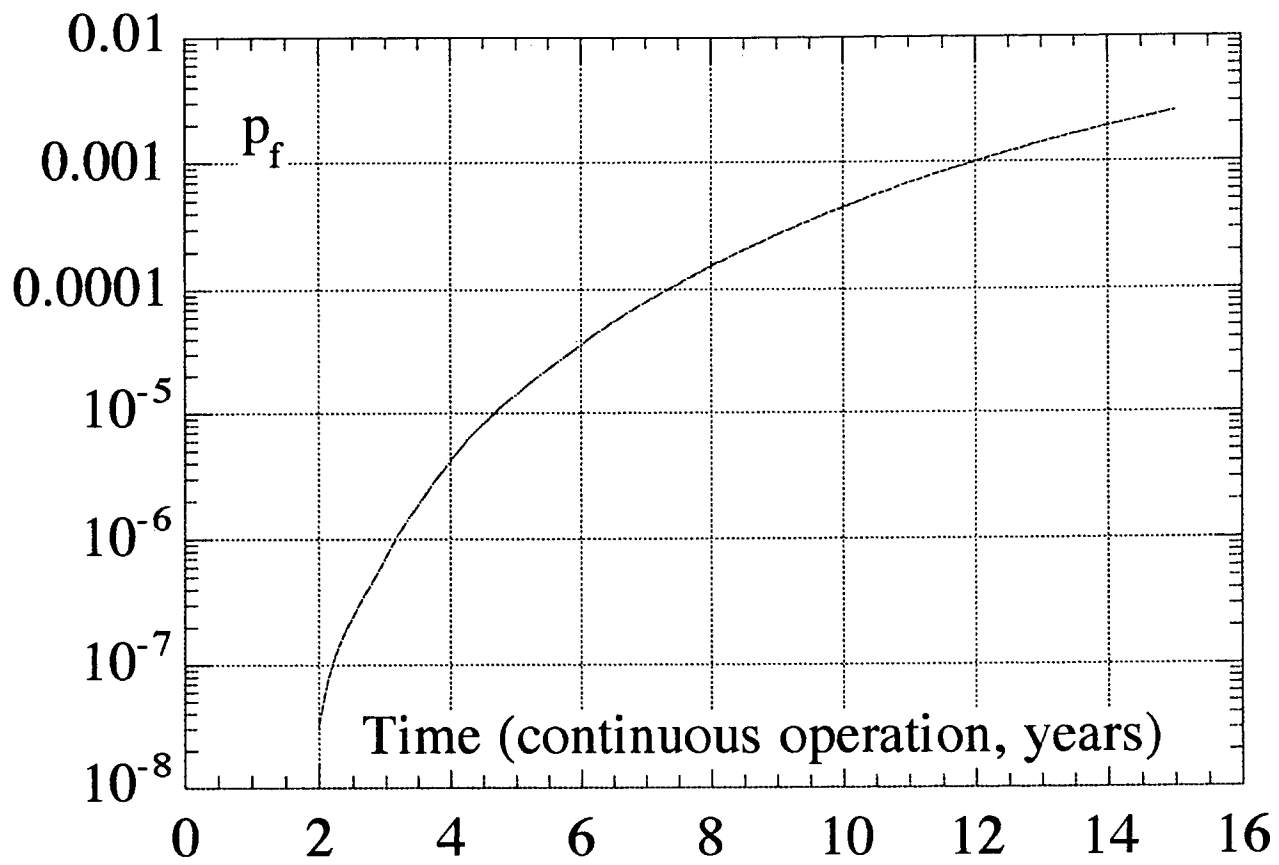| RELIABILITY ASSESSMENT (including stress endurance limit)		
	Stress endurance limit, S_Q (ksi)	14.8
	Safety index, β	2.80
	Probability of failure, p_f	0.0025

Figure 7.43 Probability of Fatigue Cracking as a Function of Time

Cruiser 2. Hatch opening

Case 7   Tanker Longitudinal Stiffeners in Deck

Commentary:

Fatigue reliability analyses were performed for the welded joints in the longitudinal stiffeners at the deck where the fatigue stresses are expected to be a maximum.* The detail considered is shown in Figure 7.44.

Two sites for fatigue are considered:

- Case 7a   Fatigue in the welds which are parallel to the direction of loading and for which the DEn C-curve applies.

- Case 7b   Fatigue in the welds which are perpendicular to the fatigue loading and for which the DEn F-curve applies. Clearly this case will have the lower reliability.

Fatigue reliability analysis for both cases are summarized in Tables 7.16 and 7.17. Analysis with and without a stress endurance limit was performed for both cases.

The probability of fatigue cracking as a function of time is given for Case 7a in Figure 7.45 and for Case 7b in Figure 7.46.

---

* For the TAPS routes where the wave climate is relatively severe, fatigue problems have been experienced in the side shell where wave bending stresses are small but oscillatory pressure loadings may be very significant.
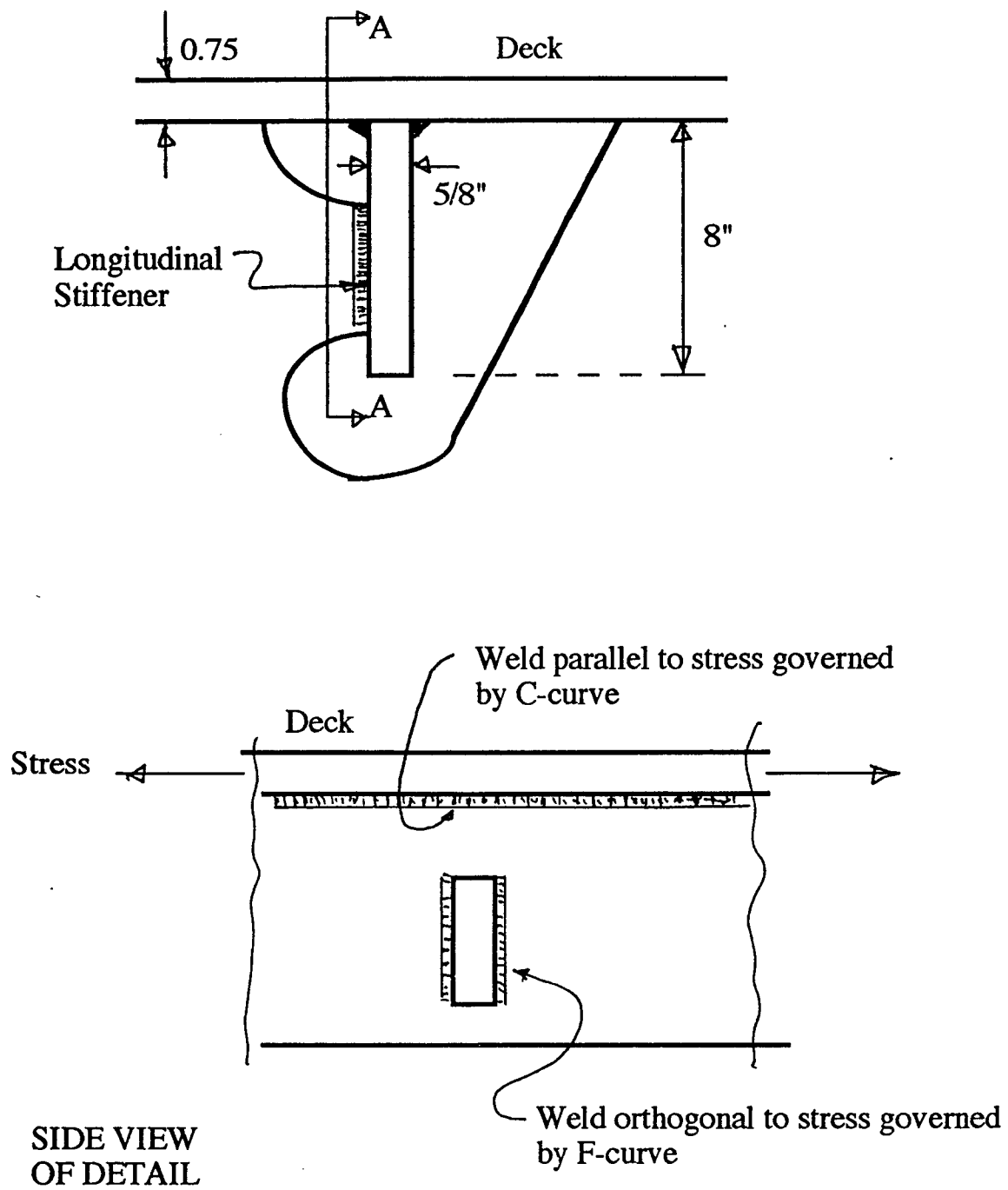
0.75

Deck

5/8"

8"

Longitudinal
Stiffener

Weld parallel to stress governed
by C-curve

Deck

Stress

SIDE VIEW
OF DETAIL

Weld orthogonal to stress governed
by F-curve

Figure 7.44 Welded Detail in Tanker

Table 7.16
Fatigue Reliability Assessment, Case 7a

SHIP	Tanker		
Description of the detail:	Weld in longitudinal deck stiffener parallel to the direction of stress		
Long term distribution of stress ranges in the deck		S_O (ksi)	48.0
		N_T	5.99E7
		ξ	0.918
SCF due to increased plate thickness			1.0
SCF due to detail			1.0
Miner's stress		S_e (ksi)	4.74
Stress modeling error		$\tilde{B}$	1.0
		C_B	0.155
Strength modeling error (uncertainty in Miner's rule)		$\tilde{\Delta}$	1.0
		C_Δ	0.3
Fatigue strength (DEn C-curve)		m	3.5
		$\tilde{A}$ (ksi units)	1.25E11
		C_A	0.50
RELIABILITY ASSESSMENT			
	Safety Index, β		2.83
	Probability of Failure, p_f		2.3E-3

RELIABILITY ASSESSMENT (including stress endurance limit)		
	Stress endurance limit, S_Q (ksi)	14.8
	Safety index, β	4.64
	Probability of failure, p_f	1.7E-6

Table 7.17
Fatigue Reliability Assessment, Case 7b

SHIP	Tanker		
Description of the detail:	Weld in longitudinal deck stiffener perpendicular to the direction of stress		
Long term distribution of stress ranges in the deck		S_O (ksi)	48.0
		N_T	5.99E7
		ξ	0.918
SCF due to increased plate thickness			1.0
SCF due to detail			1.0
Miner's stress		S_e (ksi)	4.22
Stress modeling error		$\tilde{B}$	1.0
		C_B	0.155
Strength modeling error (uncertainty in Miner's rule)		$\tilde{\Delta}$	1.0
		C_Δ	0.3
Fatigue strength (DEn F-curve)		m	3.0
		$\tilde{A}$ (ksi units)	5.28E9
		C_A	0.54
RELIABILITY ASSESSMENT			
	Safety Index, β		0.209
	Probability of Failure, p_f		0.417

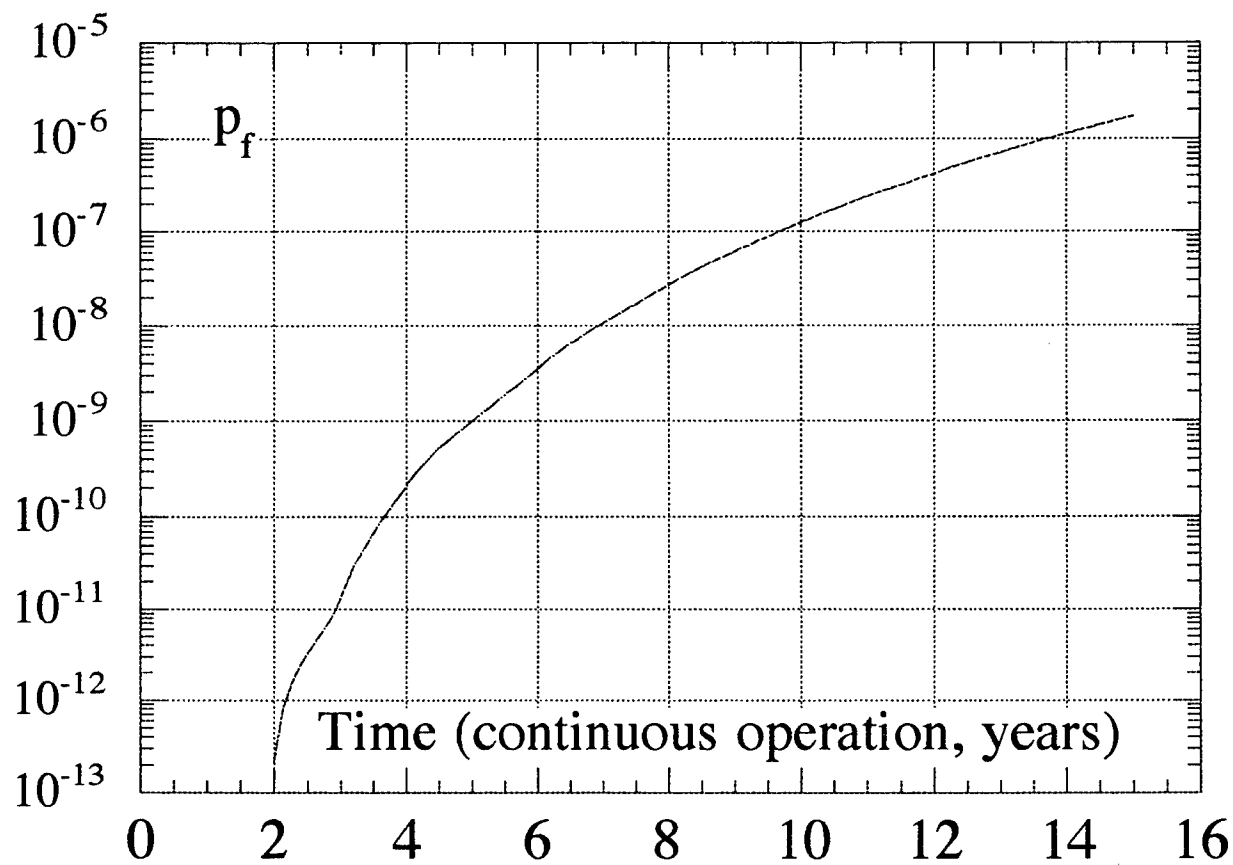| RELIABILITY ASSESSMENT (including stress endurance limit)		
	Stress endurance limit, S_Q (ksi)	8.1
	Safety Index, β	0.91
	Probability of Failure, p_f	0.18

Figure 7.45 Probability of Fatigue Cracking as a Function of Time

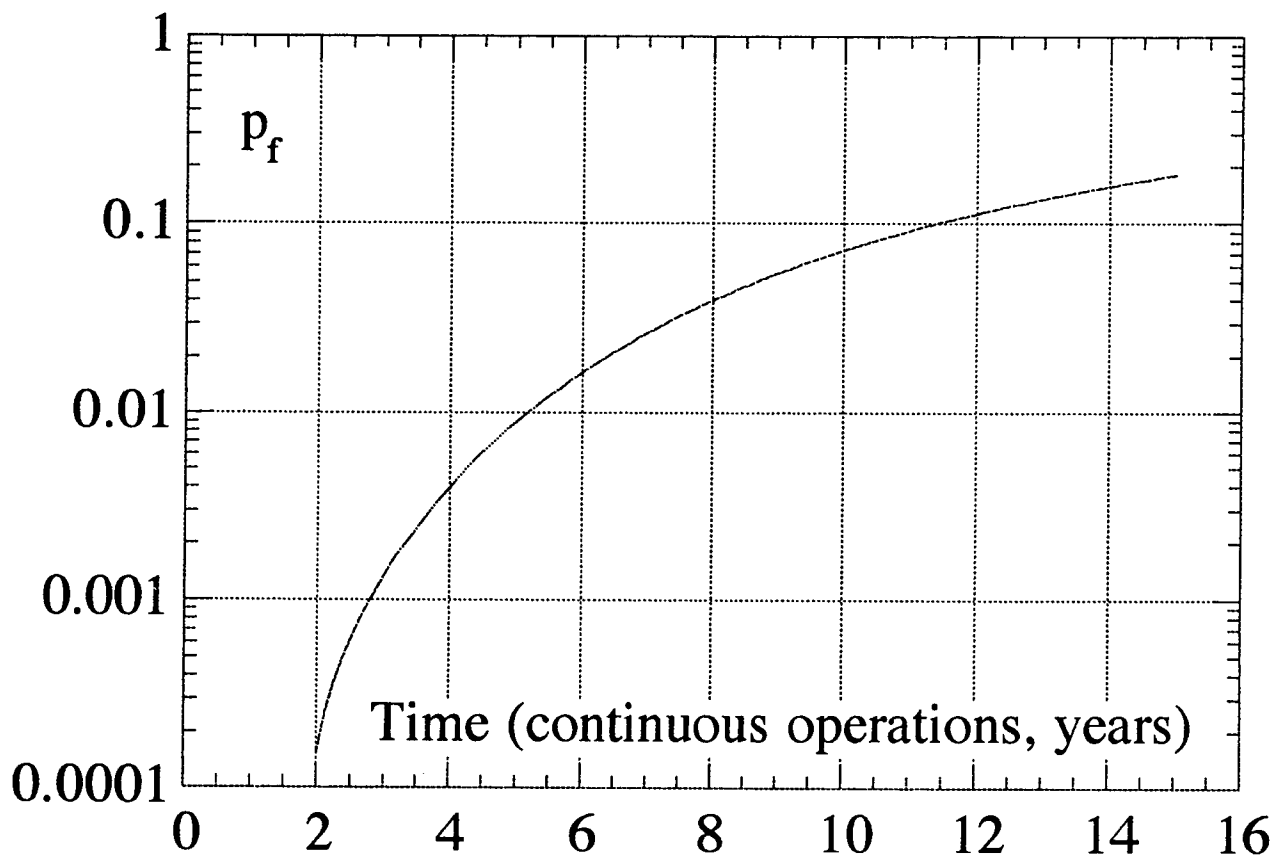Tanker. Weld parallel to direction of stress

Figure 7.46 Probability of Fatigue Cracking as a Function of Time

Tanker. Weld perpendicular to direction of stress

Case 8   SL-7 Original Hatch Opening

Commentary:

Early in the operational lives, the SL-7 Class container ships experienced fatigue at the corners of the hatch openings. Failure analyses suggested a failure mode associated with torsional stresses. Because of the deck openings, the polar moment of inertia and therefore the torsional stiffness was reduced. Fatigue was observed at the corner of the forward (closest to the bow) hatch.* The polar moment of inertial is a minimum there, and therefore torsional induced stresses are a maximum.

In this analysis, it is assumed that the ship has sufficient torsional stiffness so that the maximum stresses occur at midship and are associated with wave induced bending.

In a fatigue analysis performed as an SSC project (SSC-338), the SCF at a hatch corner associated with hull vertical plane bending was 2.2.

The hatch opening has a faceplate welded to the deck. Therefore, fatigue is assumed to occur first in these welded joints, whose direction is parallel to the direction of stress. Therefore, the DEn C-curve applies.

Fatigue reliability analysis, with and without a stress endurance limit, is summarized in Table 7.17.

The probability of fatigue cracking as a function of time is given in Figure 7.47.

---

* The ship which experienced fatigue problems and which was studied was the SEALAND McLEAN.

Table 7.17
Fatigue Reliability Assessment, Case 8

SHIP	SL-7		
Description of the detail: Hatch opening (original)			
Long term distribution of stress ranges in the deck	S_O (ksi)	39.5	
	N_T	5.56E7	
	ξ	0.888	
SCF due to increased plate thickness		1.0	
SCF due to detail		2.2	
Miner's stress	S_e (ksi)	8.19	
Stress modeling error	$\tilde{B}$	1.0	
	C_B	0.155	
Strength modeling error (uncertainty in Miner's rule)	$\tilde{\Delta}$	1.0	
	C_Δ	0.3	
Fatigue strength (DEn C-curve for continuous welds parallel to the direction of applied stress)	m	3.5	
	$\tilde{A}$ (ksi units)	1.25E11	
	C_A	0.50	
RELIABILITY ASSESSMENT			
	Safety Index, β		0.46
	Probability of Failure, p_f		0.32

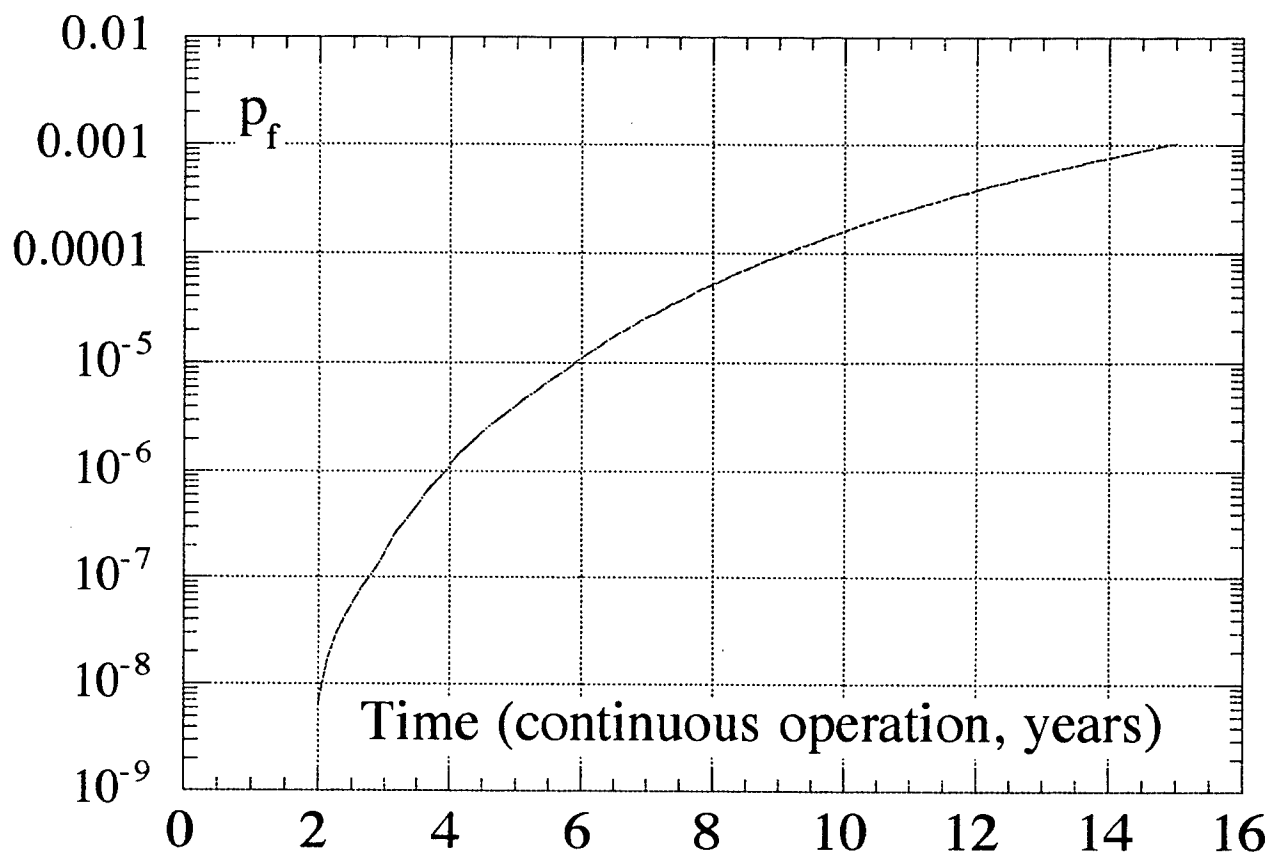| RELIABILITY ASSESSMENT (including stress endurance limit)		
	Stress endurance limit, S_Q (ksi)	14.8
	Safety Index, β	3.07
	Probability of Failure, p_f	0.001

Figure 7.47 Probability of Fatigue Cracking as a Function of Time

SL-7. Original hatch opening

Case 9   SL-7 Modified Hatch Opening

Commentary:

In an attempt to mitigate the fatigue problems associated with the hatch opening, the hatch opening was modified by reinforcing the faceplate and providing doublers.* The revised structure then had an estimated SCF at the hatch opening of 1.2 (reduced from 2.2).

Again, the DEn C-curve was considered to define the fatigue strength.

Fatigue reliability analysis is summarized in Table 7.18.

When a stress endurance limit is included in the analysis, the computed failure probability is extremely small ($\approx 10^{-9}$).

---

* Actually there were a series of modifications to the structure.

Table 7.18
Fatigue Reliability Assessment, Case 9

SHIP SL-7			
Description of the detail: Hatch opening (modified)			
Long term distribution of stress ranges in the deck		S_0 (ksi)	39.5
		N_T	5.56E7
		ξ	0.888
SCF due to increased plate thickness			1.0
SCF due to detail			1.2
Miner's stress		S_e (ksi)	4.47
Stress modeling error		$\tilde{B}$	1.0
		C_B	0.155
Strength modeling error (uncertainty in Miner's rule)		$\tilde{\Delta}$	1.0
		C_Δ	0.3
Fatigue strength (DEn C-curve for continuous welds parallel to the direction of applied stress)		m	3.5
		$\tilde{A}$ (ksi units)	1.25E11
		C_A	0.50
RELIABILITY ASSESSMENT			
	Safety Index, β		3.20
	Probability of Failure, p_f		6.9E-4

SUMMARY

Results of fatigue reliability assessments of details of the four ships are summarized in Table 7.19. The introduction of the stress endurance limit (SEL) clearly suggests a significant improvement in predicted reliability.

Table 7.19
A Comparison of Reliability Estimates With and Without Stress Endurance Limit

Case	Detail	Without SEL		With SEL	
		β	p_f	β	p_f
1a	Cruiser 1: Original hatch opening, HY-80 data	3.81	6.8E-5	–	–
1b	Cruiser 1: Original hatch opening, DEn B-curve	-2.46	≈1.0	-1.19	0.88
2	Cruiser 1: Modified hatch opening	0.514	0.30	1.65	0.049
3	Cruiser 1: Original deck house corner	-1.15	0.88	-0.78	0.78
4	Cruiser 1: Modified deck house corner	1.24	0.107	1.62	0.05
5	Cruiser 2: Deck house corner	-1.47	0.93	-0.15	0.56
6	Cruiser 2: Hatch opening	-0.149	0.56	2.80	.0025
7a	Tanker: Deck stiffener, weld perp. to stress direction	2.83	2.3E-3	4.64	1.7E-6
7b	Tanker: Deck stiffener, weld perp. to stress direction	0.209	0.417	0.91	0.18
8	SL-7: Original hatch opening	0.46	0.32	3.07	0.001
9	SL-7: Modified hatch opening	3.20	6.9E-4		

7.7 Fatigue Reliability Analysis Using the Munse Data

W. H. Munse has developed a library of welded joint fatigue data; a digest of his library is provided in SSC-318 (Munse, 1983). He has defined 52 different types of welded joints and has an S-N curve plus summary statistics for each. In this "cartoon" approach, not unlike the UK-DEn rules, the analyst will identify the picture associated with his physical problem and then use the corresponding S-N curve.

What is noteworthy about the Munse data is, while it is difficult to match S-N curves to the UK curves, there appears to be very poor agreement between the two. While the international fatigue community has by consensus accepted the UK curves, the Munse data is extensive and is difficult to ignore.

In this analysis, the Munse equivalent C and F curves are identified. The summary statistics are given in Figures 7.48 and 7.49. A plot of the Munse and UK curves, provided in Figure 7.50, illustrates the poor agreement between the two. Note the differences in the F-curves.

The fatigue reliability analysis is now performed substituting the Munse C and F curves for the UK curves where appropriate. A summary of all of the results, i.e., a comparison of safety indices and probabilities of failure from both curves, is provided in Table 7.19.
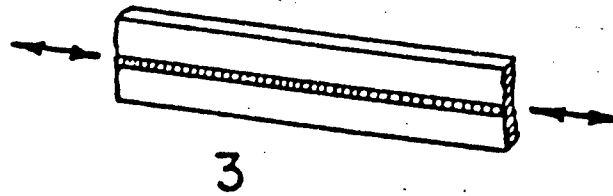
Note: In Case 1b, Cruiser 1 original hatch opening, the flame cut S-N curve of Munse was used. The statistics are,

$$m = 4.805$$
$$\tilde{A} = 6.03E13$$
$$C_A = 0.60$$

and the median curve is given in Figure 7.50.

Munse "C-Curve"

Weld parallel to the direction of the applied stress
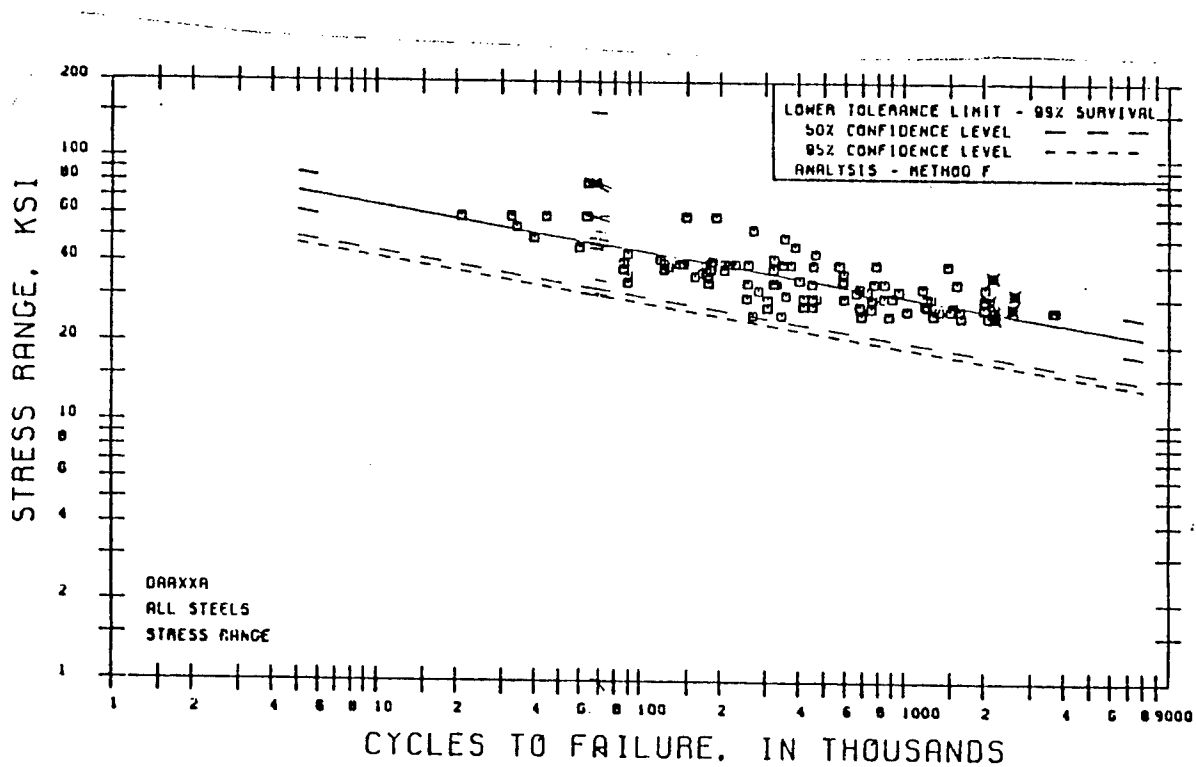

Summary statistics:

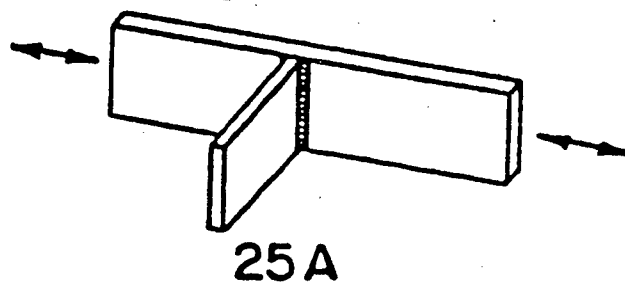$m = 5.95$

$\tilde{A} = 6.31E14$ (ksi units)

$C_A = 0.63$

Detail No. 3

Figure 7.48 The Equivalent Munse C-Curve

Munse "F-Curve"

Weld perpendicular to the direction of the applied stress
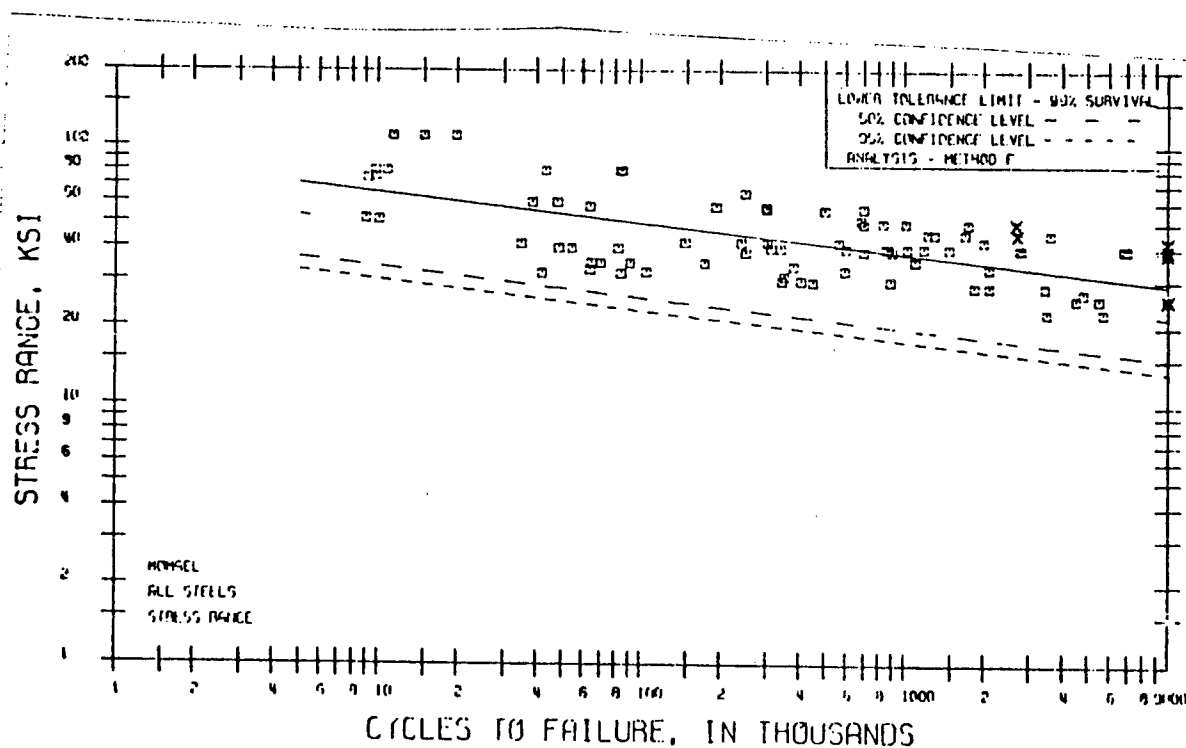

25A

Summary statistics:

$$m = 8.518$$

$$\tilde{A} = 2.95E19 \quad (\text{ksi units})$$

$$C_A = 0.91$$

Detail No. 25A

Figure 7.49 The Equivalent Munse F-Curve

UK Department of Energy S-N Curves
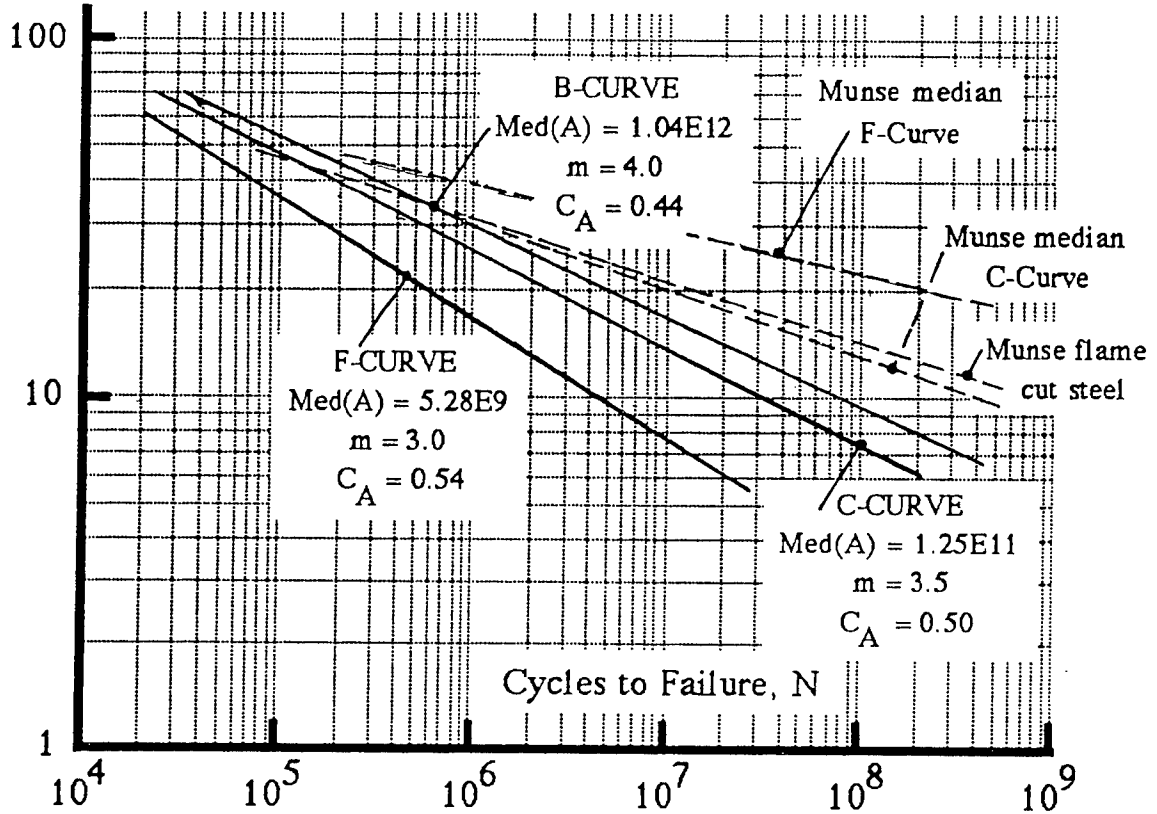
Stress Range, S (ksi)

Figure 7.50 Munse S-N Curves

Table 7.19
A Comparison of Reliability Estimates Using DEn versus Munse S-N Data

Case	Detail	β	p_f	Munse Curves	
1a	Cruiser 1: Original hatch opening, HY-80 data	3.81	6.8E-5	–	–
1b	Cruiser 1: Original hatch opening, DEn B-curve	-2.46	≈1.0	-11	≈1.0
2	Cruiser 1: Modified hatch opening	0.514	0.30	1.41	0.08
3	Cruiser 1: Original deck house corner	-1.15	0.88	3.33	4.3E-4
4	Cruiser 1: Modified deck house corner	1.24	0.107	6.60	2.14E-11
5	Cruiser 2: Deck house corner	-1.47	0.93	2.28	0.011
6	Cruiser 2: Hatch opening	-0.149	0.56	0.33	0.37
7a	Tanker: Longitudinal stiffeners in deck	2.83	2.3E-3	3.86	5.58E-5
7b	Tanker:	0.209	0.417	4.69	1.36E-6
8	SL-7: Original hatch opening	0.46	0.32	0.941	0.173
9	SL-7: Modified hatch opening	3.20	6.9E-4	4.15	1.64E-3

7.8 Sensitivity Analysis Relative to Fatigue

7.8.1 <u>Factors which Influence Fatigue Life</u>:

It is assumed that fatigue failure (significant cracking) occurs at stress concentration, usually but not always, at welded detail. The major factors that influence fatigue reliability at structural detail are:

1. Stress at the detail level. Of all of the factors that influence fatigue life, stress is perhaps the most important. For a typical S-N slope of 3.0 (based on log-log plot) a decrease of stress by a factor of two leads to an increase in estimated life by a factor of eight. In theory, it is possible to reduce stress at a point by:

   a. A plate insert having a larger thickness.

   b. Reducing a stress concentration.

   c. Reinforcement, e.g., face plate on hatch opening.

2. Fatigue strength of the joint or detail. In theory it is possible to increase the fatigue strength of a detail by:

   a. Avoiding the use of a welded joint. S-N curves for welds fall significantly below those of plain steel. There are some cases when a welded joint can be avoided, e.g., at hatch opening.

   b. Use of high tensile strength steel for plain steel. Generally there is little improvement in fatigue strength at a weld, but for non welded joints, there can be significant improvement.

   c. Improving the quality of the weld

      i. Post weld heat treatment (PWHT)

      ii. Weld toe TIG dressing

      iii. Weld toe burr grinding or machining

      iv. Weld toe hammer peening

      v. Manual rather than automatic

7.8.2 Examples of Fatigue Sensitivity Analysis:

As an example, Case 2, the modified hatch opening of Cruiser 1 will be considered. Each of the items in Section 7.8.1 will be considered.

7.8.2.1 *Sensitivity of probability of cracking to stress*

The stress level will be defined by the peak nominal stress range in the deck, S_o, defined as the stress having a return period of N_T (see eqn. (7.19)). For Cruiser 1, this stress range is $S_o = 61.9$ ksi. Using the analysis as described in Section 7.5, the safety index and probability of failure are computed as a function of S_o and plotted in Figures 7.51 and 7.52, respectively. The results clearly show that reliability has a high level of sensitivity to stress.

Nominal stress in the neighborhood of the hatch opening can be reduced by a plate insert, adding thickness to the deck. This has already been done in Cruiser 1, increasing the plate thickness of the deck from 5/16 to ½ inch. A thicker plate will improve reliability as described in Figures 7.53 for beta and 7.54 for the probability of failure.

7.8.2.2 *Sensitivity of probability of cracking to strength*

This discussion will focus on the improvement in reliability relative to the improvement in the quality of the weld. [Mohr, Tsai, and Tso (1995), BS 7608 (1993)]. Reliability estimates with the weld quality improvements described below are summarized in Table 7.20. Dramatic improvements in reliability result from post weld treatments.

Post weld heat treatment is used to remove the majority of welding residual stresses. While little life improvement can be realized for positive stress ratios, R, improvement in fatigue life by a factor of 2.0 is expected for fully reversed stress, which is the case in the deck of Cruiser 1.

Weld toe TIG dressing is used to remove the previous weld toe, with its unfavorable combination of external geometry and internal defects and replace it with a more benign weld toe. A factor of 2.2 on life is observed, with an even higher factor for steels having yield strengths in excess of 85 ksi.

Weld toe burr grinding removes initial defects along the weld toe and increases the radius at the junction between the weld metal and the base metal. Improvement in fatigue life depends upon the depth and shape of the resulting grove. Caution needs to be exercised to avoid overgrinding which can be more damaging than the initial defects. An improvement in fatigue life by a factor of 2.2 can be realized.
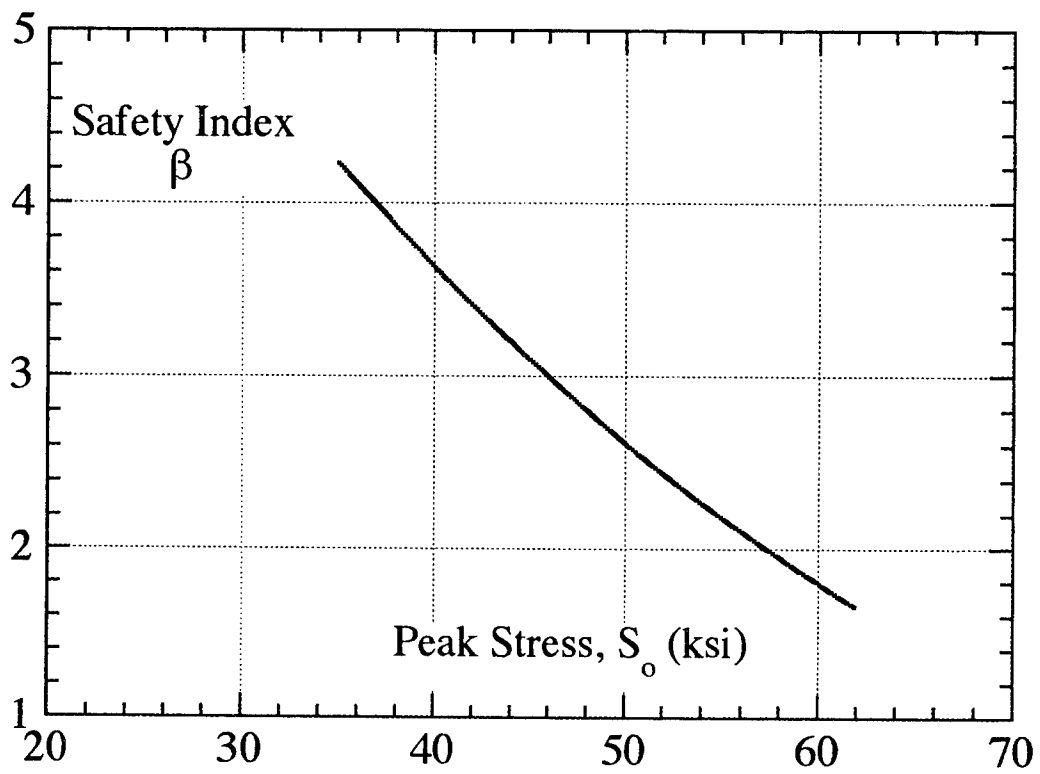
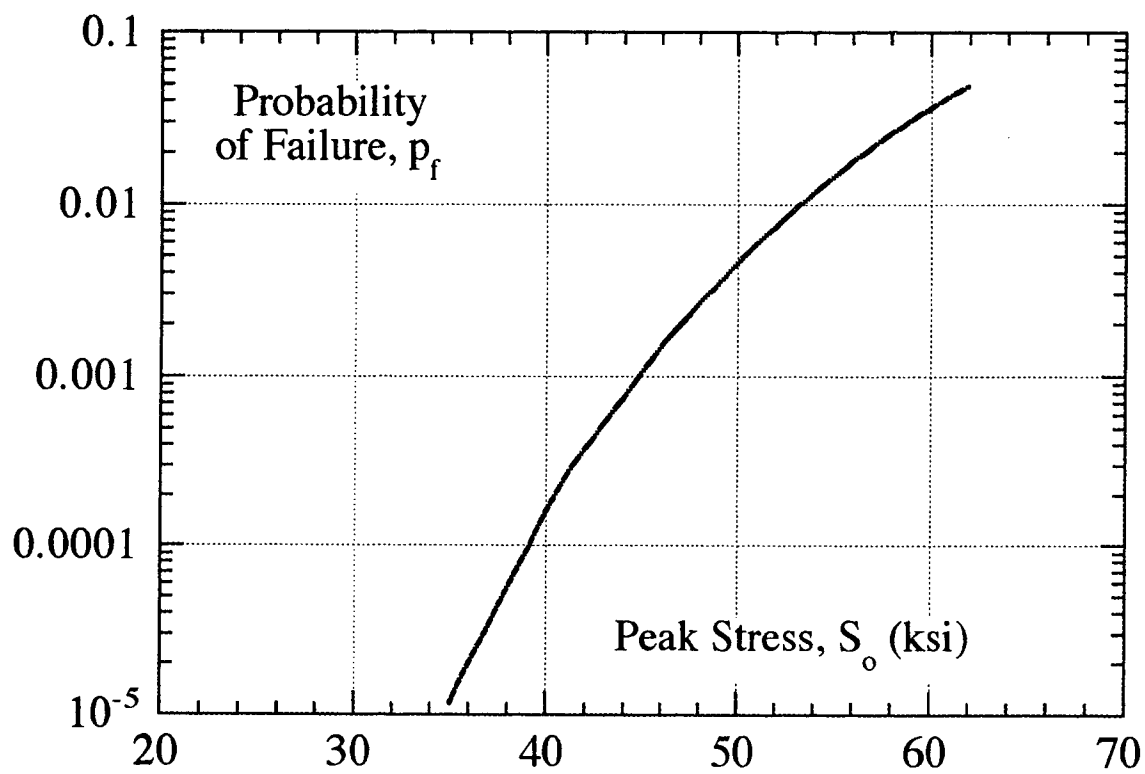Figure 7.51 Safety Index vs. Peak Stress:

Cruiser 1

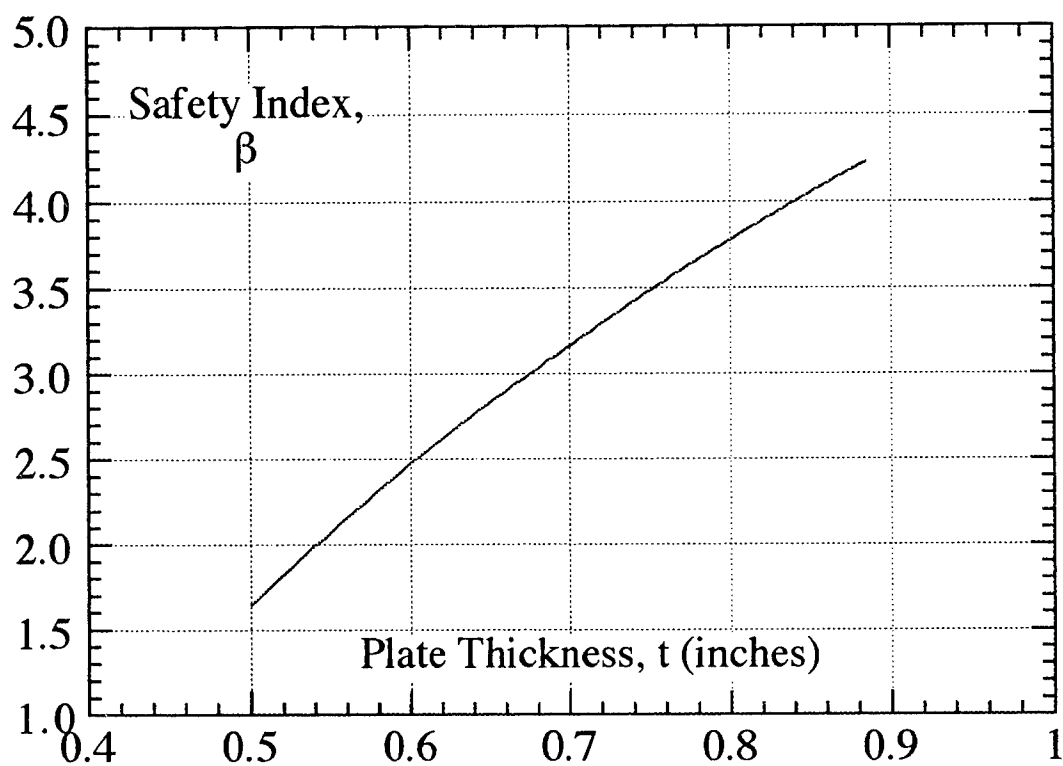Figure 7.52 Probability of Failure Versus Peak Stress

Cruiser 1

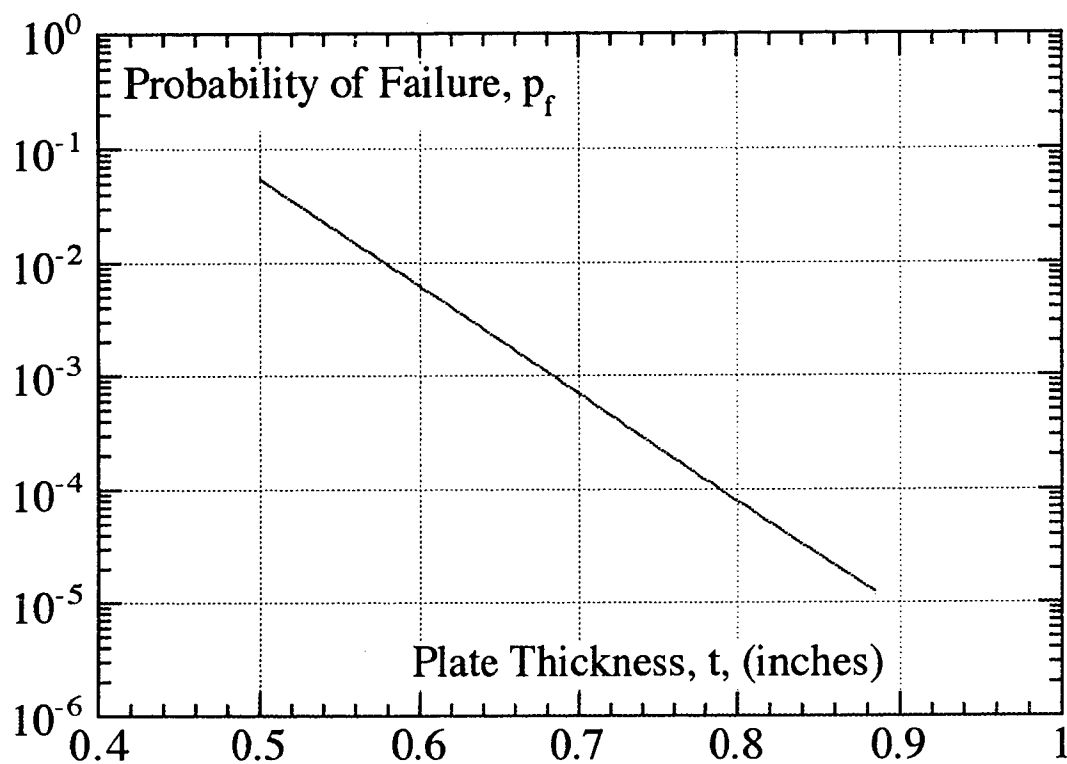Figure 7.53 Safety Index Versus Plate Thickness

Cruiser 1

Figure 7.54 Probability of Failure Versus Plate Thickness

Cruiser 1

Table 7.20
A Summary of Reliability Improvement
as a Function of Weld Treatment

	Life Factor	Beta	pf
As-welded	1.0	1.65	0.049
PWHT	2.0	2.55	0.0054
TIG Dressing	2.2	2.67	0.0037
Grinding	2.2	2.67	0.0037
Hammer peening	4.0	3.45	0.00029

Weld toe hammer peening introduces near yield compressive residual stresses at the weld surface, with more improves expected for lower stress ratios. Initial defects may remain or be deformed by the plastic deformation under the hammer, which will also slightly improve the radius at the weld toe. An improvement in life by approximately a factor of 4.0 can be realized.

Automatic versus manual welds [Gurney (1979)]. An examination of the results obtained on transverse butt welds in the as-welded condition reveals one outstanding feature, namely the relatively poor performance of automatic welds compared to that of welds made manually. The reason for this poor performance is the reinforcement shape associated with automatic welds. Gurney indicates an improvement in strength of manual welds of about 3.0 ksi at a life of two million cycles. No life factor is considered.

8.   RECOMMENDED MINIMUM ACCEPTABLE SAFETY LEVELS

8.1   Introductory Remarks

Guidelines are provided for ship designers on acceptable risks associated with each failure mode, i.e., maximum allowable estimated probabilities of failure or minimum allowable safety indices, frequently referred to as "target reliabilities". Recommendations on acceptable risks are established on the basis of information from four sources.

1. A synthesis and interpretation of the results of the reliability analysis performed in this study and reported herein. This study has indicated the level of risk associated with past successful design practice on the ships under consideration.

2. Analysis that has been performed in other ship reliability studies (e.g., Mansour, 1972, 1974, 1975, 1981, 1990; Mansour and Faulkner, 1973; Faulkner et al., 1979; Soares and Moan, 1985; Stiansen and Mansour, 1975; Stiansen et al., 1980; Thayamballi, 1990; Thayamballi et al., 1984, 1986; Diadola and Basar, 1981; Nickolaidis and Kaplan, 1991; White and Ayyum, 1985; Wirsching and Chen, 1988; Kim and Kim, 1995).

3. Experiences on other systems. The results of other exercises in which the level of risk has been estimated for large structures will be helpful in calibrating the figures that are presented.

4. Professional judgment on the part of the investigators of this study. In this regard, the team has over one-half century experience in structural reliability analysis.

Following discussions provide general background for the problem of determining target reliabilities. A review of the sources of information on target reliabilities is provided, followed by recommendations of minimum acceptable levels.

8.2   Target Values

To establish probability-based design criteria, it is necessary to define a maximum allowable risk (or probability of failure), p_0. Define

p_0 = target risk, or probability of failure
p_f = the probability of failure (as estimated from analyses)

Then, for a safe design,

$$p_f \leq p_0 \tag{8.1}$$

Alternatively, the safety index can be used. In fact, its use is more common for design criteria development. Define

β_0 = target safety index

β = safety index (as estimated from analysis based on transforming non-Normal variats to Normal variats; see Madsen, 1986, or Mansour, 1990)

$$\beta_0 = -\Phi^{-1}(p_0) \quad \beta = -\Phi^{-1}(p_f) \tag{8.2}$$

Φ is the standard normal cumulative distribution function (cdf). Then, for a safe design,

$$\beta \geq \beta_0 \tag{8.3}$$

It should be emphasized that in order for eqn. (8.2) to be valid, all non-Normal variates must be transformed to Normal variates when calculating β, using Rosenblatt transformation or any other method (see, e.g., Ang and Tang, 1984).

The selection of target reliabilities is a difficult task (Payer *et al.*, 1994). These values are not readily available and need to be generated or selected. Also, these levels might vary from one industry to another due to factors such as the implied reliability levels in currently used design practices by industries, failure consequences, public and media sensitivity, or response to failures that can depend on the industry type, types of users or owners, design life of a structure, and other political, economic, and societal factors.

8.3   Method of Selecting Target Values

Target reliability values will be chosen by the authors of this report. The process by which they will do this is described in the following.

What values should be chosen for the target reliability (or target safety index)? In general, there are no easy answers. There are three methods which have been employed:

(1) The code writers and/or the profession agrees upon a "reasonable" value. This method is used for novel structures where there is no prior history.

(2) Code calibration (calibrated reliability levels that are implied in currently used codes). The level of risk is estimated for each provision of a successful code. Safety margins are adjusted to eliminate inconsistencies in the requirements. This method has been commonly used for code revisions.

(3) Economic value analysis (cost benefit analysis). Target reliabilities are chosen to minimize total expected costs over the service life of the structure. In theory, this would be the preferred method, but it is impractical because of the data requirements for the model.

The second approach was commonly used to develop reliability-based codified design such as the LRFD format. The target reliability levels, according to this approach, are based

on calibrated values of implied levels in a currently used design practice. The argument behind this approach is that a code represents a documentation of an *accepted* practice. Therefore, since it is accepted, it can be used as a launching point for code revision and calibration. Any adjustments in the implied levels should be for the purpose of creating consistency in reliability among the resulting designs according to the reliability-based code. Using the same argument, it can be concluded that target reliability levels used in one industry might not be fully applicable to another industry.

The third approach is based on cost-benefit analysis. This approach was used effectively in dealing with designs for which failures result in only economic losses and consequences. Because structural failures might result in human injury or loss, this method might be very difficult to use because of its need for assigning a monetary value to human life. Although this method is logical on an economic basis, a major shortcoming is its need to measure the value of human life. Consequently, the second approach is favored for this study and is discussed further in the following sections.

An important consideration in the choice of design criteria is the consequences of failure. Clearly the target reliability relative to collapse of the hull girder should be larger than that of a non-critical welded detail relative to fatigue.

In this exercise, a combination of (1) and (2) will be used. The following section provides a summary of the sources of information that will be used to make decisions on target reliabilities for the structural systems and subsystems considered.

8.4   Calibrated Reliability Levels

A number of efforts, in which target reliability levels (i.e., safety indices or β values) were developed for the purpose of calibrating a new generation structural design code to an existing code, have been completed.

According to *Structural Reliability: Analysis and Prediction* (Melchers, 1987), the general methodology for code calibration based on specific reliability theories, using second-moment reliability concepts, is discussed by Allen (1975), Baker (1986), CIRIA (1977), Hawrenenk and Rackwitz (1976), Guiffre and Pinto (1976), Ravindra and Galambos (1978), Ellingwood *et al.* (1980), Lind (1976), and Ravindra *et al.* (1969). The key steps in the process, following the discussion in Melchers (1987), are as follows. First, the scope of the design situation must be identified (e.g., material, loads, structural type) and narrowed to fit the specific situation. Next, a design space reflecting all key variables (nominal yield stresses, range of applied loads, continuity conditions, etc.) is chosen and divided into discrete zones. These zones are used to develop typical designs using existing codes. Next, performance functions for the failure modes, expressed in terms of the basic variables, are defined. The statistical properties (distributions, means, variances, and average-point-in-time values) of the basic variables are used for the determination of the β indices using a specified method for reliability analysis (e.g., moment methods).

8-3

Next, each of the designs obtained above, together with the performance functions and the statistical data derived above, are used to determine β for each zone. Repeated analyses will yield the variation of β. From these data, a weighted β is obtained and used as a target reliability level β_0. Melchers notes that frequently the information is insufficient for this determination and one must make a "semi-intuitive" judgment in selecting β_0 values; for example, recognizing a value is used for dead, live, and snow load combinations as compared to dead, live, and wind load combinations or dead, live, and earthquake load combinations. Divergent β_0 values should be corrected by means of the partial factor(s) on material strength or resistance (e.g., through the strength reduction factor).

8.5   Sources of Information Used to Establish Target Reliabilities

8.5.1   SSC Project SR-1344:

This current project (SR-1344) provided a main input to the selection of target safety indices for the various failure modes of ship structures. A determination was made of the level of risk for four ships: two cruisers, a containership and a tanker. Primary, secondary and tertiary modes of failure were considered and two time frames (short- and long-term) were investigated. The results have been discussed in Chapter 5 of this report. Safety indices for critical cases are summarized in Tables 5.4.3 to 5.4.5 of Chapter 5.

Fatigue safety indices of certain details in the four ships were also analyzed and discussed in Chapter 7. The main results of the determined safety indices are given in Tables 7.10 through 7.19.

8.5.2   Studies by A. E. Mansour:

Mansour (1994) performed a preliminary study of the safety index relative to initial yield of the hull girder (primary) over the service life of eighteen ships consisting of tankers, bulk carriers and cargo ships. The results are plotted in Figures 8.5.1 and 8.5.2.

Other studies were conducted in collaboration with the American Bureau of Shipping (Mansour, Jan, Zigelman, Chen and Harding, 1984). One of the objectives of the study is to estimate the safety level implied in the Rules for primary hull structure. Rule values for the loads and strength were used in the study. The results are shown in Figure 8.5.3.

A more recent study was conducted for the Ship Structure Committee under Project SR-1330 — Probability Based Ship Design Procedures – A Demonstration (Mansour, Hovem and Thayamballi, 1993, SSC 367). Safety indices of a tanker were determined using a simplified approach for primary and fatigue modes of failure. Safety index values ranging from 1.5 to 3.5 were obtained for primary strength depending on the failure mode and 2.4 for the fatigue mode. Other reliability studies and the corresponding safety indices are given in Mansour and Faulkner (1972) and Mansour (1990).
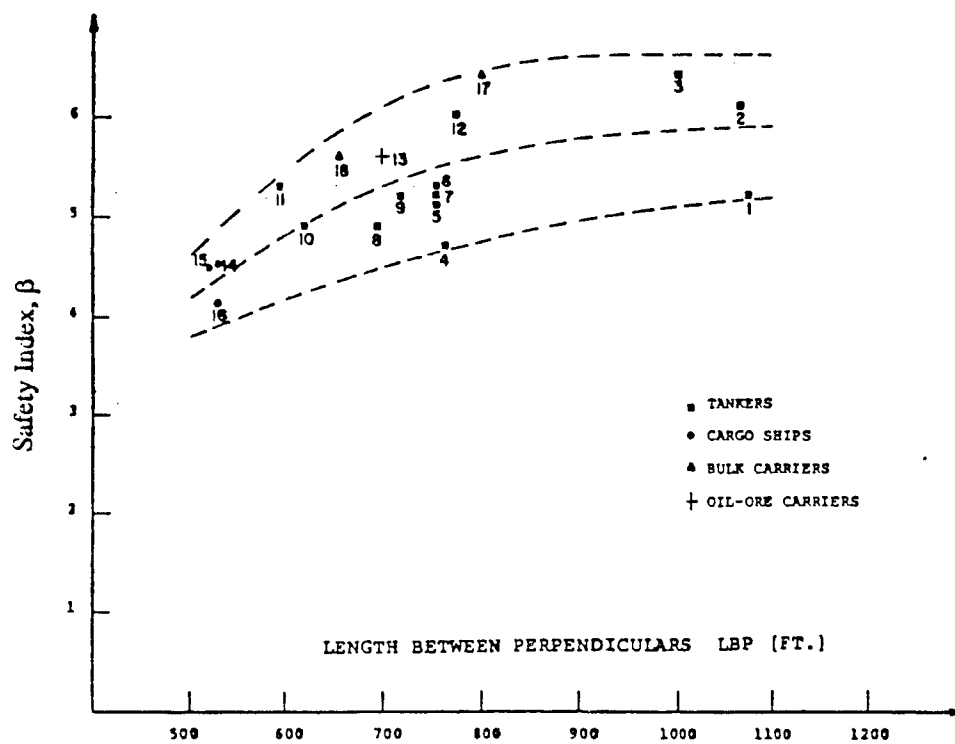
Figure 8.5.1 Safety Index β for 18 Ships as a Function of the Length Between Perpendiculars
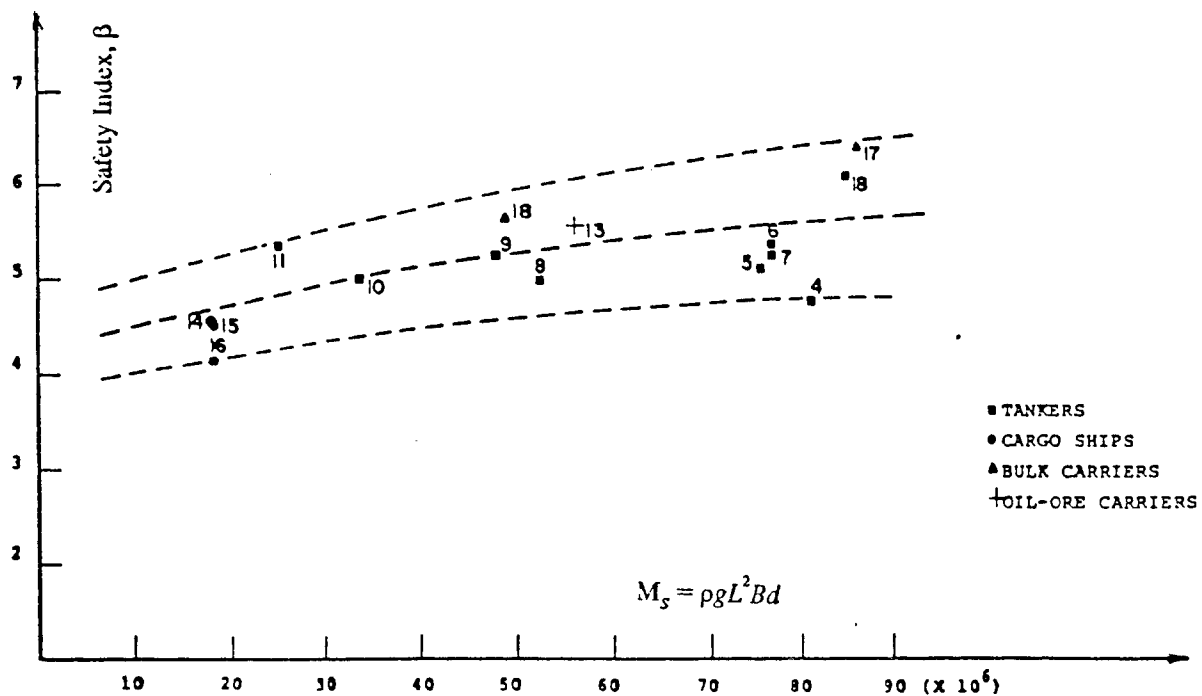(Mansour, 1974)

Figure 8.5.2 Safety Index β for 15 Ships as a Function of M_S (Mansour, 1974)
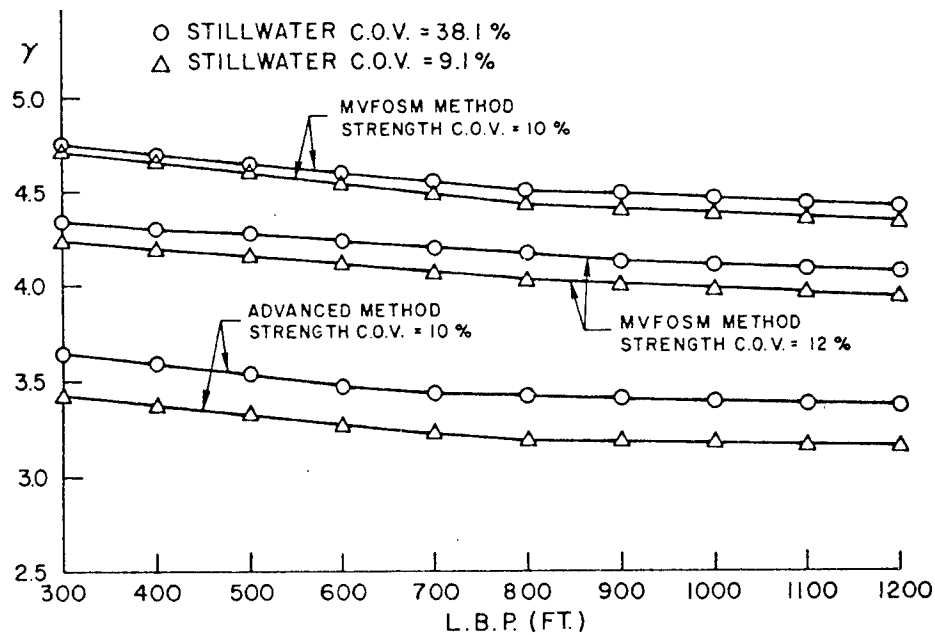
Figure 8.5.3   Safety Index (ABS) versus Length Between Perpendiculars of Ships (Mansour
et al., 1984)

8.5.3   Studies by Hyundai Heavy Industries:

A simplified reliability analysis was performed for primary and fatigue failure modes
in 34 ships (Kim and Kim, 1995). Half of these ships were tankers and the other half bulk
carriers. For the primary hull failure modes, the results are shown in Tables 8.5.1 and 8.5.2
and Figure 8.5.4, reproduced from their paper (Kim and Kim, 1995).

In these Tables and Figure, mode I refers to initial yield of the upper deck, mode II
refers to compressive buckling of upper deck using an approximate formulation and modes
III and IV refer to ultimate strength of a ship hull girder in sagging and hogging conditions,
respectively, using an approximate equation.

Fatigue reliability indices for class F joints, corresponding to ship life of 20 years, are
shown in Figure 8.5.5 for the 34 ships (Kim and Kim, 1995).

8-6

Ship no.	Tanker					Bulk Carrier				
	Design Date	DWT	LBP	B	D	Design Date	DWT	LBP	B	D
1	83. 7	40,000	184.0	30.4	17.8	83. 7	45,000	185.0	32.24	16.5
2	83.11	65,000	220.8	32.2	18.2	84. 5	168,500	282.4	45.0	23.8
3	84. 2	88,900	236.0	42.0	19.2	84. 8	144,600	260.2	42.97	23.77
4	85. 1	84,000	234.0	42.67	19.8	85. 7	127,000	267.3	42.5	22.2
5	85.10	38,500	169.0	32.2	17.45	85. 7	365,000	328.0	63.5	30.2
6	86. 3	125,000	238.0	45.0	23.35	85. 7	200,000	298.0	50.0	24.0
7	86. 9	114,200	234.0	42.67	21.5	85.11	36,500	175.0	28.0	16.1
8	87. 2	239,800	305.0	58.0	28.8	86. 2	186,000	280.0	48.0	24.5
9	86.12	254,000	310.0	56.0	29.5	87.11	64,000	215.6	32.2	18.0
10	87. 4	39,720	177.0	27.43	17.0	88. 6	122,000	256.0	40.42	21.2
11	87.12	148,000	258.0	43.2	24.9	88. 6	69,000	219.7	32.2	18.3
12	89. 9	281,000	310.0	56.0	31.4	88. 7	148,100	259.0	43.0	23.8
13	90. 3	153,000	264.0	43.9	24.4	88.12	37,000	178.0	28.4	17.2
14	92. 4	280,000	317.0	59.0	31.5	89. 5	41,400	176.0	30.5	15.95
15	92. 8	300,000	318.0	58.0	31.5	91. 7	150,000	270.0	45.0	23.8
16	93. 5	29,990	170.0	30.0	14.4	91. 7	207,000	300.0	50.0	25.7
17	93. 5	18,130	152.0	25.8	10.8	93. 6	72,000	219.8	32.25	19.0

Table 8.5.1 Principal Particulars of the Selected Ships for Reliability Analysis (in MT, m)

Mode / Ship	Tanker				Bulk Carrier			
	I	II	III	IV	I	II	III	IV
1	6.12	3.71	4.43	6.19	5.16	3.47	5.16	6.20
2	4.54	2.40	3.39	4.95	4.94	3.22	4.44	5.55
3	4.49	1.92	2.88	4.94	4.95	2.70	4.15	5.63
4	4.94	2.16	3.03	5.11	4.88	3.12	5.00	5.98
5	4.77	3.00	5.41	6.47	4.69	3.19	4.46	5.56
6	4.51	1.19	2.60	5.44	5.15	3.62	4.67	5.53
7	4.38	2.27	3.11	4.64	5.28	1.92	3.56	6.31
8	4.53	2.31	3.46	5.29	4.75	3.33	4.56	5.10
9	4.51	1.54	2.80	5.39	4.53	2.52	3.68	5.29
10	5.94	3.73	4.65	6.16	4.88	3.30	4.21	5.09
11	4.65	2.24	3.27	5.15	5.07	2.17	3.36	5.29
12	4.49	2.18	3.28	5.05	4.87	2.74	4.30	5.77
13	4.57	1.27	2.37	5.16	5.09	2.47	4.27	6.23
14	3.84	2.58	4.64	5.89	4.87	2.54	4.21	5.82
15	4.22	2.43	3.35	4.79	4.90	2.81	4.01	5.50
16	4.62	2.61	2.94	4.18	5.23	3.80	4.56	5.32
17	5.10	3.11	3.03	4.34	4.86	2.20	3.76	5.45
Mean	4.72	2.39	3.45	5.24	4.95	2.89	4.26	5.63
COV	0.12	0.30	0.24	0.12	0.04	0.19	0.11	0.07

Table 8.5.2 Results of Reliability Analysis for Ultimate Strength

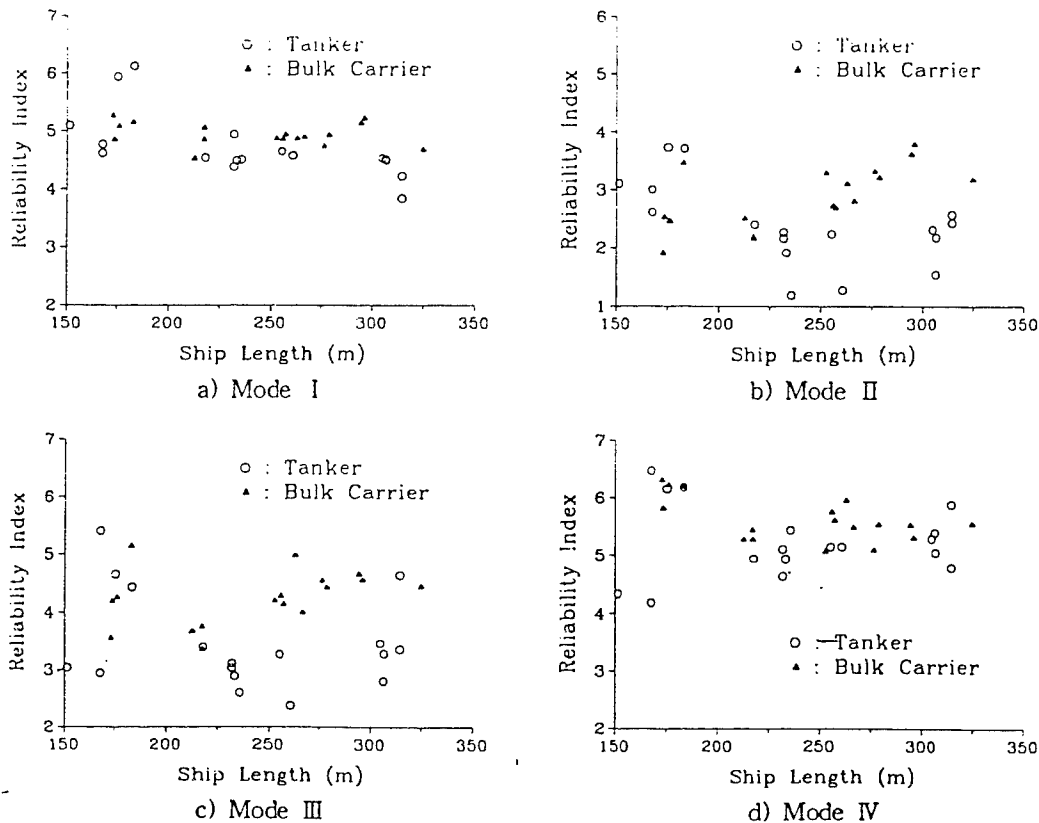a) Mode I

b) Mode II

c) Mode III

d) Mode IV

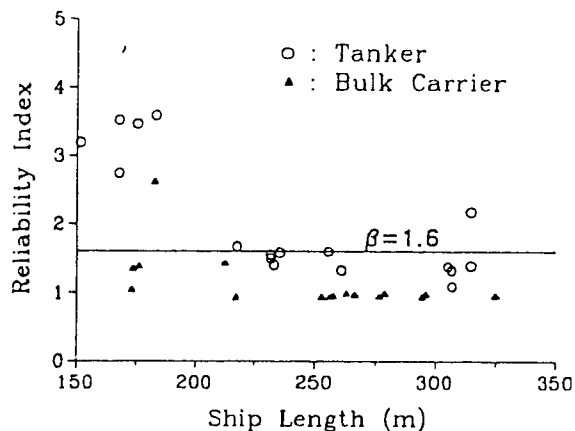Figure 8.5.4 Results of Reliability Analysis for Ultimate Strength (Kim and Kim, 1995)

Figure 8.5.5 Results of Fatigue Reliability Analysis for Joint Class F
(Kim and Kim, 1995)

8.5.4   LRFD Requirements:

In the code calibration process of Load and Resistance Factor Design, Galambos and Ravindra (1978) recommended a default value of β_0 = 3.0 as a general requirement. It is assumed by the authors that this would be for a component of a highly redundant structure. It should not apply if the consequences of failure are serious.

Reed and Brown (1992) provide a summary of the target reliability levels used in the AISC LRFD specifications. In addition to the values provided in Tables 8.5.3 and 8.5.4, values for high strength bolts in tension and shear were given as 5.0 and 5.1, and 5.9 to 6.0, respectively. Also, a value for fillet welds of 4.4 is given. Detailed information about these values are provided by Galambos (1989).

8.5.5   ANS (American National Standard) A58:

While the specific reliabilities will be a function of the strength criteria needed for specified materials and load combinations within designated structures, it is useful to have an indication of the range of possible target reliability levels. Ellingwood et al. (1980) present ranges for reliability levels for metal structures, reinforced and prestressed concrete structures, heavy timber structures, and masonry structures, as well as discussions of issues that should be considered when making the calibration. Table 8.5.3 provided typical values for target reliability levels. This table was developed based on values provided by Ellingwood et al. (1980). The target reliability levels shown in Table 8.5.4 were also used by Ellingwood and Galambos (1982) to demonstrate the development of partial safety factors. The β_0 values in Tables 8.5.3 and 8.5.4 are for structural members designed for 50 years of service.

Structural Type	Target Reliability Level (β_0)
Metal structures for buildings (dead, live, and snow loads)	3
Metal structures for buildings (dead, live, and wind loads)	2.5
Metal structures for buildings (dead, live and snow, and earthquake loads)	1.75
Metal connections for buildings (dead, live, and snow loads)	4 to 4.5
Reinforced concrete for buildings (dead, live, and snow loads) • ductile failure • brittle failure	 3 3.5

Table 8.5.3 Target Reliability Levels

Member, Limit State	Target Reliability Level (β_0)
Structural Steel	
Tension member, yield	3.0
Beams in flexure	3.0
Column, intermediate slenderness	3.5
Reinforced Concrete	
Beam in flexure	3.0
Beam in shear	3.0
Tied column, compressive failure	3.5
Masonry, unreinforced	
Wall in compression, inspected	5.0
Wall in compression, uninspected	7.5

Table 8.5.4 Target Reliability Levels Used by Ellingwood and Galambos (1982)

8.5.6   Canadian Standard Association (CSA) Deliberations:

The following figures were presented for review for possible adoption by the CSA for design criteria for offshore installations in Canadian waters.

10^{-5}/year   Safety Class 1. Failure results in a great loss of life or a high potential for environmental damage.

10^{-3}/year   Safety Class 2. Failure would result in small risk to life and a low potential for environmental damage.

8.5.7 National Building Code of Canada:

Madsen *et al.* (1986) discuss target reliability levels that were used by the National Building Code of Canada (1977) for hot-rolled steel structures. The target reliability values were selected as follows: $\beta_0 = 4.00$ for yielding in tension and flexure. $\beta_0 = 4.75$ for compression and buckling failure, and $\beta_0 = 4.25$ for shear failures. These values are larger than the values in Tables 8.5.3 and 8.5.4 because they reflect different environmental loading conditions and possibly different design life.

8.5.8 A.S. Veritas Research:

A.S. Veritas Research was a subsidiary of Det norske Veritas. Target annual probabilities, recommended by this agency, are given in Table 8.5.5 (see also Lotsberg, 1991). Note that these values are *annual* probabilities. Thus, for example, if the failure is Type 1 (ductile failure with reserve capacity) and serious, then the annual target is $p_1 = 10^{-4}$. But if the service life is 20 years, then the target for the service life would be $p_0 = 20 (10^{-4})$ or $2 \cdot 10^{-3}$.

8.5.9 Nordic Building Committee:

Madsen *et al.* (1986) also discuss target reliability levels that were used by the Nordic Building Code Committee (1978). The target reliability values were selected depending on the failure consequences of a building in the following ranges: $\beta_0 = 3.1$ for less serious failure consequences, $\beta_0 = 5.2$ for very serious failure consequences, and $\beta_0 = 4.27$ for common cases.

8.5.10 AASHTO Specifications:

Moses and Verma (1987) suggested target reliability levels in calibrating bridge codes (i.e., AASHTO Specifications). Assuming that bridge spans of less than 100 ft. are most common, a β_0 of 2.5 to 2.7 is suggested for redundant bridges, and a β_0 of 3.5 for non-redundant bridges.

8.5.11 API Fatigue Studies:

Using the best data available at the time, Wirsching (1984) estimated the safety index as $\beta_0 \approx 2.5$ implied by the API RP2A (for fixed offshore structures) fatigue design guidelines in tubular welded joints. The reality is that the reference wave designs most members (at least for platforms in water depths less than 300 feet), so that few joints have a safety index that low.

Ref.:   A.S. Veritas Research (Report No. 91-2000); Norwegian agency that certifies large scale structures worldwide.

Target (Annual) Failure Probabilities
(Target safety index in parentheses)

Failure Consequences	Failure Type		
	1	2	3
Not Serious	10^{-3} (3.09)	10^{-4} (3.71)	10^{-5} (4.26)
Serious	10^{-4} (3.71)	10^{-5} (4.26)	10^{-6} (4.75)
Very Serious	10^{-5} (4.26)	10^{-6} (4.75)	10^{-7} (5.20

FAILURE TYPE:

1. Ductile failure with reserve strength capacity resulting from strain hardening.

2. Ductile failure with no reserve capacity.

3. Brittle fracture and instability

FAILURE CONSEQUENCES:

Not serious. A failure implying small possibility for personal injuries; the possibility for pollution is small and the economic consequences are considered to be small.

Serious. A failure implying possibilities for personal injuries/fatalities or pollution or significant economic consequences.

Very serious. A failure implying large possibilities for several personal injuries/fatalities or significant pollution or very large economic consequences.

Table 8.5.5 Veritas Target Failure Probabilities

8.6   Recommended Target Safety Indices for Primary, Secondary and Tertiary Failure Modes of Ship Structures

Recommended target safety indices for hull girder (primary), stiffened panel (secondary) and unstiffened plate (tertiary) modes of failure and the corresponding notional probabilities of failure are summarized in Table 8.6.1. These lifetime values are based on professional judgment in view of the extensive reliability analysis performed in this project together with the values reviewed in the literature.

Failure Mode	Commercial Ships	Naval Ships
Primary (initial yield)	5.0 (2.9×10^{-7})	6.0 (1.0×10^{-9})
Primary (ultimate)	3.5 (2.3×10^{-4})	4.0 (3.2×10^{-5})
Secondary	2.5 (6.2×10^{-3})	3.0 (1.4×10^{-3})
Tertiary	2.0 (2.3×10^{-2})	2.5 (6.2×10^{-3})

Table 8.6.1 Recommended Target Safety Indices (Failure Probabilities) for Ultimate Strength

The consequences of the ultimate strength failure are considered as follows: primary ultimate, very serious; secondary, serious and tertiary, not serious. The primary initial yield failure mode is listed here only because it represents state-of-the-art design practice.

The probabilities of failure associated with the β values given in Table 8.6.1 were determined using the standard Gaussian cumulative distribution function (see eqn. (2.3.4) and Figure 2.3.1A).

8.7   Recommended Safety Levels for Fatigue

Recommended target safety indices for fatigue are summarized in Table 8.6.2. These are considered to be lifetime values, i.e. related to the probability of failure during the intended service life, as predicted prior to service. These values are based on professional judgment supported by the analyses reported herein, as well as a comprehensive review of the literature. A detailed commentary on the development of probability-based design criteria for ships is provided by Mansour et al. (1995).

	Description	Commercial Ships	Naval Combatants
Category 1	A significant fatigue crack is not considered to be dangerous to the crew, will not compromise the integrity of the ship structure, will not result in pollution; repairs should be relatively inexpensive.	1.0 (1.6×10^{-1})	1.5 (6.7×10^{-2})
Category 2	A significant fatigue crack is not considered to be immediately dangerous to the crew, will not immediately compromise the integrity of the ship, and will not result in pollution; repairs will be relatively expensive.	2.5 (6.2×10^{-3})	3.0 (1.4×10^{-3})
Category 3	A significant fatigue crack is considered to compromise the integrity of the ship and put the crew at risk and/or will result in pollution. Severe economic and political consequences will result from significant growth of the crack.	3.0 (1.4×10^{-3})	3.5 (2.3×10^{-4})

Table 8.6.2 Recommended Target Safety Indices (Probabilities of Failure) for Fatigue Design

8.8 Derivation of Safety Check Expressions from Target Reliabilities

The target reliabilities defined in Table 8.6.1 and 8.6.2 can be used as a design goal on an *ad hoc* basis. A designer performing a comprehensive reliability assessment, relative to the failure modes addressed, can compare these results with the suggested targets.

These values can also be used to derive safety check expressions for use in a structural design code. A Ship Structure Committee study (Mansour *et al.*, 1995) specifically addressed this topic. The operations which translate target reliabilities to partial safety factors are described in considerable detail in the report. The report also gives design formulae in partial safety factor form and develops and calibrates the partial safety factors for a wide range of the design variables. These values may be used directly in design (rather than assessment of an existing design).

9. SUMMARY, GUIDELINES, CONCLUSIONS, AND GENERAL RECOMMENDATIONS

9.1 Summary

Two major tasks have been considered in this project. The first is to further develop existing methods of assessment of ship structural safety; and the second is to apply the developed methodology to four ships. Several new developments have been presented in this report in connection with the first task. On the load component of the reliability analysis, a method for determining an extreme wave load that recognizes the difference between hogging and sagging moments has been developed in section 2.1.2. The method is based on a non-linear quadratic strip theory. Design charts based on parametric study are provided in section 2.1.3 in order to facilitate the application of the method to ships. Combination of slightly non-linear wave loads have also been investigated and some simple formulations are suggested for determining the combined load taking into consideration the correlation between the different components (section 2.1.2). For slamming loads, several existing methods have been reviewed. The review indicated that a need exists for further research and development in this area.

On the strength component of the reliability analysis, a method has been developed in section 2.2.3 for estimating the global hull strength taken into consideration buckling and yielding of the hull components such as stiffeners, plates, girders, etc. The formulation has been compared with experimental and numerical results in order to test its accuracy. New interaction relations are proposed in section 2.2.6 that account for buckling collapse of a hull subjected to both vertical and horizontal moments. The interaction equations have been tested with numerical results to determine the level of accuracy.

In connection with the methodology for estimating ship failure probabilities, a new procedure has been developed to determine the probability of a ship encountering a severe storm to be used in the short-term reliability analysis. The encounter probability has been formulated in terms of the return period of the storm as well as the operational profile of the ship and wave statistics along her route. The encounter probability is a better criterion to determine a design storm than the usually used return period of the storm.

In the development of reliability methodology, it was recognized that a designer may lack the time to prepare the required data and to learn how to run one or several computer codes in order to assess the safety of a ship. Therefore, one important consideration during the work of this project was to provide, parallel to the more accurate computer codes, simplified methods for quick estimates of the required reliability inputs. For example, in addition to the second order strip theory computer code "SOST", a simplified method for estimating the hog/sag wave bending moments was presented with accompanying design charts. A new, simple formula was also developed for combining non-linear wave loads. For the non-linear ultimate strength estimation, a simple approach has been developed in addition to the more accurate computer code ALPS/ISUM. Finally, two simple methods are provided

to estimate the reliability index and the probability of failure instead of the more accurate computer code CALREL.

In the second major task of the project, the developed reliability methodology was applied to four ships selected in consultation with the Project Technical Committee. First, a data base on the loads was developed for the four ships (2 cruisers, a tanker and an SL-7 ship). Existing data have been collected on stillwater bending moments, wave loads and slamming loads, whenever available. Non-linear wave hog and sag bending moments were determined for each ship using the second order strip theory computer code SOST. Both short term (storm based design criterion) and long term (lifetime design criterion) loads have been determined using SOST. In addition to several semi-empirical formulations, slamming loads were also estimated using a specialized computer program SLAM. This specialized software estimated also the combined wave and slamming loads.

Ultimate strengths of the four ships have been determined using a non-linear idealized structural unit method (ISUM), which is basically an efficient non-linear finite element program that specializes in plated structures. The computer code ALPS/ISUM was used to determine the primary strength (hull girder), the secondary strength (stiffened panel) and the tertiary strength (unstiffened panel) for each of the four ships. Hull strength under combined vertical and horizontal moments was also determined and the proposed interaction relation developed in the methodology task was verified for each ship using the ALPS/ISUM code.

Limit state equations for each ship have been formulated for use in the reliability and sensitivity analysis. The reliability computer code CALREL was used to determine the reliability indices for each ship in each failure mode (primary, secondary and tertiary) and for the two time frames considered (short and long term). A parametric study was conducted to investigate any detectable trend of the safety index with various design parameters. Sensitivity parameters and importance factors were calculated, also using the CALREL code. Based on these factors, critical design variables that have large impact on ship structural safety have been identified.

Whenever possible, the simple formulations for estimating the wave loads, load combinations, ultimate strength and the safety index, which were developed in the methodology task, were applied to the four ships in parallel with the more accurate computer codes SOST, SLAM, ALPS/ISUM and CALREL. The results based on the simplified methods were compared with the computer codes results.

Reliability assessment relative to fatigue was conducted for several structural details for each ship. For both cruisers, the structural details were at points where fatigue might be a problem. One is a bracket at the deck house/deck interface and the other is a hatch opening forward of the deck house. In the case of Cruiser 1, detail before and after structural modifications were considered. For the SL-7 and the Tanker, the fatigue reliability analysis was performed at the corner of a hatch opening in the SL-7 deck and at a longitudinal stiffener intersection with a web frame (Tanker). The long-term stress range distribution was determined for each location using the second order strip theory computer code SOST. The

software ProEngineer linked with the ANSYS finite element program were employed to derive the stress concentration factors. The results of these investigations were used to conduct fatigue reliability and sensitivity analyses for each structural detail in each ship.

A literature survey was conducted on safety indices associated with existing ships and current design practice. Minimum acceptable (target) safety indices available in the literature were also reviewed. These, together with the values determined in this project for the four ships, provided the basis for a recommended set of ultimate strength target reliabilities for each failure mode (primary, secondary and tertiary) and for the fatigue failure mode.

9.2 Design Parameters that Have the Highest Impact on Safety — General Guidelines

Table 9.2.1, obtained from Chapter 6, shows the three most important variables for each type of ship according to the sensitivity analysis conducted in that chapter. This is interesting information, but how can this be used to improve the ship design process? It is necessary to go one step further and examine what factors affect these variables and whether or not they are under the control of the designer.

	Cruiser 1 and *Cruiser 2*	*SL-7* and *Tanker*
First	wave bending moment (M_w)	strength $(M_U, S_{u,2}, \text{ or } S_{u,3})$
Second	strength $(M_U, S_{u,2}, \text{ or } S_{u,3})$	wave bending moment (M_w)
Third	dynamic bending moment (M_d)	stillwater bending moment (M_{sw})

Table 9.2.1 Top Three Most Important Variables

The most important variable for the naval ships (and second for the commercial ship) is the wave bending moment. Wave bending moment depends on variables such as the environmental and operating conditions, the hull form of the ship, and the ship's weight distribution. Controlling environmental and operational conditions is rather difficult for a designer. This would require such measures as limiting the ship's operating areas and/or speed and headings in severe sea states. While this *may* be possible for commercial ships, the operating requirements of warships preclude this sort of limitation. The engineer has some control over the hull form of the ship, although the interactions between specific hull features and wave loads is not fully understood. While it might seem that weight distribution is a relatively controllable parameter, this is not always the case. The weight distribution is mostly influenced by the arrangement of equipment and cargo spaces in the ship, something that is often difficult to modify as it is necessary to change the radius of gyration substantially to have a noticeable effect on the wave loads. This leads to the conclusion that effectively reducing the wave loads may not be a viable option.

The second most important group of variables for the cruisers (first for the civilian ships) are the strength variables. These are dependent primarily on the section modulus of

the hull girder, the yield strength of the material, the design of the stiffening system, and the quality control during construction. The first three are very much under the control of the designer, while the buyer of the vessel can certainly influence the fourth. Increasing the section modulus, yield strength, and stiffening system will increase the mean values of the strength variables, while improvements in quality control at the shipyard will decrease the coefficients of variation. A quick perusal of the critical sensitivity factors given in Chapter 6 (Tables 6.2.1 to 6.2.8) shows that the strength variables are *very* sensitive to changes in both mean and coefficient of variation. This means that small improvements in these areas can result in significant improvements in reliability.

Third on the list of important variables (for the cruisers) is the dynamic bending moment. The slamming loads that are represented by this moment are governed by parameters such as the environmental and operating conditions, the weight distribution, and the shape of the hull near the bow. While, as discussed above, environmental, operating, and weight issues are largely beyond the control of the engineer, the relations between various bow shapes and slamming loads are well documented. Features such as bow flare, flat of bottom near the forefoot, and the slope of the hull at the waterline are all very much controlled by the designer. Reducing the slamming loads can provide important increases in reliability.

The final variable we shall consider is the stillwater bending moment. This is much more an issue for the commercial ships than the military ships. The nominal values of stillwater bending moment can be somewhat affected by design choices. The two factors that influence the stillwater moment are the hull form and the weight distribution. The weight distribution can be controlled for commercial ships by specifying various acceptable loading conditions for the ship in different situations. The interactions between changes in the hull shape and corresponding changes in the buoyancy distribution are well documented in design literature. Appendix J lists the critical design variables and discusses their controllability.

With regard to improvement that results in the highest payoff with respect to fatigue reliability, the following are some comments on possible methods or design modifications that reduce the risk of failure due to fatigue.

1. *Reduction of Stress Ranges.* In an example it was demonstrated that roughly a 15% reduction in stress range resulted in an order of magnitude reduction in the probability of failure. Perhaps the easiest way to achieve this reduction is using a plate insert, i.e., a plate thicker than the global plate thickness. This was done to beef up critical detail in Cruiser 1.

2. *Improvement of Strength.* In an example, it was demonstrated that roughly an order of magnitude reduction in probability of failure could be achieved by post weld treatment that resulted in an increase of average life by a factor of roughly 2.0. One of the treatments, hammer peening, resulted in a reduction of risk of two orders of magnitude.

9.3 Conclusions

9.3.1 Ultimate Strength:

A common thread running throughout the entire project is the differences between the two warships — Cruiser 1 and Cruiser 2 — and the two commercial ships — SL-7 and Tanker. Some general observations and comparisons can be made between the two categories. First, the naval vessels are more strongly constructed than the commercial ships. This shows up in the reliabilities of the military ships being somewhat higher than those of the civilian ships.

Second, the stillwater bending is a much more significant factor in the design of the commercial ships. This can be seen in two places. Analysis of the importance factors places the stillwater bending moment as number three for the civilian ships, while it is dead last in all of the critical cases for the cruisers. Also, the sensitivity-to-variation study shows that making the stillwater bending moment a deterministic parameter would have little effect on the warships, while this is simply not acceptable for the commercial ships.

Failure direction is another contrasting area. For the fine-formed warships, sagging wave loads are the most critical cases, despite the hogging stillwater bending moments. SL-7 and Tanker show a predominance of hogging condition failures in the critical cases. This observation is not quite as solidly based as that for the cruisers, as secondary and tertiary sagging was not investigated for SL-7 and the long term results for Tanker show two critical sagging cases.

Another area of interesting comparisons is between Cruiser 1 and Cruiser 2. The combination of replacing portions of the steel in the structure with high-strength steel and adding about 15 percent to the displacement for Cruiser 1 increased the structural strength while decreasing the sagging wave loads. As sagging loads are the dominant failure cases for these ships, these changes make Cruiser 1 more structurally reliable than Cruiser 2 in the global ultimate strength mode of failure. The gain in strength is not all that it could be, though. The ratio M_U/M_{IY} increases from Cruiser 2 to Cruiser 1 by fourteen percent in hogging and twenty percent in sagging. Comparing this to the increase in the nominal yield strength of the material (70%) shows that not all of the potential increase in the ultimate strength is being realized. This is primarily due to the fact that the stiffening system was not changed significantly to fully exploit the increased strength of the high-strength steel. The change is definitely positive, but could be even better. However, due to cost and problems associated with alignment of longitudinal stiffeners, changing the stiffening system is easier said than done. From these results, it seems that the use of high-strength steel as a primary structural material is a very good idea; however, the fatigue reliability analysis may show some reservations as will be discussed in section 9.3.2.

Short term extreme condition assessments appear to provide a very good predictor of the lifetime reliability of a ship. While the long term reliabilities are lower than their short term counterparts, the drop seems to be fairly consistent across different wave loadings,

ships, and failure modes. This conclusion should be viewed with caution because the long term and short term analyses are very dependent on the parameters chosen. The long term analysis depends on the operational profile selected; the speeds, headings, routes, loading conditions, number of years in operation, operational tempo, etc. The short term analysis depends on the storm condition chosen (the significant wave, average zero-crossing period) and the selected heading and speed.

Several specific conclusions and observations were made in connection with the detailed analyses described earlier for the loads, ultimate strengths, reliability and sensitivity. These are listed at the end of each of these sections and will not be repeated here.

9.3.2 Fatigue:

The following are general conclusions regarding reliability considerations with respect to fatigue:

(a) It is well recognized that the strength of welded joints is independent of the strength of the steel base material. Thus, relative to fatigue, there is no advantage in using high strength steel.

(b) Estimated fatigue reliability has a strong dependence on fatigue stress amplitude. For a typical S-N slope of 3.0 (based on log-log plot) a decrease of stress by a factor of two leads to an increase in estimated life by a factor of eight. Stated another way, roughly a 15% reduction in stress will result in an order of magnitude reduction in the probability of failure.

(c) Post weld treatments can significantly improve the quality of a weld. In an example, it was demonstrated that roughly an order of magnitude reduction in probability of failure could be achieved by post weld treatment that resulted in an increase of average life by a factor of roughly 2.0.

The following are some general conclusions based on the reliability analysis of the four ships:

(a) Some estimated reliabilities seem lower than reasonable (relatively high estimated failure probabilities). It should be noted, however, that generally "fatigue failure" refers to the development of a significant (visual) crack. This in no way implies significant loss of overall structural integrity. Also, it is a fact that fatigue cracking in ship structure is common.

(b) An issue with regard to modeling fatigue strength, ... estimated reliability based on an S-N curve having an endurance limit is significantly higher than reliability based on the assumption of no endurance limit. The existence of an endurance limit is somewhat controversial in light of the fact that structure operates in a corrosive environment and that the stresses are random. An example, ... Cruiser 1 modified hatch opening,

$$\beta = 0.514 \text{ (no endurance limit)}$$

$\beta = 1.64$ (endurance limit)

(c) Cruiser 1 modifications (change of detail and thicker plate inserts) which reduce stresses also reduce estimated failure probabilities by more than an order of magnitude.

(d) Because estimated reliabilities depend strongly on the detail, there are no conclusions that can be drawn from comparison of Cruiser 1 and 2 results. Estimated fatigue reliability of the Cruiser 1 deck house corner is higher than that of Cruiser 2. And Cruiser 2's hatch opening reliability is higher than that of Cruiser 1.

(e) From the Tanker reliability analysis, it is shown that reliability of stiffener welds in which the weld is orthogonal to the direction of stress is significantly less than the reliability of welds which are in the same direction as the stress.

(f) From the SL-7 analysis, again it was shown that strengthening the hatch opening (reducing stresses) can reduce estimated failure probabilities by several orders of magnitude.

9.3.3 General:

As mentioned earlier, a survey of literature on safety indices associated with existing ships and design practice was conducted. Based on this survey, the safety indices determined for the four ships, and the judgment of the research team that conducted this project, the following target safety indices relative to service life are recommended (Table 9.3.1):

Failure Mode	Commercial Ships	Naval Ships
Primary (initial yield)	5.0	6.0
Primary (ultimate)	3.5	4.0
Secondary	2.5	3.0
Tertiary	2.0	2.5
Fatigue		
Category 1 (not serious)	1.0	1.5
Category 2 (serious)	2.5	3.0
Category 3 (very serious)	3.0	3.5

Table 9.3.1 Recommended Target Safety Indices

The consequences of the ultimate strength failure are considered as follows: primary ultimate, very serious; secondary, serious and tertiary, not serious. The primary initial yield failure mode is listed here only because it represents state-of-the-art design practice.

Overall, it has been demonstrated that a comprehensive reliability analysis can be conducted for a ship in a reasonably short period of time, if sufficient data is available. At a minimum, it is necessary to have the ultimate strengths of the hull girder in both directions, the section moduli in both directions, buckling strengths of the gross and individual panels of the deck and bottom, the stillwater bending moment, and an estimate of the loadings (both hogging and sagging) for the ship in either a short term extreme condition or a lifetime value. A CALREL input file can be created, and the reliability of the ship in various conditions can be estimated. Using the methodology outlined in this report and the input files and code created for this project as a baseline, the reliability analysis can be completed in a few hours — assuming that the above information is available. The key here is the availability of the strength and load information. While estimations of the stillwater bending moment and section moduli are readily available for any ship past the late phases of concept design, data for wave loads and ultimate strengths are harder to determine.

9.4   General Recommendations

Reliability technology has become a powerful tool for the design engineer and is widely employed in practice. A basic recommendation is that naval architects and structural engineers involved in the decision making process be knowledgeable of reliability technology. This is likely to require additional training, and there are many opportunities available. Several short courses are offered on reliability technology and its application.

The second basic recommendation is that sufficient background work has been done to develop ship structural codes based on reliability technology for use in ship design. The code would be updated as more data and research results become available. This has been the approach in other major code development, e.g., AISC-LRFD.

More specific recommendations for the Navy and the Ship Structure Committee are detailed as follows.

It is recommended that the Navy consider the use of reliability methods in the following applications:

1) *To develop probability based design code requirements.* Structural reliability technology is employed to derive factors of safety. This has been a major application of reliability methods, e.g., AISC-LRFD. It is recommended that the work of SSC SR-1345 entitled "Probability Based Ship Design Implementation of Design guidelines for Ships: A Demonstration", and the work being carried out at the Naval Surface Warfare Center, Carderock Division, be continued with the objective of developing a reliability-based code for Naval ships.

2) *To estimate reliability in existing designs.* Frequently the question is asked "….we have been using codified factors of safety in our designs, but we don't have a clue of the implied risks…. what is the level of risk (probability of failure) of this system?" The

system may be in service, or it may be on the drawing boards. In fact, it is the goal of this project to estimate reliability relative to hull girder collapse and fatigue for four existing ships. The developed procedure and analysis given in this report can be followed to estimate the risk for existing Naval ships or ship types.

3) *To perform failure analysis.* A structural component fails. In the subsequent investigation, the question is asked, "....what was the cause of failure and the probability of occurrence of this event?" And "is the probability of this occurrence small enough that we can avoid making a significant investment to make a design change?"

4) *To compare alternative designs.* Reliability as an index of structural performance has been used very successfully by the offshore industry for the purpose of comparing competing design concepts.

5) *To support economic value analysis.* The tradeoff between cost and risk is analyzed in order to gain insights on the decision making process, i.e., in theory, decisions could be made to minimize total expected life cycle costs. A current NAVSEA project entitled, "Structural Fabrication and Structural Details", is employing economic value analysis to address fabrication tolerances.

6) *To develop a strategy for design and maintenance of structures which age (e.g., corrosion and fatigue).* Risks are reduced when a structure is periodically inspected and repaired or replaced if necessary. Economic value analysis can be also employed to develop optimal maintenance strategies that lead to minimum cost without reducing the reliability below a specified level.

The major effort currently undertaken by the Ship Structure Committee for the development of a probability-based design approach for ship structures should be continued. The results of this effort is now ready to culminate into a reliability-based design code for commercial ships. The reliability thrust area formulated by the Committee on Marine Structures (CMS) is a well thought-out program that consists of six phases. The program is detailed in the Marine Board report entitled, "Marine Structures, Research Recommendations for FY 1996-1997." For ease of reference, the program is excerpted and summarized in section 1.3 of this report entitled, Historical Review — Ship Structure Committee Previous and Future Work.

Based on the work carried out in this project (SR-1344) and the review of the CMS research recommendations, it is firmly believed that sufficient information exists to initiate phase 5, "Load and Resistance Factor Design Methods for Ship Structures" of the CMS reliability thrust area (see section 1.3). This project will include a complete and rigorous code calibration for the structural design of commercial ships. The resulting load and resistance factor design criteria are to be written in a code style that is suitable for direct use of practicing engineers. It should also be given in a format suitable for updating design criteria as more data and subsequent investigation results become available.

In addition to the specific projects in the reliability thrust area outlined in the CMS program, the following areas are suggested for further development. These areas need to be addressed in depth.

1) *A study of slamming loads for reliability based design.* This study should include an update of the literature review and development conducted in SSC projects SR-1337 and SR-1344. It should provide design formulation for the magnitude of slamming loads as well as design formulation for the combined wave and slamming loads including correlation effects.

2) *An experimental study of hull girder ultimate strength.* This study should include development of scaling laws to model ship structures, with consideration given to buckling and ultimate strength. It should also include experimental verification of analytically calculated strength reduction factors due to buckling.

3) *A study to develop a reliability-based strategy for inspection intervals and maintenance of ships.* This study should include economic value analysis that leads to optimal inspection intervals taking into consideration risk and cost of inspection.

The specific projects outlined above need not to be initiated prior to Phase 5 of the CMS program in the reliability thrust area. Phase 5 (LRFD Design Practice) should have higher priority, but the first project (slamming) may be initiated concurrently with Phase 5.

ACKNOWLEDGEMENT

BIBLIOGRAPHY

Allen, D.E. 1975. Limit States Design—A Probabilistic Study. *Canadian Journal of Civil Engineering*, Vol. 2, No. 1, pp. 36-49.

American Bureau of Shipping 1992. *Guide for Design and Evaluation of the Hull Structure of Double Skin Tankers.*

American Bureau of Shipping 1994. *Rules for Building and Classing Steel Vessels.* Part 3, Hull Construction and Equipment, Section 6.

Ang, A.H.-S. and Tang, W., 1984. Probability Concepts in Engineering Planning and Design, Volume II, *Decision, Risk and Reliability*, John Wiley and Sons, New York.

Antonides, G.P. 1972. A Computer Program for Structural Response to Ship Slamming. NSRDC Ship Acoustics Dept., Report SAD-9E.

Baker, M.J. 1976. Evaluation of Partial Safety Factors for Level I Codes—Example of Application of Methods to Reinforced Concrete Beams. Bulletin d'Information, Comite European du Beton, Paris, No. 112, pp. 190-211.

Barsom, J.M. and Rolfe, S.J. 1987. *Fracture and Fatigue Control in Structures*, Prentice-Hall Book Co., Englewood Cliffs, NJ.

Borgman, L.E. 1972. Extreme Statistics, Risk, and Reliability, Report, University of Wyoming.

Breitung, K. 1984. Asymptotic Approximations for Multinormal Integrals. *Journal of Engineering Mechanics*, ASCE, Vol. 110, No. 3, pp. 357-366.

British Standards Institute 1991. Guidance on Methods for Assessing the Acceptability of Flaws in Fusion Welded Structures. PD 6493, BSI, Linford Wood, Milton Keynes, MK14 6LE, U.K.

BS 6493. 1991. *Guidance on Methods for Assessing the Acceptability of Flaws in Fusion Welded Structures*, British Standards Institution.

BS 7608. 1993. *Code of Practice for Fatigue Design and Assessment of Steel Structures*, British Standards Institution.

Caldwell, J.B. 1965. Ultimate Longitudinal Strength. *Trans. RINA*, Vol. 107, pp. 411-430.

Cartwright, D.E. and Longuet-Higgins, M.S. 1956. The Statistical Distribution of a Maxima of a Random Function. *Proc. Royal Soc. of London*, Ser. A., Vol. 237, pp. 212-232.

CIRIA 63. 1977. Rationalisation of Safety and Serviceability Factors in Structural Codes. Construction Industry Research and Information Association, 6 Storey's Gate, London, SWIP 3AU, Report 63.

Clark, J.D. 1986. Wave Loading in Warships. *Journal of Naval Shipbuilding*, Vol. 12, No. 4; also *Proc. Advances in Marine Structures*, Elsevier Applied Science, London.

Daidola, J.C. and Basar, N.S. 1981. Probabilistic Structural Analysis of Ship Hull Longitudinal Strength. AD-A099118.

Dow, R.S. 1991. Testing and Analysis of a 1/3-Scale Welded Steel Frigate Model. *Proc. Int'l Conference on Advances in Marine Structures*, Elsevier, London:New York, pp. 749-773.

Dowling, P.J., Moulani, F.M. and Frieze, P.A. 1976. The Effect of Shear Lag on the Ultimate Strength of Box Girders. *Int'l Congress on Steel Plated Structures*, Imperial College, London, pp. 108-147.

Ellingwood, B., Galambos, T.V., MacGregor, J.C., and Cornell, C.A. 1980. Development of a Probability-Based Load Criterion for American National Standard A58. National Bureau of Standards Publication 577, Washington, D.C.

Ellingwood, B. and Galambos, T.V. 1982. Probability-Based Criteria for Structural Design. *Structural Safety*, Vol. 1, pp. 15-26.

Faulkner, D. 1967. Written Discussion to International Ship Structures Congress 1967. Report of Committee 10, Volume 2.

Faulkner, D. and Sadden, J.A. 1979. Toward a Unified Approach to Ship Structural Safety. *Trans. RINA*, Vol. 121, pp. 1-38.

Ferro, G. and Mansour, A.E. 1985. Probabilistic Analysis of Combined Slamming and Wave Induced Responses. *Journal of Ship Research*, Vol. 29, No. 3, pp. 170-188.

Flokstra, C. 1974. Comparison of Ship Motion Theories with Experiments for a Container Ship. *International Shipbuilding Progress*, Vol. 21.

Freudenthal, A.M. 1947. Safety of Structures. *Transactions of the ASCE*, Vol. 112, pp. 125-180.

Frieze, P.A., and Lin, Y.T. 1991. Ship Longitudinal Strength Modelling for Reliability Analysis. *Proc. of the Marine Structural Inspection, Maintenance, and Monitoring Symposium*, SSC/SNAME, Arlington, VA, pp. III.C.1-III.C.20.

Friis-Hansen, P. 1994. On Combination of Slamming and Wave Induced Responses. *Journal of Ship Research*, Vol. 38, No. 2, pp. 104-114.

Friis-Hansen, P. 1994. Reliability Analysis of a Midship Section. Ph.D. Dissertation, January. Department of Ocean Engineering, Technical University of Denmark, Lyngby, Denmark.

Galambos, T.V. 1989. Present and Future Developments in Steel Design Codes. *Proc. 5th Int. Conference on Structural Safety and Reliability* (ICOSSAR), ASCE, New York, pp. 2011-2018.

Galambos, T.V. and Ravindra, M.K. 1978. Properties of Steel for Use in LRFD. *Journal of Structural Engineering*, ASCE, Vol. 104, No. 9, pp. 1459-1468.

Gerritsma, J. and Beukelman, W. 1967. Analysis of the Modified Strip Theory for Calculation of Ship Motions and Bending Moments. *International Shipbuilding Progress*, Vol. 14, No. 156.

Guedes Soares, C. 1984. Probabilistic Models for Load Effects in Ship Structures. Department of Marine Technology, Norwegian Institute of Technology, Trondheim, Norway, Report No. UR-84-38.

Guedes Soares, C. and Moan, T. 1985. Uncertainty Analysis and Code Calibration of the Primary Load Effects in Ship Structures. *Proc., 4th International Conference on Structural Safety and Reliability* (ICOSSAR '85), Kobe, Japan, Vol. 3, pp. 501-512.

Guedes Soares, C. and Moan, T. 1988. Statistical Analysis of Stillwater Load Effects in Ship Structures. *Trans. SNAME*, Vol. 96, pp. 129-156.

Guiffre, N. and Pinto, P.E. 1976. Discretization from a Level II Method. Information Bulletin No. 112, CIB Joint Committee on Structural Safety, Paris, France, pp. 158-189.

Gurney, T.R. 1979. *Fatigue of Welded Structures*, 2nd Edition, Cambridge University Press, Cambridge, UK.

Gurney, T.R. 1983. Fatigue Test Under Variable Amplitude Loading. Report No. 220/83, The Welding Institute, Abington Hall, Cambridge, England, CB1 6AL.

Gurney, T.R. 1986. Summary of Variable Amplitude Fatigue Data for Welded Joints. Report 3707/3877/1/86, The Welding Institute, Cambridge, UK.

Hackmann, D. 1979. Written discussion of the 1979 paper by Jensen, J.J. and Pedersen, P.T.

Harbitz, A. 1986. An Efficient Sampling Method for Probability of Failure Calculation. *International Journal on Structural Safety*, Vol. 3, No. 2, pp. 100-115.

Hasofer, A.M. and Lind, N.C. 1974. Exact and Invariant Second Moment Code Format. *Journal of Engineering Mechanics*, ASCE, Vol. 100, No. EM1, pp. 111-121.

Hawrenek, R. and Rackwitz, R. 1976. Reliability Calculations for Steel Columns. Information Bulletin No. 112, CIB Joint Committee on Structural Safety, Paris, France, pp. 125-157.

Hess, P.E. III, Nikolaidis, E., Ayyub, B. and Hughes, O. 1994. Uncertainty in Marine Structural Strength with Application in Compressive Failure of Longitudinally Stiffened Panels. Naval Surface Warfare Center, Carderock Division, U-SSM-65-94/07, Bethesda, MD

Hogben, N., Dacunha, N.M., Olliver, G.F. 1986. *Global Wave Statistics*. British Maritime Technology, Ltd., Middlesex.

Hohenbichler, M. and Rackwitz, R. 1981. Non-Normal Dependent Vectors in Structural Safety. *Journal of Engineering Mechanics*, ASCE, Vol. 100, No. EM6, pp. 1227-1238.

Hughes, O.F. 1988. *Ship Structural Design, A Rationally-Based, Computer-Aided Optimization Approach*, The Society of Naval Architects and Marine Engineers (SNAME), New York.

Hughes, O.F., Nikolaidis, E., Ayyub, B.M., White, G.J., and Hess, P. 1994. Uncertainty in Strength Models for Marine Structures. Ship Structure Committee Report No. SSC-375, Washington, D.C.

International Ship Structures Congress 1967. Report of Committee 10, Volume 2.

International Ship Structures Congress 1973. Proceedings, Reports of Committees 3 and 10, Hamburg, Germany.

International Ship Structures Congress 1994. Report of Committee III.1, Ductile Collapse, St. John's, Canada.

Jensen, J.J. 1993. Software for Calculation of Quadratic Wave-Induced Responses of Ships in Irregular Seaways, Department of Ocean Engineering, The Technical University of Denmark, August.

Jensen, J. Juncher 1994. Dynamic Amplification of Offshore Steel Platform Responses due to Non-Gaussian Wave Loads. *Marine Structures*, Vol. 7, pp. 91-105.

Jensen, J.J., Amdahl, J., Candis, P.A., et al. 1991. Report of ISSC Committee III.1 on Ductile Collapse. *Proc. Int'l Ship and Offshore Structures Congress*, Vol. 1, St. John's, Canada, pp. 299-387.

Jensen, J. Juncher, Banke, L. and Dogliani, M. 1994. Long-Term Predictions of Wave-Induced Loads using a Quadratic Strip Theory. *Proc. NAV'94*, Rome, Italy.

Jensen, J. Juncher and Dogliani, M. 1995. Wave-Induced Ship Hull Vibrations in Stochastic Seaways. *Marine Structures*, Vol. 9, Nos. 3-4, pp. 353-388.

Jensen, J. Juncher, Mansour, A.E. and Pedersen, P. Terndrup 1991. Reliability of Jack-Up Platforms Against Overturning. *Marine Structures*, Vol. 4, pp. 203-229.

Jensen, J. Juncher and Pedersen, P. Terndrup 1979. Wave-Induced Bending Moments in Ships - A Quadratic Theory. *Trans RINA*, Supplementary Papers, Vol. 121, pp. 151-165.

Jensen, J. Juncher and Pedersen, P. Terndrup 1981. Bending Moments and Shear Forces in Ships Sailing in Irregular Waves. *Journal of Ship Research*, Vol. 24, No. 4, pp. 243-251.

Jensen, J. Juncher, Pedersen, P. Terndrup and Petersen, J. Buus 1992. Stresses in Containerships. *Jahrbuch der Schiffbautechnischen Gesellschaft*, Vol. 86, paper ST5.

Jensen, J. Juncher, Petersen, J. Buss and Pedersen, P. Terndrup 1990. Prediction of Non-Linear Wave-Induced Loads on Ships. *Proc. IUTAM Symposium on the Dynamics of Marine Vehicles and Structures in Waves*, Brunel University, London.

Kaplan, P. 1984. Analysis and Assessment of Major Uncertainties Associated with Ship Hull Ultimate Failure. Ship Structure Committee Report No. SSC-332.

Kaplan, P. and Sargent, T.P. 1972. Further Studies of Computer Simulation of Slamming and Other Wave Induced Vibratory Structural Loadings on Ships in Waves. Ship Structure Committee Report 231.

Kihl, D.P. 1993. A Comparison of Three Fatigue Assessment Procedures for Surface Ship Structures. Report No. SSPD-93-173-19, Naval Surface Warfare Center, Carderock Division, Bethesda, MD.

Kim, B-J and Kim O-H. 1995. Design Criteria of Longitudinal Hull Girder Strength Based on Reliability Analysis. *Proc. Int'l Symposium on Practical Design of Ships and Mobile Units* (PRADS '95), Seoul, **c**

Lai, K.-L. and Ayyub, B.M. 1989. Structural Reliability Assessment Using Latin Hypercube Sampling. *Proc. 5th International Conference on Structural Safety and Reliability* (ICOSSAR '89), San Francisco.

Lewis, E. 1967. Predicting Long-Term Distributions of Wave-Induced Bending Moment on Ship Hulls. Spring Meeting, SNAME.

Lewis, E.V. (ed.) 1989. *Principles of Naval Architecture*. The Society of Naval Architects and Marine Engineers (SNAME), Jersey City, NJ.

Lewis, E.V., Hoffman, D., Maclean, W.M., VanHoof, R. and Zubaly, R.B. 1973. Load Criteria for Ship Structural Design. Ship Structure Committee Report 240.

Lind, N.C. 1976. Application to Design of Level I Codes. Information Bulletin No. 112, CIB Joint Committee on Structural Safety, Paris, France, pp. 73-89.

Liu, P.L. and Kiureghian, A.D. 1986. Optimization Algorithms for Structural Reliability Analysis. Dept. of Civil Engineering, University of California at Berkeley, Report No. UCB/SESM-S6109.

Liu, P-L., Lin, H-Z. and DerKiureghian, A. 1989. CALREL User Manual. Report No. UCB/SEMM-89/18, Dept. of Civil Engineering, University of California at Berkeley.

Lotsberg, I. 1991. Target Reliability Index, A Literature Survey. Report No. 91-2023, A.S. Veritas Research, Norway.

Maddox, S.J. 1991. *Fatigue Strength of Welded Structures*, Abington Press, Cambridge, England.

Maddox, S.J. 1995. An Overview of Fatigue and Fracture Design Procedures Used in Construction Industries. *Proc. Symposium on Workshop on the Prevention of Fracture in Ship Structure*, Washington, DC, March 30-31, Marine Board, National Research Council.

Madsen, H.O., Krenk, S., and Lind, N.C. 1986. *Methods of Structural Safety*, Prentice Hall, Englewood Cliffs, NJ.

Mansour, A.E. 1970. Effective Flange Breadth of Stiffened Plates Under Axial Tensile Load or Uniform Bending Moment. *Journal of Ship Research*, Vol. 14, **pp.** _____.

Mansour, A.E. 1970. Methods of Computing the Probability of Failure Under Extreme Values of Bending Moment. M.I.T. Report No. 70-15, Sept. 1970; also *Journal of Ship Research*, 1972, Vol. 16, No. 2,

Mansour, A.E. 1972. Probabilistic Design Concepts in Ship Structural Safety and Reliability. *Trans. SNAME*, Vol. 80, pp. 64-97.

Mansour, A. and Faulkner, D. 1973. On Applying the Statistical Approach to Extreme Sea Loads and Ship Hull Strength. *RINA Trans.*, Vol. 115, pp. 277-313.

Mansour, A.E. 1974. Approximate Probabilistic Methods of Calculating Ship Longitudinal Strength. *Journal of Ship Research*, Vol. 18.

Mansour, A.E. 1975. Reliability of Marine Structure. *Proc. Third International Ocean Development Conference*, Tokyo.

Mansour, A.E. 1977. Gross Panel Strength Under Combined Loading. Ship Structure Committee Report No. SSC-270, Washington, DC.

Mansour, A.E. and Thayamballi, A. 1980. Ultimate Strength of a Ship's Hull Girder in Plastic and Buckling Modes. Ship Structure Committee, Report No. SSC-299.

Mansour, A.E. 1981. Combining Extreme Environmental Loads for Reliability-Based Designs. Invited paper, *Proc. Extreme Loads Response Symposium*, pp. 63-74.

Mansour, A. and Lozow, J. 1982. Stochastic Theory of the Slamming Response of Marine Vehicles in Random Seas. *Journal of Ship Research*, Vol. 26, No. 4, pp. 276-285.

Mansour, A.E. *et al.* 1984. Implementation of Reliability Methods to Marine Structures. *Trans. SNAME*, Vol. 92, pp. 353-382.

Mansour, A.E. 1986. Approximate Formulae for Preliminary Design of Stiffened Plates. *Proc. 5th Int'l Symposium on Offshore Mechanics and Arctic Engineering* (OMAE), Tokyo, pp. 427-434.

Mansour, A.E. 1987. Extreme Value Distributions of Wave Loads and Their Application to Marine Structures. *Marine Structural Reliability Symposium*, Arlington, VA.

Mansour, A.E. 1990. An Introduction to Structural Reliability Theory. Ship Structure Committee Report SSC 351.

Mansour, A.E., Yang, J.M. and Thayamballi, A. 1990. An Experimental Investigation on Ship Hull Ultimate Strength. *Trans. SNAME*, Vol. 98, pp. 411-440.

Mansour, A.E. 1991. Extreme Value Distributions for Linear and Non-Linear Systems and Applications to Marine Structures. The Fourth International Marine Systems Design Conference, Kobe, Japan.

Mansour, A., Thayamballi, A. and Li, M. 1992. Assessment of Reliability of Ship Structures—Phase I. Final Report on Ship Structure Committee Project SR-1344.

Mansour, A.E., Thayamballi, A., Li, M. and Jue, M. 1992. A Reliability Based Assessment of Safety Levels in the ABS Double Skin Tanker Guide. Mansour Engineering Report to ABS.

Mansour, A.E., Lin, M., Hovem, L., and Thayamballi, A. 1993. Probability-Based Ship Design Procedure: A Demonstration. Ship Structure Committee Report No. SSC-368, SR-1330.

Mansour, A.E. and Thayamballi, A. 1994. Loads and Load Combinations. Ship Structure Committee Report No. SSC-373.

Mansour, A.E. 1995. Extreme Loads and Load Combinations. *Journal of Ship Research*, Vol. 39, No. 1, pp. 53-61.

Mansour, A.E., Ayyub, Bilal, White, Gregory, and Wirsching, Paul H. 1995. Probability-Based Ship Design Implementation of Design Guidelines for Ships: A Demonstration. SSC Project No. SR-1345.

Mansour, A.E. and Jensen, J.J. 1995. Slightly Non-Linear Extreme Loads and Load Combinations. *Journal of Ship Research*, Vol. 39, No. 2, pp. 139-149.

Mansour, A.E., Lin, Y.H., and Paik, J.K. 1995. Ultimate Strength of Ships Under Combined Vertical and Horizontal Moments. *Proc. Int'l Symposium on Practical Design of Ships and Mobile Units* (PRADS '95), Seoul, pp. 2.844-2.851.

Mansour, A.E. and Wirsching, P.H. 1995. Sensitivity Factors and Their Application to Marine Structures. *Marine Structures*, Vol. 8, pp. 229-255.

Melchers, R.E. 1987. *Structural Reliability Analysis and Prediction*, Ellis Horwood Limited, UK.

Miner, M.A. 1945. Cumulative Damage in Fatigue. *ASME Transactions*, Vol. 67, pp. A159-164.

Mohr, W.C., Tsai, C., and Tso, C.M. 1995. *Fatigue Strength of Welds with Profile and Post-Weld Improvements*, Edison Welding Institute, Columbus, OH.

Moses, F. 1985. Implementation of a Reliability-Based API RP2A Format. Final Report, API PRAC 83-22, American Petroleum Institute.

Moses, F. 1986. Development of Preliminary Load and Resistance Design Document for Fixed Offshore Platforms. Final Report, API-PRAC 95-22, American Petroleum Institute.

Moses, F. and Verma, D. 1987. Load Capacity Evaluation of Existing Bridges. NCHRP Report 301, Transportation Research Board, Washington, DC.

Munse, W.H., Wilbur, T.W., Tellalian, M.L., Nicoll, K., and Wilson, K. 1983. Fatigue Characterization of Fabricated Ship Details for Fatigue. Ship Structure Committee, SSC-318, NTIS, Springfield, VA 22161.

National Research Council of Canada 1977. *National Building Code of Canada*, Ottawa.

Naess, A. and Ness, G.M. 1992. Second-Order Sum-Frequency Response Statistics to Tethered Platforms in Random Waves. *Applied Ocean Research*, Vol. 14, No. 1, pp. 23-32.

Nikolaidis, E. and Kaplan, P. 1991. Uncertainties in Stress Analysis on Marine Structures. Ship Structure Committee Report SSC-363.

Nikolaidis, E., Hughes, O.F., Ayyub, B.M., and White, G.J. 1993. A Methodology for Reliability Assessment of Ship Structures. *Ship Structures Symposium 93*, SSC/ SNAME, Arlington, VA, pp. H1-H10.

Nishihara, S. 1983. Analysis of Ultimate Strength of Stiffened Rectangular Plate. *J. Soc. Naval Architect Japan*, Vol. 154, pp. 367-375 (in Japanese).

Nordic Building Code Committee 1978. Recommendations for Loading and Safety Regulations for Structural Design. Report No. 36, Copenhagen, Denmark, 148 pp.

NS 3472 Norwegian Standard 1984. Design Rules for Steel Structures. Norwegian Standards Association, Oslo, Norway.

Ochi, M.K. and Motter, L.E. 1973. Predictions of Slamming Characteristics and Hull Responses for Ship Design. *Trans. SNAME*, Vol. 81, pp. 144-190.

Ochi, M.K. 1978. Wave Statistics for the Design of Ships and Ocean Structures. *Trans. SNAME*, Vol. 86, pp. 47-69.

Ochi, M.K. 1981. Principles of Extreme Value Statistics and Their Application. *Proc. Extreme Loads Response Symposium*, SNAME and SSC, pp. 15-30.

Ochi, M. and Motter, E. 1969. Prediction of Extreme Values of Impact Pressure Associated with Ship Slamming. *Journal of Ship Research*, Vol. 13, No. 2.

Paik, J.K. 1993. ALPS/ISUM: A Computer Program for Nonlinear Analysis of Large Plated Structures Using the Idealized Structural Unit Method. Pusan National University, Pusan.

Paik, J.K., Kim, D.H., Bong, H.S., et al. 1992. Deterministic and Probabilistic Safety Evaluation for a New Double-Hull Tanker with Transverseless System. *Trans. SNAME*, Vol. 100, pp. 173-198.

Paik, J.K., Lee, J.M. 1995. An Empirical Formulation for Predicting Ultimate Compressive Strength of Plates and Stiffened Plates. Submitted for publication in *Journal of Ship Research*.

Paik, J.K., Song, J.Y., and Kim, C.W. 1993. Development of Ultimate Longitudinal Strength Standard for Ships, Phase I: Prediction Method for Ultimate Collapse Strength of a Ship's Hull. Korean Register of Shipping, Report No. OR-04(1)-93.

Payer, H.G., Huppman, H., Jochum, Chr., Madsen, H.O., Nittinger, K., Shibata, H., Wild, W., and Wingender, H.-J. 1994. Plenary Panel Discussion on How Safe is Safe Enough? in *Structural Safety and Reliability*, Balkema, Rotterdam, Netherlands, pp. 57-74.

Proceedings, Symposium and Workshop on the Prevention of Fracture in Ship Structure. 1995. Washington, DC, March 30-31, 1995, Marine Board, National Research Council.

Radaj, D. 1990. *Design and Analysis of Fatigue Resistant Welded Structures*, Abington Press, Cambridge, England.

Rashed, S.M.H. 1975. An Ultimate Transverse Strength Analysis of Ship Structures (The Idealized Structural Method). Dr. Eng. Dissertation, Osaka University.

Ravindra, M. and Galambos, T.V. 1978. Load and Resistance Factor Design for Steel. *Journal of the Structural Division*, ASCE, Vol. 104, No. 9, pp. 1337-1354.

Ravindra, M.K., Heany, A.C., and Lind, N.C. 1969. Probabilistic Evaluation of Safety Factors. Final Report, *Symposium on Concepts of Safety of Structures and Methods of Design*, IABSE, London, pp. 36-46.

Reed, D.A. and Brown, C.B. 1992. Reliability in the Context of Design. *Structural Safety*, Vol. 11, pp. 109-119.

Richardson, W.M. 1992. Estimation of Parameter Values and Parameter Covariances for the Three Parameter Weibull Distribution. Research and Development Report SSPD-93-173-16, Naval Surface Warfare Center, Carderock Division, Bathesda, MD.

Rutherford, S.E. and Caldwell, J.B. 1990. Ultimate Longitudinal Strength of Ships: A Case Study. *Trans. SNAME*, Vol. 98, pp. 441-472.

St.Dennis, M. and Pierson, W.J. 1953. On the Motions of Ships in Confused Seas. *Trans. SNAME*, Vol. 6.

Salveson, N., Tuck, E.O. and Faltinsen, O. 1970. Ship Motions and Sea Loads. *Trans. SNAME*, Vol. 78.

Schade, H.A. 1951. Effective Breadth of Stiffened Plating. *Trans. SNAME*, Vol. 59.

Schütz, W. 1979. The Prediction of Fatigue in the Crack Initiation and Propagation Stages—A State of the Art Survey. *Engineering Fracture Mechanics*, Vol. 11, No. 2, pp. 405-421.

Schütz, W. 1993. Fatigue Life Prediction—A Review of the state of the Art. *Structural Failure, Product Liability, and Technical Insurance IV* (H.P. Rossmanith, Ed.), Elsevier, New York.

Shin, Y.S. and Lukens, R.W. 1983. Probability Based High Cycle Fatigue Life Predictions. *Random Fatigue Life Prediction*, ASME, New York.

Sikora, J.P. and Beach, J.E. 1989. Automated Method for Predicting Maximum Lifetime Loads and Fatigue Lives of Ships.

Sikora, J.P., Disenbacher, A., and Beach, J.E. 1983. A Method for Estimating Lifetime Loads and Fatigue Lives for SWATH and Conventional Monohulls. *Naval Engineers Journal*, ASNE, Vol. 95, No. 4, pp. 63-85.

Silvaria, W.A. and Brillinger, D.R. 1978. On the Maximum Wave Heights in Severe Seas. *Proc. of the Offshore Technology Conference*, Paper No. 3232, Houston, USA.

Siu, W.W.C., Parimi, S.R., and Lind, N.C. 1975. Practical Approach to Code Calibration. *Journal of the Structural Division*, ASCE, Vol. 101, No. ST7, pp. 1469-1480.

Smith, C.S. 1975. Compressive Strength of Welded Steel Ship Grillages. *Trans. RINA*, Vol. 117, pp. 325-359.

Smith, C.S. 1977. Influence of Local Compressive Failure on Ultimate Longitudinal Strength of a Ship's Hull. *Proc. of the Int'l Symposium on Practical Design in Shipbuilding (PRADS)*, Tokyo, pp. 73-79.

Society of Automotive Engineers 1977. *Fatigue Under Complex Loading*, AE-6, SAE, Warrendale, PA.

Stavovy, A.B. and Chuang, S.L. 1976. Analytical Determination of Slamming Pressures for High Speed Vehicles. *Journal of Ship Research*, Vol. 20, No. 4, pp. 190-198, Errata in Vol. 21, No. 4, 1977, p. 254.

Stiansen, S.G. and Mansour, A. 1975. Ship Primary Strength Based on Statistical Data Analysis. (including discussion and author's closure) *Trans. SNAME*, Vol. 83, pp. 214-243.

Stiansen, S.G., Mansour, A.E., Jan, H.Y., and Thayamballi, A. 1980. Reliability Methods in Ship Structures. *The Naval Architect, Journal of RINA*, Jul.

Thayamballi, A.K. 1990. A Simplified Fatigue Screening Procedure for Tankers. American Bureau of Shipping Report No. 90005.

Thayamballi, A.K., Chen, Y.N., and Liu, D. 1984. Fracture Mechanics Based Assessment of Fatigue Reliability in Ship Structures. *Proc. SSC-SNAME Ship Structures Symposium*, Arlington, VA, pp. 111-138.

Thayamballi, A.K., Kutt, L., and Chen, Y.N. 1986. Advanced Strength and Structural Reliability Assessment of the Ship's Hull Girder. *Proc. Advances in Marine Structures*, AERE, Dunfermline, Elsevier Applied Science Publ., London.

Thoft-Christensen, P. and Baker, M.J. 1982. *Structural Reliability Theory and Its Application*, Springer-Verlag, New York.

Timoshenko, S. and Woinowsky-Krieger. 1959. *Theory of Plates and Shells*, 2nd Edition, McGraw Hill Book Company, New York.

Turkstra, C.J. 1970. Theory of Structural Safety. SM Study No. 2, Solid Mechanics Division, University of Waterloo, Waterloo, Ontario.

Tvedt, L. 1983. Two Second Order Approximations to the Failure Probability. Veritas Report, RDIV/20-004-83, Det norske Veritas, Oslo, Norway.

Tvedt, L. 1990. Distribution of Quadratic Forms in Normal Space—Application to Structural Reliability. *Journal of Engineering Mechanics*, ASCE, Vol. 116, No. 6, pp. 1183-1197.

Ueda, Y., Rashed, S.M.H. and Katayama, M. 1975. Ultimate Strength Analysis of Double Bottom Structures by Idealized Structural Unit Method. *Journal of Soc. of Naval Architects Japan*, Vol. 138.

Ueda, Y., Rashed, S.M.H., and Paik, J.K. 1984. Plate and Stiffened Plate Units of the Idealized Structural Unit Method Under Inplane Loading. *Journal of Society of Naval Architects of Japan*, Vol. 156.

Ueda, Y., Rashed, S.M.H., and Paik, J.K. 1995. Buckling and Ultimate Strength Interaction of Plates and Stiffened Panels under Combined Inplane Biaxial and Shearing Forces. *Marine Structures*, Vol. 8, pp. 1-36.

Valsgaard, S. 1980. Numerical Design Prediction of the Capacity of Plates in Biaxial Inplane Compression. *Computers and Structures*, Vol. 12, pp. 729-739.

Valsgaard, S. and Steen, E. 1991. Ultimate Hull Girder Strength Margins in Present Class Requirements. *Proc. of the Marine Structural Inspection, Maintenance and Monitoring Symposium*, SSC/SNAME, Arlington, VA, pp. III.B.1-III.B.19.

Vasta, J. 1958. Lessons Learned from Full-Scale Structural Tests. *Trans SNAME*, Vol. 66, pp. 165-243.

Veritas, A.S. 1991. Guidelines for the Use of Reliability Methods. Report No. 91-2000, A.S. Veritas Research, Oslo, Norway.

Viner, A.C. 1986. Development of Ship Strength Formulations. *Proc. of Int'l Conference on Advances in Marine Structures*, Elsevier, London:New York, pp. 152-173.

Vroman, R.H. 1995. An Analysis into the Uncertainty of Stiffened Panel Ultimate Strength. U.S. Naval Academy Trident Scholar Report, Annapolis, MD, U.S.A.

Wang, X. and Moan, T. 1995. Stochastic and Deterministic Combinations of Stillwater and Wave Bending Moments in Ships. *Marine Structures 8*, Elsevier Science.

Wheaton, J.W. 1976. Further Analysis of Slamming Data from the *S.S. Wolverine State*. Ship Structures Committee Report 255.

White, G.J. and Ayyub, B.M. 1985. Reliability Methods for Ship Structures. *Naval Engineers Journal*, ASNE, Vol. 97, No. 4, pp. 86-96.

White, G.J. and Ayyub, B.M. 1987a. Reliability-Based Design Formats for Marine Structures. *Journal of Ship Research*, SNAME, Vol. 31, No. 1, pp. 60-69.

White, G.J. and Ayyub, B.M. 1987b. Reliability-Based Fatigue Design for Ship Structures. *Naval Engineers Journal*, ASNE, Vol. 99, No. 3, pp. 135-149.

Winterstein, S.R. 1988. Nonlinear Vibration Models for Extremes and Fatigue. *Journal of Engineering Mechanics*, Vol. 114, No. 10, 1772-1790.

Wirsching, P.H. 1984. Fatigue Reliability of Offshore Structures. *Journal of Structural Engineering*, ASCE, Vol. 110, pp. 2340-2356.

Wirsching, P.H. and Chen, Y.N. 1988. Considerations of Probability-Based Fatigue Design Criteria for Marine Structures. *Marine Structures*, Vol. 1, pp. 23-45.

Wirsching, P.H. and Mansour, A.E. 1995. Reliability in Fatigue and Fracture Analysis of Ship Structures. *Proc. Symposium and Workshop on the Prevention of Fracture in Ship Structure*, Washington, DC, March 30-31, 1995, Marine Board, National Research Council.

Wirsching, P.H., Ortiz, K. and Chen, Y.N. 1987. Fracture Mechanics Fatigue Model in a Reliability Format. *Prod. 6th Int'l Symposium on Offshore Mechanics and Arctic Engineering* (OMAE), Houston, TX.

PROJECT TECHNICAL COMMITTEE MEMBERS

The following persons were members of the committee that represented the Ship Structure Committee to the Contractor as resident subject matter experts. As such they performed technical review of the initial proposals to selec the contractor, advised the contractor in cognizant matters pertaining to the contract of which the agencies were aware, performed technical review of the work in progress and edited the final report.

Chairman

Dr. William Richardson -   Naval Surface Warfare Center, Carderock Diviosion

Members

Dr. H. H. Chen   American Bureau of Shipping

Mr. Chris Morlan   American Bureau of Shipping

LCDR Rob Holzman   U. S. Coast Guard

Mr. Bob Sedat   U. S. Coast Guard

Mr. Fred Seibold   Maritime Administration

Dr. Neil Pegg   Defence Research Establishment Atlantic

Mr. Tom Packard   Naval Sea Systems Command

Dr. Kieth Hjelmstad   University of Illinois

Dr. Solomon Yim   Oregon State University

Mr. William Siekierka   Naval Sea Systems Command,
                Contracting Officer's
                Technical Representative

Dr. Robert Sielski   National Academy of Science,
Mr. Alex Stavovy   Marine Board Liaison

LT Thomas C. Miller   U.S. Coast Guard, Executive Director
CDR Steve Sharpe   Ship Structure Committee
CDR Mike Parmelee

COMMITTEE ON MARINE STRUCTURES

Commission on Engineering and Technical Systems

National Academy of Sciences - National Research Council

The **COMMITTEE ON MARINE STRUCTURES** has technical cognizance over the interagency Ship Structure Committee's research program.

Dr. John Landes, *Chairman*, University of Tennessee, Knoxville, TN

Mr. Howard M. Bunch, University of Michigan, Ann Arbor, MI

Dr. Dale G. Karr, University of Michigan, Ann Arbor, MI

Mr. Andrew Kendrick, NKF Services, Montreal, Quebec

Dr. John Niedzwecki, Texas A & M University, College Station, TX

Dr. Alan Pense, NAE, Lehigh University, Bethlehem, PA

Dr. Barbara A. Shaw, Pennsylvania State University, University Park, PA

Dr. Robert Sielski, National Research Council, Washington, DC

CDR Stephen E. Sharpe, Ship Structure Committee, Washington, DC

LT Thomas Miller, Ship Structure Committee, Washington, DC

DESIGN WORK GROUP

Dr. John Niedzwecki, *Chairman*, Texas A&M University, College Station, TX

Dr. Bilal Ayyub, University of Maryland, College Park, MD

Mr. Ovide J. Davis, Pascagoula, MS

Mr. Andy Davidson, NASSCO, San Diego, CA

Dr. Maria Celia Ximenes, Chevron Shipping Co., San Francisco, CA

Mr. Jeffrey Geiger, Bath Iron Works, Bath, ME

Mr. Hugh Rynn, Sea-Land Services, Elizabeth, NJ

MATERIALS WORK GROUP

Dr. Barbara A. Shaw, *Chairman*, Pennsylvania State University, University Park, PA

Dr. David P. Edmonds, Edison Welding Institute, Columbus, OH

Dr. John F. McIntyre, Advanced Polymer Sciences, Avon, OH

Dr. Harold S. Reemsnyder, Bethlehem Steel Corp., Bethlehem, PA

Dr. Bruce R. Somers, Lehigh University, Bethlehem, PA

RECENT SHIP STRUCTURE COMMITTEE PUBLICATIONS

Ship Structure Committee Publications - A Special Bibliography This bibliography of SSC reports may be downloaded from the internet at: "http://www.dot.gov/dotinfo/uscg/hq/nmc/nmc/ssc1/index.htm".

SSC-397   **Commercial Ship Design and Fabrication for Corrosion Control** J. Parente, J. Daidola, N. Basar, R. Rodi 1997

SSC-396   **Optimized Design Parameters for Welded TMCP Steels** L. Malik, R. Yee, B. Graville, A. Dinovitzer 1997

SSC-395   **Ship's Maintenance Project, Pt II & III** B. Bea, T. Xu, K. Ma, R. Shulte-Strathaus 1997

SSC-394   **Strength Assessment of Pitted Plate Panels** J. Daidola, J. Parente, I. Orisamolu, K-t. Ma 1997

SSC-393   **Evaluation of Ductile Fracture Models** R. Dexter, M. Gentilcore 1997

SSC-392   **Probability Based Ship Design: Implementation of Design Guidelines** A. Mansour, P. Wirsching, G. White, B. Ayyub 1996

SSC-391   **Evaluation of Marine Structures Education in North America** R. Yagle 1996

SSC-390   **Corrosion Control of Inter-hull Structures** M. Kikuta, M. Shimko, D Ciscom 1996

SSC-389   **Inspection of Marine Structures** L. Demsetz, R. Cario, R. Schulte-Strathaus, B. Bea 1996

SSC-388   **Ship Structural Integrity Information System-Phase II** M. Dry, R. Schulte-Strathaus, B. Bea 1996

SSC-387   **Guideline for Evaluation of Finite Elements and Results** R. I. Basu, K. J. Kirkhope, J. Srinivasan 1996

SSC-386   **Ship's Maintenance Project** R. Bea, E. Cramer, R. Schulte-Strauthaus, R. Mayoss, K. Gallion, K. Ma, R. Holzman, L. Demsetz 1995

SSC-385   **Hydrodynamic Impact on Displacement Ship Hulls - An Assessment of the State of the Art** J. Daidola, V. Mishkevich 1995

SSC-384   **Post-Yield Strength of Icebreaking Ship Structural Members** C. DesRochers, J. Crocker, R. Kumar, D. Brennan, B. Dick, S. Lantos 1995